Robust Controller Design and Evaluation for a Small Underwater Vehicle

by

Cedric Leonard Logan

B.S., Electrical Engineering, The University of Alabama, (1989)

SUBMITTED TO THE DEPARTMENT OF
ELECTRICAL ENGINEERING AND COMPUTER SCIENCE
IN PARTIAL FULFILLMENT OF THE REQUIREMENTS FOR THE DEGREES OF

ELECTRICAL ENGINEER

and

MASTER OF SCIENCE
IN ELECTRICAL ENGINEERING AND COMPUTER SCIENCE

at the

MASSACHUSETTS INSTITUTE OF TECHNOLOGY
February 1993

Signature of Author____
Department of Electrical Engineering
and Computer Science, January 1993

Certified by____
Dr. Michael Athans
Thesis Supervisor
Professor of Systems Science and Engineering
Department of Electrical Engineering and Computer Science

Certified by____
William F. Bonnice
Technical Supervisor
The Charles Stark Draper Laboratory

Accepted by____
Professor Campbell L. Searle
Chairman, Departmental Graduate Committee
Department of Electrical Engineering and Computer Science

Robust Controller Design and Evaluation for a Small Underwater Vehicle

by

Cedric Leonard Logan

Submitted to the Department of Electrical Engineering and Computer Science
on February 2, 1993 in Partial Fulfillment of the Requirements for
the Degrees of Electrical Engineer and
Master of Science in Electrical Engineering and Computer Science

ABSTRACT

A comparison of the H_∞/μ-Synthesis design methodology, the Sliding-Mode design methodology, and the Sliding-Mode Augmented design methodology, was done for heading and depth control of the Draper Laboratory/MIT Sea Grant *Sea Squirt* autonomous underwater vehicle (AUV). The H_∞/μ-Synthesis approach required the use of an uncertain full-order linear-time invariant approximation to the AUV full-order nonlinear model, which was converted into a suitable design model by adding a set of frequency-domain "loopshaping" weighting functions as design parameters. The Sliding-Mode approach required the use of a reduced-order nonlinear approximation to the full-order nonlinear AUV model, together with a reduced-order uncertainty representation. The Sliding-Mode parameter selection process was based on several design "rule-of-thumb" guidelines from the literature. The approximate decoupling of the AUV heading and depth dynamics allowed for decoupled heading and depth designs for both the H_∞/μ-Synthesis and the Sliding-Mode methodologies. The Sliding-Mode Augmented approach for the *Sea Squirt* AUV control design used an H_∞ designed linear time-invariant controller augmented by a Sliding-Mode based nonlinear control law.

The H_∞/μ-Synthesis based controllers and the Sliding-Mode based controllers were implemented and tested by using a simulation of the AUV full-order nonlinear model (including thruster and sensor dynamics). The performance of the controllers was analyzed (for a simultaneous depth and heading maneuver) over the approximate range of "typical" axial velocities commanded by the AUV. The performance of the controllers in the face of additive sensor noise was also analyzed. For the Sea Squirt design example, the H_∞/μ-Synthesis based controllers exhibited consistently better heading performance than the Sliding-Mode based controllers (due to incorporating the effects of an approximately linear Munk moment uncertainty into the design). The Sliding-Mode based controllers exhibited consistently better depth performance than the H_∞/μ-synthesis based controllers (due to incorporating the effects of the state-dependent nonlinear hydrodynamic "drag" forces into the design process). The Sliding-Mode Augmented controller exhibited better overall heading performance (due to incorporating both the Munk-moment dynamic uncertainty and the hydrodynamic-drag forces into the designs).

Thesis Supervisor:	Dr. Michael Athans
Title:	Professor of Systems Science and Engineering
Technical Supervisor	William F. Bonnice
Title:	Autonomous Systems Chief The Charles Stark Draper Laboratory

This report was prepared at the Charles Stark Draper Laboratory, Inc. under Independent Research and Development Program Nos. 276 and 438. Publication of this report does not constitute approval by Draper Laboratory of the findings or the conclusions contained herein. It is published solely for the exchange and stimulation of ideas.

Acknowledgments

I would like to first thank the Charles Stark Draper Laboratory for providing me with the opportunity to further my education at MIT through the financial and technical support of the Draper Fellow Program. I would like to also thank the MIT Sea Grant College Program for providing me with the necessary technical information and technical support for the *Sea Squirt* autonomous underwater vehicle (AUV). In addition, I would like to thank both the National Consortium for Graduate Degrees for Minorities in Engineering and Science, Inc. (GEM) and Schlumberger Well Services for providing me with both financial support and technical experience through the GEM Fellowship Program.

I would like to thank my Draper supervisor, Bill Bonnice, for his guidance and patience with me for the long time it took to finish this thesis (showing me grace when he should have showed me the door..). I would like to also thank him for helping learn how to organize my thoughts in a clear and concise manner (especially as related to the conclusions presented in this thesis). I would like to thank my MIT supervisor, Professor Michael Athans, for his guidance and expertise in "real-world" control-system design. I would especially like to thank him for always calling me to a high standard of excellence in my research. I would like to also thank Brent Appleby for helping me understand many of the basic concepts of H_∞/μ-Synthesis (as well as writing much of the H_∞/μ-Synthesis control-design software). In addition, I would like to thank Walt Baker for providing me with financial support under his Learning Augmented Control IR&D program (as well as encouraging me not to get too distracted when finishing this thesis).

I would like to thank my parents, Sidney Jr. and Earlean Logan, for their constant love, devotion, and patience during the years of my "exile" at MIT. I would also like to thank my sisters: Marcella, Cassandra, Mildred, and Arnell, and my brothers: Winfred, Rodney, and Sidney III, for their love and devotion as well.

I would like to thank my Draper officemates, Alfredo (Dino) DeAngelis and Kortney (DLFB) Leabourne for making everyday in the office an exciting day. I would also like to thank them for putting up with a marginal psychotic who hangs old circular-saw blades on his wall. I also would like to thank the others at Draper (past and present) who have encouraged me and helped me along the way: Bernd Clauberg (for much of the technical support for the operation of the *Sea Squirt*), Doug Humphrey (for writing and

organizing virtually all of the *Sea Squirt* planning and control software), Pete Millington, Bob Regan, Mark Koenig, Dave Hanson, Bill Hall, Bob Beaton, Naz Bedrossian, Mitch Livstone, Jay Farrell, Torsten Berger, Greg Chamitoff, Susan Champagne, Eva Moody, Achille Messac, Thomas Glenn, Rami Mangoubi, Ruth Caswell, Dan Fonte, J.P. Babka, Dean Cerrato, Steve Mark, Steve Atkins, Steve Stephanides, Bryan Kang, Joe Wall, Karl Flueckiger, Paul Motyka, Jim Harrison, Eli Gai, Bill Goldenthal, John Dowdle, and Fred Boelitz, et al. I would also like to thank those brave men and women who keep Draper safe for democracy: Rod Clark ("Best Haircuts in Boston.."), Tony Martin, Mike Trent, Armando Colon, Robin Glavickas, Pat Silveira, Joseph Salterio, Eugene Varallo, William Bourqault, William Mattos, and Robert Welch (Author's note: If any of you was either left out or had your name misspelled, take it up with Tony since he made up the list....). I would like to thank Steve Morales and Percell Porcey for cleaning up after my slob officemates and myself.

I would like to thank all members of the MIT Sea Grant AUV Lab, as well as the publications and administrative offices of MIT Sea Grant. I would especially like to thank Tom Consi for being a great friend and foil for political and social discussions (as well as introducing me to East African and Brazilian cuisine). I also would like to thank Jim Bellingham for his sound professional and technical advice, as well as helping me learn what the important issues are when designing systems for "real-world" underwater vehicles. In addition I would like to thank Rita Queen for always encouraging me to persevere toward my goals. I would like to thank Diane DiMassa for doing a great job of organizing *Sea Squirt* operations, as well as organizing much of the necessary technical support. Of course, I would like to thank (nearly) everyone else as well at Sea Grant (past and present): Professor Chrys Chryssostomidis, ReRe Quinn, Jim Bales, John Leonard, Carolyn Levi, Cliff Goudey, Brian Tracey, Dave Gerson, Drew Bennett, Joice Himawan, Brad Moran, Karen Hartley, Tekla McInerny, Leah McGavern, Max Defenbaugh, Omar Green, Chad Brown, Erick Alvarado, Dave Chen, Norm Doelling, Christine McDonald, Christof Rehling, Michel Perrier, Chelle Gentemann, Gina Middaugh, Chris Smith, Madeline Hall-Arber, Tim Downes, John Moore, Kathy Seaward, Bill Upthegrove, Hope Abramson, Don Atwood, Kathy King, Kathleen Heide, Julie Eastman, and E. Ray Pariser.

I would to thank Randy Saunders for being a best friend to me and encouraging me through the darker days of writing this thesis (especially over coffee at the 24 Hour Coffee Haus). I would also like to thank Dan Zachary for helping me learn how to be joyful in the midst of the most trying of circumstances. I also would like to thank everyone else at

Harvard/MIT/Tufts (past and present. I apologize if I missed anyone..) who have been my family away from home, especially Vic Gobbell, Howard and Ann (Black) Loree, Dean Farmer, Kim Horowitz, Randy and Kay Mckean, Peter Rothschild, Allan Marshall, Harris Gilliam, Rob Grace, Kim Oakberg, Joanne Liu, Kristine Drobot, John Oates, Rob Kim, Bryan Klassen, Byron Stewart, Rob Banks, Brett Krieder, Mike Domroese, Elsa Mak, Greg Adams, Ethan Wenger, Jim Ryan, Lisa Chou, Susan Park, Micheal and Vicky (Brant) Wynne, Ted and Yuri Sung, Mike Lee, Jude Federspiel, Chris Lee, Mark Wintersmith, Mark Rawizza, Andrew Romain, Jon Hardy, Jose Elizondo, Isaac Hand, Kristy Jensen, Scott Sweeney, Steve Body, Danielle Dunlap, Dave Houston, Rick Rodriguez, Esther Furmin, Donna Johnson, Deborah Flynn, Amber Smith, Chelsea Wilkins, Suzanne Bedoin, Alisha James, Wendy Wai, Jee-Lian Yap, Rosemary Kelly, Omar Richard-Sutherland, Benoit DeGouville, Tim Resch, and Sandy Reed.

I would like to thank Hugh and Lee Herr for being great friends, as well opening their home to me in my times of need. I also would like to thank many others at Ashdown and elsewhere at MIT (and various other places) for their encouragement and support (I apologize if I missed anyone..): Kathy Misovec, John Matz, Brian Eidson, Jee-Hoon Yap, Thomas Kettler, Dan Frost, Virgil Foster, Gilbert Chiang, Monika Gorkani, Ben Bacon, Christ Richmond, Gerald Prioleau, Dean Isaac Colbert, Frank Espinoza, Charles Lee, Jose Lopez, Joel Douglas, Kirk Gilpin, Mike Perrott, Tom Lee, Duncan Reijnen, Jim McCarrick, Vipul Bhushan, S. Papa Rao, Joel Johnson, Dan Crews, James Njeru, Oumar Ndiaye, Jarvis Jacobs, Monica Choi, Diane Ho, Rulane Merz, Larry Hsu, Charles Huang, Carmen Turner, Professor Vernon and Beth Ingram, Adam Powell, Mohammed Farnish, Greg Troxel, Kevin Ressler, Caryl Brown, Paul Martin, Esteban Torres, Angela Longo, Lynn McDonough, Professor Jeff Shapiro (for his sound professional advice), Marilyn Pierce, Carmen O'Brien, Jerry and Zelda Fruzia, Foy Barge, Doug Robinson, Dr. Mario Magana (for advising me to come to MIT in the first place), David Smithermann, Billy Stapleton, Kim Draughn, et al..

I would like to thank the teachers and staff of the Central High School (Hayneville, AL) for preparing me at an early age, as well as the teachers and staff of the Lowndes County Area Vocational School. I would like to thank the University of Alabama for allowing me to further my undergraduate engineering education. I would like to thank Bill Flanagan, Clay Jordan, Larry Lloyd, Cathy Gadomski, Michael Greenberg, Guy Vachon, Diane Wallace, et al at Houston Downhole Sensors.

Praise be to the God and Father of our Lord Jesus Christ, the Father of compassion and the God of all comfort, who comforts us in all our troubles, so that we can comfort those in any trouble with the comfort we ourselves have received from God. For just as the sufferings of Christ flow over into our lives, so also through Christ our comfort overflows. If we are distressed, it is for your comfort and salvation; if we are comforted, it is for your comfort, which produces in you patient endurance of the same sufferings we suffer. And our hope for you is firm, because we know that just as you share in our sufferings, so also you share in our comfort.

We do not want you to be uninformed, brothers, about the hardships we suffered in the province of Asia . We were under great pressure, far beyond our ability to endure, so that we despaired even of life. Indeed, in our hearts we felt the sentence of death. But this happened that we might not rely on ourselves, but on God, who raises the dead. He has delivered us from such a deadly peril, and He will deliver us. On Him we have set our hope that He will continue to deliver us, as you help us by your prayers. Then many will give thanks on our behalf for the gracious favor granted us in answer to the prayers of many.

II Corinthians 1:3-11 (NIV)

Table of Contents

Chapter 1

Introduction

The *Sea Squirt* is a small, autonomous underwater vehicle (AUV) originally developed in January of 1988 as part of a joint educational project between the Charles Stark Draper Laboratory (CSDL) and the M.I.T. Sea Grant Program. The purpose of this vehicle is to act as a testbed for control-system, planning, and sensor design for autonomous underwater systems. Some of the missions typically performed by this vehicle include underwater surveys, water-quality measurements, and undersea obstacle detection.

1.1 DESIGN PROBLEM AND APPROACH

The control of underwater vehicles, such as the *Sea Squirt* AUV, presents several challenging design issues. First, and foremost, the dynamics of such vehicles are often nonlinear and difficult to model accurately. Second, underwater vehicles are subjected to underwater currents, waves, and other disturbances that are also difficult to model. Third, such a vehicle may have varying physical configurations, depending on its particular mission. Thus, it would be advantageous for the control system used for an underwater vehicle to be robust, i.e., maintain stability (and hopefully, performance) even with the design challenges described above.

There are many existing methodologies for robust control system design. Two of these methodologies are based on H_∞/μ-Synthesis Control and Sliding Mode Control. H_∞ Control is a linear control design methodology. It tries to achieve its design goals by finding the stabilizing linear controller that minimizes the frequency-domain effects of disturbances on the stability and/or performance of the system. When used in conjunction with the so-called Small-Gain Theorem, H_∞ control can produce designs that are robust to bounded, linear time-invariant (LTI) modeling errors. μ-Synthesis is an extension of H_∞ Control that attempts to reduce the design conservatism that occurs when there are multiple sources of LTI uncertainty, while preserving the H_∞ robustness properties.

Sliding-Mode Control is a robust nonlinear control design methodology. It tries to achieve its design objectives by constraining the dynamics of the system to a linear hypersurface in state-space, thereby forcing these dynamics to behave in a linear fashion. When used in conjunction with Lyapunov system theory, Sliding-Mode Control produces control designs with guaranteed robustness properties in the face of plant parametric uncertainty. In addition, if an interpolating "boundary-layer" is added, a direct tradeoff can be made between performance and stability robustness to bounded high-frequency unmodeled dynamics.

With a suitable design model, the H_∞/μ-Synthesis and Sliding-Mode design methodologies can be used to design robust controllers for the vehicle. Such a model can be developed by first examining the physical Equations-of-Motion (EOM) for the AUV in order to determine the revelant dynamics. These Equations-of-Motion can then be simplified by considering what the normal modes of operation of the vehicle would be. From this simplification, a suitable nonlinear model for applying the Sliding-Mode methodology can be obtained. Bounded modeling uncertainty, as well as bounded disturbances can be included in this model. This uncertain reduced-order nonlinear model can then be linearized around some nominal operating point of the AUV to produce an uncertain linear time-invariant (LTI) model. By adding frequency-domain weighting functions and making the appropriate definitions, this uncertain linear model can be converted into the so-called Standard-Form model for H_∞/μ-synthesis design. The H_∞/μ-Synthesis methodology can then be applied to this model to produce a robust LTI controller. In addition, several frequency-domain tests can be applied to the closed-

loop form of this model in order to determine, *a priori*, the stability and/or performance robustness properties of the final design.

A performance comparison of the resulting robust control designs can be done by using the actual vehicle and/or computer simulations of the vehicle dynamics. The results of such a comparative study can then be used to determine which of the design methodologies is best suited for control problems, such as the AUV.

1.2 THESIS OVERVIEW AND OUTLINE

In summary, the goal of this thesis was to conduct a rigorous comparison of the design, implementation, and performance of the H_∞/μ-Synthesis and Sliding-Mode robust control-system design methodologies for heading and depth control of the *Sea Squirt* AUV. Even though the robust control designs presented in this thesis were specifically for the *Sea Squirt*, it is hoped that the conclusions can be generalized to robust control design for other types of systems as well.

Chapter 2 of this thesis begin with a presentation of the H_∞/μ-synthesis design methodology for robust control systems. First, a survey of the Standard Form (SF) representation is given. Some techniques for representing modeling uncertainty in linear time-invariant (LTI) systems are presented. This modeling-uncertainty presentation also details the development of a technique for representing parametric type uncertainty for a "generalized" LTI state-space system. The Small-Gain Theorem and its role in robust control system design and analysis are discussed. An H_∞ robust design technique based on the Small-Gain Theorem is presented. The Structured Singular Value (μ) is defined and its use as a measure of robust stability and performance is discussed. Finally, an algorithm for μ-based robust control design is presented.

Chapter 3 presents the Sliding-Mode design methodology for robust nonlinear control systems. It begins with a brief survey of the so-called Descriptor/Companion class of nonlinear systems. This survey also includes a representation of the modeling uncertainty that can be incorporated into the Sliding-Mode design process. The Sliding-Mode control law for the Descriptor/Companion class of systems is presented, together

with a description of the so-called "boundary layer". Lastly, a technique is presented for designing control systems where a Sliding-Mode based controller augments a linear, time-invariant (LTI) dynamic controller.

Chapter 4 describes the *Sea Squirt* vehicle and the design models (full-order and reduced order, linear and nonlinear) developed from the physical Equations-of-Motion. This chapter also presents some analysis results (e.g., time-domain simulation analysis, eigenstructure analysis, frequency response analysis, etc.) for these models. In addition, this chapter discusses the models used for the vehicle's sensors and actuators.

Chapter 5 describes the design of H_∞/μ-Synthesis based robust heading and depth controllers for the AUV using the full-order LTI model developed in Chapter 4. It begins with a discussion of some of the general AUV control system requirements and performance goals. The derivation of the H_∞/μ-synthesis Standard-Form design model from the full-order LTI model is described. The design of the full-order AUV controller using the H_∞ design methodology is detailed. Lastly, the design of the full-order AUV controller using μ-synthesis is detailed.

Chapter 6 discusses the design of the Sliding-Mode robust controller. It begins in with a review of some of the general AUV control system requirements and performance goals. The design of the AUV depth and heading controllers using the Sliding-Mode methodology is described. Lastly, the performance of the AUV Sliding-Mode controllers illustrated by a computer simulation of the "nominal" design model.

Chapter 7 describes the robust control designs where an H_∞/μ-Synthesis based LTI controller is augmented by a Sliding-Mode based controller.

Chapter 8 presents the results of a computer simulation comparison of the robust control designs. These results are shown for combined heading and depth control during a full scale autonomous test. This chapter also presents some issues involved in implementing the robust control designs on the AUV.

Chapter 9 presents the conclusions from the comparison between the robust control designs for the Sea Squirt AUV.

Chapter 2

H_∞/μ-Synthesis Robust Control

H_∞/μ-Synthesis is one of the more recent developments in the field of control-system design. H_∞ control is an optimization technique for finding the stabilizing linear control law (if it exists) that minimizes the effects of a set of exogenous disturbance inputs upon a set of "performance" outputs, where these disturbance inputs and "performance" outputs are defined in accordance with the so-called Standard Form (SF) plant representation for linear systems. Together with the "Small-Gain" theorem and/or several frequency-domain "loop-shaping" techniques, H_∞ control can be used to design control systems with guaranteed stability and performance robustness properties (if the uncertainty in the system is assumed bounded, stable, and linear time invariant).

One important drawback, however, of H_∞ control is that it has a tendency to produce unnecessarily conservative control designs for plant models containing multiple sources of uncertainty. To reduce this design conservatism for multiple-uncertainty plants, Doyle[3] introduced the idea of the Structured Singular Value (μ) as a measure of robust stability and performance. From this idea followed the μ-Synthesis design methodology [4], which, in many respects, is an extended version of H_∞ control. The μ-Synthesis design methodology is a "double" optimization technique that involves solving a standard H_∞ optimization problem together with a convex optimization of a series of frequency-dependent weights (where these weights are defined at each source of bounded LTI modeling uncertainty in the system).

This chapter presents the H_∞/μ-synthesis design methodology for robust control systems. A survey of the Standard Form (SF) representation is given in Section 2.1. Section 2.2 presents some techniques used for representing modeling uncertainty in linear time-invariant (LTI) systems. This section also details the development of a technique for representing parametric type uncertainty for a "generalized" LTI state-space system. Section 2.3 discusses the Small-Gain Theorem and its role in robust control system design and analysis. An H_∞ robust design technique based on the Small-Gain Theorem is presented in Section 2.4. Section 2.5 defines the Structured Singular Value (μ) and discusses its use as a measure of robust stability and performance. Finally, an algorithm for μ-based robust control design is presented in Section 2.6.

2.1 STANDARD FORM MODEL FOR ROBUSTNESS ANALYSIS AND DESIGN

The Standard Form (SF) Model for robustness analysis and design has the general form shown in Figure 2.1. Here, **P**(s) is the "open-loop" SF system, **K**(s) is a linear time-invariant controller and $\Delta(s)$ is a norm-bounded block-diagonal perturbation matrix given by

$$\Delta(s) = \begin{bmatrix} \Delta_1(s) & 0 & \cdots & 0 \\ 0 & \Delta_2(s) & & \vdots \\ \vdots & & \ddots & 0 \\ 0 & \cdots & 0 & \Delta_m(s) \end{bmatrix} \qquad (2.1)$$

where each block element term, $\Delta_i(s)$, (which can be multi-input, multi-output) represents a single source of bounded LTI modeling uncertainty in the system. In order to simplify any robustness analysis, the $\Delta_i(s)$ terms are usually normalized such that

$$\bar{\sigma}[\Delta_i(j\omega)] < 1 \quad \forall\ \omega \qquad (2.2)$$

where $\bar{\sigma}$ denotes the maximum singular value.

In most cases, this normalization is done by augmenting the open-loop SF model, **P**(s) with a series of frequency-domain weighing functions.

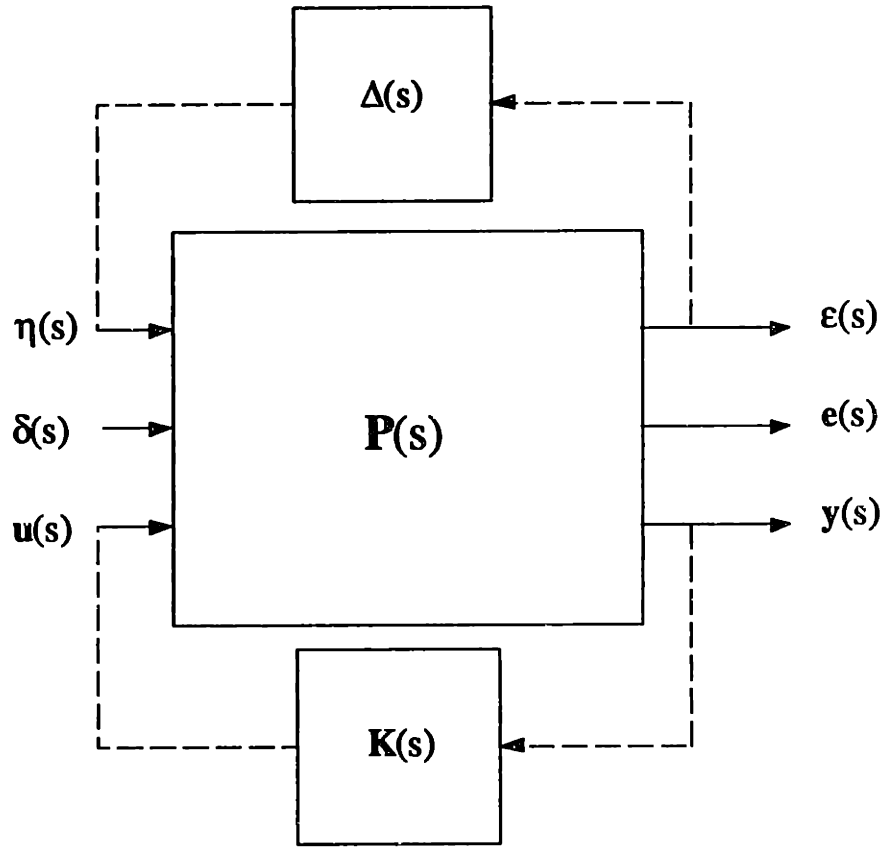

Figure 2.1: Standard Form Model

The outputs of the SF model of Figure 2.1 are an observation output vector, **y**, and a performance measure vector, **e**. The vector **e** consists of variables that are desired to be "small" (e.g., weighted tracking errors, control magnitudes, etc.). The inputs of the SF model are a control input vector, **u**, and a system disturbance vector, δ. The vector δ consists of all inputs external to the closed-loop system (e.g., weighted disturbance forces, reference signals, sensor-noise signals, etc.). The nine-block transfer-function for the SF open-loop system, **P**(s), is given by

$$\begin{bmatrix} \varepsilon \\ e \\ y \end{bmatrix} = \begin{bmatrix} P_{11}(s) & P_{12}(s) & P_{13}(s) \\ P_{21}(s) & P_{22}(s) & P_{23}(s) \\ P_{31}(s) & P_{32}(s) & P_{33}(s) \end{bmatrix} \begin{bmatrix} \eta \\ \delta \\ u \end{bmatrix} \tag{2.3}$$

The open-loop SF model and a given linear controller K(s) can be combined to form the closed-loop representation shown in Figure 2.2.

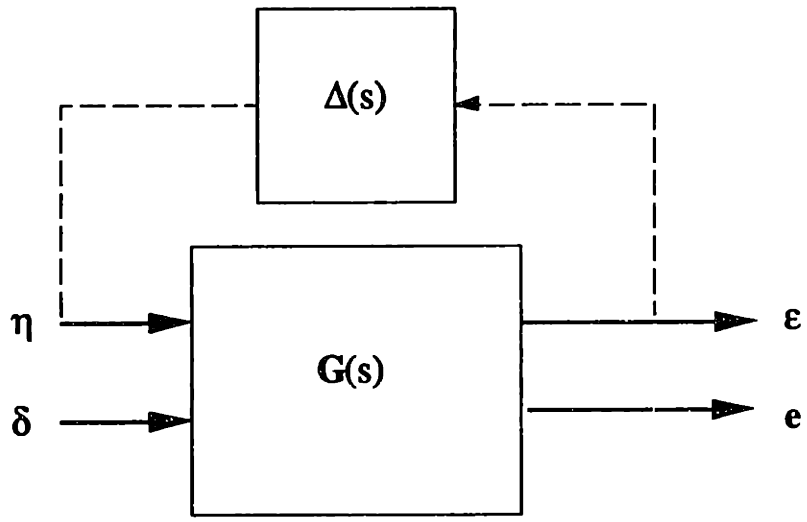

Figure 2.2: Closed-Loop SF Representation

The four-block transfer function of the closed-loop SF system of Figure 2.2 is given by

$$\begin{bmatrix} \varepsilon \\ e \end{bmatrix} = \begin{bmatrix} G_{11}(s) & G_{12}(s) \\ G_{21}(s) & G_{22}(s) \end{bmatrix} \begin{bmatrix} \eta \\ \delta \end{bmatrix} \tag{2.4}$$

where

$$G_{11}(s) = P_{11}(s) + P_{13}(s)K(s)(I - P_{33}(s)K(s))^{-1}P_{31}(s) \tag{2.5}$$

$$G_{12}(s) = P_{12}(s) + P_{13}(s)K(s)(I - P_{33}(s)K(s))^{-1}P_{32}(s) \tag{2.6}$$

$$\mathbf{G_{21}(s) = P_{21}(s) + P_{23}(s)K(s)(I - P_{33}(s)K(s))^{-1}P_{31}(s)} \qquad (2.7)$$

$$\mathbf{G_{22}(s) = P_{22}(s) + P_{23}(s)K(s)(I - P_{33}(s)K(s))^{-1}P_{32}(s)} \qquad (2.8)$$

The performance transfer-function matrix (i.e., the transfer function matrix from the disturbance input, δ, to the performance measure output, **e**), of the nominal closed-loop system is given by $\mathbf{G_{22}(s)}$ and the performance transfer-function matrix of the perturbed closed-loop system is given by

$$\mathbf{G_{ed}(s) = G_{22}(s) + G_{21}(s)\Delta(s)[I - G_{11}(s)\Delta(s)]^{-1}G_{12}(s)} \qquad (2.9)$$

The performance goal for the SF system is to minimize the effects of the disturbances, δ, on the performance-measure vector, **e**. This implies that the desired design goal for the SF system is to find the stabilizing controller, **K(s)**, which minimizes, in some fashion, the performance transfer-function matrix given by (2.9). However, from (2.9), the uncertainty, $\Delta(s)$, also affects the performance of the SF system. Then for "robust" performance, the desired design goal is to now find the stabilizing controller that not only minimizes the performance transfer-function matrix, but which also makes it as insensitive as possible to changes in $\Delta(s)$.

2.2 MODELING UNCERTAINTY IN LTI SYSTEMS

Modeling uncertainty can occur in a linear time-invariant (LTI) dynamic system in many forms. However, for the stability and performance robustness measures of this chapter (Small Gain and μ), the modeling uncertainty must be restricted to stable LTI perturbations. This class of perturbations still covers a wide range of modeling errors, such as plant parameter errors, unmodeled sensor and actuator dynamics, and errors due to using reduced-order plant models. This class of perturbations can be broken down into two main classes: parametric uncertainty and uncertain dynamic models.

2.2.1 Parametric State-Space Uncertainty

The first class of modeling perturbations to be considered is state-space parametric uncertainty. Here, the LTI plant model is assumed to be given by the following generalized state-space description [1](unmodeled dynamics are assumed to be neglected)

$$\mathbf{E}\dot{\mathbf{x}} = \mathbf{A}_1\mathbf{x} + \mathbf{B}_1\mathbf{u} + \mathbf{L}_1\mathbf{d} \tag{2.10}$$

$$\mathbf{y} = \mathbf{C}_1\mathbf{x} + \mathbf{D}_1\mathbf{u} + \mathbf{D}_2\mathbf{d} \tag{2.11}$$

where **x** is the state vector, **u** is a "control" input vector, and **d** is a "disturbance" input vector. The matrix **E** is assumed to be nonsingular. In the literature, **E** is usually assumed to be the identity matrix [2]. However, for many physical systems, **E** can be modelled directly (and somewhat easily) as a "mass and inertia" matrix, with the condition of it being nonsingular. For this more generalized "physical" representation, parametric uncertainty can be modeled as

$$\begin{aligned}\left(\mathbf{E}_o - \sum_{j=1}^{m} \Delta\mathbf{E}_j\delta_j\right)\dot{\mathbf{x}} = &\left(\mathbf{A}_{1o} + \sum_{i=1}^{k} [\Delta\mathbf{A}_1]_i\delta_i\right)\mathbf{x} \\ &+ \left(\mathbf{B}_{1o} + \sum_{i=1}^{k} [\Delta\mathbf{B}_1]_i\delta_i\right)\mathbf{u} \\ &+ \left(\mathbf{L}_{1o} + \sum_{i=1}^{k} [\Delta\mathbf{L}_1]_i\delta_i\right)\mathbf{d}\end{aligned} \tag{2.12}$$

[1] This also referred to as the descriptor form.

$$\mathbf{y} = \left(\mathbf{C}_{1o} + \sum_{i=1}^{k} [\Delta \mathbf{C}_1]_i \delta_i\right)\mathbf{x} + \left(\mathbf{D}_{1o} + \sum_{i=1}^{k} [\Delta \mathbf{D}_1]_i \delta_i\right)\mathbf{u} + \left(\mathbf{D}_{2o} + \sum_{i=1}^{k} [\Delta \mathbf{D}_2]_i \delta_i\right)\mathbf{d} \tag{2.13}$$

Each of the scalars, δ_i and δ_j, represent normalized parameter errors of the form

$$-1 < \delta_i < 1 \quad \forall\, i \tag{2.14}$$

$$-1 < \delta_j < 1 \quad \forall\, j \tag{2.15}$$

The perturbation matrices associated with each uncertain parameter can be combined into the following "master" uncertainty matrices

$$\begin{bmatrix} [\Delta \mathbf{A}_1]_i & [\Delta \mathbf{B}_1]_i & [\Delta \mathbf{L}_1]_i \\ [\Delta \mathbf{C}_1]_i & [\Delta \mathbf{D}_1]_i & [\Delta \mathbf{D}_2]_i \end{bmatrix} \in R^{(n_x + n_y)\times(n_x + n_u + n_d)} \tag{2.16}$$

$$[\Delta \mathbf{E}_j] \in R^{(n_x)\times(n_x)} \tag{2.17}$$

where n_x, n_y, n_u, and n_d are the dimensions of **x**, **y**, **u**, and **d**, respectively. Note that for this generalized model, errors in the "mass and inertia" matrix, **E**, were assumed to be independent of errors in the other matrices.

In general, a single parameter error will rarely affect all of the states and outputs of the model given by (2.10) and (2.11). This implies that the "master" uncertainty matrices will not be of full rank. From this, these matrices can be written in the following reduced forms

$$\begin{bmatrix} [\Delta \mathbf{A}_1]_i & [\Delta \mathbf{B}_1]_i & [\Delta \mathbf{L}_1]_i \\ [\Delta \mathbf{C}_1]_i & [\Delta \mathbf{D}_1]_i & [\Delta \mathbf{D}_2]_i \end{bmatrix} = \begin{bmatrix} \mathbf{Q}_i \\ \mathbf{R}_i \end{bmatrix} [\Delta_i] [\mathbf{S}_i \; \mathbf{T}_i \; \mathbf{V}_i] \tag{2.18}$$

$$[\Delta \mathbf{E}_j] = [\mathbf{P}_j][\Delta_j][\mathbf{N}_j] \tag{2.19}$$

where $\mathbf{Q}_i \in R^{n_x \times n_i}$, $\mathbf{R}_i \in R^{n_y \times n_i}$, $\mathbf{S}_i \in R^{n_i \times n_x}$, $\mathbf{T}_i \in R^{n_i \times n_u}$, $\mathbf{V}_i \in R^{n_i \times n_d}$, $\mathbf{P}_j \in R^{n_x \times n_j}$, $\mathbf{N}_j \in R^{n_j \times n_x}$, $\Delta_i = \delta_i \mathbf{I}^{n_i \times n_i}$, and $\Delta_j = \delta_j \mathbf{I}^{n_j \times n_j}$. The scalars, n_i and n_j, are the respective ranks of the uncertainty matrices, (2.16) and (2.17). Using this form, the state-space description, (2.12)-(2.13), of the parametrically-perturbed system can then be written as

$$\begin{aligned} \mathbf{E}_o \dot{\mathbf{x}} - \begin{bmatrix} \mathbf{P}_1 & \cdots & \mathbf{P}_m \end{bmatrix} \begin{bmatrix} \eta_{k+1} \\ \vdots \\ \eta_{k+m} \end{bmatrix} &= \mathbf{A}_{1o}\mathbf{x} \\ + \mathbf{B}_{1o}\mathbf{u} + \mathbf{L}_{1o}\mathbf{d} + \begin{bmatrix} \mathbf{Q}_1 & \cdots & \mathbf{Q}_k \end{bmatrix} &\begin{bmatrix} \eta_1 \\ \vdots \\ \eta_k \end{bmatrix} \end{aligned} \tag{2.20}$$

$$\mathbf{y} = \mathbf{C}_{1o}\mathbf{x} + \mathbf{D}_{1o}\mathbf{u} + \mathbf{D}_{2o}\mathbf{d} + [\mathbf{R}_1 \cdots \mathbf{R}_k] \begin{bmatrix} \eta_1 \\ \vdots \\ \eta_k \end{bmatrix} \tag{2.21}$$

$$\begin{bmatrix} \varepsilon_1 \\ \vdots \\ \varepsilon_k \end{bmatrix} = \begin{bmatrix} \mathbf{S}_1 \\ \vdots \\ \mathbf{S}_k \end{bmatrix} \mathbf{x} + \begin{bmatrix} \mathbf{T}_1 \\ \vdots \\ \mathbf{T}_k \end{bmatrix} \mathbf{u} + \begin{bmatrix} \mathbf{V}_1 \\ \vdots \\ \mathbf{V}_k \end{bmatrix} \mathbf{d} \tag{2.22}$$

$$\begin{bmatrix} \varepsilon_{k+1} \\ \vdots \\ \varepsilon_{k+m} \end{bmatrix} = \begin{bmatrix} \mathbf{N}_1 \\ \vdots \\ \mathbf{N}_m \end{bmatrix} \dot{\mathbf{x}} \tag{2.23}$$

where, in accordance with the SF model presented in Section 2.1, the ε 's and η 's are defined as the input and output, respectively, of the normalized, parameter-error uncertainty blocks, Δ_i and Δ_j. Using the assumption that the "mass and inertia" matrix $\mathbf{E}$ is nonsingular (which implies that its nominal value, $\mathbf{E_0}$, is also nonsingular), (2.20) can be solved directly for the derivative of the state vector, $\mathbf{x}$. If the expression for the derivative of $\mathbf{x}$ is substituted into (2.23), the parametrically-perturbed system can be reduced to the following generalized uncertainty representation.

$$\dot{\mathbf{x}} = \mathbf{E}_o^{-1}\mathbf{A}_{1o}\mathbf{x} + \mathbf{E}_o^{-1}\mathbf{B}_{1o}\mathbf{u} + \mathbf{E}_o^{-1}\mathbf{L}_{1o}\mathbf{d} + \mathbf{E}_o^{-1}\begin{bmatrix} \mathbf{Q}_1 & \cdots & \mathbf{Q}_k \end{bmatrix}\begin{bmatrix} \eta_1 \\ \vdots \\ \eta_k \end{bmatrix} + \mathbf{E}_o^{-1}\begin{bmatrix} \mathbf{P}_1 & \cdots & \mathbf{P}_m \end{bmatrix}\begin{bmatrix} \eta_{k+1} \\ \vdots \\ \eta_{k+m} \end{bmatrix} \tag{2.24}$$

$$\mathbf{y} = \mathbf{C}_{1o}\mathbf{x} + \mathbf{D}_{1o}\mathbf{u} + \mathbf{D}_{2o}\mathbf{d} + [\mathbf{R}_1 \cdots \mathbf{R}_k]\begin{bmatrix} \eta_1 \\ \vdots \\ \eta_k \end{bmatrix} \tag{2.25}$$

$$\begin{bmatrix} \varepsilon_1 \\ \vdots \\ \varepsilon_k \end{bmatrix} = \begin{bmatrix} \mathbf{S}_1 \\ \vdots \\ \mathbf{S}_k \end{bmatrix}\mathbf{x} + \begin{bmatrix} \mathbf{T}_1 \\ \vdots \\ \mathbf{T}_k \end{bmatrix}\mathbf{u} + \begin{bmatrix} \mathbf{V}_1 \\ \vdots \\ \mathbf{V}_k \end{bmatrix}\mathbf{d} \tag{2.26}$$

$$\begin{bmatrix} \varepsilon_{k+1} \\ \vdots \\ \varepsilon_{k+m} \end{bmatrix} = \begin{bmatrix} \mathbf{N}_1 \\ \vdots \\ \mathbf{N}_m \end{bmatrix} \left[\mathbf{E}_o^{-1}\mathbf{A}_{1o}\mathbf{x} + \mathbf{E}_o^{-1}\mathbf{B}_{1o}\mathbf{u} + \mathbf{E}_o^{-1}\mathbf{L}_{1o}\mathbf{d} \right] + \begin{bmatrix} \mathbf{N}_1 \\ \vdots \\ \mathbf{N}_m \end{bmatrix} \mathbf{E}_o^{-1} \begin{bmatrix} \mathbf{Q}_1 & \cdots & \mathbf{Q}_k \end{bmatrix} \begin{bmatrix} \eta_1 \\ \vdots \\ \eta_k \end{bmatrix} + \begin{bmatrix} \mathbf{N}_1 \\ \vdots \\ \mathbf{N}_m \end{bmatrix} \mathbf{E}_o^{-1} \begin{bmatrix} \mathbf{P}_1 & \cdots & \mathbf{P}_m \end{bmatrix} \begin{bmatrix} \eta_{k+1} \\ \vdots \\ \eta_{k+m} \end{bmatrix} \quad (2.27)$$

2.2.2 Uncertain Dynamics

The second class of LTI perturbations, uncertain dynamics, are usually represented by dynamic model errors in the plant transfer function rather than by parametric uncertainty in the state-space model. Perturbations belonging to this class of modeling uncertainty are assumed to be bounded, stable transfer functions of the form

$$\mathbf{E}_i(s) = \mathbf{W}_i(s)\Delta_i(s) \quad (2.28)$$

where $\mathbf{W}_i(s)$ is a weighting function and Δ_i (s) is a normalized perturbation with norm bound

$$\bar{\sigma}[\Delta_i(j\omega)] < 1 \quad \forall\, i, \forall\, \omega \quad (2.29)$$

In the literature, there are usually two methods of representing these types of perturbations in the plant transfer function: the additive error model and the multiplicative error model. Given a nominal plant transfer function, $\mathbf{G}_O(s)$, the additive-error model has the form

$$\mathbf{G}(s) = \mathbf{G}_o(s) + \mathbf{E}_a(s) \tag{2.30}$$

The input multiplicative-error model has the form

$$\mathbf{G}(s) = \mathbf{G}_o(s)[\mathbf{I} + \mathbf{E}_{im}(s)] \tag{2.31}$$

while the output-multiplicative error model has the form

$$\mathbf{G}(s) = [\mathbf{I} + \mathbf{E}_{om}(s)]\mathbf{G}_o(s) \tag{2.32}$$

Frequency-domain upper bounds for these types of modeling perturbations can be found by

$$\bar{\sigma}[\mathbf{E}_a(j\omega)] = \bar{\sigma}[\mathbf{G}(j\omega) - \mathbf{G}_o(j\omega)] \tag{2.33}$$

$$\bar{\sigma}[\mathbf{E}_{im}(j\omega)] = \bar{\sigma}[\mathbf{G}_o^{\dagger}(j\omega)\{\mathbf{G}(j\omega) - \mathbf{G}_o(j\omega)\}] \tag{2.34}$$

$$\bar{\sigma}[\mathbf{E}_{om}(j\omega)] = \bar{\sigma}[\{\mathbf{G}(j\omega) - \mathbf{G}_o(j\omega)\}\mathbf{G}_o^{\dagger}(j\omega)] \tag{2.35}$$

where $\mathbf{G}_0^{\dagger}(j\omega)$ is defined as the generalized inverse of the matrix $\mathbf{G}_0(j\omega)$.

One disadvantage of the previously discussed error models (additive and multiplicative) is the difficulty of modeling bounded perturbations that *destabilize* the open-loop plant. In some cases, a better representation for this type of perturbation is the feedback error model, as shown in Figure 2.3

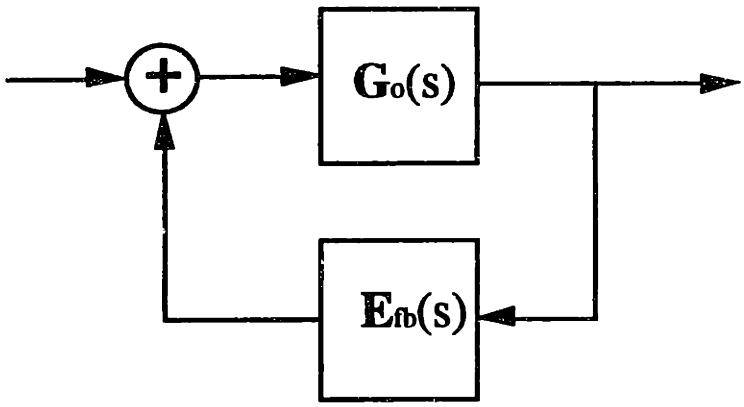

Figure 2.3: Feedback Uncertainty Model

This implies that the actual plant transfer function, G(s), is given by

$$\mathbf{G(s) = \left(I - G_o(s)E_{fb}(s) \right)^{-1} G_o(s)} \qquad \textbf{(2.36)}$$

Even if the plant is nominally stable, it is still usually possible to find some bounded, stable $E_{fb}(s)$ that will destabilize it. Unfortunately, finding the frequency-domain upper bounds for this type of error representation is not quite as straightforward as it is for either the additive error model, or the multiplicative error model (when only G(s) and Go(s) are known).

2.3 THE SMALL-GAIN THEOREM

Most feedback systems can be represented by the general feedback system shown in Figure 2.4. The vectors, $\mathbf{u}_1$ and $\mathbf{u}_2$, are defined as exogenous inputs, and the vectors, $\mathbf{e}_1$ and $\mathbf{e}_2$, are defined as "error" signals. This system is bounded-input, bounded-output stable if both error signals, $\mathbf{e}_1$ and $\mathbf{e}_2$, are bounded, given that the inputs, $\mathbf{u}_1$ and $\mathbf{u}_2$, are bounded.

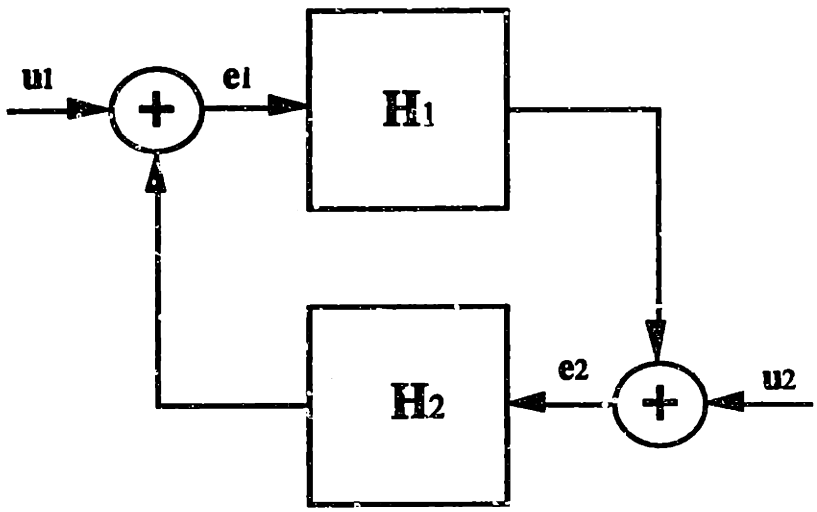

Figure 2.4: General Feedback System for Small-Gain Theorem

From Figure 2.4, the following representations of these error signals can be found

$$\begin{aligned}\mathbf{e}_1 &= \mathbf{u}_1 + \mathbf{H}_2(\mathbf{u}_2 + \mathbf{H}_1\mathbf{e}_1) \\ &= (\mathbf{I} - \mathbf{H}_2\mathbf{H}_1)^{-1}(\mathbf{u}_1 + \mathbf{H}_2\mathbf{u}_2)\end{aligned} \tag{2.37}$$

$$\begin{aligned}\mathbf{e}_2 &= \mathbf{u}_2 + \mathbf{H}_1(\mathbf{u}_1 + \mathbf{H}_2\mathbf{e}_2) \\ &= (\mathbf{I} - \mathbf{H}_1\mathbf{H}_2)^{-1}(\mathbf{H}_1\mathbf{u}_1 + \mathbf{u}_2)\end{aligned} \tag{2.38}$$

Using these equations, the corresponding norms of the error signals are then given by

$$\begin{aligned}\|\mathbf{e}_1\| &= \left\|(\mathbf{I} - \mathbf{H}_2\mathbf{H}_1)^{-1}(\mathbf{u}_1 + \mathbf{H}_2\mathbf{u}_2)\right\| \\ &\le \left\|(\mathbf{I} - \mathbf{H}_2\mathbf{H}_1)^{-1}\right\|(\|\mathbf{u}_1\| + \|\mathbf{H}_2\|\,\|\mathbf{u}_2\|)\end{aligned} \tag{2.39}$$

$$\begin{aligned} \|e_2\| &= \left\|(I - H_1H_2)^{-1}(H_1u_1 + u_2)\right\| \\ &\le \left\|(I - H_1H_2)^{-1}\right\|(\|H_1\|\,\|u_1\| + \|u_2\|) \end{aligned} \tag{2.40}$$

The norms of the transfer functions, H_1 and H_2, are defined as induced norms of the form

$$\|H\| = \max_{\|u\| \neq 0} \frac{\|y\|}{\|u\|} \qquad \text{for } y = Hu \tag{2.41}$$

From (2.39) and (2.40), the general feedback system is bounded-input, bounded-output stable if and only if

$$\left\|(I - H_1H_2)^{-1}\right\| < \infty \tag{2.42}$$

and

$$\left\|(I - H_2H_1)^{-1}\right\| < \infty \tag{2.43}$$

with the additional assumption that the induced norms of H_1 and H_2 are also bounded (i.e., H_1 and H_2 are themselves input-output stable). The norm-bound conditions of (2.42) and (2.43) are satisfied if the following induced-norm bounds are satisfied.

$$\|H_1H_2\| < 1 \tag{2.44}$$

$$\|H_2H_1\| < 1 \tag{2.45}$$

Since the norms for H_1 and H_2 are defined as induced norms, the following submultiplicative inequalities can be used

$$\|H_1H_2\| \le \|H_1\|\,\|H_2\| \tag{2.46}$$

$$\|H_2H_1\| \le \|H_1\|\,\|H_2\| \tag{2.47}$$

These inequalities then imply that a sufficient condition for closed-loop, bounded-input, bounded-output stability of the general feedback system is

$$\|\mathbf{H}_1\| \, \|\mathbf{H}_2\| < 1 \tag{2.48}$$

Obviously, one condition that satisfies (2.48) is

$$\|\mathbf{H}_1\| < 1 \tag{2.49}$$

$$\|\mathbf{H}_2\| < 1 \tag{2.50}$$

This condition is the Small-Gain test for operators with bounded induced norms. For a physical system, the Small-Gain test implies that the signals, $\mathbf{e}_1$ and $\mathbf{e}_2$, cannot grow without bound if they are constantly attenuated in "energy" by each of the subsystems, $\mathbf{H}_1$ and $\mathbf{H}_2$.

For a "nominal" linear system M(s) with a linear perturbation Δ(s), shown in Figure 2.5, any induced norm can be used with the Small-Gain theorem to guarantee bounded-input, bounded-output stability.

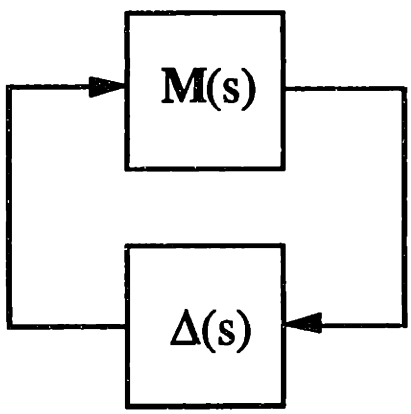

Figure 2.5: Perturbed Linear system for Small-Gain Theorem

One such induced norm would, of course, be the H_∞ norm, which is defined as the induced 2-norm.

$$\begin{aligned} \|\mathbf{H}(s)\|_\infty &\equiv \sup_\omega \bar{\sigma}[\mathbf{H}(j\omega)] \\ &= \sup_\omega \left[\sup_{\|u\|_2 \neq 0} \frac{\|y\|_2}{\|u\|_2} \right] \end{aligned} \tag{2.51}$$

The 2-norm is defined as the "energy" present in a vector signal, i.e.,

$$\|x(t)\|_2 = \left[\int_{-\infty}^{\infty} x^H(t)x(t)dt \right]^{1/2} \tag{2.52}$$

where x^H represents the Hermitian (complex-conjugate transpose) of the vector, x. Then the Small-Gain theorem states that the general perturbed linear system of Figure 2.5 will be bounded-input, bounded-output stable if the respective H_∞ norms of both M(s) and $\Delta(s)$ are less than unity.

2.4 H_∞ ROBUST CONTROL DESIGN USING THE SMALL-GAIN THEOREM

As discussed in Section 2.3, the Small-Gain Theorem provides means of analyzing the stability-robustness of a LTI control system design to bounded, stable, LTI perturbations. With the appropriate normalization, the properties of the Small Gain Theorem can also be exploited for analyzing the performance-robustness of a control design as well. In addition, by using H_∞ optimization, the Small-Gain Theorem can be used to design a control system for both stability and performance-robustness.

2.4.1 Small-Gain Stability and Performance Robustness Tests

Consider the Standard Form (SF) Model discussed in Section 2.1. Recall that the four-block transfer-function matrix of the closed-loop system, G(s), is given by

$$\begin{bmatrix} \varepsilon \\ e \end{bmatrix} = \begin{bmatrix} G_{11}(s) & G_{12}(s) \\ G_{21}(s) & G_{22}(s) \end{bmatrix} \begin{bmatrix} \eta \\ \delta \end{bmatrix} \tag{2.53}$$

This model, plus the perturbation matrix, Δ(s), can also be drawn as shown in Figure 2.6

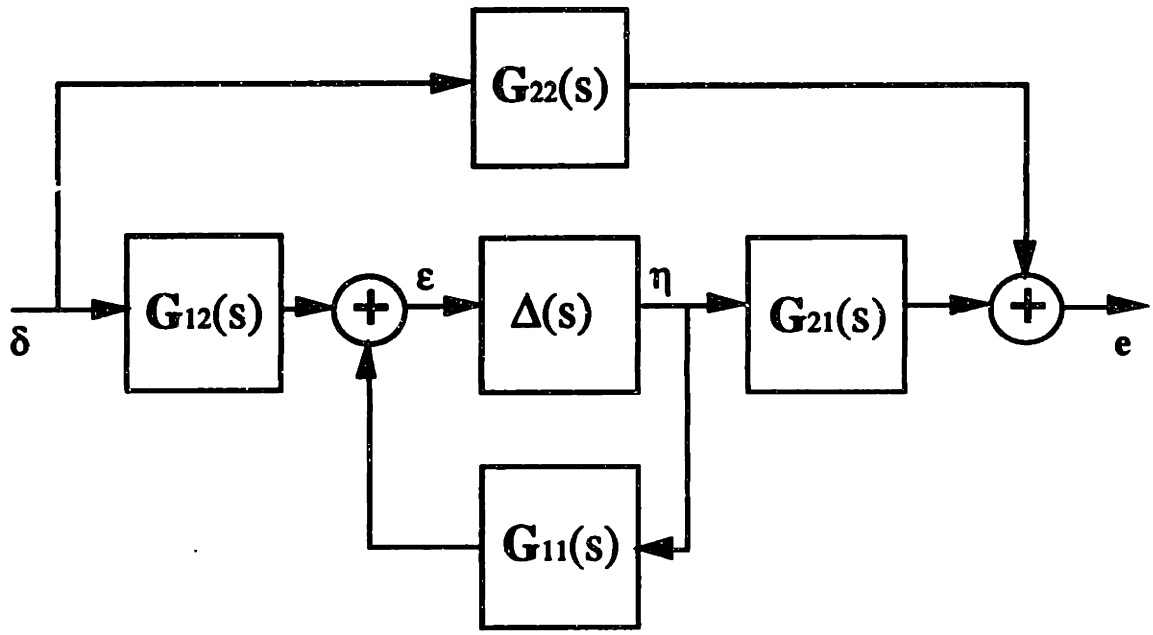

Figure 2.6: Closed-Loop SF Model Plus Perturbation

By definition, if the controller, K(s) is stabilizing, each of the four transfer-function submatrices of G(s) is stable and bounded. This implies, as shown in Figure 2.6, that the robust stability of the perturbed system depends solely on the loop given by $G_{11}(s)$ and Δ(s). From the Small-Gain Theorem, the following sufficient condition for robust stability of the closed-loop SF system can be derived (the perturbation, Δ(s), is also assumed stable and bounded)

$$\|G_{11}(s)\|_\infty \|\Delta(s)\|_\infty < 1 \tag{2.54}$$

If Δ is normalized such that its H_∞ norm is less than or equal unity, then a sufficient condition for robust stability is simply

$$\|G_{11}(s)\|_\infty < 1 \qquad (2.55)$$

Now, assume that a "fictitious" unity norm-bounded uncertainty block, $\Delta_p(s)$, is added to the SF model, as shown in Figure 2.7, with the input of $\Delta_p(s)$ being the performance-measure vector, **e**, and the output being the system-disturbance vector, δ.

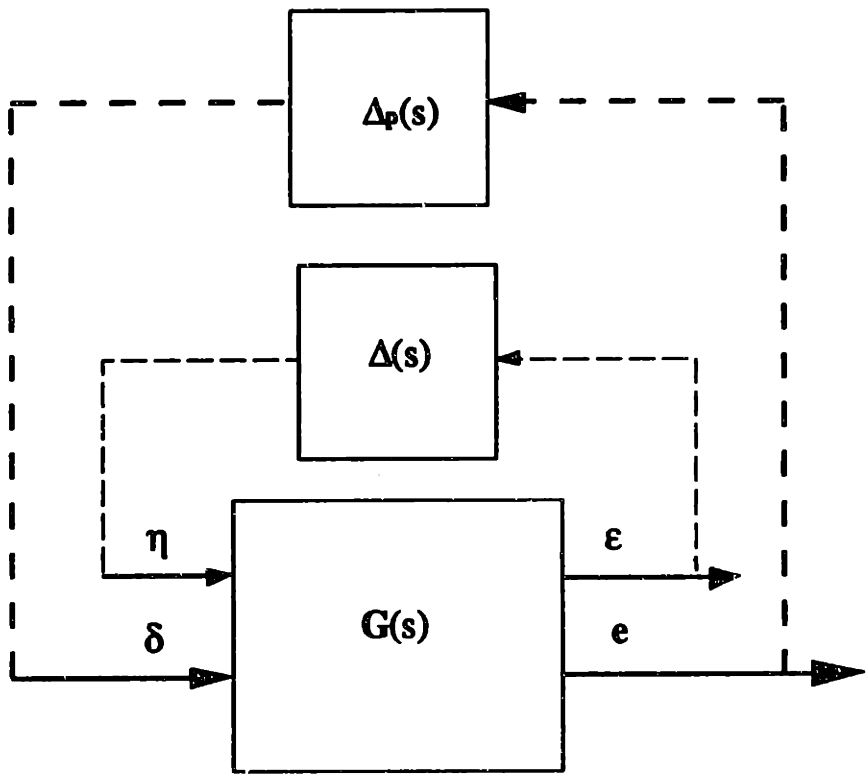

Figure 2.7: Closed-Loop SF System with Performance "Uncertainty" Block

This fictitious performance uncertainty block, plus the "real" uncertainty block, $\Delta(s)$, can be combined together to form a block-diagonal "total" uncertainty matrix, $\Delta_T(s)$, given by

$$\Delta_T(s) = \begin{bmatrix} \Delta(s) & 0 \\ 0 & \Delta_p(s) \end{bmatrix} \qquad (2.56)$$

Since $\Delta_T(s)$ is block-diagonal, it can be shown that its H_∞ norm is given by

$$\|\Delta_T(s)\|_\infty = \max\left(\|\Delta(s)\|_\infty, \|\Delta_p(s)\|_\infty\right) \qquad (2.57)$$

Recall that the H_∞ norm of both $\Delta(s)$ and $\Delta_p(s)$ are each assumed to be less than or equal unity. Therefore, the H_∞ norm of $\Delta_T(s)$ is also less than or equal unity. From this result, and the Small-Gain Theorem, a sufficient-condition for the stability of the system given by Figure 2.7 (with the fictitious performance uncertainty) is given by

$$\|G(s)\|_\infty = \left\| \begin{bmatrix} G_{11}(s) & G_{12}(s) \\ G_{21}(s) & G_{22}(s) \end{bmatrix} \right\|_\infty < 1 \qquad (2.58)$$

If this stability condition is met, it can be shown that the H_∞ norm of the transfer function from δ to e, given by (2.59), is also less than unity [2].

$$G_{ed}(s) = G_{22}(s) + G_{21}(s)\Delta(s)[I - G_{11}(s)\Delta(s)]^{-1}G_{12}(s) \qquad (2.59)$$

This implies that the system achieves robust performance in the face of the perturbation, $\Delta(s)$, where the performance of the system is defined as the 2-norm "gain" (H_∞-norm) of (2.59).

2.4.2 Frequency-Domain Loopshaping

From the discussion of the previous section, performance-robustness for the SF model is defined as the H_∞ norm of the closed-loop transfer-function from δ to **e** being less than or equal unity, in the face of the perturbation, $\Delta(s)$. In other words, performance-robustness implies simply keeping the maximum magnitude of this closed-loop transfer function less than unity for *all* frequencies. However, in control-design practice, it is usually desirable to increase (or decrease) the performance (command following, etc.) at some frequencies relative to others. This requires "loopshaping" the performance transfer function in some manner to have the desired frequency-domain properties.

Many methods exist for performing frequency-domain loopshaping. Some methods [1,6] try to shape the closed-loop performance transfer-function by using low-frequency and high-frequency open-loop approximations. However, by using frequency-domain weighting functions together with the submultiplicative property of the H_∞ norm, closed-loop loopshaping can be done directly with H_∞ optimization [5,6].

Consider the weighted closed-loop model shown in Figure 2.8.

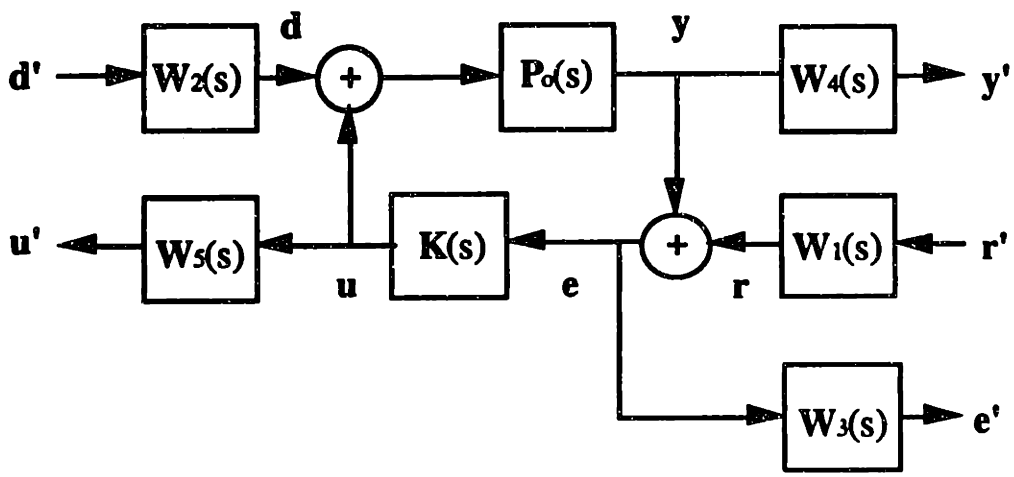

Figure 2.8: Weighted Closed-Loop Model

Here, $\mathbf{P_0}(s)$ is a nominal open-loop LTI plant model (without any modeling uncertainty) and $\mathbf{K}(s)$ is a stabilizing LTI controller. The vector $\mathbf{r}$ represents a "reference" signal and the vector $\mathbf{d}$ represents a "disturbance" signal. The vector $\mathbf{e}$ represents an "error" signal to the controller. The "control" input to the plant is given by $\mathbf{u}$, while the output of the plant is given by $\mathbf{y}$. The resulting weighted closed-loop transfer function, $\mathbf{G'}(s)$, of this model can be represented by

$$\begin{bmatrix} \mathbf{e'} \\ \mathbf{y'} \\ \mathbf{u'} \end{bmatrix} = \begin{bmatrix} \mathbf{W_3}(s)\mathbf{G_{er}}(s)\mathbf{W_1}(s) & \mathbf{W_3}(s)\mathbf{G_{ed}}(s)\mathbf{W_2}(s) \\ \mathbf{W_4}(s)\mathbf{G_{yr}}(s)\mathbf{W_1}(s) & \mathbf{W_4}(s)\mathbf{G_{yd}}(s)\mathbf{W_2}(s) \\ \mathbf{W_5}(s)\mathbf{G_{ur}}(s)\mathbf{W_1}(s) & \mathbf{W_5}(s)\mathbf{G_{ud}}(s)\mathbf{W_2}(s) \end{bmatrix} \begin{bmatrix} \mathbf{r'} \\ \mathbf{d'} \end{bmatrix} \qquad (2.60)$$

Suppose that a stabilizing controller, K(s), can be found such that the H_∞ norm of this transfer function is less than unity (e.g.. by using the H_∞ optimization algorithm with a SF model performance transfer-function defined by $\delta^T = [r'^T \; d'^T]$ and $e^T = [e'^T \; y'^T \; u'^T]$), which leads to

$$\left\| \begin{bmatrix} W_3(s)G_{er}(s)W_1(s) & W_3(s)G_{ed}(s)W_2(s) \\ W_4(s)G_{yr}(s)W_1(s) & W_4(s)G_{yd}(s)W_2(s) \\ W_5(s)G_{ur}(s)W_1(s) & W_5(s)G_{ud}(s)W_2(s) \end{bmatrix} \right\|_\infty < 1 \qquad (2.61)$$

This norm bound also implies that the H_∞ norm of each of the transfer-function submatrices contained in (2.60) is also less than unity. Then, by using the submultiplicative properties of the H_∞ norm, and by using the appropriate weightings, the actual closed-loop transfer function, G(s), can be "shaped" in some desired fashion in the frequency domain.

As an example of this approach, consider the case where $W_1(s) = -I$ and $W_2(s) = 0$. The weighted closed-loop transfer-function norm bound given by (2.61) reduces to

$$\left\| \begin{bmatrix} W_3(s)G_{er}(s) \\ W_4(s)G_{yr}(s) \\ W_5(s)G_{ur}(s) \end{bmatrix} \right\|_\infty < 1 \qquad (2.62)$$

In the literature, this is known as the weighted-control mixed-sensitivity problem [5]. In a classical design sense, $G_{er}(s)$ represents the sensitivity transfer function from the reference signal to the tracking error and $G_{yr}(s)$ represents the complementary sensitivity transfer-function from the reference signal to the plant output. From the submultiplicative and "dilation and contraction" properties of the H_∞ norm, i.e.,

$$\|[A]\|_\infty \le \left\| \begin{bmatrix} [A] \\ [B] \end{bmatrix} \right\|_\infty \le \left\| \begin{bmatrix} [A] & [C] \\ [B] & [D] \end{bmatrix} \right\|_\infty \qquad (2.63)$$

the following bounds can be derived

$$\|W_3(s)\|_\infty \|G_{er}(s)\|_\infty < 1 \tag{2.64}$$

$$\|W_4(s)\|_\infty \|G_{yr}(s)\|_\infty < 1 \tag{2.65}$$

Since the H_∞ norm of a transfer function is by definition the maximum magnitude over all frequencies, it follows that

$$\bar{\sigma}[W_3(j\omega)]\ \bar{\sigma}[G_{er}(j\omega)] < 1 \ \ \forall\ \omega \tag{2.66}$$

$$\bar{\sigma}[W_4(j\omega)]\ \bar{\sigma}[G_{yr}(j\omega)] < 1 \ \ \forall\ \omega \tag{2.67}$$

From this relation, the following magnitude bounds can be derived both for the sensitivity and the complementary sensitivity

$$\bar{\sigma}[G_{er}(j\omega)] < \frac{1}{\bar{\sigma}[W_3(j\omega)]} \ \forall\ \omega \tag{2.68}$$

$$\bar{\sigma}[G_{yr}(j\omega)] < \frac{1}{\bar{\sigma}[W_4(j\omega)]} \ \forall\ \omega \tag{2.69}$$

Therefore, these transfer functions can be "shaped" by choosing the weights, $W_3(s)$ and $W_4(s)$, to be the respective approximate inverses of the desired sensitivity and complementary sensitivity. For example, if the sensitivity is desired to be "small" in a frequency range of interest, $W_3(s)$ is chosen to be "large" in that frequency range.

However, there are some disadvantages of this loopshaping method. First, it is not always obvious how to choose an appropriate set of weights for a given open-loop plant. Second, and most important, this method can produce controllers containing zeros that try to cancel out lightly damped stable modes of the open-loop plant [6] (which can produce hidden, undesirable oscillations).

2.4.3 Gamma Iteration/Two Riccatti H_∞ Minimization Algorithm

Given the open-loop system, **P**(s), it can be deduced from the Small Gain test of (2.57) that the desired robust performance design goal is to find a stabilizing linear controller, **K**(s), where the H_∞ norm of closed-loop SF system, **G**(s), is minimized (and less than unity). Many algorithms have been developed for performing this minimization. The earliest algorithms[5,6], involved redefining the H_∞ minimization problem as a model-matching problem (e.g., approximating an unstable transfer function by a stable one) in the frequency domain. Later, these model-matching algorithms were refined to perform this minimization by using state-space versions of Youla parameterization and Hankel norm approximation[7,8]. An important development came with the development of simpler state-space algorithms involving the solution of just two matrix Riccatti equations[9]. These "two-Riccatti" algorithms had the advantage of synthesizing H_∞ optimal controllers with the same state dimension as the open-loop SF system, which eliminated most of the model reduction work that had to be performed with some of the earlier state-space algorithms. For the results of this thesis, a descriptor-system variant [10] of the "two-Riccatti" based algorithms is used in conjunction with a "gamma-iteration" technique. This algorithm produces a family of stabilizing controllers in the "descriptor" generalized state-space form (i.e., where the state derivatives are multiplied by a non-identity "descriptor" matrix). One advantage of using the descriptor-system variant is that it is somewhat more numerically robust than other two-Riccatti algorithms for H_∞ designs that approach their limits of performance[11]. The descriptor-system two-Riccatti algorithm is presented in more detail in Appendix A. An outline of the gamma-iteration/two-Riccatti H_∞ minimization algorithm is shown in Figure 2.9.

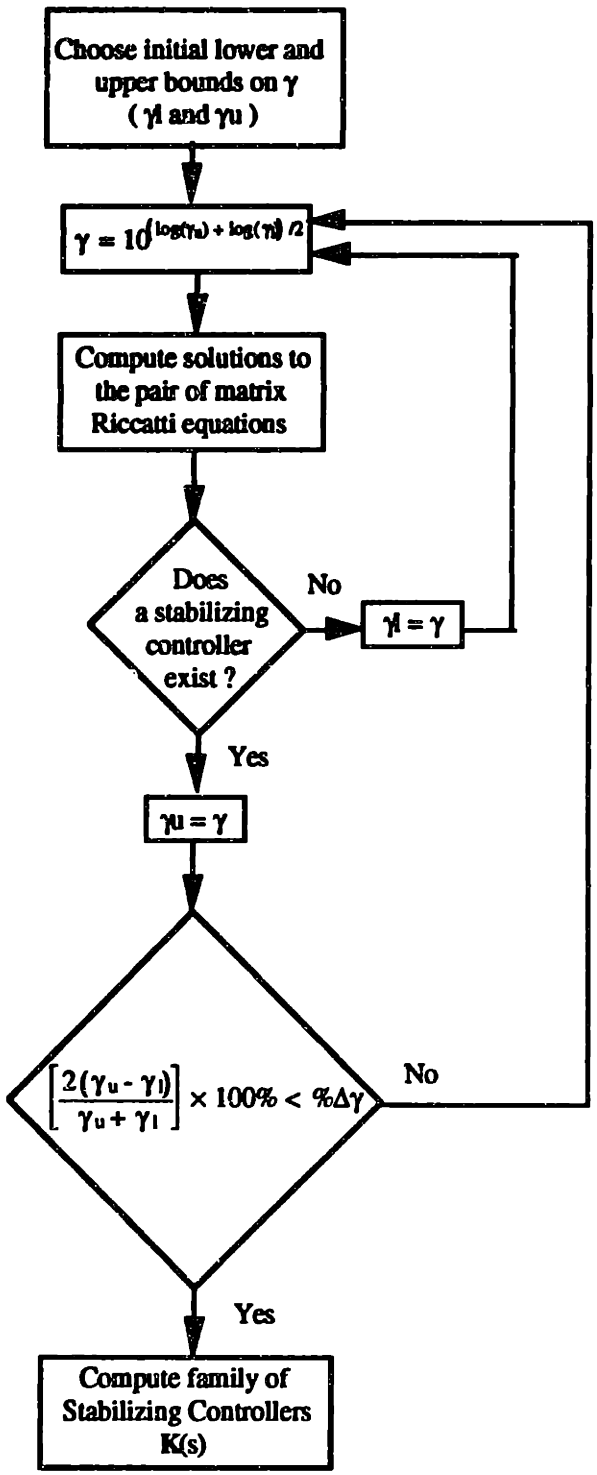

Figure 2.9: Gamma Iteration/Two-Riccatti Algorithm

For this particular H_∞ minimization algorithm, the goal is to find the smallest upper bound, γ, on the H_∞ norm of the closed-loop SF system, G(s), for which a stabilizing controller exists. The first step is to choose an initial upper bound, γ_u, and lower bound, γ_l, for γ. Next, a value for γ is chosen between these two bounds. One method for doing this, especially if there is a wide separation between γ_l and γ_u, is by logarithmic bisection

$$\gamma = 10^{(\log(\gamma_u) + \log(\gamma_l))/2} \tag{2.70}$$

Given a value for γ, the descriptor-system two-Riccatti algorithm attempts to find a stabilizing linear controller, K(s), such that, for the closed-loop system, G(s),

$$\|G(s)\|_\infty = \left\| \begin{bmatrix} G_{11}(s) & G_{12}(s) \\ G_{21}(s) & G_{22}(s) \end{bmatrix} \right\|_\infty < \gamma \tag{2.71}$$

This is done by finding the solutions, $\hat{P}$ and $\hat{S}$, of the following pair of normalized matrix Riccatti equations.

$$A_{r1}^T\hat{P} + \hat{P}A_{r1} - \hat{P}R_{r1}\hat{P} + Q_{r1} = 0 \tag{2.72}$$

$$A_{r2}\hat{S} + \hat{S}A_{r2}^T - \hat{S}R_{r2}\hat{S} + Q_{r2} = 0 \tag{2.73}$$

These equations are described in more detail in Appendix A. If these solutions are "stabilizing", and if the other existence conditions described in Appendix A are satisfied, then a stabilizing linear controller exists that satisfies (2.71). If such a stabilizing controller exists, γ is now the new upper bound (i.e., $\gamma_u = \gamma$) for the H_∞ norm of G(s). If not, then γ is now the new lower bound (i.e., $\gamma_l = \gamma$). The gamma-iteration/two-Riccatti algorithm is then repeated until the difference between γ_l and γ_u converges to within some specified tolerance, e.g.,

$$\left[\frac{(\gamma_u - \gamma_l)}{\left(\frac{\gamma_u + \gamma_l}{2}\right)}\right] < \Delta\gamma \tag{2.74}$$

Given that the bounds for γ have converged (and the existence conditions are satisfied), the final step in the algorithm is to compute the state-space parameterization of a rational stabilizing linear controller, **K**, that satisfies the condition

$$\|G(s)\|_\infty = \left\| \begin{bmatrix} G_{11}(s) & G_{12}(s) \\ G_{21}(s) & G_{22}(s) \end{bmatrix} \right\|_\infty < \gamma_u \tag{2.75}$$

One such controller in the parameterized family of linear controllers that satisfy (2.75) is the so-called *central* or *maximum-entropy* controller [6]. One useful property of the central controller is that it has the same state dimension as the original open-loop Standard-Form model, **P**(s).

This central controller can be represented in descriptor form as

$$\mathbf{E_k}\dot{\mathbf{x}}_\mathbf{k} = \mathbf{A_k x_k} + \mathbf{B_{k1}y} \tag{2.76}$$

$$\mathbf{u} = \mathbf{C_{k1}x_k} + \mathbf{D_{k11}y} \tag{2.77}$$

Once the H_∞ controller, **K**(s), is found, it is usually converted from the descriptor form into a standard state-space representation. For example, if **K**(s) is the central controller, it can be converted into the following standard state-space system

$$\dot{\mathbf{x}}_\mathbf{k} = \mathbf{A_c x_k} + \mathbf{B_c y} \tag{2.78}$$

$$\mathbf{u} = \mathbf{C_c x_k} + \mathbf{D_c y} \tag{2.79}$$

If the "descriptor" matrix, $\mathbf{E_k}$, is nonsingular, this can be done by

$$\mathbf{A_c} = \mathbf{E_k^{-1}A_k} \tag{2.80}$$

$$\mathbf{B_c = E_k^{-1} B_{k1}} \tag{2.81}$$

$$\mathbf{C_c = C_{k1}} \tag{2.82}$$

$$\mathbf{D_c = D_{k11}} \tag{2.83}$$

However, if $\mathbf{E_k}$ happens to be singular (but nonzero), different procedures are used. These procedures usually involve converting the system into Singular-Value Decomposition (SVD) coordinates[11,12].

2.5 THE STRUCTURED SINGULAR VALUE (μ)

For the control designs described in Section 2.4, the Small-Gain tests provide sufficient conditions for both robust stability and performance. Moreover, these tests are valid for *any* given complex perturbation, $\Delta(s)$, with an H_∞-norm less than unity. However, when there are multiple sources of uncertainty in the system, Δ is known (and restricted) to be block-diagonal. This implies that the Small-Gain based robust stability and performance tests (and the resulting control designs) can be unnecessarily conservative.

One means for reducing this conservatism is to use stability and performance tests based on the Structured Singular Value (μ). Originally developed by Doyle[3], μ is defined for the perturbed linear system shown in Figure 2.10

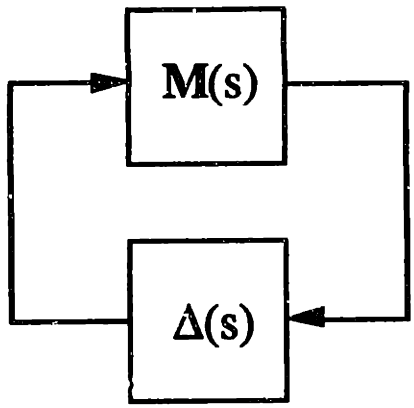

Figure 2.10: Perturbed Linear System for μ

as

$$\mu[\mathbf{M}(j\omega)] = \begin{cases} 0 & \text{if } \det[\mathbf{I} - \mathbf{M}(j\omega)\Delta(j\omega)] \neq 0 \text{ for all } \Delta \in \mathbf{B}\Delta \\ \{\min_{\Delta \in \mathbf{B}\Delta} \bar{\sigma}[\Delta(j\omega)]\}^{-1} & \text{s.t. } \det[\mathbf{I} - \mathbf{M}(j\omega)\Delta(j\omega)] = 0 \text{ otherwise} \end{cases} \quad (2.84)$$

where $\mathbf{B}\Delta$ is defined as the set of all unity-norm bounded, block-diagonal, stable perturbations. A *necessary* and sufficient condition for the stability of the system defined by Figure 2.10 is given by

$$\mu[\mathbf{M}(j\omega)] < 1 \quad \forall\ \omega \quad (2.85)$$

When the perturbation, $\Delta(s)$, has a block-diagonal structure (and is complex-valued), μ provides a *nonconservative* test for use in the robust stability and performance tests. Unfortunately, μ is not a norm and is not easily found. However, upper bounds for μ can be computed and used in practice. Stability and performance robustness tests using these upper bounds are sufficient, but not necessary; therefore they will add some conservatism into the control designs. Also, μ-based tests tend to be conservative when real-valued perturbations are considered, since $\Delta(j\omega)$ is allowed to be complex. This type of conservatism can be especially troublesome for nominal design models that have lightly damped poles, since for this case, the robust stability and performance goals may be impossible to achieve (e.g., lightly damped poles tend to produce open-loop systems with

relatively large H_∞ norms).

Many methods have been developed for computing an upper bound to μ. The following method[4] involves solving the weighted Small-Gain problem shown in Figure 2.11.

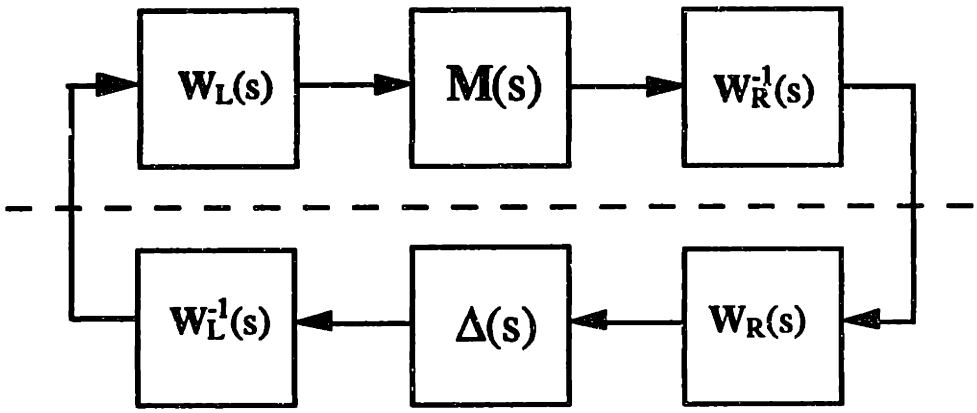

Figure 2.11: Weighted Small-Gain Problem

As with the previous sections, the perturbation matrix, $\Delta(s)$, is assumed to have the block-diagonal form

$$\Delta(s) = \begin{bmatrix} \Delta_1(s) & 0 & \cdots & 0 \\ 0 & \Delta_2(s) & & \vdots \\ \vdots & & \ddots & 0 \\ 0 & \cdots & 0 & \Delta_m(s) \end{bmatrix} \qquad (2.86)$$

with each of the $\Delta_i(s)$ terms normalized such that

$$\bar{\sigma}[\Delta_i(j\omega)] < 1 \quad \forall\ \omega \qquad (2.87)$$

The weighting matrices are chosen so as to preserve the structure of $\Delta(s)$, i.e.,

$$W_L^{-1}\Delta W_R \text{ maps the space } B\Delta \text{ to } B\Delta \qquad (2.88)$$

where $\mathbf{B}\Delta$ is defined as the set of all stable perturbations that have the block-diagonal structure of (2.86) and the normalized norm bound of (2.87). If the weights are chosen in this fashion, then it can be shown that

$$\mu\left[\mathbf{W}_R^{-1}(j\omega)\mathbf{M}(j\omega)\mathbf{W}_L(j\omega)\right] = \mu\left[\mathbf{M}(j\omega)\right] \tag{2.89}$$

For any given matrix, μ has the property that it is always bounded from above by the maximum singular value. Using this property, the following weighted-norm upper bound can be defined

$$\mu\left[\mathbf{M}(j\omega)\right] \le \bar{\mu}\left[\mathbf{M}(j\omega)\right] \equiv \bar{\sigma}\left[\mathbf{W}_R^{-1}(j\omega)\mathbf{M}(j\omega)\mathbf{W}_L(j\omega)\right] \tag{2.90}$$

Robustness tests based on this upper bound will be less conservative than the previous Small-Gain based tests since the weights, $\mathbf{W}_L$ and $\mathbf{W}_R$, can be chosen to minimize the weighted norm given by (2.90).

One practical constraint for choosing the set of weights, $\mathbf{W}_L$ and $\mathbf{W}_R$, that satisfy the mapping property of (2.88) is

$$\left|\mathbf{W}_L(j\omega)\right| = \mathbf{D}_L(\omega) \tag{2.91}$$

$$\left|\mathbf{W}_R(j\omega)\right| = \mathbf{D}_R(\omega) \tag{2.92}$$

where

$$\mathbf{D}_R(\omega) = \begin{bmatrix} d_1(\omega)\mathbf{I}_{c_1} & 0 & \cdots & 0 \\ 0 & d_2(\omega)\mathbf{I}_{c_2} & & \vdots \\ \vdots & & \ddots & 0 \\ 0 & \cdots & 0 & d_m(\omega)\mathbf{I}_{c_m} \end{bmatrix} \tag{2.93}$$

$$\mathbf{D}_L(\omega) = \begin{bmatrix} d_1(\omega)\mathbf{I}_{r_1} & 0 & \cdots & 0 \\ 0 & d_2(\omega)\mathbf{I}_{r_2} & & \vdots \\ \vdots & & \ddots & 0 \\ 0 & \cdots & 0 & d_m(\omega)\mathbf{I}_{r_m} \end{bmatrix} \quad (2.94)$$

with the assumption $\Delta_i(j\omega) \in C^{n_i \times c_i}$. The $d_i(\omega)$ are defined to be real, frequency-dependent, positive scalars. By using this constraint on the choice of weighting matrices, the upper bound calculation for μ can be reduced to the following convex optimization problem

$$\bar{\mu}[\mathbf{M}(j\omega)] = \min_{d_i \in R_+} \bar{\sigma}[\mathbf{D}_R^{-1}(\omega)\mathbf{M}(j\omega)\mathbf{D}_L(\omega)] \quad (2.95)$$

where R_+ is the space of positive, real numbers. This upper bound for μ has been found to give reasonable answers, with errors generally less than about 15%[6].

2.6 ROBUST CONTROL DESIGN USING μ

As discussed in Section 2.5, the Small-Gain based H_∞ robustness tests described in Section 2.4 are unnecessarily conservative for the cases of block-diagonal $\Delta(s)$. This also implies that the corresponding H_∞ control designs based on these robustness tests would also be unnecessarily conservative. However, it also follows from the discussion that it is possible to exploit the perturbation structure in order to reduce this conservatism.

2.6.1 μ-Based Stability and Performance Robustness Tests

From the discussion of μ in Section 2.5, a less conservative test for robust stability of the Standard Form closed-loop system is given by

$$\mu[\mathbf{G}_{11}(j\omega)] < 1 \quad \forall\ \omega \quad (2.96)$$

Similarly, a less conservative test for robust performance is given by

$$\mu[G(j\omega)] = \mu\left(\begin{bmatrix} G_{11}(j\omega) & G_{12}(j\omega) \\ G_{21}(j\omega) & G_{22}(j\omega) \end{bmatrix}\right) < 1 \quad \forall\ \omega \tag{2.97}$$

However, recall from the discussion that μ is not a norm and is not easily computed. Therefore, for control-system robustness analysis and design, the weighted-norm upper bound for μ derived in Section 2.5 is typically used in practice.

Consider the weighted-norm Standard Form model shown in Figure 2.12.

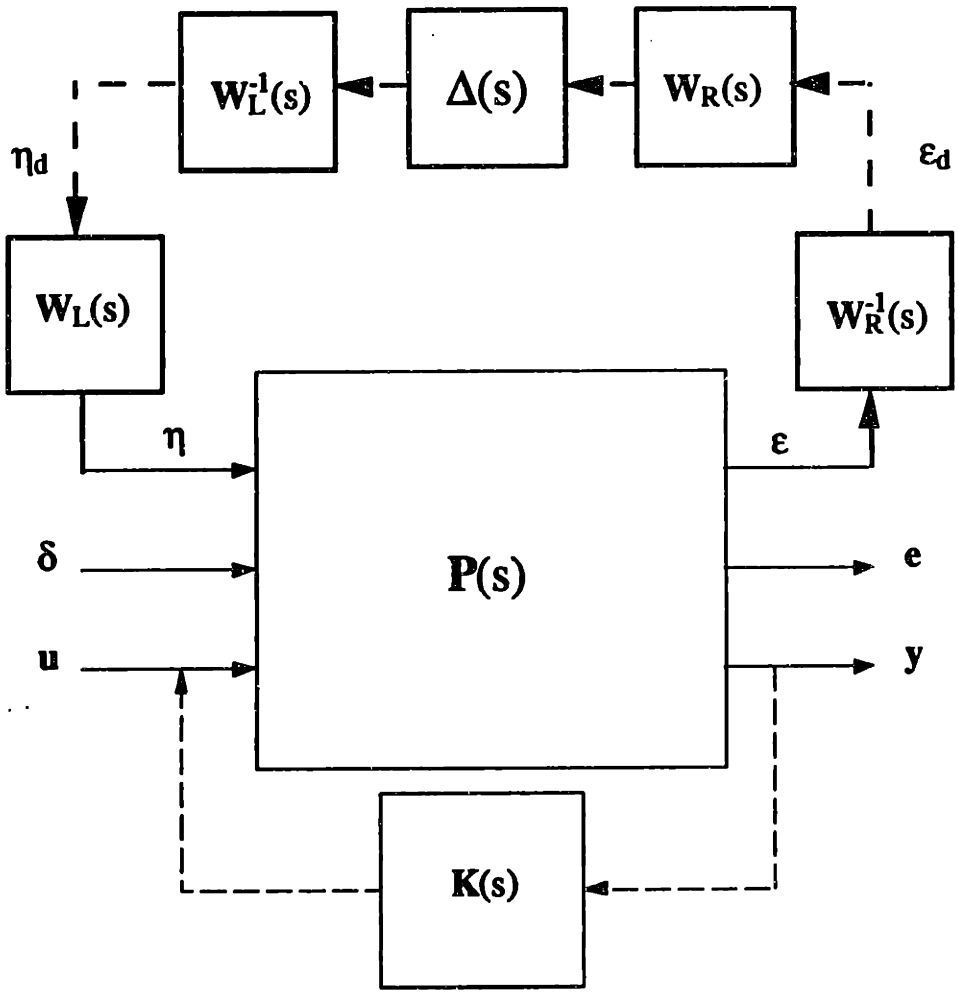

Figure 2.12: Weighted Standard Form Model

From the discussion of μ, if the weights $W_L(s)$ and $W_R(s)$ are chosen according to the

criterion of (2.93)-(2.94), then it can be shown that

$$\mu\left[\mathbf{W}_R^{-1}(j\omega)\mathbf{G}_{11}(j\omega)\mathbf{W}_L(j\omega)\right] = \mu\left[\mathbf{G}_{11}(j\omega)\right] \tag{2.98}$$

from which follows the weighted-norm upper bound

$$\mu\left[\mathbf{G}_{11}(j\omega)\right] \le \bar{\mu}\left[\mathbf{G}_{11}(j\omega)\right] = \bar{\sigma}\left[\mathbf{W}_R^{-1}(j\omega)\mathbf{G}_{11}(j\omega)\mathbf{W}_L(j\omega)\right] \tag{2.99}$$

This implies that a test for robust stability would be the H_∞-norm of the weighted closed-loop system, i.e.,

$$\left\|\mathbf{W}_R^{-1}(s)\mathbf{G}_{11}(s)\mathbf{W}_L(s)\right\|_\infty < 1 \tag{2.100}$$

Now, let the disturbance input vector, δ, be scaled by $1/\alpha$, where α is a real, positive scalar. Then the open-loop transfer function, $\mathbf{P}_D(s)$, of the weighted open-loop system would be given by

$$\mathbf{P}_D(s) = \begin{bmatrix} \mathbf{W}_R^{-1}(s)\mathbf{P}_{11}(s)\mathbf{W}_L(s) & \frac{1}{\alpha}\mathbf{W}_R^{-1}(s)\mathbf{P}_{12}(s) & \mathbf{W}_R^{-1}(s)\mathbf{P}_{13}(s) \\ \mathbf{P}_{21}(s)\mathbf{W}_L(s) & \frac{1}{\alpha}\mathbf{P}_{22}(s) & \mathbf{P}_{23}(s) \\ \mathbf{P}_{31}(s)\mathbf{W}_L(s) & \frac{1}{\alpha}\mathbf{P}_{32}(s) & \mathbf{P}_{33}(s) \end{bmatrix} \tag{2.101}$$

A test for *robust* performance would be the weighted-norm

$$\max_\omega \bar{\mu}\left[\mathbf{G}(j\omega)\right] = \max_\omega \bar{\mu}\left[\mathbf{G}_D(j\omega)\right] \le \left\|\mathbf{G}_D(s)\right\|_\infty < 1 \tag{2.102}$$

where $\mathbf{G}_D(s)$ is the closed-loop weighted SF system. If the original unweighted open-loop system, $\mathbf{P}(s)$, is scaled in a manner such that the desired closed-loop H_∞-norm from δ to $\mathbf{e}$ is less than unity, then it can be shown that the system performance has the upper bound

$$\frac{\|e\|_2}{\|d\|_2} < \alpha \quad \forall \Delta \in \mathbf{B}\Delta \tag{2.103}$$

This performance robustness test will be more conservative than the actual μ-based test of (2.97) since only an upper bound for μ is being used, but it will be less conservative than the Small-Gain based test, since the weights are chosen to minimize the closed-loop H_∞-norm of $G_D(s)$.

2.6.2 μ-Based Robust Design Algorithm

The performance test given by (2.100) implies that the robust design objective would be the solution of the following optimization problem

$$\min_{K(s)} \min_{W_R(s),\, W_L(s)} \left\{ \max_{\omega} \bar{\sigma}[G_D(j\omega)] \right\} \tag{2.104}$$

where K(s) is the set of all stabilizing, rational controllers. This problem, however, is not easy to solve since it is not convex for $\{K(s)\}$ and $\{W_R(s), W_L(s)\}$[3]. However, it is convex for $\{K(s)\}$ and $\{W_R(s), W_L(s)\}$ *separately.*

There are many methods that are based on this optimization problem for performing robust-control design. An iterative-based robust design algorithm[2], shown in Figure 2.13, is used for the results of this thesis.

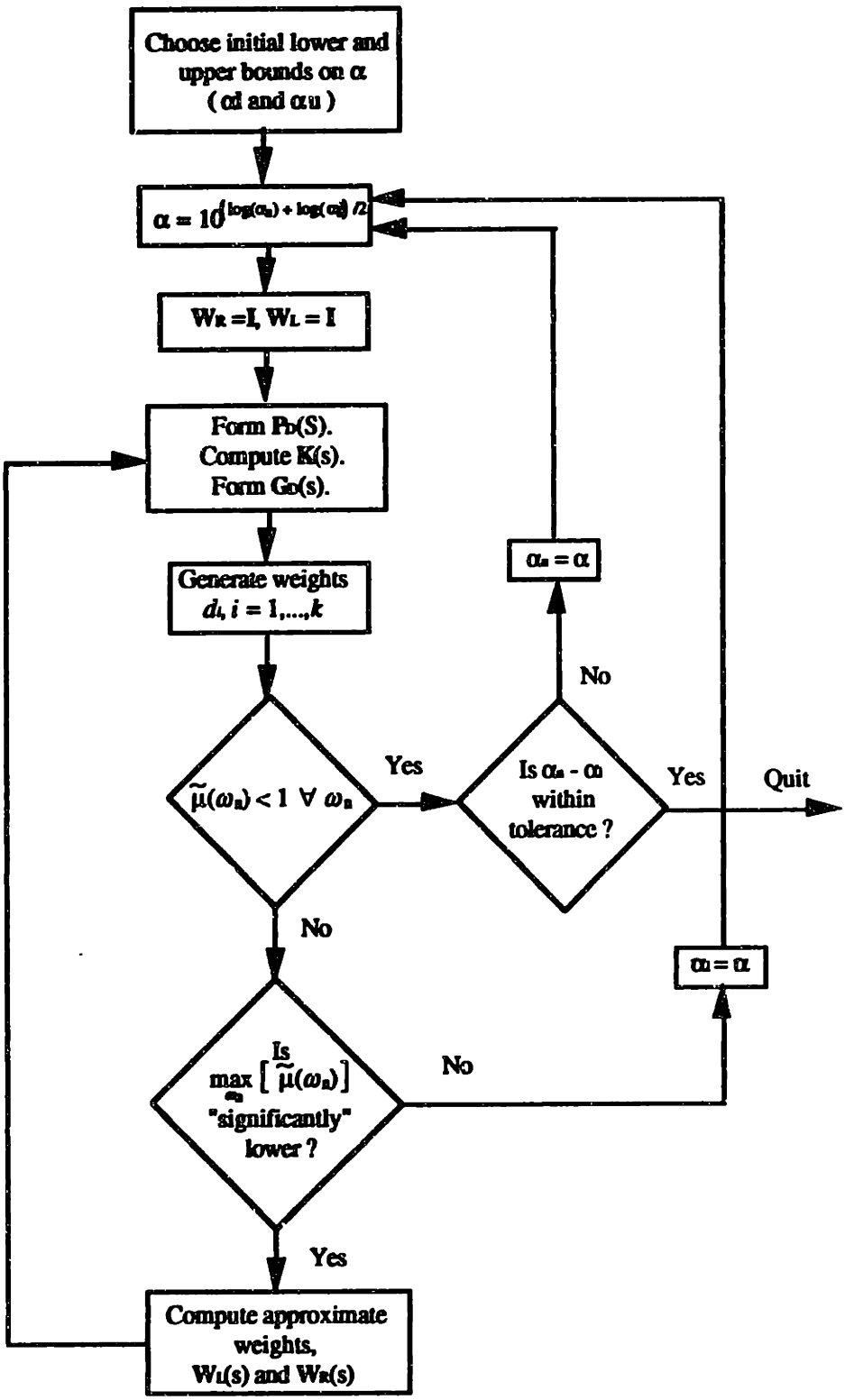

Figure 2.13: Robust Design Algorithm

This particular algorithm exploits the fact that the minimization is convex for $\{\mathbf{K}(s)\}$ and $\{\mathbf{W_R}(s),\mathbf{W_L}(s)\}$, separately. In this iterative approach, an initial set of weights is first selected (e.g., $\mathbf{W_L}(s) = \mathbf{I}$, $\mathbf{W_R}(s) = \mathbf{I}$). Now, using this set of weights, a state-space representation for $\mathbf{P_D}(s)$ is formed and a controller, $\mathbf{K}(s)$, is found to minimize the H_∞ norm of the closed-loop system, $\mathbf{G_D}(s)$. Then, a *new* set of weights is selected to further minimize the weighted H_∞-norm of $\mathbf{G}(s)$, which is the closed-loop system formed by the combination of this controller, $\mathbf{K}(s)$, and the original unweighted SF plant, $\mathbf{P}(s)$. Next, a new state-space representation for $\mathbf{P_D}(s)$ is formed from the combination of the original $\mathbf{P}(s)$ and the new weights. Then, a *new* H_∞ controller, $\mathbf{K}(s)$, is found for this new $\mathbf{P_D}(s)$, and so on. This iteration between $\mathbf{K}(s)$ and the weights is continued until the closed-loop H_∞-norm converges.

The first step in the robust design algorithm is to choose an initial lower bound, α_l, and upper bound, α_u, on α, the H_∞-norm of the closed-loop transfer function from the disturbance vector, δ, to the performance-measure vector, $\mathbf{e}$. Then, an α is chosen between α_l and α_u by logarithmic bisection.

$$\alpha = 10^{(\log(\alpha_u) + \log(\alpha_l))/2} \tag{2.105}$$

Next, an initial set of weights is selected, $\mathbf{W_L}(s) = \mathbf{I}$, $\mathbf{W_R}(s) = \mathbf{I}$. This choice of weights, together with $\mathbf{P}(s)$ and α, is then used to form $\mathbf{P_D}(s)$.

$$\mathbf{P_D}(s) = \begin{bmatrix} \mathbf{W_R^{-1}}(s)\mathbf{P_{11}}(s)\mathbf{W_L}(s) & \frac{1}{\alpha}\mathbf{W_R^{-1}}(s)\mathbf{P_{12}}(s) & \mathbf{W_R^{-1}}(s)\mathbf{P_{13}}(s) \\ \mathbf{P_{21}}(s)\mathbf{W_L}(s) & \frac{1}{\alpha}\mathbf{P_{22}}(s) & \mathbf{P_{23}}(s) \\ \mathbf{P_{31}}(s)\mathbf{W_L}(s) & \frac{1}{\alpha}\mathbf{P_{32}}(s) & \mathbf{P_{33}}(s) \end{bmatrix} \tag{2.106}$$

Then, a stabilizing $\mathbf{K}(s)$ is then found to minimize the H_∞-norm of the closed-loop system, $\mathbf{G_D}(s)$, by using the gamma-iteration/two-Riccatti algorithm of Section 2.4.

Now, a direct frequency-domain representation for the weights, $\mathbf{W_L}(s)$ and $\mathbf{W_R}(s)$, that minimize the upper bound of μ cannot be easily found. Instead, this robust-design algorithm circumvents this difficulty by using algorithms[2] that find a sequence of approximations to the weights at number of frequencies, $\{\omega_n\}$,

$$\mathbf{d_R}(\omega_n) = \begin{bmatrix} d_1(\omega_n)\mathbf{I}_{R_1} & & 0 \\ & \ddots & \\ 0 & & d_k(\omega_n)\mathbf{I}_{R_k} \end{bmatrix} \qquad (2.107)$$

$$\mathbf{d_L}(\omega_n) = \begin{bmatrix} d_1(\omega_n)\mathbf{I}_{L_1} & & 0 \\ & \ddots & \\ 0 & & d_k(\omega_n)\mathbf{I}_{L_k} \end{bmatrix} \qquad (2.108)$$

Each approximate weight is chosen so as to minimize a corresponding upper bound in a sequence of approximate upper bounds for μ of the closed-loop system, **G**(s), formed by the combination of the controller, **K**(s), and the original unweighted SF plant, **P**(s)

$$\tilde{\mu}(\omega_n) \equiv \min_{d_i,\, i=1,\ldots,k} \bar{\sigma}\begin{bmatrix} \mathbf{d_R^{-1}}(\omega_n)\mathbf{G}_{11}(j\omega_n)\mathbf{d_L}(\omega_n) & \mathbf{d_R^{-1}}(\omega_n)\mathbf{G}_{12}(j\omega_n) \\ \mathbf{G}_{21}(j\omega_n)\mathbf{d_L}(\omega_n) & \mathbf{G}_{22}(j\omega_n) \end{bmatrix} \qquad (2.109)$$

If the following approximate performance robustness test is satisfied at each element of the sequence of approximate upper bounds

$$\tilde{\mu}(\omega_n) < 1 \;\forall\; \omega_n \qquad (2.110)$$

then the present value of α becomes the new upper bound α_u. If the lower and upper bounds of α are sufficiently close, then the robust-design algorithm has converged to a solution of the minimization problem.

However, if (2.110) is not satisfied and the maximum of the sequence of μ upper bounds is not "significantly" lower than its previous value (which implies that (2.110) cannot be attained with the present value of α), then α becomes the new lower bound, α_l. The new bounds are then used to choose a new value of α. This new value of α is now used by the robust-design algorithm to begin a new design iteration.

If (2.110) is not satisfied, but the maximum of the sequence of computed μ upper bounds is "significantly" lower (or this is the initial set of weights), then a set of finite-order, stable, non-minimum phase, single-input, single-output(SISO) transfer functions, $D_i(s)$, are constructed from the set of scalar weights, $d_i(\omega_n)$, such that the frequency-domain errors

$$e_i(j\omega_n) = \left| |D_i(j\omega_n)| - d_i(j\omega_n) \right| \qquad (2.111)$$

are as small as possible over the frequency set. The new weights, $W_L(s)$ and $W_R(s)$ (which are constructed from this set of SISO transfer functions), are now appended to the original SF plant, $P(s)$, to form a new $P_D(s)$. This new $P_D(s)$ is then used to find a new stabilizing controller, $K(s)$.

It has been shown that under ideal conditions[2], this approximate weight-computation algorithm does converge to a stabilizing controller, $K(s)$, such that, point-wise,

$$\tilde{\mu}(\omega_n) \rightarrow \bar{\mu}(\omega_n) \qquad (2.112)$$

However, local minima may exist, which implies

$$\max_{\omega_n} \tilde{\mu}(\omega_n) \geq \max_{\omega} \bar{\mu}(\omega) \qquad (2.113)$$

Note that this increases the conservatism of the design. Also note that an unfortunate "side-effect" of this approximate approach is that the state order of the final μ-based controller, **K**(s), is the same as the state order of the *weighted* open-loop plant, $\mathbf{P_D}(s)$, which implies that the controller state order is *increased* by the state order of *both* weights (over the state order of a corresponding H_∞ controller designed using only the original plant, **P**(s)). For systems containing more than a modest number of individual perturbations, this increase in state order can be quite substantial. This side-effect can be partially alleviated by performing model reduction on **K**(s) after each iteration; however, this could slow down the convergence rate to the upper bound of μ.

Chapter 3

Sliding-Mode Robust Control

Sliding-Mode Control (SMC) is a robust nonlinear control-system design methodology. This methodology, a subset of "variable-structure" control theory, was first studied by Filippov[13] and Utkin[14] in the Soviet Union. The Sliding-Mode technique tries to achieve its desired design goals by constraining the nonlinear-system state-variable motion to a linear hyperplane in state-space, called a "sliding surface", thereby forcing these dynamics to behave in a linear fashion. When used in conjunction with Lyapunov theory, the Sliding-Mode methodology produces control designs with guaranteed stability and performance robustness properties. However, some early sliding-mode designs exhibited undesirable high-frequency control signal "chattering" due to discontinuities in the control law at the sliding surface boundary. To reduce this chattering effect, Slotine[15] introduced the idea of the sliding surface "boundary layer". The boundary layer provides a means of "interpolating" the control law across the sliding surface boundary, thereby "smoothing out" the control signals. The boundary layer also provides a direct means of quantifying the tradeoff between control-system performance and stability-robustness.

This chapter presents the Sliding-Mode design methodology for robust nonlinear control systems. Sliding-Mode Control requires the controlled nonlinear system to belong to the so-called Descriptor/Companion class of nonlinear systems; therefore, a brief survey of this class of systems is presented in Section 3.1. This survey also includes a representation of the modeling uncertainty that can be incorporated into the SMC design process. The Sliding-Mode control law for the Descriptor/Companion class of systems is presented in Section 3.2, together with a description of the boundary layer. Lastly, a technique is presented in Section 3.3 for designing control systems where a Sliding-Mode based controller augments a linear, time-invariant (LTI) dynamic controller.

3.1 DESCRIPTOR/COMPANION MODEL WITH UNCERTAINTY

For a multi-input, multi-output (MIMO) plant, the state-space description of the Descriptor/Companion model is given by

$$\begin{aligned}
\frac{d}{dt}(\hat{\mathbf{x}}) &= \hat{\mathbf{x}} \\
\frac{d}{dt}(\hat{\dot{\mathbf{x}}}) &= \hat{\ddot{\mathbf{x}}} \\
&\vdots \\
\frac{d}{dt}\left(\hat{\mathbf{x}}^{(n-2)}\right) &= \hat{\mathbf{x}}^{(n-1)} \\
\mathbf{E}(\mathbf{x})\left[\frac{d}{dt}\left(\hat{\mathbf{x}}^{(n-1)}\right)\right] &= \mathbf{E}(\mathbf{x})\,\hat{\mathbf{x}}^{(n)} = \mathbf{f}(\mathbf{x}) + \mathbf{B}(\mathbf{x})\mathbf{u} + \mathbf{d}
\end{aligned} \tag{3.1}$$

The Descriptor/Companion model is composed of a set of n-th order linear "integrator" subsystems coupled at their respective inputs by the nonlinear matrix functions, $\mathbf{f}(\mathbf{x})$, $\mathbf{E}(\mathbf{x})$, and $\mathbf{B}(\mathbf{x})$, as shown in Figure 3.1.

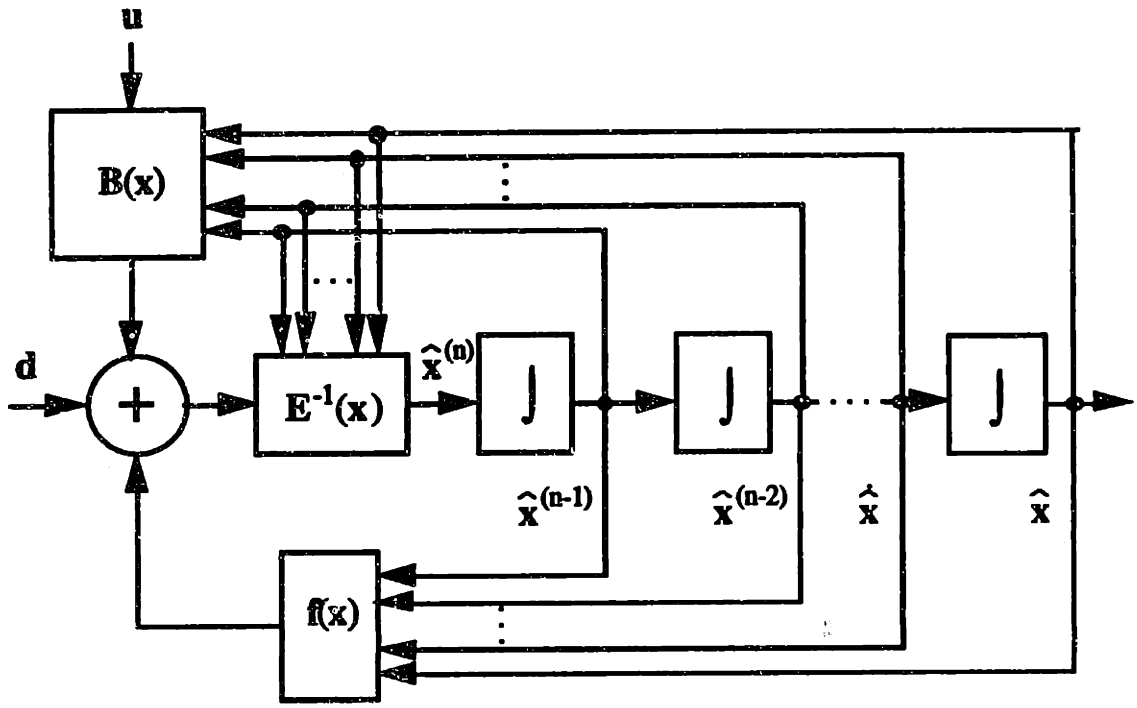

Figure 3.1: Descriptor/Companion Model

For this model, $\hat{\mathbf{x}}$, is defined as a vector of subsystem "output" states, given by

$$\hat{\mathbf{x}} = \begin{bmatrix} \hat{x}_1 \\ \vdots \\ \hat{x}_k \end{bmatrix} \tag{3.2}$$

where k is the total number of integrator subsystems. The total state vector, x, is defined to be

$$\mathbf{x} = \begin{bmatrix} \hat{\mathbf{x}} \\ \vdots \\ \hat{\mathbf{x}}^{(n-1)} \end{bmatrix} \tag{3.3}$$

This total state vector contains all the output states, plus all their respective derivatives up to n-1.

The control input vector, **u**, for this model is simply given by

$$\mathbf{u} = \begin{bmatrix} u_1 \\ \vdots \\ u_k \end{bmatrix} \tag{3.4}$$

Note that the Descriptor/Companion model has the same number of controls as output states. The disturbance input vector, **d**, of this model is given by

$$\mathbf{d} = \begin{bmatrix} d_1 \\ \vdots \\ d_k \end{bmatrix} \tag{3.5}$$

Again, note that this model has the same number of disturbance inputs as output states (and controls).

The "descriptor" matrix, $\mathbf{E}(\mathbf{x})$, has dimension $k \times k$, the control input matrix, $\mathbf{B}(\mathbf{x})$, has dimension $k \times k$, while the state feedback matrix, $\mathbf{f}(\mathbf{x})$, has dimension $k \times 1$. $\mathbf{E}(\mathbf{x})$ is assumed to be symmetric positive-definite for all **x**. The real part of the eigenvalues of $\mathbf{B}(\mathbf{x})$ is assumed to be positive for all **x** (i.e., $\mathbf{B}(\mathbf{x})$ is nonsingular and "positive" for all x). For this model, this condition on $\mathbf{B}(\mathbf{x})$ implies that all of the states of the system are controllable from the control input, **u**. In addition, this nonsingularity condition implies that **u** can compensate for all of the disturbance inputs given by **d**. Lastly, all of the system states described by the vector, **x**, are assumed to be available for feedback.

Bounded parameter uncertainty for the Descriptor/Companion class of nonlinear systems can be represented in many ways. One such representation is the additive uncertainty representation, where the uncertainties in the matrices, $\mathbf{E}(\mathbf{x})$, $\mathbf{f}(\mathbf{x})$, and $\mathbf{B}(\mathbf{x})$, are assumed to have the following forms

$$\mathbf{E}(\mathbf{x}) = \hat{\mathbf{E}}(\mathbf{x}) - \Delta\mathbf{E}(\mathbf{x}) \tag{3.6}$$

$$\mathbf{f}(\mathbf{x}) = \hat{\mathbf{f}}(\mathbf{x}) + \Delta\mathbf{f}(\mathbf{x}) \tag{3.7}$$

$$\mathbf{B}(\mathbf{x}) = \hat{\mathbf{B}}(\mathbf{x}) + \Delta\mathbf{B}(\mathbf{x}) \tag{3.8}$$

The matrices, $\hat{\mathbf{E}}(\mathbf{x})$, $\hat{\mathbf{f}}(\mathbf{x})$, and $\hat{\mathbf{B}}(\mathbf{x})$, represent the respective nominal values. The magnitude of the additive uncertainty in $\mathbf{E}(\mathbf{x})$, $\mathbf{f}(\mathbf{x})$, and $\mathbf{B}(\mathbf{x})$ is assumed to be bounded element-wise by the matrices, $\Delta\mathbf{E}(\mathbf{x})$, $\Delta\mathbf{f}(\mathbf{x})$, and $\Delta\mathbf{B}(\mathbf{x})$, i.e.,

$$|\Delta e_{ij}(\mathbf{x})| \le \overline{\Delta e}_{ij}(\mathbf{x}) \tag{3.9}$$

$$|\Delta f_i(\mathbf{x})| \le \overline{\Delta f}_i(\mathbf{x}) \tag{3.10}$$

$$|\Delta b_{ij}(\mathbf{x})| \le \overline{\Delta b}_{ij}(\mathbf{x}) \tag{3.11}$$

In addition, the magnitude of the disturbance vector, $\mathbf{d}$, is assumed to be bounded element-wise by $\bar{\mathbf{d}}$, i.e.,

$$|d_i(t)| \le \bar{d}_i(t) \tag{3.12}$$

For the Descriptor/Companion model, there are no direct uncertainty representations for unmodeled dynamics such as sensor or actuator dynamics. Usually in the literature[16], these dynamics are assumed to be bounded, stable, and of a sufficiently high frequency such that they will not be excited by the dominant closed-loop dynamics of the model. On the other hand, the effects of lower-frequency bounded unmodeled dynamics are usually lumped together (if possible) with the disturbance, $\mathbf{d}$.

3.2 THE SLIDING-MODE CONTROL LAW FOR THE DESCRIPTOR/COMPANION MODEL

The control-system design goal is for the state output, $\hat{\mathbf{x}}$, of the Descriptor/Companion model of Section 3.1 to track some time-varying state reference, $\hat{\mathbf{x}}_d$. This implies that the design goal is to minimize the magnitude of the output tracking-error vector, $\tilde{\hat{\mathbf{x}}}$, given by

$$\tilde{\hat{\mathbf{x}}} = \hat{\mathbf{x}} - \hat{\mathbf{x}}_d \tag{3.13}$$

However, if $\hat{\mathbf{x}}_d$ is n-differentiable, a more suitable design goal would be "perfect" tracking, where the entire state, $\mathbf{x}$, of the Descriptor/Companion model exactly tracks a time-varying state "trajectory", $\mathbf{x}_d$, given by

$$\mathbf{x}_d = \begin{bmatrix} \hat{\mathbf{x}}_d \\ \vdots \\ \hat{\mathbf{x}}_d^{(n-1)} \end{bmatrix} \tag{3.14}$$

which implies minimizing the magnitude the "total" state tracking-error vector, $\tilde{\mathbf{x}}$, given by

$$\tilde{\mathbf{x}} = \mathbf{x} - \mathbf{x}_d \tag{3.15}$$

The order of this state tracking-error vector is higher than the number of controls given by $\mathbf{u}$. This implies that it is generally impossible to force the system to "perfectly" track the reference state-trajectory, especially in the presence of nonzero initial conditions. On the other hand, recall from Section 3.1 that all of the states of the Descriptor/Companion model are controllable from $\mathbf{u}$. This implies it may be possible to stabilize the tracking-error dynamics in a manner such that the total-state tracking-error *decays* eventually to zero. Then, for all practical purposes, "perfect" tracking may be achieved, but only after some transient, and only if the reference trajectory is not too "fast".

One way [15] to accomplish this design goal is to force the state tracking error to be constrained to a sliding surface in state space, $s(\tilde{x}) = 0$, where $s(\tilde{x})$ is described by following matrix equation of dimension $k \times 1$ in state-space

$$s(\tilde{x}) = \sum_{p=0}^{n-1} \binom{n-1}{p} \Lambda^p \tilde{\tilde{x}}^{(n-1-p)} \tag{3.16}$$

This matrix equation is a weighted vector sum of the output-tracking error vector, plus its first (n-1) derivatives. In other words, this equation is a simply a weighted vector sum of the components of the total-state tracking error vector.

If Λ is chosen such that the matrix, $-\Lambda$, is Hurwitz, then the state-tracking error will decay eventually to zero, with dynamics governed by the linear matrix differential equation

$$\left(\frac{d}{dt} + \Lambda\right)^{n-1} \tilde{\tilde{x}} = 0 \tag{3.17}$$

Then "perfect" state-tracking can be achieved, but only after a transient, and only if the reference is not "faster" than the dynamics of (3.17). In addition, if the state-tracking error vector satisfies the following Lyapunov-based *Sliding-Condition* relation

$$\frac{1}{2}\frac{d}{dt} s^T(\tilde{x}) s(\tilde{x}) \leq -\eta s^T(\tilde{x}) \mathrm{sgn}(s(\tilde{x})) \quad \text{for } \tilde{x} \in \left(R^{(n)\times k} - S(t)\right) \tag{3.18}$$

for all states "off" the sliding surface, it can be shown [15] that the system is guaranteed to reach the stable sliding-surface in a finite time, and remain there. Note that sgn(z) is defined as the vector signum function. The Sliding-Condition relation is discussed in further detail in Appendix B.

The Sliding-Mode Control Law for the Descriptor/Companion model that satisfies the Sliding-Condition of (3.18) can be shown [15] to have the following form

$$\mathbf{u} = \hat{\mathbf{u}} - \mathbf{K}(\tilde{\mathbf{x}})\mathrm{sgn}(\mathbf{s}(\tilde{\mathbf{x}})) \tag{3.19}$$

where $\mathbf{K}(\tilde{\mathbf{x}})$ is a diagonal matrix given by

$$\mathbf{K}(\tilde{\mathbf{x}}) = \begin{bmatrix} K_1(\tilde{\mathbf{x}}) & \cdots & 0 \\ \vdots & \ddots & \vdots \\ 0 & \cdots & K_k(\tilde{\mathbf{x}}) \end{bmatrix} \tag{3.20}$$

The "nominal" control law, $\hat{\mathbf{u}}$, maintains zero steady-state tracking error when the system is on the sliding surface (in the absence of modeling errors or disturbances). The discontinuous term, $\mathbf{K}(\tilde{\mathbf{x}})\mathrm{sgn}(\mathbf{s}(\tilde{\mathbf{x}}))$, forces the system to be attracted to and remain on the sliding surface.

The nominal control law can be derived by assuming that the system is on the sliding surface (i.e., $\mathbf{s}(\tilde{\mathbf{x}}) = \mathbf{0}$). This implies that the time-derivative of $\mathbf{s}(\tilde{\mathbf{x}})$ is also zero.

$$\frac{d}{dt}\mathbf{s}(\tilde{\mathbf{x}}) = \sum_{p=0}^{n-1} \binom{n-1}{p} \Lambda^p \tilde{\mathbf{x}}^{(n-p)} = 0 \tag{3.21}$$

This expression can be factored into

$$\sum_{p=0}^{n-1} \binom{n-1}{p} \Lambda^p \tilde{\mathbf{x}}^{(n-p)} = \hat{\mathbf{x}}^{(n)} - \hat{\mathbf{x}}_d^{(n)} + \sum_{p=1}^{n-1} \binom{n-1}{p} \Lambda^p \tilde{\mathbf{x}}^{(n-p)} = 0 \tag{3.22}$$

Substitution of the nominal Descriptor/Companion system, i.e., $\mathbf{E}(\mathbf{x}) = \hat{\mathbf{E}}(\mathbf{x})$, $\mathbf{f}(\mathbf{x}) = \hat{\mathbf{f}}(\mathbf{x})$, $\mathbf{B}(\mathbf{x}) = \hat{\mathbf{B}}(\mathbf{x})$, and $\mathbf{d} = \mathbf{0}$, into (3.22) gives

$$\hat{\mathbf{E}}^{-1}(\mathbf{x})\left(\hat{\mathbf{f}}(\mathbf{x}) + \hat{\mathbf{B}}(\mathbf{x})\hat{\mathbf{u}} \right) - \hat{\mathbf{x}}_d^{(n)} + \sum_{p=1}^{n-1} \binom{n-1}{p} \Lambda^p \tilde{\mathbf{x}}^{(n-p)} = 0 \tag{3.23}$$

Solving (3.23) for $\hat{\mathbf{u}}$ then yields

$$\hat{\mathbf{u}} = \hat{\mathbf{B}}^{-1}(\mathbf{x})\left(-\hat{\mathbf{f}}(\mathbf{x}) + \hat{\mathbf{E}}(\mathbf{x})\left(\hat{\mathbf{x}}_d^{(n)} - \sum_{p=1}^{n-1} \binom{n-1}{p} \Lambda^p \tilde{\mathbf{x}}^{(n-p)} \right) \right) \tag{3.24}$$

The discontinuous term can be found by first substituting the Sliding-Mode Control Law of (3.19) together with the nominal control term, (3.24), into the uncertain Descriptor/Companion system, i.e., where

$$\mathbf{E}(\mathbf{x}) = \hat{\mathbf{E}}(\mathbf{x}) - \Delta\mathbf{E}(\mathbf{x}) \tag{3.25}$$

$$\mathbf{f}(\mathbf{x}) = \hat{\mathbf{f}}(\mathbf{x}) + \Delta\mathbf{f}(\mathbf{x}) \tag{3.26}$$

$$\mathbf{B}(\mathbf{x}) = \hat{\mathbf{B}}(\mathbf{x}) + \Delta\mathbf{B}(\mathbf{x}) \tag{3.27}$$

which then gives the following expression for the derivative of $s(\tilde{\mathbf{x}})$

$$\begin{aligned} \frac{d}{dt} s(\tilde{\mathbf{x}}) = \hat{\mathbf{E}}^{-1}(\mathbf{x})\big(& \Delta\mathbf{E}(\mathbf{x})\hat{\mathbf{x}}^{(n)} + \Delta\mathbf{f} + \mathbf{d} + \Delta\mathbf{B}(\mathbf{x})\hat{\mathbf{u}} \\ & - (\hat{\mathbf{B}}(\mathbf{x}) + \Delta\mathbf{B}(\mathbf{x}))\mathbf{K}(\tilde{\mathbf{x}})\mathrm{sgn}(s(\tilde{\mathbf{x}}))\big) \end{aligned} \tag{3.28}$$

Substitution of (3.28) into the Sliding Condition of (3.18), implies that a lower bound on the diagonal elements of $\mathbf{K}(\tilde{\mathbf{x}})$ is given by

$$K_i(\tilde{x}) \geq \max_{\Delta B \in \Delta B} \left[(\hat{B}(x) + \Delta B(x))^{-1} (\overline{\Delta E}(x)\bar{\tilde{x}}^{(n)} + \overline{\Delta f}(x) + \bar{d} + \Delta B(x)\hat{u} + \eta \hat{E}(x) \begin{bmatrix} 1 \\ \vdots \\ 1 \end{bmatrix}) \right]_i \tag{3.29}$$

where $\overline{\Delta E}(x)$, $\overline{\Delta f}(x)$, and $\overline{\Delta B}(x)$, are upper bounds to the additive uncertainty. Note that the magnitude of $\hat{x}^{(n)}$ is assumed to be bounded (element-wise) by $\bar{\tilde{x}}^{(n)}$, i.e.,

$$\left| \hat{x}^{(n)} \right| \leq \bar{\tilde{x}}^{(n)} \tag{3.30}$$

For the Descriptor/Companion model, the idealized sliding-mode control law given by (3.19) provides "perfect" asymptotic tracking of the desired state trajectory, in the face of the model-parameter uncertainties described by (3.25)-(3.27), plus any unmodeled low-frequency dynamics included in **d**. However, the discontinuous portion of this control law can cause undesirable high-frequency control signal "chattering". This implies that this controller will not be guaranteed to be robust to higher-frequency unmodeled dynamics.

To alleviate this chattering effect (and provide robustness to unmodeled high-frequency dynamics), the discontinuous control term can be modified by adding a sliding-surface "boundary layer" [15] of sufficient "width". The resulting sliding-mode control law is then given by

$$u = \hat{u} - K(\tilde{x})\mathrm{sat}(s(\tilde{x})\Phi^{-1}) \tag{3.31}$$

where

$$\mathrm{sat}(s(\tilde{x})\Phi^{-1}) = \begin{bmatrix} \mathrm{sat}(s_1(\tilde{x})/\Phi_1) \\ \vdots \\ \mathrm{sat}(s_k(\tilde{x})/\Phi_k) \end{bmatrix} \tag{3.32}$$

The "boundary-layer" matrix, Φ, is assumed to be diagonal, real, and positive, while the "saturation" function is assumed to be defined by

$$\text{sat}(s_i(\tilde{x})/\Phi_i) = \begin{cases} s_i(\tilde{x})/\Phi_i & |s_i(\tilde{x})| \le \Phi_i \\ \text{sgn}(s_i(\tilde{x})) & |s_i(\tilde{x})| \ge \Phi_i \end{cases} \tag{3.33}$$

As shown in Figure 3.2, the modified control law given by (3.31) linearly interpolates the idealized sliding-mode control law across the boundary layer

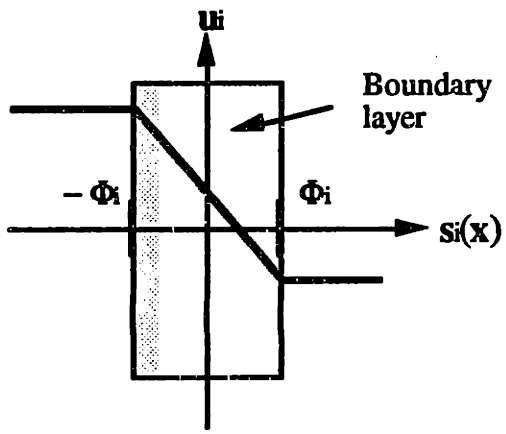

Figure 3.2: Control Law Interpolation Inside Boundary Layer

It can be shown [15] that if the dynamics of the system are confined to be within the boundary layer, the magnitude of the output tracking error is bounded element-wise by

$$|\tilde{x}| = |\hat{x} - \hat{x}_d| \le \Lambda^{1-n}\text{diag}(\Phi) \tag{3.34}$$

With the Sliding-Mode Control Law of (3.31), the derivative of $s(\tilde{x})$ while inside the boundary layer is given by

$$\frac{d}{dt}s(\tilde{x}) = \hat{E}^{-1}(x)\Big(\big[-(\hat{B}(x) + \Delta B(x))K(\tilde{x})\Phi^{-1}(s(\tilde{x})) \big] + \big[\Delta E(x)\hat{x}^{(n)} + \Delta f + d + \Delta B(x)\hat{u} \big] \Big) \tag{3.35}$$

It can be shown [16] using this equation (and the assumptions on the eigenvalues of $\mathbf{B}(\mathbf{x})$ and $\mathbf{E}(\mathbf{x})$) that $s(\tilde{\mathbf{x}})$ can be represented as the output of a stable system with its input given by the additive parameter uncertainty. It can also be shown that the "dominant" dynamics of this system are directly influenced by the boundary layer matrix. If the boundary layer matrix is chosen such that the dominant dynamics of this system do not excite any unmodeled dynamics present in the actual nonlinear system, chattering can be eliminated. Therefore, the boundary layer provides a direct way of quantifying the trade-off between stability-robustness (i.e., elimination of chattering) and performance (i.e., tracking precision).

3.3 AUGMENTATION OF LTI CONTROLLERS USING THE SLIDING-MODE METHODOLOGY

For nonlinear systems such as the Descriptor/Companion model of Section 3.1, the usual procedure for designing linear time-invariant (LTI) control systems is to linearize the nonlinear model about some nominal "operating point", and then use a linear control system technique to design the controller. However, the control performance can degrade considerably when the system moves away from the nominal region of operation.

One means of alleviating this performance degradation is by using feedback linearization [16,17], where a nonlinear feedback law directly compensates for the nonlinearities. The controlled nonlinear system can (in certain cases) be made to appear linear. The Sliding-Mode Law of Section 3.2 is a special case of feedback linearization, where the nonlinear Descriptor/Companion model is made to appear as a linear "sliding-surface" model.

For the Descriptor/Companion system, suppose the LTI controller is designed using the following LTI model

$$\frac{d}{dt}\left(\hat{\mathbf{x}}\right) = \dot{\hat{\mathbf{x}}}$$

$$\frac{d}{dt}\left(\dot{\hat{\mathbf{x}}}\right) = \ddot{\hat{\mathbf{x}}}$$

$$\vdots$$

$$\frac{d}{dt}\left(\hat{\mathbf{x}}^{(n-2)}\right) = \hat{\mathbf{x}}^{(n-1)}$$

$$\mathbf{E}_p\hat{\mathbf{x}}^{(n)} = \mathbf{A}_p\mathbf{x} + \mathbf{B}_p\mathbf{u} + \mathbf{d} \qquad (3.36)$$

with the goal of the controller being state-tracking (i.e., forcing the state vector, $\mathbf{x}$, to track a reference state vector, $\mathbf{x}_d$, which implies the minimization of the tracking error vector, $\tilde{\mathbf{x}} = \mathbf{x} - \mathbf{x}_d$). This implies that the LTI controller has the following standard state-space form

$$\dot{\mathbf{x}}_c = \mathbf{A}_c\mathbf{x}_c + \mathbf{B}_c\tilde{\mathbf{x}}$$

$$\mathbf{u}_{LTI} = \mathbf{C}_c\mathbf{x}_c + \mathbf{D}_c\tilde{\mathbf{x}} \qquad (3.37)$$

where the "measured" input to this controller is the state-tracking error. For the "perfect model" case without uncertainties and disturbances, the feedback-linearization control law is given by

$$\hat{\mathbf{u}} = \hat{\mathbf{B}}^{-1}(\mathbf{x})\left(-\hat{\mathbf{f}}(\mathbf{x}) + \hat{\mathbf{E}}(\mathbf{x})\left(\mathbf{E}_p^{-1}\mathbf{A}_p\mathbf{x} + \mathbf{E}_p^{-1}\mathbf{B}_p\mathbf{u}_{LTI}\right)\right) \qquad (3.38)$$

This control law is very similar to the "nominal" term of the Sliding-Mode control law of Section 3.2. Intuitively, this control law "cancels out" all of the known nonlinear dynamics of the Descriptor/Companion system, and replaces them with the linear dynamics of the LTI design model.

For the actual Descriptor/Companion model (with the additive uncertainty described by (3.6)-(3.11)), the control law given by (3.38) may not necessarily compensate for any modeling errors or disturbances (depending on the design of the LTI controller). This implies that there may be some performance degradation for the actual model. The Sliding-

Mode control law of Section 3.2 suggests one means of alleviating this problem. Specifically, it suggests defining a "sliding-surface" linear function of the form

$$s(\tilde{x}) = \sum_{p=0}^{n-1} \binom{n-1}{p} \Lambda^p \tilde{x}^{(n-1-p)} \tag{3.39}$$

When this function is bounded, the state tracking-error vector is also guaranteed to be bounded. This suggests that the control law given by (3.38) can be modified to

$$u = \hat{u} - K(\tilde{x})\,dsgn(s(\tilde{x}),\Phi) \tag{3.40}$$

where the "dead-zone boundary" matrix, Φ, is real diagonal. The "dead-zone" signum function is given by

$$dsgn(s_i(\tilde{x}),\Phi_i) = \begin{cases} 0 & |s_i(\tilde{x})| \le \Phi_i \\ sgn(s_i(\tilde{x})) & |s_i(\tilde{x})| \ge \Phi_i \end{cases} \tag{3.41}$$

$K(\tilde{x})$ is a diagonal matrix given by

$$K(\tilde{x}) = \begin{bmatrix} K_1(\tilde{x}) & \cdots & 0 \\ \vdots & \ddots & \vdots \\ 0 & \cdots & K_k(\tilde{x}) \end{bmatrix} \tag{3.42}$$

Using the Sliding Condition of (3.18), it can be shown that if the diagonal elements of $K(\tilde{x})$ satisfy the lower bound condition given by

$$K_i(\tilde{x}) \geq \max_{\Delta B \in \Delta B} \Big[\Big(\widehat{B}(x) + \Delta B(x) \Big)^{-1} \Big(\overline{\Delta E}(x) \tilde{\bar{x}}^{(n)} + \overline{\Delta f}(x) + \bar{d} + \Delta B(x) \big| \hat{u} \big| + \widehat{E}(x) \Big| E_p^{-1} A_p x + E_p^{-1} B_p u_{LTI} - \hat{x}_d^{(n)} + \sum_{p=1}^{n-1} \binom{n-1}{p} \Lambda^p \tilde{x}^{(n-p)} \Big| + \eta \widehat{E}(x) \begin{bmatrix} 1 \\ \vdots \\ 1 \end{bmatrix} \Big) \Big]_i \tag{3.43}$$

then the sliding-surface function given by (3.39) is guaranteed to be bounded by Φ, which implies that the tracking error will also be bounded. Therefore, Φ can be chosen so as to meet a specific tracking-error performance goal, so long as both the modeling uncertainty and disturbances are bounded. Note that the lower bound condition on $K(\tilde{x})$ is also very similar to the lower bound condition found for the Sliding-Mode control law of Section 3.2.

As with the Sliding-Mode control law, the discontinuous portion of the modified control law of (3.40) can cause undesirable high-frequency control signal "chattering". This can be alleviated by modifying the control law to linearly interpolate across the discontinuities. The modified control law is given by

$$u = \hat{u} - K(\tilde{x}) dsat(s(\tilde{x}), \Phi_{inner}, \Phi_{outer}) \tag{3.42}$$

where the "dead-zone" saturation function is defined to be

$$dsat(s_i(\tilde{x}), \Phi_i) = \begin{cases} 0 & |s_i(\tilde{x})| \leq [\Phi_{inner}]_i \\ (s_i(\tilde{x}) - [\Phi_{inner}]_i \, sgn(s_i(\tilde{x})))/([\Phi_{outer}]_i - [\Phi_{inner}]_i) & [\Phi_{inner}]_i \leq |s_i(\tilde{x})| \leq [\Phi_{outer}]_i \\ sgn(s_i(\tilde{x})) & |s_i(\tilde{x})| \geq [\Phi_{outer}]_i \end{cases} \tag{3.43}$$

Thus the control law has a "double" boundary layer, as shown in Figure 3.3.

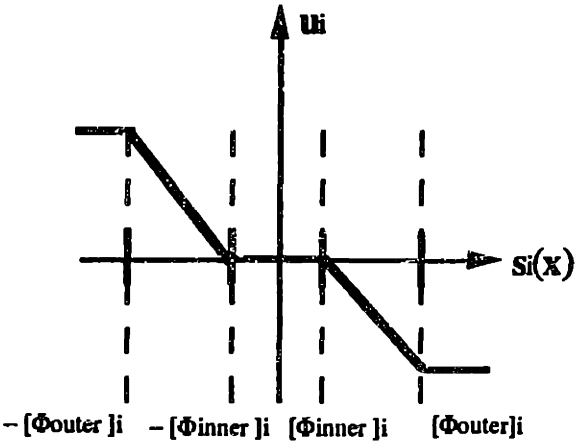

Figure 3.3: Modified Control Law

The inner layer is chosen so as to give increased robust performance, without sacrificing the nominal performance characteristics of the LTI controller. The outer layer is chosen so as to eliminate chattering, in a similar fashion to the Sliding-Mode control law.

In summary, the general form of the Sliding-Mode Augmented control law, given by (3.42), can be represented by the block diagram shown in Figure 3.4.

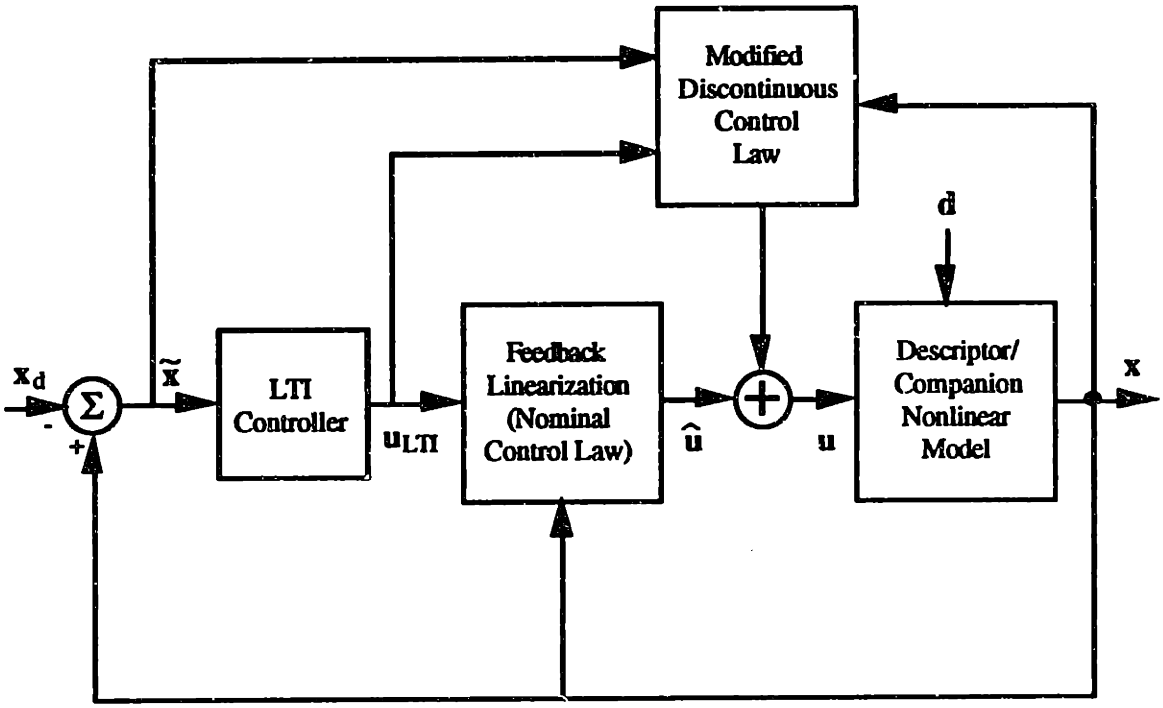

Figure 3.4: The Sliding-Mode Augmented Control Law

The feedback-linearization nominal term of the Sliding-Mode Augmented control law modifies the output of the LTI controller so as to compensate for all of the known nonlinearities of the Descriptor/Companion model. The discontinuous term of the control law then tries to compensate for bounded modeling errors and disturbances.

Chapter 4

Model Development and Analysis

The appropriate tradeoff between system-model accuracy and model-development effort is one of the most important considerations for any control system design. "Good" system model accuracy is desirable for a number of reasons. For example, the performance of a control system design is often determined by the accuracy of the system model used in the design process. Even for "robust" control design methodologies, such as H_∞/μ-Synthesis Control and Sliding Mode Control, the "best" obtainable control system performance is still directly affected by the system model accuracy. Also, accurate system models can be very useful for validating the performance and stability of the control system design in computer simulations prior to testing in the actual physical system. While model accuracy is desirable for these reasons, it often requires significant model complexity and increased effort in determining the model parameters. Model complexity also tends to increase the control-system design effort.

This chapter discusses some of these modeling tradeoffs as related to the development of the system models used in the design and evaluation of the control systems for the *Sea Squirt* AUV. It begins with a brief physical description of the vehicle and then details the development and analysis of both nonlinear and linear system models, both full-order and reduced-order.

4.1 PHYSICAL DESCRIPTION OF VEHICLE

The MIT Sea Grant/CSDL *Sea Squirt* AUV is a modified Benthos Mark II Minirover (Figure 4.1) approximately three feet in length. It has three thrusters (starboard, port, and vertical) which are used for direct yaw and depth control. The *Sea Squirt's* pitch and roll are passively stabilized by locating the center of buoyancy (cb) above the center of gravity (cg). There are no hydrodynamic control surfaces such as rudders or stern planes. The *Sea Squirt* sensors include a forward-looking sonar, a bottom-looking sonar (altimeter), a depth transducer, a magnetic flux-gate compass, a yaw-rate gyroscope, and pitch and roll inclinometers. Depth rate is estimated by back-differencing and filtering the sensed depth. The onboard computer for the *Sea Squirt* is a GESPAC 68020-based system using the OS-9 multi-tasking operating system.

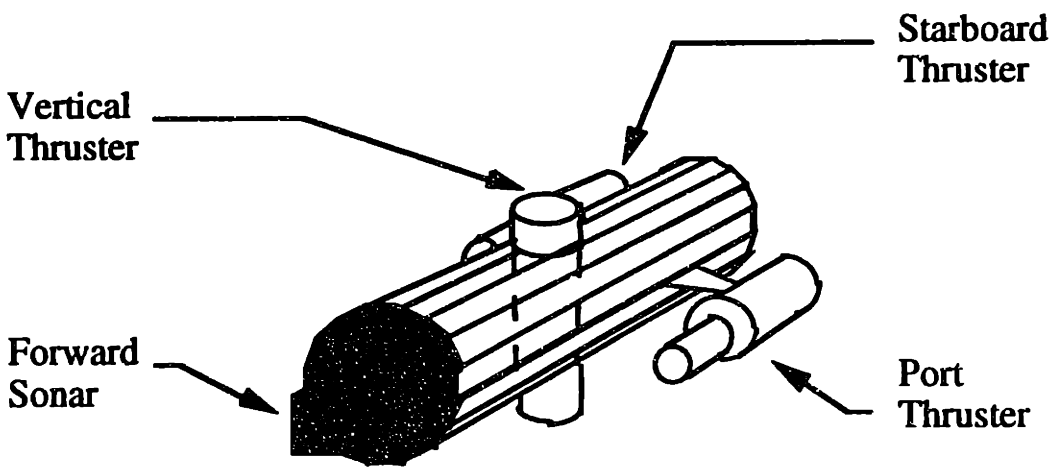

Figure 4.1: The Sea Squirt AUV

4.2 FULL-ORDER SIX DEGREE-OF-FREEDOM NONLINEAR MODEL

The first step in developing a suitable mathematical model of an underwater vehicle, such as the *Sea Squirt*, was to obtain a set of differential equations of motion (EOM). One method for obtaining the EOM for an underwater vehicle is to derive them directly from basic rigid-body mechanics and hydrodynamics. A more straightforward way would be to take the equations of motion of a similar vehicle, then modify them as needed.

4.2.1 AUV Equations of Motion

As outlined in [18], a set of EOM for the *Sea Squirt* AUV was developed, based upon the U. S. Navy's Standard Equations-of-Motion for Free-Swimming Underwater Vehicles[19]. These Standard EOM are a general Taylor-Series expansion of the forces and moments acting on the vehicle along three independent body axes, with the assumptions of "small" angle of attack and "small" sideslip angle motion. These equations include hydrodynamic effects (e.g., drag), hydrostatic effects (e.g., vehicle buoyancy), plus "added mass" effects due to the mass of the water accelerated along with the vehicle. For the AUV EOM, control surface terms, plus hydrodynamic terms whose contribution was assumed "small" were neglected. Disturbance force and torque terms were added. The EOM for the *Sea Squirt* AUV are shown here in their final form

Axial Force

$$\begin{aligned} &m[\dot{u} - vr + wq - X_g(q^2 + r^2) + Y_g(pq - \dot{r}) + Z_g(pr + \dot{q})] \\ &\quad = X_{\dot{u}}\dot{u} + X_{u|u|}u|u| + (W - B)\sin\theta + T_p + T_s + D_u \end{aligned} \tag{4.1}$$

Lateral Force

$$\begin{aligned} &m[\dot{v} - wp + ur - Y_g(r^2 + p^2) + Z_g(qr - \dot{p}) + X_g(qp + \dot{r})] \\ &\quad = Y_{\dot{v}}\dot{v} + Y_{\dot{p}}\dot{p} + Y_{\dot{r}}\dot{r} + Y_{v|v|}v|v| + Y_{ur}ur + Y_{uv}|u|v \\ &\qquad + (W - B)\cos\theta\sin\phi + D_v \end{aligned} \tag{4.2}$$

Vertical Force

$$\begin{aligned} m[\dot{w} - uq + vp - Z_g(p^2 + q^2) + X_g(rp - \dot{q}) + Y_g(rq + \dot{p})] \\ = Z_{\dot{w}}\dot{w} + Z_{\dot{q}}\dot{q} + Z_{w|w|}w|w| + Z_{uw}|u|w + Z_{uq}uq \\ + (W - B)\cos\theta\cos\phi + T_v + D_w \end{aligned} \quad (4.3)$$

Rolling Moment

$$\begin{aligned} I_{xx}\dot{p} + (I_{zz} - I_{yy})qr - (\dot{r} + pq)I_{zx} + (r^2 - q^2)I_{yz} \\ + (pr - \dot{q})I_{xy} + m[Y_g(\dot{w} - uq + vp) - Z_g(\dot{v} - wp + ur)] \\ = K_{\dot{p}}\dot{p} + K_{\dot{v}}\dot{v} + K_{p|p|}p|p| + (Y_gW - Y_bB)\cos\theta\cos\phi \\ - (Z_gW - Z_bB)\cos\theta\sin\phi + T_vY_g + D_p \end{aligned} \quad (4.4)$$

Pitching Moment

$$\begin{aligned} I_{yy}\dot{q} + (I_{xx} - I_{zz})rp - (\dot{p} + qr)I_{xy} + (p^2 - r^2)I_{yz} \\ + (qp - \dot{r})I_{yz} + m[Z_g(\dot{u} - vr + wq) - X_g(\dot{w} - uq + vp)] \\ = M_{\dot{q}}\dot{q} + M_{\dot{w}}\dot{w} + M_{q|q|}q|q| + M_{uw}uw + M_{uq}|u|q \\ - (X_gW - X_bB)\cos\theta\cos\phi \\ - (Z_gW - Z_bB)\sin\theta - (T_p + T_s)Z_g + T_vX_g + D_q \end{aligned} \quad (4.5)$$

Yawing Moment

$$\begin{aligned} I_{zz}\dot{r} + (I_{yy} - I_{xx})pq - (\dot{q} + rp)I_{yz} + (q^2 - p^2)I_{xy} \\ + (rq - \dot{p})I_{zx} + m[X_g(\dot{v} - wp + ur) - Y_g(\dot{u} - vr + wq)] \\ = N_{\dot{r}}\dot{r} + N_{\dot{v}}\dot{v} + N_{r|r|}r|r| + N_{ur}ur + N_{uv}uv \\ + (X_gW - X_bB)\cos\theta\sin\phi \\ + (Y_gW - Y_bB)\sin\theta + Y_T(T_p - T_s) + D_r \end{aligned} \quad (4.6)$$

The variables, u, v, and w, are the linear velocities defined in the vehicle-relative coordinate frame, and p, q, and r are the angular velocities in the vehicle-relative coordinate frame. The positive directions of these velocities are defined according to the right-hand rule as shown in Figure 4.2.

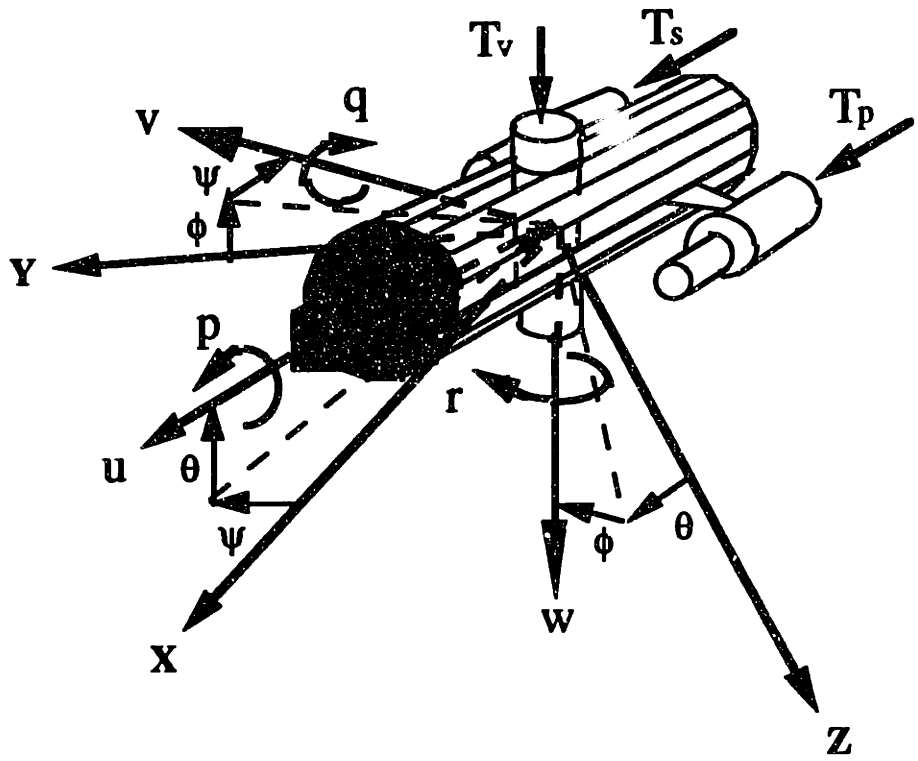

Figure 4.2: Definition of AUV EOM Variables

The vehicle's earth-frame relative angular positions (roll, pitch, and heading) are represented by the Euler angles, ϕ, θ, and ψ, which are defined in the manner also shown in Figure 4.2. T_S, T_P, and T_V represent the propulsion forces produced by the starboard, port, and vertical thrusters. D_u, D_v, D_w, D_p, D_q, and D_r represent the disturbance forces and torques with positive directions defined in the vehicle-relative coordinate frame exactly like u, v, w, p, q, and r. Derivatives with respect to time are represented by the dotted terms. The mass of the vehicle is given by m, while the mass moments of inertia are given by I_{xx}, I_{yy}, and I_{zz}. B and W are the AUV's buoyancy and weight, respectively. The locations of the vehicle's center-of-gravity (cg) and center-of-buoyancy (cb) are defined in the vehicle-relative coordinate frame by (X_g, Y_g, Z_g) and (X_b, Y_b, Z_b). The remaining terms in the EOM are the various hydrodynamic coefficients of the AUV (i.e., $Y_{|v|v}$, N_{ur}, etc.). These terms are used to describe effects such as drag forces, lift forces, and "added mass" forces which act on the AUV.

The kinematic relationships between the vehicle-relative velocities and the Earth-relative positions and Euler angles can be defined by the following equations.

$$\dot{X} = u \cos\theta \cos\psi + v(\sin\phi \sin\theta \cos\psi - \cos\phi \sin\psi) + w(\sin\phi \sin\psi + \cos\phi \sin\theta \cos\psi) \quad (4.7)$$

$$\dot{Y} = u \cos\theta \sin\psi + v(\cos\theta \cos\psi + \cos\phi \sin\theta \sin\psi) + w(\cos\phi \sin\theta \cos\psi - \sin\phi \cos\psi) \quad (4.8)$$

$$\dot{Z} = - u \sin\theta + v \cos\theta \sin\phi + w \cos\theta \cos\phi \quad (4.9)$$

$$\dot{\phi} = p + \left[\frac{r \cos\phi + q \sin\phi}{\cos\theta}\right] \sin\theta \quad (4.10)$$

$$\dot{\theta} = q \cos\phi + r \sin\phi \quad (4.11)$$

$$\dot{\psi} = \frac{r \cos\phi + q \sin\phi}{\cos\theta} \quad (4.12)$$

The full-order, six degree-of-freedom nonlinear vehicle model consists of the force and moment equations, (4.1)-(4.6), together with the kinematic equations, (4.9)-(4.12). Note that the earth-frame relative linear positions, X and Y, were not included in this model, since they were not revelant to the AUV design effort (i.e., they are not controlled), plus they do not affect any of the other dynamic states. This model can alternately be expressed in the vector form

$$\mathbf{E}\dot{\mathbf{x}} = \mathbf{f}(\mathbf{x},\mathbf{u},\mathbf{d}) \quad (4.13)$$

$$\mathbf{y} = \mathbf{C}\mathbf{x} \quad (4.14)$$

where the full-order state vector is defined by

$$\mathbf{x} = [\, u\ v\ w\ p\ q\ r\ Z\ \phi\ \theta\ \psi\,]^T \tag{4.15}$$

and the input vector is defined by

$$\mathbf{u} = [T_v\ \ (T_p - T_s)\ \ (T_p + T_s)]^T \tag{4.16}$$

with a disturbance vector defined by

$$\mathbf{d} = [\, D_u\ D_v\ D_w\ D_p\ D_q\ D_r]^T \tag{4.17}$$

The output vector is then defined as the vector of variables actually measured or estimated by the vehicle's sensor suite

$$\mathbf{y} = [Z\ \psi\ \dot{Z}\ r\ \phi\ \theta]^T \tag{4.18}$$

4.2.2 Simulation Analysis of the Full-Order Nonlinear Model

From previous control-system design efforts for the *Sea Squirt* AUV [18], the full-order nonlinear model appears to provide a reasonably accurate mathematical approximation of the dynamic behavior of this vehicle. Many useful design insights into the dynamics of the AUV (plus an awareness of some of the physical limitations) can be gained by analyzing this model. A direct mathematical analysis of this nonlinear model, however, can be both difficult and time-consuming. A more convenient means of analyzing this model is to examine some of its time-domain responses by using a computer simulation.

For the full-order nonlinear model, a computer simulation analysis was performed (using a fourth-order Runge-Kutta numerical integration MATLAB™ package). The coefficients of this model were given the approximate numerical values contained in [18]

(and reprinted in Appendix D for convenience). Sensor and thruster dynamics were neglected.

Unforced Response

The first case to be considered is the unforced response of the model to non-zero initial conditions. The vehicle-relative velocities, u, v, and w, were each given an initial value of 1.0 ft/sec, while the vehicle-relative angular positions, p, q, and r, were each given an initial value of 10 deg/s. All of the position variables were each given an initial value of zero, and all of the thruster and disturbance forces were each given a value of zero, as well. The resulting time-domain response is shown in the plots of Figure 4.3.

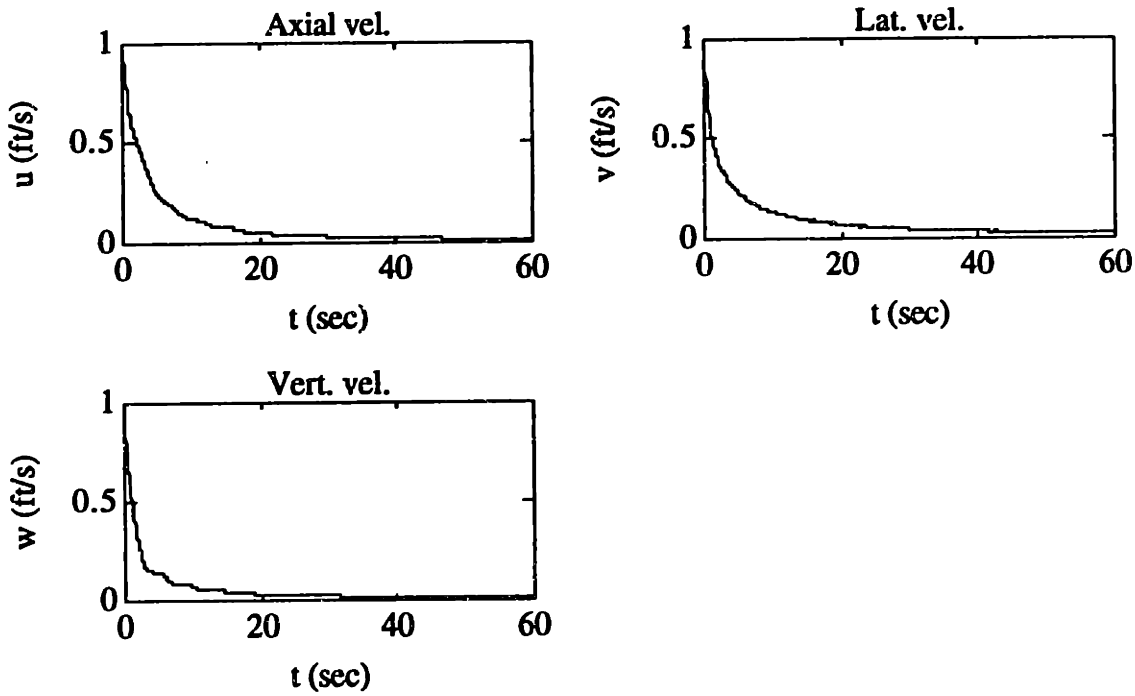

Figure 4.3: Full-Order Nonlinear Unforced Response

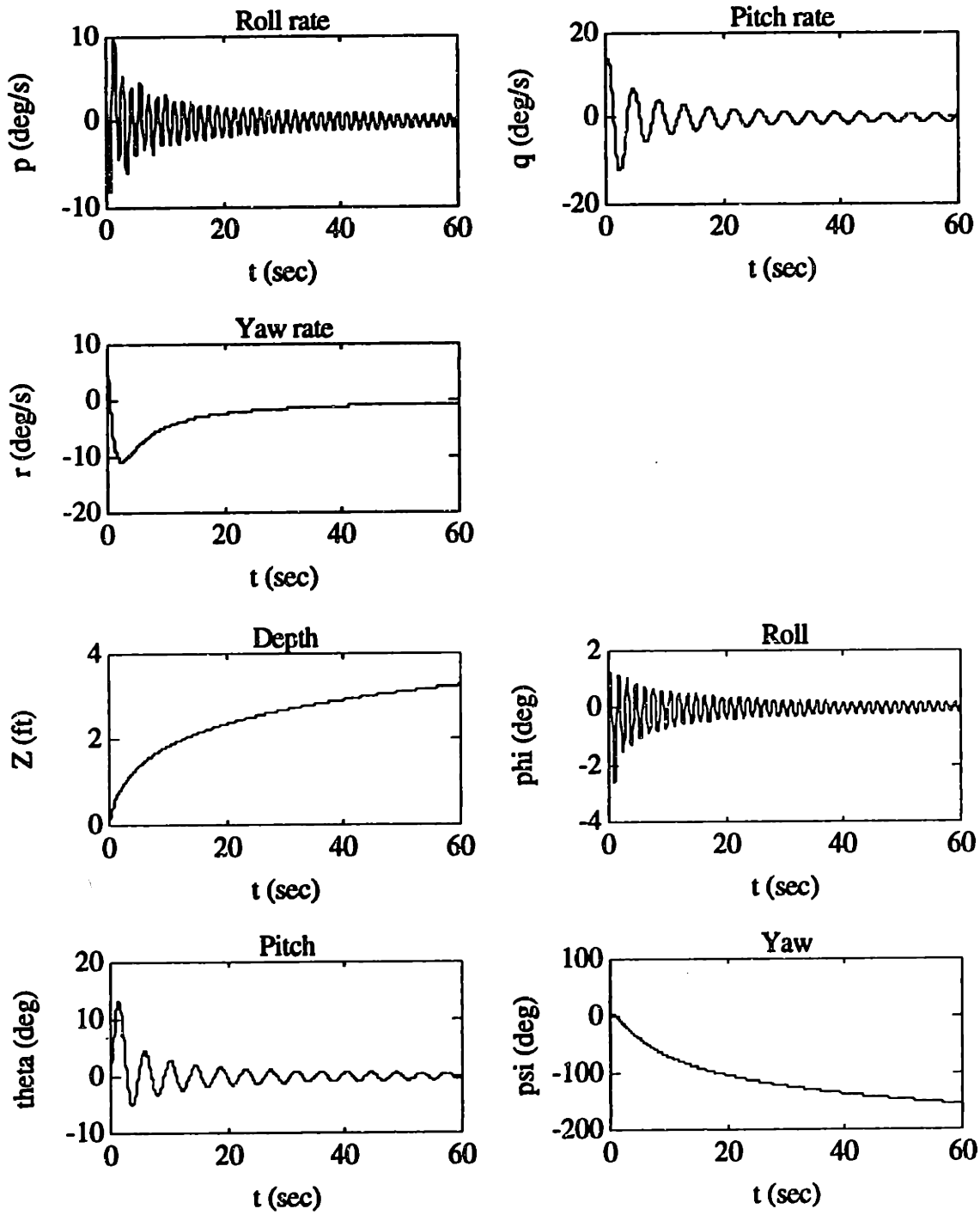

Figure 4.3: Full-Order Nonlinear Unforced Response (continued)

Several conclusions can be reached about the AUV model from these particular time-response plots. First, this model is second-order and marginally stable (i.e., the earth-relative positions are approximately the integrals of the respective vehicle-relative velocities). Note that the vehicle-relative linear velocities, by themselves, appear to have a stable first-order response (with a damping dependent upon the hydrodynamic drag).

In addition, there appear to be two stable oscillatory modes of interest. The first mode affects the roll angle, ϕ, and has a frequency of approximately 4.4 rad/sec (0.7 Hz). The second mode affects the pitch angle, θ, and has a frequency of approximately 1.4 rad/sec (0.23 Hz). These modes result from the restoring moment caused by the AUV's passive stabilization scheme (i.e., locating the center-of-buoyancy (cb) above the center-of-gravity (cg)).

Vertical Thrust Step Response

Next, the response of the AUV model to step control inputs was considered. All states of the vehicle were given an initial value of zero and all disturbance forces were assumed to be zero. Again, both sensor and thruster dynamics were neglected. For the first simulation case, a step of 1.0 lb.. was applied to the vertical thrust input, T_V. T_P and T_S were both set to zero. The resulting time-domain response is shown in the plots of Figure 4.4.

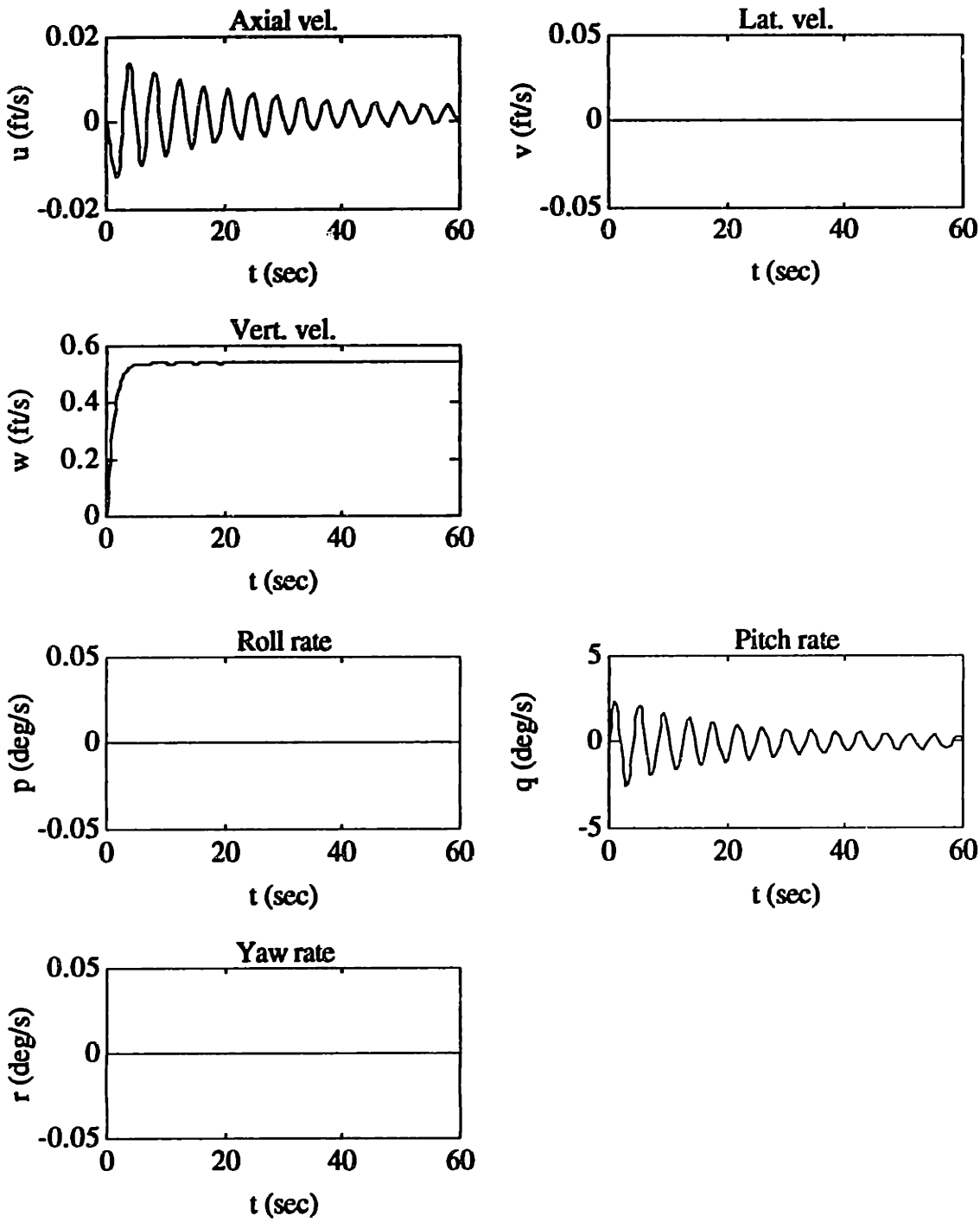

Figure 4.4: Full-Order Nonlinear Vertical Step Response

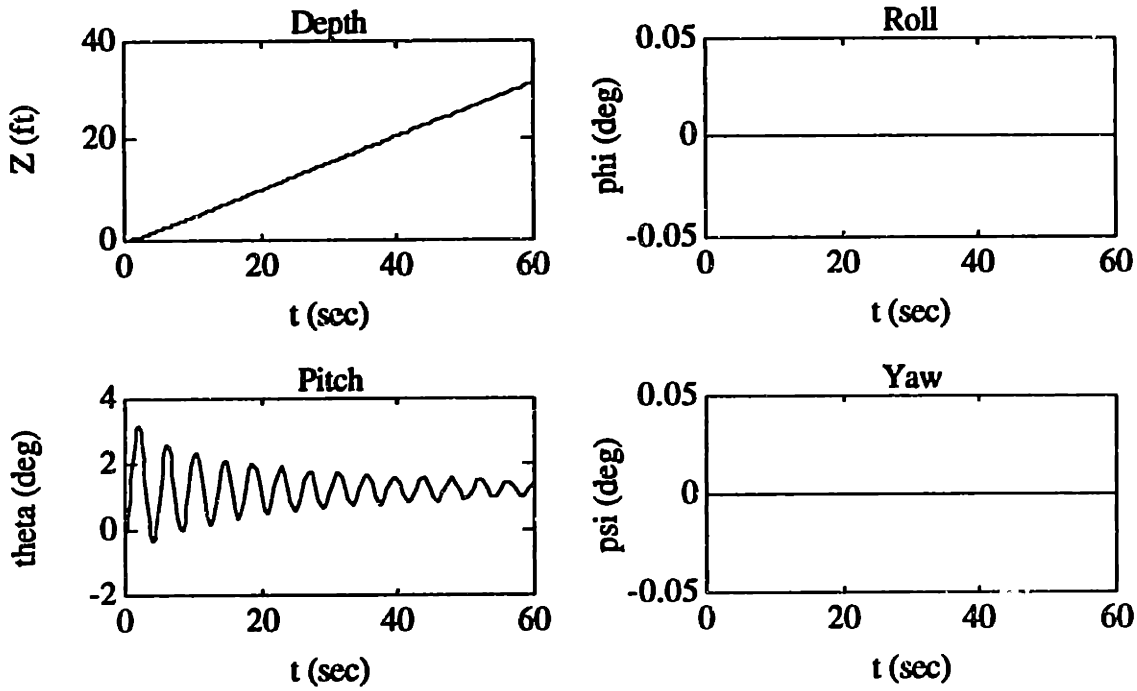

Figure 4.4: Full-Order Nonlinear Vertical Step Response (continued)

From these plots, the most apparent feature of design interest is the almost total decoupling of the heading and roll dynamics from the vertical thrust input. Physically, this corresponds to the fact that the vertical thruster is located along the centerline of the vehicle. For the "hovering" condition with a zero roll angle, this implies that the vertical thrust force will be almost completely parallel to the Z-axis of the vehicle.

Another feature of design interest is the excitation of the oscillatory mode associated with the pitch dynamics by the vertical thrust input. Physically this corresponds to the vertical thruster being located along the vehicle centerline, but slightly away from the cg. This excitation also implies that large vertical thrust inputs can cause undesirable oscillations in the pitch angle, especially if applied at the approximate frequency of this particular mode.

Differential Thrust Step Response

The next simulation case was done with the same zero initial-state and zero disturbance conditions as previously. The port thrust, T_p, was set to 0.5 lb.. and the starboard thrust, T_s, was set to -0.5 lb (which gave a total "positive differential" thrust of 1.0 lb., but which also gave a total forward thrust of zero). The vertical thrust, T_v, was set equal to zero. The resulting time-domain response is shown in Figure 4.5.

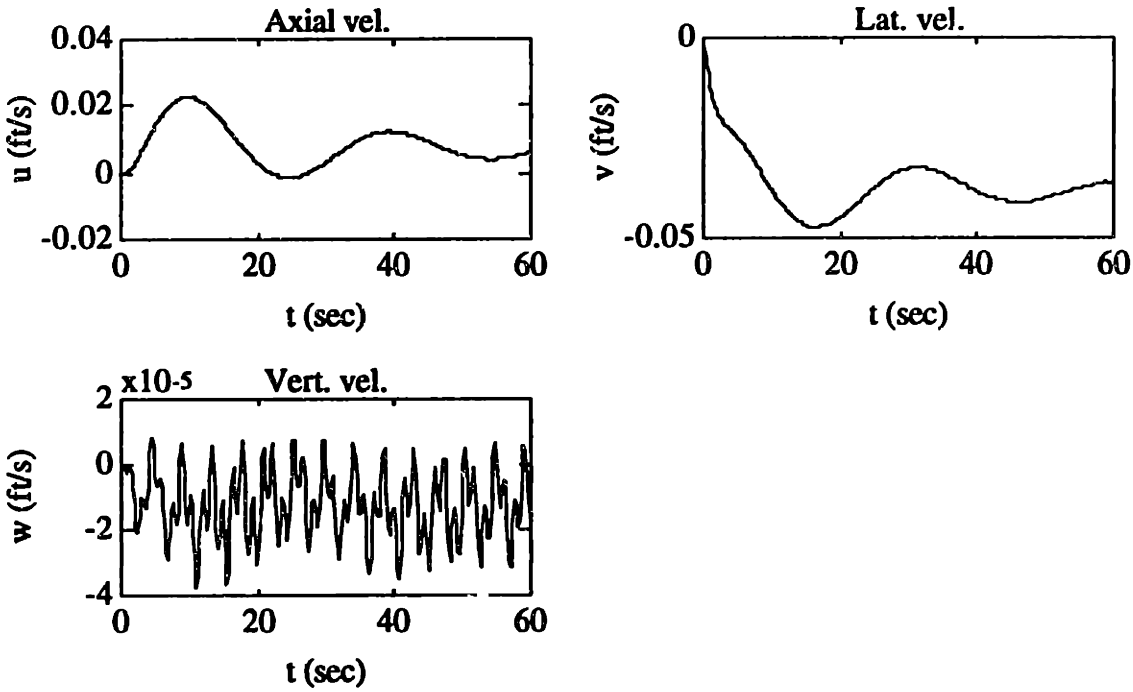

Figure 4.5: Full-Order Nonlinear Differential Step Response

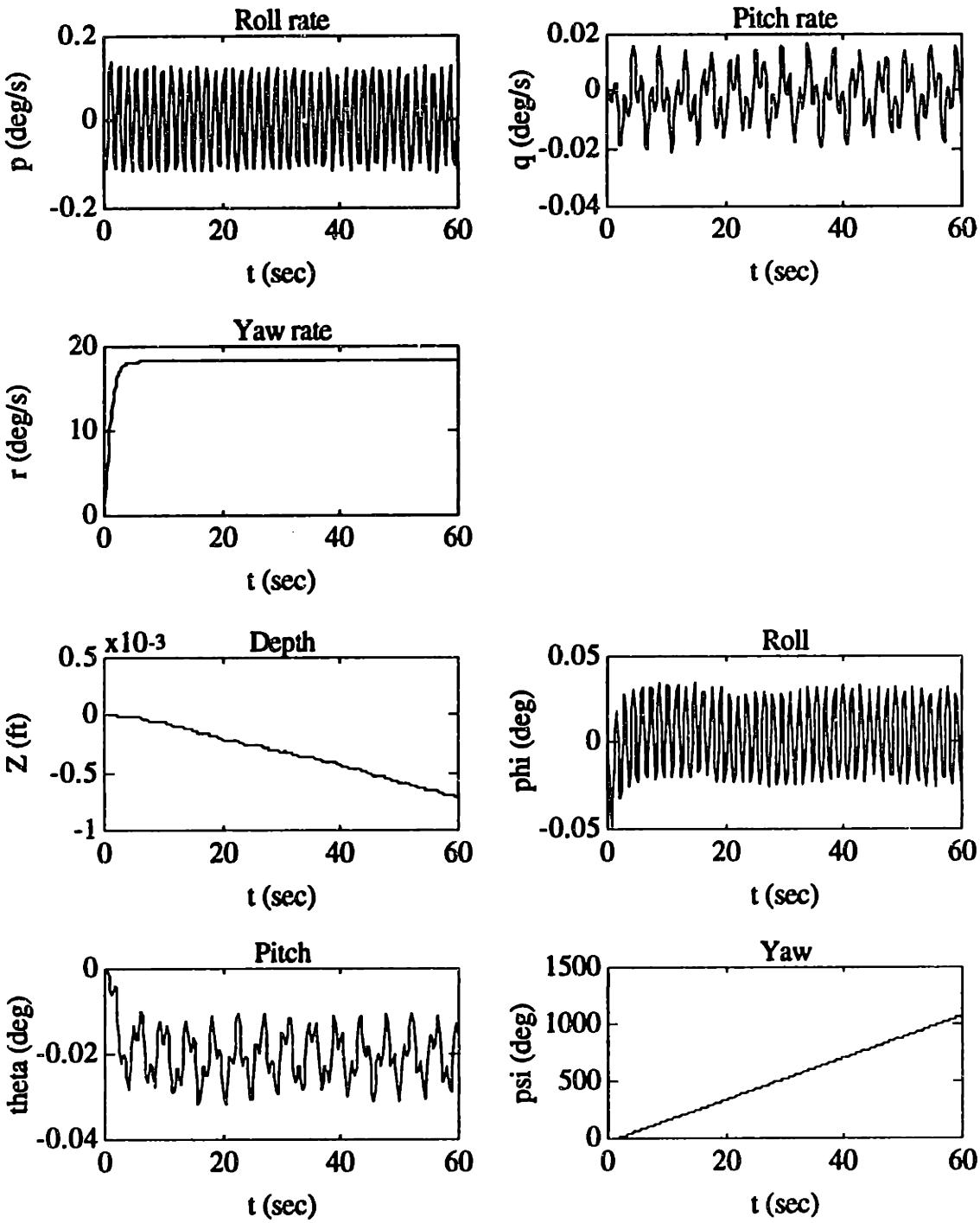

Figure 4.5: Full-Order Nonlinear Differential Step Response (continued)

From these plots, apparently the pitch and depth dynamics are nearly unaffected by the "differential thrust" when the vehicle is in the "hover" condition, except for a small oscillation caused by the excitation of the roll dynamics. For all practical design purposes, this data (plus the simulation data from the previous simulation case) implies that the depth dynamics and the heading dynamics are virtually decoupled from each other, at least for the "hovering" condition. Therefore, it may be possible to design separate heading and depth controllers for the AUV.

Note the presence of a low-frequency oscillation in the axial and lateral velocities. This oscillation is due to what is known in rigid-body dynamics as the Coriolis effect, which in this case is caused by the coupling of the axial and lateral velocities by the yaw rate. Physically, the Coriolis effect causes the vehicle to slowly "wobble" as it yaws in place.

"Full-Ahead" Step Response

The next simulation case was done with the objective of examining the step response of the model for a "significant" forward axial speed, u. Again, the state initial conditions and the disturbances were all assumed zero, and the sensor and thruster dynamics were neglected. T_V was again set to 1.0 lb., and the "differential thrust" (T_P - T_S) was again set equal to 1.0 lb. However, the "total" forward thrust ($T_P + T_S$) was set equal to 1.0 lb. as well, which then gave T_P equal to 1.0 lb. and T_S equal to 0.0 lb. The resulting time-domain response is shown in the plots of Figure 4.6.

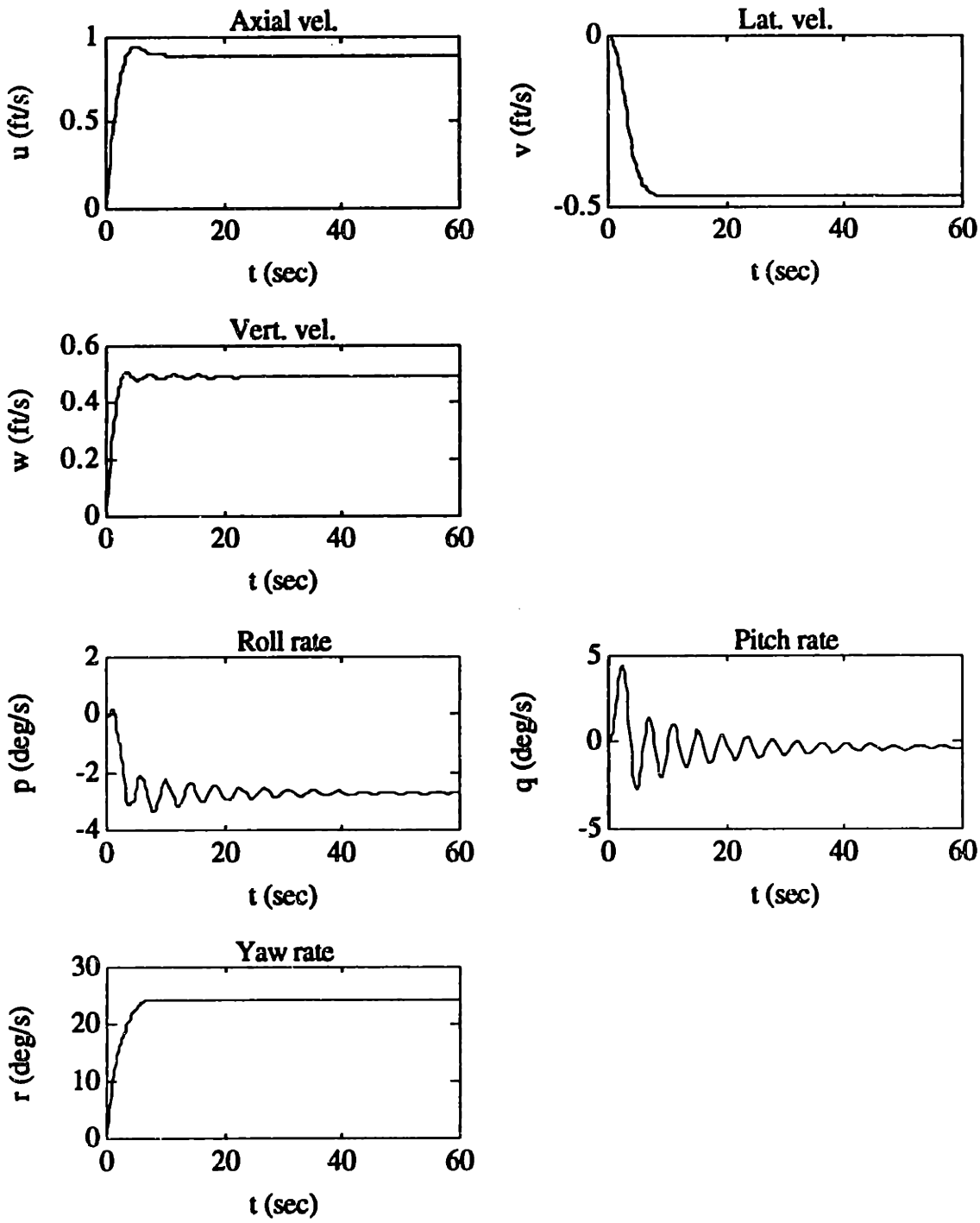

Figure 4.6: Full-Order Nonlinear "Full-Ahead" Step Response

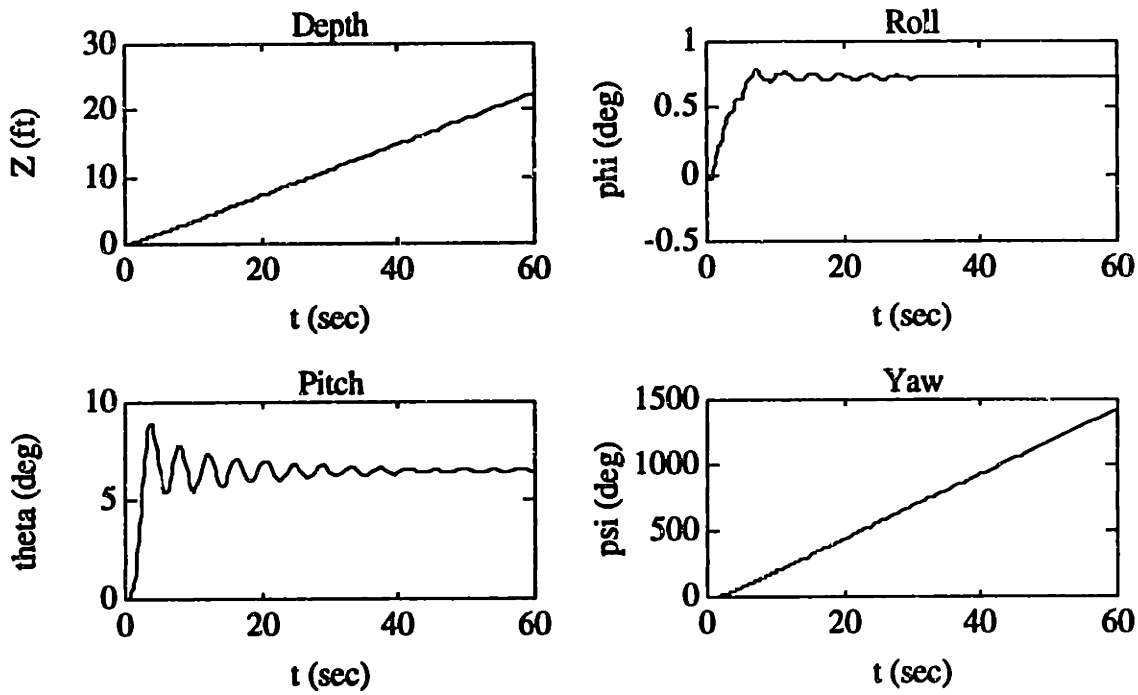

Figure 4.6: Full-Order Nonlinear "Full-Ahead" Step Response (continued)

From this set of plots, the fairly weak coupling of the heading and depth dynamics is still readily apparent. The response of the model for this case is, in many respects, the superposition of the previous two simulation cases. This implies that it may still be possible to design separate heading and depth controllers for the AUV. However, there are several additional effects due to the nonzero axial speed that must be considered.

The first effect of interest is the increased lateral velocity, v. This is caused by the centripetal forces acting on the vehicle when it performs a turn. Physically, this lateral velocity implies that the vehicle is "side-slipping" outward from the center of the turn. In the literature [18], this sideslip velocity (together with the axial velocity, u) can potentially cause a destabilizing moment in heading known as the Munk moment.

The steady-state value of the yawing angular velocity, r, is about 30 percent larger for this operating condition, as compared to the "hovering" condition. One explanation for this increase in the yaw rate is the effect of the Munk moment described previously.

The next effect of design interest is on the pitch dynamics. In this case, there is a significant steady-state pitch angle of about 6.3 degrees. This is due to the Munk moment effect caused by the interaction of the axial velocity, u, with the vertical velocity, w. The effect of this pitch angle is to change the kinematic relationship slightly between w and the depth, Z. In addition, another axial velocity effect (due to hydrodynamic "lift" forces) is a slight reduction in the steady-state depth rate.

"Full-Reverse" Step Response

The final simulation case was done with the objective of examining the response of the model for negative axial speeds (a requirement for some of the typical missions performed by the AUV). The state initial conditions and the disturbances were all assumed zero, and the sensor and thruster dynamics were neglected. T_V was again set to 1.0 lb., and the "differential thrust" (T_P - T_S) was again set equal to 1.0 lb. The "total" forward thrust (T_P + T_S) was set equal to -1.0 lb., which gave T_P equal to 0.0 lb. and T_S equal to -1.0 lb. The resulting time-domain response is shown in the plots of Figure 4.7.

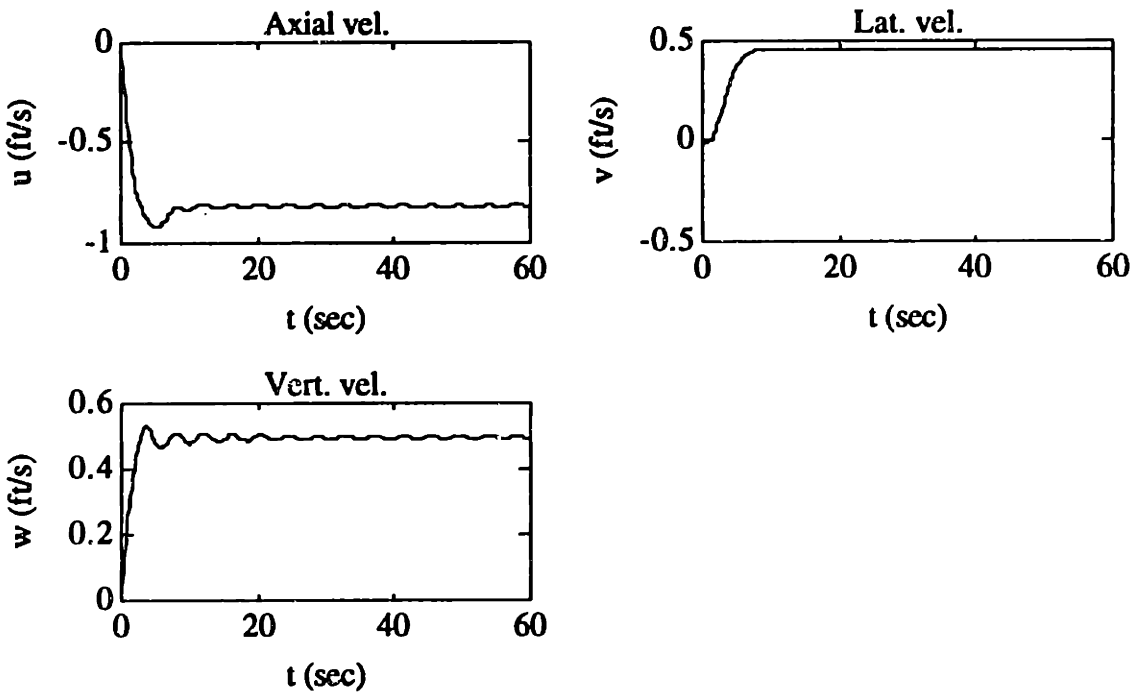

Figure 4.7: Full-Order Nonlinear "Full-Reverse" Step Response

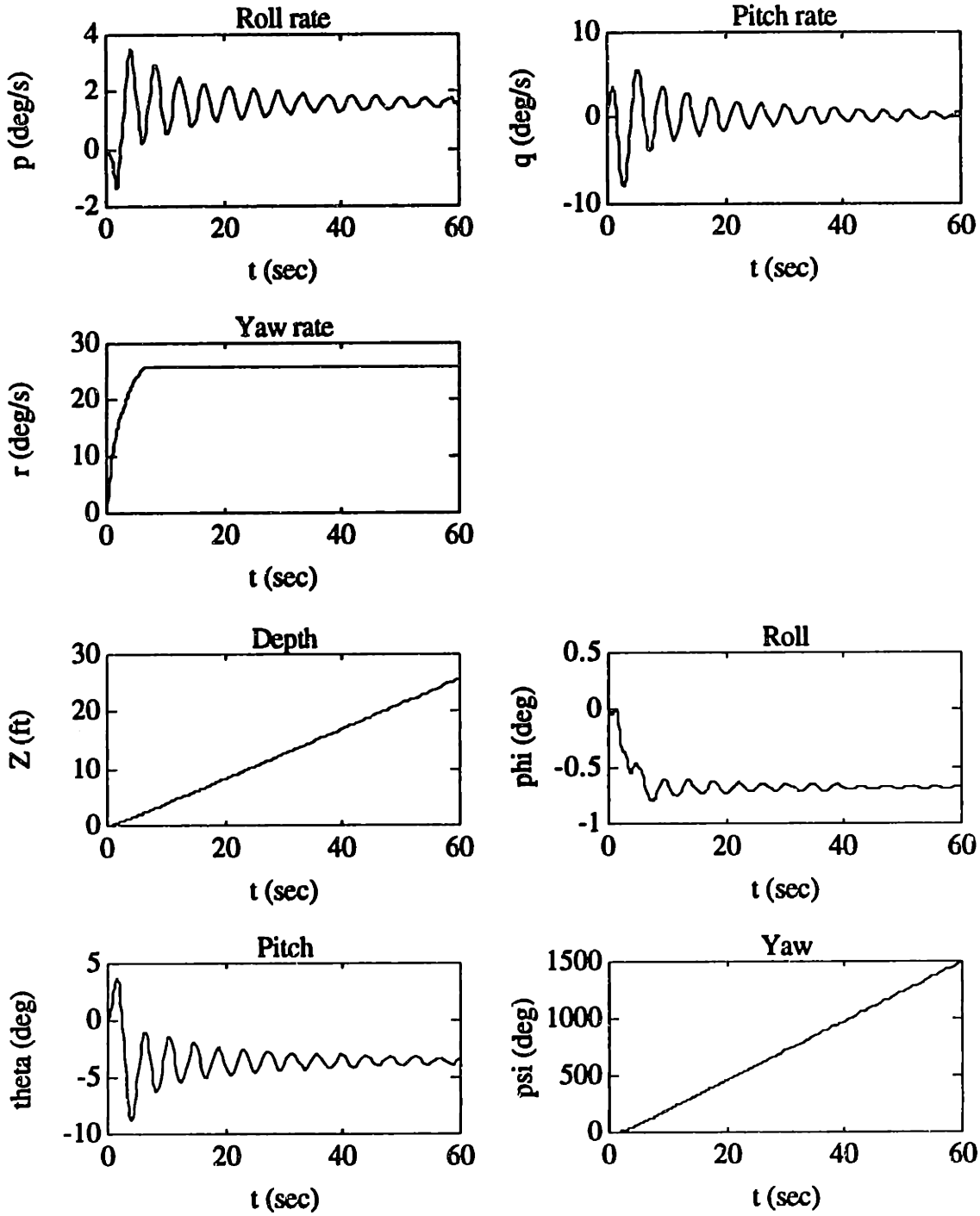

Figure 4.7: Full-Order Nonlinear "Full-Reverse" Step Response (continued)

For this simulation case, the response is very similar to the response of the previous simulation case with the positive axial velocity. The lateral velocity has approximately the same magnitude (but opposite sign). Physically, this implies that the vehicle is still "side-slipping" outward from the center of the turn. Therefore, the heading still exhibits the effects of the Munk moment (which implies that the heading dynamics will be less stable for negative axial velocities than for the "hovering" condition). The steady-state pitch angle is also opposite in sign (but with a slightly smaller magnitude).

4.3 REDUCED-ORDER DESCRIPTOR-COMPANION NONLINEAR MODEL

The six degree-of-freedom nonlinear AUV model described in the previous section provides a reasonable approximation to the dynamic behavior of the vehicle. However, there are several somewhat obvious incompatibilities of this model with the modeling assumptions used by the Sliding-Mode control methodology. Perhaps the most obvious is the unavailability of some of the states for feedback. In addition, there are several structural incompatibilities (e.g., the "velocity" variables are defined in the *vehicle-relative* coordinate system, while the "position" variables are defined in the *earth-relative* coordinate system, etc.).

4.3.1 Development of Reduced-Order Descriptor/Companion Nonlinear Model

A compatible reduced-order Descriptor/Companion nonlinear model was derived for the *Sea Squirt* AUV. First, several "practical" simplifying assumptions were made about the behavior of the vehicle, following [18]. Pitch and roll were assumed to have a steady-state value of zero, with all thrusters turned off. This implied that the vehicle is properly ballasted (i.e., the cb is located directly above the cg, and both the cb and cg are located along the centerline of the vehicle). In terms of the model parameters, this implied

$$X_g \cong X_b \tag{4.19}$$

$$Y_g \cong Y_b \cong 0 \tag{4.20}$$

$$Z_g \geq Z_b \tag{4.21}$$

The AUV's pitch and roll angles could not be directly controlled. Therefore, their respective angular velocities were assumed small and were neglected. This led to

$$\dot{\theta} \cong 0 \tag{4.22}$$

$$\dot{\phi} \cong 0 \tag{4.23}$$

Next, the pitch and roll angles themselves were also assumed small (i.e., a magnitude of less than about 10 degrees). Therefore, the kinematic equations (4.9)-(4.12) were simplified (using the Small-Angle Condition) to

$$\dot{Z} \cong w \tag{4.24}$$

$$p \cong \dot{\phi} \cong 0 \tag{4.25}$$

$$q \cong \dot{\theta} \cong 0 \tag{4.26}$$

$$\dot{\psi} \cong r \tag{4.27}$$

By using both the model-parameter assumptions and the Small-Angle Condition assumptions, the AUV EOM (4.1)-(4.3) plus (4.6) were simplified to

Axial Force

$$[m - X_{\dot{u}}]\dot{u} = m[v\psi + X_g\psi^2] + X_{u|u|u|u|} + T_p + T_s + D_u \tag{4.28}$$

Lateral Force

$$[m - Y_{\dot{v}}]\dot{v} = [Y_{\dot{r}} - mX_g]\dot{\psi} + Y_{v|v|}v|v| + [Y_{ur} - m]u\psi + Y_{uv}|u|v + D_v \quad (4.29)$$

Vertical Force

$$[m - Z_{\dot{w}}]\dot{Z} = Z_{w|w|}\dot{Z}|\dot{Z}| + Z_{uw}|u|\dot{Z} + (W - B) + T_v + D_w \quad (4.30)$$

Yawing Moment

$$[I_{zz} - N_{\dot{r}}]\ddot{\psi} = [N_{\dot{v}} - mX_g]\dot{v} + N_{\dot{r}|\dot{r}|}\dot{\psi}|\dot{\psi}| + [N_{ur} - mX_g]u\dot{\psi} + N_{uv}uv + Y_T(T_p - T_s) + D_r \quad (4.31)$$

In this particular reduced-order nonlinear model, the AUV's depth dynamics described by (4.30) were essentially decoupled from its heading dynamics described by (4.29) and (4.31).

However, the heading dynamics of this reduced-order model, described by the combination of the lateral force and the yawing moment, are still incompatible with the assumptions of the Descriptor/Companion model. Both the lateral force equation (4.29) and the yawing moment equation (4.31) contain the unmeasured velocities u and v.

To simplify the heading dynamics further, the lateral force equation, (4.29) was substituted into the yawing moment equation, (4.31), to obtain

$$\left[\frac{(I_{ZZ} - N_{\dot{r}})(m - Y_{\dot{v}}) - (N_{\dot{v}} - mX_g)(Y_{\dot{r}} - mX_g)}{(m - Y_{\dot{v}})}\right]\ddot{\psi} = \left[\frac{N_{\dot{v}} - mX_g}{m - Y_{\dot{v}}}\right][Y_{v|v|}v|v| + (Y_{ur} - m)u\dot{\psi} + Y_{uv}|u|v + D_v] + N_{\dot{r}|\dot{r}|}\dot{\psi}|\dot{\psi}| + (N_{ur} - mX_g)u\dot{\psi} + N_{uv}uv + Y_T(T_p - T_s) + D_r \quad (4.32)$$

Also the yawing moment equation was substituted into the lateral force equation to obtain

$$\left[\frac{(I_{ZZ} - N_{\dot{r}})(m - Y_{\dot{v}}) - (N_{\dot{v}} - mX_g)(Y_{\dot{r}} - mX_g)}{(I_{ZZ} - N_{\dot{r}})}\right]\dot{v}$$
$$= \left[\frac{Y_{\dot{r}} - mX_g}{I_{ZZ} - N_{\dot{r}}}\right][\, N_{r|r|}\dot{\psi}|\dot{\psi}| + (N_{ur} - mX_g)u\dot{\psi}$$
$$+ N_{uv}uv + Y_T(T_p - T_s) + D_r\,]$$
$$+ Y_{v|v|}v|v| + (Y_{ur} - m)u\dot{\psi} + Y_{uv}|u|v + D_v \qquad (4.33)$$

This substitution had the effect of "decoupling" the heading angular acceleration from the lateral acceleration, which implied that the heading dynamics could be described solely by (4.32).

On the vehicle, there are no sensors to measure or to estimate either the lateral velocity, v, or the axial velocity, u. Therefore, both the modified yawing moment equation (4.32) and the vertical force equation (4.30) were simplified even further to eliminate these unmeasurable variables. This was done by "lumping" all terms containing either of these velocities into the yawing disturbance torque, D_r, and the vertical disturbance force. This formed a new disturbance force, D_w', and a new disturbance torque, D_r'. The resulting simplified equations are given by (4.34) and (4.35).

$$[m - Z_{\dot{w}}]\ddot{Z} = Z_{w|w|}\dot{Z}|\dot{Z}| + (W - B) + T_v + D_w' \qquad (4.34)$$

$$\left[\frac{(I_{ZZ} - N_{\dot{r}})(m - Y_{\dot{v}}) - (N_{\dot{v}} - mX_g)(Y_{\dot{r}} - mX_g)}{(m - Y_{\dot{v}})}\right]\ddot{\psi}$$
$$= N_{r|r|}\dot{\psi}|\dot{\psi}| + Y_T(T_p - T_s) + D_r' \qquad (4.35)$$

Lastly, equations (4.34) and (4.35) were rewritten as

$$[m - Z_{\dot{w}}]\ddot{Z} = Z_{w|w|}\dot{Z}|\dot{Z}| + (W - B) + U_Z + d_Z(t) \qquad (4.36)$$

$$\left[\frac{(I_{ZZ} - N_{\dot{r}})(m - Y_{\dot{v}}) - (N_{\dot{v}} - mX_g)(Y_{\dot{r}} - mX_g)}{(m - Y_{\dot{v}})}\right]\ddot{\psi}$$
$$= N_{r|r|}\dot{\psi}|\dot{\psi}| + Y_T U_\psi + d_\psi(t) \qquad (4.37)$$

with D_w' replaced by $d_Z(t)$, D_r' replaced by $d_\psi(t)$, T_v replaced by U_Z, and $(T_p - T_s)$ replaced by U_ψ in order to simplify notation. Finally, the reduced-order AUV model can be written in the following 2nd order Descriptor/Companion system

$$\frac{d}{dt}(\hat{\mathbf{x}}) = \hat{\mathbf{x}}$$

$$\mathbf{E}\left[\frac{d}{dt}(\hat{\mathbf{x}})\right] = \mathbf{E}\,\ddot{\hat{\mathbf{x}}} = \mathbf{f(x)} + \mathbf{Bu} + \mathbf{d} \qquad \textbf{(4.38)}$$

where the reduced-order total state vector is given by

$$\mathbf{x} = [\, Z\ \psi\ \dot{Z}\ \dot{\psi}\,]^T \qquad \textbf{(4.39)}$$

and the reduced-order output state vector is given by

$$\hat{\mathbf{x}} = [\, Z\ \psi\,]^T \qquad \textbf{(4.40)}$$

The control input vector is given by

$$\mathbf{u} = [\, U_Z\ U_\psi\,]^T \qquad \textbf{(4.41)}$$

and the disturbance vector is given by

$$\mathbf{d} = [\, d_Z(t)\ \ d_\psi(t)]^T \qquad \textbf{(4.42)}$$

The descriptor matrix, **E**, for this model is therefore given by

$$\mathbf{E} = \begin{bmatrix} [m - Z_{\dot{w}}] & 0 \\ 0 & \left[\dfrac{(I_{ZZ} - N_{\dot{r}})(m - Y_{\dot{v}}) - (N_{\dot{v}} - mX_g)(Y_{\dot{r}} - mX_g)}{(m - Y_{\dot{v}})}\right] \end{bmatrix} \qquad \textbf{(4.43)}$$

and **f(x)** is given by

$$\mathbf{f(x)} = \begin{bmatrix} Z_{w|w|}\dot{z}|\dot{z}| + (W - B) & 0 \\ 0 & N_{q|q|}\dot{\psi}|\dot{\psi}| \end{bmatrix} \tag{4.44}$$

The control-input matrix, **B**, is given by

$$\mathbf{B} = \begin{bmatrix} 1 & 0 \\ 0 & Y_T \end{bmatrix} \tag{4.45}$$

4.2.2 Simulation Analysis of the Reduced-Order Descriptor/Companion Nonlinear Model

For the AUV control-design effort, it would be useful to analyze the validity of the reduced-order nonlinear model, as compared to the full-order model. One means of doing this is compare the time-responses of this reduced-order model versus the time-responses of the full-order model.

For the reduced-order nonlinear model, a computer simulation analysis was performed (again by using a fourth-order Runge-Kutta numerical integration MATLAB™ package). The coefficients of this model were again given the approximate numerical values contained in [18]. Sensor and thruster dynamics were neglected.

Unforced Response

The first case to be considered is the unforced response of the reduced-order model to non-zero initial conditions. As with the full-order model, the depth rate was given an initial value of 1.0 ft/sec, while the heading rate was given an initial value of 10 deg/s. Both the depth and the heading were given an initial value of zero, and all of the thruster and disturbance forces were given a value of zero, as well. The resulting time-domain response is shown in the plots of Figure 4.8.

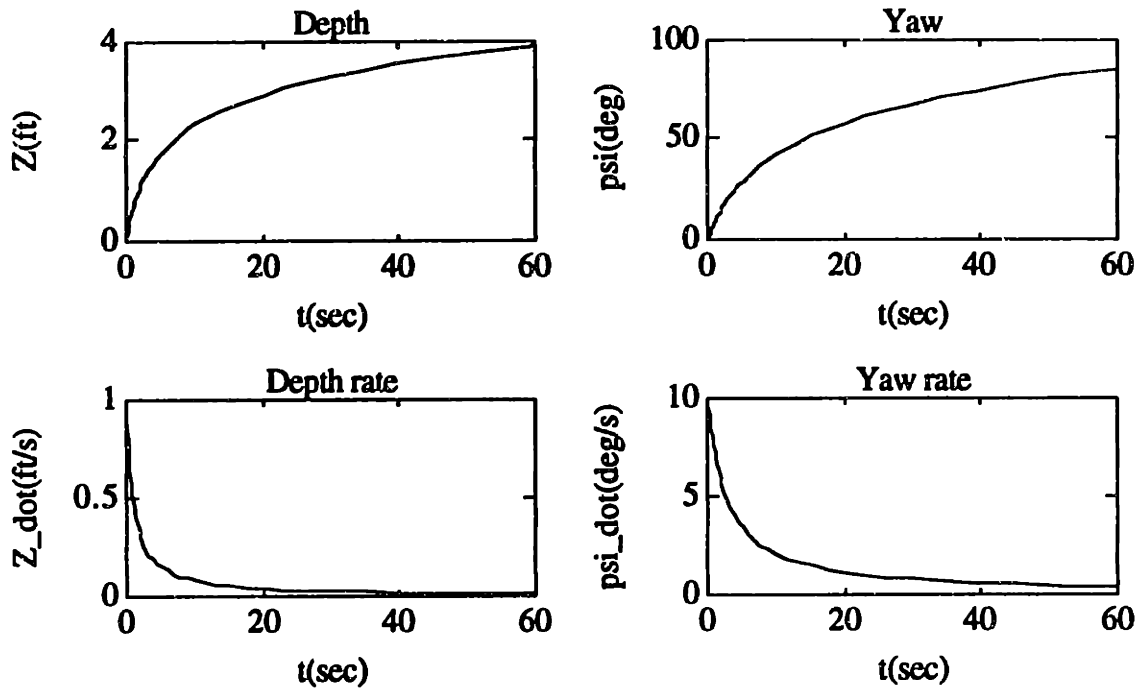

Figure 4.8: Reduced-Order Nonlinear Unforced Response

From these particular time-response plots, both the depth rate and heading rate appear to have a stable first-order response (with a damping probably dependent upon the hydrodynamic drag). The reduced-order unforced depth response appears to be very similar to the unforced full-order depth response of Figure 4.3. However, the unforced heading response is quite different (due to the effects of the nonzero lateral velocity). Note the absence of the oscillatory modes associated with the pitch and roll dynamics.

Vertical Thrust Step Response

Next, the response of the reduced-order AUV model to step control inputs was considered. All the states of the vehicle were given an initial value of zero and all disturbance forces were assumed to be zero. Again, both sensor and thruster dynamics were neglected. For the first simulation case, a step of 1.0 lb. was applied to U_Z (i.e., a step of 1.0 lb. to Tv). U_ψ was set to zero. The resulting time-domain response is shown in the plots of Figures 4.9.

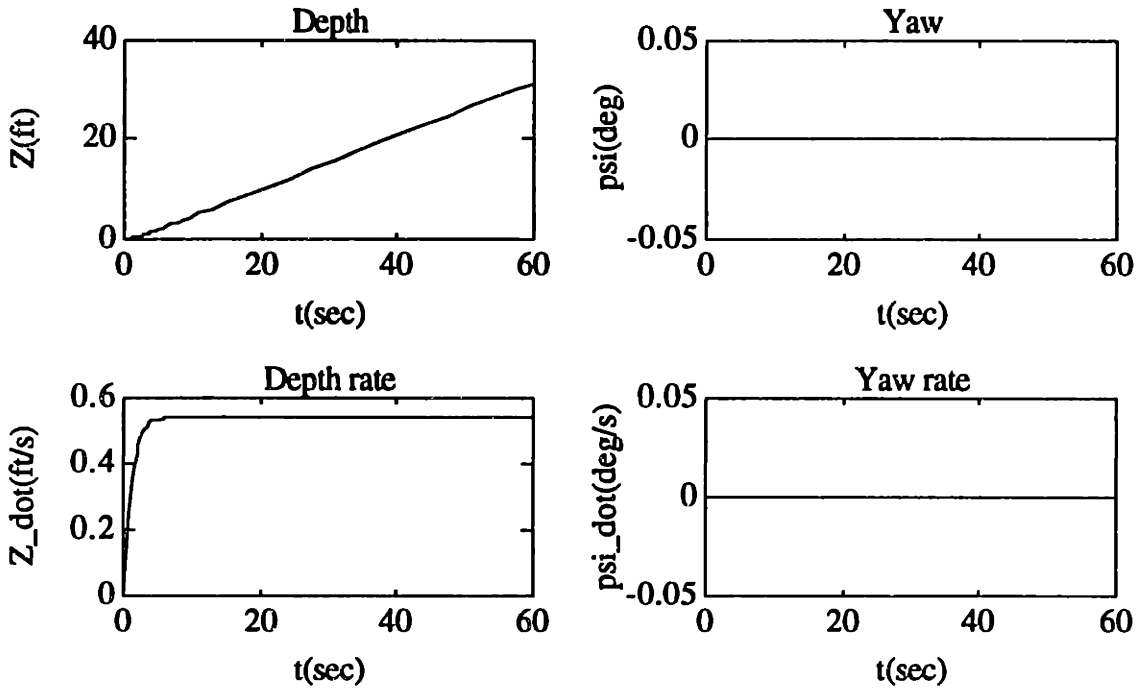

Figure 4.9: Reduced-Order Nonlinear Vertical Step Response

From these plots, the heading dynamics are completely decoupled from the depth control input, as expected. This depth response appears to be almost identical to the full-order depth response during the "hovering" condition, except for the absence of the oscillations due to the mode associated with the pitching dynamics. This implies that the reduced-order model provides a "good" approximation to the depth dynamics of the AUV for "small" axial velocities, so long as the inputs do not excite the pitch oscillatory mode.

Differential Thrust Step Response

For the next simulation case, a step of 1.0 lb. was applied to U_ψ (i.e., a differential thrust of 1.0 lb.). U_Z was set to zero. The resulting time-domain response is shown in the plots of Figures 4.10.

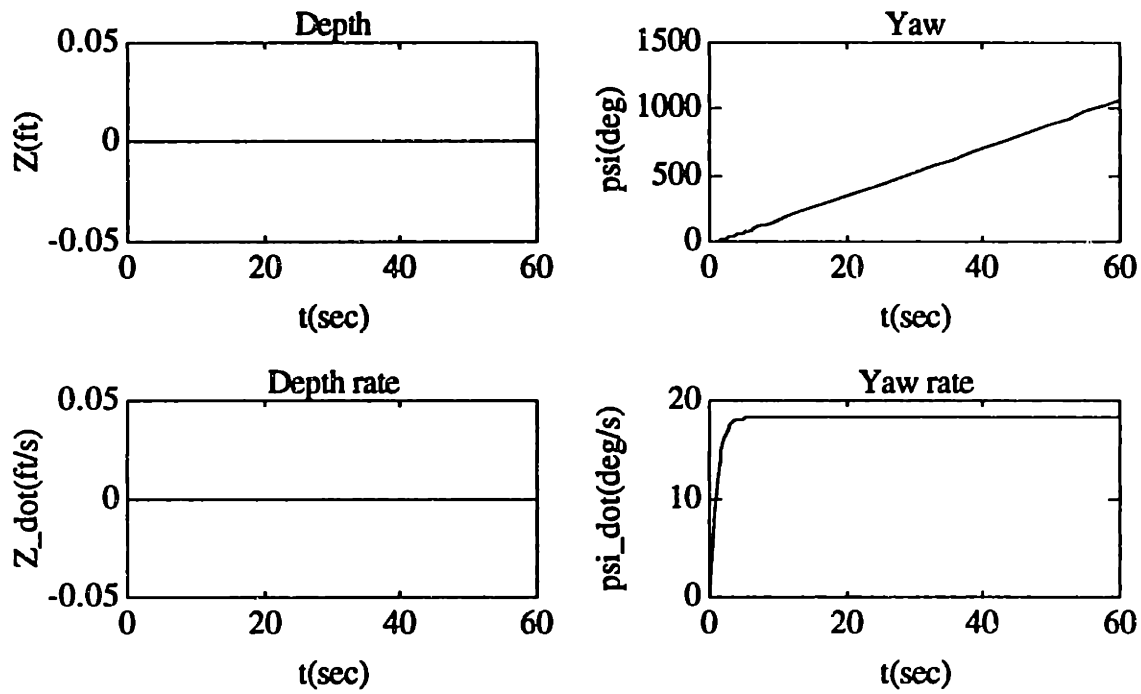

Figure 4.10: Reduced-Order Nonlinear Differential Step Response

For this case, the heading response appears to be almost identical to the full-order heading response during the "hovering" condition. This implies that the reduced-order model also provides a "good" approximation to the heading dynamics of the AUV for "small" axial velocities.

4.4 FULL-ORDER LTI MODEL

For the linear control-system design methodologies presented in Chapter 2, the nonlinear AUV models developed in Sections 4.2 and 4.3 cannot be directly used. In order to use these methodologies, recall that the dynamics of the AUV must be converted into a linear time-invariant (LTI) model of the form

$$\mathbf{E}_1\dot{\mathbf{x}} = \mathbf{A}_1\mathbf{x} + \mathbf{B}_1\mathbf{u} + \mathbf{L}_1\mathbf{d} \tag{4.46}$$

$$\mathbf{y} = \mathbf{C}_1\mathbf{x} + \mathbf{D}_1\mathbf{u} + \mathbf{D}_2\mathbf{d} \tag{4.47}$$

4.4.1 Development of Full-Order LTI Model

The standard procedure for doing this linearization is to expand the nonlinear model in a first-order Taylor series about some nominal operating point. Recall that the full-order nonlinear AUV model is described by the general vector form

$$\mathbf{E}\dot{\mathbf{x}} = \mathbf{f}(\mathbf{x},\mathbf{u},\mathbf{d}) \tag{4.48}$$

$$\mathbf{y} = \mathbf{C}\mathbf{x} \tag{4.49}$$

where the full-order state vector is defined by

$$\mathbf{x} = [\, u\ v\ w\ p\ q\ r\ Z\ \phi\ \theta\ \psi\,]^T \tag{4.50}$$

and the input vector is defined by

$$\mathbf{u} = [T_v\ \ (T_p - T_s)\ \ (T_p + T_s)]^T \tag{4.51}$$

with a disturbance vector defined by

$$\mathbf{d} = [\, D_u\ D_v\ D_w\ D_p\ D_q\ D_r]^T \tag{4.52}$$

The output vector is then defined as the vector of variables actually measured and/or estimated by the vehicle's sensor suite

$$\mathbf{y} = [Z\ \psi\ \dot{Z}\ r\ \phi\ \theta]^T \tag{4.53}$$

For this nonlinear model, the first-order Taylor series is given by

$$\mathbf{E}\dot{\mathbf{x}}_o + \mathbf{E}\delta\dot{\mathbf{x}} = \mathbf{f}(\mathbf{x}_o,\mathbf{u}_o,\mathbf{d}_o) + \frac{\partial \mathbf{f}}{\partial \mathbf{x}}(\mathbf{x}_o,\mathbf{u}_o,\mathbf{d}_o)\delta\mathbf{x} + \frac{\partial \mathbf{f}}{\partial \mathbf{u}}(\mathbf{x}_o,\mathbf{u}_o,\mathbf{d}_o)\delta\mathbf{u} + \frac{\partial \mathbf{f}}{\partial \mathbf{d}}(\mathbf{x}_o,\mathbf{u}_o,\mathbf{d}_o)\delta\mathbf{d} \tag{4.54}$$

$$\mathbf{y}_o + \delta\mathbf{y} = \mathbf{C}\mathbf{x}_o + \mathbf{C}\delta\mathbf{x} \tag{4.55}$$

where $\delta\mathbf{x}$, $\delta\mathbf{u}$, and $\delta\mathbf{d}$ are defined as "perturbations" of the form

$$\mathbf{x} = \mathbf{x}_o + \delta\mathbf{x} \tag{4.56}$$

$$\mathbf{u} = \mathbf{u}_o + \delta\mathbf{u} \tag{4.57}$$

$$\mathbf{d} = \mathbf{d}_o + \delta\mathbf{d} \tag{4.58}$$

If the operating point satisfies the relations

$$\mathbf{E}\dot{\mathbf{x}}_o = \mathbf{f}(\mathbf{x}_o,\mathbf{u}_o,\mathbf{d}_o) \tag{4.59}$$

$$\mathbf{y}_o = \mathbf{C}\mathbf{x}_o \tag{4.60}$$

then the first-order series can be rewritten as

$$\mathbf{E}\delta\dot{\mathbf{x}} = \frac{\partial \mathbf{f}}{\partial \mathbf{x}}(\mathbf{x}_o,\mathbf{u}_o,\mathbf{d}_o)\delta\mathbf{x} + \frac{\partial \mathbf{f}}{\partial \mathbf{u}}(\mathbf{x}_o,\mathbf{u}_o,\mathbf{d}_o)\delta\mathbf{u} + \frac{\partial \mathbf{f}}{\partial \mathbf{d}}(\mathbf{x}_o,\mathbf{u}_o,\mathbf{d}_o)\delta\mathbf{d} \tag{4.61}$$

$$\delta\mathbf{y} = \mathbf{C}\delta\mathbf{x} \tag{4.62}$$

This first-order series can then be used to directly write the "descriptor" form of the AUV LTI model, given by

$$\mathbf{E}_1\delta\dot{\mathbf{x}} = \mathbf{A}_1\delta\mathbf{x} + \mathbf{B}_1\delta\mathbf{u} + \mathbf{L}_1\delta\mathbf{d} \tag{4.63}$$

$$\delta\mathbf{y} = \mathbf{C}_1\delta\mathbf{x} \tag{4.64}$$

This descriptor model can also be converted into the conventional state-space form, as shown below

$$\begin{aligned}\delta\dot{\mathbf{x}} &= \mathbf{E}_1^{-1}\mathbf{A}_1\delta\mathbf{x} + \mathbf{E}_1^{-1}\mathbf{B}_1\delta\mathbf{u} + \mathbf{E}_1^{-1}\mathbf{L}_1\delta\mathbf{d} \\ &= \mathbf{A}_0\delta\mathbf{x} + \mathbf{B}_0\delta\mathbf{u} + \mathbf{L}_0\delta\mathbf{d}\end{aligned} \tag{4.65}$$

Note that (4.61)-(4.65) imply that the dynamic behavior of the LTI model will directly depend upon the selection of the nominal operating point of the nonlinear model.

4.4.2 Analysis of Full-Order LTI Model

The full-order LTI model developed in the previous section can be used by the linear control-design methodologies of Chapter 2. However, it would be useful to analyze this model, especially as related to the choice of the nominal operating point. By comparing the results of this analysis to the known dynamics of the full-order nonlinear model, it can be determined how much information is "lost", in terms of using the first-order linear approximation.

The open-loop stability of this model can be analyzed by an examination of the eigenstructure of $\mathbf{A}_0$. Controllability and observability can be determined from the eigenstructure, together with $\mathbf{B}_0$ and $\mathbf{C}_1$. The transmission zeros of this model can also be analyzed. The frequency-response can be analyzed from plotting the singular values versus frequency.

"Hovering" Model

An analysis of the full-order AUV LTI model was performed at three separate nominal conditions. The first case was at the zero forward speed "hovering" condition (i.e., $\mathbf{x}_0 = \mathbf{0}$, $\mathbf{u}_0 = \mathbf{0}$, and $\mathbf{d}_0 = \mathbf{0}$). The open-loop eigenvalues are shown in Table 4.1 and the plot of Figure 4.11. The normalized magnitudes of the right and left eigenvectors are shown in the plots of Figures 4.12-4.13.

Table 4.1: Eigenvalues of Full-Order LTI Model ("Hovering" Model)

0
0
0
0
0
0
0 + 4.2784i
0 - 4.2784i
0 + 1.4658i
0 - 1.4658i

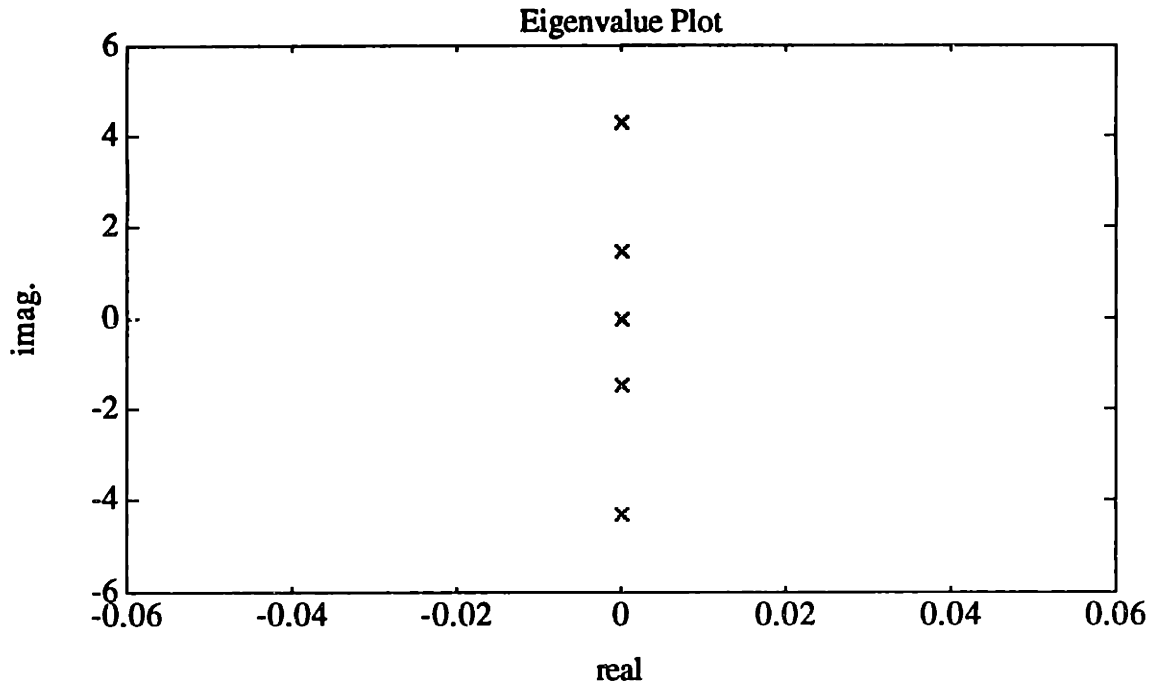

Figure 4.11: Eigenvalues of Full-Order LTI Model ("Hovering" Model)

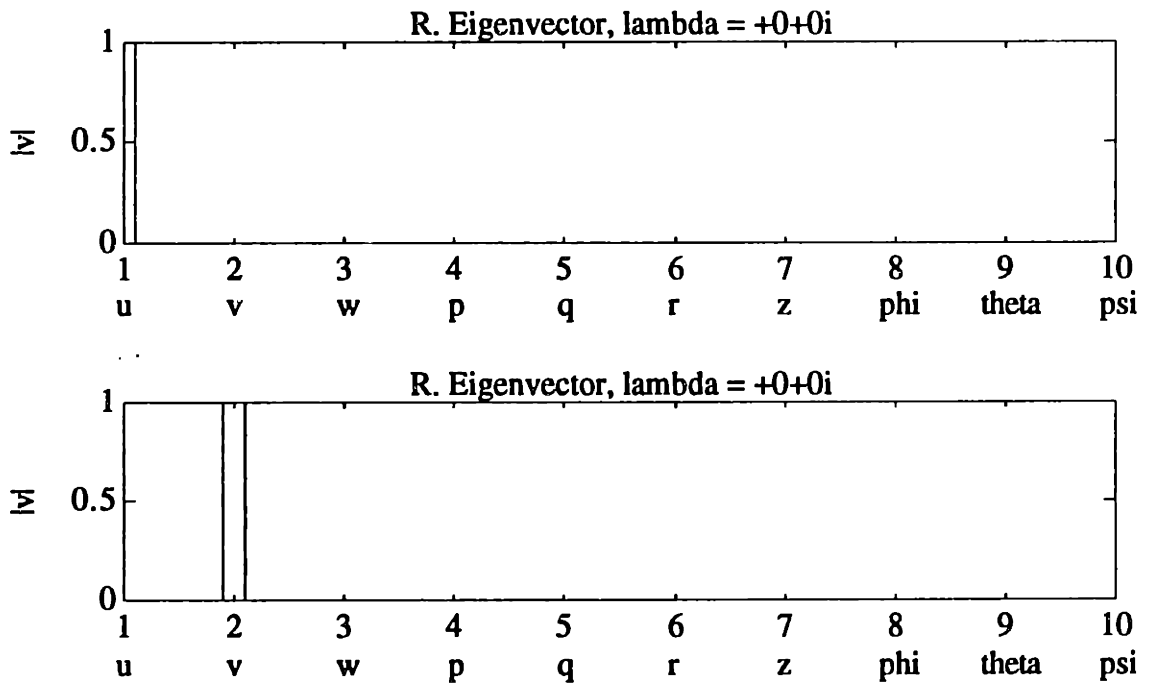

Figure 4.12: Right Eigenvectors of Full-Order LTI Model ("Hovering" Model)

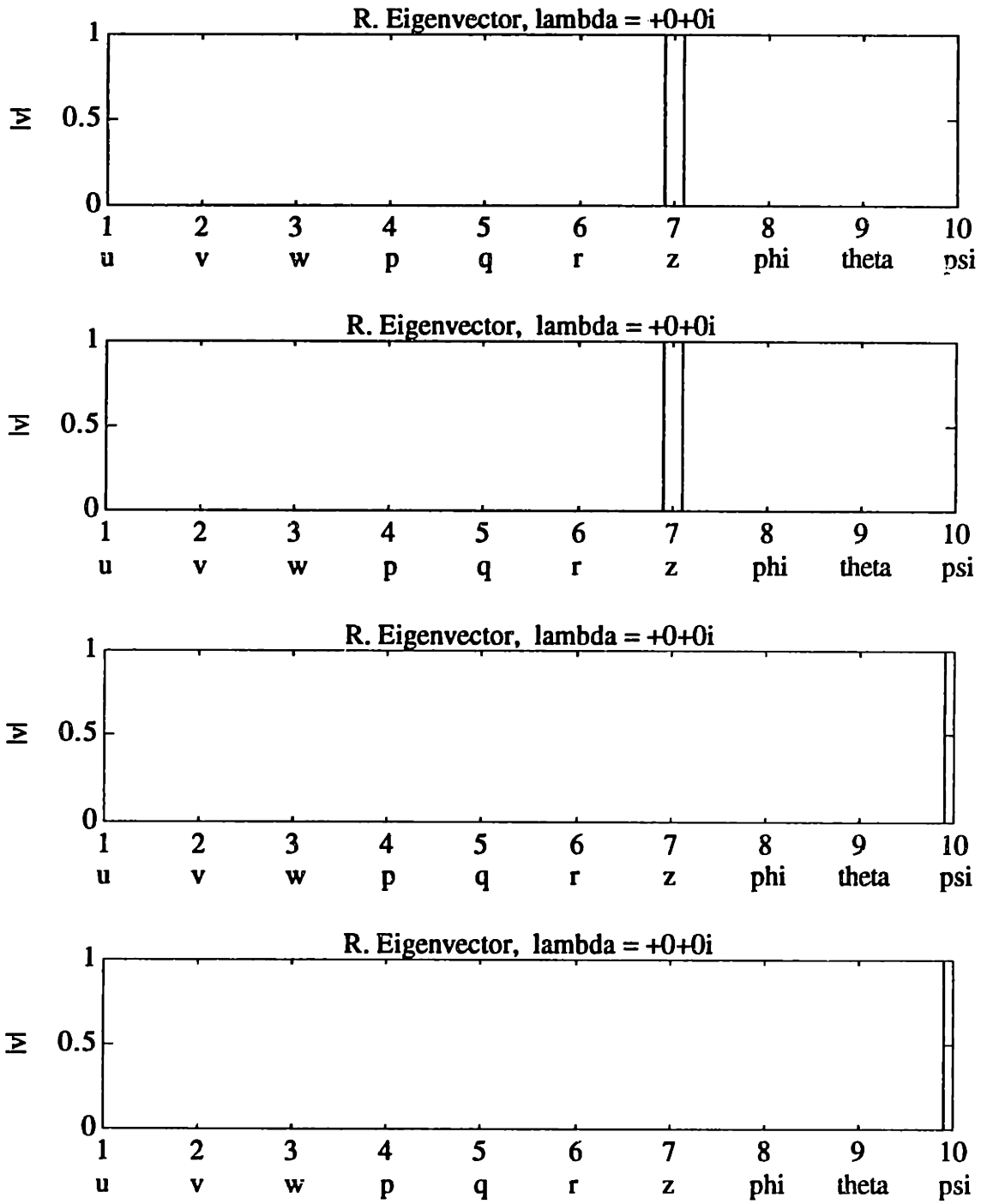

Figure 4.12: Right Eigenvectors of Full-Order LTI Model ("Hovering" Model) (continued)

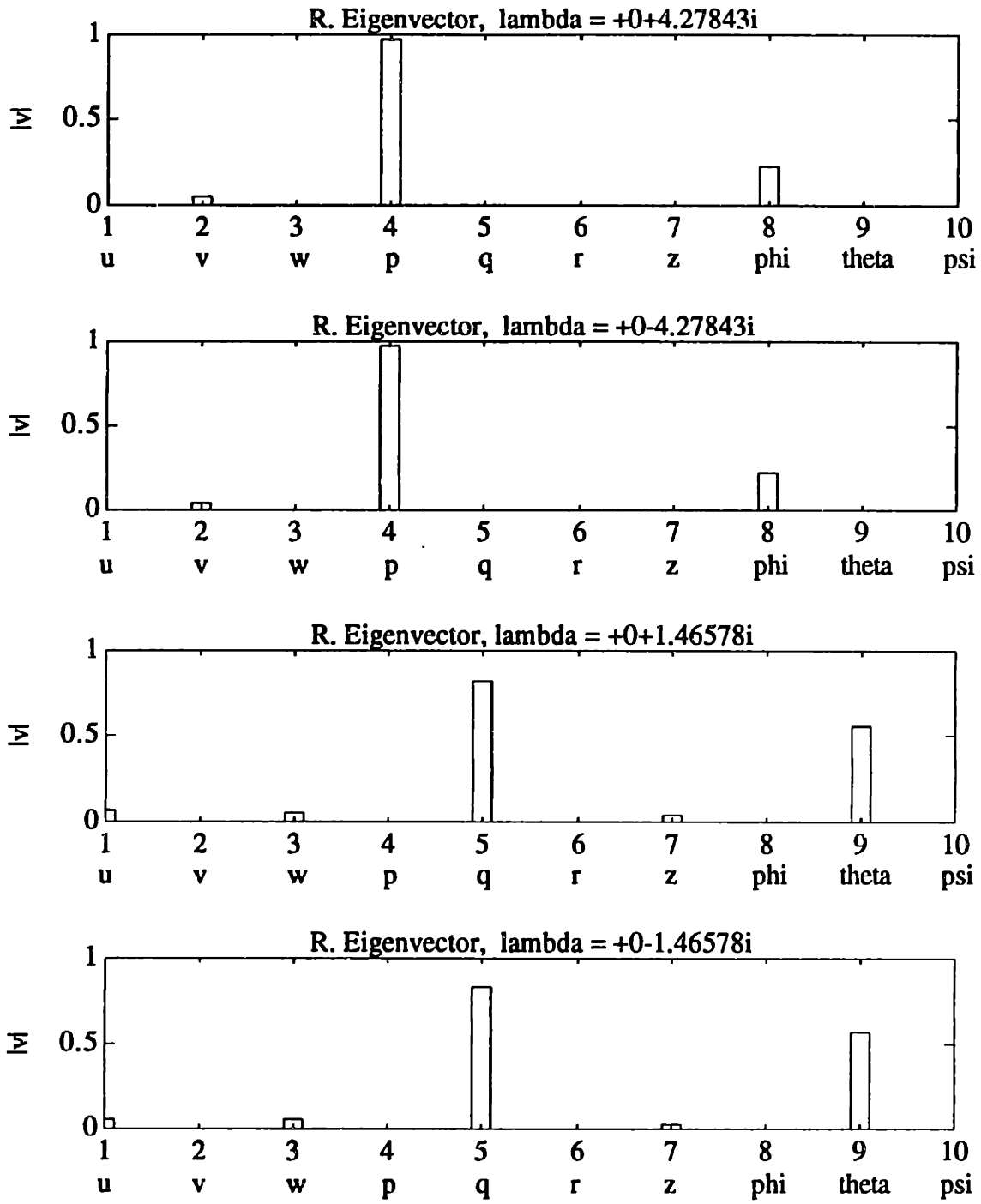

Figure 4.12 Right Eigenvectors of Full-Order LTI Model ("Hovering" Model) (continued)

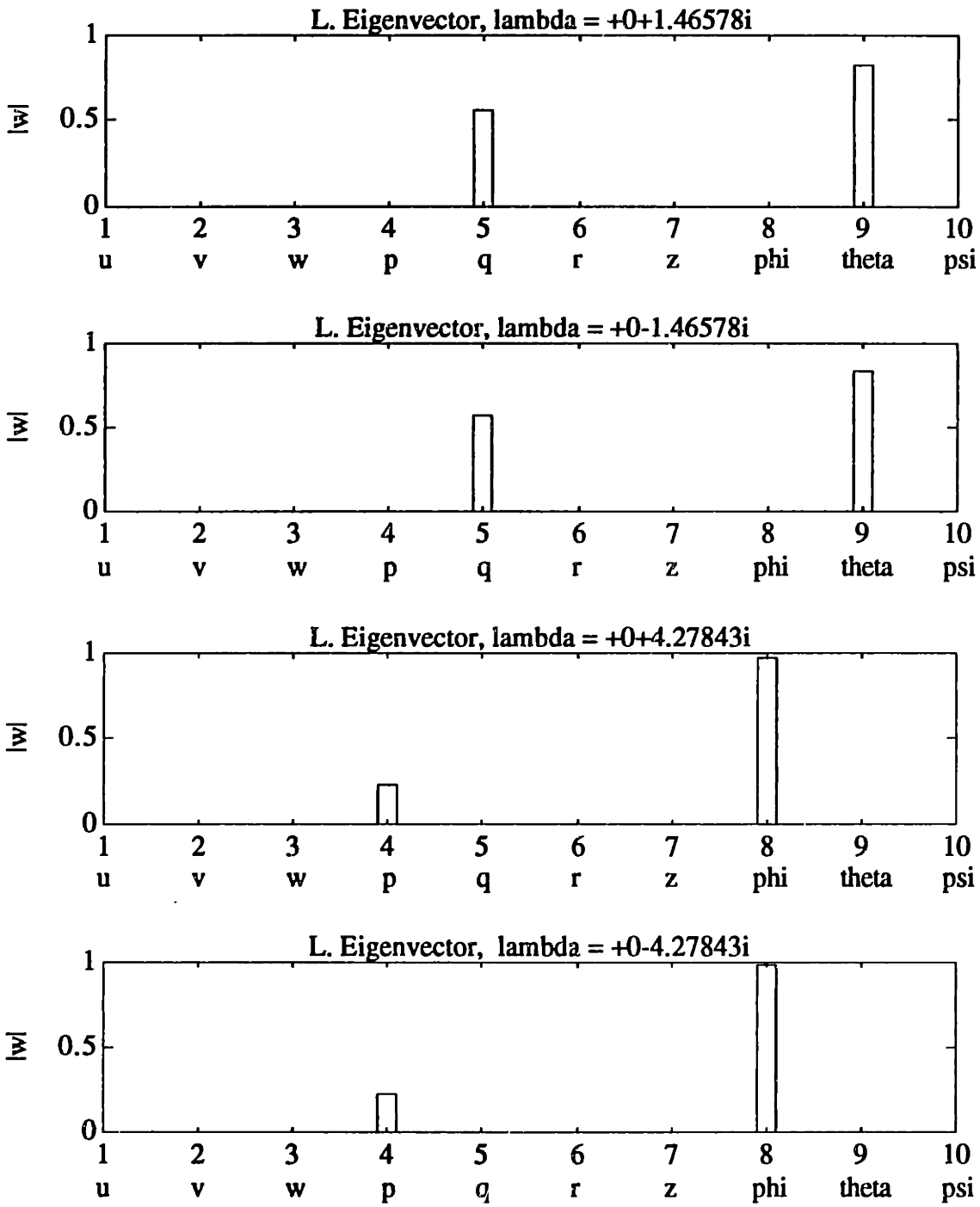

Figure 4.13: Left Eigenvectors of Full-Order LTI Model ("Hovering" Model)

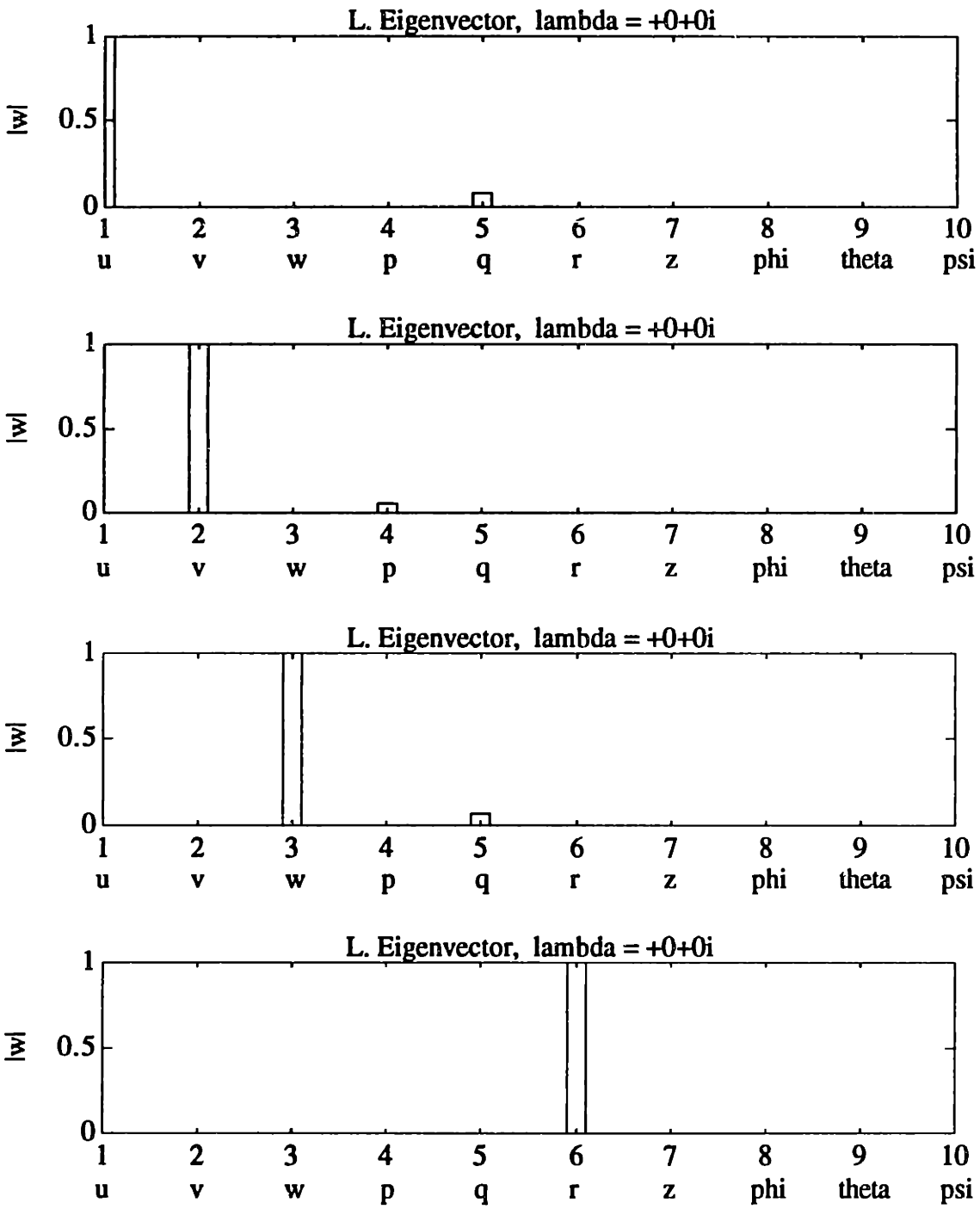

Figure 4.13: Left Eigenvectors of Full-Order LTI Model ("Hovering" Model) (continued)

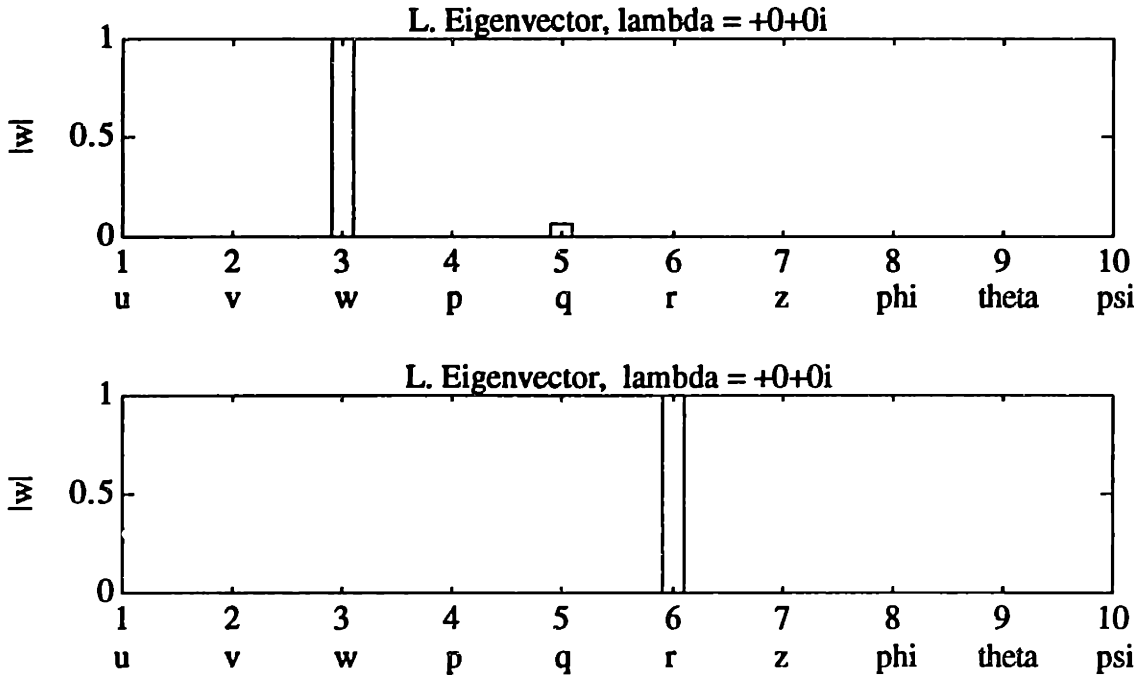

Figure 4.13: Left Eigenvectors of Full-Order LTI Model ("Hovering" Model) (continued)

For this case, each of the eigenvalues of this system are on the imaginary axis (which implies that the model is marginally stable). There are six eigenvalues at the origin. Physically (from the left eigenvalue plots), this partially corresponds to the fact that the depth and the heading do not affect the AUV dynamics. If there is a perturbation in either of these quantities, the AUV will not return to the nominal point. These zero eigenvalues also correspond to the fact that damping effects (e.g., hydrodynamic drag) for the AUV are velocity-dependent.

There are also two undamped oscillatory modes as well. The first mode has a frequency of approximately 1.47 rad/s and is associated with the pitch dynamics. The second mode has a frequency of approximately 4.28 rad/s and is associated with the roll dynamics. As with the oscillatory modes observed for the nonlinear full-order model, these modes are caused by the restoring moment associated with the passive stabilization scheme for pitch and roll.

The controllability of the modes of the LTI model can be determined by examining the rows of the matrix product, $\mathbf{WB_0}$, where the rows of **W** are the left eigenvectors. The element-by-element magnitude of this matrix product is shown in Table 4.2 (together with the corresponding eigenvalues and thrust inputs).

Table 4.2: $|\mathbf{WB_0}|$ for the "Hovering" LTI Model

Eigenvalue	$\lvert\mathbf{WB_0}\rvert$		
	(T_v)	$(T_p - T_s)$	$(T_p + T_s)$
0 + 1.4658i (Pitch)	0.0390	0	0.0354
0 - 1.4658i (Pitch)	0.0390	0	0.0354
0 + 4.2784i (Roll)	0	0.0019	0
0 - 4.2784i (Roll)	0	0.0019	0
0 (Axial velocity)	0.0000	0	0.4298
0 (Lateral velocity)	0	0.0144	0
0 (Depth)	0.3033	0.0000	0.0000
0 (Heading)	0	0.2102	0
0 (Depth)	0.3033	0.0000	0.0000
0 (Heading)	0	0.2102	0

From this table, all of the modes of this model are controllable from the control input, **u**. However, note that the rows associated with the oscillatory roll mode, the oscillatory pitch mode, and the lateral velocity mode have a smaller magnitude than the rows associated with the heading and depth modes (which, as expected, implies that the roll, pitch, and lateral velocity are more difficult to control with the present AUV thruster configuration).

The observability of the modes of the LTI model can be determined by examining the columns of the matrix product, $\mathbf{C_1V}$ (i.e., the rows of $\mathbf{V^TC_1^T}$) where the columns of

V are the right eigenvectors. The element-by-element magnitude of $V^T C_1^T$ is shown in Table 4.3 (together with the corresponding eigenvalues and measured outputs).

Table 4.3: $|V^T C_1^T|$ for "Hovering" LTI Model

Eigenvalue	$\|V^T C_1^T\|$					
	(Z)	(psi)	(Z_dot)	(r)	(phi)	(theta)
0 (Axial velocity)	0	0	0	0	0	0
0 (Lateral velocity)	0	0	0	0	0	0
0 (Depth)	1.0000	0	0	0	0	0
0 (Depth)	1.0000	0	0.0000	0	0	0
0 (Heading)	0	1.0000	0	0	0	0
0 (Heading)	0	1.0000	0	0.0000	0	0
0 + 4.2784i (Roll)	0	0.0011	0	0.0047	0.2273	0
0 - 4.2784i (Roll)	0	0.0011	0	0.0047	0.2273	0
0 + 1.4658i (Pitch)	0.0369	0	0.0541	0	0	0.5612
0 - 1.4658i (Pitch)	0.0369	0	0.054i	0	0	0.5612

From this table, the oscillatory roll and pitch modes are observable, as well as the "double integrator" modes associated with depth and heading. The modes associated with the axial and lateral velocities, however, are unobservable, which implies that direct control of these velocities is impossible in the "hovering" condition with the present set of measurements.

Using the MATLAB™ software, the following finite transmission zeros were found for this condition.

Table 4.4: Transmission Zeros of Full-Order LTI Model ("Hovering" Model)

0
0

These zeros were found to be associated with the axial and lateral velocity. Recall that the modes associated with these velocities were found to be unobservable (since axial and lateral velocity sensors were not part of the AUV sensor suite, and since these velocities do not affect any of the other (measured) state variables). This implies that these transmission zeros "cancel" these particular modes.

The transfer-function singular values versus frequency (from the controls to the output of this model) are shown in Figure 4.14.

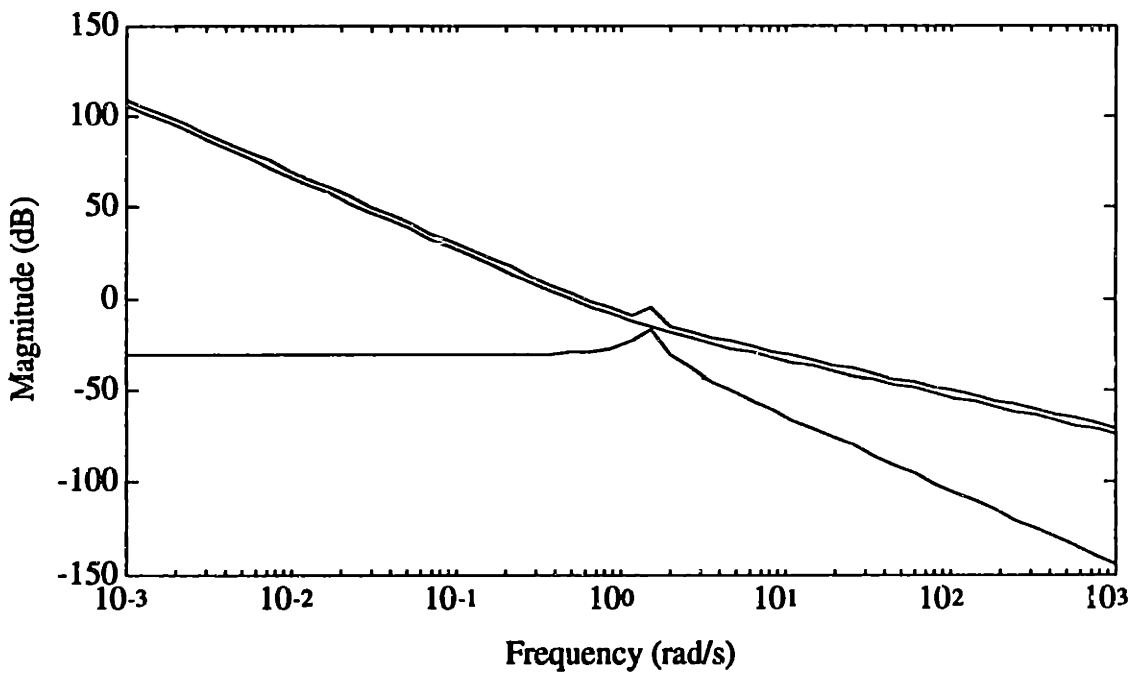

Figure 4.14: Frequency Response of LTI Model from **u** to **y** ("Hovering" Model)

Several aspects of this model are apparent from this plot. At the lower frequencies, the maximum singular value corresponds to the 40 db/decade "two integrator" response from the controls to depth and yaw. At the higher frequencies, the maximum singular value

corresponds to the 20 db/decade "one integrator" response from the controls to the depth rate and the yawing angular velocity. The minimum singular value corresponds to the response from the controls to the pitch and roll angles. Note the presence of the "bump" at approximately 1.5 rad/s. This is also due to the response from the controls to the oscillatory pitch mode.

"Full-Ahead" Model

The next case was the "full-ahead" condition, at an axial velocity of 1.0 ft/s. This approximately gave $\mathbf{x}_0 = [\ 1\ 0\ 0\ 0\ 0\ 0\ 0\ 0\ 0\ 0\ ]^T$, $\mathbf{u}_0 = [0\ 0.84\ 0]^T$, and $\mathbf{d}_0 = \mathbf{0}$. The open-loop eigenvalues are shown in Table 4.5 and the plot of Figure 4.15. The normalized magnitudes of the right and left eigenvectors are shown in the plots of Figures 4.16- 4.17.

Table 4.5: Eigenvalues of Full-Order LTI Model ("Full-Ahead" Model)

0
0
-0.0546 + 1.3443i
-0.0546 - 1.3443i
-0.1009
-0.7250
-0.0014 + 4.2793i
-0.0014 - 4.2793i
0.4640
-0.6704

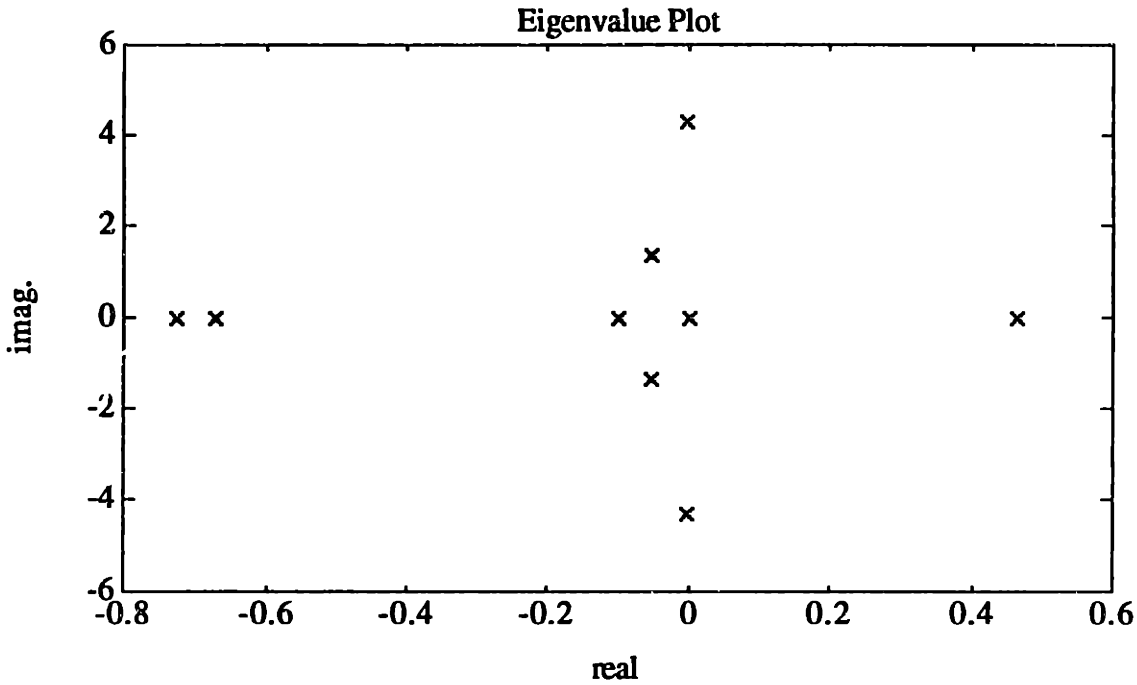

Figure 4.15: Eigenvalues of Full-Order LTI Model ("Full-Ahead" Model)

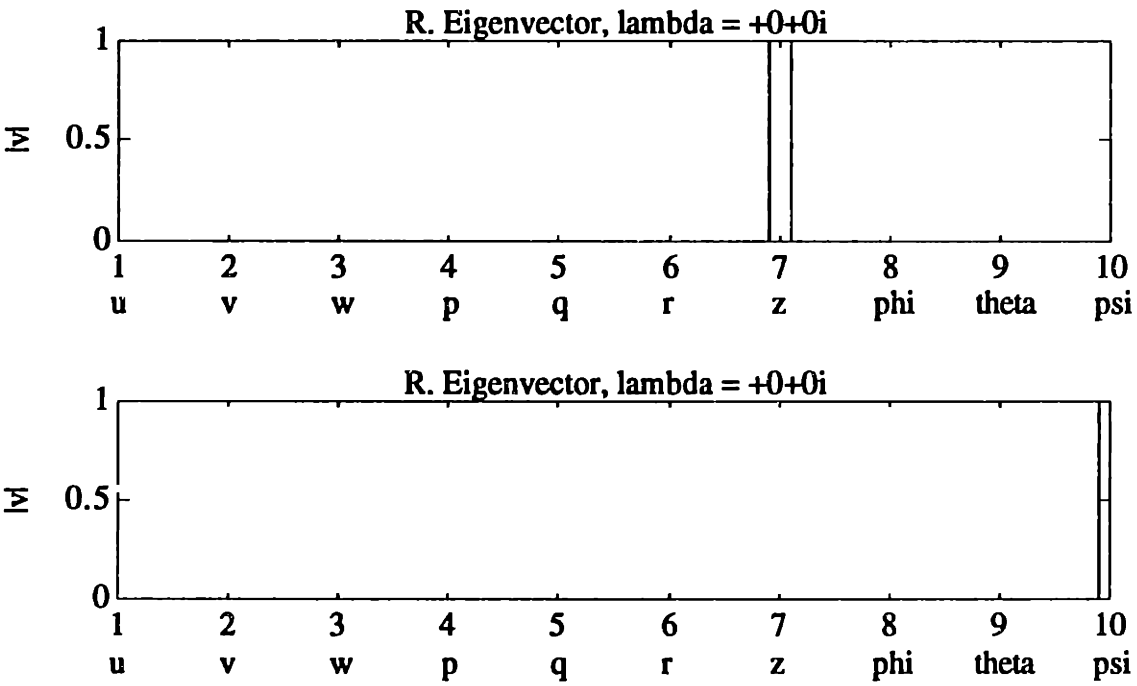

Figure 4.16: Right Eigenvectors of Full-Order LTI Model ("Full-Ahead" Model)

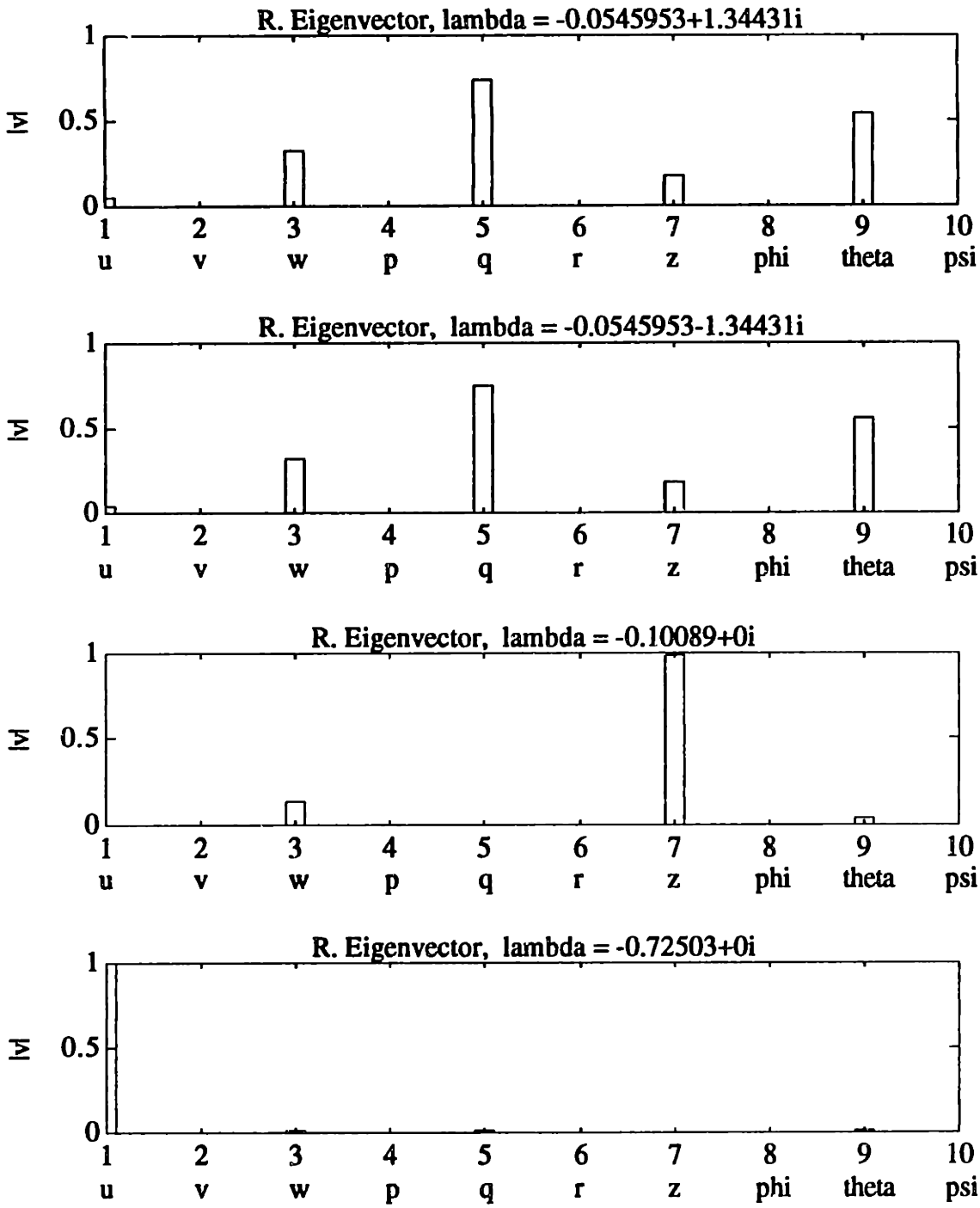

Figure 4.16: Right Eigenvectors of Full-Order LTI Model ("Full-Ahead" Model)

(continued)

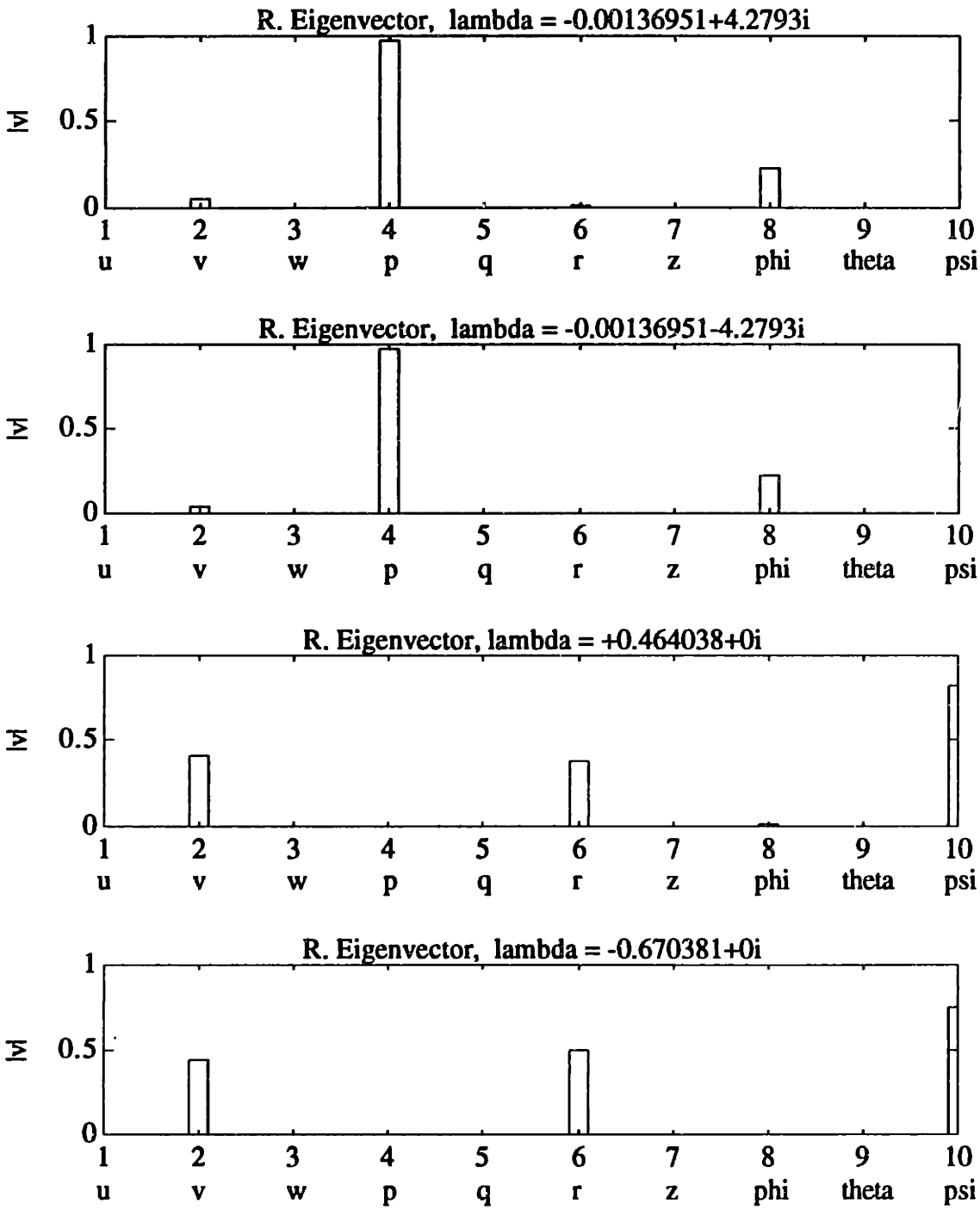

Figure 4.16: Right Eigenvectors of Full-Order LTI Model ("Full-Ahead" Model)

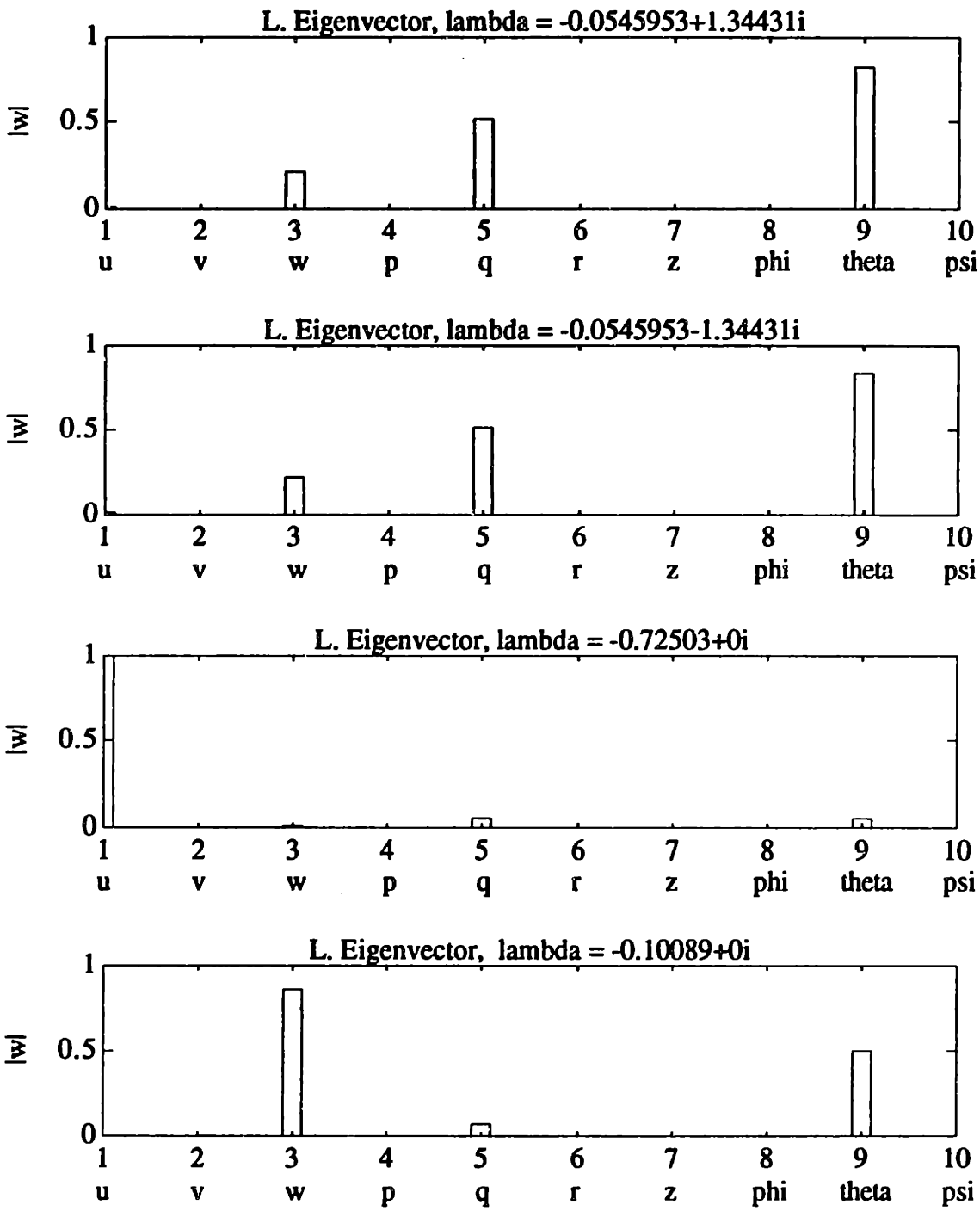

Figure 4.17: Left Eigenvectors of Full-Order LTI Model ("Full-Ahead" Model)

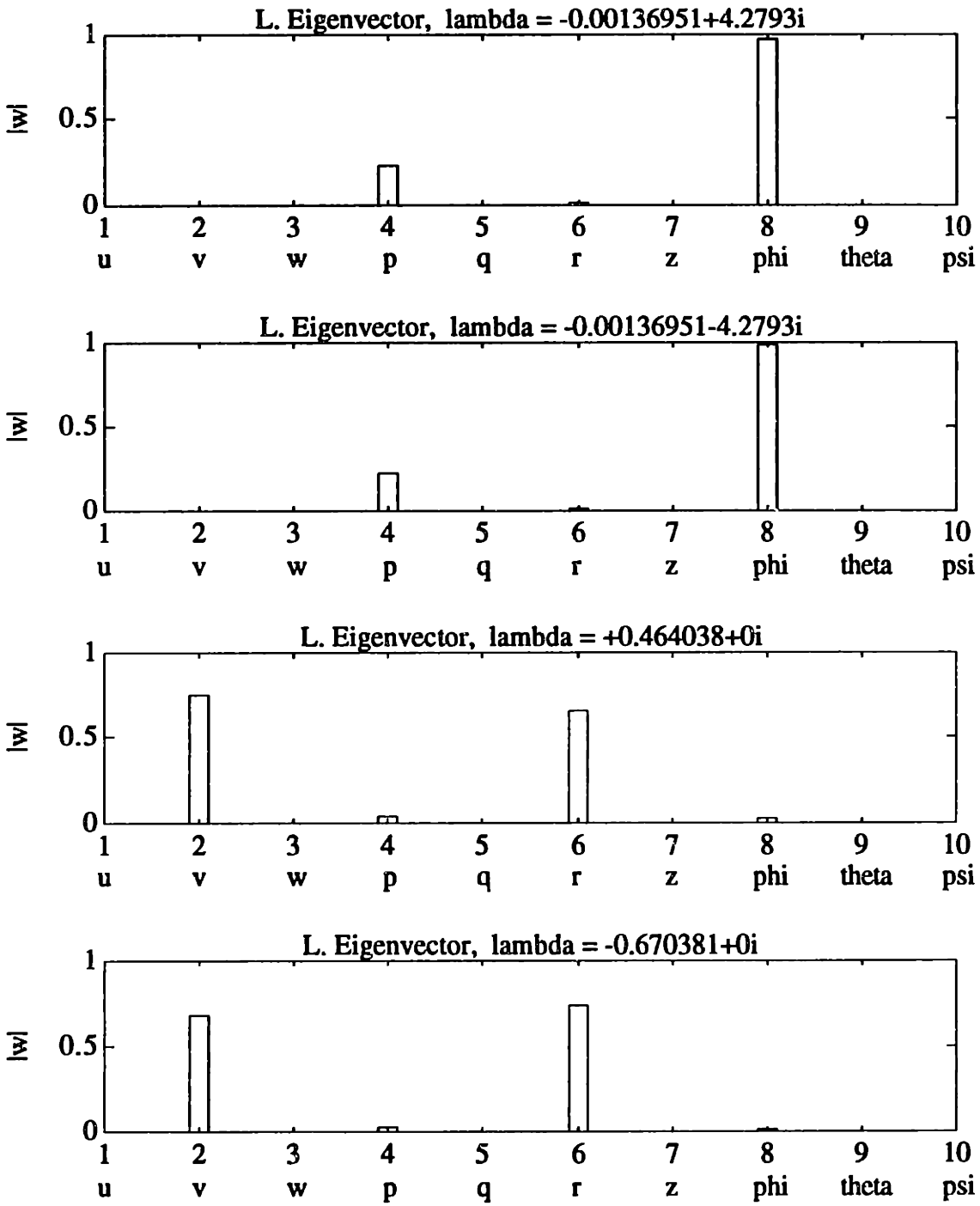

Figure 4.17: Left Eigenvectors of Full-Order LTI Model ("Full-Ahead" Model) (continued)

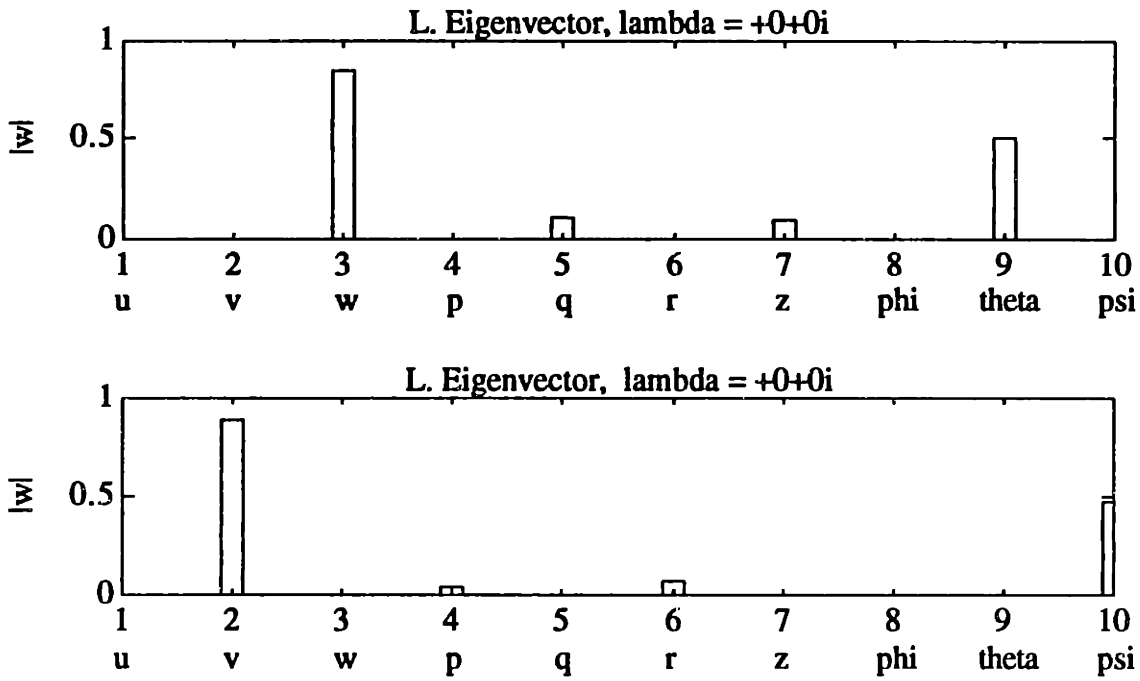

Figure 4.17: Left Eigenvectors of Full-Order LTI Model ("Full-Ahead" Model) (continued)

For this case, the only eigenvalues at the origin are two eigenvalues associated with the depth and heading, respectively. The modes that are associated with the axial velocity and vertical velocity appear to now be stable (due to the effects of hydrodynamic drag). In addition, the oscillatory pitch and roll modes also appear to be slightly damped as well (also due to hydrodynamic drag).

However, there is an unstable mode associated with the heading rate, together with the lateral velocity. The most probable cause of this unstable mode is the Munk moment effect, discussed in the earlier sections on the full-order nonlinear model. Whenever "side-slippage" of the vehicle occurs (i.e., a nonzero lateral velocity), the Munk moment reflects the tendency of the cylindrical-shaped AUV to turn "broadside" to the resulting linear direction of travel. Note that this unstable mode also very slightly affects the roll as well (due to gyroscopic coupling between the heading rate and the roll rate).

Again, the controllability of the modes of the "full-ahead" LTI model can be determined by examining the rows of the matrix product, $\mathbf{WB_O}$, where the rows of W are

the left eigenvectors. The element-by-element magnitude of this matrix product is shown in Table 4.6 (together with the corresponding eigenvalues and thrust inputs).

Table 4.6: $|WB_O|$ for the "Full-Ahead" Model

Eigenvalue	$\|WB_O\|$		
	(T_V)	$(T_P - T_S)$	$(T_P + T_S)$
-0.0546 + 1.3443i (Pitch)	0.0773	0	0.0299
-0.0546 - 1.3443i (Pitch)	0.0773	0	0.0299
-0.7250 (Axial Velocity)	0.0038	0	0.4308
-0.1009 (Depth)	0.2603	0	0.0007
-0.0014 + 4.2793i (Roll)	0.0000	0.0033	0
-0.0014 - 4.2793i (Roll)	0.0000	0.0033	0
0.4640 (Heading & Lateral Vel.)	0.0000	0.1494	0
-0.6704 (Heading & Lateral Vel.)	0.0000	0.1437	0
0 (Depth)	0.2554	0	0.0016
0 (Heading)	0.0000	0.0276	0

From this table, all of the modes of this model are controllable from the control input. Especially note that the unstable mode associated with the heading and lateral velocity is controllable from the differential thrust input, $(T_P - T_S)$ (but not from the vertical thrust input, T_V). This implies that a controller designed purely for heading can stabilize it.

The observability of the modes of the "straight ahead" LTI model can be determined by examining the columns of the matrix product, $\mathbf{C_1 V}$ (i.e., the rows of $\mathbf{V^T C_1^T}$). The element-by-element magnitude of $\mathbf{V^T C_1^T}$ is shown in Table 4.7 (together with the corresponding eigenvalues and measured outputs).

Table 4.7: $|V^T C_1 T|$ for the "Full-Ahead" Model

Eigenvalue	$\|V^T C_1 T\|$					
	(Z)	(psi)	(Z_dot)	(r)	(phi)	(theta)
0 (Depth)	1.0000	0	0	0	0	0
0 (Heading)	0	1.0000	0	0	0	0
-0.0546 + 1.3443i (Pitch)	0.1816	0.0000	0.2443	0.0000	0.0000	0.5526
-0.0546 - 1.3443i (Pitch)	0.1816	0.0000	0.2443	0.0000	0.0000	0.5526
-0.1009 (Depth)	0.9899	0.0000	0.0999	0.0000	0.0000	0.0369
-0.7250 (Axial Velocity)	0.0118	0.0000	0.0086	0.0000	0.0000	0.0219
-0.0014 + 4.2793i (Roll)	0.0000	0.0020	0.0000	0.0085	0.2272	0.0000
-0.0014 - 4.2793i (Roll)	0.0000	0.0020	0.0000	0.0085	0.2272	0.0000
0.4640 (Heading & Lateral Vel.)	0.0000	0.8268	0.0000	0.3837	0.0057	0.0000
-0.6704 (Heading & Lateral Vel.)	0.0000	0.7461	0.0000	0.5002	0.0058	0.0000

For this case, all of the modes are observable with this set of measurements (even though the axial velocity mode is relatively less observable than all the other modes). Note that the unstable mode is observable from the heading measurement, which again implies that a controller designed purely for heading can stabilize it.

Using the MATLAB™ software, the following finite transmission zeros were found for this condition.

Table 4.8: Transmission Zeros of Full-Order LTI Model ("Full-Ahead" Model)

-0.3916

This zero was found to be associated with the axial velocity. Note that this zero is not equal to any of the eigenvalues of this model shown in Table 4.5. This verifies that all the modes are both controllable and observable (i.e., there are no pole-zero cancellations). In

addition, this implies that there are no performance limitations due to non-minimum phase zeroes.

The transfer-function singular values versus frequency (from the controls to the output of this model) are shown in Figure 4.18.

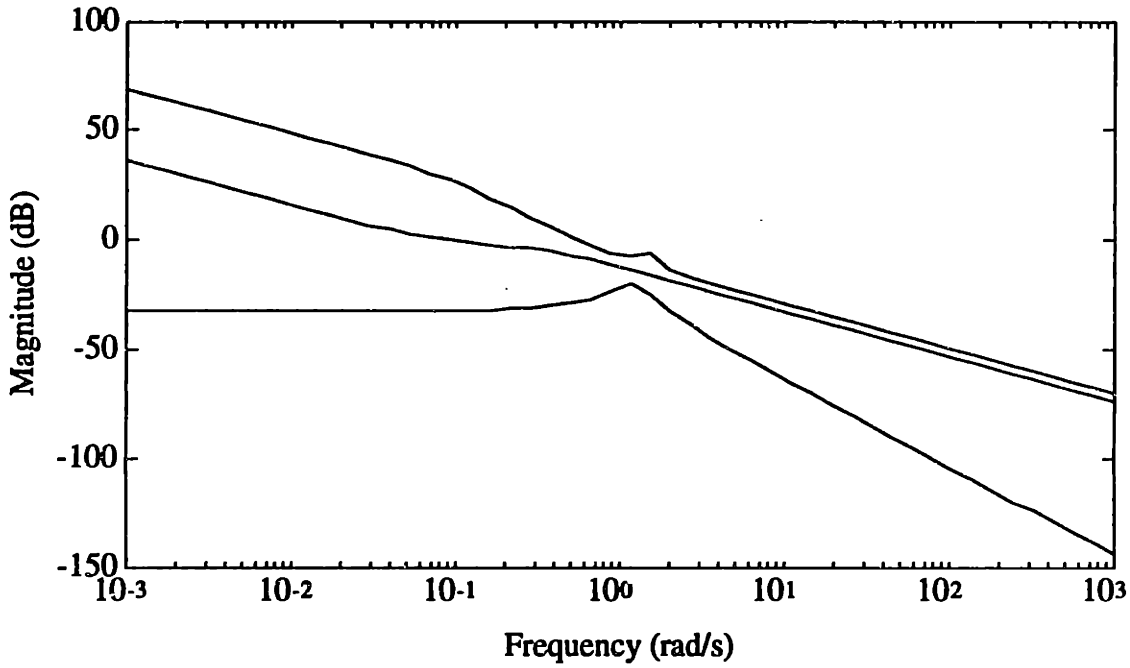

Figure 4.18: Frequency Response of LTI Model from **u** to **y** ("Full-Ahead" Model)

Several aspects of this model (due the effects of the nominal axial speed) are apparent from this plot. At the lower frequencies, both the maximum singular-value and the center singular-value correspond to a 20 db/decade "one pole" response from the controls to depth and yaw (due the migration of the "velocity" pole from the origin). At the higher frequencies, the maximum singular value corresponds to the 20 db/decade "one-pole" response from the controls to the depth rate and the yawing angular velocity. The minimum singular value corresponds to the response from the controls to the pitch and roll angles. Again, note the presence of the "bump" at approximately 1.5 rad/s (due to the response from the controls to the pitch angle).

Full-Reverse Model

The last case was the "full-reverse" condition, at an axial velocity of -1.0 ft/s. This was done to determine the effects of negative axial velocity, since some normal modes of vehicle operation require such velocities. The operating condition was approximately $\mathbf{x}_0 = [\,-1\ 0\ 0\ 0\ 0\ 0\ 0\ 0\ 0\ 0\ 0\,]^T$, $\mathbf{u}_0 = [0\ -0.84\ 0]^T$, and $\mathbf{d}_0 = \mathbf{0}$. The open-loop eigenvalues are shown in Table 4.9 and the plot of Figure 4.19. The normalized magnitudes of the right and left eigenvectors are shown in the plots of Figures 4.20-4.21.

Table 4.9: Eigenvalues of Full-Order LTI Model ("Full-Reverse" Model)

0
0
-0.0518 + 1.3390i
-0.0518 - 1.3390i
-0.1017
-0.7250
-0.0015 + 4.2792i
-0.0015 - 4.2792i
0.4765
-0.6853

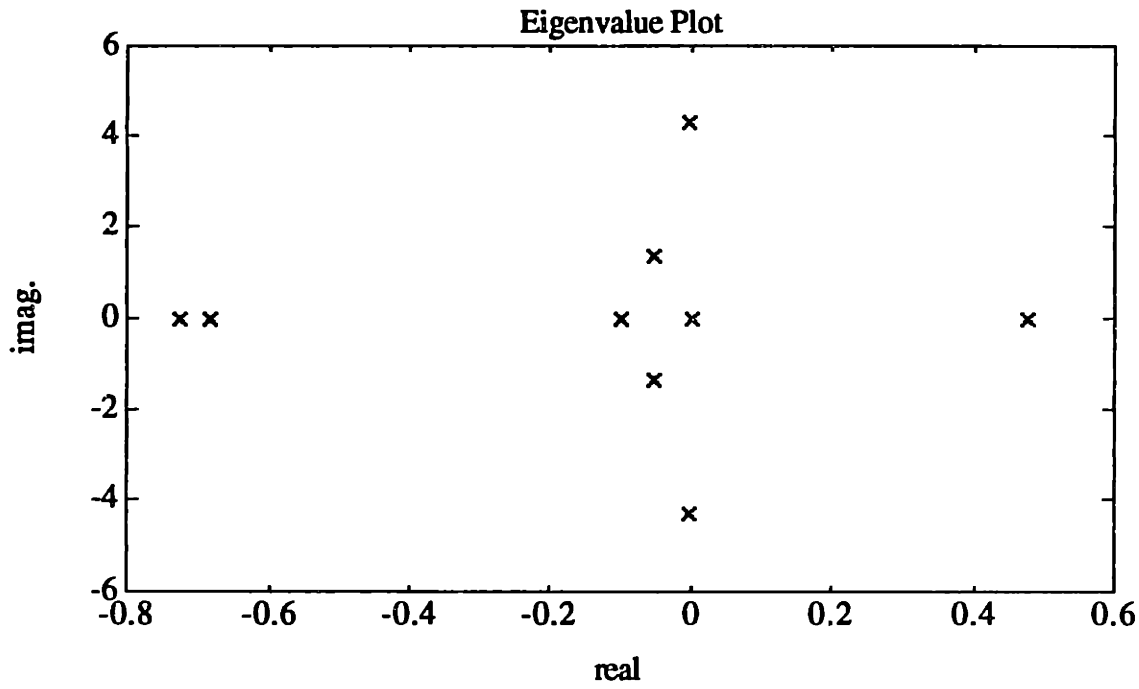

Figure 4.19: Eigenvalues of Full-Order LTI Model ("Full-Reverse" Model)

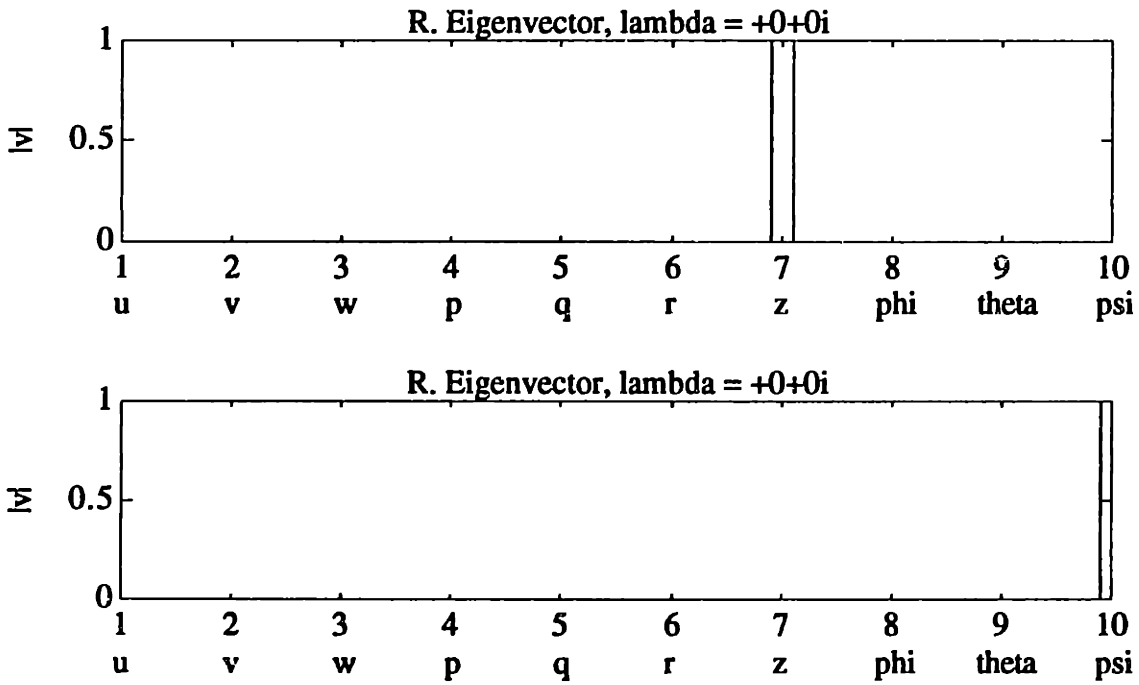

Figure 4.20: Right Eigenvectors of Full-Order LTI Model ("Full-Reverse" Model)

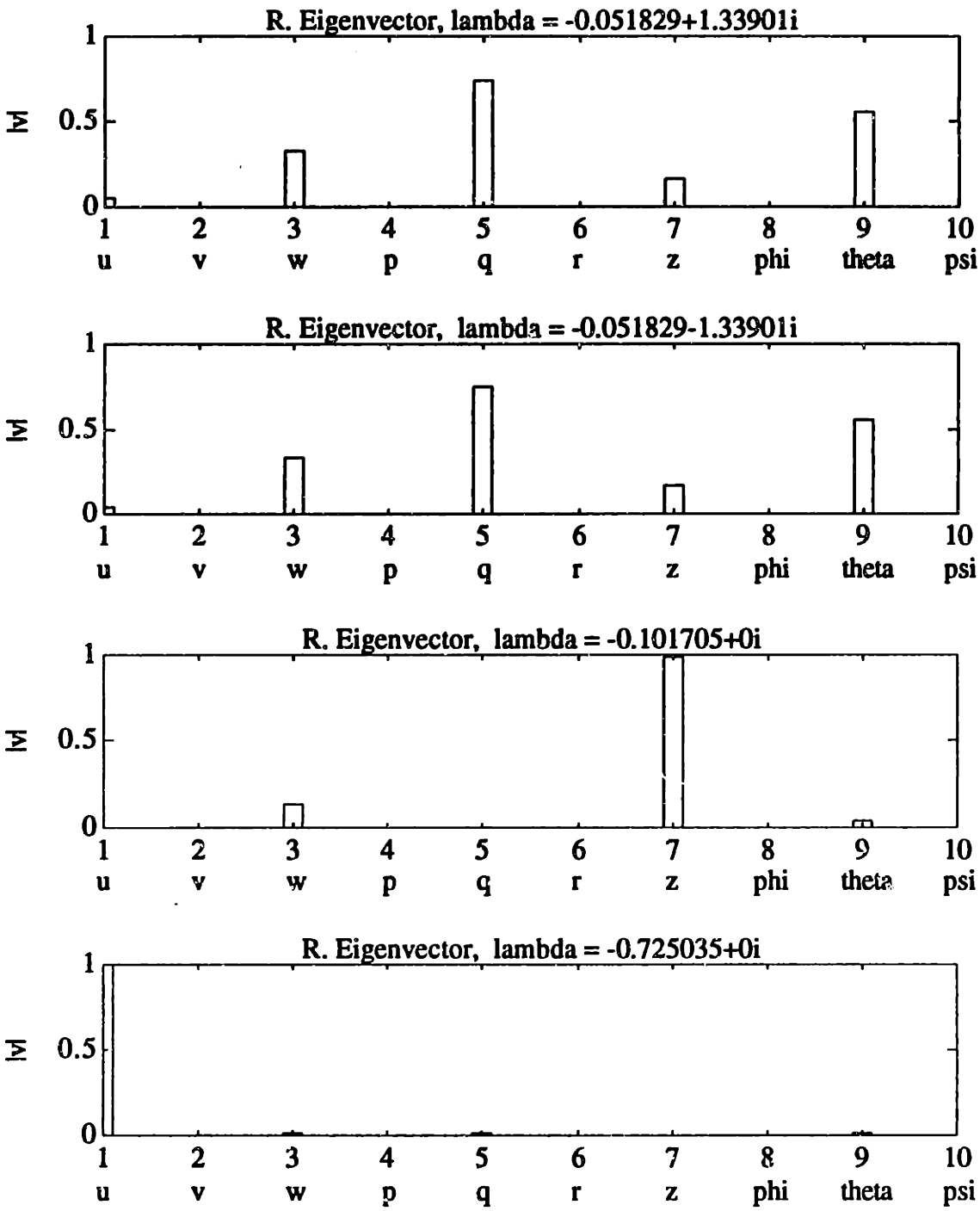

Figure 4.20: Right Eigenvectors of Full-Order LTI Model ("Full-Reverse" Model)

(continued)

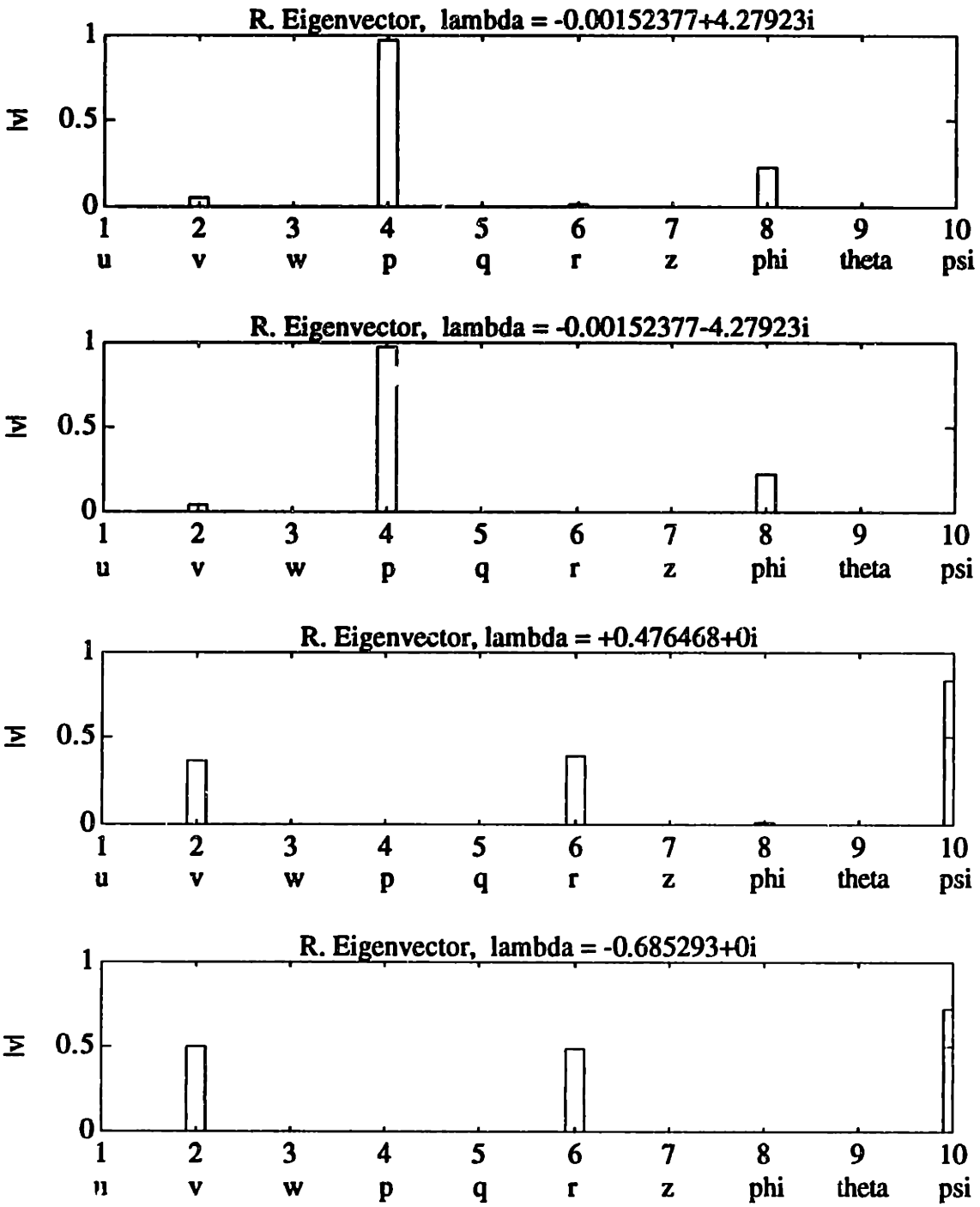

Figure 4.20: Right Eigenvectors of Full-Order LTI Model ("Full-Reverse" Model)

(continued)

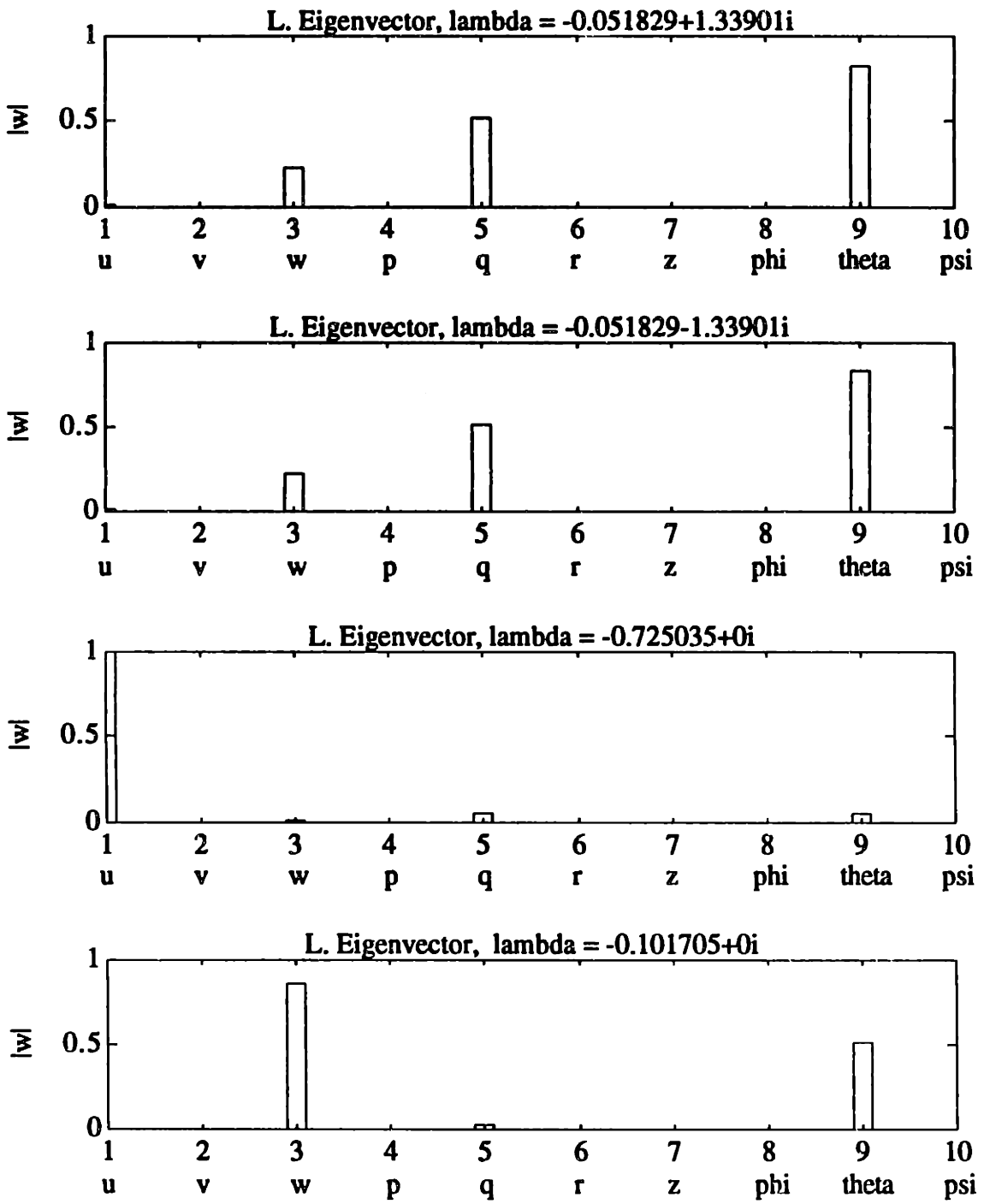

Figure 4.21: Left Eigenvectors of Full-Order LTI Model ("Full-Reverse" Model)

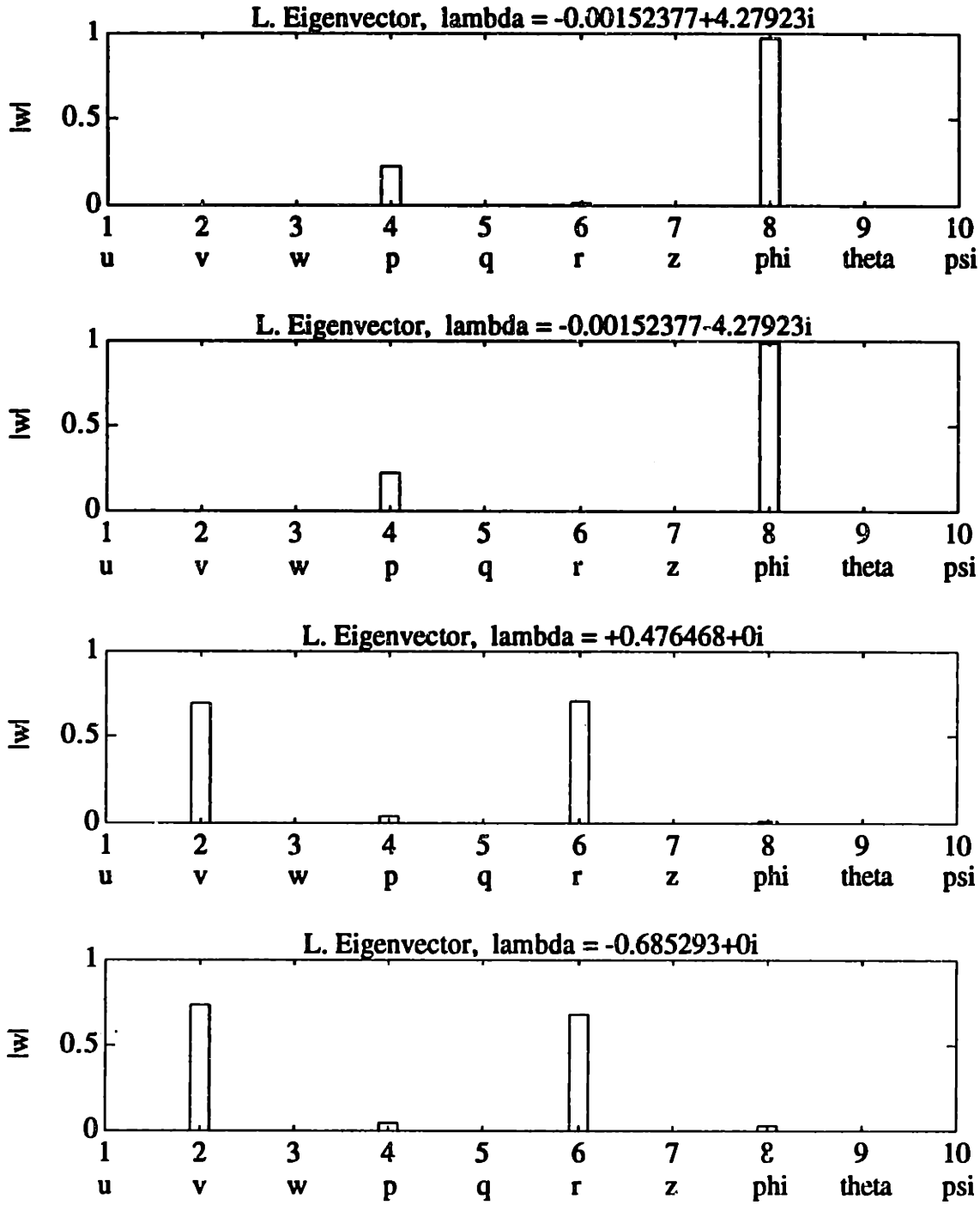

Figure 4.21 Left Eigenvectors of Full-Order LTI Model ("Full-Reverse" Model)

(continued)

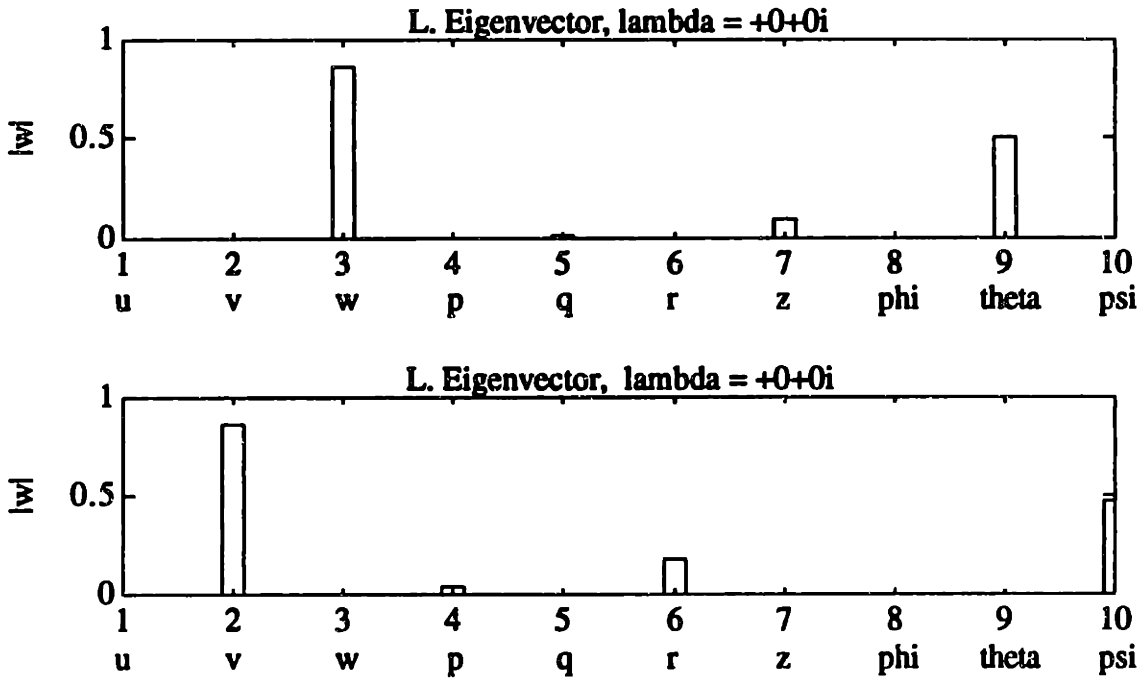

Figure 4.21: Left Eigenvectors of Full-Order LTI Model ("Full-Reverse" Model)

(continued)

For this case, the general form of the eigenstructure appears to be almost identical to the eigenstructure for the previous "full ahead" case. Again, the only eigenvalues at the origin are two eigenvalues associated with depth and heading. The modes associated with the axial velocity and vertical velocity still appear to be stable. The oscillatory pitch and roll modes also are significantly damped as well. The unstable mode associated with the heading rate and the lateral velocity still appears. All of this implies that the stability effects of the nominal axial velocity are nearly independent of the sign of this particular velocity. This is due to the fact that the AUV is nearly symmetric along each of its three main axes.

The controllability of the modes of the "full reverse" LTI model was determined by examining the rows of the matrix product, WB_0. The element-by-element magnitude of this matrix product is shown in Table 4.10 (together with the corresponding eigenvalues and thrust inputs).

Table 4.10: $|WB_0|$ for the "Full-Reverse" Model

Eigenvalue	$\|WB_0\|$		
	(T_v)	$(T_p - T_s)$	$(T_p + T_s)$
-0.0518 + 1.3390i (Pitch)	0.0771	0	0.0298
-0.0518 - 1.3390i (Pitch)	0.0771	0	0.0298
-0.7250 (Axial Velocity)	0.0065	0	0.4307
-0.1017 (Depth)	0.2631	0	0.0007
-0.0015 + 4.2792i (Roll)	0.0000	0.0032	0
-0.0015 - 4.2792i (Roll)	0.0000	0.0032	0
0.4765 (Heading & Lateral Vel.)	0.0000	0.1393	0
-0.6853 (Heading & Lateral Vel.)	0.0000	0.1538	0
0 (Depth)	0.2637	0	0.0016
0 (Heading)	0.0000	0.0264	0

As with the "full ahead" case, all of the modes of this model appear to be controllable from the control input. Again, especially note that the unstable mode associated with the yaw rate and the lateral velocity is controllable from the port and starboard thrust inputs, which implies that a controller designed purely for heading can stabilize it (even for negative axial velocities).

The observability of the modes of the "full reverse" LTI model was determined by examining the columns of the matrix product, $\mathbf{C_1 V}$ (i.e., the rows of $\mathbf{V^T C_1^T}$). The element-by-element magnitude of $\mathbf{V^T C_1^T}$ is shown in Table 4.11 (together with the corresponding eigenvalues and measured outputs).

Table 4.11: $|V^T C_1 T|$ for the "Full-Reverse" Model

Eigenvalue	$\|V^T C_1 T\|$					
	(Z)	(psi)	(Z_dot)	(r)	(phi)	(theta)
0 (Depth)	1.0000	0	0	0	0	0
0 (Heading)	0	1.0000	0	0	0	0
-0.0518 + 1.3390i (Pitch)	0.1692	0.0000	0.2268	0.0000	0.0000	0.5545
-0.0518 - 1.3390i (Pitch)	0.1692	0.0000	0.2268	0.0000	0.0000	0.5545
-0.1017 (Depth)	0.9896	0.0000	0.1006	0.0000	0.0000	0.0382
-0.7250 (Axial Velocity)	0.0086	0.0000	0.0062	0.0000	0.0000	0.0221
-0.0015 + 4.2792i (Roll)	0.0000	0.0020	0.0000	0.0085	0.2272	0.0000
-0.0015 - 4.2792i (Roll)	0.0000	0.0020	0.0000	0.0085	0.2272	0.0000
0.4765 (Heading & Lateral Vel.)	0.0000	0.8377	0.0000	0.3991	0.0066	0.0000
-0.6853 (Heading & Lateral Vel.)	0.0000	0.7160	0.0000	0.4907	0.0041	0.0000

For the "full reverse" case, all of the modes are observable with this set of measurements. The unstable mode is observable from the heading measurement, which again implies that a controller designed purely for heading can stabilize it.

Using the MATLAB™ software, the following finite transmission zeros were found for this condition.

Table 4.12: Transmission Zeros of Full-Order LTI Model ("Full-Reverse" Model)

-0.3916

This zero was found to be associated with the axial velocity. This zero is also not equal to any of the eigenvalues of this model shown in Table 4.9. This verifies that all the modes

are both controllable and observable and that there are no performance limitations due to non-minimum phase zeroes.

The singular values of the transfer-function from the controls to the output of this model versus frequency are shown in Figure 4.22

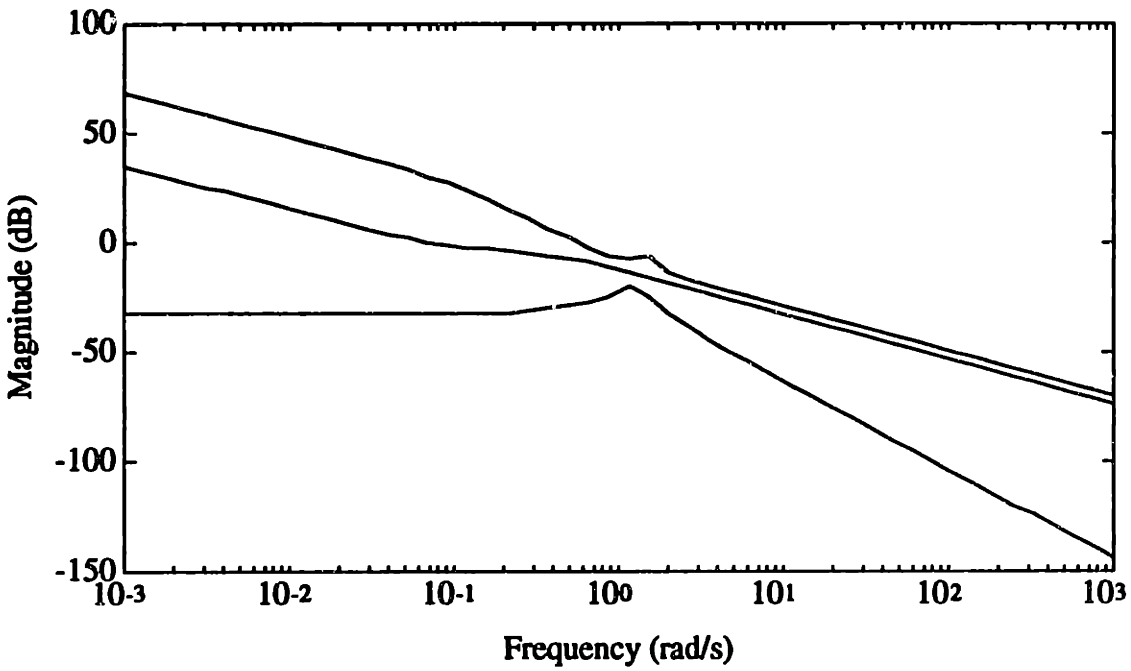

Figure 4.22: Frequency Response of LTI Model from **u** to **y** ("Full-Reverse" Model)

At the lower frequencies, (as with the "full ahead" case), the maximum singular-value and the center singular-value correspond to a 20 db/decade "one pole" response from the controls to depth and yaw (due the migration of the "velocity" pole from the origin). At the higher frequencies, the maximum singular value corresponds to the 20 db/decade "one-pole" response from the controls to the depth rate and the yawing angular velocity. The minimum singular value corresponds to the response from the controls to the pitch and roll angles. Again, note the presence of the "bump" at approximately 1.5 rad/s (due to the response from the controls to the pitch angle).

4.5 REDUCED-ORDER LTI MODEL

For the Sliding-Mode augmented control-design method presented in Section 3.3, the LTI controller must be designed using the following linear version of the Descriptor/Companion model.

$$\frac{d}{dt}\left(\hat{x}\right) = \hat{\dot{x}}$$

$$\frac{d}{dt}\left(\hat{\dot{x}}\right) = \hat{\ddot{x}}$$

$$\vdots$$

$$\frac{d}{dt}\left(\hat{x}^{(n-2)}\right) = \hat{x}^{(n-1)}$$

$$E_p\hat{x}^{(n)} = A_p x + B_p u + d \qquad (4.66)$$

There are several possible procedures for deriving this model. One procedure would be to simplify the previously developed full-order linear model using the assumptions of Section 4.3. A somewhat simpler procedure is to linearize the reduced-order Descriptor/Companion nonlinear model already developed.

4.5.1 Derivation of the Reduced-Order LTI Model

Recall that for the AUV, the reduced-order Descriptor/Companion nonlinear model is given by the following 2nd-order system

$$\frac{d}{dt}\left(\hat{x}\right) = \hat{\dot{x}}$$

$$E\left[\frac{d}{dt}\left(\hat{\dot{x}}\right)\right] = E\,\hat{\ddot{x}} = f(x) + Bu + d \qquad (4.67)$$

The reduced-order total state vector is given by

$$\mathbf{x} = [\, Z \;\psi\; \dot{Z} \;\dot{\psi}\,]^T \tag{4.68}$$

and the reduced-order output state vector is given by

$$\hat{\mathbf{x}} = [\, Z \;\psi\,]^T \tag{4.69}$$

The control input vector is given by

$$\mathbf{u} = [\, U_Z \; U_\psi\,]^T \tag{4.70}$$

and the disturbance vector is given by

$$\mathbf{d} = [\, d_Z(t) \;\; d_\psi(t)]^T \tag{4.71}$$

This linearization was also done using a first-order Taylor series approximation about a nominal "operating point". For this model, if the point is chosen such that the "acceleration" variables were zero, i.e.,

$$\frac{d}{dt}(\hat{\mathbf{x}}_o) = \dot{\hat{\mathbf{x}}}_o$$

$$0 = \mathbf{f}(\mathbf{x}_o) + \mathbf{B}\mathbf{u}_o + \mathbf{d}_o \tag{4.72}$$

then the first-order Taylor-series approximation is given by

$$\frac{d}{dt}(\delta\hat{\mathbf{x}}) = \delta\dot{\hat{\mathbf{x}}}$$

$$\mathbf{E}\left[\frac{d}{dt}\left(\delta\dot{\hat{\mathbf{x}}}\right)\right] = \frac{\partial \mathbf{f}}{\partial \mathbf{x}}(\mathbf{x}_o)\,\delta\mathbf{x} \;+\; \mathbf{B}\delta\mathbf{u} \;+\delta\mathbf{d} \tag{4.73}$$

where as in the derivation of the full-order LTI model, $\delta\mathbf{x}$, $\delta\mathbf{u}$, and $\delta\mathbf{d}$ are defined as "perturbations" of the form

$$\mathbf{x} = \mathbf{x_o} + \delta\mathbf{x} \tag{4.74}$$

$$\mathbf{u} = \mathbf{u_o} + \delta\mathbf{u} \tag{4.75}$$

$$\mathbf{d} = \mathbf{d_o} + \delta\mathbf{d} \tag{4.76}$$

Then (4.73) was used to directly write the AUV LTI model

$$\begin{aligned} \frac{d}{dt}(\delta\hat{\mathbf{x}}) &= \delta\dot{\hat{\mathbf{x}}} \\ \mathbf{E_p}\left[\frac{d}{dt}(\delta\hat{\mathbf{x}})\right] &= \mathbf{A_p}\delta\mathbf{x} + \mathbf{B_p}\delta\mathbf{u} + \delta\mathbf{d} \end{aligned} \tag{4.77}$$

This descriptor model can also be converted into the conventional state-space form shown below

$$\begin{aligned} \frac{d}{dt}(\delta\hat{\mathbf{x}}) &= \delta\dot{\hat{\mathbf{x}}} \\ \left[\frac{d}{dt}(\delta\hat{\mathbf{x}})\right] &= \mathbf{E_p^{-1}A_p}\delta\mathbf{x} + \mathbf{E_p^{-1}B_p}\delta\mathbf{u} + \mathbf{E_p^{-1}}\delta\mathbf{d} \end{aligned} \tag{4.78}$$

if the LTI "descriptor" matrix, $\mathbf{E_p}$ is assumed to be nonsingular.

4.5.2 Analysis of the Reduced-Order Linear Model

The reduced-order LTI model developed in the previous section can be used by Sliding-Mode augmented-LTI control-design methodology of Chapter 3 (and the linear control-design methodologies of Chapter 2). However, it would be useful to analyze the characteristics of this reduced-order model (as with the full-order model), especially as related to the choice of the nominal operating point. The open-loop stability of this model can be analyzed by examining the eigenvalues of $\mathbf{E_p^{-1}A_p}$. The frequency-response can be analyzed from plots of the transfer-function singular values.

The eigenvalues of this model as a function of the nominal depth rate are shown in Table 4.13 and are shown in the plot of Figure 4.23

Table 4.13: Variation of the Eigenvalues of the Reduced-Order LTI Model as a Function of Depth Rate.

$\dot{Z}$(ft/s)	Eigenvalues			
-2.0	0 (Heading)	0 (Heading)	-4.2432 (Depth)	0 (Depth)
-1.0	0 (Heading)	0 (Heading)	-2.1216 (Depth)	0 (Depth)
0.0	0 (Heading)	0 (Heading)	0 (Depth)	0 (Depth)
1.0	0 (Heading)	0 (Heading)	-2.1216 (Depth)	0 (Depth)
2.0	0 (Heading)	0 (Heading)	-4.2432 (Depth)	0 (Depth)

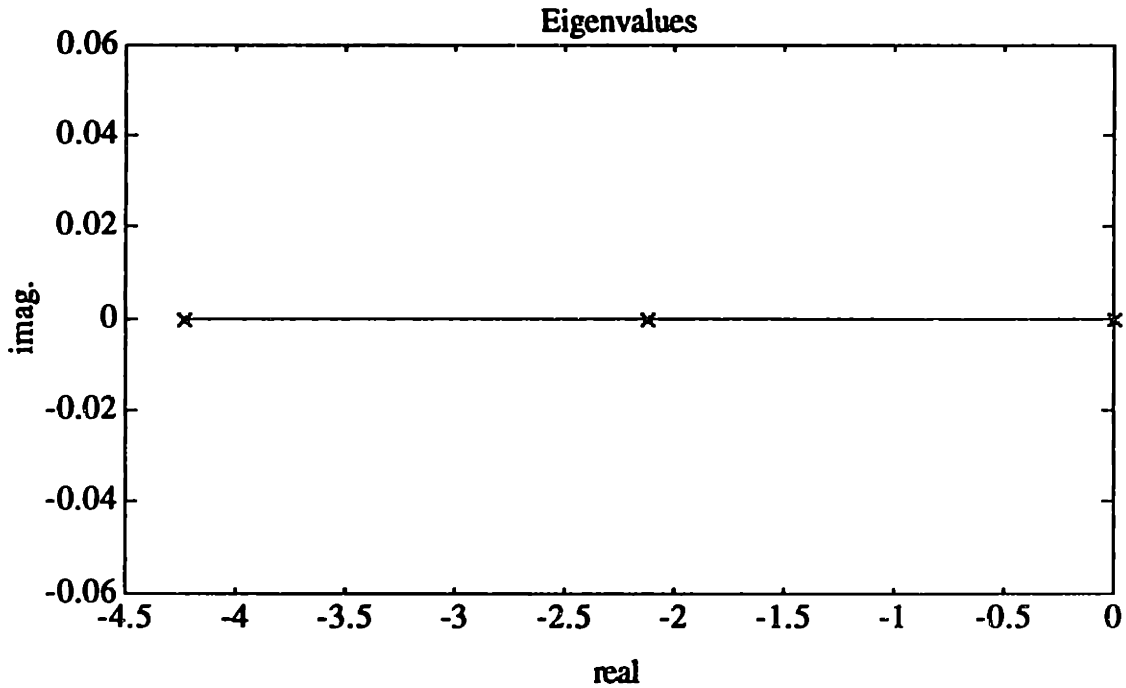

Figure 4.23: Variation of the Eigenvalues of the Reduced-Order LTI Model as a Function of Depth Rate.

Here, the eigenvalue associated with the depth has a damping directly dependent on the magnitude of the nominal value of the depth rate.

The eigenvalues of this model (as a function of the nominal yaw rate) are shown in Table 4.14 and are shown in the plot of Figure 4.24.

Table 4.14: Variation of the Eigenvalues of the Reduced-Order LTI Model as a Function of Yaw Rate

$\dot{\Psi}$(deg/s)	Eigenvalues			
-20.0	0 (Depth)	0 (Depth)	0 (Heading)	-1.4677 (Heading)
-10.0	0 (Depth)	0 (Depth)	0 (Heading)	-0.7338 (Heading)
0.0	0 (Depth)	0 (Depth)	0 (Heading)	0 (Heading)
10.0	0 (Depth)	0 (Depth)	0 (Heading)	-1.4677 (Heading)
20.0	0 (Depth)	0 (Depth)	0 (Heading)	-0.7338 (Heading)

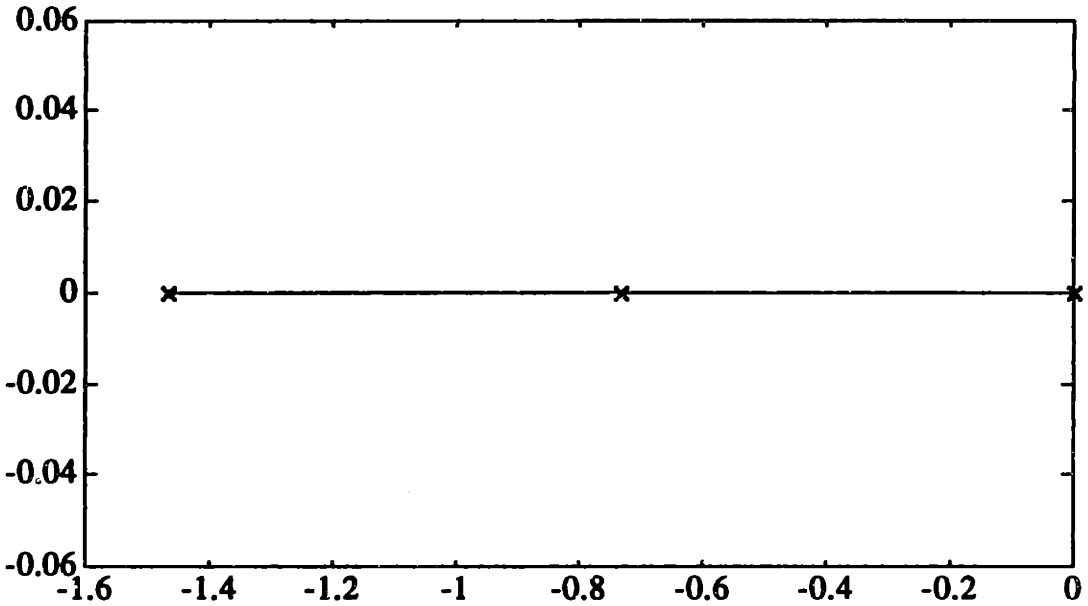

Figure 4.24: Variation of the Eigenvalues of the Reduced-Order LTI Model as a Function of Yaw Rate

The eigenvalue associated with the heading also appears to have a damping directly dependent on the magnitude of the nominal value of the yaw rate. For both the full-order linear model and the full-order nonlinear model, there is a destabilizing Munk moment (and consequently an unstable mode) dependent on the axial velocity. For this reduced-order model, however, this destabilizing moment does not appear. From a design perspective, this can be a somewhat serious issue (since for nonzero axial velocities, a stable reduced-order LTI model is being used to approximate an unstable full-order LTI model). However, if the robust LTI control design methodologies presented in Chapter 2 are used for the design of the reduced-order LTI controller, one possible solution to this issue would be to use the fairly accurate "hovering" model as the nominal design model, while including the Munk moment effect as a dynamic model error.

Since all the states are assumed to be available for feedback, the output vector, **y**, of this model is identical to the system state vector, **x**. Therefore, the reduced-order LTI

model transfer-function singular values (from the controls, **u**, to the system state, **x**) are shown in the plots of Figures 4.25 to 4.26. The first plot was done at the "hovering" condition of zero nominal depth rate and zero nominal heading rate.

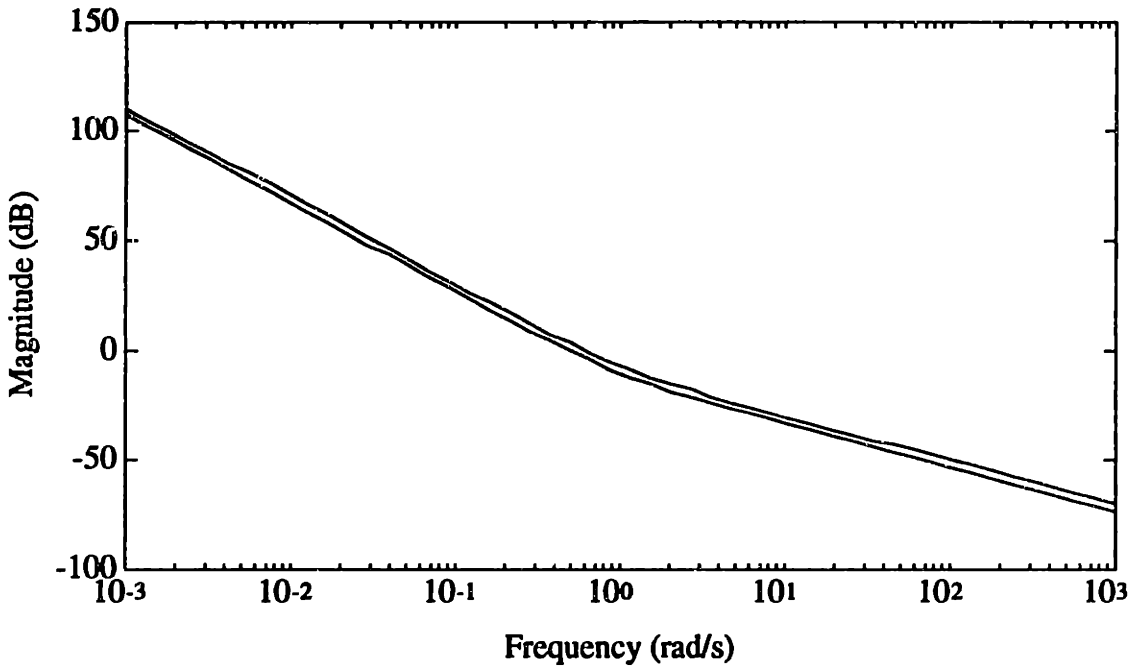

Figure 4.25: Frequency Response of the Reduced-Order LTI Model from **u** to **x** (Hovering Condition)

Upon closer examination, the singular values of this frequency response are nearly identical to the maximum singular values of the full-order model at the "hovering" condition (minus the "bump" caused by the pitch dynamics). This implies that the reduced-order model provides a reasonable approximation to the "hovering" full-order model for frequency-domain control design, so long as the pitch dynamics are not excited. The next plot was done with a nominal depth rate of 1.0 ft/s and with the nominal values of all the other states set to zero.

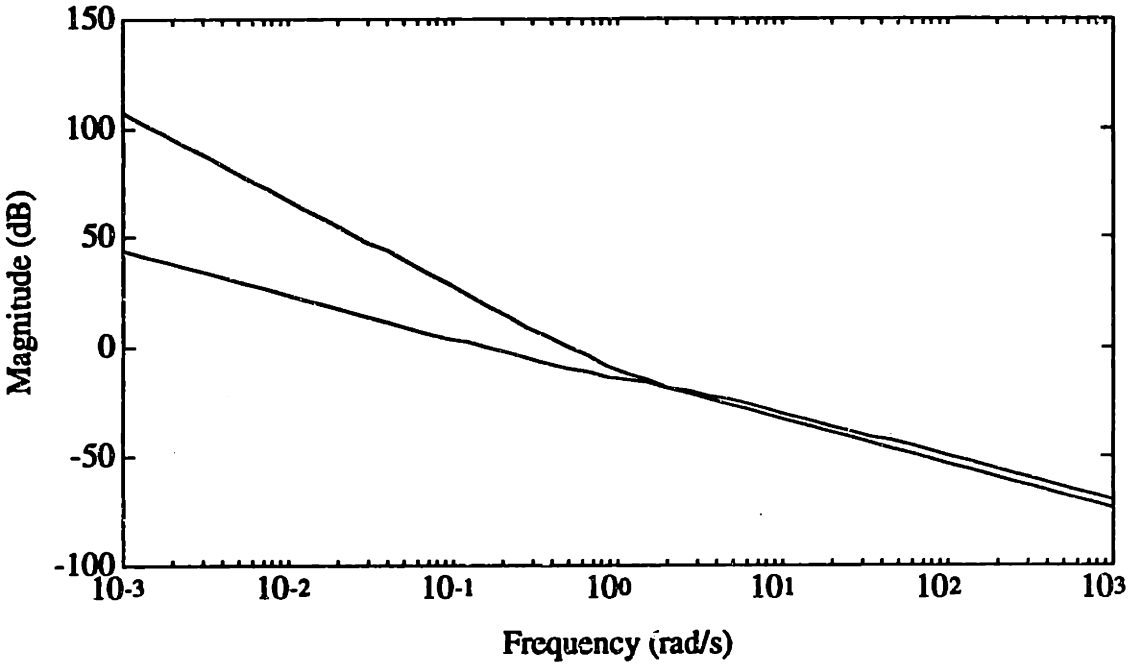

Figure 4.26: Frequency Response of the Reduced-Order LTI Model from **u** to **x**

(Depth Rate = 1.0 ft/s)

The minimum singular value of this plot corresponds to the response from the controls to the depth and depth rate. At the lower frequencies, the minimum singular value exhibits a 20 db/dec "one pole" response due to the shift of the depth rate pole from the origin. Note that the maximum singular value, which corresponds to the response from the controls to the heading and heading rate, is unchanged from the previous "hovering" case.

The last plot was done with a nominal heading rate of 10.0 deg/s and with the nominal values of all the other states set to zero.

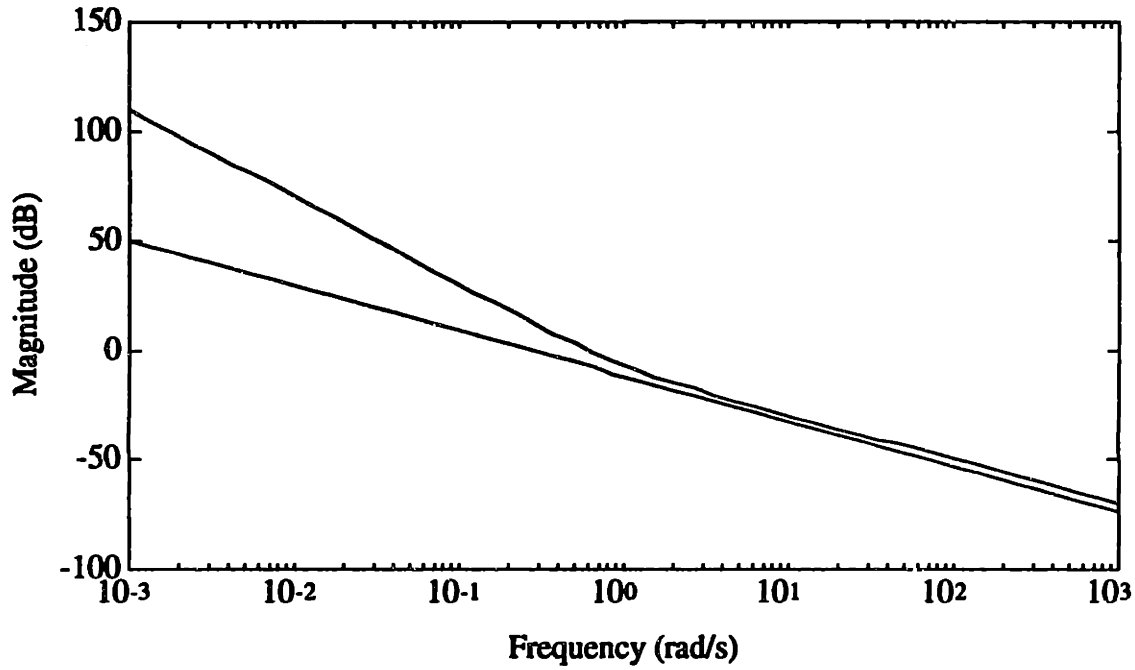

Figure 4.27: Frequency Response of the Reduced-Order LTI Model from **u** to **x**

(Heading Rate = 10.0 deg/s)

For this plot, the minimum singular value corresponds to the response from the controls to the heading and heading rate. At the lower frequencies, the minimum singular value exhibits a 20 db/dec "one pole" response due to the shift of the heading rate pole from the origin. The maximum singular value, which now corresponds to the response from the controls to the depth and depth rate, is again unchanged from the "hovering" case.

4.6 THRUSTER AND SENSOR MODELS

For the design and the evaluation of the AUV control system, the sensors can be modeled as first-order systems with unity gain and a time constant(τ), with an additive gaussian white noise input with mean, $\overline{m}$, and standard deviation, σ, as shown in Figure 4.28. The thrusters can also be modeled as first-order systems with unity gain and a time constant(τ), but with an additional time delay given by T_d.

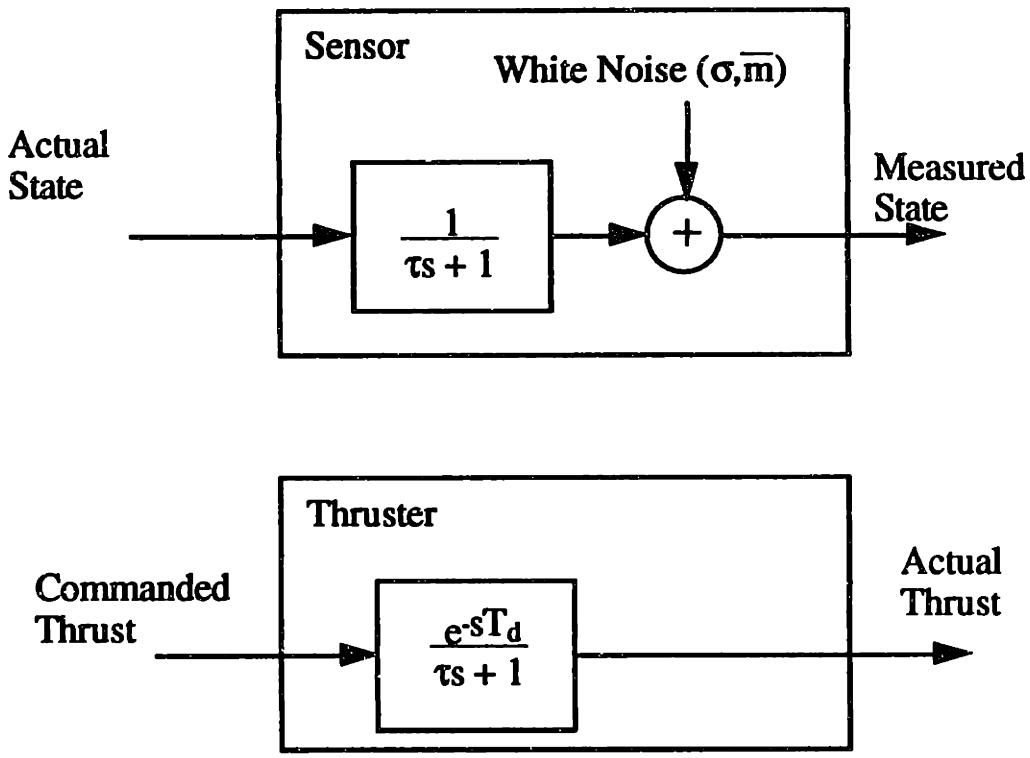

Figure 4.28: AUV Thruster and Sensor Models

For a control system design (such as the AUV), the dynamics of the thrusters and sensors play a significant role. For example, if the thruster dynamics are neglected in the control system design, the closed-loop bandwidth of the AUV control system should be below the bandwidth of the thrusters, given by the inverse of τ, or else the performance (and possibly the stability) of the system may suffer. In addition, these models are extremely useful for evaluating in simulation the effects of noise, time lags and time delays on the performance of the control system before it is tested in the vehicle.

Numerical values for these models are reproduced below in Tables 4.15 and 4.16 from [18]. These values were obtained, whenever possible, from the manufacturer's specifications. In cases where this information was lacking, a realistic estimate was made based on observation of actual vehicle testing data.

Table 4.15 Sensor Characteristics

Sensor	τ	σ	$\overline{m}$
Inclinometers	0.3 sec	1.0 deg	0.0 deg
Compass	0.2 sec	1.5 deg	0.0 deg
Yaw Rate Gyro	0.15 sec	0.4 deg/sec	0.0 deg/sec
Depth Sensor	0.2 sec	0.1 ft	0.0 ft

Table 4.16 Thruster Characteristics

t	T_d
0.75 sec	0.2 sec

Chapter 5

Full-Order H_∞/μ-Synthesis Vehicle Controller Design

The goal of this design effort is to synthesize heading and depth controllers for the *Sea Squirt* AUV (using the H_∞/μ-synthesis robust control-system design methodology described in Chapter 2 together with the full-order LTI model developed in Chapter 4). This chapter presents the issues involved in this design process. Section 5.1 discusses some of the general AUV control system requirements and performance goals. Section 5.2 describes the derivation of the H_∞/μ-synthesis Standard-Form design model from the full-order LTI model. Next, Section 5.3 details the design of the full-order AUV controller using the H_∞ design methodology. Lastly, Section 5.4 details the design of the full-order AUV controller using μ-synthesis.

5.1 CONTROL SYSTEM SPECIFICATIONS

For the AUV control system design, the goal is to design a controller that accepts commands from the higher-level behavioral "planning" programs and tries to force the vehicle to follow these commands. As discussed in Chapter 4, sensors are available on the AUV for measuring depth, heading, heading rate, pitch and roll. Depth rate is estimated by back-differencing and filtering the sensed depth. Since an axial velocity transducer is not included in the AUV sensor suite, the forward speed of the vehicle is controlled with an open-loop strategy.

The most important requirement for the AUV control system is stability throughout the vehicle's ranges and modes of operation. This means that the controller must exhibit stability robustness for all valid bounded modeling perturbations. In terms of performance, the control system must be able to accept and follow with reasonable accuracy any and all combinations of valid heading and depth commands over the entire range of forward speeds commanded by the open-loop speed controller.

In classical control-design, LTI control-system performance is frequently defined in terms of quantitative measures (such as maximum steady-state error, percentage overshoot, and response time to step inputs). Target values for these classical performance measures are shown in Table 5.1.

Table 5.1: Preliminary AUV Control System Goals

Steady-State Depth Error	5%
Steady-State Heading Error	5%
Depth Overshoot	10 %
Heading Overshoot	10 %
Depth Response	10.0 seconds
Heading Response	5.0 seconds

These performance goals are based on what would be required for the AUV to complete a "typical" mission. Also, these goals are influenced by the maximum performance levels of the vehicle hardware, such as the thrusters. In addition, it is desirable to obtain these performance goals with minimum excitation of the pitch and roll dynamics of the vehicle.

5.2 DERIVATION OF THE FULL-ORDER STANDARD-FORM MODEL

Recall from Chapter 2 that the Standard Form (SF) model for robustness analysis and design is given by the general form shown in Figure 5.1.

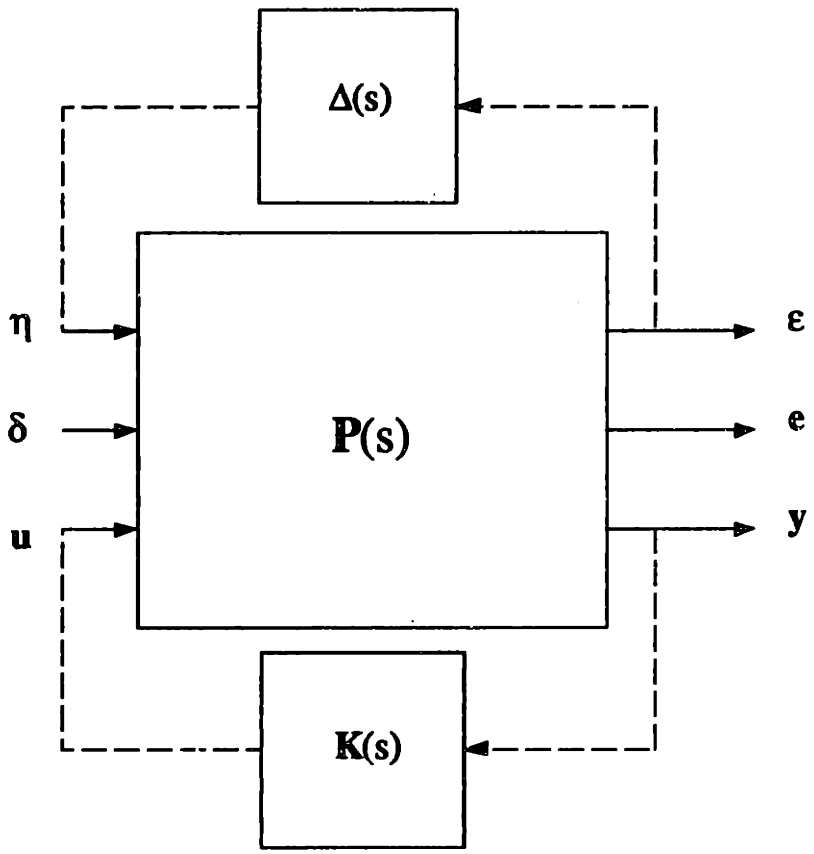

Figure 5.1: Standard Form Model

P(s) is the open-loop SF system, K(s) is a linear time-invariant (LTI) controller and Δ(s) is a norm-bounded perturbation matrix constructed with the block diagonal form

$$\Delta(s) = \begin{bmatrix} \Delta_1(s) & 0 & \cdots & 0 \\ 0 & \Delta_2(s) & & \vdots \\ \vdots & & \ddots & 0 \\ 0 & \cdots & 0 & \Delta_m(s) \end{bmatrix} \qquad (5.1)$$

Each block element term, $\Delta_i(s)$, (which can be multi-input, multi-output) represents a single source of bounded LTI modeling uncertainty in the system. The $\Delta_i(s)$ terms are normalized with frequency-dependent scaling weights (which are imbedded in P(s)) such that for each $\Delta_i(s)$,

$$\bar{\sigma}[\Delta_i(j\omega)] < 1 \quad \forall\ \omega \tag{5.2}$$

The outputs of the SF model of Figure 5.1 are an observation output vector, **y**, and a performance measure vector, **e**. The vector **e** consists of variables that are desired to be "small" (e.g., weighted tracking errors, control magnitudes, etc.). The inputs of the SF model are a control input vector, **u**, and a system disturbance vector, δ. The vector δ consists of all inputs external to the closed-loop system (e.g., weighted disturbance forces, reference signals, sensor-noise signals, etc.). The goal of the H_∞/μ-synthesis design methodology is to find the causal, stabilizing controller, K(s), that minimizes the influence of the external disturbances, δ, on the performance output, **e**, in the face of the perturbation $\Delta(s)$.

In order to apply the H_∞/μ-synthesis methodology to the design of the *Sea Squirt* AUV control system, the full-order LTI model derived in Chapter 4 must be converted into the Standard Form model described above. This involves defining both a parametric state-space uncertainty model and a frequency -domain "loop shaping" performance formulation.

5.2.1 Derivation of the AUV Parametric State-Space Uncertainty Model

Recall from Chapter 4 that the full-order AUV model (without sensor or thruster dynamics) is given by the following generalized state-space description

$$\mathbf{E_1\dot{x} = A_1x + B_1u + L_1d} \tag{5.3}$$

$$\mathbf{y = C_1x} \tag{5.4}$$

where the full-order state vector is defined by

$$\mathbf{x} = [\, u\ v\ w\ p\ q\ r\ Z\ \phi\ \theta\ \psi\,]^T \tag{5.5}$$

with a disturbance vector defined by

$$\mathbf{d} = [\, D_u\ D_v\ D_w\ D_p\ D_q\ D_r]^T \tag{5.6}$$

The input vector is defined by

$$\mathbf{u} = [T_v\ \ (T_p - T_s)\ \ (T_p + T_s)]^T \tag{5.7}$$

From the full-order eigenstructure analysis of Chapter 4, the total forward thrust given by T_p+T_s only strongly affects the stable, nearly unobservable mode associated with the axial velocity, u. Therefore, for the AUV design effort, only the vertical thrust, T_v, and the differential thrust, T_p-T_s, were used. The "reduced" input vector is then given by

$$\mathbf{u} = [T_v\ \ (T_p - T_s)]^T \tag{5.8}$$

The output vector is defined as the vector of variables actually measured and/or estimated by the vehicle's sensor suite

$$\mathbf{y} = [Z\ \psi\ \dot{Z}\ r\ \phi\ \theta]^T \tag{5.9}$$

From Chapter 2, parametric uncertainty in the full-order LTI system can be described by the following uncertainty model

$$\left(\mathbf{E}_{1o} - \sum_{j=1}^{m} [\Delta \mathbf{E}_1]_j \delta_j\right)\dot{\mathbf{x}} = \left(\mathbf{A}_{1o} + \sum_{i=1}^{k} [\Delta \mathbf{A}_1]_i \delta_i\right)\mathbf{x} + \left(\mathbf{B}_{1o} + \sum_{i=1}^{k} [\Delta \mathbf{B}_1]_i \delta_i\right)\mathbf{u} + \left(\mathbf{L}_{1o} + \sum_{i=1}^{k} [\Delta \mathbf{L}_1]_i \delta_i\right)\mathbf{d} \tag{5.10}$$

$$\mathbf{y} = \left(\mathbf{C}_{1o} + \sum_{i=1}^{k} [\Delta \mathbf{C}_1]_i \delta_i\right)\mathbf{x} \tag{5.11}$$

This uncertainty model consists of a set of nominal dynamics, $[\mathbf{E}_{1o},\mathbf{A}_{1o},\mathbf{B}_{1o},\mathbf{L}_{1o},\mathbf{C}_{1o}]$, plus a set of bounded parametric perturbation matrices, $[\Delta\mathbf{E}_1,\Delta\mathbf{A}_1,\Delta\mathbf{B}_1,\Delta\mathbf{L}_1,\Delta\mathbf{C}_1]$. The scalars, δ_i and δ_j, represent normalized parameter errors of the form

$$-1 < \delta_i < 1 \quad \forall\, i \tag{5.12}$$

$$-1 < \delta_j < 1 \quad \forall\, j \tag{5.13}$$

For a tenth-order system such as the AUV full-order model, the overall total number of parametric perturbations can be quite substantial (which has the effect of increasing the complexity of the design effort). In order to reduce the total number of perturbations, several simplifications were made. First, all of the "cross-coupling" uncertainties in the "descriptor" matrix, $\mathbf{E}_{1o}$, were assumed to be zero (which implied that all of the uncertainty was concentrated along the main diagonal of this matrix). Next, all of the parametric uncertainties in the pitch and roll dynamics were ignored, since control of the modes associated with these dynamics was not included as a specified goal of this design effort. These simplifications give the following structure for the bound on the parametric uncertainty in $\mathbf{E}_1$ and $\mathbf{A}_1$.

$$\left| \sum_{j=1}^{m} [\Delta E_1]_j \delta_j \right| \leq \begin{bmatrix} \left|\begin{matrix} \Delta e_{11} & 0 & 0 & 0 & 0 & 0 \\ 0 & \Delta e_{22} & 0 & 0 & 0 & 0 \\ 0 & 0 & \Delta e_{33} & 0 & 0 & 0 \\ 0 & 0 & 0 & 0 & 0 & 0 \\ 0 & 0 & 0 & 0 & 0 & 0 \\ 0 & 0 & 0 & 0 & 0 & \Delta e_{66} \end{matrix}\right| & \begin{matrix} \\ \\ \\ 0 \\ \\ \\ \end{matrix} \\ \begin{matrix} \\ \\ \\ \\ \\ \\ \end{matrix} & \begin{matrix} \\ \\ \\ \\ \\ \\ \end{matrix} \\ \begin{matrix} \\ \\ \\ 0 \\ \\ \\ \end{matrix} & \begin{matrix} \\ \\ \\ 0 \\ \\ \\ \end{matrix} \end{bmatrix} \tag{5.14}$$

$$\left| \sum_{i=1}^{k} [\Delta A_1]_i \delta_i \right| \leq \begin{bmatrix} \left|\begin{matrix} \Delta a_{11} & 0 & 0 & 0 & 0 & 0 \\ 0 & \Delta a_{22} & 0 & 0 & 0 & \Delta a_{26} \\ 0 & 0 & \Delta a_{33} & 0 & 0 & 0 \\ 0 & 0 & 0 & 0 & 0 & 0 \\ 0 & 0 & 0 & 0 & 0 & 0 \\ 0 & \Delta a_{62} & 0 & 0 & 0 & \Delta a_{66} \end{matrix}\right| & \begin{matrix} \\ \\ \\ 0 \\ \\ \\ \end{matrix} \\ \begin{matrix} \\ \\ \\ \\ \\ \\ \end{matrix} & \begin{matrix} \\ \\ \\ \\ \\ \\ \end{matrix} \\ \begin{matrix} \\ \\ \\ 0 \\ \\ \\ \end{matrix} & \begin{matrix} \\ \\ \\ 0 \\ \\ \\ \end{matrix} \end{bmatrix} \tag{5.15}$$

Note that the diagonal terms of $\Delta\mathbf{E}_1$ correspond to errors in the "added mass" hydrodynamic coefficients, while the diagonal terms of $\Delta\mathbf{A}_1$ correspond to errors in the "drag" coefficients. The off-diagonal terms, Δa_{26} and Δa_{62}, correspond to errors in the Munk moment coupling terms between the lateral velocity and the yaw rate. The "gain" properties of both the thrusters and sensors were assumed to be well known, which implied that uncertainties in the control-input matrix, $\mathbf{B}_1$, and uncertainties in the measured-output matrix, $\mathbf{C}_1$, could also be neglected. Uncertainties in the disturbance input matrix, $\mathbf{L}_1$, were neglected as well (since any uncertainty in this matrix can be "lumped" together with the uncertain disturbance vector, **d**).

For this design, the nominal operating point of the AUV was chosen to be the "straight ahead" condition at axial velocity of 1.0 ft/s (which corresponds to the "straight-ahead" model of Section 4.4.2). Bounds on the $\Delta\mathbf{E}_1$ perturbation matrices were chosen by assuming that each corresponding term in $\mathbf{E}_1$ has a 50% maximum uncertainty. Bounds on the $\Delta\mathbf{A}_1$ perturbation matrices were determined by performing a numerical comparison between the nominal design model and the full-order models corresponding to the "hovering" case and the "straight-reverse" case, described in Section 4.4.2. The nominal model was also numerically compared with an additional model corresponding to the case of a "full-speed" dive of 1.0 ft/sec and a "full-speed" turn of 15 deg/sec. From this comparison, the following numerical bounds were selected.

Table 5.2: Parametric Uncertainty Bounds for Full-Order LTI Model

Uncertainty Term	Perturbation Bound
Δe_{11}	1.1600
Δe_{22}	1.7250
Δe_{33}	1.6450
Δe_{66}	1.3400
Δa_{11}	1.6800
Δa_{22}	0.3000
Δa_{33}	7.2600
Δa_{66}	2.7964
Δa_{26}	3.8560
Δa_{62}	3.1400

These bounds were then used to convert the parametric-uncertainty matrices into the following representations

$$\sum_{j=1}^{m} [\Delta \mathbf{E}_1]_j \delta_j = [\mathbf{P}][\Delta_1][\mathbf{N}] \tag{5.16}$$

$$\sum_{i=1}^{k} [\Delta \mathbf{A}_1]_i \delta_i = [\mathbf{Q}][\Delta_2][\mathbf{S}] \tag{5.17}$$

For this uncertainty representation, **P**, **N**, **Q**, and **S** are constant-valued weighting matrices and Δ_1 and Δ_2 are complex perturbations with norm bounds

$$\bar{\sigma}[\Delta_1(j\omega)] < 1 \;\forall\; \omega \tag{5.18}$$

$$\bar{\sigma}[\Delta_2(j\omega)] < 1 \;\forall\; \omega \tag{5.19}$$

The AUV uncertainty model of (5.10) can be simplified to the form

$$\begin{aligned}
\dot{\mathbf{x}} &= \mathbf{E}_{1o}^{-1}\mathbf{A}_{1o}\mathbf{x} + \mathbf{E}_{1o}^{-1}\mathbf{B}_{1o}\,\mathbf{u} + \mathbf{E}_{1o}^{-1}\mathbf{L}_{1o}\mathbf{d} + \mathbf{E}_{1o}^{-1}\mathbf{P}\eta_1 + \mathbf{E}_{1o}^{-1}\mathbf{Q}\eta_2 \\
\varepsilon_1 &= \mathbf{N}\dot{\mathbf{x}} \\
&= \mathbf{N}\mathbf{E}_{1o}^{-1}\mathbf{A}_{1o}\mathbf{x} + \mathbf{N}\mathbf{E}_{1o}^{-1}\mathbf{B}_{1o}\mathbf{u} + \mathbf{N}\mathbf{E}_{1o}^{-1}\mathbf{L}_{1o}\mathbf{d} + \mathbf{N}\mathbf{E}_{1o}^{-1}\mathbf{P}\eta_1 \\
&\quad + \mathbf{N}\mathbf{E}_{1o}^{-1}\mathbf{Q}\eta_2 \\
\varepsilon_2 &= \mathbf{S}\mathbf{x}
\end{aligned} \tag{5.20}$$

where η_1 is the output of Δ_1, η_2 is the output of Δ_2, ε_1 is the input of Δ_1, and ε_2 is the input of Δ_1. A block diagram of this uncertainty model is shown in Figure 5.2.

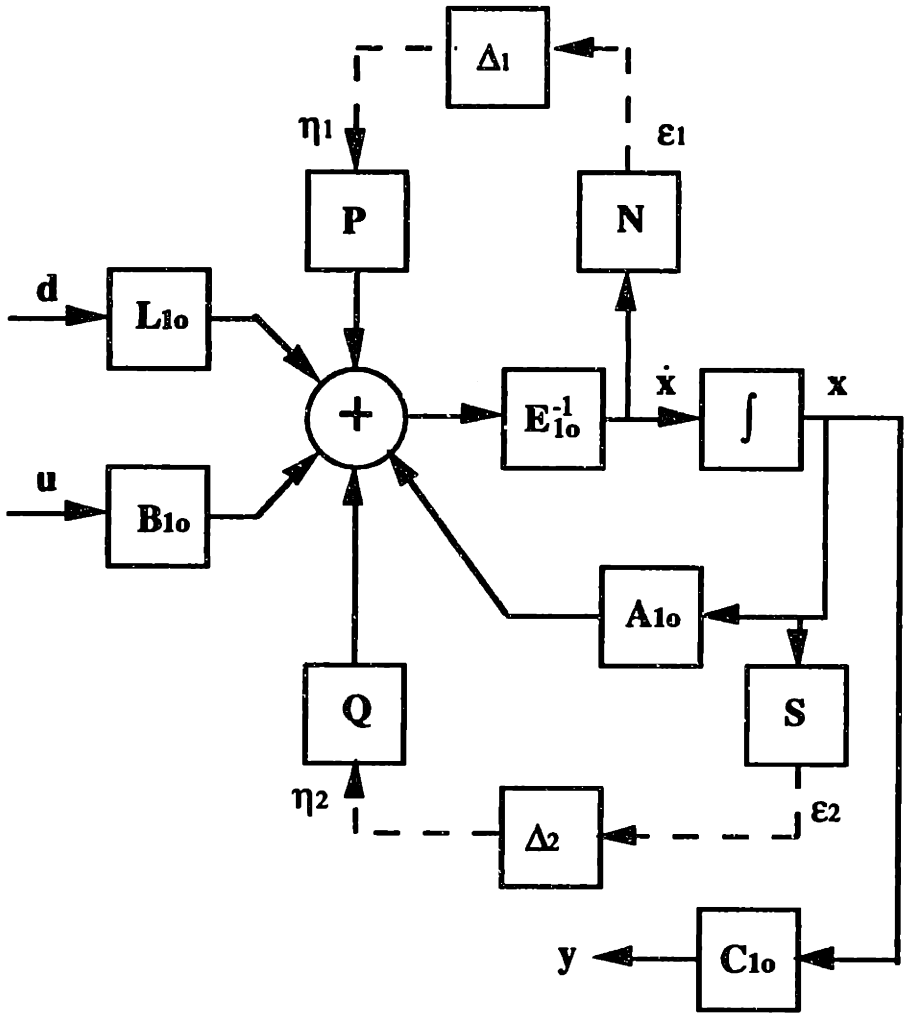

Figure 5.2: AUV Parametric State-Space Uncertainty Representation

5.2.2 Frequency-Domain Loop shaping Formulation

The AUV uncertainty model of Figure 5.2 cannot be directly used by the H_∞/μ-synthesis methodology to develop a reasonable design for the AUV control system. For example, this representation does not include tracking error, whose minimization is one of the specified goals of the AUV control-system design effort. In addition, this representation neglects any frequency-domain characteristics of the input variables. Since the H_∞/μ-synthesis design methodology tries to minimize the performance-measure function of the design plant over all frequencies, this can result in a design that is much too conservative.

Recall from Chapter 2 that one solution for this dilemma is to "loop shape" the performance transfer function using frequency-domain weighting functions. For the AUV H_∞/μ-Synthesis control design effort, the following structure (shown in Figure 5.3) was used for the "loopshaping" weighting functions.

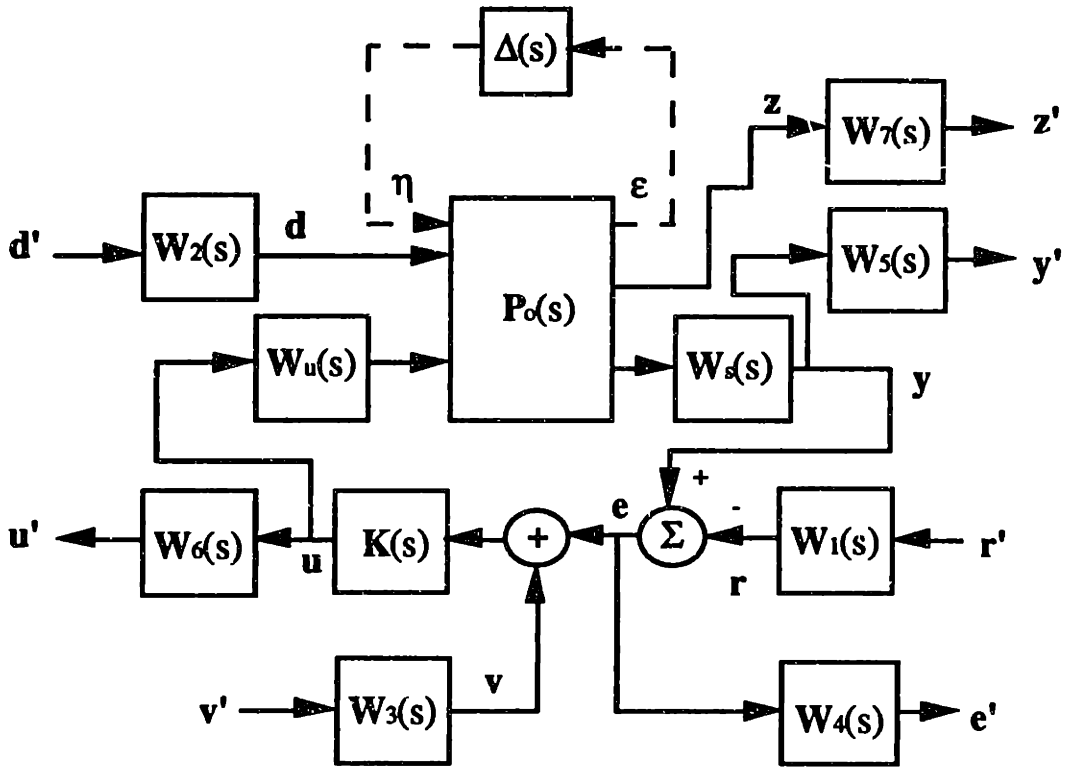

Figure 5.3: Weighted Closed-Loop Model

Here, $\mathbf{P_0}(s)$ is the full-order AUV parametric uncertainty model (with $\eta^T = [\,\eta_1{}^T\,\eta_2{}^T\,]$ and $\varepsilon^T = [\,\varepsilon_1{}^T\,\varepsilon_2{}^T\,]$) and $\mathbf{K}(s)$ is a stabilizing LTI controller. The vector **r** represents a "reference" signal, while the vector **e** represents the "tracking error" signal to the controller. The vector **v** represents a "measurement noise" input. The vector **z** represents the "unmeasured" states of the AUV (i.e., states not included in **y**). The vectors, **r'**, **d'**, and **v'**, represent unity-norm, "white noise" inputs, while the vectors, **e'**, **y'**, **u'**, and **z'**, are simply "weighted" performance" outputs. Note that this model also includes the thruster actuator dynamics, given by $\mathbf{W_u}(s)$, plus the sensor dynamics, given by $\mathbf{W_S}(s)$.

One means of representing the "nominal" (i.e., $\Delta(s) = 0$) closed-loop transfer function of this system is given by

$$\begin{bmatrix} \mathbf{e}' \\ \mathbf{y}' \\ \mathbf{u}' \\ \mathbf{z}' \end{bmatrix} = \begin{bmatrix} W_4(s)G_{er}(s)W_1(s) & W_4(s)G_{ed}(s)W_2(s) & W_4(s)G_{ev}(s)W_3(s) \\ W_5(s)G_{yr}(s)W_1(s) & W_5(s)G_{yd}(s)W_2(s) & W_5(s)G_{yv}(s)W_3(s) \\ W_6(s)G_{ur}(s)W_1(s) & W_6(s)G_{ud}(s)W_2(s) & W_6(s)G_{uv}(s)W_3(s) \\ W_7(s)G_{zr}(s)W_1(s) & W_7(s)G_{zd}(s)W_2(s) & W_7(s)G_{zv}(s)W_3(s) \end{bmatrix} \begin{bmatrix} \mathbf{r}' \\ \mathbf{d}' \\ \mathbf{v}' \end{bmatrix} \tag{5.21}$$

If a stabilizing controller, $\mathbf{K}(s)$, can be found such that the H_∞ norm of this weighted transfer function is less than unity, the actual closed-loop transfer function, $\mathbf{G}(s)$, of the AUV control system can be "shaped" in the desired fashion in the frequency domain.

It is not generally possible to simultaneously shape all of the elements of the transfer function matrix given by (5.21). However, by the appropriate choice of weights, an emphasis can be placed on shaping selected elements relative to all the others. For example, the "sensitivity" transfer function, $G_{er}(s)$, can be shaped by $W_1(s)$ and $W_4(s)$, while the "complementary sensitivity" transfer function, $G_{yr}(s)$, can be shaped by $W_1(s)$ and $W_5(s)$.

From this loopshaping formulation, the Standard-Form performance-measure vector, $\mathbf{e}$, for the full-order H_∞/μ-synthesis AUV control-design effort was chosen to be the output of (5.21), i.e.,

$$\mathbf{e} = \begin{bmatrix} \mathbf{e}' \\ \mathbf{y}' \\ \mathbf{u}' \\ \mathbf{z}' \end{bmatrix} \tag{5.22}$$

The Standard-Form "disturbance" input, δ, was simply chosen to be the input of (5.21), i.e.,

$$\delta = \begin{bmatrix} \mathbf{r}' \\ \mathbf{d}' \\ \mathbf{v}' \end{bmatrix} \tag{5.23}$$

5.3 H_∞ CONTROLLER DESIGN

Given the AUV Standard-Form (SF) design model of Section 5.2, a robust H_∞ controller was designed using the Small-Gain Theorem, together with other ideas from Chapters 2. The actual design procedure for the H_∞ controller consisted of several steps.

Model Scaling

First, the state vector, $\mathbf{x}$, the control input vector, $\mathbf{u}$, and the output, $\mathbf{y}$, of the full-order AUV parametric-uncertainty model were scaled by their respective expected maximum magnitudes, which led to

$$\mathbf{E}'_{1o} = \mathbf{E}_{1o}\mathbf{S}_x^{-1} \tag{5.24}$$

$$\mathbf{A}'_{1o} = \mathbf{A}_{1o}\mathbf{S}_x^{-1} \tag{5.25}$$

$$\mathbf{B}'_{1o} = \mathbf{B}_{1o}\mathbf{S}_u^{-1} \tag{5.26}$$

$$\mathbf{C}'_{1o} = \mathbf{S}_y\mathbf{C}_{1o}\mathbf{S}_x^{-1} \tag{5.27}$$

$$\mathbf{S}' = \mathbf{S}\mathbf{S}_x^{-1} \tag{5.28}$$

$$\mathbf{N}' = \mathbf{N}\mathbf{S}_x^{-1} \tag{5.29}$$

The disturbance input, **d**, and the perturbation matrices, **Q** and **P**, were left unscaled.

For the AUV control-design effort, the maximum expected values for the "controlled" states were assumed to be the maximum expected tracking error (which was assumed to be 1.0 ft. for depth, 1.0 ft/sec for depth rate, 10.0 deg. (0.175 rad) for heading, and 10.0 deg/sec (0.175 rad/sec) for heading rate). The maximum expected value for both roll and pitch was 10.0 deg., and the maximum expected value of both the roll rate and pitch rate was assumed to be 10.0 deg/sec. The maximum expected value for both the axial velocity and the lateral velocity was assumed to be 1.0 ft/sec. The maximum allowed thrust value for each thruster was 5.0 lb. Therefore, the scaling matrices were given by

$$\mathbf{S}_x = \begin{bmatrix} 1 & 0 & 0 & 0 & 0 & 0 & 0 & 0 & 0 & 0 & 0 & 0 \\ 0 & 1 & 0 & 0 & 0 & 0 & 0 & 0 & 0 & 0 & 0 & 0 \\ 0 & 0 & 1 & 0 & 0 & 0 & 0 & 0 & 0 & 0 & 0 & 0 \\ 0 & 0 & 0 & \frac{1}{0.175} & 0 & 0 & 0 & 0 & 0 & 0 & 0 & 0 \\ 0 & 0 & 0 & 0 & \frac{1}{0.175} & 0 & 0 & 0 & 0 & 0 & 0 & 0 \\ 0 & 0 & 0 & 0 & 0 & \frac{1}{0.175} & 0 & 0 & 0 & 0 & 0 & 0 \\ 0 & 0 & 0 & 0 & 0 & 0 & 1 & 0 & 0 & 0 & 0 & 0 \\ 0 & 0 & 0 & 0 & 0 & 0 & 0 & \frac{1}{0.175} & 0 & 0 & 0 & 0 \\ 0 & 0 & 0 & 0 & 0 & 0 & 0 & 0 & \frac{1}{0.175} & 0 & 0 & 0 \\ 0 & 0 & 0 & 0 & 0 & 0 & 0 & 0 & 0 & \frac{1}{0.175} & 0 & 0 \\ 0 & 0 & 0 & 0 & 0 & 0 & 0 & 0 & 0 & 0 & \frac{1}{0.175} & 0 \\ 0 & 0 & 0 & 0 & 0 & 0 & 0 & 0 & 0 & 0 & 0 & \frac{1}{0.175} \end{bmatrix} \tag{5.30}$$

$$\mathbf{S}_u = \begin{bmatrix} \frac{1}{5.0} & 0 \\ 0 & \frac{1}{5.0} \end{bmatrix} \tag{5.31}$$

$$\mathbf{S_y} = \begin{bmatrix} 1 & 0 & 0 & 0 & 0 & 0 \\ 0 & \frac{1}{0.175} & 0 & 0 & 0 & 0 \\ 0 & 0 & 1 & 0 & 0 & 0 \\ 0 & 0 & 0 & \frac{1}{0.175} & 0 & 0 \\ 0 & 0 & 0 & 0 & \frac{1}{0.175} & 0 \\ 0 & 0 & 0 & 0 & 0 & \frac{1}{0.175} \end{bmatrix} \tag{5.32}$$

Thruster and Sensor Dynamics

For the thruster dynamics, the unity-gain model presented in Section 4.6 was used, but with a first-order Pade approximation for the 0.2 second time-delay. Therefore, the thruster dynamics model, $\mathbf{W_u}(s)$, was given by

$$\mathbf{W_u}(s) = \begin{bmatrix} \frac{(-0.1s+1)}{(0.75s+1)(0.1s+1)} & 0 \\ 0 & \frac{(-0.1s+1)}{(0.75s+1)(0.1s+1)} \end{bmatrix} \tag{5.33}$$

From Section 4.6, the sensor dynamics were approximately the frequency order of the AUV sampling rate, which meant that they can be ignored for design purposes (so long as the final closed-loop bandwidth is sufficiently low). Therefore, the sensor dynamics model, $\mathbf{W_s}(s)$ was simply given by

$$\mathbf{W_s}(s) = \mathbf{I} \tag{5.34}$$

5.3.1 Selection of Weighting Functions

The next (and most important) step in the H_∞ design procedure was the selection of the frequency-dependent performance weighting functions. The depth dynamics and the heading dynamics of the AUV full-order linear model were essentially decoupled, which allowed for separate (but concurrent) designs of the AUV's depth and heading control systems.

From this decoupling effect, the reference input and the (scaled) "reference" weighting function, $W_1(s)$, were reduced to the following form

$$\mathbf{r} = \mathbf{S_y W_1}(s)\mathbf{r}'$$

$$= \begin{bmatrix} w_{111}(s) & 0 \\ 0 & \frac{1}{0.175} w_{122}(s) \\ s(w_{111}(s)) & 0 \\ 0 & s\left(\frac{1}{0.175} w_{122}(s)\right) \\ 0 & 0 \\ 0 & 0 \end{bmatrix} \begin{bmatrix} Z_d' \\ \psi_d' \end{bmatrix} \qquad (5.35)$$

The weight $w_{111}(s)$ was used for depth control design and the weight $w_{122}(s)$ was used for heading control design. The structure of this weighting function reflects the fact that the rate references are given by the corresponding derivatives of the position references. In addition, this function also reflects the desire to keep the pitch and roll angles as small as possible. Note that the structure of $W_1(s)$ implies that both the weights, $w_{111}(s)$ and $w_{122}(s)$, must be strictly proper (i.e., at least 20 dB/dec roll-off), in order for (5.35) to be proper.

The decoupling of the depth and heading dynamics also meant that the (scaled) "measurement noise" weight, $W_3(s)$, the (scaled) "error" weight, $W_4(s)$, and the (scaled) "output" weight, $W_5(s)$, could be simplified to the following diagonal forms

$$\mathbf{v} = \mathbf{S_y W_3(s) v'}$$

$$= \begin{bmatrix} w_{311}(s) & 0 & 0 & 0 & 0 & 0 \\ 0 & \frac{1}{0.175}w_{322}(s) & 0 & 0 & 0 & 0 \\ 0 & 0 & w_{333}(s) & 0 & 0 & 0 \\ 0 & 0 & 0 & \frac{1}{0.175}w_{344}(s) & 0 & 0 \\ 0 & 0 & 0 & 0 & \frac{1}{0.175}w_{355}(s) & 0 \\ 0 & 0 & 0 & 0 & 0 & \frac{1}{0.175}w_{366}(s) \end{bmatrix} \begin{bmatrix} v'_Z \\ v'_\psi \\ v'_{\dot{Z}} \\ v'_r \\ v'_\phi \\ v'_\theta \end{bmatrix} \quad \textbf{(5.36)}$$

$$\mathbf{e' = S_y^{-1} W_4(s) e}$$

$$= \begin{bmatrix} w_{411}(s) & 0 & 0 & 0 & 0 & 0 \\ 0 & 0.175w_{422}(s) & 0 & 0 & 0 & 0 \end{bmatrix} \begin{bmatrix} Z - Z_d \\ \psi - \psi_d \\ \dot{Z} - \dot{Z}_d \\ r - \dot{\psi}_d \\ \phi - \phi_d \\ \theta - \theta_d \end{bmatrix} \quad \textbf{(5.37)}$$

$$\mathbf{y' = S_y^{-1} W_5(s) y}$$

$$= \begin{bmatrix} w_{511}(s) & 0 & 0 & 0 & 0 & 0 \\ 0 & 0.175w_{522}(s) & 0 & 0 & 0 & 0 \\ 0 & 0 & 0 & 0 & 0.175w_{535}(s) & 0 \\ 0 & 0 & 0 & 0 & 0 & 0.175w_{546}(s) \end{bmatrix} \begin{bmatrix} Z \\ \psi \\ \dot{Z} \\ r \\ \phi \\ \theta \end{bmatrix} \quad \textbf{(5.38)}$$

The structure of $W_3(s)$ implies that the measurement noises in the depth tracking error, in the heading tracking error, in the depth rate tracking error, in the heading rate tracking error, in the roll angle, and in the pitch angle, are decoupled from each other.

Recall from Section 5.2.2 that if a stabilizing controller, K(s), can be found such that the H_∞ norm of (5.21) is less than unity, the actual closed-loop transfer function, G(s), of the AUV control system can be "shaped" in the desired fashion in the frequency domain. For this design effort, the sensitivity (i.e., from the position reference to the position error) closed-loop transfer function was shaped by $W_1(s)$ and $W_4(s)$, while the complementary sensitivity (i.e., from the position measurement-noise input to the position output) transfer function, was shaped by $W_3(s)$ and $W_5(s)$. Therefore, the structures of $W_4(s)$ and $W_5(s)$ were chosen such that the emphasis of the H_∞ loopshaping was placed on the depth and heading position control loop (even though the depth rate and the heading rate were used as part of the input to the controller).

For this case, the weights, $w_{311}(s)$, $w_{411}(s)$, $w_{433}(s)$, and $w_{511}(s)$, were used for depth control design and the weights, $w_{322}(s)$, $w_{344}(s)$, $w_{422}(s)$, and $w_{522}(s)$, were used for heading control design. The weights, $w_{535}(s)$ and $w_{546}(s)$, were used simply as a penalty on the roll and pitch (for numerical computational-robustness purposes). Using the submultiplicative and "dilation and contraction" properties of the H_∞ norm (discussed in Section 2.4.2), it can be shown that the upper bounds for singular-value frequency response of the depth position sensitivity and complementary sensitivity transfer functions are given by

$$\bar{\sigma}[G_{(Z-Z_d)Z_d}(j\omega)] < \frac{1}{(\bar{\sigma}[W_{111}(j\omega)])(\bar{\sigma}[W_{411}(j\omega)])} \quad \forall\ \omega \tag{5.39}$$

$$\bar{\sigma}[G_{Zv_Z}(j\omega)] < \frac{1}{(\bar{\sigma}[W_{311}(j\omega)])(\bar{\sigma}[W_{511}(j\omega)])} \quad \forall\ \omega \tag{5.40}$$

Similarly, the upper bounds for the singular-value frequency response of the heading position sensitivity and complementary transfer functions can be shown to be given by

$$\bar{\sigma}[G_{(\psi - \psi_d)\psi_d}(j\omega)] < \frac{1}{(\bar{\sigma}[W_{122}(j\omega)])(\bar{\sigma}[W_{422}(j\omega)])} \quad \forall \omega \tag{5.41}$$

$$\bar{\sigma}[G_{\psi v_\psi}(j\omega)] < \frac{1}{(\bar{\sigma}[W_{322}(j\omega)])(\bar{\sigma}[W_{522}(j\omega)])} \quad \forall \omega \tag{5.42}$$

For the AUV control design effort, it was desired to have a closed-loop bandwidth of approximately 0.5 rad/sec for the depth control loop and a closed-loop bandwidth of approximately 1.0 rad/sec for the heading control loop (in order to be below the bandwidth of the thrusters and in order to not excite the pitching dynamics). In addition, it was desired for the position complementary sensitivity transfer function to have a 40 dB/dec "roll off", and be below 40 dB at 5.0 rad/sec for the depth control loop, and be below 10.0 rad/sec for the heading control loop, while reducing the position-sensitivity transfer function as much as possible.

For this design effort, the position reference inputs were assumed to be bandlimited and low-frequency. Therefore, the reference weights were chosen to be low-pass with an upper cutoff frequency equal to the target closed-loop bandwidths

$$w_{111}(s) = \frac{0.5^2}{(s + 0.5)^2} \tag{5.43}$$

$$w_{122}(s) = \frac{1}{(s + 1)^2} \tag{5.44}$$

The position measurement noise weights were chosen to be high-pass with a lower cutoff frequency equal to the target closed-loop bandwidths.

$$w_{311}(s) = \frac{(s + 0.05)^2}{(s + 0.5)^2} \tag{5.45}$$

$$w_{322}(s) = \frac{(s + 0.1)^2}{(s + 1)^2} \tag{5.46}$$

A plot of these weighting functions is shown in Figures 5.4-5.5. Note that the sum of the magnitude of the reference weight and the magnitude of the corresponding measurement noise weight is approximately equal to unity.

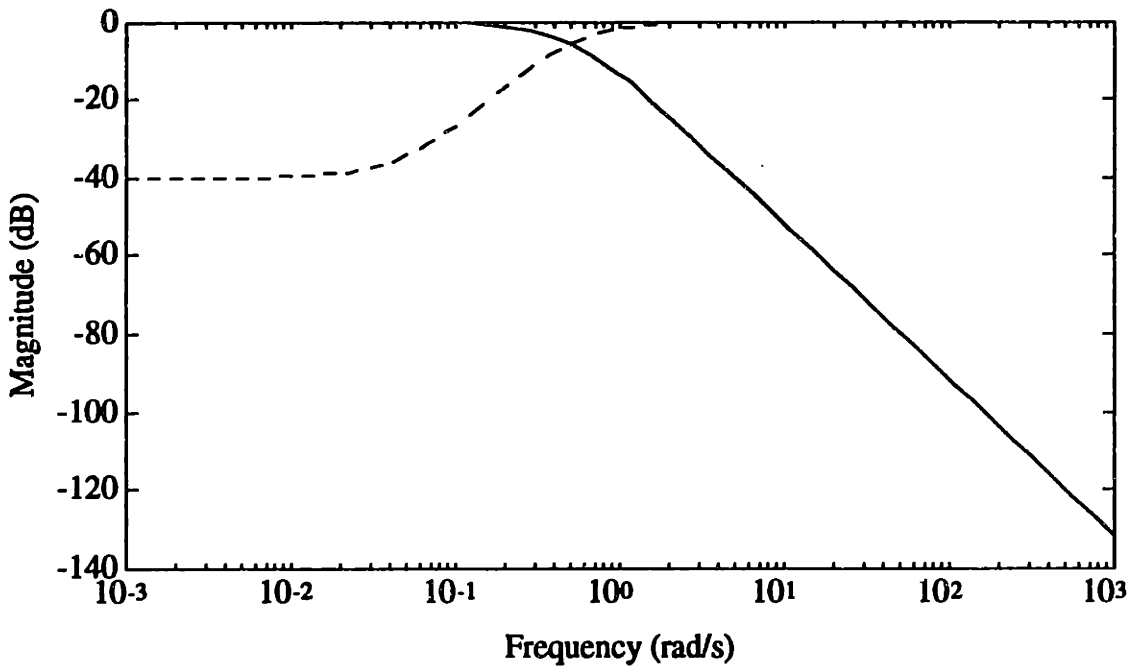

Figure 5.4 : Reference (-) & Measurement noise (--) weights ($W_{111}(s)$ & $W_{311}(s)$)

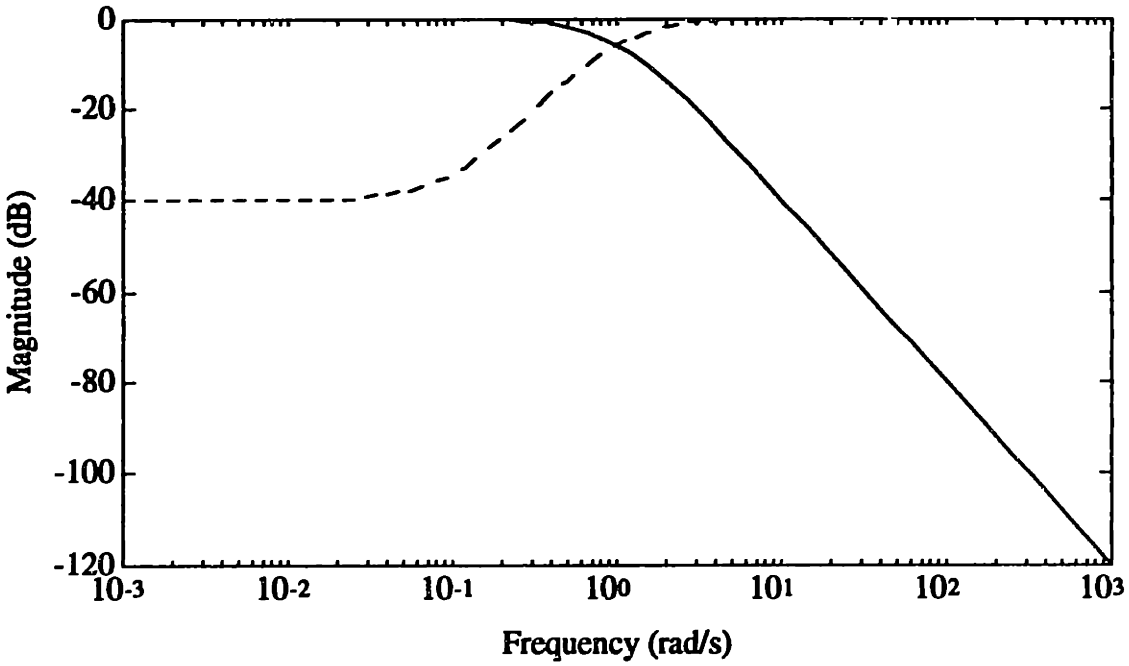

Figure 5.5 : Reference (-) & Measurement noise (--) weights ($W_{122}(s)$ & $W_{322}(s)$)

In addition, the "velocity" measurement noise weight (plus the roll and pitch measurement noise weights) was chosen to be high-pass, with a lower cutoff frequency equal to the target closed-loop bandwidths. This gave

$$w_{333}(s) = \frac{1.5(s + 0.05)^2}{(s + 0.5)^2} \qquad (5.47)$$

$$w_{344}(s) = \frac{(s + 0.1)^2}{(s + 1)^2} \qquad (5.48)$$

$$w_{355}(s) = \frac{5(s + 0.1)^2}{(s + 1)^2} \qquad (5.49)$$

$$w_{366}(s) = \frac{5(s + 0.1)^2}{(s + 1)^2} \qquad (5.50)$$

The measurement noise for roll and pitch were scaled by 5.0 in order to decrease the relative loop gain of the roll and pitch control loops. In an intuitive sense, this scaling forces the controller to rely more on the "less noisy" depth and heading measurements. The measurement noise for the depth rate was scaled in a similar fashion by 1.5 (in order to decrease the controller's reliance on the relatively "noisy" back-differenced depth rate estimate). Note that these measurement noise weights do not bear any relationship to the actual sensor noise models, but are simply used as a design tool in the loopshaping process.

Next, the position "error" weights and the position "output weights were chosen (with the condition that the loopshaping upper bounds for the position sensitivity and complementary sensitivity satisfy the frequency-domain design specifications stated earlier). This gave

$$w_{411}(s) = \frac{\gamma_{411}(s + 0.5)^2}{(s + 0.05)^2} \tag{5.51}$$

$$w_{422}(s) = \frac{\gamma_{422}(s + 1)^2}{(s + 0.1)^2} \tag{5.52}$$

$$w_{511}(s) = \frac{\gamma_{511}[10(s + 0.5)]^2}{(s + 5)^2} \tag{5.53}$$

$$w_{522}(s) = \frac{\gamma_{522}[10(s + 1)]^2}{(s + 10)^2} \tag{5.54}$$

Plots of the upper bounds for the position sensitivity and complementary sensitivity are shown in Figures 5.6-5.7 (for the case of where all the "γs" are equal to unity). Note that both these bounds cross the 0.0 dB line at the target closed-loop bandwidths.

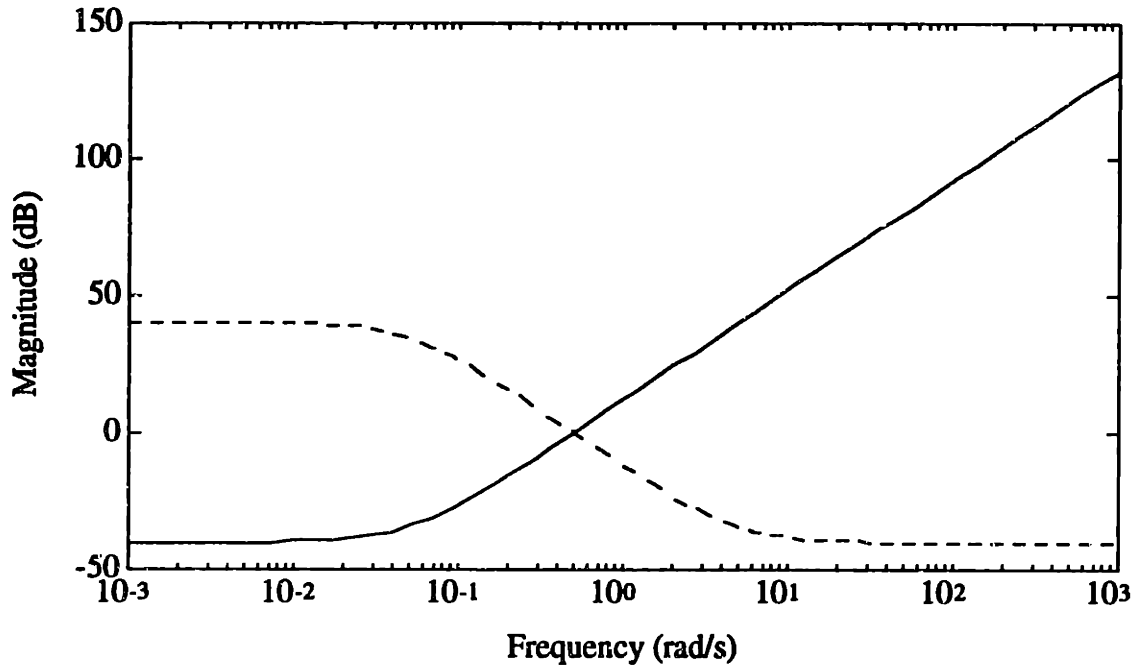

Figure 5.6: Depth Sensitivity (-) and Complementary Sensitivity (--) Bounds

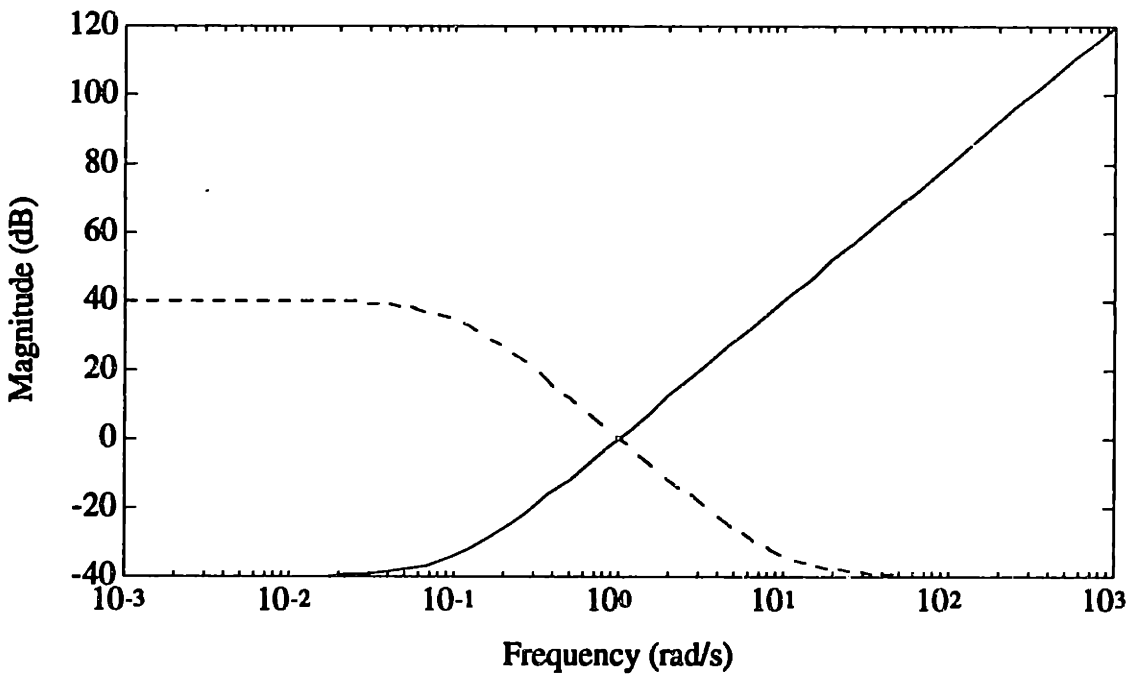

Figure 5.7: Heading Sensitivity (-) and Complementary Sensitivity (--) Bounds

These upper bounds imply that the sensitivity is primarily shaped in the low-frequency range, while the complementary sensitivity is primarily shaped in the high-frequency range. However, they *do not* imply that the singular-value frequency responses of the sensitivity and complementary sensitivity will have the exact shapes given by Figures 5.6-5.7.

The output weights for roll and pitch, $w_{535}(s)$ and $w_{546}(s)$, were simply chosen to be scalars (since control of roll and pitch is not one of the specified goals of the AUV design effort). This gave

$$w_{535}(s) = \gamma_{535} \tag{5.55}$$

$$w_{546}(s) = \gamma_{546} \tag{5.56}$$

The disturbance weighting function was reduced to the following form

$$\mathbf{d} = \mathbf{W}_2(s)\mathbf{d}'$$

$$= \begin{bmatrix} 0 & 0 \\ 0 & 0 \\ w_{231}(s) & 0 \\ 0 & 0 \\ 0 & 0 \\ 0 & w_{262}(s) \end{bmatrix} \begin{bmatrix} D_w' \\ D_r' \end{bmatrix} \tag{5.57}$$

In a physical sense, this function reflects the desire to only consider the disturbances that directly affect the AUV's depth and heading (i.e., the vertical disturbance force, D_w, and the yawing disturbance moment, D_r). For this design effort, both disturbances were assumed to be low-frequency, with bandwidths approximately equal to the target closed-loop bandwidths. This gave

$$w_{231}(s) = \frac{0.01(s + 50)}{(s + 0.5)} \tag{5.58}$$

$$w_{262}(s) = \frac{0.01(s + 100)}{(s + 1)} \tag{5.59}$$

The control input, weighting function, $W_6(s)$, was reduced to the following diagonal form (from the decoupling of the depth and heading dynamics).

$$\begin{aligned} \mathbf{u}' &= W_6(s)S_u^{-1}\mathbf{u} \\ &= \begin{bmatrix} 5w_{611}(s) & 0 \\ 0 & 5w_{622}(s) \end{bmatrix} \begin{bmatrix} T_v \\ (T_p - T_s) \end{bmatrix} \end{aligned} \tag{5.60}$$

Both the vertical thrust weight, w611(s), and the differential thrust weight, w622(s), were chosen to be high-pass transfer functions of the form

$$w_{611}(s) = \frac{\gamma_{611}100(s + 0.05)}{(s + 50)} \tag{5.61}$$

$$w_{622}(s) = \frac{\gamma_{622}100(s + 0.1)}{(s + 100)} \tag{5.62}$$

Note that this selection of weights implies that both control inputs are penalized more at the higher frequencies.

For the AUV control design effort, the "unmeasured-state" output vector, **z**, consisted of the vehicle-relative axial and lateral velocities, plus the vehicle-relative roll rate and pitch rate. The following structure was then chosen for the unmeasured-state weighting function, $W_7(s)$ (with the appropriate scaling, S_z, on **z**),

$$\mathbf{z}' = \mathbf{W}_7(s)\mathbf{S}_z^{-1}\mathbf{z}$$

$$= \begin{bmatrix} w_{711}(s) & 0 & 0 & 0 \\ 0 & w_{722}(s) & 0 & 0 \\ 0 & 0 & 0.175w_{733}(s) & 0 \\ 0 & 0 & 0 & 0.175w_{744}(s) \end{bmatrix} \begin{bmatrix} u \\ v \\ p \\ q \end{bmatrix} \quad (5.63)$$

Each of the weights, w711(s), w722(s),w733(s), and w744(s), was chosen for simplicity to be scalars (since no frequency-domain characteristics were specified for z)

$$w_{711}(s) = \gamma_{711} \quad (5.64)$$

$$w_{722}(s) = \gamma_{722} \quad (5.65)$$

$$w_{733}(s) = \gamma_{733} \quad (5.66)$$

$$w_{744}(s) = \gamma_{744} \quad (5.67)$$

5.3.2 H_∞ Compensator Synthesis Using Gamma Iteration

The next step in the H_∞ design procedure was to synthesize the H_∞ compensator from the AUV Standard-Form design model (with the set of weighting functions from the previous section) using the gamma-iteration algorithm from Chapter 2. A balanced-fractional model reduction algorithm (described in Appendix E) was also used in order to increase the numerical robustness of the compensator synthesis (in addition to removing any uncontrollable or unobservable states in either the design model or the controller).

Recall from Chapter 2 that the Small-Gain based H_∞ design algorithm tends to produce unnecessarily conservative control designs for real, structured perturbations (such as the AUV parametric uncertainty model). This implies that it may not be possible, using the H_∞ design technique, to find a stabilizing controller for the AUV that is guaranteed to be

robust over the full range of parametric modeling uncertainty. Therefore, the perturbation matrices were scaled in the following manner

$$\mathbf{N}'' = \sqrt{\gamma_{\Delta E}}\,\mathbf{N}' \tag{5.68}$$

$$\mathbf{P}' = \sqrt{\gamma_{\Delta E}}\,\mathbf{P} \tag{5.69}$$

$$\mathbf{Q}' = \sqrt{\gamma_{\Delta A}}\,\mathbf{Q} \tag{5.70}$$

$$\mathbf{S}'' = \sqrt{\gamma_{\Delta A}}\,\mathbf{S}' \tag{5.71}$$

For the first compensator design iteration, a "small" initial value of 0.01 was chosen for all the performance γ's. Then, the perturbation γ's were increased from zero until the control design began to fail the Small-Gain robustness test. From this procedure, the following values were selected for $\gamma_{\Delta E}$ and $\gamma_{\Delta A}$.

$$\gamma_{\Delta E} = 0.025 \tag{5.72}$$

$$\gamma_{\Delta A} = 0.025 \tag{5.73}$$

For this case, from the model-reduction algorithm, the bounds on the additive model error versus model order are shown in Figure 5.8.

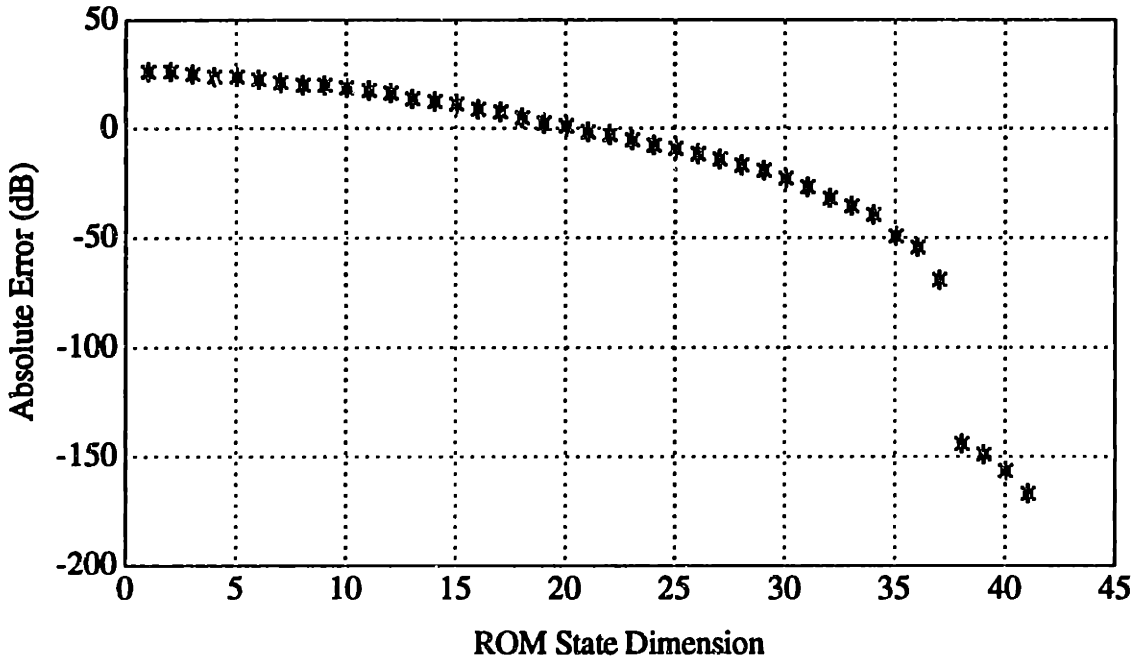

Figure 5.8: Fractional-Balanced Additive Error Bounds

Note the fairly sharp increase in the model error from the 38-state level to the 37-state level. This implies that the 37-state model is a significantly less accurate representation than the 38-state model. Also note that there is relatively little improvement in the model accuracy beyond the 38-state level. Therefore, the 38-state SF model was judged to be sufficiently accurate for the H_∞ design.

The plot of the normalized Hankel singular-values of the SF model versus model order is shown in Figure 5.9.

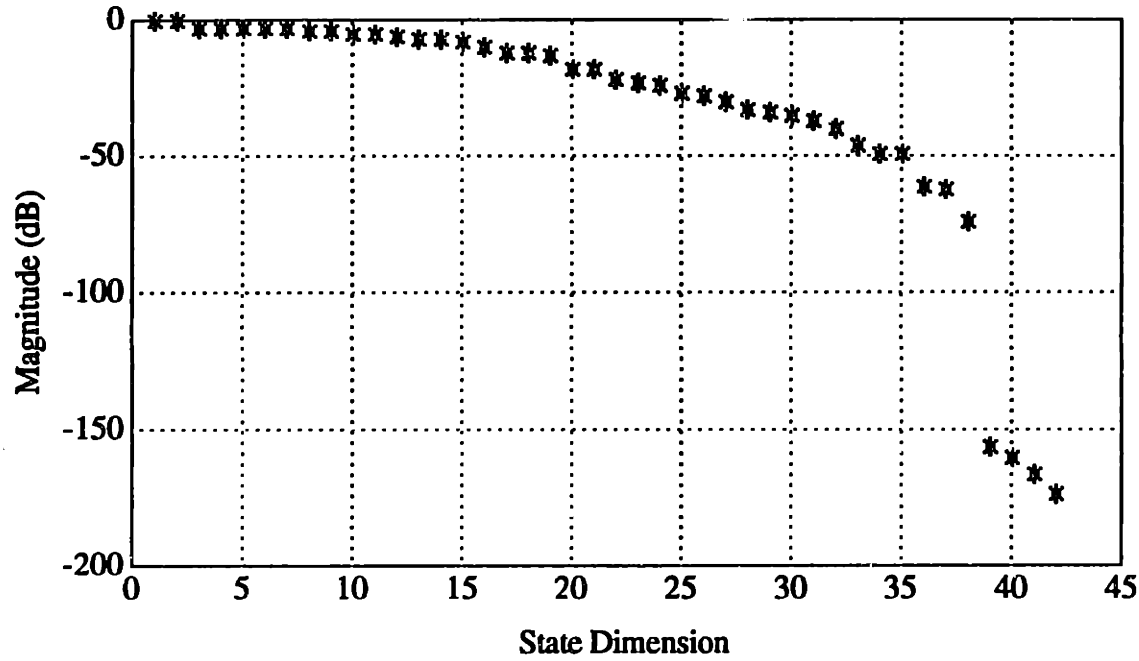

Figure 5.9: Hankel Singular Values

From this plot, all of the Hankel singular values of the 38-state model are nonzero. From Appendix E, this implies that the 38-state model is minimal (as desired). Again, note the sharp drop-off around the 38-state level. From Appendix E, this confirms that the states beyond this level are much less controllable or observable than the lower order states and can be truncated without difficulty.

For this reduced-order SF model, an H_∞ compensator was then synthesized using gamma iteration. Initial upper and lower bounds of 10 and 0.1, respectively, on the H_∞ norm were used for this design, with a convergence tolerance of 1%. After several iterations, the algorithm converged to an H_∞ norm bound of approximately 0.8131. The singular-value frequency response of this controller is shown in Figure 5.10

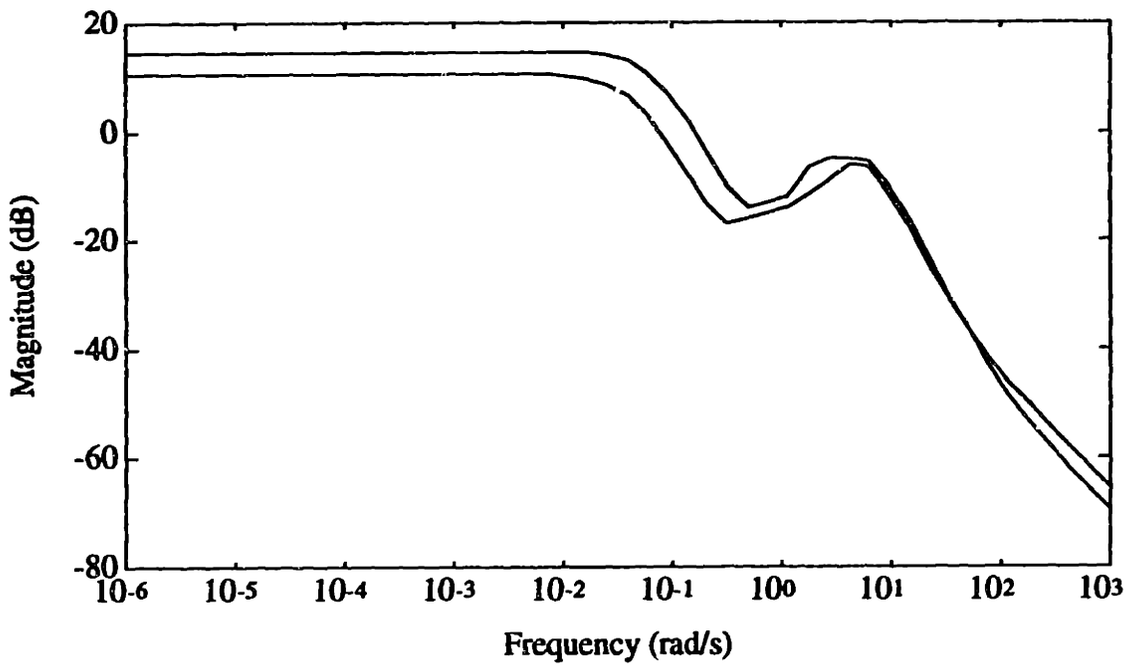

Figure 5.10: Unscaled Compensator Frequency Response (Initial Design)

The position sensitivity and complementary sensitivity of this initial design are shown in Figure 5.11

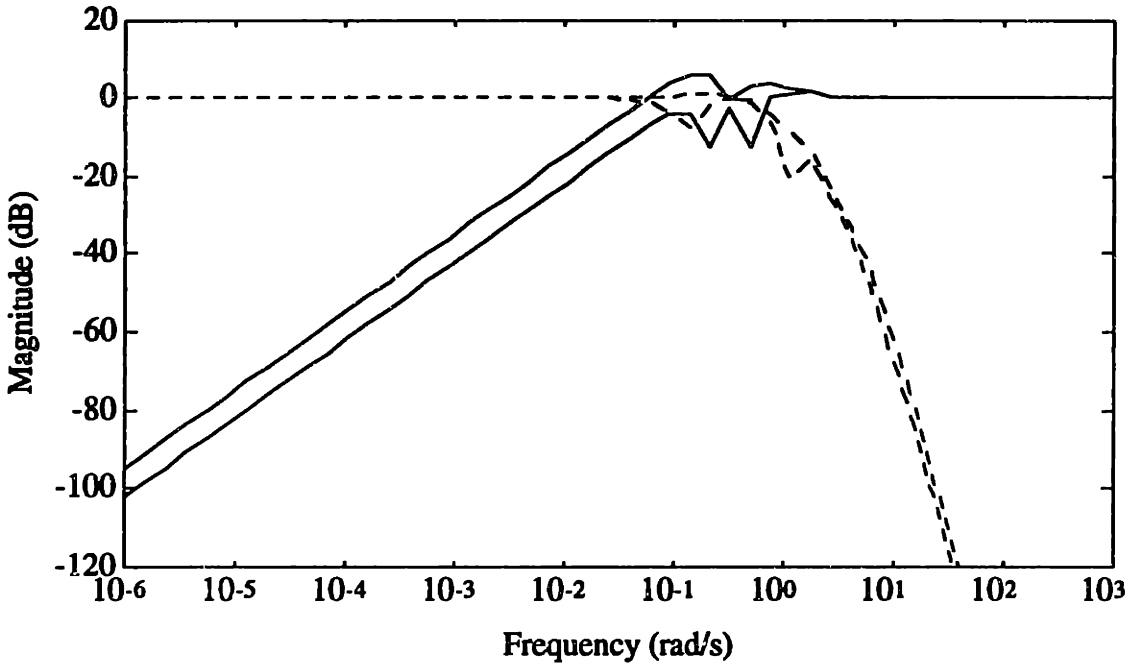

Figure 5.11: Sensitivity (-) and Complementary Sensitivity (--) (Initial Design)

From this plot, the initial design appears to approximately meet the nominal bandwidth requirements, with closed-loop bandwidths of about 0.5 rad/sec and 1.0 rad/sec, respectively for depth and heading. Interestingly, the sensitivity has a 20 dB/dec roll off, while the complementary sensitivity has an 80 dB/dec roll-off. The peak magnitude of the sensitivity is approximately 6.0 dB (i.e., a peak magnitude of approximately 2.0). This indicates that it may be possible to reduce the bound on this transfer function even further (as well as possibly reducing the bound on the complementary sensitivity).

For the next design iteration, the weightings on the position error and position output were increased by 10 (i.e., $\gamma_{411} = 0.1$, $\gamma_{422}=0.1$, $\gamma_{511}=0.1$, $\gamma_{522}=0.1$). Again, by using the fractional-balanced model-reduction algorithm, a 38-state reduced-order SF model was judged to be sufficiently accurate for the H_∞ design.

Next, a new H_∞ compensator was synthesized using gamma iteration. Initial upper and lower bounds of 10 and 0.1, respectively, on the H_∞ norm were used for this design, with a convergence tolerance of 1%. After several iterations, the gamma-iteration algorithm converged to an H_∞ norm bound of approximately 0.8131. The frequency response of this controller is shown in Figure 5.12

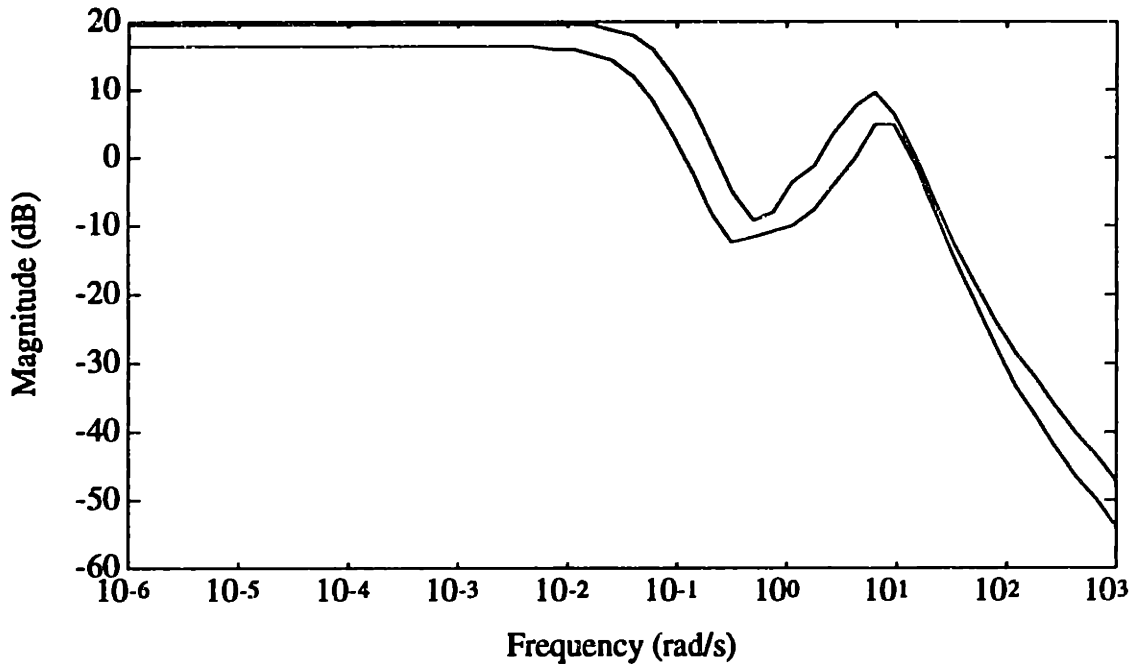

Figure 5.12: Unscaled Compensator Frequency Response (Second Design)

The frequency response of this controller is very similar to the initial controller, but with a lower gain at the low frequencies.

The position sensitivity and complementary sensitivity of this design are shown in Figure 5.13

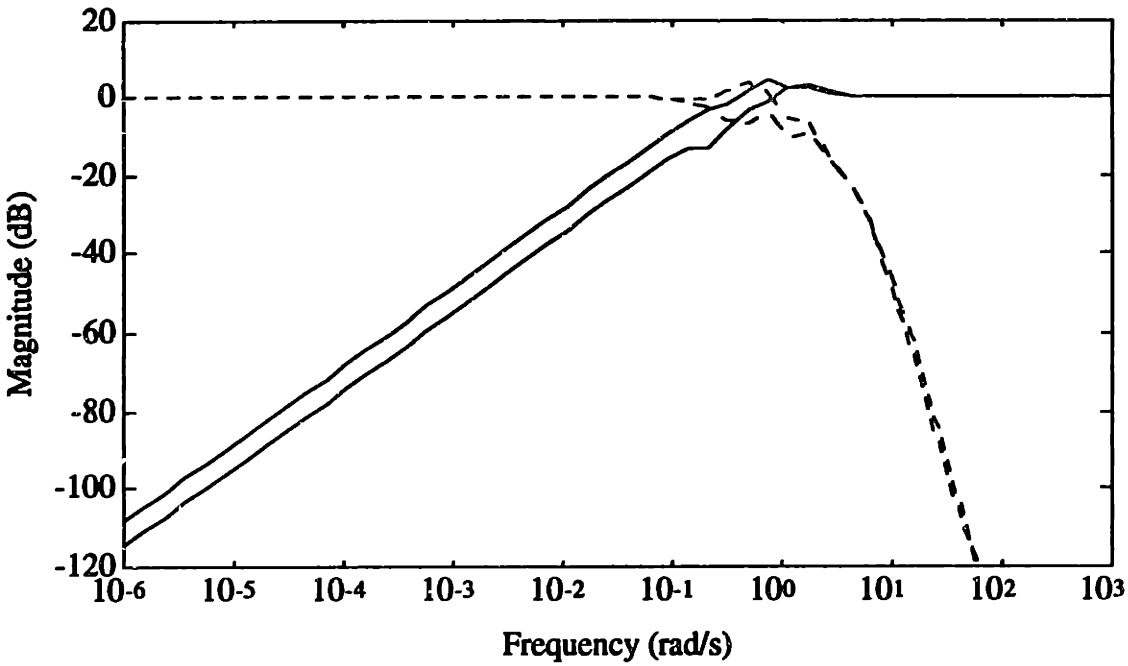

Figure 5.13: Sensitivity (-) and Complementary Sensitivity (--) (Second Design)

From this plot, the second design meets the nominal bandwidth requirements quite well, with closed-loop bandwidths of approximately 0.5 rad/sec and 1.0 rad/sec, respectively for depth and heading. Again, note that the sensitivity has a 20 dB/dec roll off, while the complementary sensitivity has an 80 dB/dec roll-off. The peak magnitude characteristics of both the sensitivity and complementary sensitivity are somewhat better than the initial design (i.e., a peak magnitude of less than 3 dB). The complementary sensitivity also meets the specification of being below 40 dB at 10 rad/sec for heading (but does not quite meet the corresponding specification at 5.0 rad/sec for depth). The complementary sensitivity also appears to have a "notch" at 1.0 rad/sec. This is probably caused by the controller attempting to suppress the effects of the pitching dynamics.

5.3.3 H_∞ Closed-Loop Linear Performance

Given the compensator synthesized in Section 5.3.2, the final step in the H_∞ design process was to evaluate its time-domain performance for the full-order LTI models of Section 4.4, in order to determine if it meets the specifications of Section 5.1. This was done by evaluating the separate time-domain responses of the closed-loop system to a 1.0 ft. step in depth and a 10.0 deg. step in heading.

Nominal Performance

The first performance evaluation was done using the nominal "full ahead" LTI model linearized about an axial velocity, u_0, of 1.0 ft/s. The depth step response of this model is shown in Figure 5.14, and the heading step response is shown in Figure 5.15. Numerical values for the step performance are shown in Table 5.3.

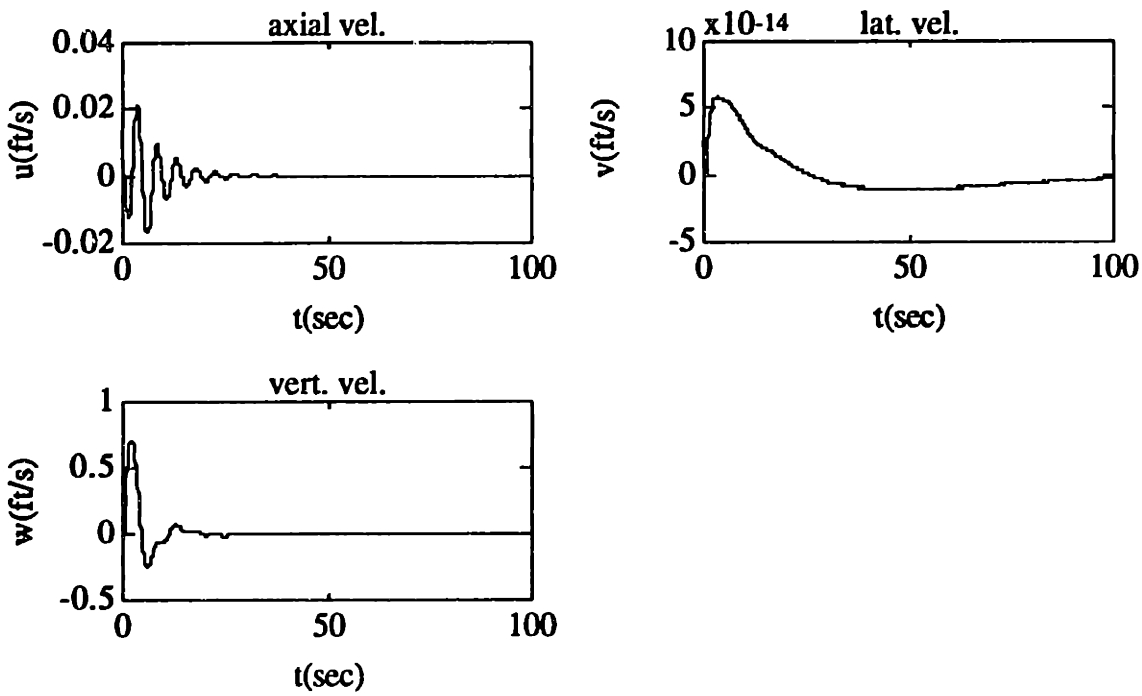

Figure 5.14: Nominal Depth Step Response

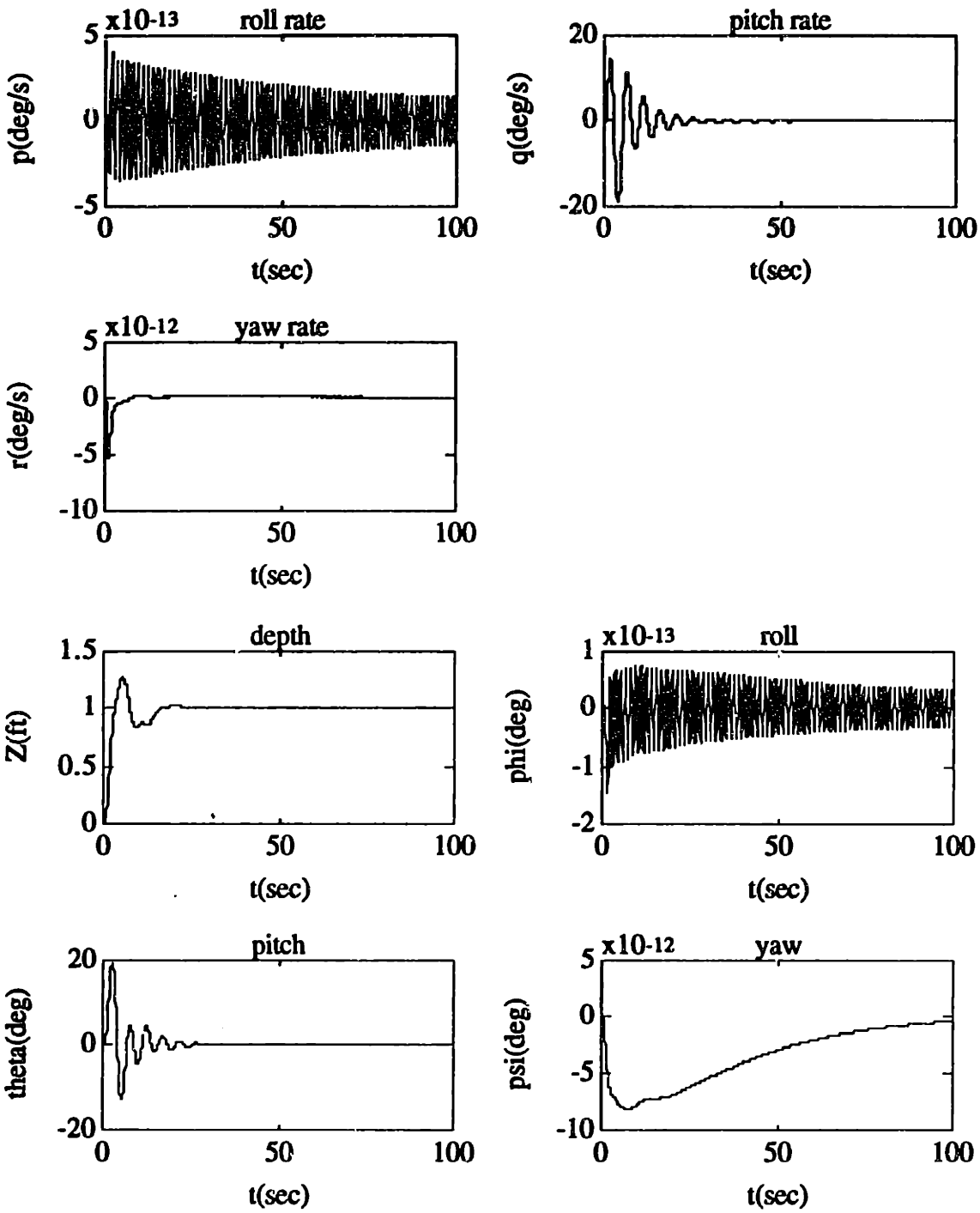

Figure 5.14: Nominal Depth Step Response (continued)

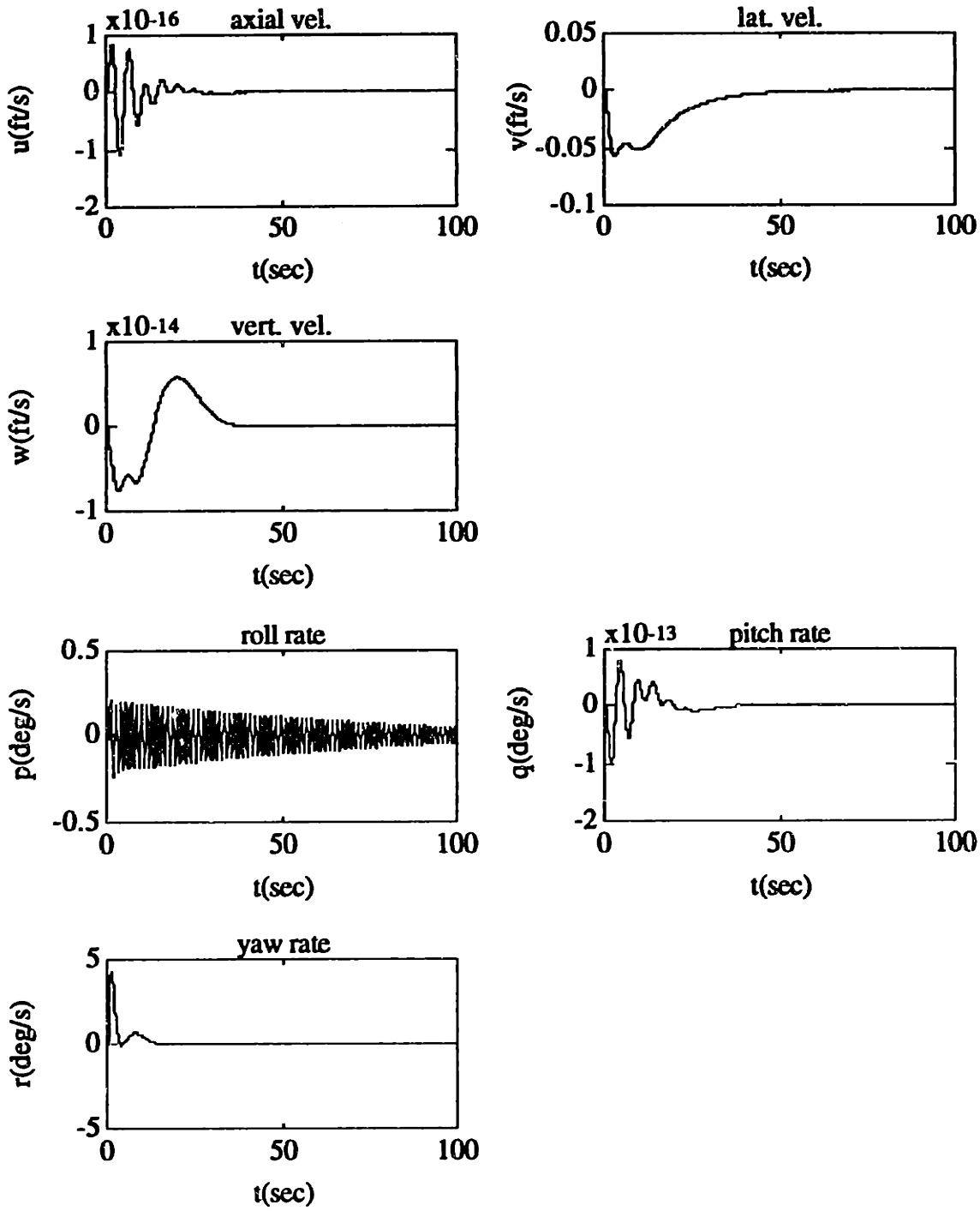

Figure 5.15: Nominal Heading Step Response

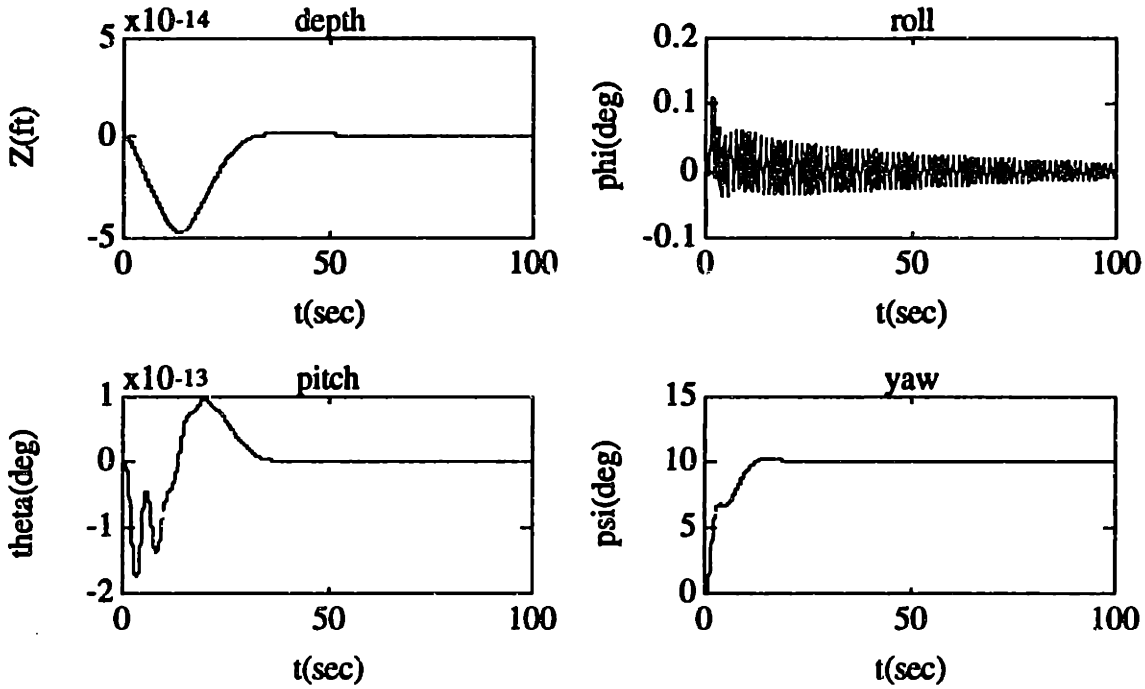

Figure 5.15: Nominal Heading Step Response (continued)

Table 5.3: Nominal AUV Control System Performance for u_0 = 1.0 ft/s
(with Performance Specifications in Parentheses)

Steady-State Depth Error	< 1.0% (5.0 %)
Steady-State Heading Error	< 1.0% (5.0 %)
Depth Overshoot	26.5 % (10.0 %)
Heading Overshoot	1.53% (10.0 %)
Depth Response	3.0 seconds (10.0 seconds)
Heading Response	13.0 seconds (5.0 seconds)

It appears for the nominal model that the H_∞ controller meets most of the design specifications of Section 5.1. Note the somewhat large depth overshoot. One probable cause is the decreased reliance of the controller on the "noisy" depth rate estimate (which, in a classical control sense, implies difficulty in using the depth rate for velocity damping of

the depth response). This implies that any attempt to decrease the depth overshoot would probably increase the sensitivity of the depth control loop to sensor noise. Even though the heading response time was slower than the specification, it was still judged to be reasonably fast enough for a "typical" mission of the AUV. In addition, if the response time was decreased any further, there would be (by definition) a corresponding increase in the closed-loop bandwidth, which could then excite some of the unmodeled dynamics of the AUV.

For this control design, the roll and pitch dynamics do not appear to be unnecessarily excited. Note that axial and lateral velocities also appear to be stabilized by this controller.

Robust Performance (Axial Velocity Perturbations)

The next performance evaluation was done in order to test the robustness of the H_∞ design to off-nominal axial velocities. For this evaluation, the "hovering" model, linearized about an axial velocity, u_0, of 0.0 ft/sec, and the "full-reverse" model, linearized about an axial velocity, u_0, of -1.0 ft/sec, were used. The depth step responses for these models are shown in Figure 5.16 (together with the nominal depth response), and the heading step responses are shown in Figure 5.17 (together with the nominal heading response).

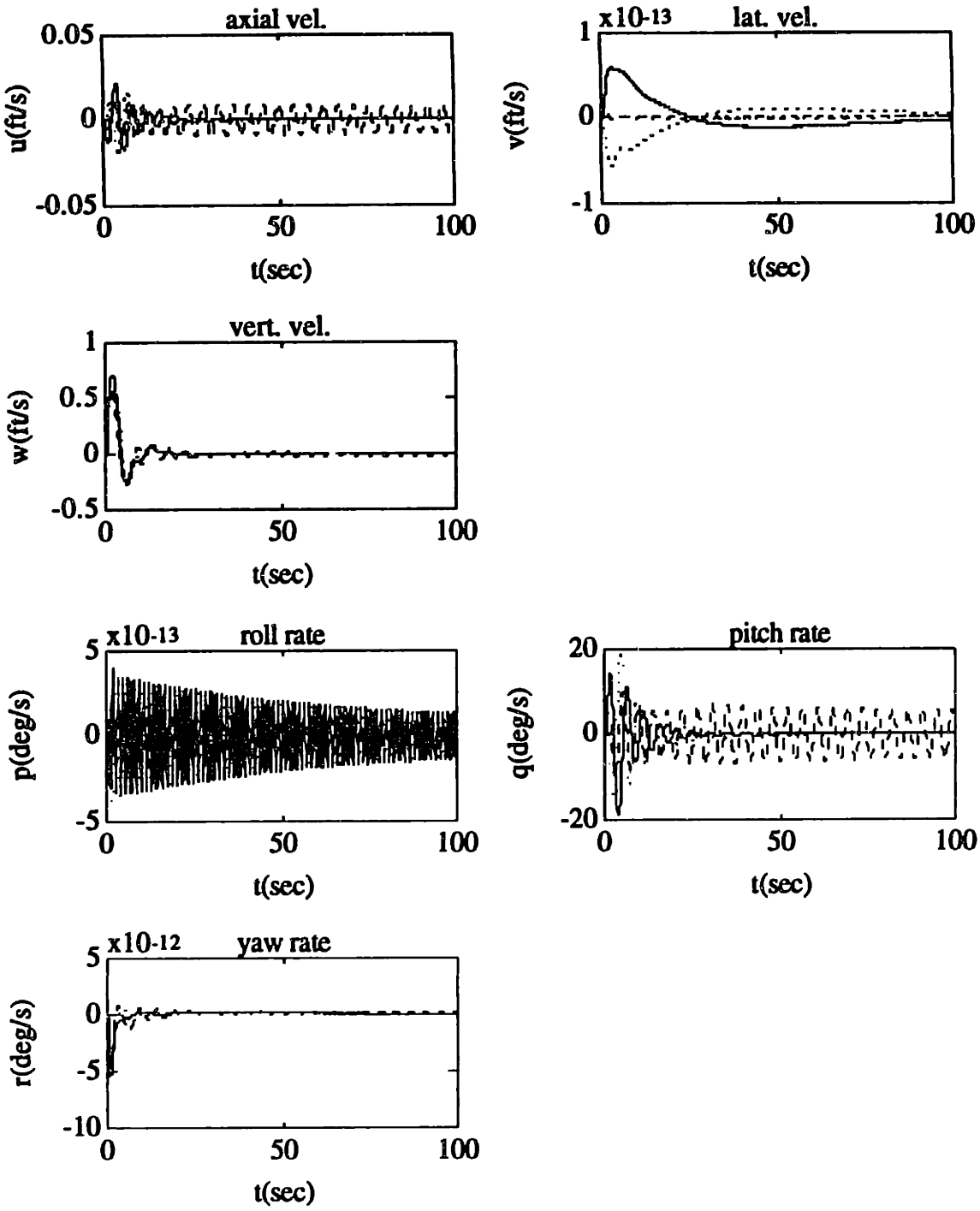

Figure 5.16: Robust Depth Step Response

Nominal (-), "Hovering" (--), "Full-Reverse" (..)

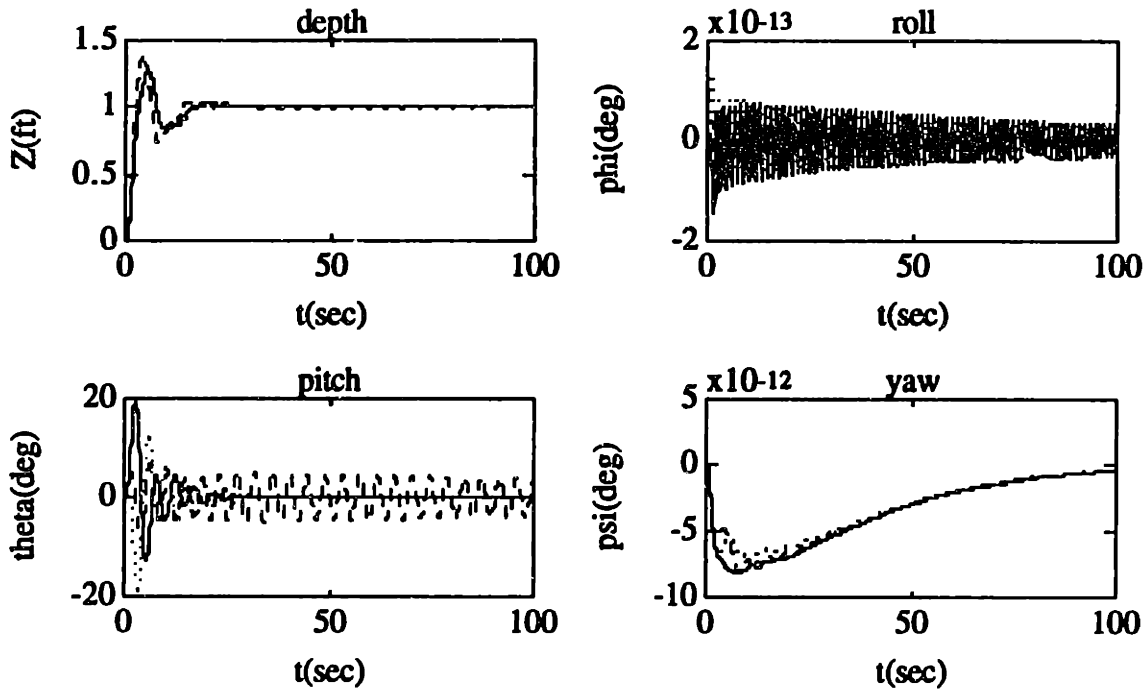

Figure 5.16: Robust Depth Step Response (continued)

Nominal (-), "Hovering" (--), "Full-Reverse" (..)

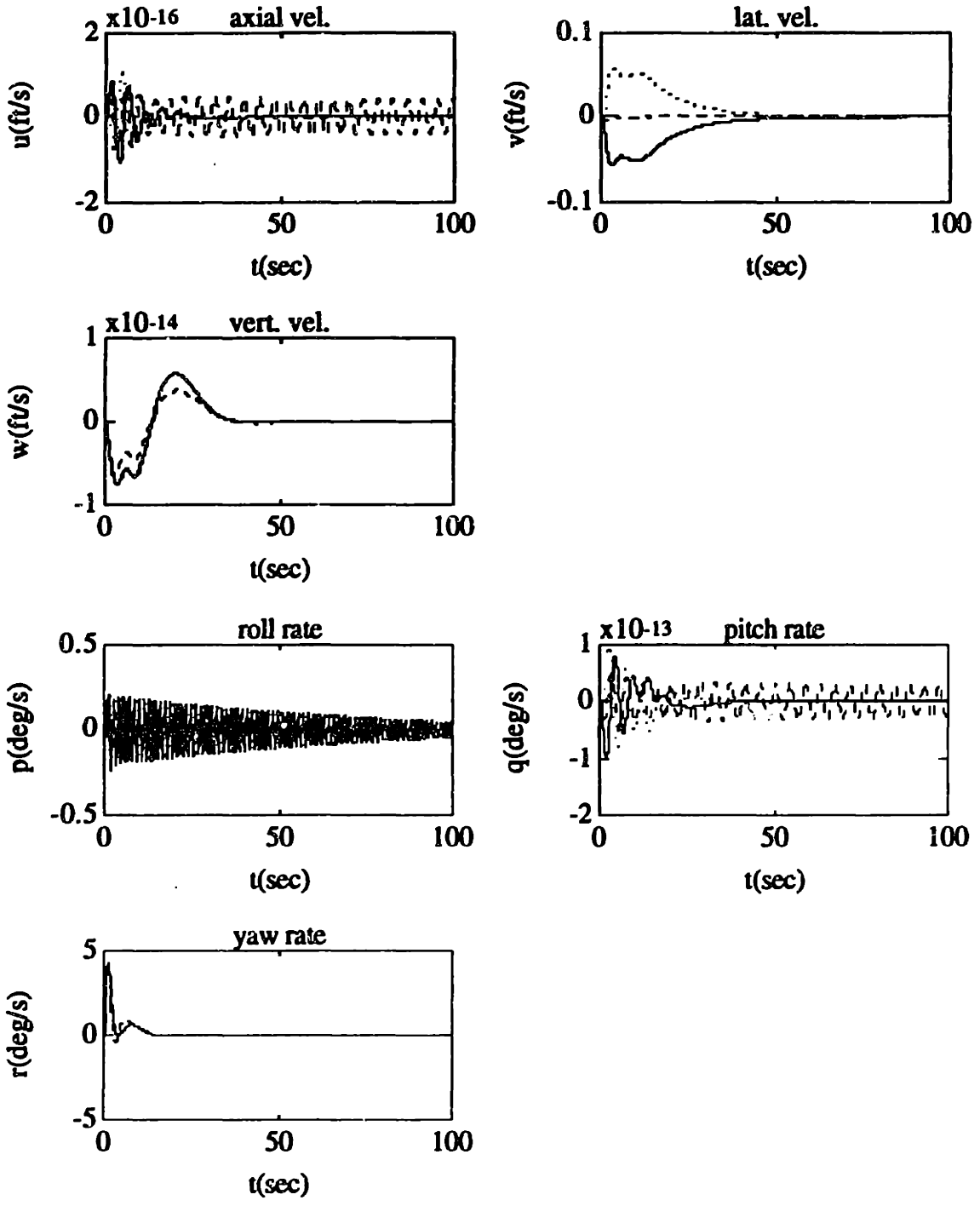

Figure 5.17: Robust Heading Step Response

Nominal (-), "Hovering" (--), "Full-Reverse" (..)

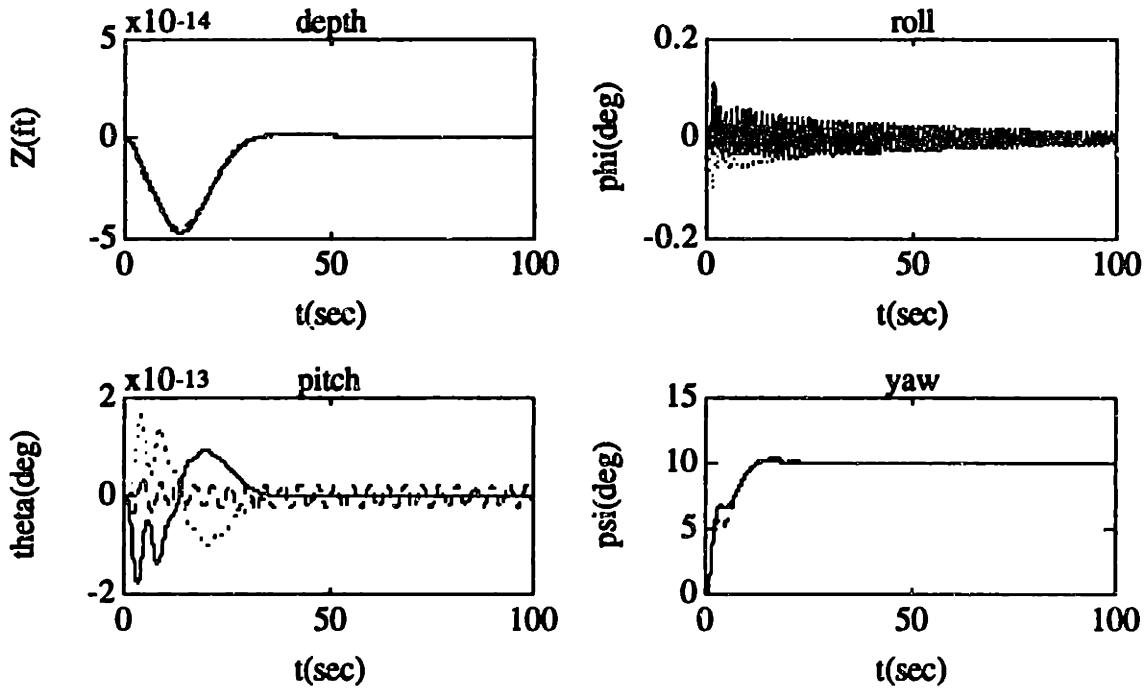

Figure 5.17: Robust Heading Step Response (continued)

Nominal (-), "Hovering" (--), "Full-Reverse" (..)

For the "hovering" model, the H_∞ controller appears to perform reasonably well. Again (with the exception of the somewhat high depth overshoot and the slower heading response time), it still meets the specifications of Section 5.1. However, note that the roll and pitch appear to be somewhat more oscillatory, but stable (from an eigenstructure analysis of the closed-loop system, even though the pitch is nearly undamped). From the eigenstructure analysis of Chapter 4, this is caused by the fact that the modes associated with roll and pitch are undamped for the "hovering" model. The axial and lateral velocities are also stabilized by this controller. However, they also have a somewhat more oscillatory response (due to coupling effects from the roll and pitch oscillations).

For the "full-reverse" model, the H_∞ controller also appears to perform reasonably well. Again, as for the nominal model, it still meets the specifications of Section 5.1, with the exception of the depth overshoot and the heading response time. Interestingly, the roll

and pitch responses, plus the axial and lateral velocity responses, appear to be nearly the "mirror" images of the corresponding responses for the nominal case.

Robust Performance ("Added-Mass" Perturbations)

The next performance evaluation was done in order to test the robustness of the H_∞ design to perturbations in the AUV's "added mass" hydrodynamic coefficients. For the first model ("vehicle-light" model) used in this evaluation, the vehicle was assumed to have a negative 30% perturbation in the diagonal elements of the "mass and inertia" matrix, $\mathbf{E}_1$, corresponding to the axial, lateral, and vertical velocities and the yaw rate. From the AUV parametric uncertainty model of Section 5.2.1, this corresponds to $\Delta_1 = 0.6\mathbf{I}$ (i.e., $\mathbf{E}_1 = \mathbf{E}_{1o} - 0.6\mathbf{PN}$). For the second model ("vehicle-heavy" model), the vehicle was assumed to have a positive 50% perturbations in these elements (i.e., $\Delta_1 = -\mathbf{I}$, $\mathbf{E}_1 = \mathbf{E}_{1o} + \mathbf{PN}$). The depth step responses for these models are shown in Figure 5.18 (together with the nominal depth response), and the heading step response is shown in Figure 5.19 (together with the nominal heading response). Note that both the "vehicle-light" model and the "vehicle-heavy" model were linearized about the nominal axial velocity, u_0, of 1.0 ft/s.

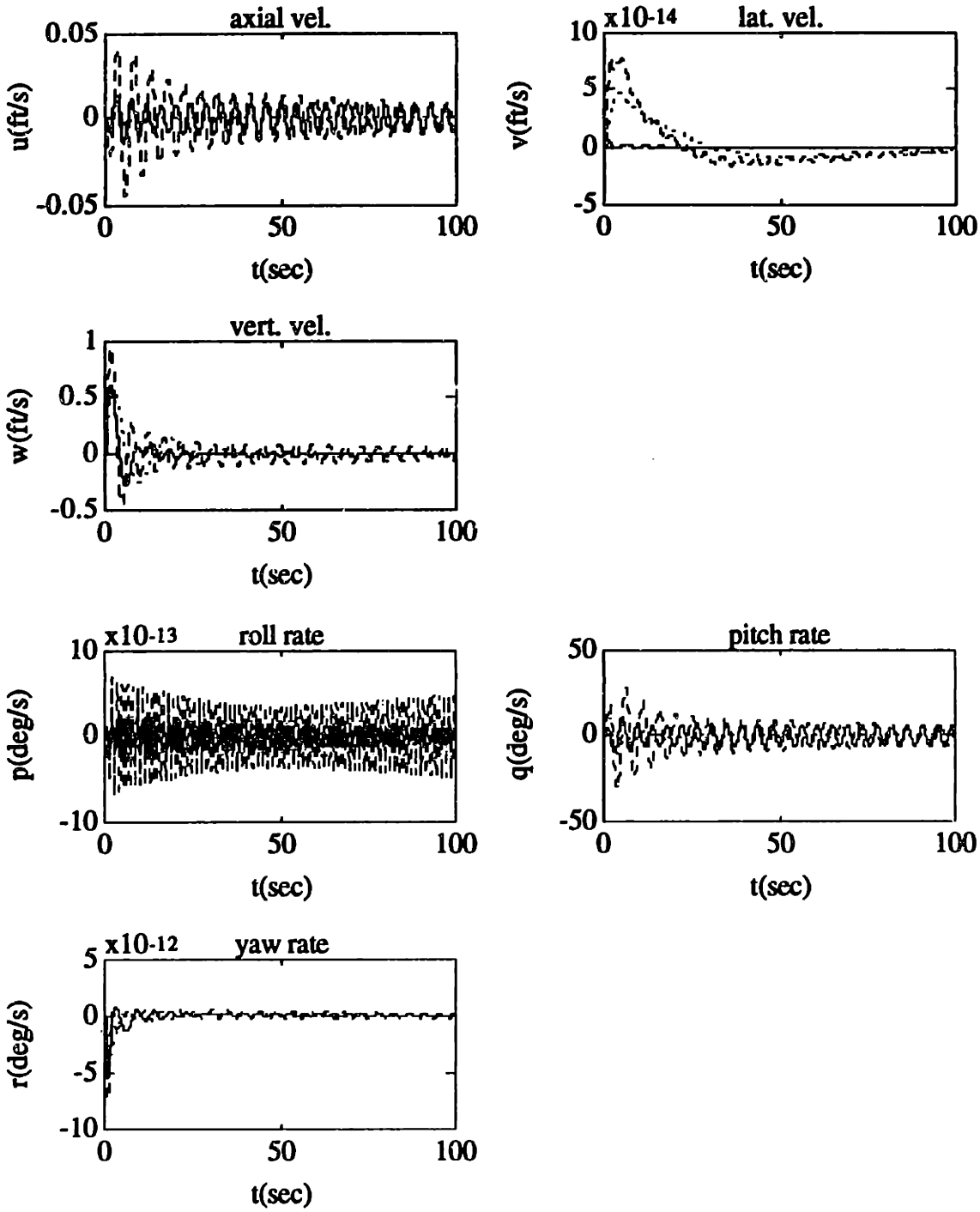

Figure 5.18: Robust Depth Step Response

Nominal (-), "Vehicle-Light" (--), "Vehicle-Heavy" (..)

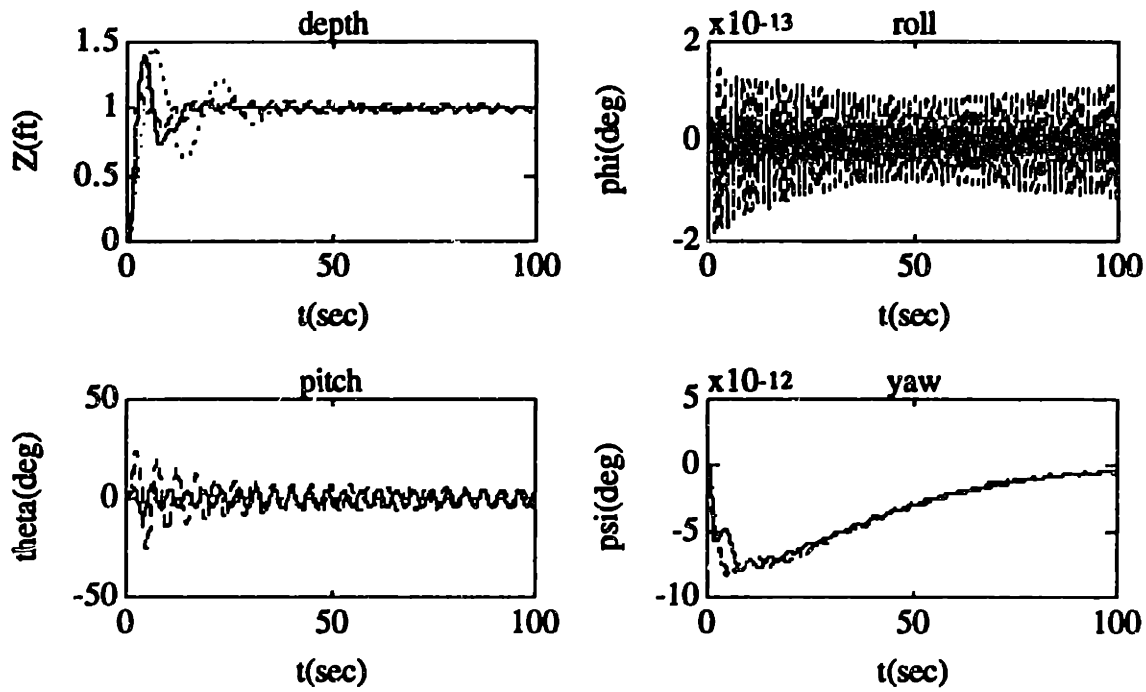

Figure 5.18: Robust Depth Step Response (continued)

Nominal (-), "Vehicle-Light" (--), "Vehicle-Heavy" (..)

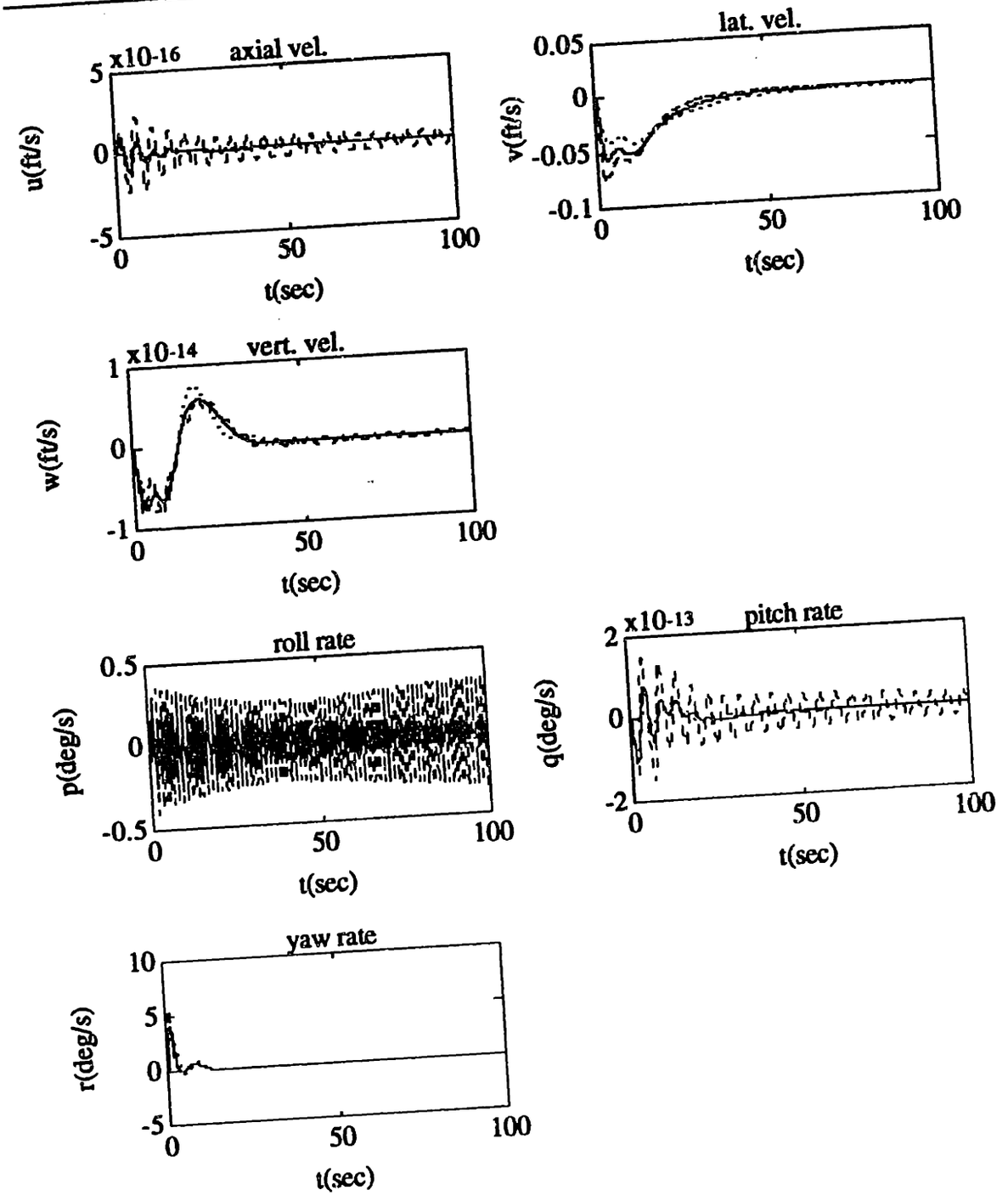

Figure 5.19: Robust Heading Step Response

Nominal (-), "Vehicle-Light" (--), "Vehicle-Heavy" (..)

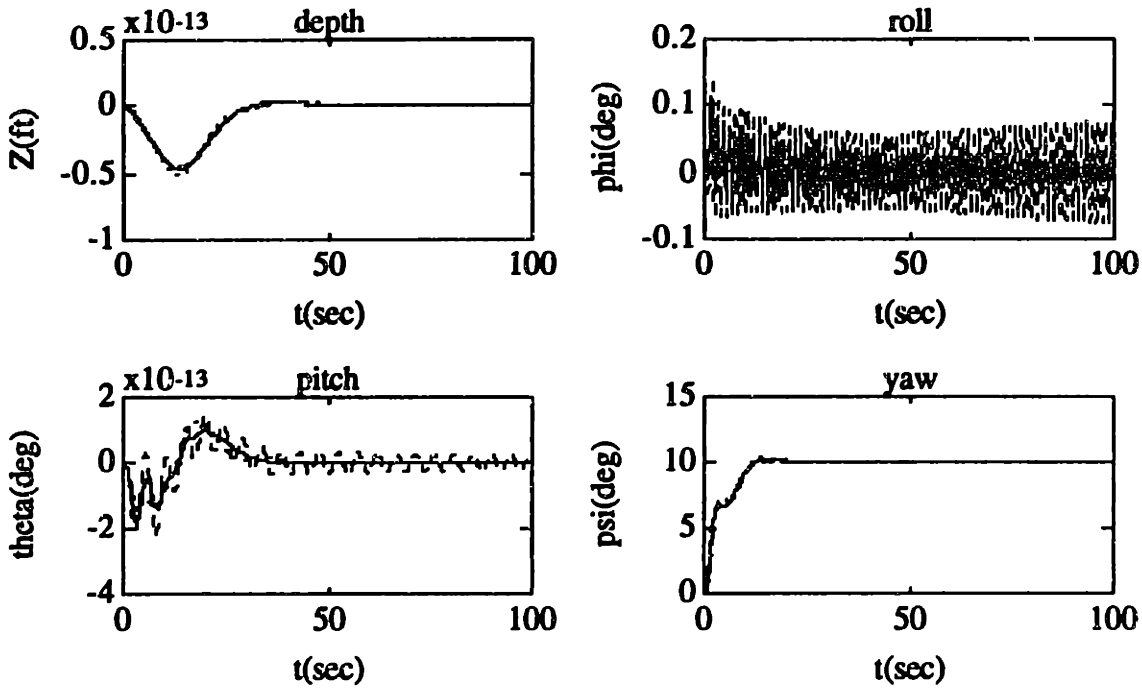

Figure 5.19: Robust Heading Step Response

Nominal (-), "Vehicle-Light" (--), "Vehicle-Heavy" (..)

For both the "vehicle-light" model and the "vehicle-heavy" model, the H_∞ controller appears to perform reasonably well. Again, as for the nominal model, it still meets the specifications of Section 5.1., with the exception of the high depth overshoot and slower heading response time. However, the depth response and pitch response appear to be somewhat more oscillatory. The roll response is significantly more oscillatory, but stable (by an eigenstructure analysis of the closed-loop system). Note that it would be difficult to dampen the roll oscillations, since direct roll control of the AUV is not possible.

One implication of these responses is that the H_∞ controller is somewhat more robust to positive perturbations in the "added-mass" terms. This implies, for robust control-system design, that it is better to underestimate the "added-mass" coefficients rather than overestimate them.

5.4 μ-SYNTHESIS CONTROLLER DESIGN

Given the AUV Standard-Form (SF) design model of Section 5.2, a μ-Synthesis controller was designed using the μ-based robust design algorithm presented in Section 2.6.2. For purposes of comparison (between the unstructured Small-Gain design approach and the structured μ-based design approach), all of the weighting functions, scaling matrices, performance γ's, and perturbation γ's of the SF design model had the exact values as those used in the SF design model for the Small-Gain based H_∞ controller of the previous section.

5.4.1 Compensator Synthesis Using the μ-Based Robust Design Algorithm

Recall from Chapter 2 that the μ-based robust design algorithm attempts to minimize α, where α is the upper bound for the robust system performance, i.e.,

$$\frac{\|e\|_2}{\|\delta\|_2} < \alpha \quad \forall \Delta \in \mathbf{B}\Delta \tag{5.74}$$

The first step in this algorithm was to obtain a lower bound and an upper bound for α. To obtain the lower bound for α, an H_∞ controller was designed using only the "nominal" part of the SF plant model (i.e., $\Delta = 0$), given by

$$\begin{bmatrix} \mathbf{e} \\ \mathbf{y} \end{bmatrix} = \begin{bmatrix} \mathbf{P}_{22}(s) & \mathbf{P}_{23}(s) \\ \mathbf{P}_{32}(s) & \mathbf{P}_{33}(s) \end{bmatrix} \begin{bmatrix} \delta \\ \mathbf{u} \end{bmatrix} \tag{5.75}$$

The closed-loop H_∞ norm from δ to **e** of this design was found to be 0.4573, which was then used as the lower bound for α (since this is the *absolute* limit of robust performance for any H_∞-based design using this particular SF model). For simplicity, the upper bound for α was chosen to be 1.0000 (since for this value of α, the μ-synthesis SF design model is identical to the original H_∞ design model of the previous section). Using logarithmic bisection, an initial value of α = 0.6762 was chosen. As shown in Table 5.4, for this

value of α, the robust design algorithm found a compensator that satisfied the approximate μ-based performance test, given by

$$\tilde{\mu}(\omega_n) < 1 \; \forall \; \omega_n \tag{5.76}$$

Note that for each iteration shown in Table 5.4, 200 logarithmically-spaced frequency points were used for ω_n, with a range between 0.001 rad/s and 100 rad/s.

Using this initial value of α as the new upper bound, a value of $\alpha = 0.5561$ was chosen. After two iterations, the approximate upper-bound for μ failed to converge to a level satisfying the performance-robustness test. Therefore, this value for α was chosen as the new lower bound. Again, by using logarithmic bisection, a value of a = 0.6132 was chosen. For this case, the algorithm again converged to a design that failed to satisfy the approximate robust-performance test after two iterations. Note that for this value of α, the approximate upper bound for μ was significantly *higher* for the second iteration, due to using somewhat poor first-order curve fits to the weights generated by the μ-analysis of the closed-loop system. Unexpectedly, higher-order fits were found to produce closed-loop system with even higher bounds for μ (probably due to the nonconvexity of the μ-based optimization algorithm). Therefore, this value of α was chosen as the new lower bound. Since the new lower and upper bounds for α were within approximately 10% of each other, the upper bound value of $\alpha = 0\ 6732$ was judged to be acceptable as the final value of α. The plots of Figure 5.20 through 5.22 show the sequence of μ upper bounds, the weights, and the curve fit at each iteration for this choice of α.

Table 5.4: Results of μ-Based Robust Design Algorithm

α	γ_1	$\max_{\omega_n} \tilde{\mu}_1(\omega_n)$	γ_2	$\max_{\omega_n} \tilde{\mu}_2(\omega_n)$
0.6762	1.046	1.0397	0.939	0.9374
0.5561	1.263	1.2634	1.084	1.0782
0.6132	1.144	1.1405	55.23	3.9088

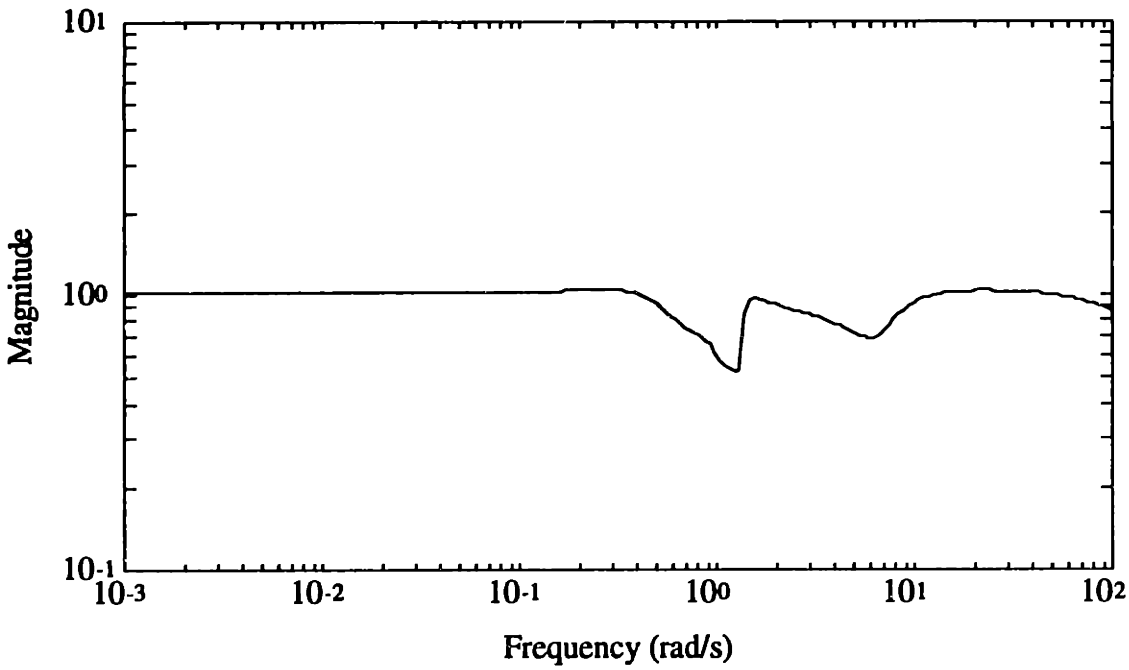

Figure 5.20: Approximate μ Upper Bound for First Iteration

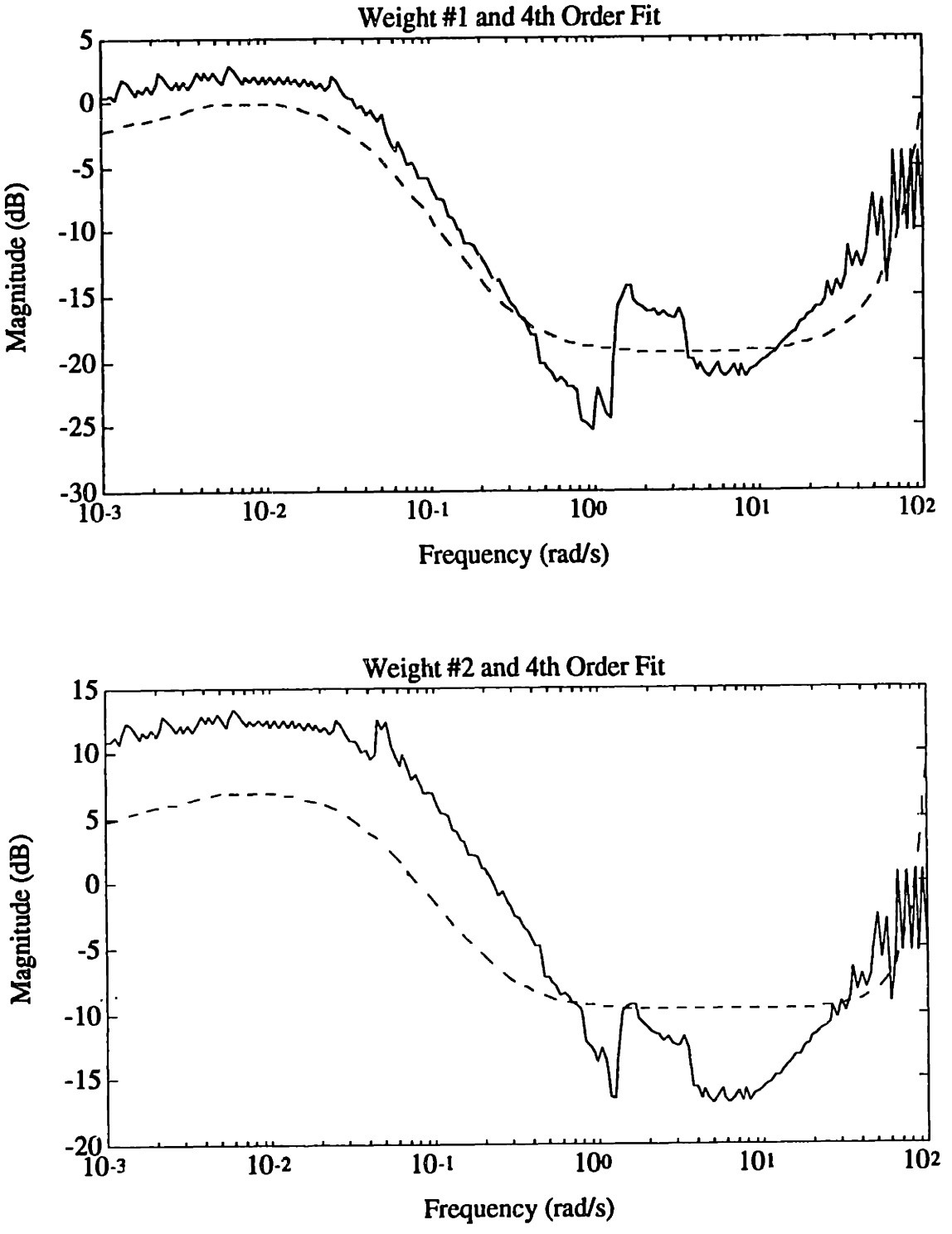

Figure 5.21: Curve Fits After First Iteration

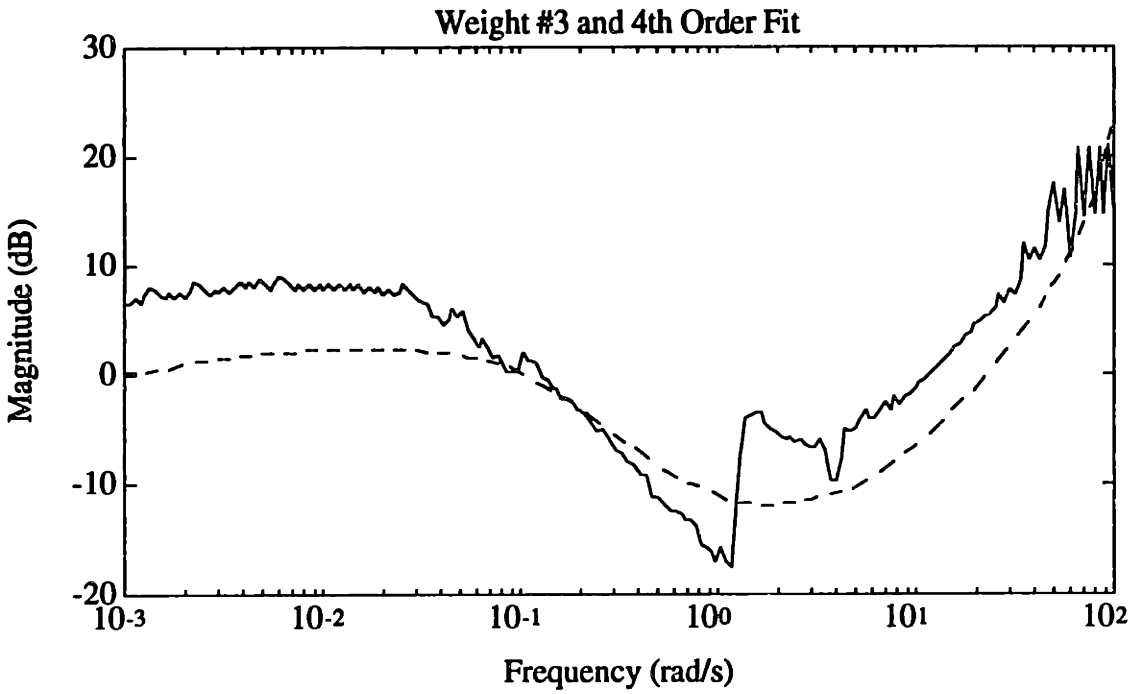

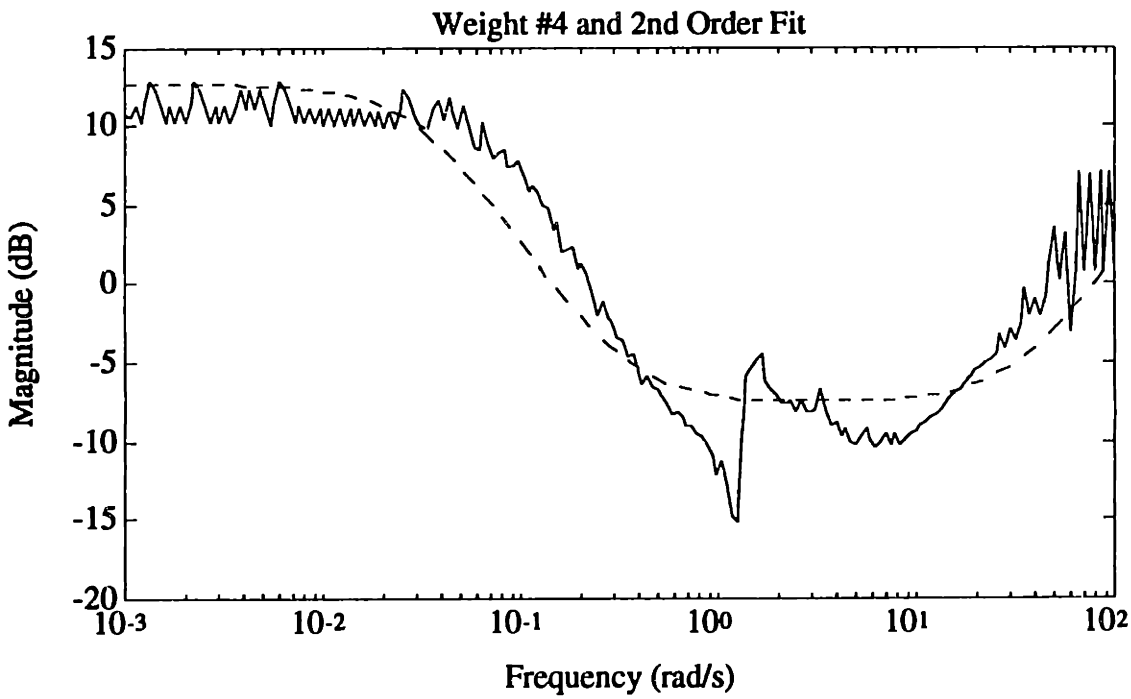

Figure 5.21: Curve Fits After First Iteration (continued)

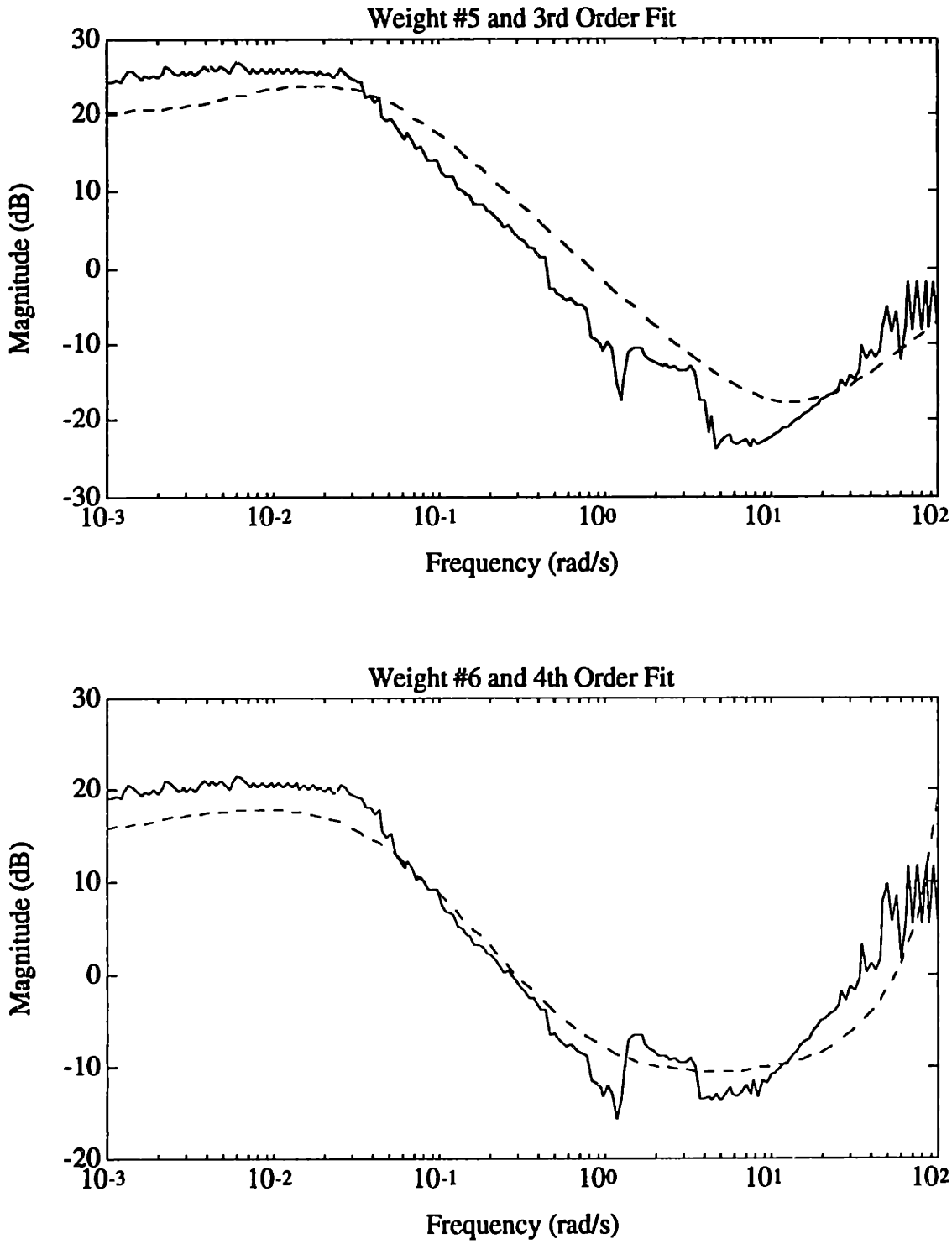

Figure 5.21: Curve Fits After First Iteration (continued)

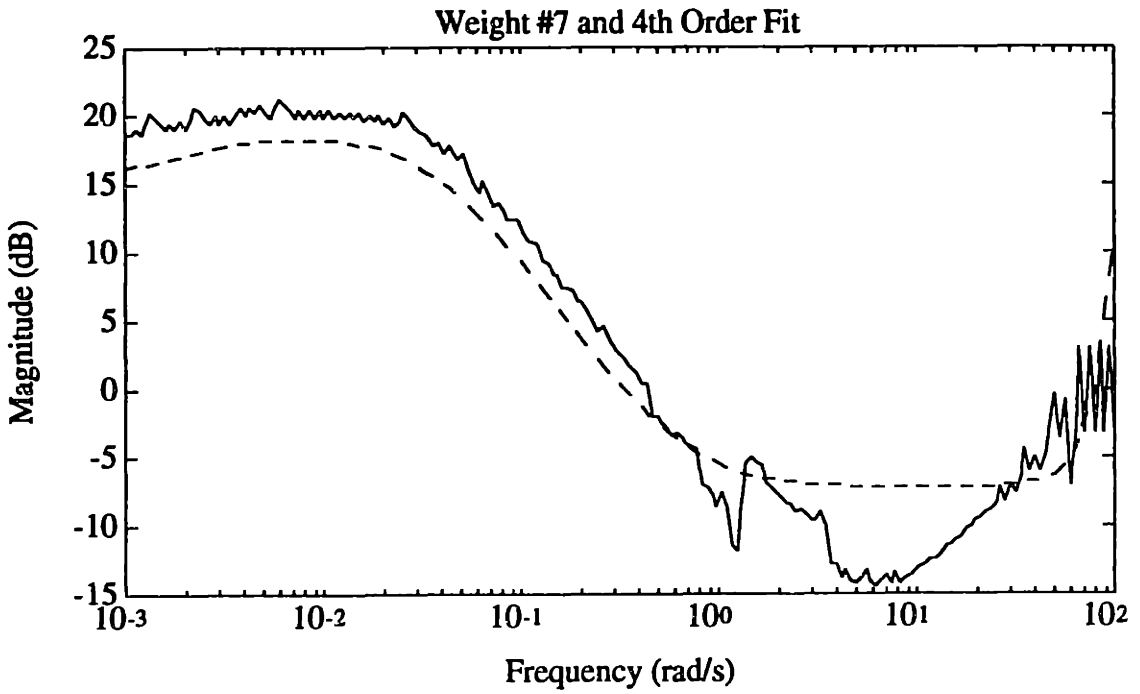

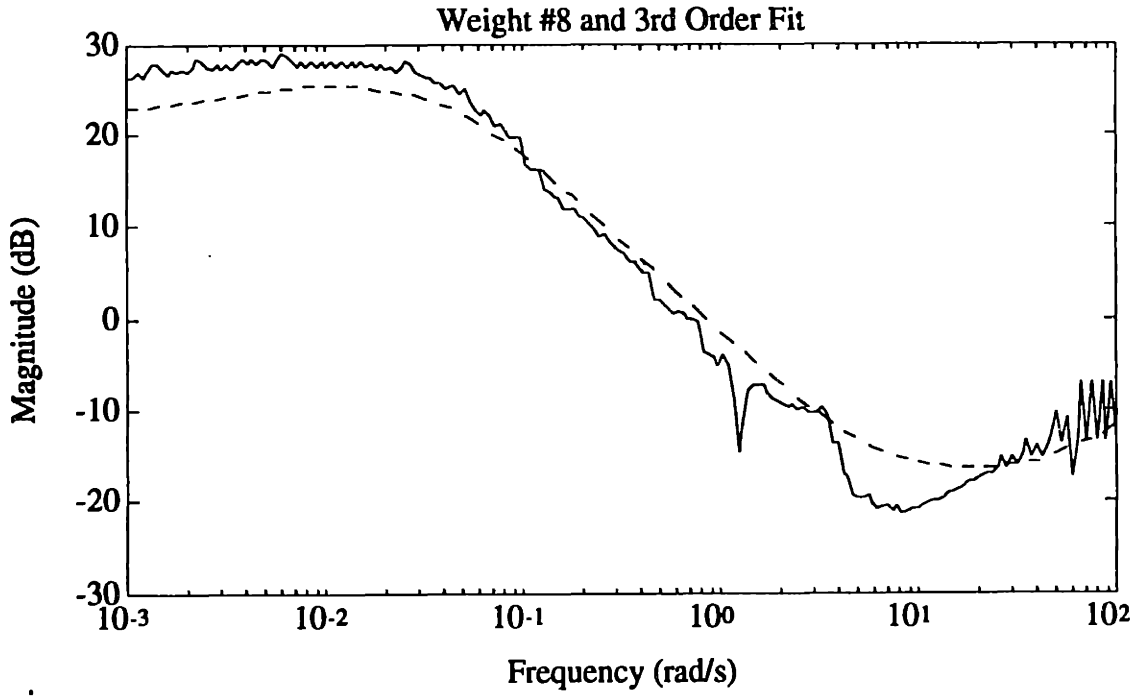

Figure 5.21: Curve Fits After First Iteration (continued)

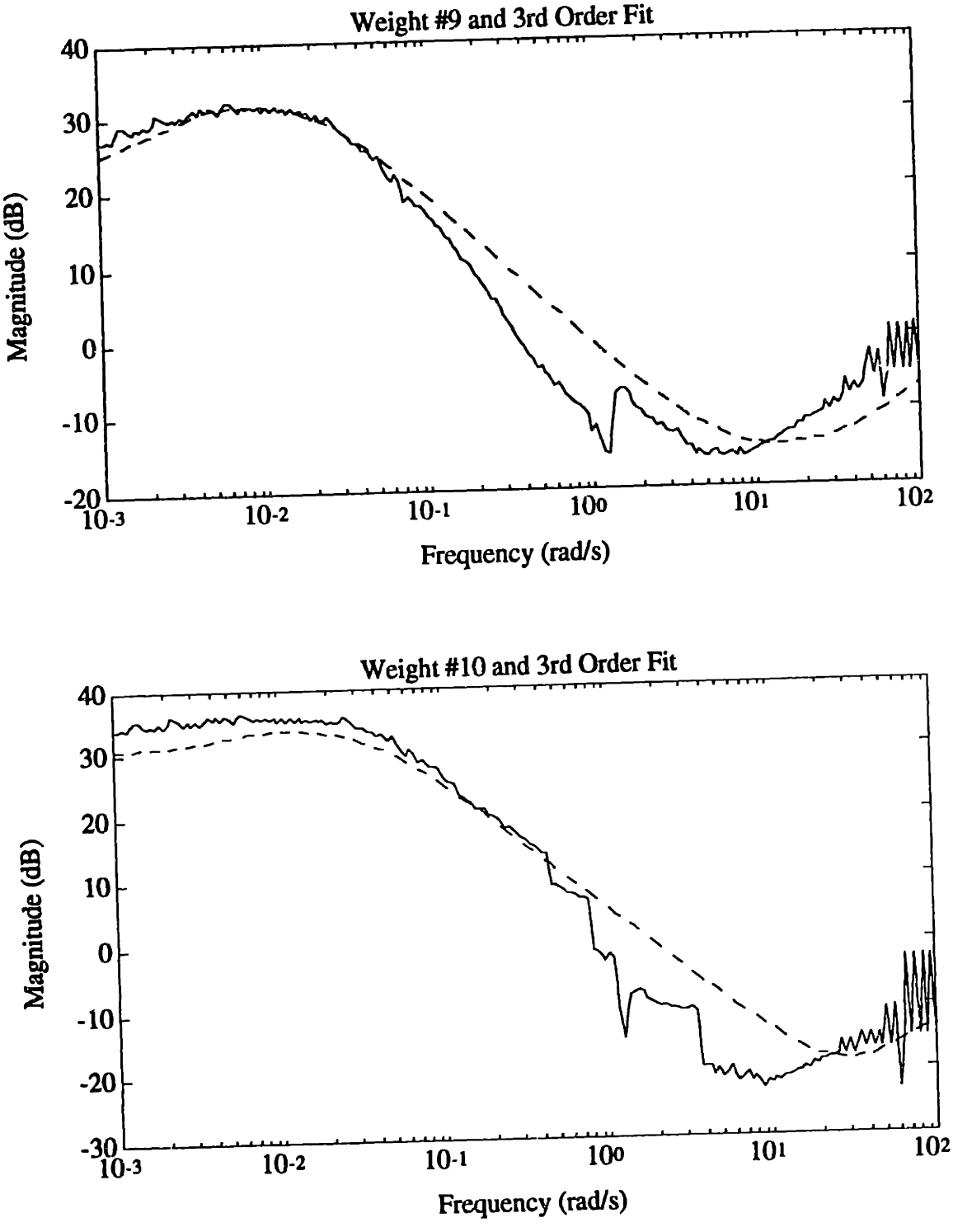

Figure 5.21: Curve Fits After First Iteration (continued)

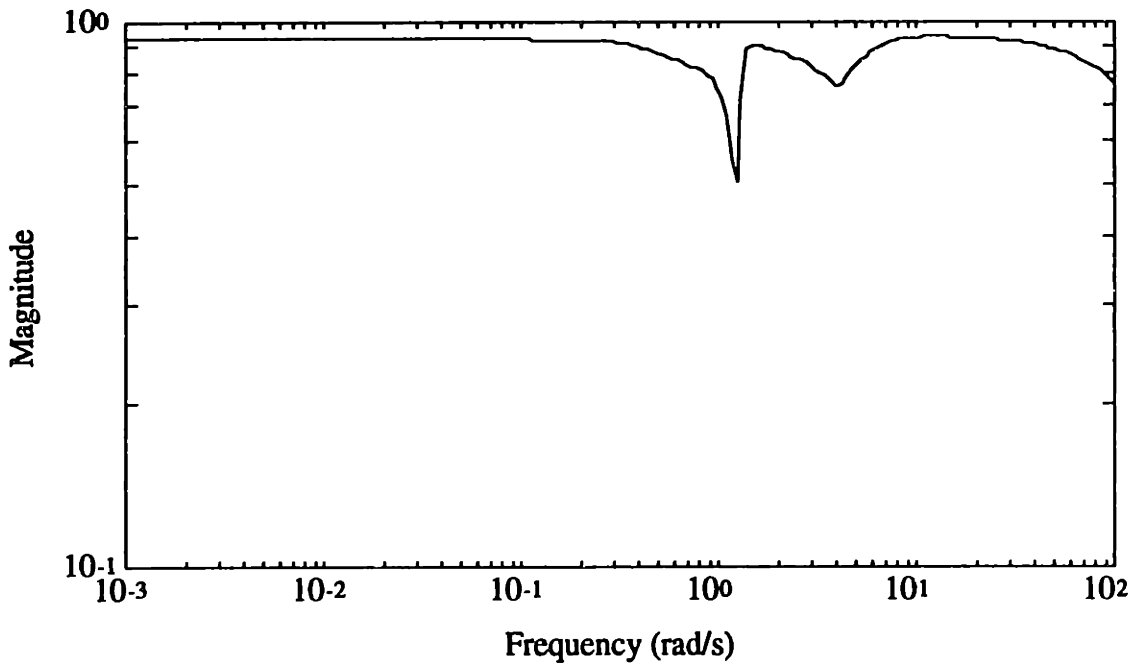

Figure 5.22: Approximate μ Upper Bound for Second Iteration

The next step in the μ-synthesis design process was to reduce the somewhat high-order (91 state) compensator from the second iteration down to a more manageable state-level. For purposes of comparison to the 38-state robust H_∞ compensator developed in Section 5.3, the μ-based compensator was also reduced down to that state level. The bounds on the additive error versus model order are shown in Figure 5.23. From this plot, the additive error at the 38-state level is less than 100 dB, which was judged to be reasonably small. For this reduced-order compensator, the approximate μ upper-bound on the closed-loop system was essentially unchanged from the full-order case (with a maximum value of 0.9374). The plot of the normalized Hankel singular values of this compensator are shown in Figure 5.24. From this plot, all of the Hankel singular values of the 38-state compensator are nonzero, which implies that this compensator is minimal (as desired).

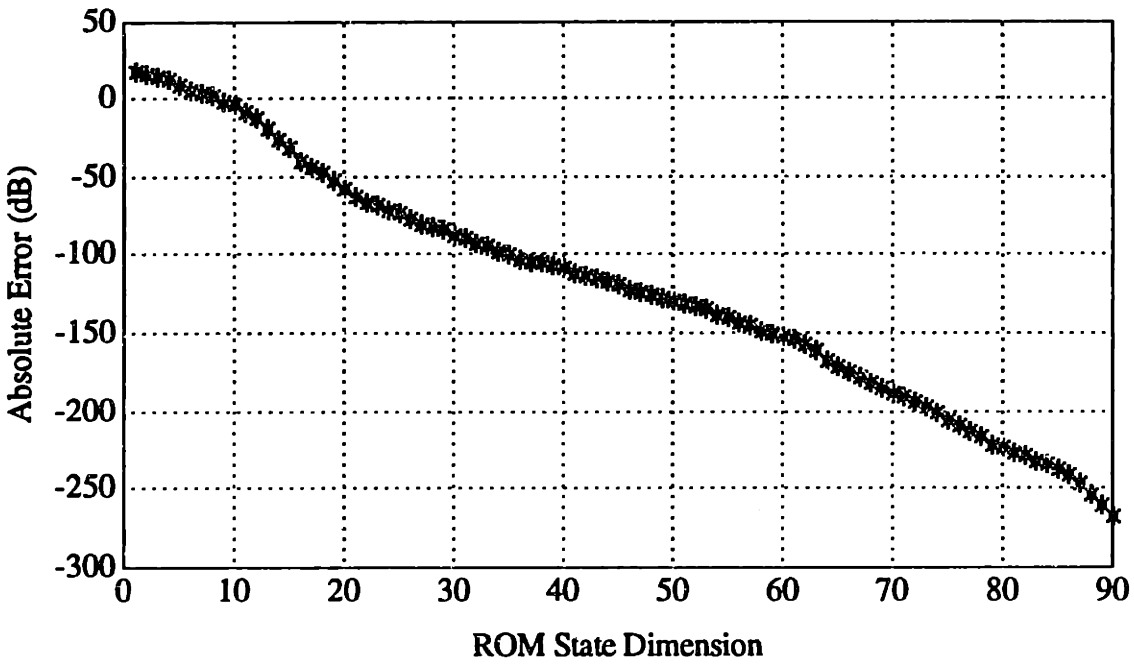

Figure 5.23: Fractional-Balanced Additive-Error Bounds

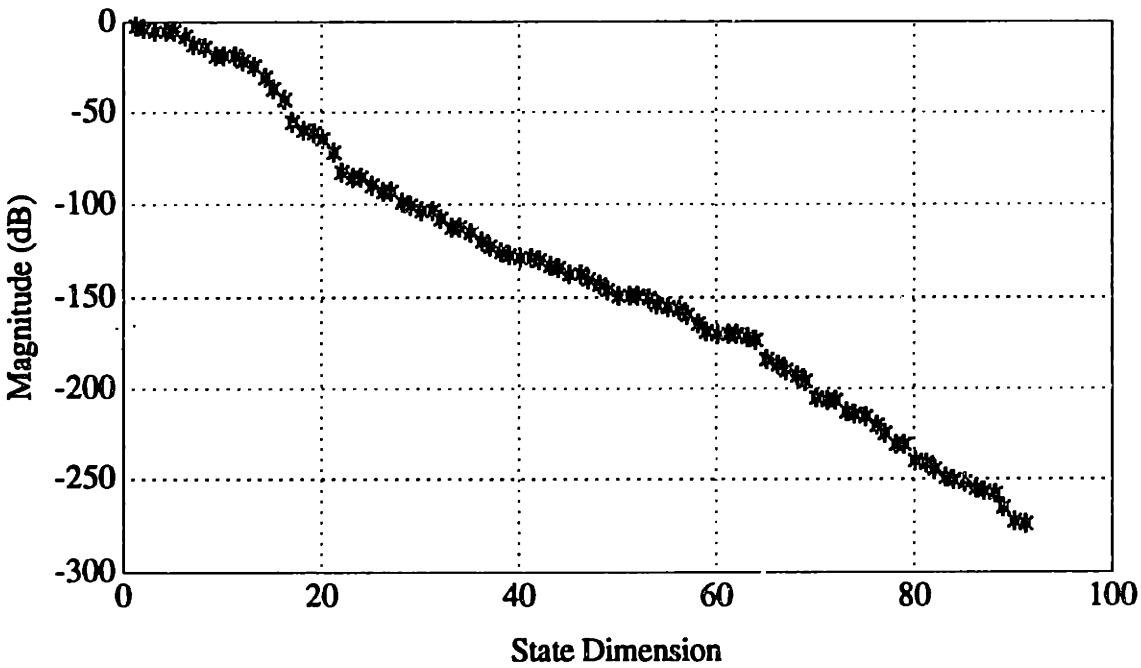

Figure 5.24: Hankel Singular Values

The frequency response of the 38-state μ-synthesis controller is shown below in Figure 5.25.

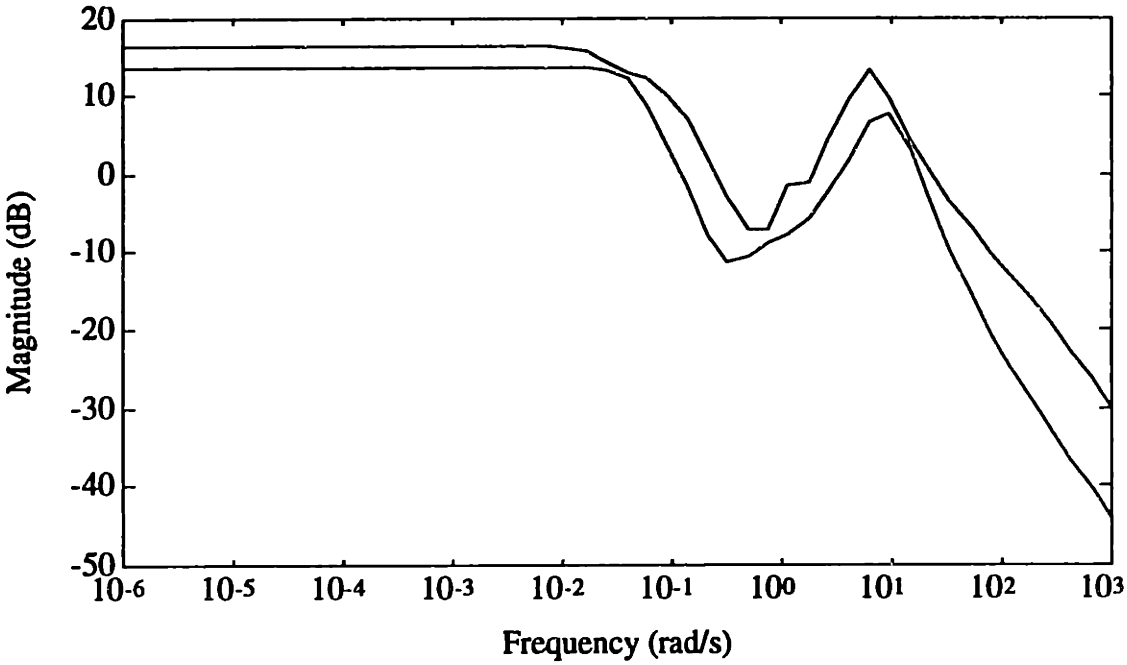

Figure 5.25: Unscaled μ-Synthesis Compensator Frequency Response

The μ-synthesis compensator frequency response is very similar to the original robust H_∞ compensator frequency response shown in Figure 5.12. However, the "depth control" portion (from the depth, depth rate, and pitch to the vertical thrust) of this (nearly decoupled) compensator has a higher low-frequency gain (as compared to the H_∞ compensator). On the other hand, the "heading control" portion (from the heading, yaw rate, and roll to the differential thrust) has a lower low-frequency gain (as compared to the H_∞ compensator).

The position sensitivity and complementary-sensitivity of this design are shown in Figure 5.26.

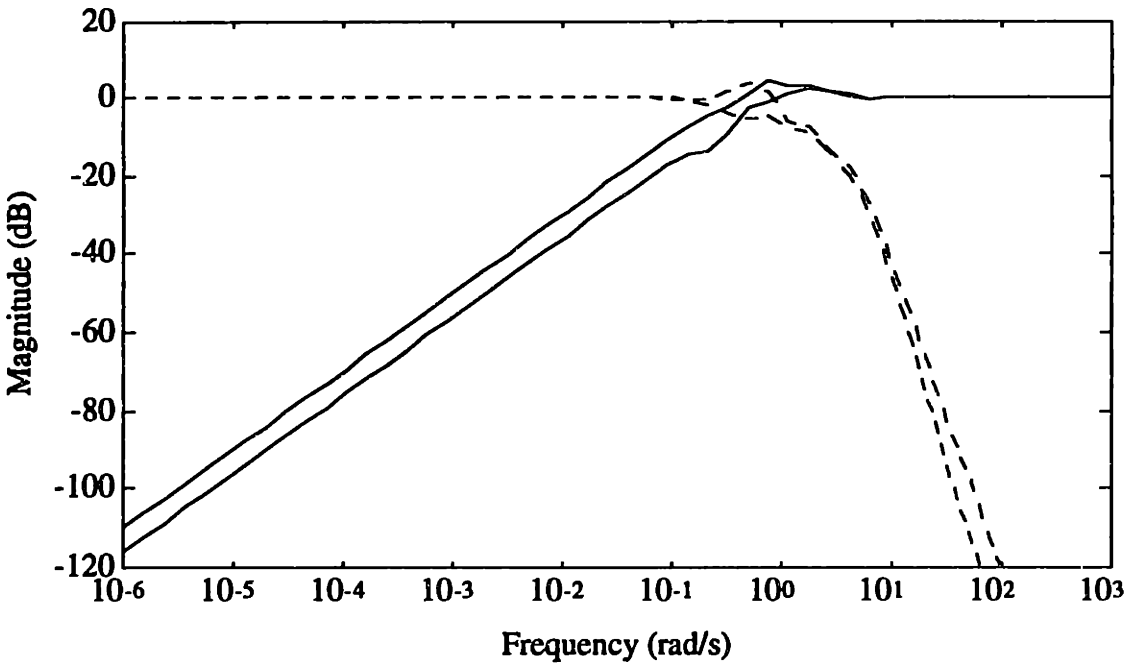

Figure 5.26: Sensitivity (-) and Complementary Sensitivity (--) (μ-Synthesis Design)

From this plot, the μ-synthesis design appears to have a closed-loop frequency response also similar to the robust H_∞ design, with closed-loop bandwidths of approximately 0.5 rad/sec and 1.0 rad/sec, respectively for depth and heading. Again, note that the sensitivity has a 20 dB/dec roll off, while the complementary sensitivity has an 80 dB/dec roll-off. The peak magnitude characteristics of both the sensitivity and complementary sensitivity are also similar to the robust H_∞ design (i.e., a peak magnitude of less than 3 dB). The complementary sensitivity also meets the H_∞ design specification of being below 40 dB at 10 rad/sec for heading (but does not meet the corresponding specification at 5.0 rad/sec for depth).

5.4.2 μ-Synthesis Closed-Loop Linear Performance

Given the compensator synthesized in Section 5.4.1, the final step in the design process was to evaluate its time-domain performance for the full-order LTI models of Section 4.4. This was done in order to determine if the μ-Synthesis compensator meets the design specifications of Section 5.1 (as well as to compare its performance characteristics to the performance characteristics of the robust H_∞ design). As with the H_∞ design, the performance evaluation was done examining the separate closed-loop time-domain responses to a 1.0 ft. step in depth and a 10.0 deg. step in heading.

Nominal Performance

The first performance evaluation was done using the nominal "full ahead" LTI model linearized about an axial velocity, u_0, of 1.0 ft/s. The depth step response of this model is shown in Figure 5.27, and the heading step response is shown in Figure 5.28. Numerical values for the step performance are shown in Table 5.5.

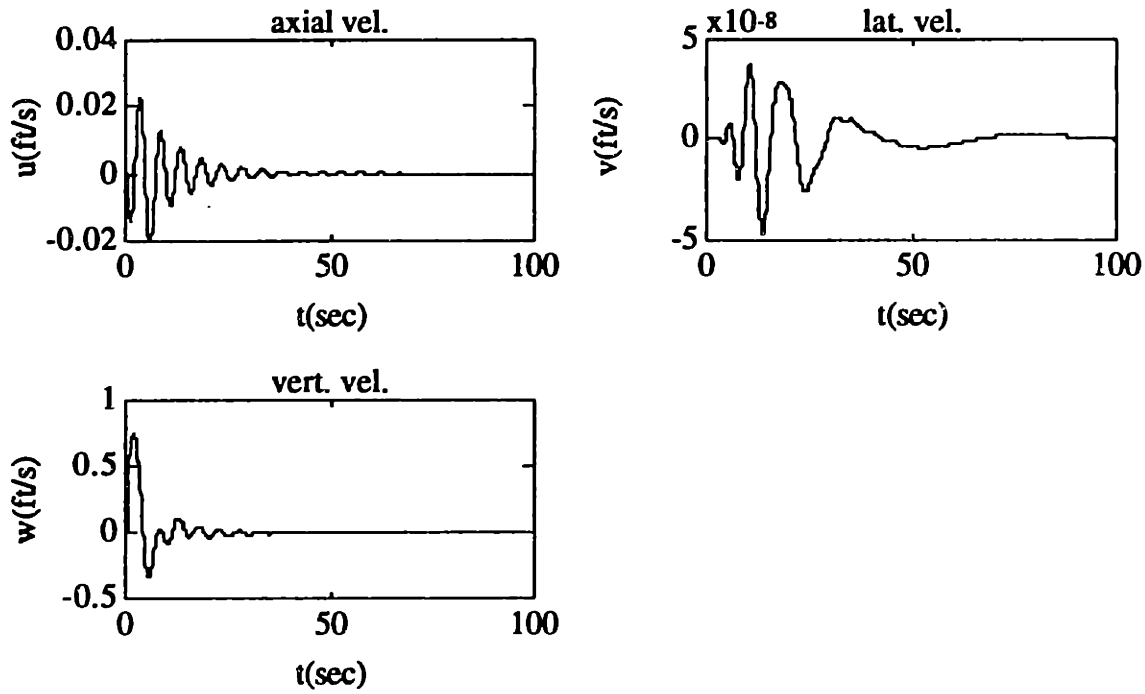

Figure 5.27: Nominal Depth Step Response

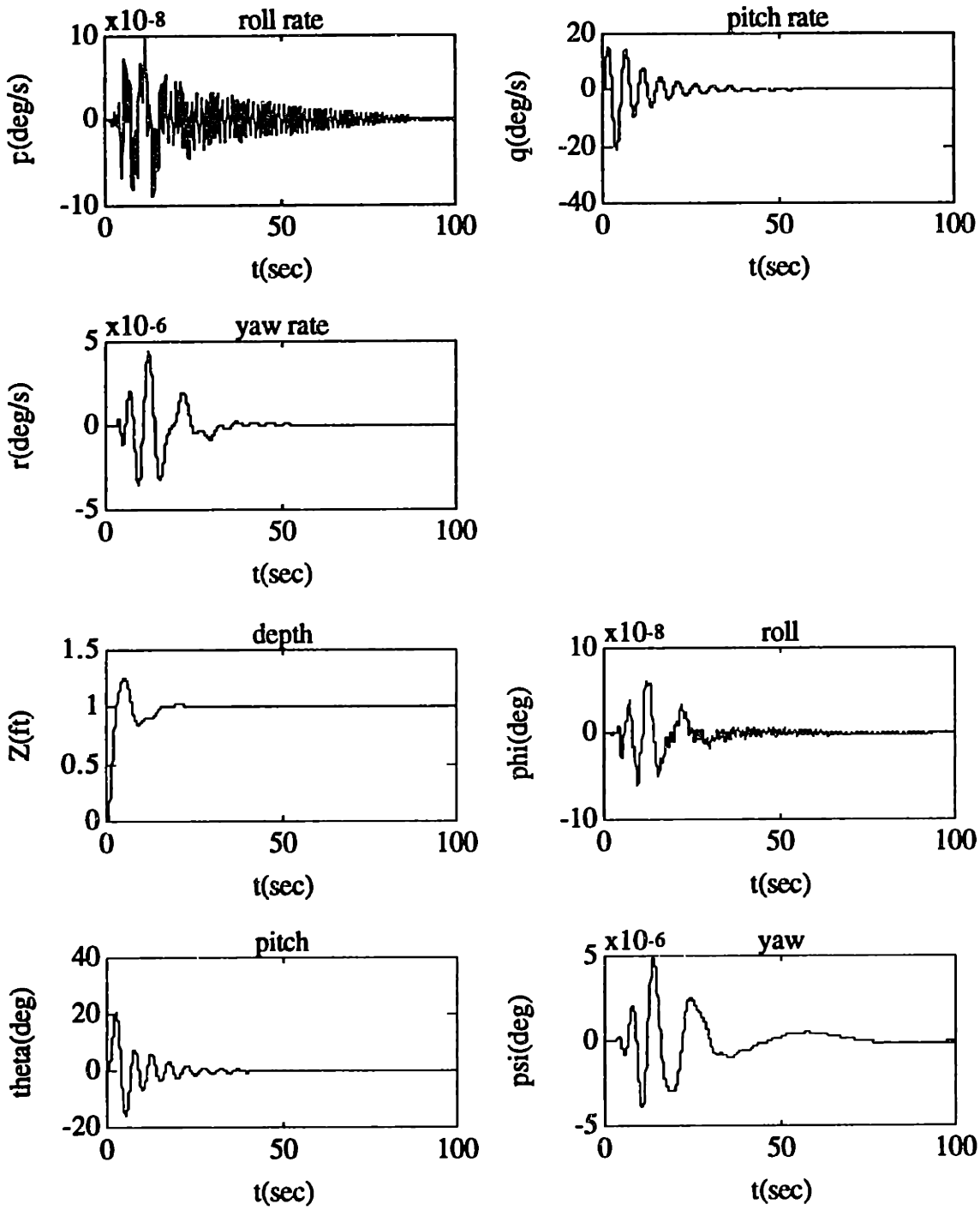

Figure 5.27: Nominal Depth Step Response (continued)

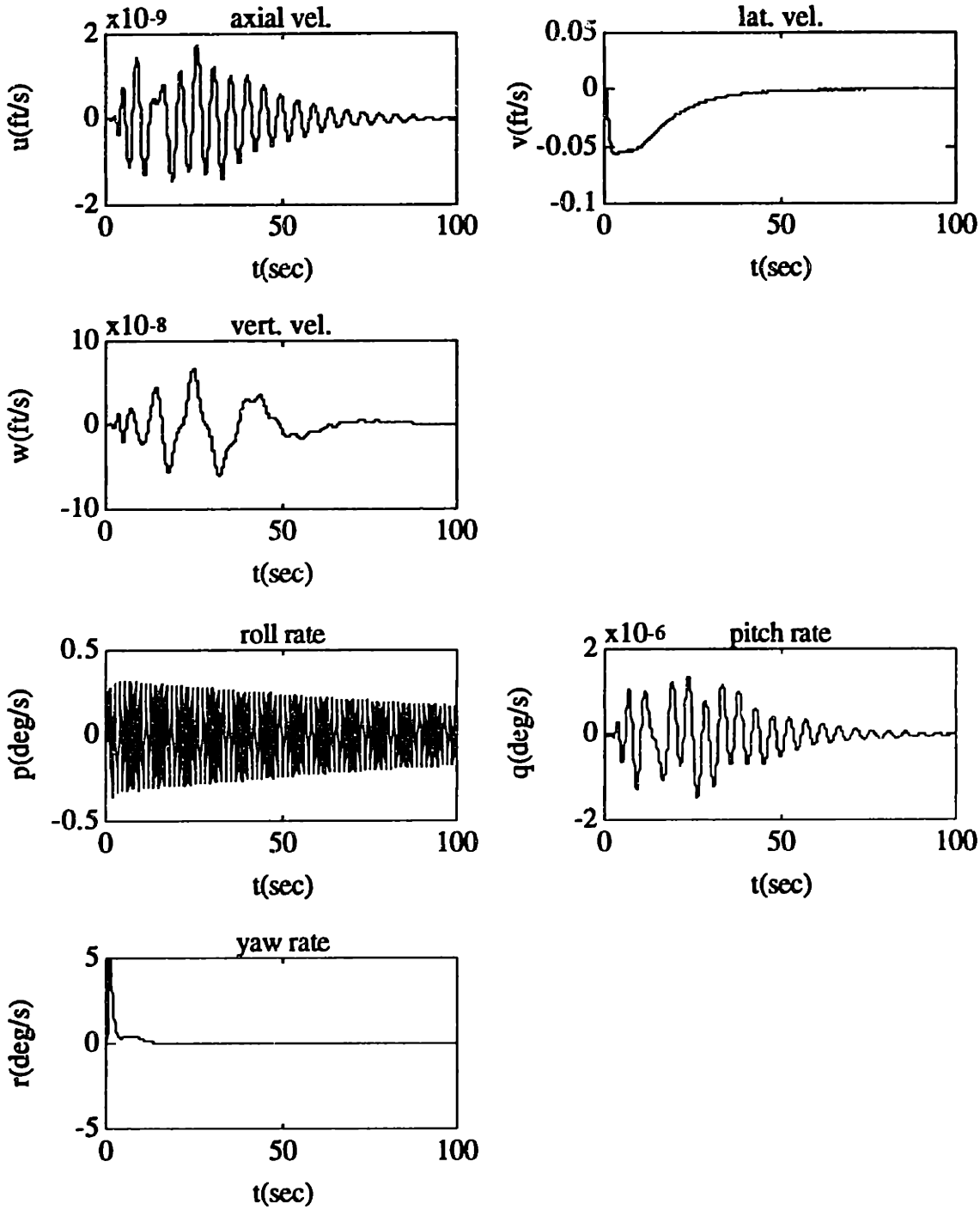

Figure 5.28: Nominal Heading Step Response

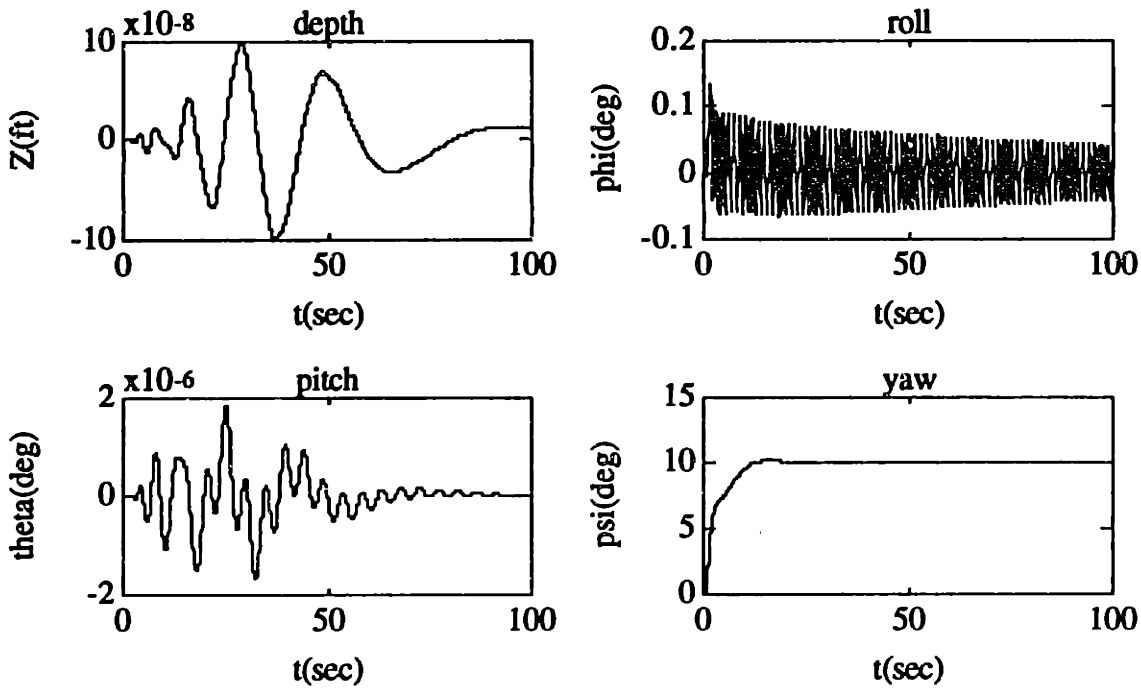

Figure 5.28: Nominal Heading Step Response (continued)

Table 5.5: Nominal AUV Control System Performance for u_0 = 1.0 ft/s (with Performance Specifications in Parentheses)

Steady-State Depth Error	< 1.0% (5.0 %)
Steady-State Heading Error	< 1.0% (5.0 %)
Depth Overshoot	25.3 % (10.0 %)
Heading Overshoot	0.92% (10.0 %)
Depth Response	1.0 seconds (10.0 seconds)
Heading Response	13.0 seconds (5.0 seconds)

It appears that the response of the μ-synthesis controller is almost identical to the response of the robust H_∞ controller for the nominal model (meeting most of the design specifications of Section 5.1). The depth overshoot is still somewhat large, but slightly less than the depth overshoot for the H_∞ controller. The heading response time was

identical to the H_∞ heading response time (which was slower than the specification, but still judged to be reasonably fast enough for a "typical" mission of the AUV).

For this control design, the roll and pitch dynamics do not appear to be unnecessarily excited. However, the pitch response is slightly more oscillatory, due to the increased gain of the "depth control" portion of the μ-synthesis controller. Note that the axial and lateral velocities are stabilized by this controller, just as with the H_∞ case.

Robust Performance (Axial Velocity Perturbations)

The next performance evaluation was done in order to test the robustness of the μ-synthesis design to off-nominal axial velocities. For this evaluation, as with the evaluation of the H_∞ compensator, the "hovering" model, linearized about an axial velocity, u_0, of 0.0 ft/sec, and the "full-reverse" model, linearized about an axial velocity, u_0, of -1.0 ft/sec, were used. The depth step responses for these models are shown in Figure 5.29 (together with the nominal depth response), and the heading step responses are shown in Figure 5.30 (together with the nominal heading response).

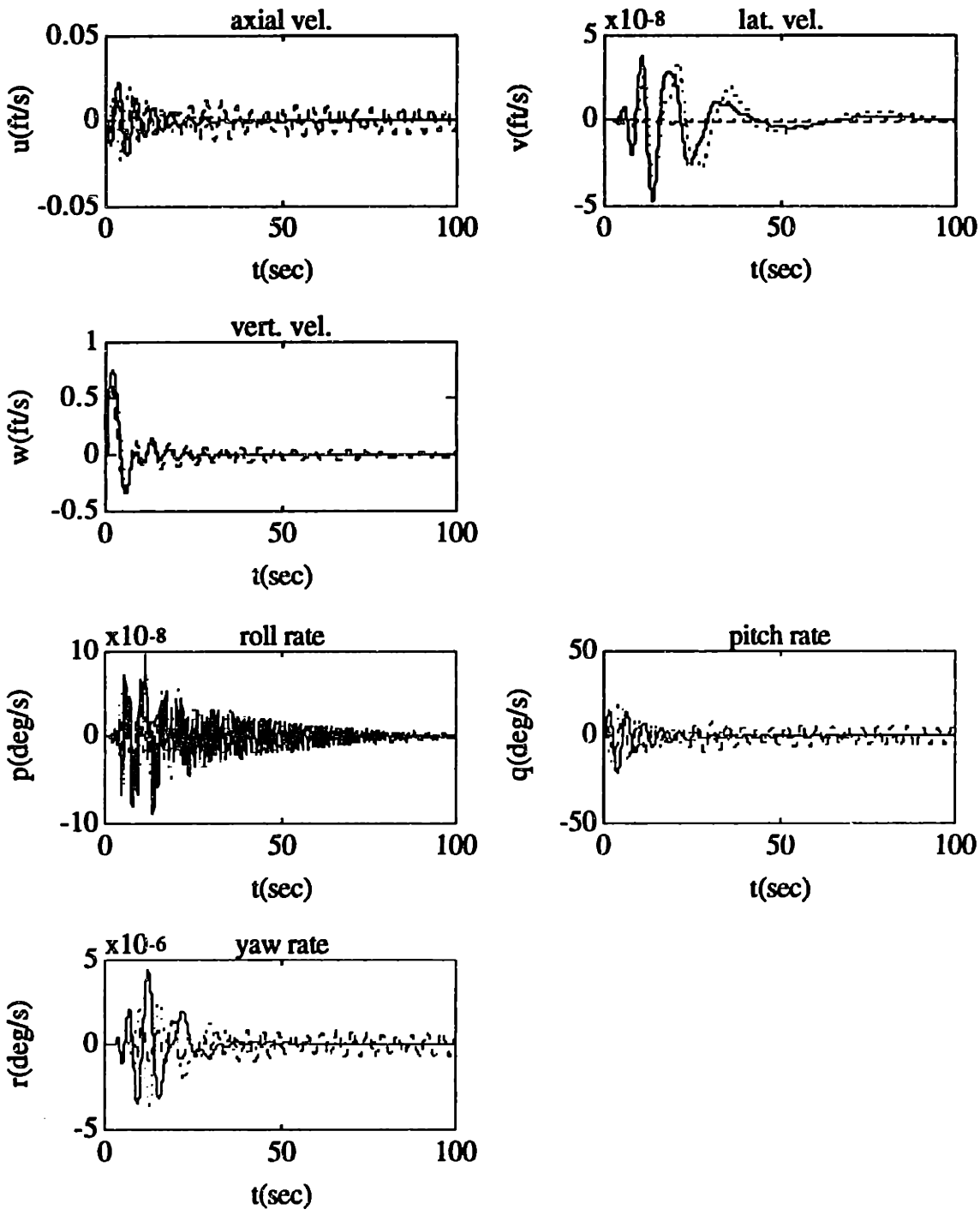

Figure 5.29: Robust Depth Step Response

Nominal (-), "Hovering" (--), "Full-Reverse" (..)

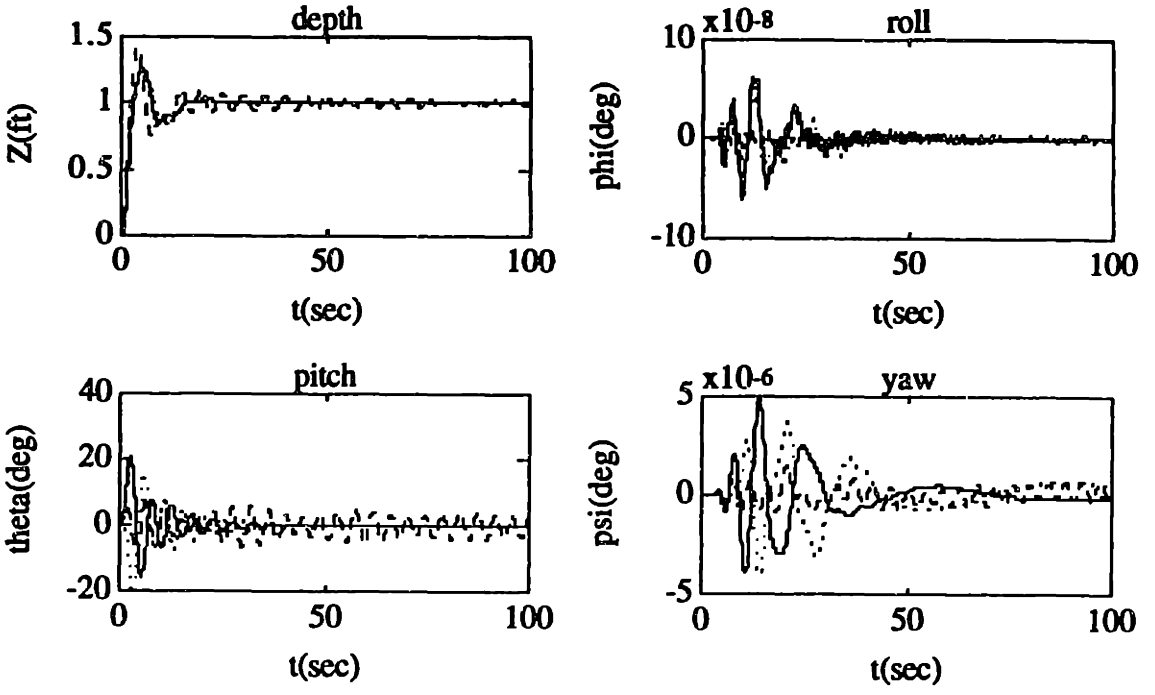

Figure 5.29: Robust Depth Step Response (continued)

Nominal (-), "Hovering" (--), "Full-Reverse" (..)

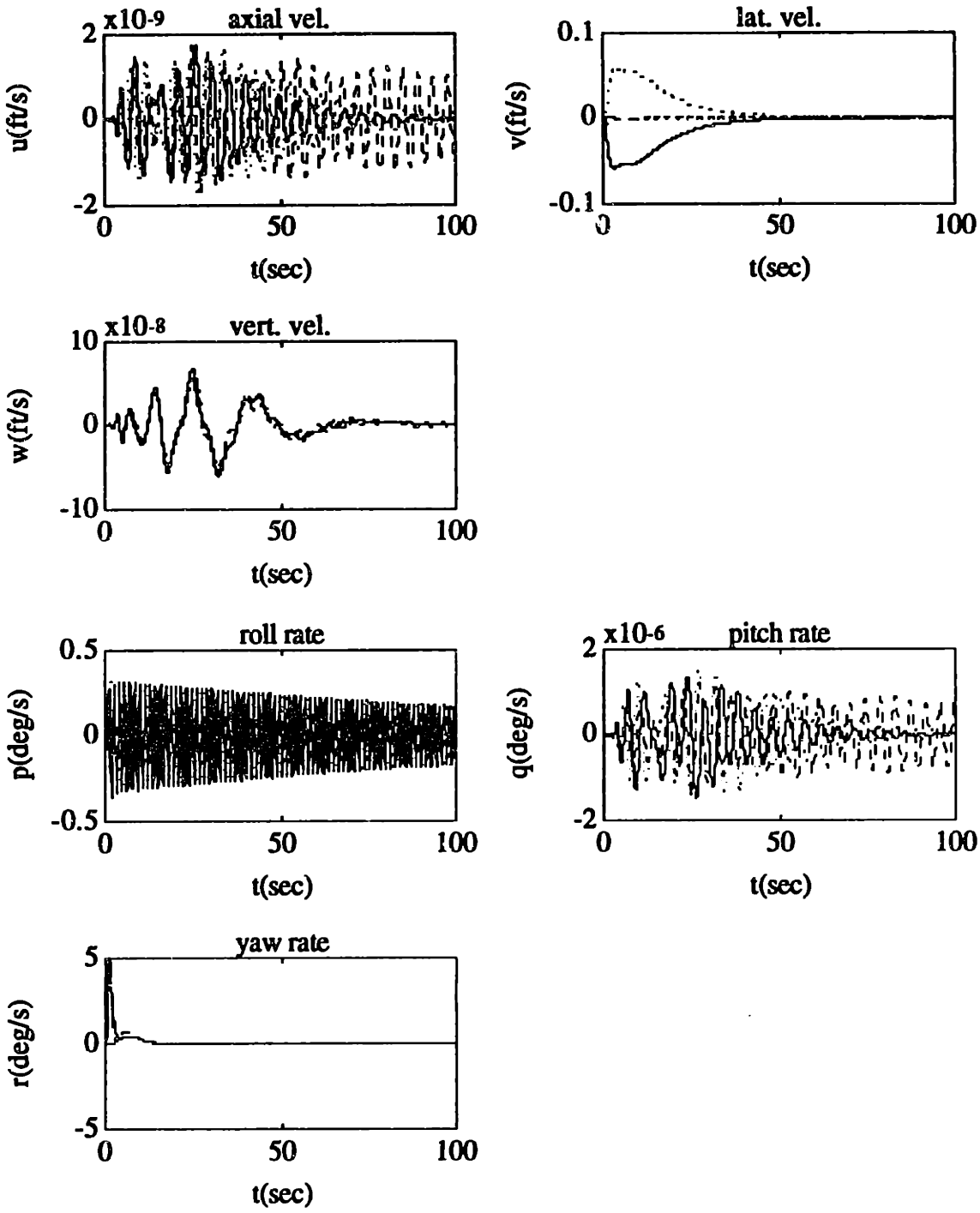

Figure 5.30: Robust Heading Step Response

Nominal (-), "Hovering" (--), "Full-Reverse" (..)

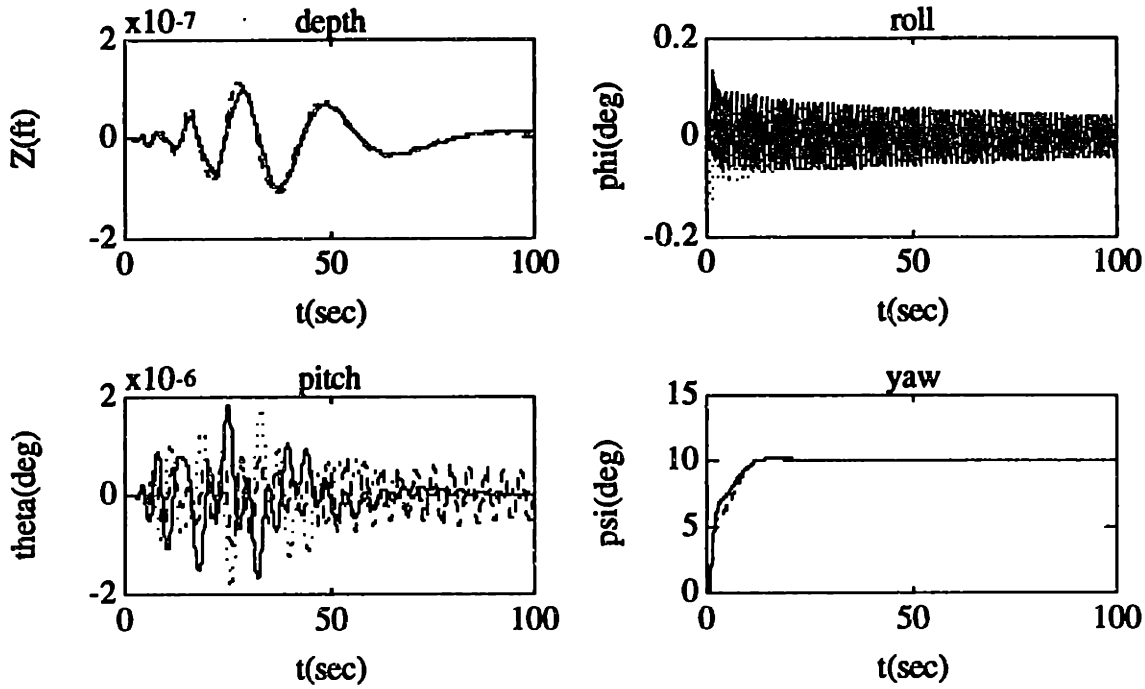

Figure 5.30: Robust Heading Step Response (continued)

Nominal (-), "Hovering" (--), "Full-Reverse" (..)

For the "hovering" model, the μ-synthesis controller appears to perform reasonably well, similarly to the robust H_∞ controller. Again, with the exception of the somewhat high depth overshoot and the slower heading response time, it still meets the specifications of Section 5.1 The pitch is somewhat more oscillatory than for the H_∞ controller, but stable (from an eigenstructure analysis of the closed-loop system, even though the pitch is nearly undamped). This is caused by the higher depth control gain. The axial and lateral velocities are also stabilized by this controller.

For the "full-reverse" model, the μ-synthesis controller also appears to perform reasonably well. As with the nominal model, it still meets the specifications of Section 5.1, with the exception of the depth overshoot and the heading response time. As with the H_∞ controller, the roll and pitch responses, plus the axial and lateral velocity responses, appear to be nearly the "mirror" images of the corresponding responses for the nominal case.

Robust Performance ("Added-Mass" Perturbations)

The next performance evaluation was done in order to test the robustness of the μ-synthesis design to perturbations in the AUV's "added mass" hydrodynamic coefficients. For the first model ("vehicle-light" model) used in this evaluation, the vehicle was assumed to have a negative 25% perturbation in the diagonal elements of the "mass and inertia" matrix, $\mathbf{E}_1$, corresponding to the axial, lateral, and vertical velocities and the yaw rate. From the AUV parametric uncertainty model of Section 5.2.1, this corresponds to $\Delta_1 = 0.5\mathbf{I}$ (i.e., $\mathbf{E}_1 = \mathbf{E}_{1o} - 0.5\mathbf{PN}$). For the second model ("vehicle-heavy" model), the vehicle was assumed to have a positive 50% perturbations in these elements (i.e., $\Delta_1 = -\mathbf{I}$, $\mathbf{E}_1 = \mathbf{E}_{1o} + \mathbf{PN}$). The depth step responses for these models are shown in Figure 5.31 (together with the nominal depth response), and the heading step response is shown in Figure 5.32 (together with the nominal heading response). Note that both the "vehicle-light" model and the "vehicle-heavy" model were linearized about the nominal axial velocity, u_0, of 1.0 ft/s.

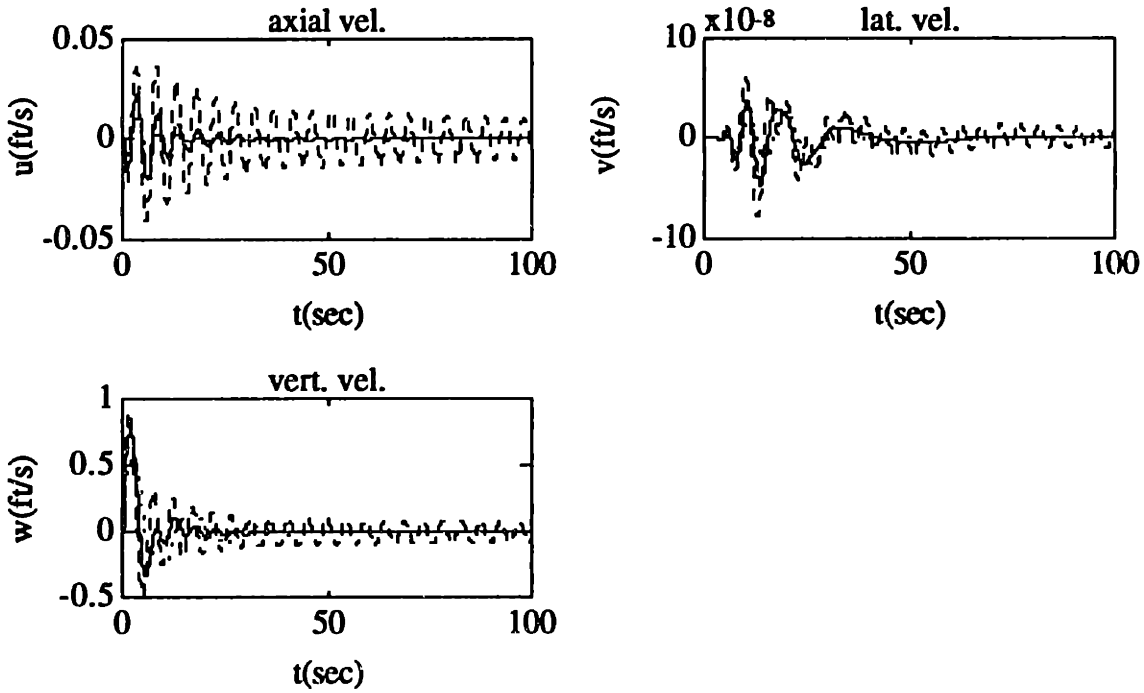

Figure 5.31: Robust Depth Step Response

Nominal (-), "Vehicle-Light" (--), "Vehicle-Heavy" (..)

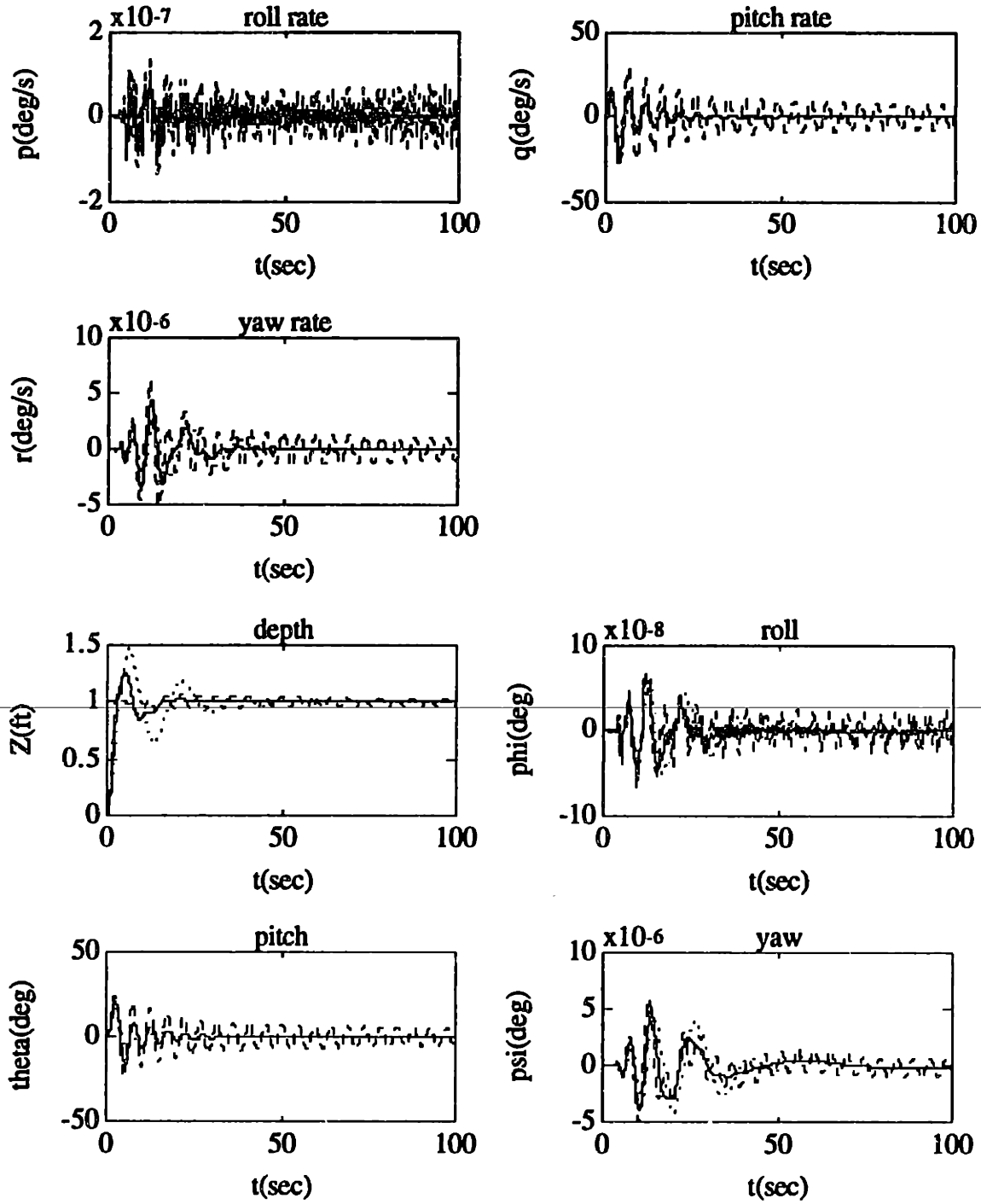

Figure 5.31: Robust Depth Step Response (continued)

Nominal (-), "Vehicle-Light" (--), "Vehicle-Heavy" (..)

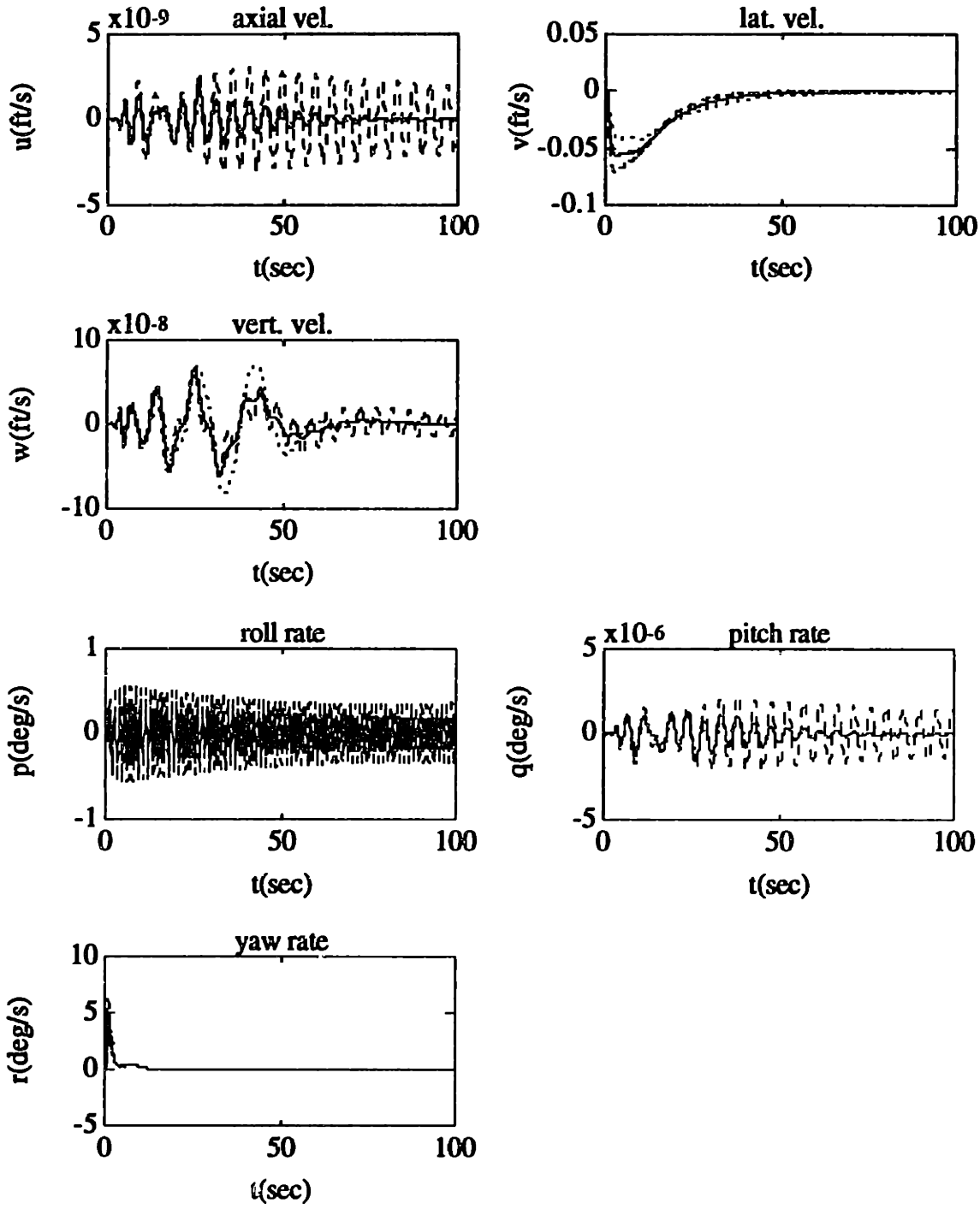

Figure 5.32: Robust Heading Step Response

Nominal (-), "Vehicle-Light" (--), "Vehicle-Heavy" (..)

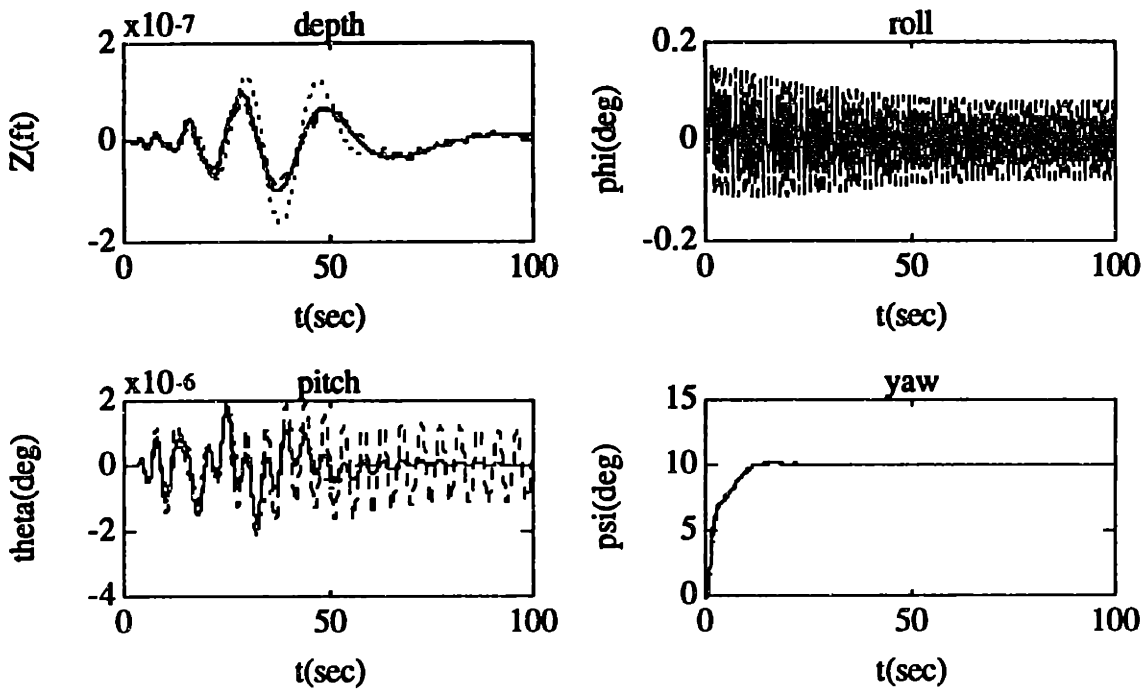

Figure 5.32: Robust Heading Step Response (continued)

Nominal (-), "Vehicle-Light" (--), "Vehicle-Heavy" (..)

For both the "vehicle-light" model and the "vehicle-heavy" model, the μ-synthesis controller appears to perform reasonably well. As with the H_∞ controller, it still meets the design specifications of Section 5.1, with the exception of the high depth overshoot and slower heading response time. However, the depth response and pitch response appear to be somewhat more oscillatory (especially for the "vehicle-light" case), due to the increased low-frequency depth-control gain.

Chapter 6

Sliding-Mode Vehicle Controller Design

The goal of this design effort is to synthesize heading and depth controllers for the *Sea Squirt* AUV using the Sliding-Mode robust control-design methodology described in Chapter 3. This chapter presents the revelant issues involved in the AUV Sliding-Mode design process. Section 6.1 reviews some of the general AUV control-system requirements and performance goals. Section 6.2 describes the design of the AUV depth and heading controllers using the Sliding-Mode methodology. Lastly, Section 6.3 illustrates the performance of the AUV Sliding-Mode controllers by using a computer simulation of the "nominal" design model.

6.1 CONTROL SYSTEM SPECIFICATIONS

The goal of the AUV control design effort is to design a controller that accepts commands from the higher-level behavioral "planning" programs and tries to force the vehicle to follow these commands. Recall from Chapter 4 that sensors are available on the AUV for measuring depth, heading, heading rate, pitch and roll. Depth rate is estimated by back-differencing and filtering the sensed depth. Since an axial speed transducer is not included in the AUV sensor suite, the forward speed of the vehicle is open-loop controlled.

Stability throughout all the vehicle's ranges and modes of operation is the most important requirement for the AUV control system. In other words, the controller must exhibit stability robustness for all valid bounded modeling perturbations. In terms of performance, the control system must be able to accept and follow with reasonable accuracy any and all combinations of valid heading and depth commands over the entire range of vehicle forward speeds.

In classical control-design, control system performance is frequently defined in terms of quantitative measures (such as maximum steady-state error, percentage overshoot, and response time). However, quantifying these performance measures are somewhat complicated by the fact that Sliding-Mode is a nonlinear tracking-control design technique. Instead, the AUV control system performance can be quantified by how well it tracks its "reference" state trajectory. This means that overshoot and steady-state error can be defined in an absolute sense rather than as percentages. Response time can be defined as the time required for the controller to reasonably "catch up" to and track the "reference" trajectory.

Numerical values for these performance measures are shown in Table 6.1.

Table 6.1: Preliminary AUV Control System Goals

Steady-State Depth Error	$\pm$1.0 feet
Steady-State Heading Error	$\pm$ 5.0 degrees
Depth Overshoot	1.0 feet
Heading Overshoot	10.0 degrees
Depth Response	10.0 seconds
Heading Response	5.0 seconds

These ad hoc performance goals are based on the "typical" mission requirements of the AUV. In addition, these goals are also influenced by the maximum performance levels of the actual vehicle hardware, such as the thrusters. Note that the depth response-time goal and the heading response-time goal are identical to the LTI performance goals presented in Section 5.1, whereas the steady-state error goals and overshoot goals are defined in the absolute sense stated earlier in this section.

6.2 SLIDING-MODE CONTROL LAW DESIGN

For the AUV Sliding-Mode robust control design, the reduced-order Descriptor/Companion nonlinear model developed in Chapter 4 was used. Recall that this 2nd-order model was given by

$$\frac{d}{dt}(\hat{\mathbf{x}}) = \dot{\hat{\mathbf{x}}}$$

$$\mathbf{E}\left[\frac{d}{dt}(\dot{\hat{\mathbf{x}}})\right] = \mathbf{E}\,\ddot{\hat{\mathbf{x}}} = \mathbf{f}(\mathbf{x}) + \mathbf{B}\mathbf{u} + \mathbf{d} \qquad (6.1)$$

The reduced-order total state vector was given by

$$\mathbf{x} = [\, Z\ \psi\ \dot{Z}\ \dot{\psi}\,]^T \qquad (6.2)$$

and the reduced-order output state vector was given by

$$\hat{\mathbf{x}} = [\, Z\ \psi\,]^T \qquad (6.3))$$

The control input vector was given by

$$\mathbf{u} = [\, U_Z\ U_\psi\,]^T \qquad (6.4)$$

and the disturbance vector was given by

$$\mathbf{d} = [\, d_Z(t)\ \ d_\psi(t)]^T \qquad (6.5)$$

The goal of the design effort is to find the Sliding-Mode controller that will force the output state of this reduced-order nonlinear model to track a "reference" trajectory, in the face of bounded parametric modeling-errors and disturbances.

6.2.1 Parametric Modeling-Error and Disturbance Bounds

For this AUV model, the "mass" matrix, **E**, had the following additive-uncertainty form

$$\mathbf{E} = \widehat{\mathbf{E}} - \Delta\mathbf{E} \tag{6.6}$$

with a nominal value, $\widehat{\mathbf{E}}$, given by

$$\widehat{\mathbf{E}} = \begin{bmatrix} [m - Z_{\dot{w}}] & 0 \\ 0 & \left[\dfrac{(I_{ZZ} - N_{\dot{r}})(m - Y_{\dot{v}}) - (N_{\dot{v}} - mX_g)(Y_{\dot{r}} - mX_g)}{(m - Y_{\dot{v}})}\right] \end{bmatrix} \tag{6.7}$$

For ease of computation, the matrix **E** was simply assumed to have a 50% uncertainty in each of its diagonal elements. The "off-diagonal" elements were assumed to be always zero (i.e., no coupling between the depth and heading dynamics). Then the upper bound matrix for the magnitude of the additive uncertainty in **E** is given by

$$\overline{\Delta\mathbf{E}} = 0.5\,|\mathbf{E}|$$

$$= \begin{bmatrix} 0.5\,|\,[m - Z_{\dot{w}}]\,| & 0 \\ 0 & 0.5\left|\left[\dfrac{(I_{ZZ} - N_{\dot{r}})(m - Y_{\dot{v}}) - (N_{\dot{v}} - mX_g)(Y_{\dot{r}} - mX_g)}{(m - Y_{\dot{v}})}\right]\right| \end{bmatrix} \tag{6.8}$$

The nonlinear vector transfer-function, **f(x)**, also had a similar additive-uncertainty form, with

$$\mathbf{f}(\mathbf{x}) = \widehat{\mathbf{f}}(\mathbf{x}) + \Delta\mathbf{f}(\mathbf{x}) \tag{6.9}$$

The nominal value of this transfer function was given by

$$\hat{\mathbf{f}}(\mathbf{x}) = \begin{bmatrix} Z_{w|w|}\dot{Z}|\dot{Z}| + (W - B) \\ N_{q|q|}\dot{\psi}|\dot{\psi}| \end{bmatrix} \tag{6.10}$$

For the 2nd-order Descriptor Companion nonlinear model described by (6.1), the following upper-bound vector was derived for magnitude of the additive uncertainty in f(x)

$$\overline{\Delta\mathbf{f}}(\mathbf{x}) = \begin{bmatrix} \left| \overline{\Delta Z_{w|w|}}\dot{Z}|\dot{Z}| + \overline{\Delta(W - B)} \right| \\ \left| \overline{\Delta N_{q|q|}}\dot{\psi}|\dot{\psi}| \right| \end{bmatrix}$$

$$= \begin{bmatrix} \left|\overline{\Delta Z_{w|w|}}\right| |\dot{Z}|^2 + \left|\overline{\Delta(W - B)}\right| \\ \left|\overline{\Delta N_{q|q|}}\right| |\dot{\psi}|^2 \end{bmatrix} \tag{6.11}$$

For this design, the hydrodynamic coefficients were assumed to have a maximum uncertainty of 50%. The magnitude of the error in the "net" buoyancy, (W-B), was assumed to be less than 1.0 lb. Then the upper-bound vector for the uncertainty in f(x) was simply given by

$$\overline{\Delta\mathbf{f}}(\mathbf{x}) = \begin{bmatrix} 0.5\,|Z_{w|w|}|\,|\dot{Z}|^2 + 1.0 \\ 0.5\,|N_{q|q|}|\,|\dot{\psi}|^2 \end{bmatrix} \tag{6.12}$$

The control-input matrix, B, of the 2nd-order Descriptor Companion nonlinear model was given by

$$\mathbf{B} = \begin{bmatrix} 1 & 0 \\ 0 & Y_T \end{bmatrix} \tag{6.13}$$

Uncertainty in this matrix was neglected since the "gain" errors of the thrusters were assumed to be small. The thruster moment-arm length, Y_T was also assumed to be well known.

For the AUV model, the disturbance input, **d**, must account for factors such as environmental disturbances and nonlinearities not included in previous parametric modeling-error description. Finding the corresponding upper bound for these factors, however, is not as straightforward as finding the upper bound for the parametric uncertainty. In addition, if the disturbance upper bound is chosen larger than the maximum force that the thrusters can deliver, the performance of the control design will possibly suffer.

Therefore, for this design, the upper bound for the magnitude of the depth disturbance force was simply chosen to be one-half the maximum vertical thrust force. Similarly, the upper bound for the magnitude of the heading disturbance torque was assumed to be one-half the maximum torque generated by the port and starboard thrusters. The disturbance upper-bound vector was then given by

$$\bar{\mathbf{d}} = \begin{bmatrix} 0.5 \max |T_V| \\ 0.5 \max |Y_T(T_p - T_s)| \end{bmatrix} \tag{6.14}$$

For the AUV, the maximum thrust force for all the thrusters was assumed to be 5.0 lb., which then gave a disturbance upper bound of

$$\bar{\mathbf{d}} = \begin{bmatrix} 2.5 \\ 5.0\ Y_T \end{bmatrix} \tag{6.15}$$

6.2.2 Development of the AUV Sliding-Mode Control Law

The goal of the Sliding-Mode control design is for the state vector given by **x** to track a time-varying reference "trajectory" vector given by $\mathbf{x}_d$. The design of the Sliding-Mode controller consisted of several steps. A linear sliding-surface of the form

$$s(\tilde{x}) = \sum_{p=0}^{n-1} \binom{n-1}{p} \Lambda^p \tilde{\tilde{x}}^{(n-1-p)} \tag{6.16}$$

was developed. For the AUV model, the sliding-surface was defined to be a first-order surface, given by

$$s(\tilde{x}) = \dot{\tilde{x}} + \Lambda \tilde{x} \tag{6.17}$$

Recall that the AUV depth and heading dynamics were essentially decoupled. This implies that if Λ is given by the following diagonal form

$$\Lambda = \begin{bmatrix} \lambda_{11} & 0 \\ 0 & \lambda_{22} \end{bmatrix} \tag{6.18}$$

then the design of the AUV depth and heading control systems can be done separately (but concurrently). For this case, λ_{11} can be used for the design of the depth control system, and λ_{22} can be used for the design of the heading control system.

From Chapter 3, the Sliding-Mode Control Law with "boundary-layer" for the Descriptor/Companion model is given by

$$u = \hat{u} - K(\tilde{x})\mathrm{sat}(s(\tilde{x})\Phi^{-1}) \tag{6.19}$$

For the AUV control design using the first-order sliding-surface, the "nominal" control law had the form

$$\hat{u} = B^{-1}\left(-\hat{f}(x) + \hat{E}\left(\ddot{\tilde{x}}_d - \Lambda \dot{\tilde{x}}\right)\right) \tag{6.20}$$

while the diagonal "feedback" matrix had the form

$$\text{diag}[\mathbf{K}(\tilde{\mathbf{x}})] = \mathbf{B}^{-1}\left(\overline{\Delta\mathbf{E}}\,\overline{\ddot{\tilde{\mathbf{x}}}} + \overline{\Delta\mathbf{f}}(\mathbf{x}) + \bar{\mathbf{d}} + \eta\hat{\mathbf{E}}\begin{bmatrix}1\\1\end{bmatrix}\right) \tag{6.21}$$

The maximum depth acceleration was assumed to be less than 0.2 ft/s^2, while the maximum heading acceleration was assumed to be less than 5.0 deg/s^2 (approximately 0.1 rad/s^2). Then the upper-bound acceleration vector is simply given by

$$\overline{\ddot{\tilde{\mathbf{x}}}} = \begin{bmatrix} 0.2 \\ 0.1 \end{bmatrix} \tag{6.22}$$

The scalar η was chosen to be zero.

6.2.3 Controller Bandwidth Selection

Recall from Chapter 3 that if Λ is chosen such that the matrix, $-\Lambda$, is Hurwitz, then the state-tracking error will decay eventually to zero, with dynamics governed by the linear matrix differential equation

$$\left(\frac{d}{dt} + \Lambda\right)^{n-1}\tilde{\tilde{\mathbf{x}}} = 0 \tag{6.23}$$

in the absence of modeling errors or disturbances. For the first-order sliding-surface described by (6.17), this implies that the "nominal" tracking-error dynamics are governed by the first-order linear matrix differential equation

$$\dot{\tilde{\tilde{\mathbf{x}}}} + \Lambda\tilde{\tilde{\mathbf{x}}} = 0 \tag{6.24}$$

The eigenvalues of the diagonal matrix, Λ, given by (6.18), are simply the coefficients, λ_{11} and λ_{22}. Equation (6.24) implies (in the absence of modeling errors or disturbances) the depth tracking-error will decay to zero with a time constant given by the inverse of λ_{11}. Similarly, the heading tracking-error will decay to zero with a time

constant given by the inverse of λ_{22}. From classical control theory for a first-order system, this then implies that the nominal closed-loop bandwidth of the depth control system is given by λ_{11} and the nominal bandwidth of the closed-loop heading control system is given by λ_{22}.

As with classical control design, selection of the Sliding-Mode control-system bandwidth involves a number of tradeoffs The higher the bandwidth, the better the system performance, in terms of both tracking error and response time. However, "chattering" and/or instability may result if the bandwidth is chosen too high (exciting some unmodeled dynamic mode). Also, the bandwidth is constrained by both unmodeled time delays and the controller sampling rate (if the controller is implemented in discrete-time).

In the literature [15,16] several quantitative design "rule-of-thumb" constraints have been developed as aids in choosing the Sliding-Mode bandwidth. For unmodeled modes, the constraint is given by

$$\omega_b < 0.4\ [\omega_{\text{unmodeled mode}}]_{\min} \tag{6.25}$$

where ω_b is the system bandwidth. For unmodeled time-delays, the corresponding constraint is given by

$$\omega_b < \frac{1}{3\ [T_d]_{\max}} \tag{6.26}$$

The bandwidth constraint due to the controller sampling rate is given by

$$\omega_b < \frac{\omega_s}{5} \tag{6.27}$$

For the *Sea Squirt* AUV, the controller has a sampling rate of approximately 31.4 rad/s (5.0 Hz). From (6.25), this implies that the Sliding-Mode closed-loop bandwidth should be less than about 6.0 rad/s. From Chapter 4, the largest unmodeled time-delay is a 0.2 second time-delay associated with the thruster dynamics. From (6.26), this gives a

bandwidth constraint of about 1.7 rad/s. The lowest-frequency unmodeled mode is a first-order lag of about 1.3 rad/s (also associated with the thruster dynamics). From (6.27), this gives a bandwidth constraint of about 0.5 rad/s, which is the smallest of all the constraints. Therefore, this constraint value was used as the Sliding-Mode closed-loop bandwidth for both the depth control system and the heading control system. This then gave λ_{11} equal to 0.5 rad/s and λ_{22} equal to 0.5 rad/s.

6.2.4 Controller Boundary-Layer Selection

From Chapter 3, the elements of the diagonal "interpolating" boundary layer matrix Φ must be chosen large enough so as to eliminate undesirable high-frequency control "chattering". However, also recall that the guaranteed output tracking precision (for the AUV 2nd order system) is given by

$$\left|\tilde{x}\right| = \left|x - x_d\right| \leq \Lambda^{-1}\mathrm{diag}(\Phi) \tag{6.28}$$

Thus, Φ provides a direct tradeoff between stability-robustness and performance. In the literature [16], for diagonal Λ and $K(\tilde{x})$, Φ is usually chosen to be

$$\begin{aligned}\mathrm{diag}[\Phi] &= \max_{\tilde{x}} \mathrm{diag}\left[K(\tilde{x})\Lambda^{-1}\right] \\ &= \max_{\tilde{x}} \mathrm{diag}\left[B^{-1}\left(\overline{\Delta E}\,\tilde{\tilde{x}} + \overline{\Delta f}(x) + \bar{d}\right)\Lambda^{-1}\right]\end{aligned} \tag{6.29}$$

For the AUV, the maximum depth rate was assumed to be 1.0 ft/s, and the maximum heading rate was assumed to be 15.0 deg/s (approximately 0.26 rad/s). Using the numerical parameter values of Appendix D, the following value for Φ was calculated

$$\Phi = \begin{bmatrix} 11.2 & 0 \\ 0 & 11.1 \end{bmatrix} \tag{6.30}$$

From (6.28) and (6.30), the guaranteed output tracking precision is then given by

$$|\tilde{x}| = |x - x_d| \leq \begin{bmatrix} 22.4 \\ 22.2 \end{bmatrix} \tag{6.31}$$

provided that the modeling-error and disturbance bounds are not exceeded. Note that this bound is quite conservative (as to be essentially useless from a robustness standpoint) in that it gives a depth tracking-error bound of *22.4 feet* and a heading tracking-error bound of *22.2 radians* (approximately *1272 degrees*). One implication of (6.31) is that it may be necessary to decrease the boundary-layer width for the final AUV Sliding-Mode control design.

6.3 NOMINAL SIMULATION PERFORMANCE OF THE AUV SLIDING-MODE CONTROLLER

A preliminary test of the nominal performance of the AUV Sliding-Mode controller was done in order to see how well this particular controller meets the design goals specified in Section 6.1. This test was performed using a MATLAB™ computer simulation based on the reduced-order Descriptor/Companion nonlinear design model. This simulation also included the model of the thruster dynamics presented in Chapter 4. The sensor dynamics were neglected. The model coefficients were given the nominal values shown in Appendix D. The commanded depth trajectory was from 0.0 to 10.0 ft. (with a maximum depth rate of 0.5 ft/sec and a maximum depth acceleration of 0.2 ft/sec^2), and the commanded heading trajectory was from 0.0 to 180.0 degrees (with a maximum heading rate of 15.0 deg/sec and a maximum heading acceleration of 5.0 deg/sec^2).

The results of this test are shown in Figure 6.1 and Table 6.2. For the numerical values shown in Table 6.2, the response time was defined as the time period starting where the reference trajectory reaches its final value (within 0.1 feet for depth and within 0.5 degrees for heading) and ending where the vehicle first obtains this value (within 0.1 feet for depth and within 0.5 degrees for heading). The maximum overshoot was defined as

the difference between the maximum value reached by the vehicle and the maximum value reached by the reference trajectory.

The nominal steady-state error performance of the Sliding-Mode controller met the design goal specified in Table 6.1, as well as the depth overshoot and heading overshoot. Both the depth and heading response times were slower than specified. However, the response times were judged to be acceptable since any attempt at improving them would probably increase the overshoot (due to the lag caused by the thruster dynamics).

Table 6.2: Nominal Performance Test of the AUV Sliding-Mode Controller (with Performance Specifications in Parentheses)

Steady-State Depth Error	0.0 feet ($\pm$1.0 feet)
Steady-State Heading Error	0.0 degrees ($\pm$5.0 degrees)
Depth Overshoot	0.395 feet (1.0 feet)
Heading Overshoot	6.20 degrees (10.0 degrees)
Depth Response	12.0 seconds (10.0 seconds)
Heading Response	20.0 seconds (5.0 seconds)

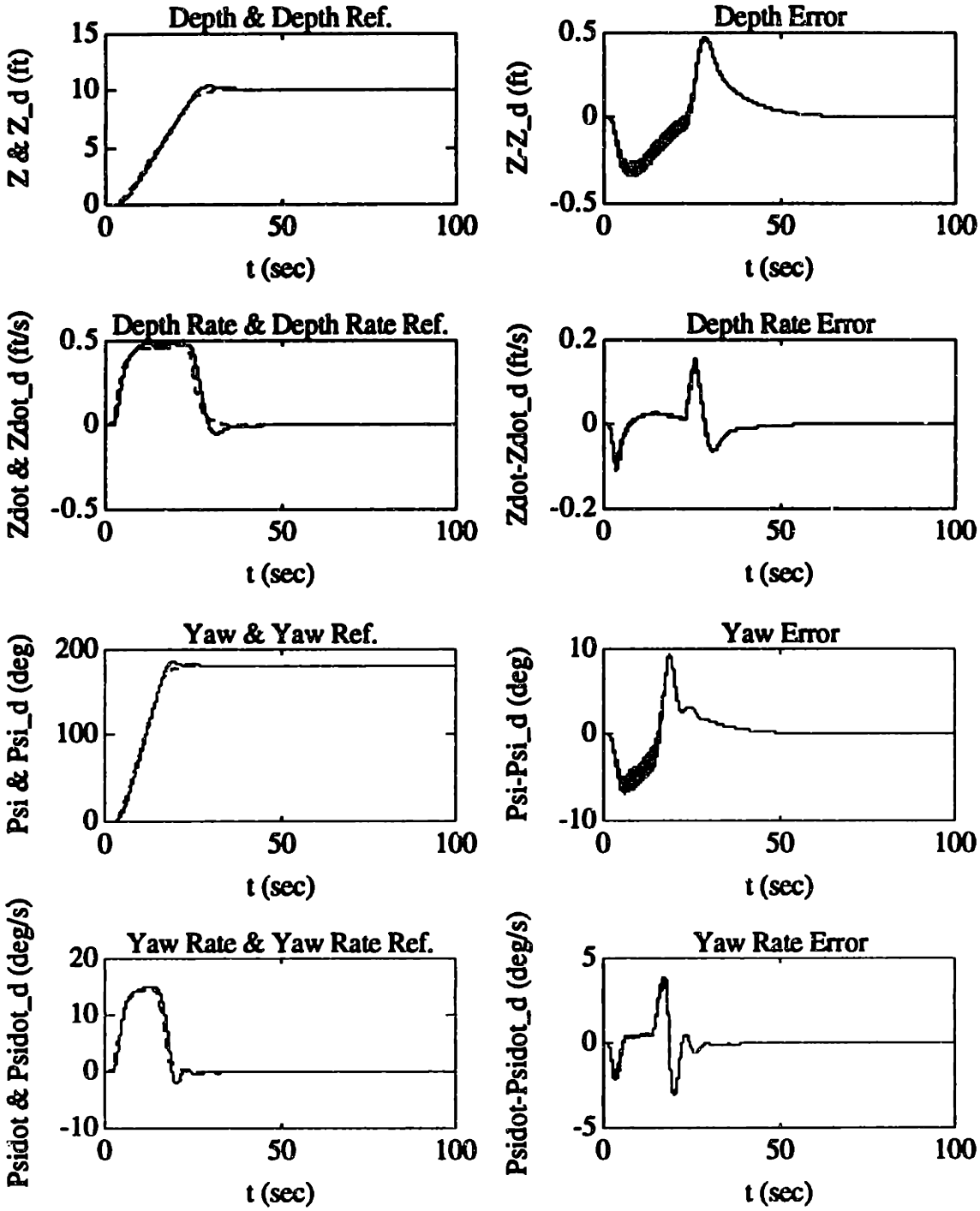

Figure 6.1: Nominal Performance Test of the AUV Sliding-Mode Controller

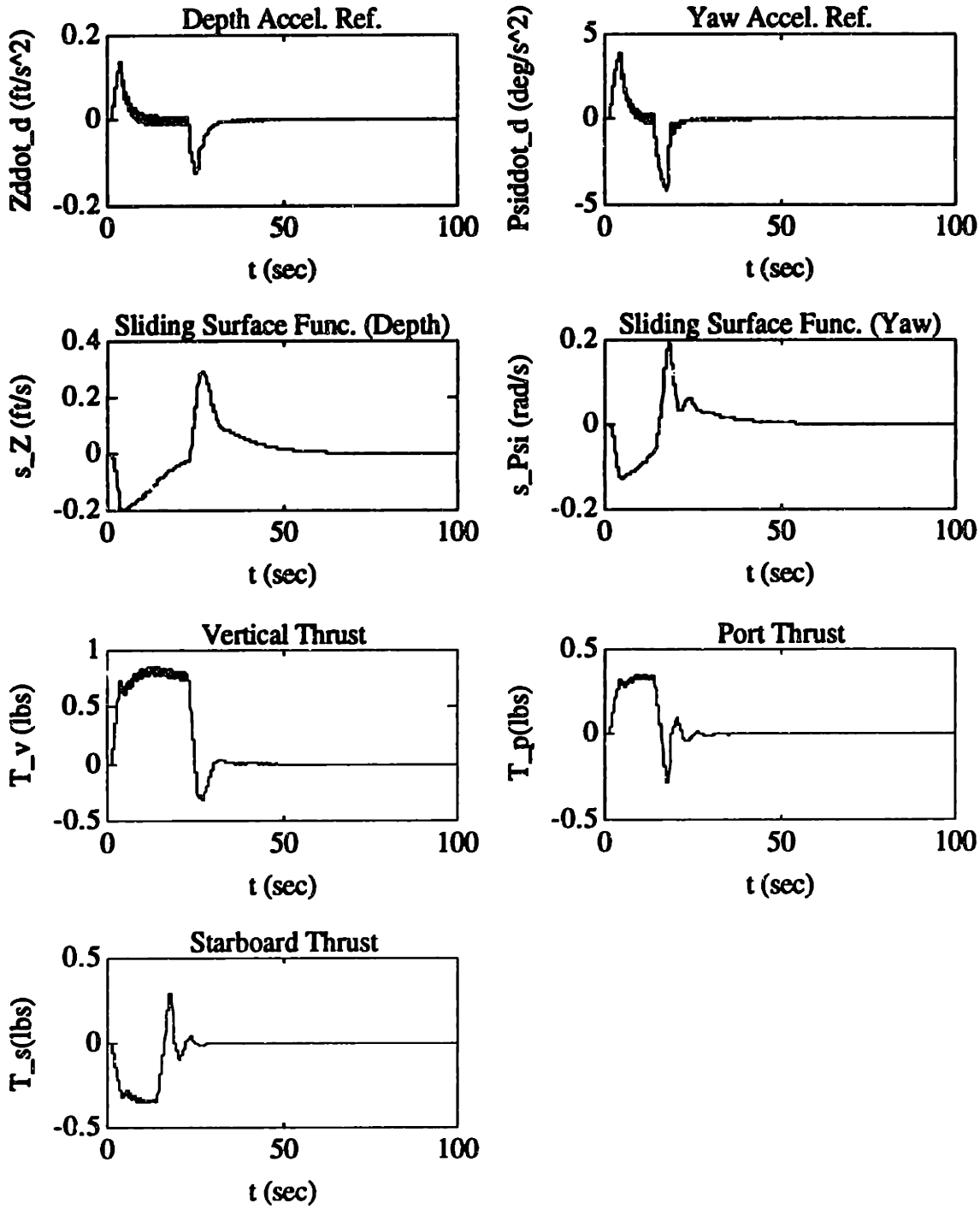

Figure 6.1: Nominal Performance Test of the AUV Sliding-Mode Controller (continued)

Chapter 7

Sliding-Mode Augmented Vehicle Controller Design

The goal of this design effort is to synthesize heading and depth controllers for the *Sea Squirt* AUV using the Sliding-Mode Augmented robust control-system design methodology described in Chapter 3, together with the reduced-order models developed in Chapter 4. This chapter presents the issues involved in this design process. Section 7.1 reviews some of the general AUV control system requirements and performance goals. Section 7.2 describes the design of the augmented LTI controller using H_∞/μ-synthesis and the reduced-order LTI model. Next, Section 7.3 details the design of the AUV Sliding-Mode Augmented control law. Lastly, Section 7.4 details the performance of the Sliding-Mode Augmented AUV controller using a simulation of the "nominal" nonlinear design model.

7.1 CONTROL SYSTEM SPECIFICATIONS

For the AUV control system design, the goal is to design a controller that accepts commands from the higher-level behavioral "planning" programs and tries to force the vehicle to follow these commands. As discussed previously, sensors are available on the AUV for measuring depth, heading, heading rate, pitch and roll. The AUV's depth rate is estimated by back-differencing and filtering the sensed depth. The forward speed of the vehicle is controlled with an open-loop strategy (since an axial velocity transducer is not included in the AUV sensor suite).

Recall from the previous design efforts of Chapter 5 and Chapter 6 that the most important requirement for the AUV control system is stability throughout the vehicle's ranges and modes of operation. This means that the controller must exhibit stability robustness for all valid bounded modeling perturbations. In terms of performance, the control system must be able to accept and follow with reasonable accuracy any and all combinations of valid heading and depth commands over the entire range of forward speeds commanded by the open-loop speed controller.

For a LTI control system, performance is frequently defined in terms of quantitative measures such as maximum steady-state error, percentage overshoot, and response time to step inputs. As with the Sliding-Mode design effort of Chapter 6, quantifying these performance measures are somewhat complicated by the fact that Sliding-Mode (and Sliding-Mode Augmented) is essentially a nonlinear tracking-control design technique. A solution is to quantify the AUV control system performance by how well it tracks its "reference" state trajectory. Overshoot and steady-state error can be defined in an absolute sense rather than as percentages. Response time can be defined as the time required for the controller to reasonably "catch up" to and track the "reference" trajectory.

Numerical values for these performance measures are shown in Table 7.1.

Table 7.1: Preliminary AUV Control System Goals

Steady-State Depth Error	$\pm$1.0 feet
Steady-State Heading Error	$\pm$ 5.0 degrees
Depth Overshoot	1.0 feet
Heading Overshoot	10.0 degrees
Depth Response	10.0 seconds
Heading Response	5.0 seconds

Note that these goals are the same as the performance goals of the Sliding-Mode design effort of Chapter 6.

7.2 LTI CONTROLLER DESIGN

In order to apply the H_∞/μ-synthesis methodology to the design of the augmented linear controller for the *Sea Squirt* AUV control system, the reduced-order LTI model derived in Chapter 4 must be converted into the Standard Form model described in Chapter 2. This involves defining both an uncertainty model and a frequency-domain "loop shaping" performance formulation.

7.2.1 Derivation of the Reduced-Order AUV Uncertainty Model

Recall from Chapter 4 that the reduced-order AUV model (without sensor or thruster dynamics) is given by the following generalized state-space description

$$\frac{d}{dt}(\hat{\mathbf{x}}) = \dot{\hat{\mathbf{x}}}$$

$$\mathbf{E}_p\left[\frac{d}{dt}(\dot{\hat{\mathbf{x}}})\right] = \mathbf{E}_p\ddot{\hat{\mathbf{x}}} = \mathbf{A}_p\mathbf{x} + \mathbf{B}_p\mathbf{u} + \mathbf{d} \qquad (7.1)$$

The reduced-order total state vector is given by

$$\mathbf{x} = [\, Z \;\psi\; \dot{Z} \;\dot{\psi}\,]^T \qquad (7.2)$$

and the reduced-order "controlled-output" state vector is given by

$$\hat{\mathbf{x}} = [\, Z \;\psi\,]^T \qquad (7.3)$$

The control input vector is given by

$$\mathbf{u} = [\, U_Z \; U_\psi\,]^T$$

$$= [\, T_v \;\; (T_s - T_p)\,]^T \qquad (7.4)$$

and the disturbance vector is given by

$$\mathbf{d} = [\, d_Z(t) \;\; d_\psi(t)]^T \tag{7.5}$$

Note that all of the states given by (7.2) were assumed to be available for feedback (i.e., y = x).

The reduced-order LTI model given by (7.1) can also be written in the form

$$\begin{bmatrix} \mathbf{I} & \mathbf{0} \\ \mathbf{0} & \mathbf{E_p} \end{bmatrix} \dot{\mathbf{x}} = \begin{bmatrix} [\, \mathbf{0} \;\; \mathbf{I} \,] \\ \mathbf{A_p} \end{bmatrix} \mathbf{x} + \begin{bmatrix} \mathbf{0} \\ \mathbf{B_p} \end{bmatrix} \mathbf{u} + \begin{bmatrix} \mathbf{0} \\ \mathbf{I} \end{bmatrix} \mathbf{d} \tag{7.6}$$

which can be simplified to

$$\mathbf{E_1}\dot{\mathbf{x}} = \mathbf{A_1}\mathbf{x} + \mathbf{B_1}\mathbf{u} + \mathbf{L_1}\mathbf{d} \tag{7.7}$$

Parametric State-Space Uncertainty

From Chapter 2, parametric uncertainty in the reduced-order LTI system given by (7.7) can be described by the following uncertainty model

$$\left(\mathbf{E_{1o}} - \sum_{j=1}^{m} [\Delta \mathbf{E_1}]_j \delta_j\right)\dot{\mathbf{x}} = \left(\mathbf{A_{1o}} + \sum_{i=1}^{k} [\Delta \mathbf{A_1}]_i \delta_i\right)\mathbf{x} + \left(\mathbf{B_{1o}} + \sum_{i=1}^{k} [\Delta \mathbf{B_1}]_i \delta_i\right)\mathbf{u} + \mathbf{L_1}\mathbf{d} \tag{7.8}$$

This uncertainty model consists of a set of nominal dynamics, $[\mathbf{E_{1o}}, \mathbf{A_{1o}}, \mathbf{B_{1o}}]$, plus a set of bounded parametric perturbation matrices, $[\Delta \mathbf{E_1}, \Delta \mathbf{A_1}, \Delta \mathbf{B_1}]$. The scalars, δ_i and δ_j, represent normalized parameter errors of the form

$$-1 < \delta_i < 1 \quad \forall\, i \tag{7.9}$$

$$-1 < \delta_j < 1 \quad \forall\, j \tag{7.10}$$

For this AUV model, the nominal value of the "mass" matrix, $\mathbf{E}_p$, was given by

$$\mathbf{E}_{po} = \begin{bmatrix} [m - Z_{\dot{w}}] & 0 \\ 0 & \left[\dfrac{(I_{ZZ} - N_{\dot{r}})(m - Y_{\dot{v}}) - (N_{\dot{v}} - mX_g)(Y_{\dot{r}} - mX_g)}{(m - Y_{\dot{v}})}\right] \end{bmatrix} \tag{7.11}$$

while the nominal value of the matrix, $\mathbf{A}_p$, was given by

$$\mathbf{A}_{po} = \begin{bmatrix} 0 & 0 & 2Z_{w|w|}|\dot{Z}_o| & 0 \\ 0 & 0 & 0 & 2N_{q|q|}|\dot{\psi}_o| \end{bmatrix} \tag{7.12}$$

For this model, it was assumed that there was no coupling between the depth and heading dynamics. This gave the following structure for the bounds on the parametric uncertainty in $\mathbf{E}_1$ and $\mathbf{A}_1$

$$\left| \sum_{j=1}^{m} [\Delta \mathbf{E}_1]_j \delta_j \right| \leq \begin{bmatrix} 0 & 0 & 0 & 0 \\ 0 & 0 & 0 & 0 \\ 0 & 0 & \Delta e_{33} & 0 \\ 0 & 0 & 0 & \Delta e_{44} \end{bmatrix} \tag{7.13}$$

$$\left| \sum_{i=1}^{k} [\Delta \mathbf{A}_1]_i \delta_i \right| \leq \begin{bmatrix} 0 & 0 & 0 & 0 \\ 0 & 0 & 0 & 0 \\ 0 & 0 & \Delta a_{33} & 0 \\ 0 & 0 & 0 & \Delta a_{44} \end{bmatrix} \tag{7.14}$$

Note that the diagonal terms of ΔE_1 correspond to errors in the "added mass" hydrodynamic coefficients (since the vehicle's center-of-gravity, mass, and inertia were assumed to be well known), while the diagonal terms of ΔA_1 correspond to errors in the "drag" coefficients.

The control-input matrix, B_p, of the reduced-order linear model was given by

$$B_p = \begin{bmatrix} 1 & 0 \\ 0 & Y_T \end{bmatrix} \tag{7.15}$$

Uncertainty in this matrix was neglected since the "gain" errors of the thrusters were assumed to be small. The thruster moment-arm length, Y_T was also assumed to be well known.

For this design, the nominal operating point of the AUV was chosen to be the "hovering" condition of zero depth rate and zero heading rate. Bounds on the ΔE_1 perturbation matrices were chosen by assuming that each corresponding term in E_1 has a 50% maximum uncertainty. Bounds on the ΔA_1 perturbation matrices were determined by performing a numerical comparison between the nominal design model and the reduced-order models corresponding to the case of a "full-speed" dive of 1.0 ft/sec and a "full-speed" turn of 15 deg/sec (with a 50% maximum uncertainty in the drag coefficients). From this comparison, the following numerical bounds were selected.

Table 7.2: Parametric Uncertainty Bounds for Reduced-Order LTI Model

Uncertainty Term	Perturbation Bound
Δe_{33}	1.6450
Δe_{44}	1.3319
Δa_{33}	10.470
Δa_{44}	4.3982

These bounds were then used to convert the parametric-uncertainty matrices into the following representations

$$\sum_{j=1}^{m} [\Delta \mathbf{E}_1]_j \delta_j = [\mathbf{P}][\Delta_1][\mathbf{N}] \tag{7.16}$$

$$\sum_{i=1}^{k} [\Delta \mathbf{A}_1]_i \delta_i = [\mathbf{Q}][\Delta_2][\mathbf{S}] \tag{7.17}$$

For this uncertainty representation, **P**, **N**, **Q**, and **S** are constant-valued weighting matrices and Δ_1 and Δ_2 are complex perturbations with norm bounds

$$\bar{\sigma}[\Delta_1(j\omega)] < 1 \ \forall \ \omega \tag{7.18}$$

$$\bar{\sigma}[\Delta_2(j\omega)] < 1 \ \forall \ \omega \tag{7.19}$$

The AUV uncertainty model of (7.8) can be simplified to the form

$$\begin{aligned} \dot{\mathbf{x}} &= \mathbf{E}_{1o}^{-1}\mathbf{A}_{1o}\mathbf{x} + \mathbf{E}_{1o}^{-1}\mathbf{B}_{1o}\,\mathbf{u} + \mathbf{E}_{1o}^{-1}\mathbf{L}_1\mathbf{d} + \mathbf{E}_{1o}^{-1}\mathbf{P}\eta_1 + \mathbf{E}_{1o}^{-1}\mathbf{Q}\eta_2 \\ \varepsilon_1 &= \mathbf{N}\dot{\mathbf{x}} \\ &= \mathbf{N}\mathbf{E}_{1o}^{-1}\mathbf{A}_{1o}\mathbf{x} + \mathbf{N}\mathbf{E}_{1o}^{-1}\mathbf{B}_{1o}\mathbf{u} + \mathbf{N}\mathbf{E}_{1o}^{-1}\mathbf{L}_1\mathbf{d} + \mathbf{N}\mathbf{E}_{1o}^{-1}\mathbf{P}\eta_1 \\ &\quad + \mathbf{N}\mathbf{E}_{1o}^{-1}\mathbf{Q}\eta_2 \\ \varepsilon_2 &= \mathbf{S}\mathbf{x} \end{aligned} \tag{7.20}$$

where η_1 is the output of Δ_1, η_2 is the output of Δ_2, ε_1 is the input of Δ_1, and ε_2 is the input of Δ_1.

Uncertain Dynamic Model (Munk Moment)

Recall from the analysis of Section 4.5.2 that the reduced-order AUV LTI model provides a reasonable approximation to the full-order AUV LTI model for low axial speeds. However, for both the full-order linear model and the full-order nonlinear model, there is a destabilizing Munk moment (and consequently an unstable mode) dependent on the axial velocity. In addition, recall that for the reduced-order LTI model, this destabilizing moment does not appear. From a design perspective, this is a somewhat serious issue (since for nonzero axial velocities, a stable reduced-order LTI model is being used to approximate an unstable full-order LTI model). However, from Section 2.2.2, one possible solution to this issue would be to include the Munk moment effect as a dynamic model error (using the feedback uncertainty representation).

From previous AUV modeling and control design efforts[18], plus the full-order AUV Equations-of-Motion presented in Section 4.2.1, the hydrodynamic expression for the Munk moment about the yawing axis is given by

$$\tau_{Munk} = N_{uv}uv \tag{7.21}$$

where u is the axial velocity and v is the lateral velocity. From Section 4.3.1, the (unsimplified) reduced-order lateral force equation is given by

$$\begin{aligned}\left[\frac{(I_{ZZ} - N_{\dot{r}})(m - Y_{\dot{v}}) - (N_{\dot{v}} - mX_g)(Y_{\dot{r}} - mX_g)}{(I_{ZZ} - N_{\dot{r}})}\right]\dot{v} \\ = \left[\frac{Y_{\dot{r}} - mX_g}{I_{ZZ} - N_{\dot{r}}}\right][\, N_{r|r|}\dot{\psi}|\dot{\psi}| + (N_{ur} - mX_g)u\dot{\psi} \\ + N_{uv}uv + Y_T(T_p - T_s) + D_r\,] \\ + Y_{v|v|}v|v| + (Y_{ur} - m)u\dot{\psi} + Y_{uv}|u|v + D_v\end{aligned} \tag{7.22}$$

If both the coupling force due to offset, Xg, of the AUV's center-of-mass and the the "added mass" term, $Y_{\dot{r}}$, are assumed to be "small", and if the lateral disturbance force, Dv, is neglected, (7.22) can be simplified to

$$\left[m - Y_{\dot{v}} \right] \dot{v} = Y_{v|v|} v|v| + Y_{uv} |u| v + (Y_{ur} - m) u \dot{\psi} \tag{7.23}$$

For constant, "straight-ahead" or "straight-reverse" motion (i.e., $u = u_o$, $v = 0$), (7.23) and (7.21) can be linearized to form the following first-order LTI system (with the heading rate as the input, the Munk moment as the output, and the lateral velocity as the state variable)

$$\left[m - Y_{\dot{v}} \right] \dot{v} = Y_{uv} |u_o| v + (Y_{ur} - m) u_o \dot{\psi} \tag{7.24}$$

$$\tau_{Munk} = N_{uv} u_o v \tag{7.25}$$

Therefore, the transfer function from the heading rate to the Munk moment can be written as

$$\begin{aligned} \tau_{Munk}(s) &= G_{Munk}(s) \dot{\psi}(s) \\ &= \left[\frac{\left(\frac{Y_{ur} - m}{m - Y_{\dot{v}}} \right) N_{uv} u_o^2}{s - \left(\frac{Y_{uv} |u_o|}{m - Y_{\dot{v}}} \right)} \right] \dot{\psi}(s) \end{aligned} \tag{7.26}$$

Note that both the gain and the bandwidth of this transfer function are directly dependent on the magnitude of the nominal axial velocity, u_o. Using the numerical values found in Appendix D for the AUV coefficients, it can be shown that an upper bound for the magnitude of this uncertain (but stable) transfer function is given by

$$|G_{Munk}(j\omega)| \leq \left| \frac{0.88}{j\omega + 0.087} \right| \quad \forall \ \omega \tag{7.27}$$

This upper bound can then be used to write the following uncertainty representation for the Munk moment

$$G_{Munk}(s) = E_{fbl}(s) \Delta_{fb}(s) E_{fbr}(s) \tag{7.28}$$

where $E_{fbl}(s)$ and $E_{fbr}(s)$ are stable, minimum-phase transfer functions that satisfy the constraint

$$|E_{fbl}(j\omega)|\,|E_{fbr}(j\omega)| = \left|\frac{0.88}{j\omega + 0.087}\right| \forall\ \omega \tag{7.29}$$

and Δ_{fb} is a complex perturbation with magnitude bound

$$|\Delta_{fb}(j\omega)| < 1\ \forall\ \omega \tag{7.30}$$

The Munk moment can now be appended to the state-space parametric uncertainty model as a yawing disturbance, as shown in the block diagram of Figure 7.1. Note that the Munk moment appears as a feedback uncertainty from the heading rate to the heading acceleration. The matrices, $\mathbf{L}_{fb}$ and $\mathbf{C}_{fb}$, represent the disturbance input and state output matrices for the Munk moment feedback uncertainty and are given by

$$\mathbf{L}_{fb} = \begin{bmatrix} 0 \\ 0 \\ 0 \\ 1 \end{bmatrix} \tag{7.31}$$

$$\mathbf{C}_{fb} = [\,0\ \ 0\ \ 0\ \ 1\,] \tag{7.32}$$

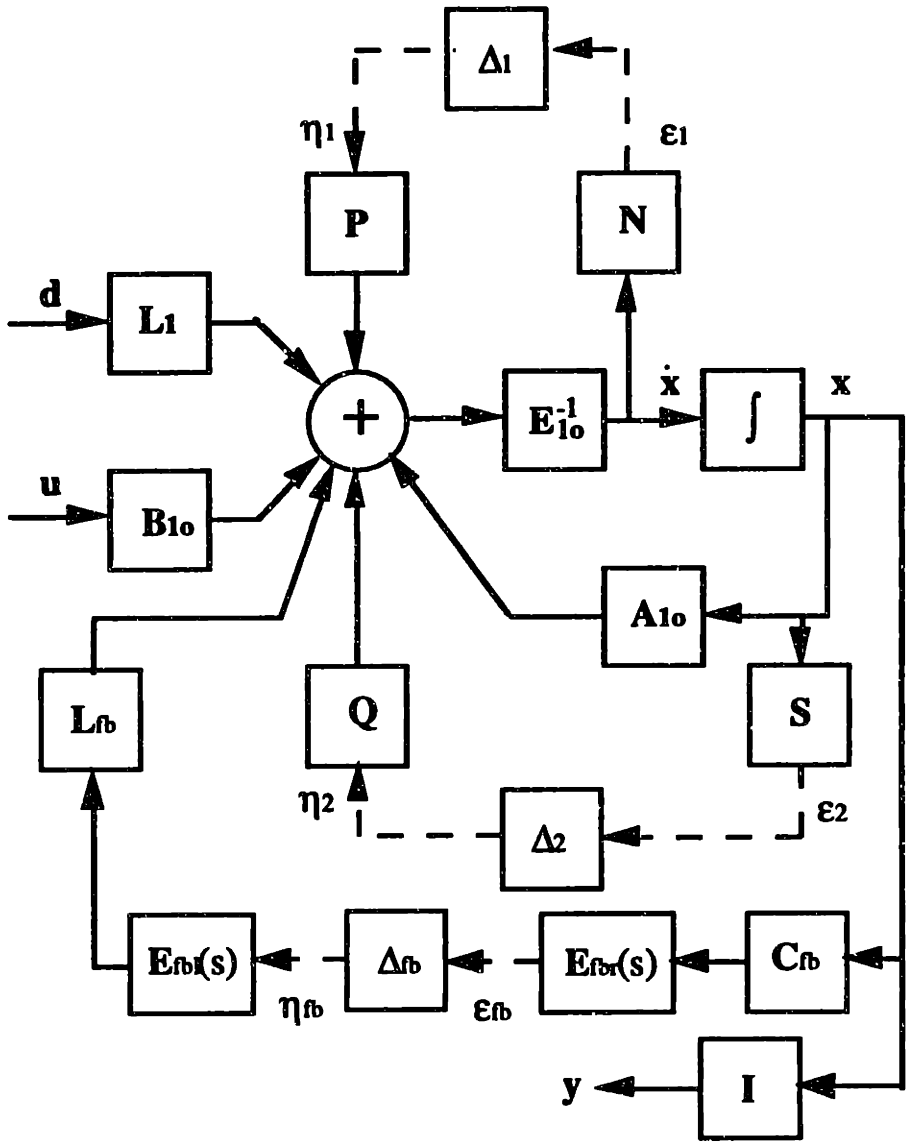

Figure 7.1: AUV Reduced-Order LTI Uncertainty Representation

7.2.2 Frequency-Domain Loop shaping Formulation

As with the design effort of Chapter 5, the AUV uncertainty model of Figure 7.1 cannot be directly used by the H_∞/μ-synthesis methodology to develop a reasonable design for the AUV control system. Recall that this representation does not include tracking error (whose minimization is one of the specified goals of the AUV control-system design effort) and neglects any frequency-domain characteristics of the input variables. Since the H_∞/μ-

synthesis design methodology tries to minimize the performance-measure function of the design plant over all frequencies, the final design can be much too conservative.

Recall from Chapter 2 and Chapter 5 that one solution for this dilemma is to "loop shape" the performance transfer function using frequency-domain weighting functions. For the reduced-order AUV H_∞/μ-Synthesis control design effort, the following structure, shown in Figure 7.2, was used for the "loopshaping" weighting functions.

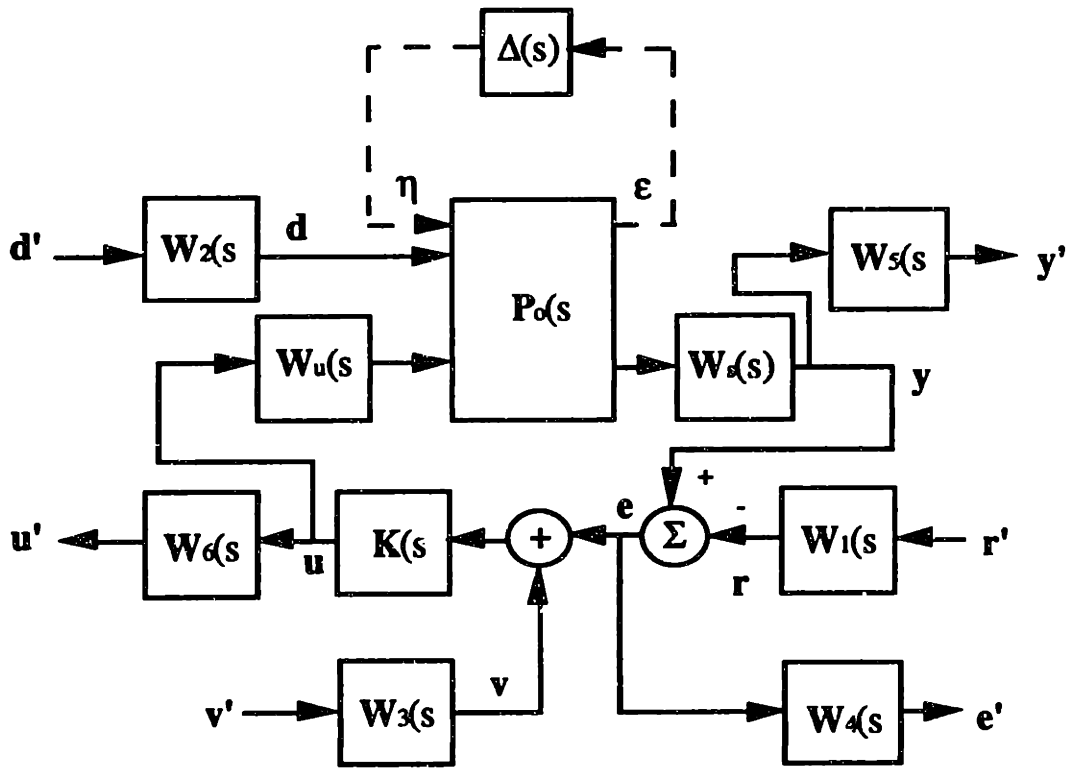

Figure 7.2: Weighted Closed-Loop Model

Here, $\mathbf{P_0}(s)$ is the reduced-order AUV uncertainty model (with $\eta^T = [\,\eta_1{}^T\ \eta_2{}^T\ \eta_{fb}{}^T]$ and $\varepsilon^T = [\,\varepsilon_1{}^T\ \varepsilon_2{}^T\ \varepsilon_{fb}{}^T]$) and $\mathbf{K}(s)$ is a stabilizing LTI controller. The vector $\mathbf{r}$ represents a "reference" signal, while the vector $\mathbf{e}$ represents the "tracking error" signal to the controller. The vector $\mathbf{v}$ represents a "measurement noise" input. The vectors, $\mathbf{r'}$, $\mathbf{d'}$, and $\mathbf{v'}$, represent unity-norm, "white noise" inputs, while the vectors, $\mathbf{e'}$, $\mathbf{y'}$, and $\mathbf{u'}$, are simply "weighted" performance" outputs. Note that this model also includes the thruster actuator dynamics, given by $\mathbf{W_u}(s)$, plus the sensor dynamics, given by $\mathbf{W_s}(s)$. The general form

of this weighted closed-loop model is exactly the same as the model used for the full-order design effort of Chapter 5, minus the weighting for the "unmeasured" states, **z** (since all the states of the reduced-order model are assumed to be available for feedback).

The "nominal" (i.e., $\Delta(s) = \mathbf{0}$) closed-loop transfer function of this system is given by

$$\begin{bmatrix} \mathbf{e}' \\ \mathbf{y}' \\ \mathbf{u}' \end{bmatrix} = \begin{bmatrix} \mathbf{W}_4(s)\mathbf{G}_{er}(s)\mathbf{W}_1(s) & \mathbf{W}_4(s)\mathbf{G}_{ed}(s)\mathbf{W}_2(s) & \mathbf{W}_4(s)\mathbf{G}_{ev}(s)\mathbf{W}_3(s) \\ \mathbf{W}_5(s)\mathbf{G}_{yr}(s)\mathbf{W}_1(s) & \mathbf{W}_5(s)\mathbf{G}_{yd}(s)\mathbf{W}_2(s) & \mathbf{W}_5(s)\mathbf{G}_{yv}(s)\mathbf{W}_3(s) \\ \mathbf{W}_6(s)\mathbf{G}_{ur}(s)\mathbf{W}_1(s) & \mathbf{W}_6(s)\mathbf{G}_{ud}(s)\mathbf{W}_2(s) & \mathbf{W}_6(s)\mathbf{G}_{uv}(s)\mathbf{W}_3(s) \end{bmatrix} \begin{bmatrix} \mathbf{r}' \\ \mathbf{d}' \\ \mathbf{v}' \end{bmatrix} \tag{7.33}$$

If a stabilizing controller, $\mathbf{K}(s)$, can be found such that the H_∞ norm of this weighted transfer function is less than unity, the actual closed-loop transfer function, $\mathbf{G}(s)$, of the AUV control system can be "shaped" in the desired fashion in the frequency domain.

From this loopshaping formulation, the Standard-Form performance-measure vector, **e**, for the full-order H_∞/μ-synthesis AUV control-design effort was chosen to be the output of (7.33), i.e.,

$$\mathbf{e} = \begin{bmatrix} \mathbf{e}' \\ \mathbf{y}' \\ \mathbf{u}' \end{bmatrix} \tag{7.34}$$

The Standard-Form "disturbance" input, δ, was chosen to be the input of (7.33), i.e.,

$$\delta = \begin{bmatrix} \mathbf{r}' \\ \mathbf{d}' \\ \mathbf{v}' \end{bmatrix} \tag{7.35}$$

7.2.3 H_∞ Controller Design

Given the design model of Section 7.2.2, a robust H_∞ controller was designed using the Small-Gain Theorem, together with other ideas from Chapters 2. The actual design procedure for the H_∞ controller consisted of several steps.

Model Scaling

First, the state vector, **x**, and the control input vector, **u**, of the reduced-order AUV parametric-uncertainty model were scaled by their respective expected maximum magnitudes, which led to

$$\mathbf{E}'_{1o} = \mathbf{E}_{1o}\mathbf{S}_x^{-1} \tag{7.36}$$

$$\mathbf{A}'_{1o} = \mathbf{A}_{1o}\mathbf{S}_x^{-1} \tag{7.37}$$

$$\mathbf{B}'_{1o} = \mathbf{B}_{1o}\mathbf{S}_u^{-1} \tag{7.38}$$

$$\mathbf{S}' = \mathbf{S}\mathbf{S}_x^{-1} \tag{7.39}$$

$$\mathbf{N}' = \mathbf{N}\mathbf{S}_x^{-1} \tag{7.40}$$

$$\mathbf{C}'_{fb} = \mathbf{C}_{fb}\mathbf{S}_x^{-1} \tag{7.41}$$

The disturbance input, **d**, and the perturbation matrices, **Q** and **P**, were left unscaled.

For the AUV control-design effort, the maximum expected values for the states were assumed to be the maximum expected tracking error (which was assumed to be 1.0 ft. for depth, 1.0 ft/sec for depth rate, 10.0 deg.(0.175 rad) for heading, and 10.0 deg/sec (0.175 rad/sec) for heading rate). The maximum allowed thrust value for each thruster was 5.0 lb. Therefore, the scaling matrices were given by

$$\mathbf{S_x} = \begin{bmatrix} 1 & 0 & 0 & 0 \\ 0 & \frac{1}{0.175} & 0 & 0 \\ 0 & 0 & 1 & 0 \\ 0 & 0 & 0 & \frac{1}{0.175} \end{bmatrix} \tag{7.42}$$

$$\mathbf{S_u} = \begin{bmatrix} \frac{1}{5.0} & 0 \\ 0 & \frac{1}{5.0} \end{bmatrix} \tag{7.43}$$

Thruster and Sensor Dynamics

For the thruster dynamics, the unity-gain model presented in Section 4.6 was used, but with a first-order Pade approximation for the 0.2 second time-delay. Therefore, the thruster dynamics model, $\mathbf{W_u}(s)$, was given by

$$\mathbf{W_u}(s) = \begin{bmatrix} \frac{(-0.1s+1)}{(0.75s+1)(0.1s+1)} & 0 \\ 0 & \frac{(-0.1s+1)}{(0.75s+1)(0.1s+1)} \end{bmatrix} \tag{7.44}$$

From Section 4.6, the sensor dynamics were approximately the frequency order of the AUV sampling rate, which meant that they can be ignored for design purposes (so long as the final closed-loop bandwidth is sufficiently low). Therefore, the sensor dynamics model, $\mathbf{W_S}(s)$ was simply given by

$$\mathbf{W_S}(s) = \mathbf{I} \tag{7.45}$$

Munk Moment Uncertainty

From the discussion of the Munk moment uncertainty in Section 7.2.1, the "upper-bound" transfer functions, $E_{fbl}(s)$ and $E_{fbr}(s)$, must be stable, minimum-phase transfer functions that satisfy the constraint

$$|E_{fbl}(j\omega)|\,|E_{fbr}(j\omega)| = \left|\frac{0.88}{j\omega + 0.087}\right| \forall\ \omega \tag{7.46}$$

For this design, these upper-bound transfer functions were simply given by

$$E_{fbl}(s) = \frac{5(0.88)}{s + 0.087} \tag{7.47}$$

$$E_{fbr}(s) = 0.2 \tag{7.48}$$

Intuitively, this selection for the upper-bound transfer functions implies that the Munk moment uncertainty is modeled as first-order, low-frequency, yawing-moment disturbance-input (mimicking the first-order dynamics of the lateral velocity, v) and a constant "penalty" weighting on the heading rate. Note that the relative weighting of 5 between the two upper-bound functions was added to increase the effect of the disturbance input portion of the Munk moment uncertainty, relative to the constant heading-rate penalty. This implies an increased low-frequency gain in the "heading control" portion of the final H_∞ controller.

Selection of Weighting Functions

The next (and most important) step in the H_∞ design procedure was the selection of the frequency-dependent performance weighting functions. Recall that the AUV reduced-order linear-model depth and heading dynamics were decoupled, which allowed decoupled designs for the AUV's depth and heading control systems.

From this decoupling effect, the reference input and the (scaled) "reference" weighting function, $W_1(s)$, were reduced to the following form

$$\mathbf{r} = \mathbf{W}_1(s)\mathbf{r}'$$

$$= \begin{bmatrix} w_{111}(s) & 0 \\ 0 & \frac{1}{0.175}w_{122}(s) \\ s(w_{111}(s)) & 0 \\ 0 & s\left(\frac{1}{0.175}w_{122}(s)\right) \end{bmatrix} \begin{bmatrix} Z_d' \\ \psi_d' \end{bmatrix} \qquad (7.49)$$

The weight $w_{111}(s)$ was used for depth control design and the weight $w_{122}(s)$ was used for heading control design. The structure of this weighting function reflects the fact that the rate references are given by the corresponding derivatives of the position references. Note that the structure of $\mathbf{W}_1(s)$ also implies that both the weights, $w_{111}(s)$ and $w_{122}(s)$, must be strictly proper (i.e., at least 20 dB/dec roll-off), in order for (7.49) to be proper.

The decoupling of the depth and heading dynamics also meant that the (scaled) "measurement noise" weight, $\mathbf{W}_3(s)$, the (scaled) "error" weight, $\mathbf{W}_4(s)$, and the (scaled) "output" weight, $\mathbf{W}_5(s)$, could be simplified to the following diagonal forms

$$\mathbf{v} = \mathbf{W}_3(s)\mathbf{v}'$$

$$= \begin{bmatrix} w_{311}(s) & 0 & 0 & 0 \\ 0 & \frac{1}{0.175}w_{322}(s) & 0 & 0 \\ 0 & 0 & w_{333}(s) & 0 \\ 0 & 0 & 0 & \frac{1}{0.175}w_{344}(s) \end{bmatrix} \begin{bmatrix} v_Z' \\ v_\psi' \\ v_{\dot{Z}}' \\ v_{\dot{\psi}}' \end{bmatrix} \qquad (7.50)$$

$$\mathbf{e}' = \mathbf{W}_4(s)\mathbf{e}$$

$$= \begin{bmatrix} w_{411}(s) & 0 & 0 & 0 \\ 0 & 0.175w_{422}(s) & 0 & 0 \end{bmatrix} \begin{bmatrix} Z - Z_d \\ \psi - \psi_d \\ \dot{Z} - \dot{Z}_d \\ \dot{\psi} - \dot{\psi}_d \end{bmatrix} \tag{7.51}$$

$$\mathbf{y}' = \mathbf{W}_5(s)\mathbf{y}$$

$$= \begin{bmatrix} w_{511}(s) & 0 & 0 & 0 \\ 0 & 0.175w_{522}(s) & 0 & 0 \end{bmatrix} \begin{bmatrix} Z \\ \psi \\ \dot{Z} \\ \dot{\psi} \end{bmatrix} \tag{7.52}$$

The structure of $\mathbf{W}_3(s)$ implies that the measurement noises in the depth tracking error, heading tracking error, depth rate tracking error, and heading rate tracking error are all decoupled from each other.

Recall from Section 7.2.2 that if a stabilizing controller, $\mathbf{K}(s)$, can be found such that the H_∞ norm of (7.33) is less than unity, the actual closed-loop transfer function, $\mathbf{G}(s)$, of the AUV control system can be "shaped" in the desired fashion in the frequency domain. For this design effort, the sensitivity (i.e., from the position reference to the position error) closed-loop transfer function was shaped by $\mathbf{W}_1(s)$ and $\mathbf{W}_4(s)$, while the complementary sensitivity (i.e., from the position measurement-noise input to the position output) transfer function, was shaped by $\mathbf{W}_3(s)$ and $\mathbf{W}_5(s)$. Therefore, the structures of $\mathbf{W}_4(s)$ and $\mathbf{W}_5(s)$ were chosen such that the emphasis of the H_∞ loopshaping was placed on the depth and heading position control loop (even though the depth rate and the heading rate were used as part of the input to the controller).

For this case, the weights, $w_{311}(s)$, $w_{411}(s)$, $w_{433}(s)$, and $w_{511}(s)$, were used for depth control design and the weights, $w_{322}(s)$, $w_{344}(s)$, $w_{422}(s)$, and $w_{522}(s)$, were used for heading control design. Using the submultiplicative and "dilation and contraction"

properties of the H_∞ norm (discussed in Section 2.4.2), the upper bounds for singular-value frequency response of the depth position sensitivity and complementary sensitivity transfer functions are given by

$$\bar{\sigma}[G_{(Z-Z_d)Z_d}(j\omega)] < \frac{1}{(\bar{\sigma}[W_{111}(j\omega)])(\bar{\sigma}[W_{411}(j\omega)])} \quad \forall\ \omega \tag{7.53}$$

$$\bar{\sigma}[G_{Z_{VZ}}(j\omega)] < \frac{1}{(\bar{\sigma}[W_{311}(j\omega)])(\bar{\sigma}[W_{511}(j\omega)])} \quad \forall\ \omega \tag{7.54}$$

Similarly, the upper bounds for the singular-value frequency response of the heading position sensitivity and complementary transfer functions are given by

$$\bar{\sigma}[G_{(\psi-\psi_d)\psi_d}(j\omega)] < \frac{1}{(\bar{\sigma}[W_{122}(j\omega)])(\bar{\sigma}[W_{422}(j\omega)])} \quad \forall\ \omega \tag{7.55}$$

$$\bar{\sigma}[G_{\psi v_\psi}(j\omega)] < \frac{1}{(\bar{\sigma}[W_{322}(j\omega)])(\bar{\sigma}[W_{522}(j\omega)])} \quad \forall\ \omega \tag{7.56}$$

For the AUV reduced-order, H_∞/μ-synthesis LTI control design effort (as with the reduced-order Sliding-Mode design effort of Chapter 6), it was desired to have a closed-loop bandwidth of approximately 0.5 rad/sec for the depth control loop and a closed-loop bandwidth of approximately 0.5 rad/sec for the heading control loop (in order to be below the bandwidth of the thrusters and in order to not excite the pitching dynamics). In addition, it was desired for the position complementary sensitivity transfer function to have a 40 dB/dec "roll off", and be below 40 dB at 5.0 rad/sec for the depth control loop, and be below 5.0 rad/sec for the heading control loop, while reducing the position-sensitivity transfer function as much as possible. Note that these specifications are exactly the same as the specifications for the full-order H_∞/μ-synthesis design effort of Chapter 5.

For this design effort, the loopshaping results presented in Chapter 5 were used as a guideline for selection of the H_∞/μ-synthesis design weights. As with the design effort of Chapter 5, the position reference inputs were assumed to be bandlimited and low-

frequency. Therefore, the reference weights were chosen to be low-pass with an upper cutoff frequency equal to the target closed-loop bandwidth

$$w_{111}(s) = \frac{0.5^2}{(s + 0.5)^2} \tag{7.57}$$

$$w_{122}(s) = \frac{0.5^2}{(s + 0.5)^2} \tag{7.58}$$

The position measurement noise weights were chosen to be high-pass with a lower cutoff frequency equal to the target closed-loop bandwidth.

$$w_{311}(s) = \frac{(s + 0.05)^2}{(s + 0.5)^2} \tag{7.59}$$

$$w_{322}(s) = \frac{(s + 0.05)^2}{(s + 0.5)^2} \tag{7.60}$$

A plot of these weighting functions is shown in Figures 7.3-7.4. Note that the sum of the magnitude of the reference weight and the magnitude of the corresponding measurement noise weight is approximately equal to unity.

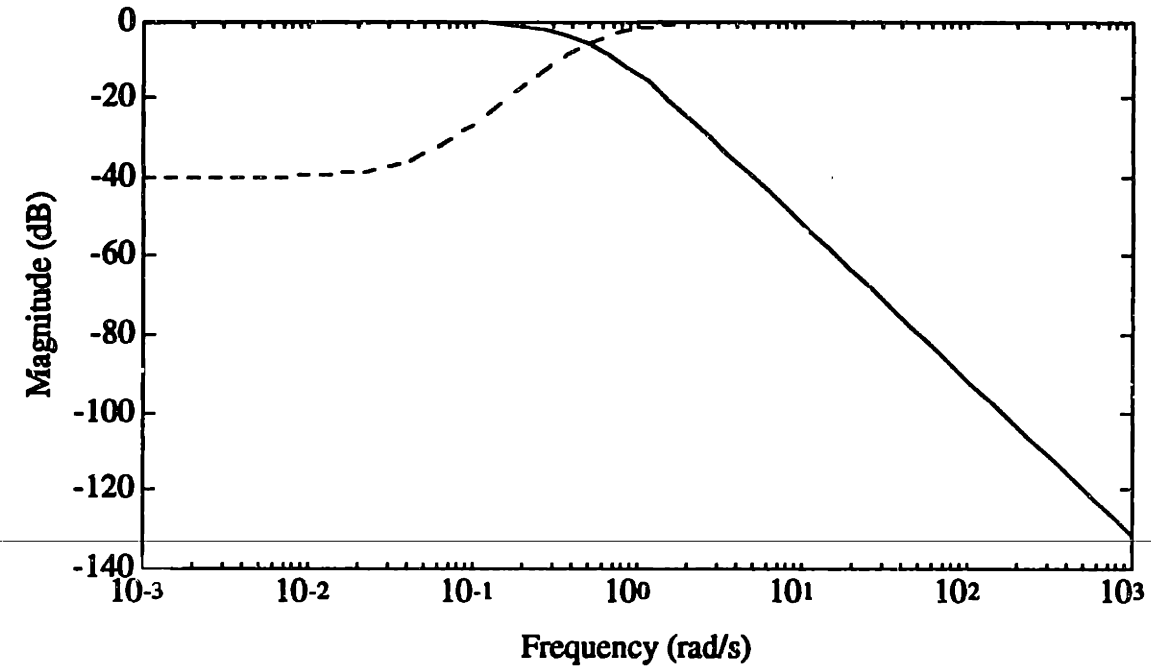

Figure 7.3 : Reference (-) & Measurement noise (--) weights ($W_{111}(s)$ & $W_{311}(s)$)

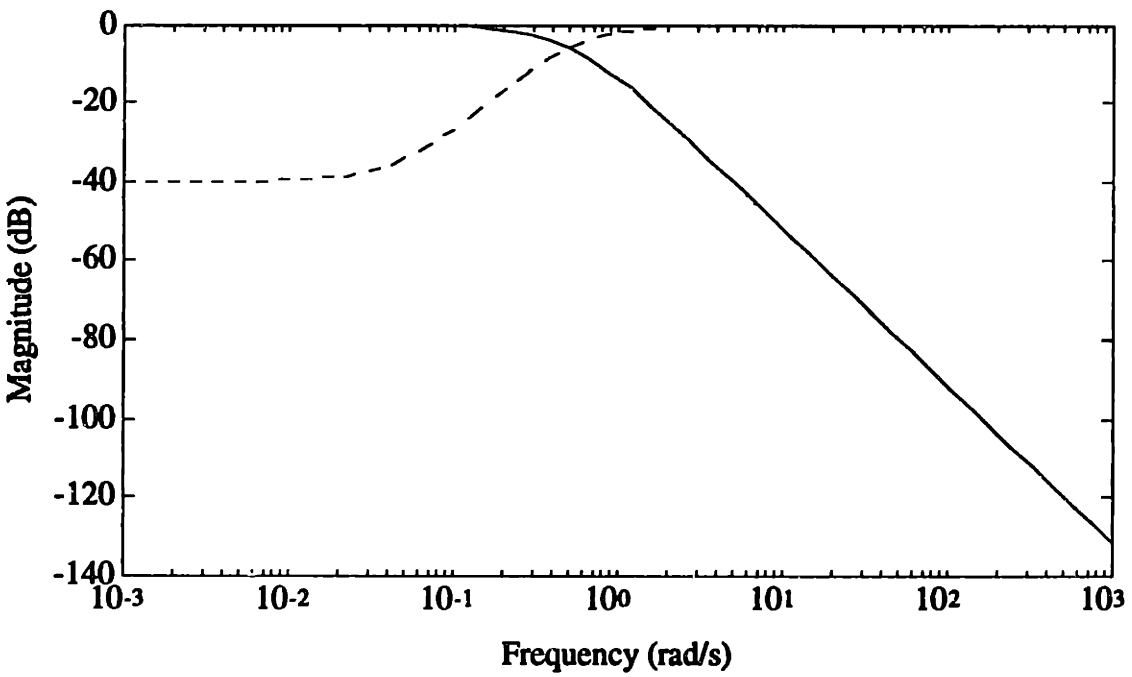

Figure 7.4 : Reference (-) & Measurement noise (--) weights ($W_{122}(s)$ & $W_{322}(s)$)

The "velocity" measurement noise weights were chosen to be high-pass, with a lower cutoff frequency equal to the target closed-loop bandwidth. This gave

$$w_{333}(s) = \frac{2(s + 0.05)^2}{(s + 0.5)^2} \tag{7.61}$$

$$w_{344}(s) = \frac{(s + 0.05)^2}{(s + 0.5)^2} \tag{7.62}$$

The measurement noise for the depth rate was scaled by 2.0 (in order to decrease the controller's reliance on the relatively "noisy" back-differenced depth rate estimate). These measurement noise weights do not bear any relationship to the actual sensor noise models, but are simply used as a design tool in the loopshaping process.

The position "error" weights and the position "output" weights were chosen such that the loopshaping upper bounds for the position sensitivity and complementary sensitivity satisfy the frequency-domain design specifications stated earlier. This gave

$$w_{411}(s) = \frac{\gamma_{411}(s + 0.5)^2}{(s + 0.05)^2} \tag{7.63}$$

$$w_{422}(s) = \frac{\gamma_{422}(s + 0.5)^2}{(s + 0.05)^2} \tag{7.64}$$

$$w_{511}(s) = \frac{\gamma_{511}[10(s + 0.5)]^2}{(s + 5)^2} \tag{7.65}$$

$$w_{522}(s) = \frac{\gamma_{522}[10(s + 0.5)]^2}{(s + 5)^2} \tag{7.66}$$

Plots of the upper bounds for the position sensitivity and complementary sensitivity are shown in Figures 7.5-7.6 (for the case of where all the "γs" are equal to unity). Note that both these bounds cross the 0.0 dB line at the target closed-loop bandwidths.

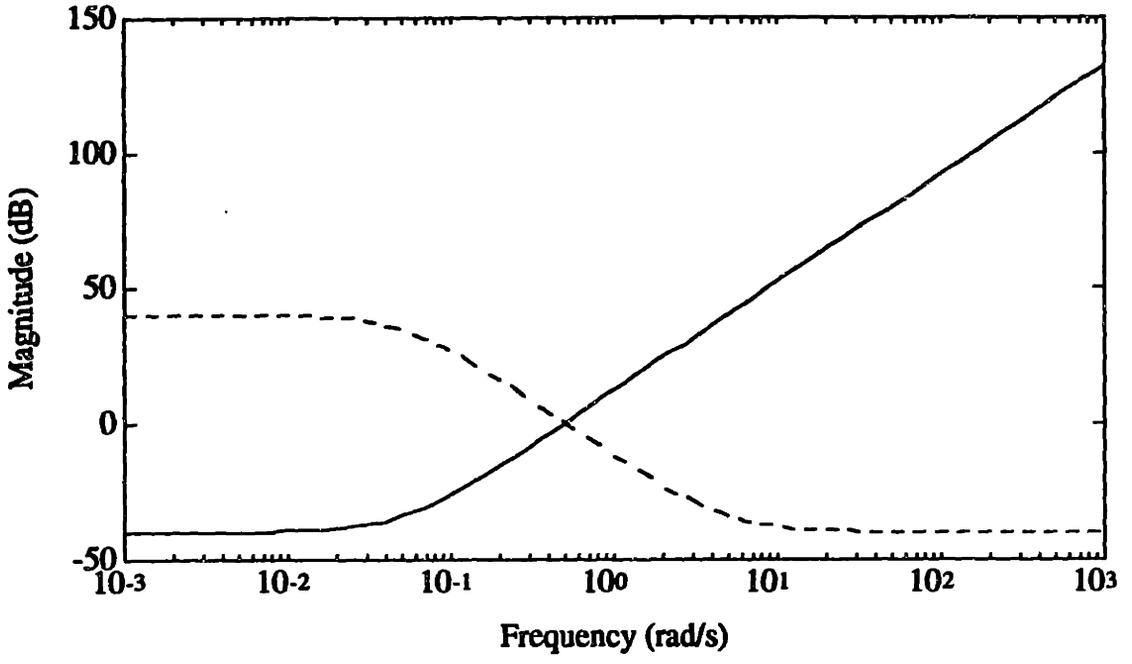

Figure 7.5: Depth Sensitivity (-) and Complementary Sensitivity (--) Bounds

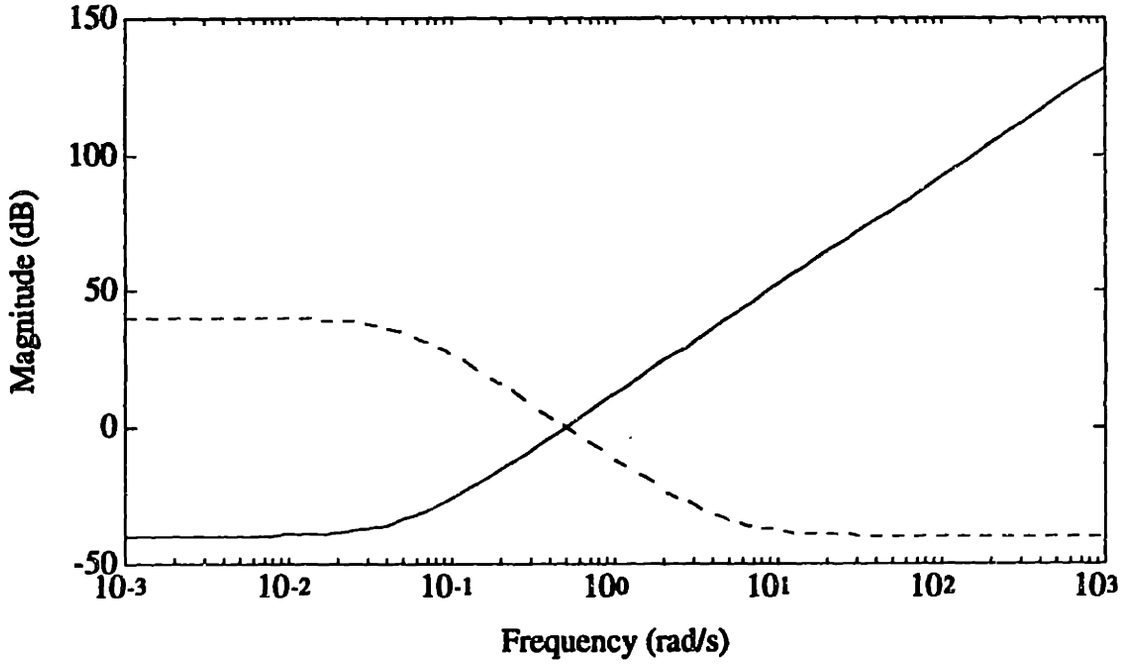

Figure 7.6: Heading Sensitivity (-) and Complementary Sensitivity (--) Bounds

These upper bounds imply that the sensitivity is primarily shaped in the low-frequency range, while the complementary sensitivity is primarily shaped in the high-frequency range. They *do not* imply that the singular-value frequency responses of the sensitivity and complementary sensitivity will have the exact shapes given by Figures 7.5-7.6.

The disturbance weighting function was reduced to the following form

$$\mathbf{d} = \mathbf{W}_2(s)\mathbf{d}' = \begin{bmatrix} w_{211}(s) & 0 \\ 0 & w_{222}(s) \end{bmatrix} \begin{bmatrix} d'_Z \\ d'_\psi \end{bmatrix} \tag{7.67}$$

Both disturbances were assumed to be low-frequency, with bandwidths approximately equal to the target closed-loop bandwidths. This gave

$$w_{211}(s) = \frac{0.01(s + 50)}{(s + 0.5)} \tag{7.68}$$

$$w_{222}(s) = \frac{0.01(s + 50)}{(s + 0.5)} \tag{7.69}$$

From the decoupling of the depth and heading dynamics, the control-input weighting function, $W_6(s)$ was reduced to the following diagonal form.

$$\mathbf{u}' = \mathbf{W}_6(s)\mathbf{u} = \begin{bmatrix} w_{611}(s) & 0 \\ 0 & w_{622}(s) \end{bmatrix} \begin{bmatrix} T_v \\ (T_p - T_s) \end{bmatrix} \tag{7.70}$$

Both the vertical thrust weight, $w_{611}(s)$, and the differential thrust weight, $w_{622}(s)$, were chosen to be high-pass transfer functions of the form

$$w_{611}(s) = \frac{\gamma_{611}100(s + 0.05)}{(s + 50)} \tag{7.71}$$

$$w_{622}(s) = \frac{\gamma_{622} 100(s + 0.05)}{(s + 50)} \tag{7.72}$$

This selection of weights implies that both control inputs are penalized more at the higher frequencies.

H_∞ Compensator Synthesis using Gamma Iteration

The next step in the H_∞ design procedure was to synthesize the H_∞ compensator from the AUV Standard-Form design model (with the set of weighting functions from the previous section) using the gamma-iteration algorithm from Chapter 2. A balanced-fractional model reduction algorithm (described in Appendix E) was also used in order to increase the numerical robustness of the compensator synthesis (in addition to removing any uncontrollable or unobservable states in either the design model or the controller).

Recall from Chapter 2 that the Small-Gain based H_∞ design algorithm tends to produce unnecessarily conservative control designs for structured perturbations (such as the reduced-order AUV uncertainty model). This implies that it may not be possible, using the H_∞ design technique, to find a stabilizing controller for the AUV that is guaranteed to be robust over the full range of modeling uncertainty. Therefore, the perturbation matrices were scaled in the following manner

$$\mathbf{N}'' = \sqrt{\gamma_{\Delta E}}\,\mathbf{N}' \tag{7.73}$$

$$\mathbf{P}' = \sqrt{\gamma_{\Delta E}}\,\mathbf{P} \tag{7.74}$$

$$\mathbf{Q}' = \sqrt{\gamma_{\Delta A}}\,\mathbf{Q} \tag{7.75}$$

$$\mathbf{S}'' = \sqrt{\gamma_{\Delta A}}\,\mathbf{S}' \tag{7.76}$$

$$\mathbf{C}''_{fb} = \sqrt{\gamma_{fb}}\,\mathbf{C}'_{fb} \tag{7.77}$$

$$L'_{fb} = \sqrt{\gamma_{fb}}\, L_{fb} \tag{7.78}$$

Similarly to the Full-Order H_∞ compensator design process presented in Chapter 5, an initial "small" value of 0.01 was selected for all the performance γ's. Bounds on the perturbation γ's were found by iterating these parameters from zero until the control design begin to fail the Small-Gain robustness test. From this procedure, the following values were selected for $\gamma_{\Delta E}$, $\gamma_{\Delta A}$, and γ_{fb}.

$$\gamma_{\Delta E} = 0.02 \tag{7.79}$$

$$\gamma_{\Delta A} = 0.05 \tag{7.80}$$

$$\gamma_{fb} = 0.1 \tag{7.81}$$

For the next design iteration, the weightings on the position error and position output were increased by a factor of 5 (i.e., $\gamma_{411} = 0.05$, γ_{422}=0.05, γ_{511}=0.05, γ_{522}=0.05). In order for the design to satisfy the Small-Gain Test, the weighting on the differential heading control was decreased by a factor of 2 (i.e., $\gamma_{622} = 0.005$). This implies an increased heading control effort in order to counteract the effects of the Munk moment uncertainty.

For this case, from the model-reduction algorithm, the bounds on the additive model error versus model order are shown in Figure 7.7.

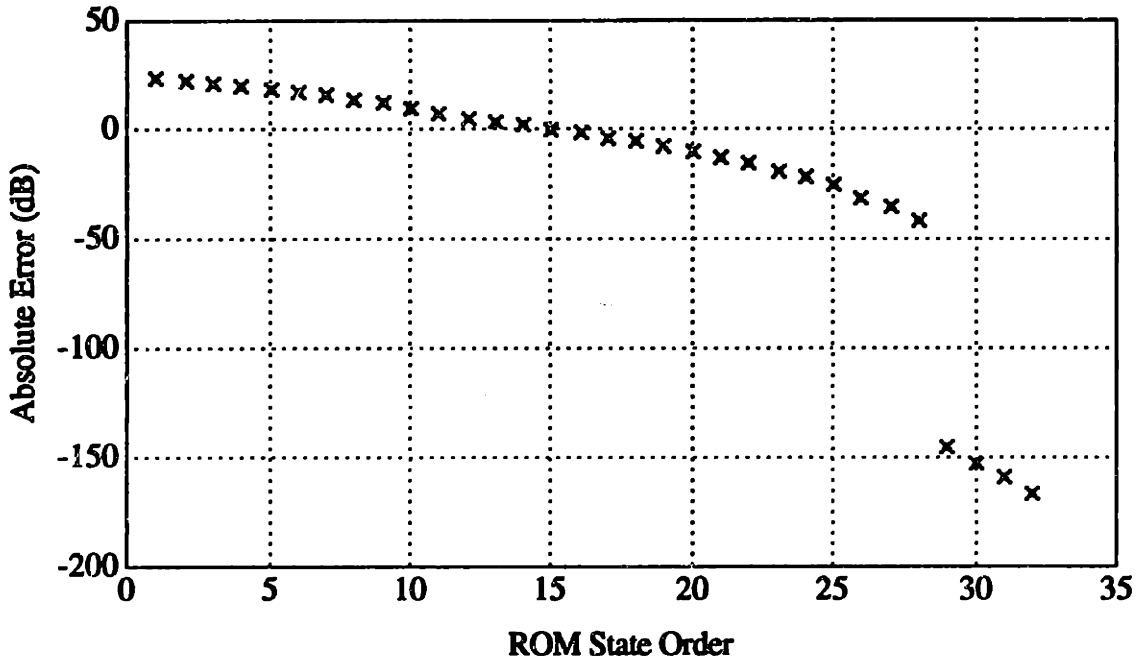

Figure 7.7: Fractional-Balanced Additive Error Bounds

Note the fairly sharp increase in the model error from the 29-state level to the 28-state level. This implies that the 28-state model is a significantly less accurate representation than the 29-state model. Also note that there is relatively little improvement in the model accuracy beyond the 29-state level. Therefore, the 29-state SF model was judged to be sufficiently accurate for the H_∞ design.

The plot of the normalized Hankel singular-values of the SF model versus model order is shown in Figure 7.8.

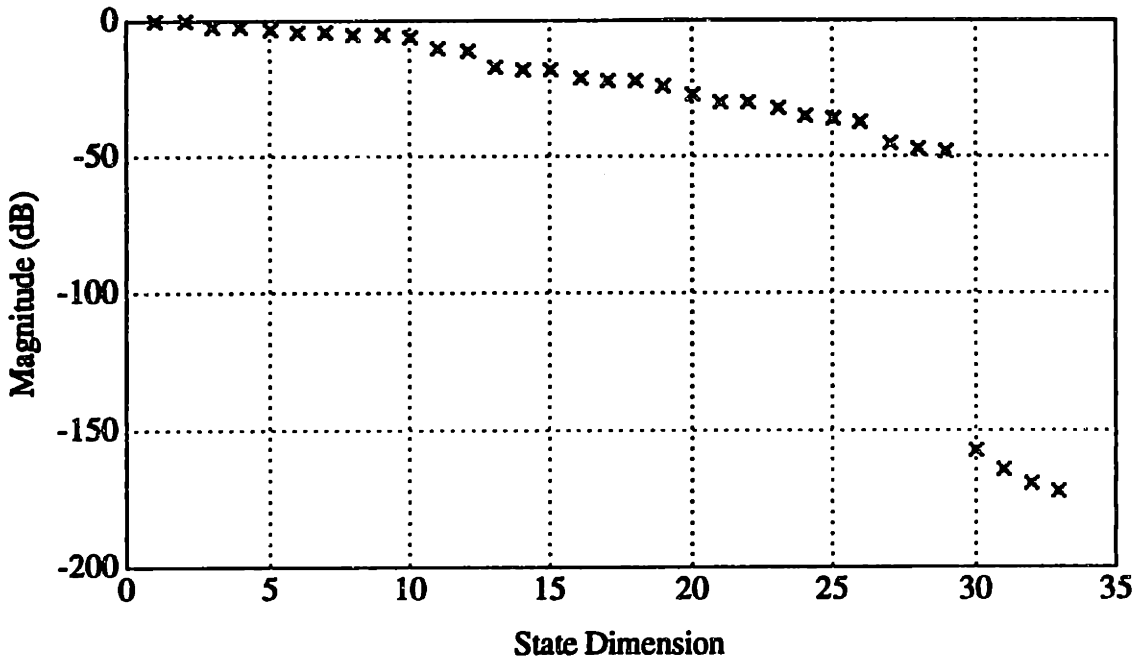

Figure 7.8: Hankel Singular Values

From this plot, all of the Hankel singular values of the 29-state model are nonzero. From Appendix E, this implies that the 29-state model is minimal (as desired). Again, note the sharp drop-off around the 29-state level. From Appendix E, this confirms that the states beyond this level are much less controllable or observable than the lower order states and can be truncated without difficulty.

For this reduced-order SF model, an H_∞ compensator was then synthesized using gamma iteration. Initial upper and lower bounds of 10 and 0.1, respectively, on the H_∞ norm were used for this design, with a convergence tolerance of 1%. After several iterations, the algorithm converged to an H_∞ norm bound of approximately 0.8429. The singular-value frequency response of this controller is shown in Figure 7.9

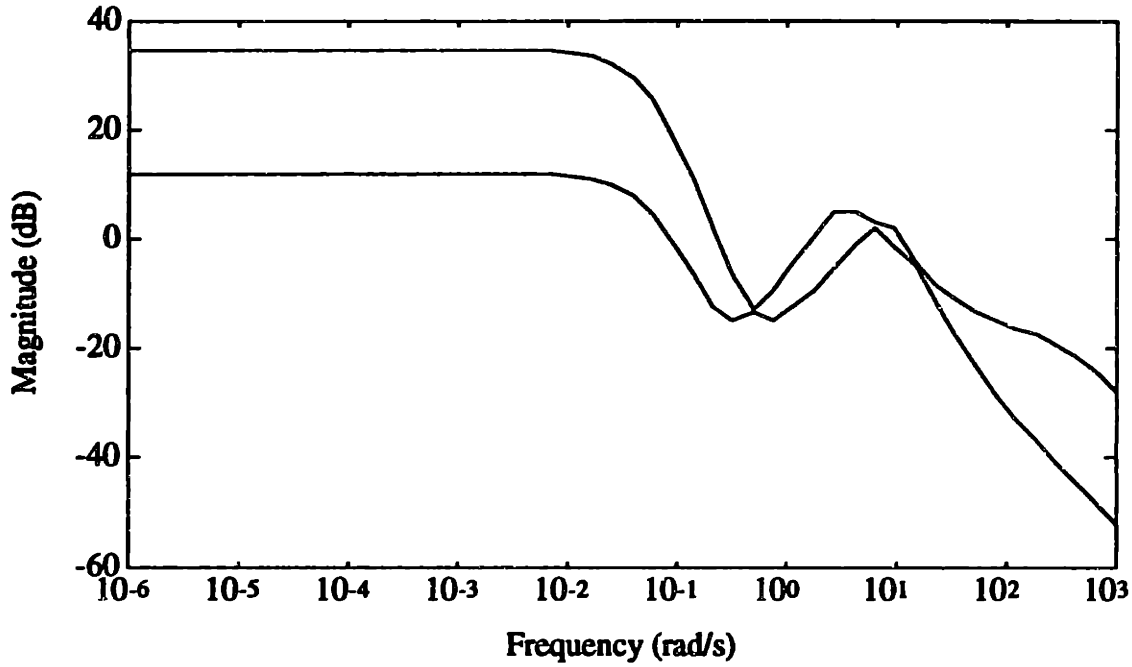

Figure 7.9: Unscaled Compensator Frequency Response

The position sensitivity and complementary sensitivity of this design are shown in Figure 7.10

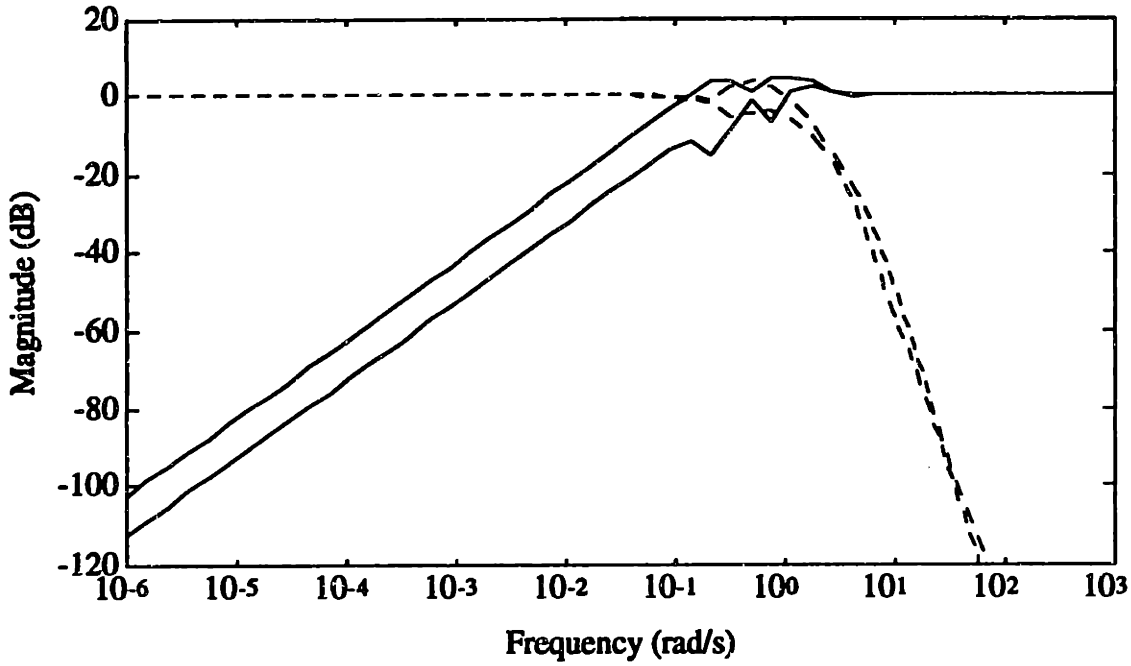

Figure 7.10: Sensitivity (-) and Complementary Sensitivity (--)

From this plot, the H_∞ design appears to approximately meet the nominal bandwidth requirements, with a closed-loop bandwidth of about 0.5 rad/sec. However, it doesn't quite meet the specification of having the complementary sensitivity below 40 dB at 5.0 rad/sec. Interestingly, the sensitivity has a 20 dB/dec roll off, while the complementary sensitivity has an 80 dB/dec roll-off. The peak magnitude of both the sensitivity and complementary sensitivity is approximately 4.5 dB (i.e., a peak magnitude of approximately 1.7).

7.3 SLIDING-MODE AUGMENTED CONTROL LAW DESIGN

For the AUV Sliding-Mode Augmented control design, the reduced-order Descriptor/Companion nonlinear model developed in Chapter 4 was used. This 2nd-order model was given by

$$\frac{d}{dt}(\hat{x}) = \dot{\hat{x}}$$

$$E\left[\frac{d}{dt}(\dot{\hat{x}})\right] = E\,\ddot{\hat{x}} = f(x) + Bu + d \tag{7.82}$$

The reduced-order total state vector was given by

$$x = [\, Z \;\psi\; \dot{Z} \;\dot{\psi}\,]^T \tag{7.83}$$

and the reduced-order output state vector was given by

$$\hat{x} = [\, Z \;\psi\,]^T \tag{7.84}$$

The control input vector was given by

$$u = [\, U_Z \;U_\psi\,]^T \tag{7.85}$$

and the disturbance vector was given by

$$d = [\, d_Z(t) \;\; d_\psi(t)]^T \tag{7.86}$$

The goal of the design effort is to find the Sliding-Mode Augmented controller that will force the output state of this reduced-order nonlinear model to track a "reference" trajectory, in the face of bounded parametric modeling-errors and disturbances.

7.3.1 Parametric Modeling-Error and Disturbance Bounds

From the Sliding-Mode control design effort presented in Chapter 6, the "mass" matrix, **E**, of the reduced-order model had the following additive-uncertainty form

$$\mathbf{E} = \widehat{\mathbf{E}} - \Delta\mathbf{E} \tag{7.87}$$

with a nominal value, $\widehat{\mathbf{E}}$, given by

$$\widehat{\mathbf{E}} = \begin{bmatrix} [m - Z_{\dot{w}}] & 0 \\ 0 & \left[\dfrac{(I_{ZZ} - N_{\dot{r}})(m - Y_{\dot{v}}) - (N_{\dot{v}} - mX_g)(Y_{\dot{r}} - mX_g)}{(m - Y_{\dot{v}})}\right] \end{bmatrix} \tag{7.88}$$

The matrix **E** was assumed to have a 50% uncertainty in each of its diagonal elements. The "off-diagonal" elements were assumed to be always zero. Then the upper bound matrix for the magnitude of the additive uncertainty in **E** is given by

$$\overline{\Delta\mathbf{E}} = 0.5\,|\mathbf{E}|$$

$$= \begin{bmatrix} 0.5\,|[m - Z_{\dot{w}}]| & 0 \\ 0 & 0.5\left|\left[\dfrac{(I_{ZZ} - N_{\dot{r}})(m - Y_{\dot{v}}) - (N_{\dot{v}} - mX_g)(Y_{\dot{r}} - mX_g)}{(m - Y_{\dot{v}})}\right]\right| \end{bmatrix} \tag{7.89}$$

The nonlinear vector transfer-function, **f(x)**, also had a similar additive-uncertainty form, with

$$\mathbf{f(x)} = \widehat{\mathbf{f}}(\mathbf{x}) + \Delta\mathbf{f(x)} \tag{7.90}$$

The nominal value of this transfer function was given by

$$\hat{\mathbf{f}}(\mathbf{x}) = \begin{bmatrix} Z_{w|w|}\dot{Z}|\dot{Z}| + (W - B) \\ N_{q|q|}\dot{\psi}|\dot{\psi}| \end{bmatrix} \tag{7.91}$$

For the AUV 2nd-order Descriptor/Companion nonlinear model, the following upper-bound vector was derived for magnitude of the additive uncertainty in $\mathbf{f}(\mathbf{x})$

$$\overline{\Delta\mathbf{f}}(\mathbf{x}) = \begin{bmatrix} \left| \overline{\Delta Z_{w|w|}}\dot{Z}|\dot{Z}| + \overline{\Delta(W - B)} \right| \\ \left| \overline{\Delta N_{q|q|}}\dot{\psi}|\dot{\psi}| \right| \end{bmatrix}$$

$$= \begin{bmatrix} \left|\overline{\Delta Z_{w|w|}}\right| |\dot{Z}|^2 + \left|\overline{\Delta(W - B)}\right| \\ \left|\overline{\Delta N_{q|q|}}\right| |\dot{\psi}|^2 \end{bmatrix} \tag{7.92}$$

The hydrodynamic coefficients were assumed to have a maximum uncertainty of 50%. The magnitude of the error in the "net" buoyancy, (W-B), was assumed to be less than 1.0 lb. Then the upper-bound vector for the uncertainty in $\mathbf{f}(\mathbf{x})$ was simply given by

$$\overline{\Delta\mathbf{f}}(\mathbf{x}) = \begin{bmatrix} 0.5\,|Z_{w|w|}|\,|\dot{Z}|^2 + 1.0 \\ 0.5\,|N_{q|q|}|\,|\dot{\psi}|^2 \end{bmatrix} \tag{7.93}$$

The control-input matrix, $\mathbf{B}$, of the 2nd-order Descriptor Companion nonlinear model was given by

$$\mathbf{B} = \begin{bmatrix} 1 & 0 \\ 0 & Y_T \end{bmatrix} \tag{7.94}$$

Uncertainty in this matrix was neglected since the "gain" errors of the thrusters were assumed to be small. The thruster moment-arm length, Y_T was also assumed to be well known.

From Chapter 6, the upper bound for the magnitude of the depth disturbance force was simply chosen to be one-half the maximum vertical thrust force. Similarly, the upper bound for the magnitude of the heading disturbance torque was assumed to be one-half the maximum torque generated by the port and starboard thrusters. The disturbance upper-bound vector was then given by

$$\bar{\mathbf{d}} = \begin{bmatrix} 0.5 \max |T_v| \\ 0.5 \max |Y_T(T_p - T_s)| \end{bmatrix} \tag{7.95}$$

For the AUV design effort, the maximum thrust force for all the thrusters was assumed to be 5.0 lb., which then gave a disturbance upper bound of

$$\bar{\mathbf{d}} = \begin{bmatrix} 2.5 \\ 5.0\ Y_T \end{bmatrix} \tag{7.96}$$

7.3.2 Development of the AUV Sliding-Mode Augmented Control Law

The goal of the Sliding-Mode Augmented control design (as with the Sliding-Mode design effort presented in Chapter 6) is for the state vector given by $\mathbf{x}$ to track a time-varying reference "trajectory" vector given by $\mathbf{x}_d$. The design of the Sliding-Mode Augmented controller consisted of several steps. A linear sliding-surface of the form

$$s(\tilde{\mathbf{x}}) = \sum_{p=0}^{n-1} \binom{n-1}{p} \Lambda^p \tilde{\mathbf{x}}^{(n-1-p)} \tag{7.97}$$

was developed. For the 2nd-order AUV model, the sliding-surface was defined to be a first-order surface, given by

$$s(\tilde{x}) = \dot{\tilde{x}} + \Lambda\tilde{x} \tag{7.98}$$

From the AUV model analysis presented in Chapter 4, the AUV depth and heading dynamics are essentially decoupled. This implies that if Λ is given by the following diagonal form

$$\Lambda = \begin{bmatrix} \lambda_{11} & 0 \\ 0 & \lambda_{22} \end{bmatrix} \tag{7.99}$$

then the design of the AUV depth and heading control systems can be done separately (but concurrently). The parameter, λ_{11} can be used for the design of the depth control system, and λ_{22} can be used for the design of the heading control system. From the discussion of the AUV Sliding-Mode controller in Chapter 6, it can be shown that these parameters give the desired closed-loop bandwidth of the Sliding-Mode design. For this Augmented design, this desired bandwidth was chosen to the same as the desired closed-loop bandwidth of the H_∞ LTI design presented in Section 7.2 (0.5 rad/s for depth, and 0.5 rad/s for heading). This then gave λ_{11} equal to 0.5 rad/s and λ_{22} equal to 0.5 rad/s. Note that these bandwidths are also identical to the desired closed-loop bandwidths of the Sliding-Mode design.

From Chapter 3, the Sliding-Mode Augmented Control Law with "boundary-layer" for the Descriptor/Companion model is given by

$$u = \hat{u} - K(\tilde{x})\text{dsat}(s(\tilde{x}),\Phi_{\text{inner}},\Phi_{\text{outer}}) \tag{7.100}$$

For the AUV control design, with the nominal LTI plant model defined by

$$\frac{d}{dt}(\hat{x}) = \dot{\hat{x}}$$

$$E_p\left[\frac{d}{dt}(\dot{\hat{x}})\right] = E_p\ddot{\hat{x}} = A_p x + B_p u + d \tag{7.101}$$

the "nominal" portion of the Sliding-Mode Augmented control law had the form

$$\hat{\mathbf{u}} = \mathbf{B}^{-1}\left(-\hat{\mathbf{f}}(\mathbf{x}) + \hat{\mathbf{E}}\left(\mathbf{E}_p^{-1}\mathbf{A}_p\mathbf{x} + \mathbf{E}_p^{-1}\mathbf{B}_p\mathbf{u}_{LTI}\right)\right) \tag{7.102}$$

From the discussion of the LTI control design presented in Section 7.2, the respective nominal "mass and inertia" matrices and the respective control input matrices for both the reduced-order nonlinear model and the reduced-order LTI model were identical. Therefore, the nominal control law given by (7.102) was simplified to

$$\hat{\mathbf{u}} = \mathbf{B}^{-1}\left(-\hat{\mathbf{f}}(\mathbf{x}) + \mathbf{A}_p\mathbf{x}\right) + \mathbf{u}_{LTI} \tag{7.103}$$

The diagonal "feedback" portion of the Sliding-Mode Augmented control law had the form

$$\begin{aligned}\mathrm{diag}[\mathbf{K}(\tilde{\mathbf{x}})] = \mathbf{B}^{-1}\Bigg(&\overline{\Delta\mathbf{E}}\ddot{\tilde{\mathbf{x}}} + \overline{\Delta\mathbf{f}}(\mathbf{x}) + \bar{\mathbf{d}} \\ &+ \hat{\mathbf{E}}\left|\mathbf{E}_p^{-1}\mathbf{A}_p\mathbf{x} + \mathbf{E}_p^{-1}\mathbf{B}_p\mathbf{u}_{LTI} - \ddot{\mathbf{x}}_d + \Lambda\dot{\tilde{\mathbf{x}}}\right| + \eta\hat{\mathbf{E}}\begin{bmatrix}1\\1\end{bmatrix}\Bigg)\end{aligned} \tag{7.104}$$

Again, by using the fact that the respective nominal "mass and inertia" matrices and the respective control input matrices for both the reduced nonlinear model and the reduced-order LTI model were identical (and by using the fact that the "mass and inertia" matrices were diagonal with positive elements), the feedback portion given by (7.104) was simplified to

$$\begin{aligned}\mathrm{diag}[\mathbf{K}(\tilde{\mathbf{x}})] = \mathbf{B}^{-1}\Bigg(&\overline{\Delta\mathbf{E}}\ddot{\tilde{\mathbf{x}}} + \overline{\Delta\mathbf{f}}(\mathbf{x}) + \bar{\mathbf{d}} \\ &+ \left|\mathbf{A}_p\mathbf{x} + \mathbf{B}_p\mathbf{u}_{LTI} + \mathbf{E}_p(-\ddot{\mathbf{x}}_d + \Lambda\dot{\tilde{\mathbf{x}}})\right| + \eta\hat{\mathbf{E}}\begin{bmatrix}1\\1\end{bmatrix}\Bigg)\end{aligned} \tag{7.105}$$

The maximum depth acceleration was assumed to be less than 0.2 ft/s^2, while the maximum heading acceleration was assumed to be less than 5.0 deg/s^2 (approximately 0.1 rad/s^2). Then the upper-bound acceleration vector is simply given by

$$\bar{\ddot{\underset{\sim}{x}}} = \begin{bmatrix} 0.2 \\ 0.1 \end{bmatrix} \tag{7.106}$$

The scalar η was chosen to be zero.

For the Sliding-Mode Augmented design, the outer boundary-layer width was chosen to be same as the boundary-layer width of the improved "second:" Sliding-Mode design presented in Chapter 8 (for purposes of comparison), which gave the following value for Φ_{outer}

$$\Phi_{outer} = \begin{bmatrix} 4.48 & 0 \\ 0 & 1.48 \end{bmatrix} \tag{7.107}$$

The inner boundary-layer width was chosen to be 10% of the respective desired maximum steady-state tracking error (i.e., 1.0 feet for depth and 5.0 degrees (0.087 rad.) for heading), which gave

$$\Phi_{inner} = \begin{bmatrix} 0.1 & 0 \\ 0 & 0.0087 \end{bmatrix} \tag{7.108}$$

7.4 NOMINAL SIMULATION PERFORMANCE OF THE AUV SLIDING-MODE AUGMENTED CONTROLLER

A preliminary test of the nominal performance of the AUV Sliding-Mode Augmented controller was done in order to see how well this particular controller meets the design goals specified in Section 7.1. This test was performed using a MATLAB™ computer simulation based on the reduced-order Descriptor/Companion nonlinear design model. This simulation also included the model of the thruster dynamics presented in Chapter 4. The sensor dynamics were neglected. The model coefficients were given the nominal values shown in Appendix D. The commanded depth trajectory was from 0.0 to 10.0 ft. (with a maximum depth rate of 0.5 ft/sec and a maximum depth acceleration of 0.2 ft/sec^2), and the commanded heading trajectory was from 0.0 to 180.0 degrees (with a maximum heading rate of 15.0 deg/sec and a maximum heading acceleration of 5.0 deg/sec^2).

The results of this test are shown in Figure 7.11 and Table 7.3. The numerical values shown in Table 7.3 were defined in the same manner as for the Sliding-Mode design of Chapter 6. The response time was defined as the time period starting where the reference trajectory reaches its final value (within 0.1 feet for depth and within 0.5 degrees for heading) and ending where the vehicle first obtains this value (within 0.1 feet for depth and within 0.5 degrees for heading). The maximum overshoot was defined as the difference between the maximum value reached by the vehicle and the maximum value reached by the reference trajectory.

The nominal steady-state error performance of the Sliding-Mode controller met the design goal specified in Table 7.3, as well as the depth overshoot. The heading overshoot was slightly greater than specified, but still acceptable. The depth response-time and heading-response time were slower than specified. However, these response times were judged to be acceptable since any attempt at improving them would probably increase the overshoot (due to the lag caused by the thruster dynamics).

Table 7.3: Nominal Performance Test of the AUV Sliding-Mode Augmented Controller (with Performance Specifications in Parentheses)

Steady-State Depth Error	0.0 feet ($\pm$1.0 feet)
Steady-State Heading Error	0.0 degrees ($\pm$5.0 degrees)
Depth Overshoot	0.395 feet (1.0 feet)
Heading Overshoot	10.29 degrees (10.0 degrees)
Depth Response	13.09 seconds (10.0 seconds)
Heading Response	27.18 seconds (5.0 seconds)

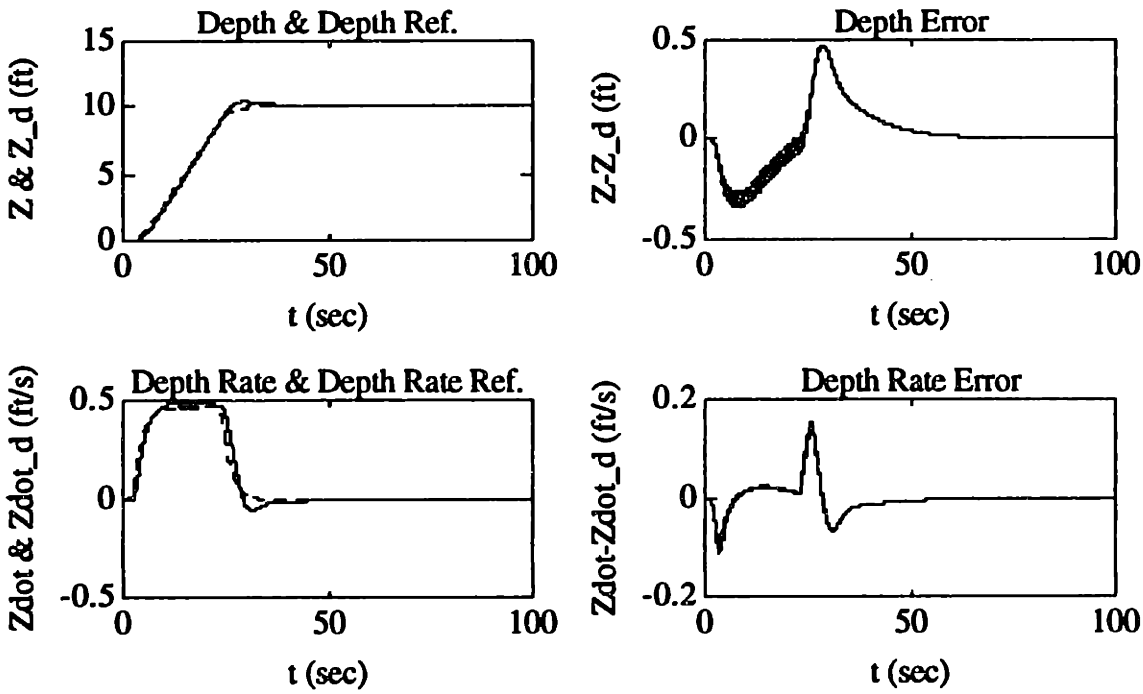

Figure 7.3: Nominal Performance Test of the AUV Sliding-Mode Augmented Controller

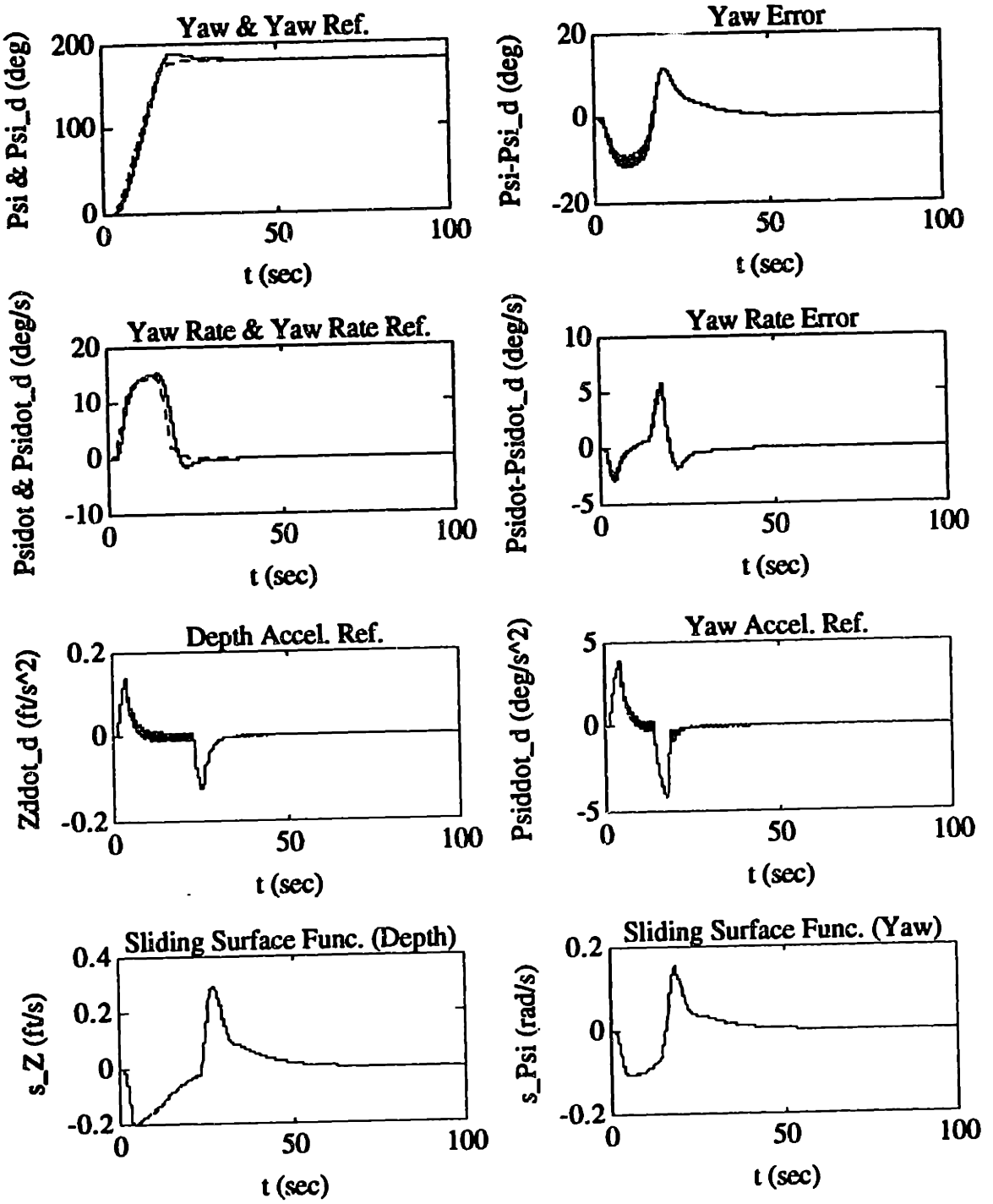

Figure 7.3: Nominal Performance Test of the

AUV Sliding-Mode Augmented Controller (continued)

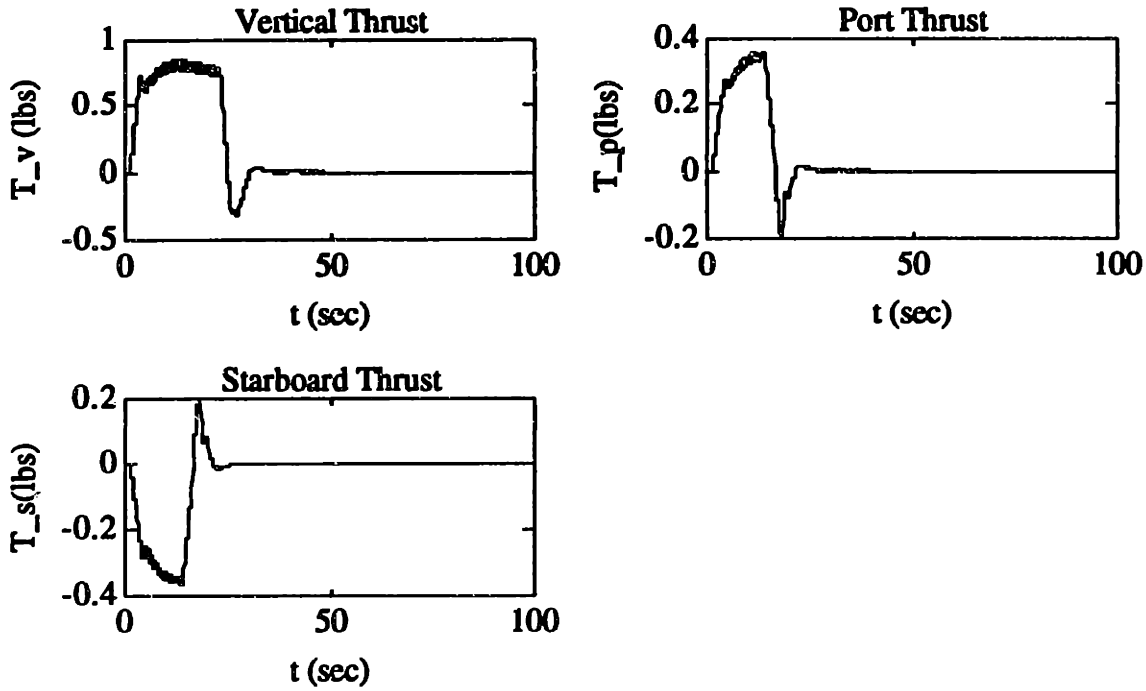

Figure 7.3: Nominal Performance Test of the

AUV Sliding-Mode Augmented Controller (continued)

Chapter 8

Simulation Comparison of Robust Controller Designs

The robust controllers, developed in Chapter 5, developed in Chapter 6, and developed in Chapter 7, were initially implemented and tested using a MATLAB™ computer simulation of the dynamics of the AUV. This simulation was based on the full-order Six-Degree-of-Freedom nonlinear model of the AUV presented in Chapter 4. This model also included the thruster models and sensor models presented in Chapter 4.

8.1 IMPLEMENTATION ISSUES

Controller Discretization

For the AUV, the LTI controllers developed in Chapter 5 and Chapter 7 will be implemented in digital form. This requires the development of a discrete-time linear state-space model of the controller. If the continuous time model is given by

$$\begin{aligned} \dot{x}_c &= A_c x_c + B_c y_1 \\ u_{LTI} &= C_c x_c + D_c y_1 \end{aligned} \tag{8.1}$$

the discrete-time model would be given by

$$\begin{aligned} x_c((n+1)T) &= G_c(T)x_c(nT) + H_c(T)y_1(nT) \\ u_{LTI}(nT) &= C_c x_c(nT) + D_c(T)y_1(nT) \end{aligned} \tag{8.2}$$

where T is the sampling period of the AUV's digital control system.

One way to derive the discrete-time model from the continuous-time linear model is by the *zero-order hold equivalence method* [21]. Here, the input, $y_1(nT)$, is assumed to change only at the sampling instants, which leads to the following relationships between the models

$$G_c(T) = e^{A_c T} \tag{8.3}$$

$$H_c(T) = \left(\int_0^T e^{A_c \lambda} \, d\lambda \right) B_c \tag{8.4}$$

$$C_c(T) = C_c \tag{8.5}$$

$$D_c(T) = D_c \tag{8.6}$$

If the matrix, A_c, happens to be nonsingular, the integral for $H_c(T)$ given by (8.4) can be simplified to

$$H_c(T) = A_c^{-1}(e^{A_c T} - I)B_c \tag{8.7}$$

For all of the simulation performance tests of this chapter, the sampling time, T, was chosen to be 0.2 seconds, which was exactly the same as the sampling time of the actual *Sea Squirt* AUV control system.

Trajectory Generation Algorithm

The controlled state trajectories, Z_d and Ψ_d, which are input into the AUV controller, must be continuous functions of time with finite time derivatives. However, the commands given to the AUV's heading and depth controllers by the high-level "planner" algorithms are steps, which do not meet the above requirement. To overcome this problem, a Trajectory Generation Algorithm(TGA) was implemented in the AUV's control system. The TGA is a nonlinear low-pass filter that generates an "optimal time" state

trajectory from the input step commands, given the maximum allowed accelerations and velocities of the AUV, as shown in Figure 8.1.

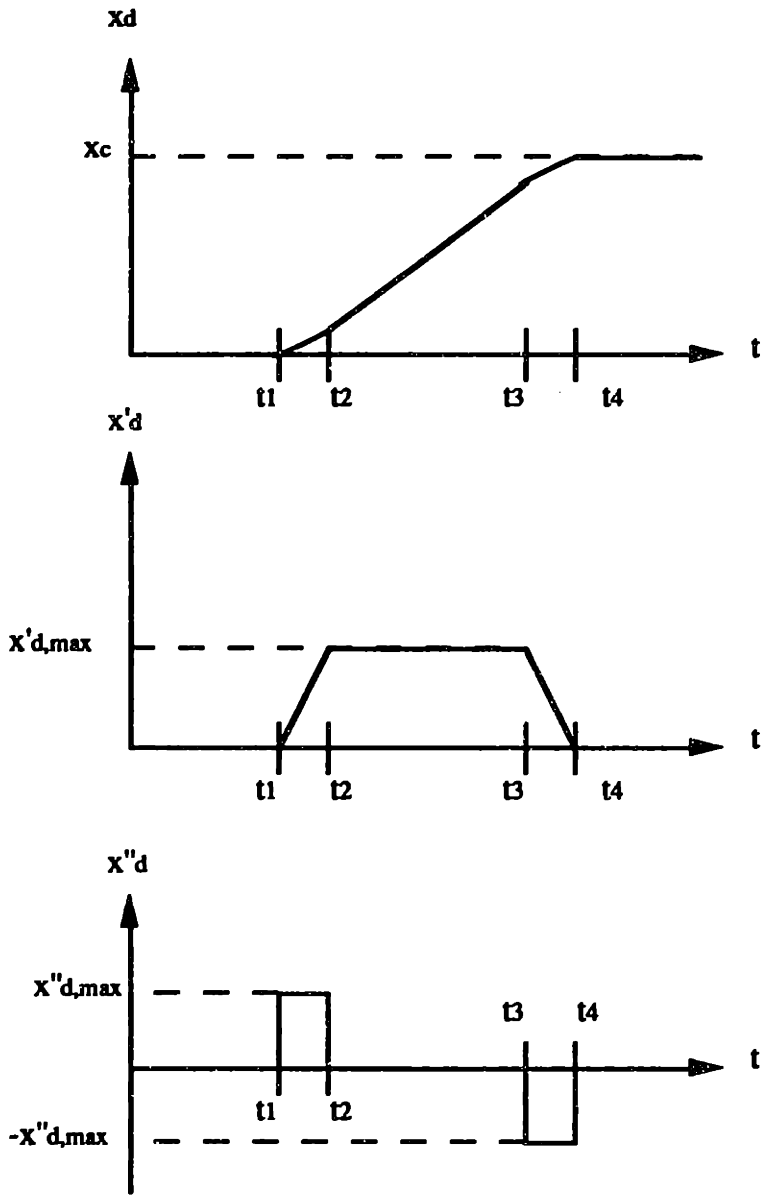

Figure 8.1 "Optimal Time" State Trajectory Generated by TGA

For all of the simulation performance tests of the AUV control system presented in this chapter, the maximum heading rate was chosen to be 15.0 deg/sec and the maximum heading acceleration was chosen to be 5.0 deg/sec^2. The maximum depth rate was chosen to be 0.5 ft/sec and the maximum depth acceleration was chosen to be 0.2 ft/sec^2. In

addition, the optimal-time trajectories generated by the TGA were filtered (by 0.5 rad/s bandwidth low-pass first-order digital filters for both depth and heading) before being sent to the AUV controller.

Depth Rate Estimator and Filter

Recall form Chapter 4 that the AUV sensor suite does not contain a depth rate sensor. Therefore, for the simulation results presented in this chapter, the AUV's depth rate was estimated by back-differencing and filtering the sensed depth using a first-order low-pass digital filter. For a sampling rate of 0.2 rad/s and a filter bandwidth of 2.5 rad/s, the discrete-time depth rate estimation and filtering algorithm was given by

$$H_{\dot{Z}}(z) = \left(\frac{1 - z^{-1}}{0.2}\right)\left(\frac{1 - e^{(-2.5)(0.2)}}{1 - z^{-1}e^{(-2.5)(0.2)}}\right)$$

$$= \frac{0.39347 - 0.39347z^{-1}}{0.2 - 0.121306z^{-1}} \qquad (8.8)$$

8.2 FULL-ORDER H_∞/μ-SYNTHESIS CONTROLLER PERFORMANCE

8.2.1 Full-Order H_∞ Controller Performance

"Full-Ahead" Simulation Performance

The first simulated test was done with a commanded forward thrust of 1.0 lb., nominal model parameters, and zero sensor noise in order to test (as close as possible) the nominal performance of the H_∞ controller. The commanded heading trajectory was from 0.0 to 180.0 degrees, and the commanded depth trajectory was from 0.0 to 10.0 ft. The results of this test are shown in Figure 8.2 and Table 8.1. For the numerical values shown in Table 8.1, the response time is defined as the time period from where the reference trajectory reaches its final value (within 0.1 feet for depth and within 0.5 degrees for heading) to the where the vehicle first attains this value (within 0.1 feet for depth and within 0.5 degrees for heading). The maximum overshoot is defined as the difference

between the maximum value reached by the vehicle and the maximum value reached by the reference trajectory. For purposes of comparison with the Sliding-mode based controllers, the numerical results of Table 8.1 are shown together with the (nonlinear) performance specifications from Chapter 6 and Chapter 7.

Table 8.1: "Full-Ahead" Performance Test of the AUV Full-Order H_∞ Controller (with Performance Specifications from Chapters 6 and 7 in Parentheses)

Steady-State Depth Error	0.0 feet ($\pm$1.0 feet)
Steady-State Heading Error	0.0 degrees ($\pm$5.0 degrees)
Depth Overshoot	1.72 feet (1.0 feet)
Heading Overshoot	5.73 degrees (10.0 degrees)
Depth Response	11.74 seconds (10.0 seconds)
Heading Response	5.83 seconds (5.0 seconds)

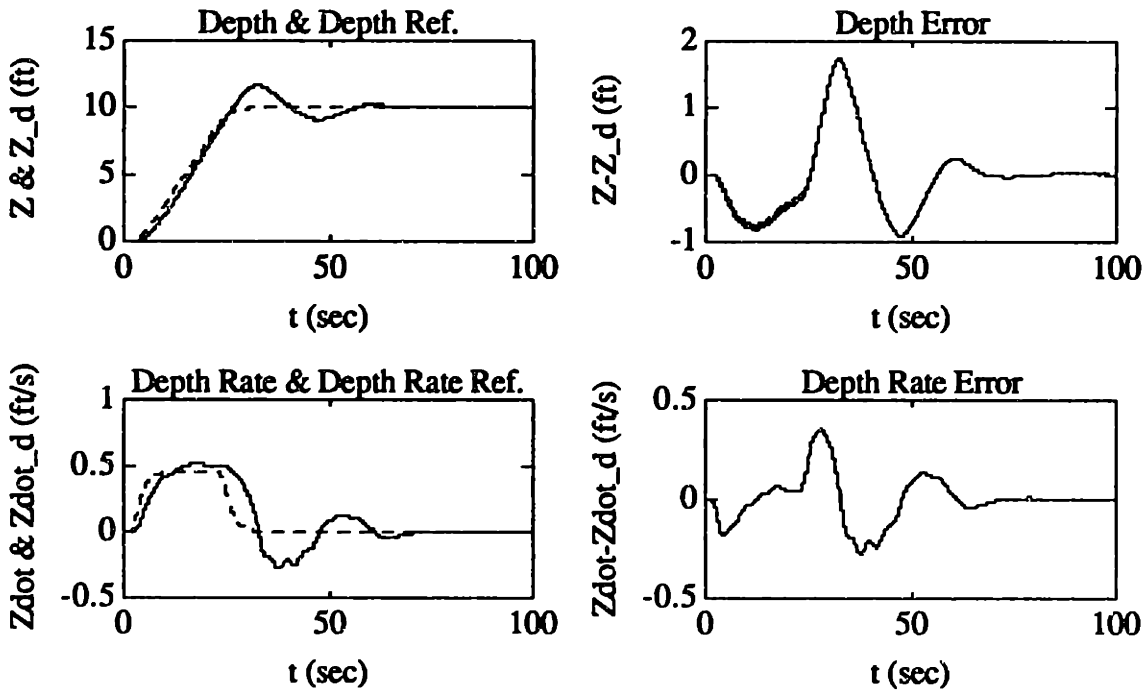

Figure 8.2: "Full-Ahead" Simulation Performance of Full-Order H_∞ Controller

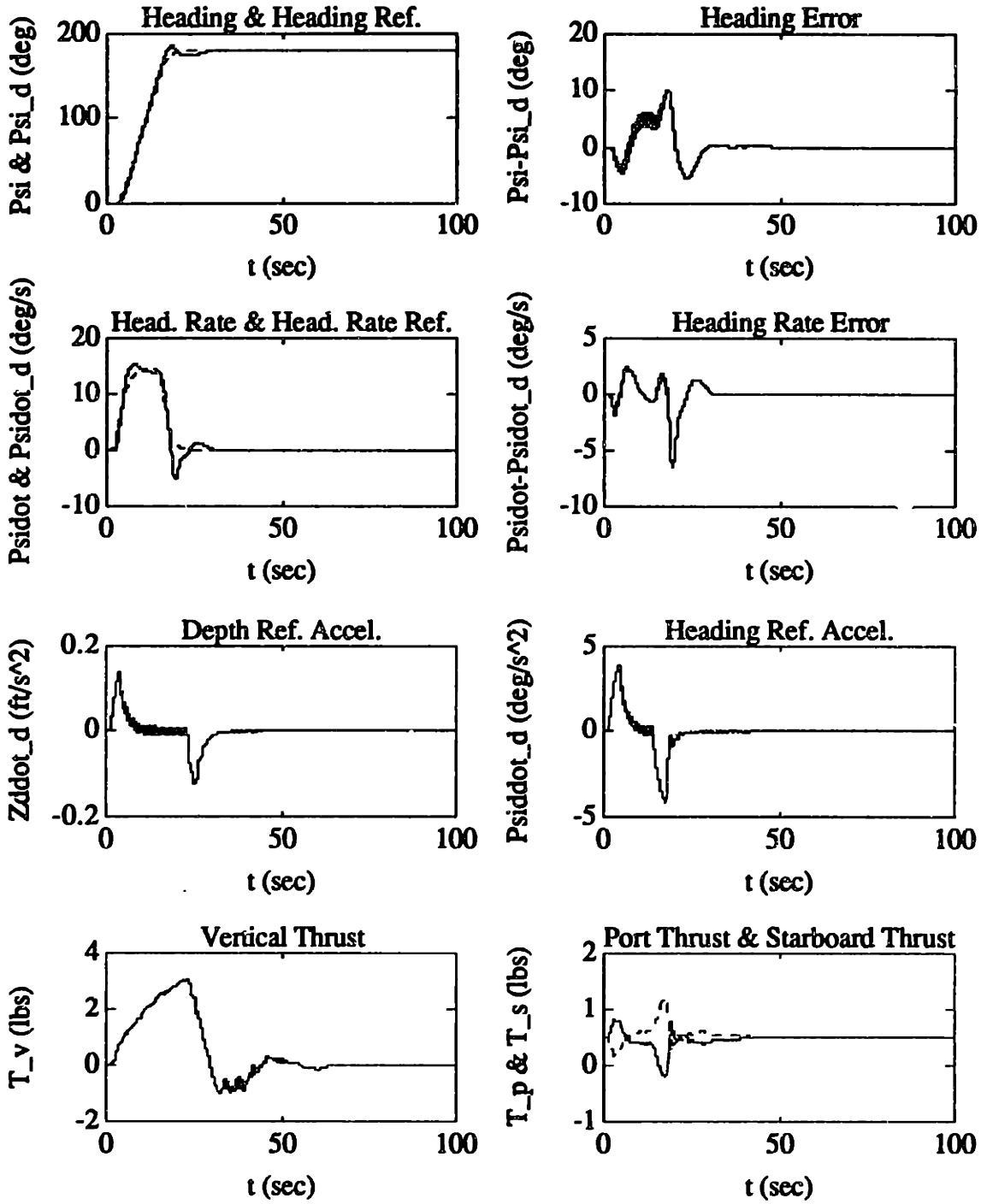

Figure 8.2: "Full-Ahead" Simulation Performance of
Full-Order H_∞ Controller (continued)

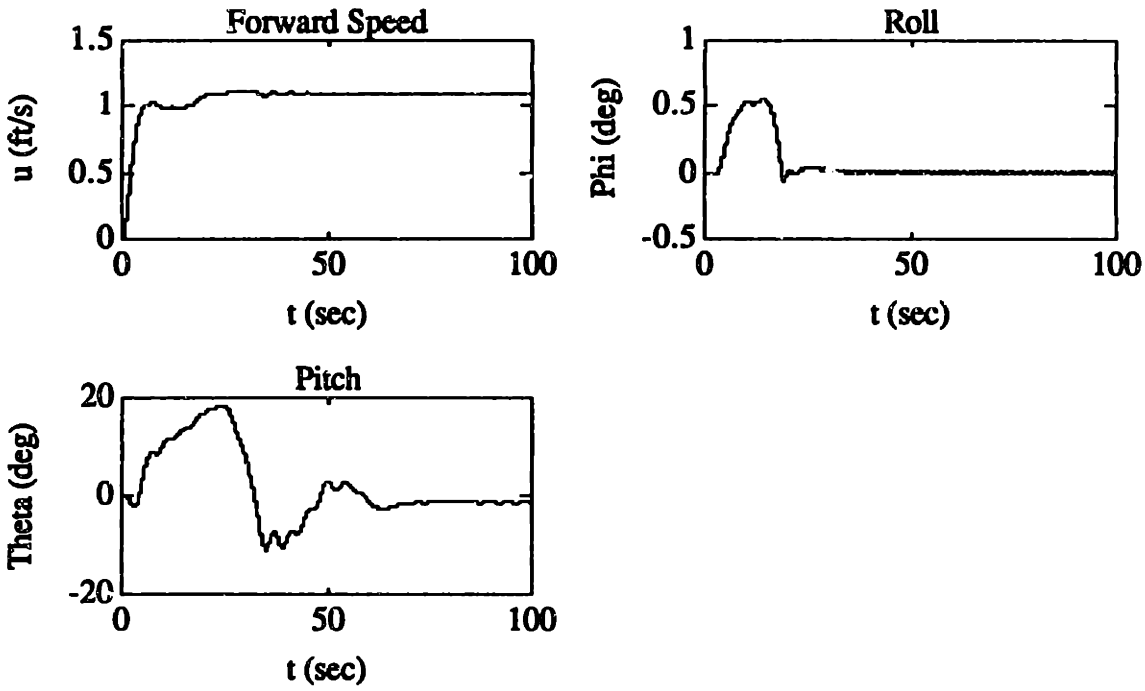

Figure 8.2: "Full-Ahead" Simulation Performance of
Full-Order H_∞ Controller (continued)

From the results of Figure 8.2 and Table 8.1, the "full-ahead" steady-state error performance of the Full-Order H_∞ controller met the nonlinear performance goals of Chapter 6 and 7, as well as the heading overshoot. Both the depth response-time and heading-response time were slightly slower than specified, but still acceptable. However, the depth overshoot was greater than specified. From the linear performance results presented in Section 5.3.3, one probable cause for this somewhat high overshoot is the decreased reliance of the H_∞ controller on the "noisy" depth rate estimate. Another probable cause for the depth overshoot is the somewhat high pitch response (with a maximum magnitude of approximately 18.1 degrees). This implies a loss of effectiveness for the vertical thruster in controlling depth (since the vertical thrust force component along the earth-relative Z-axis of the vehicle can be shown to be proportional to the cosine of the pitch angle).

"Hovering" Simulation Performance

The second simulated test was also done with nominal model parameters and zero sensor noise, but with a commanded total forward thrust of 0.0 lb. This was done in order to test the robustness of the H_∞ controller to low off-nominal axial velocities. The commanded trajectories were identical to the first test. The results of this test are shown Figure 8.3 and Table 8.2.

Table 8.2: "Hovering" Performance Test of the AUV Full-Order H_∞ Controller (with Performance Specifications from Chapters 6 and 7 in Parentheses)

Steady-State Depth Error	$\pm$0.02 feet ($\pm$1.0 feet)
Steady-State Heading Error	0.0 degrees ($\pm$5.0 degrees)
Depth Overshoot	0.60 feet (1.0 feet)
Heading Overshoot	6.07 degrees (10.0 degrees)
Depth Response	3.04 seconds (10.0 seconds)
Heading Response	0.5 seconds (5.0 seconds)

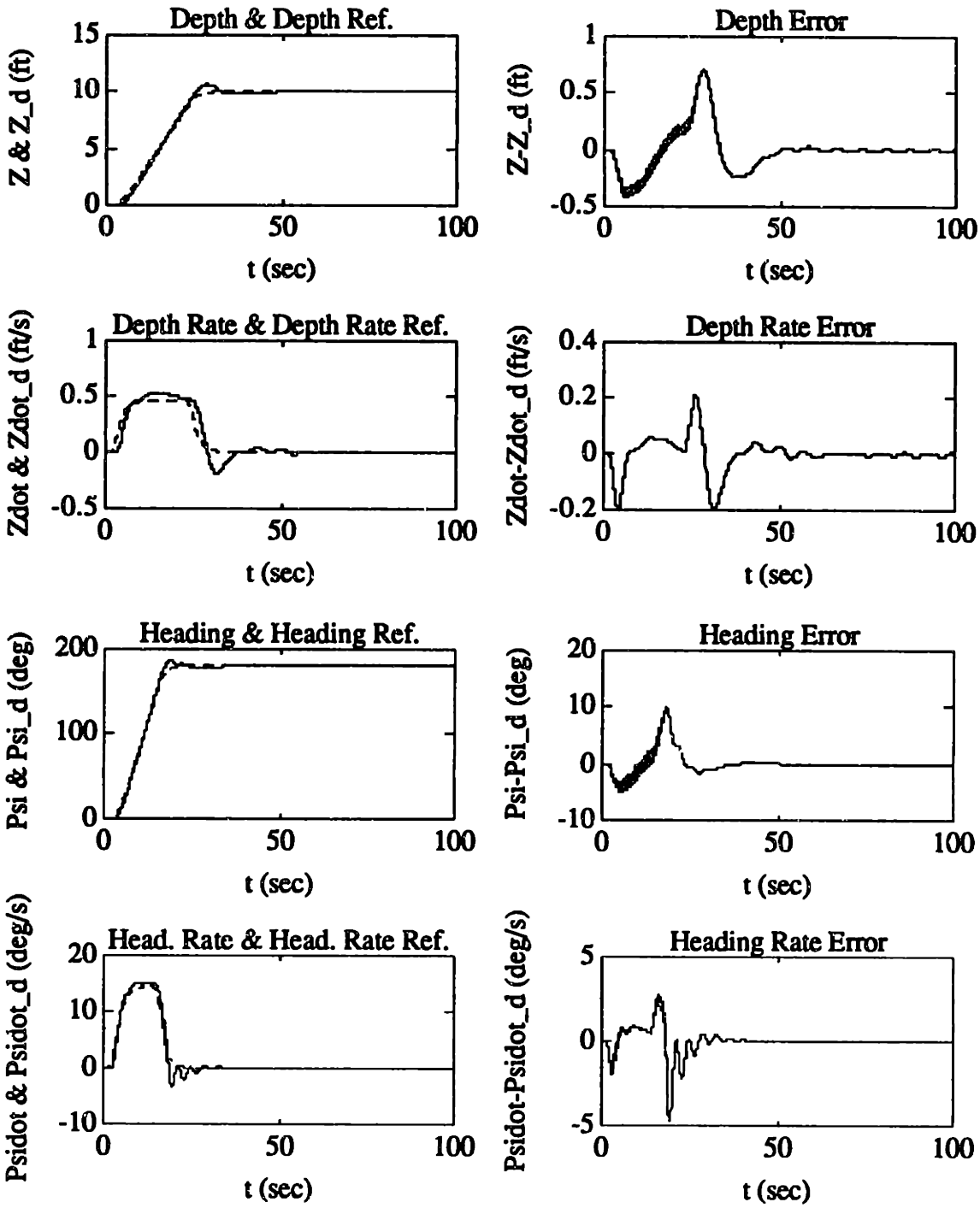

Figure 8.3: "Hovering" Simulation Performance of
Full-Order H_∞ Controller

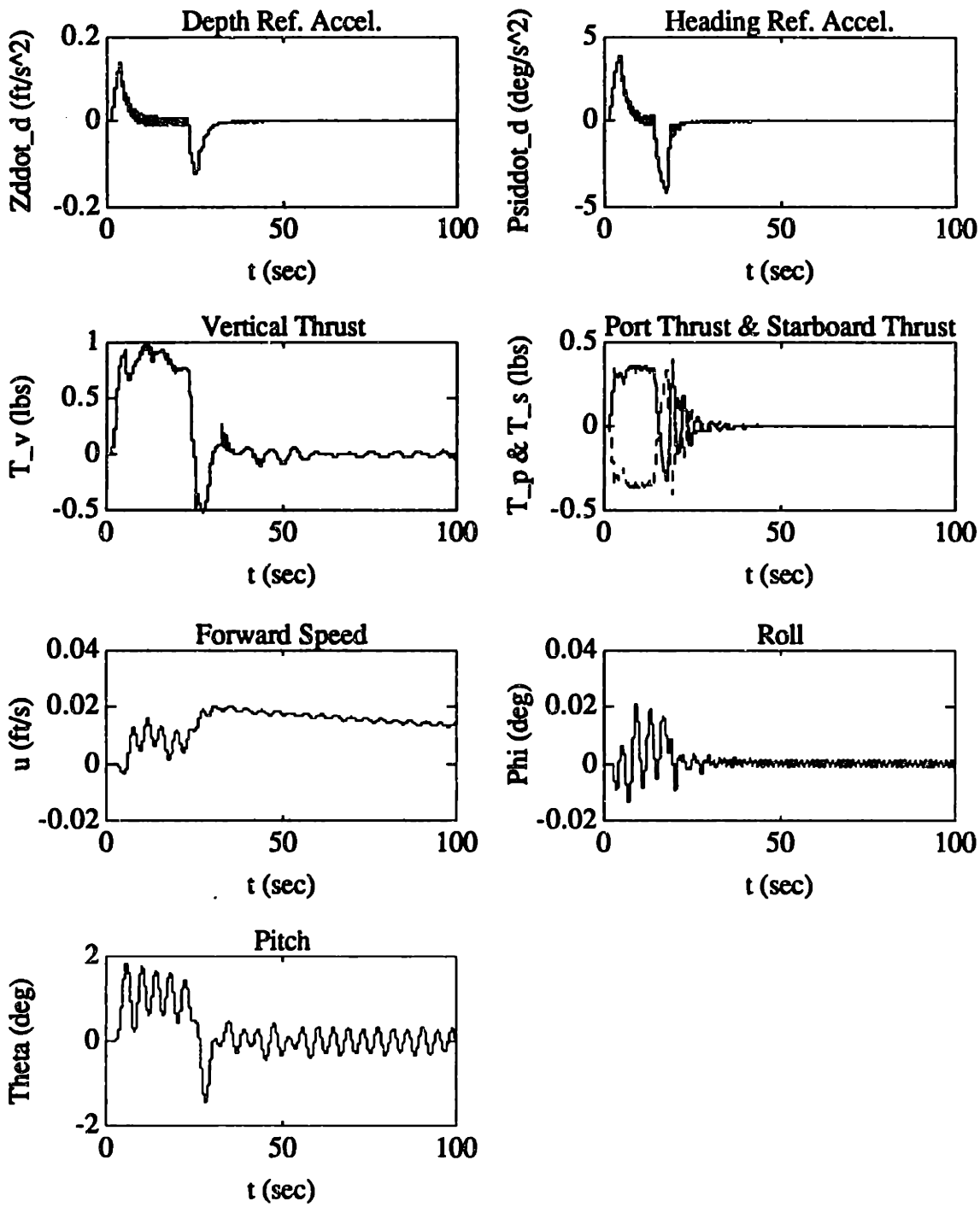

Figure 8.3: "Hovering" Simulation Performance of
Full-Order H_∞ Controller (continued)

From the results of Figure 8.3 and Table 8.2, the overall "hovering" performance of the Full-Order H_∞ controller was significantly improved, as compared to its "full-ahead" performance. For this case, the controller met all of the nonlinear performance goals of Chapter 6 and 7, including the depth overshoot. Roll and pitch were still stabilized by this controller, even though their responses were slightly more oscillatory. Note the smaller pitch response (with a maximum magnitude of approximately 1.88 degrees). This implies that the vertical thruster is more effective in controlling depth, as compared to the "full-ahead" case. Note that depth response has a slight steady-state oscillation. This is due in part to the oscillatory pitch response.

"Full-Reverse" Simulation Performance

The next simulated test was done with nominal model parameters and zero sensor noise, but with a commanded total forward thrust of -1.0 lb. This was done in order to test the robustness of the H_∞ controller to negative off-nominal axial velocities. The commanded trajectories were identical to the first test. The results of this test are shown Figure 8.4 and Table 8.3.

Table 8.3: "Full-Reverse" Performance Test of the AUV Full-Order H_∞ Controller (with Performance Specifications from Chapters 6 and 7 in Parentheses)

Steady-State Depth Error	$\pm$0.05 feet ($\pm$1.0 feet)
Steady-State Heading Error	0.0 degrees ($\pm$5.0 degrees)
Depth Overshoot	1.16 feet (1.0 feet)
Heading Overshoot	4.21 degrees (10.0 degrees)
Depth Response	7.84 seconds (10.0 seconds)
Heading Response	5.48 seconds (5.0 seconds)

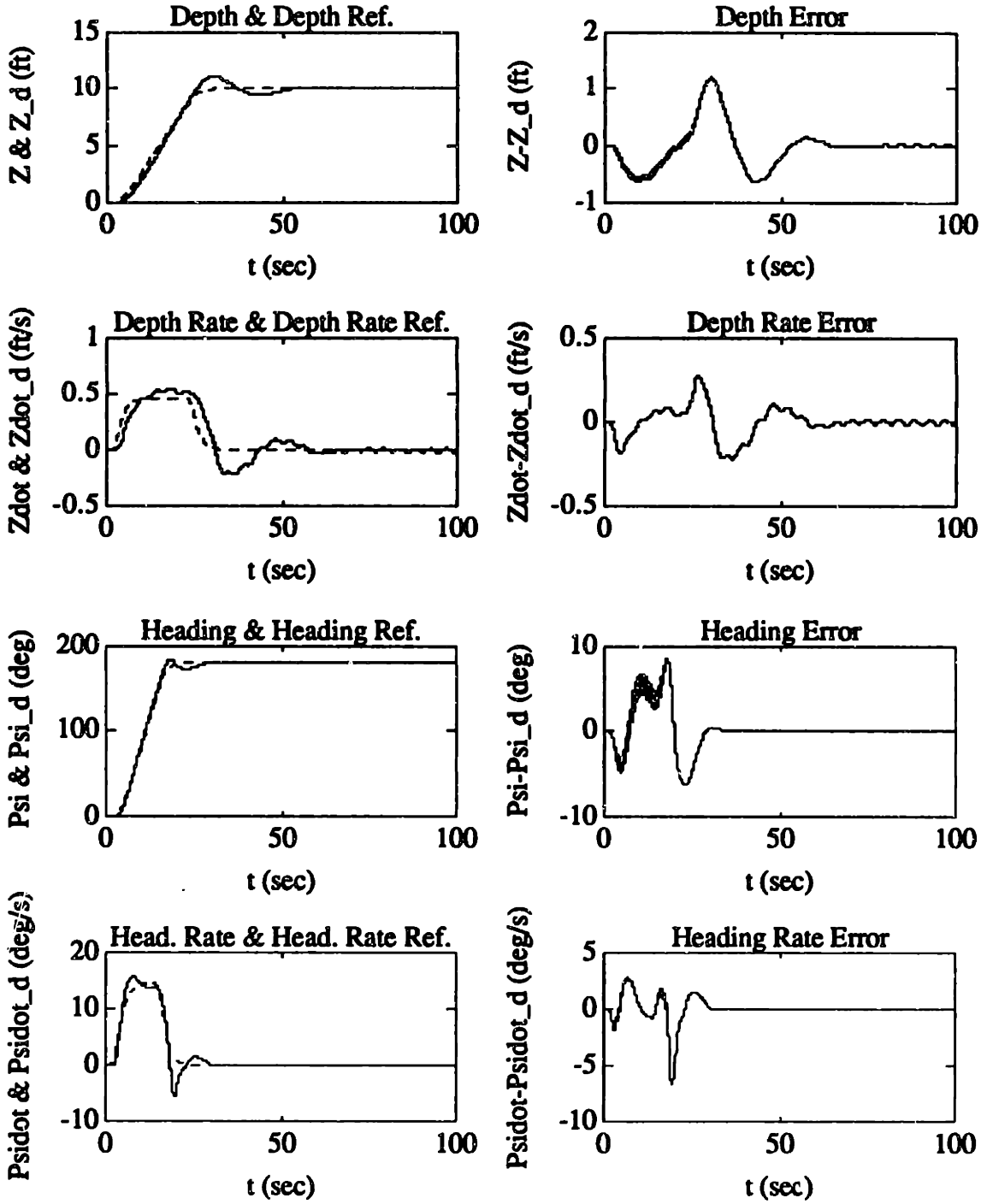

Figure 8.4: "Full-Reverse" Simulation Performance of Full-Order H_∞ Controller

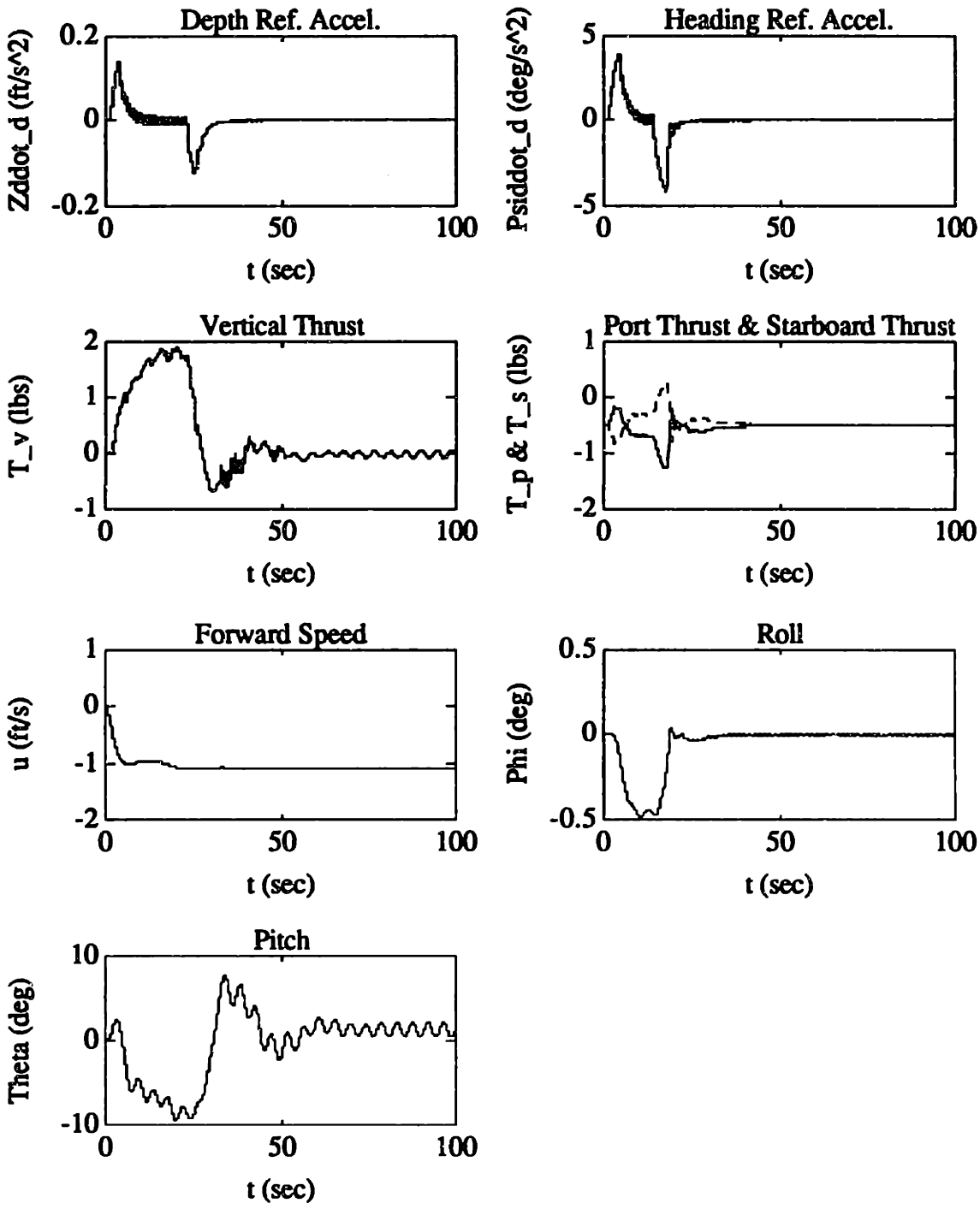

Figure 8.4: "Full-Reverse" Simulation Performance of Full-Order H_∞ Controller (continued)

From the results of Figure 8.4 and Table 8.3, the "full-reverse" steady-state error performance of the Full-Order H_∞ controller met the nonlinear performance goals of Chapter 6 and 7, as well as both the heading overshoot and the depth response time. The heading response time was slightly slower than specified, but still acceptable. The depth overshoot was greater than specified, but significantly less that the depth overshoot for the "full-ahead" case. This gives credence to the hypothesis that the depth overshoot is due in part to the loss of vertical thrust effectiveness due to the pitch response (since the pitch response has a maximum magnitude of approximately 9.4 degrees, as compared to 18.1 degrees for the "full-ahead" case). Note that the depth response has a slight steady-state oscillation. This is also due in part to the pitch response, which for this case, is more oscillatory and essentially opposite in sign to the pitch response for the "full-ahead" case. This implies that any attempts to use the pitch measurement to decrease the depth overshoot (by decreasing the "sensor noise" weighting function in the H_∞ design phase of Section 5.3.1) could cause unwanted oscillations in both the depth response and the pitch response for the case of negative axial velocities.

"Noisy Full-Ahead" Simulation Performance

The next simulated test was done using nominal model parameters, at the "nominal" commanded forward thrust of 1.0 lb. However, the Gaussian sensor noise inputs were set to the values found Section 4.6 (in order to test the noise performance of the H_∞ controller). The commanded heading trajectory was again from 0.0 to 180.0 degrees, and the commanded depth trajectory was from 0.0 to 10.0 ft. The results of this test are shown in Figure 8.5.

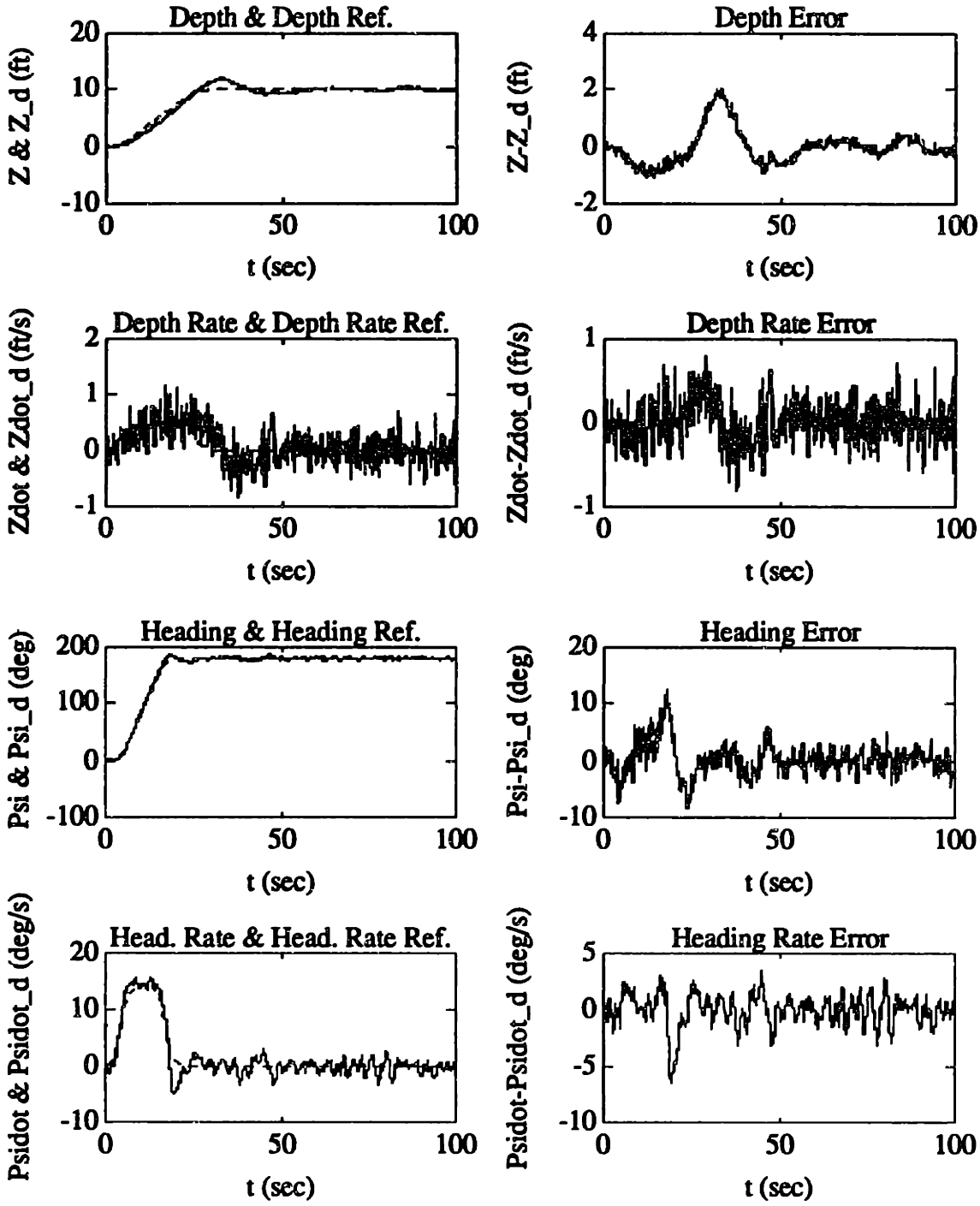

Figure 8.5: "Noisy Full-Ahead" Simulation Performance of Full-Order H_∞ Controller

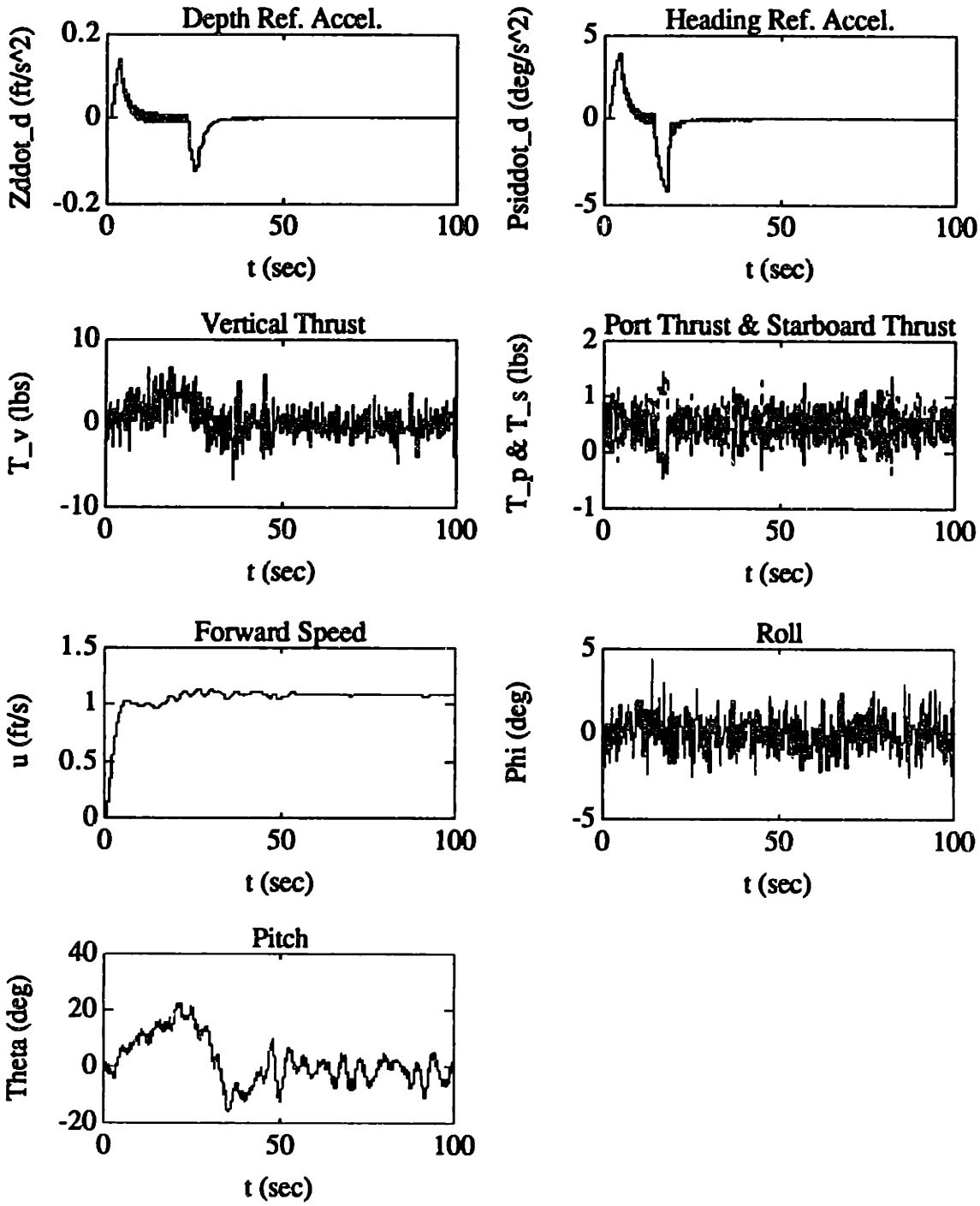

Figure 8.5: "Noisy Full-Ahead" Simulation Performance of Full-Order H_∞ Controller (continued)

From the results of Figure 8.5, it appears that the full-order H∞ controller is reasonably robust to the additive sensor noise (at least for the "full-ahead case"). With the exception of a slightly larger depth overshoot, the overshoot and response time characteristics of this control design are essentially unchanged from the noise-free case. The steady-state error in the depth and the heading are somewhat larger and more oscillatory than for the noise-free case. However, the steady-state error still meets the design specifications of ±1.0 feet and ±5.0 degrees for depth and heading, respectively. Note that the commanded thrust input signals to the AUV thrusters are significantly more oscillatory for this case. For the actual Sea Squirt vehicle, this could cause an unwanted drain by the thruster motors on the AUV's power source.

8.2.2 Full-Order μ-Synthesis Controller Performance

"Full-Ahead" Simulation Performance

The first simulated test of the AUV μ-synthesis controller was done with a commanded forward thrust of 1.0 lb., nominal model parameters, and zero sensor noise in order to test the "nominal" performance of this controller. As with the H_∞ controller of the previous section, the commanded heading trajectory was from 0.0 to 180.0 degrees, and the commanded depth trajectory was from 0.0 to 10.0 ft. The results of this test are shown in Figure 8.6 and Table 8.4.

Table 8.4: "Full-Ahead" Performance Test of the AUV Full-Order μ-Synthesis Controller (with Performance Specifications from Chapters 6 and 7 in Parentheses)

Steady-State Depth Error	0.0 feet ($\pm$1.0 feet)
Steady-State Heading Error	0.0 degrees ($\pm$5.0 degrees)
Depth Overshoot	1.50 feet (1.0 feet)
Heading Overshoot	4.36 degrees (10.0 degrees)
Depth Response	9.91 seconds (10.0 seconds)
Heading Response	6.45 seconds (5.0 seconds)

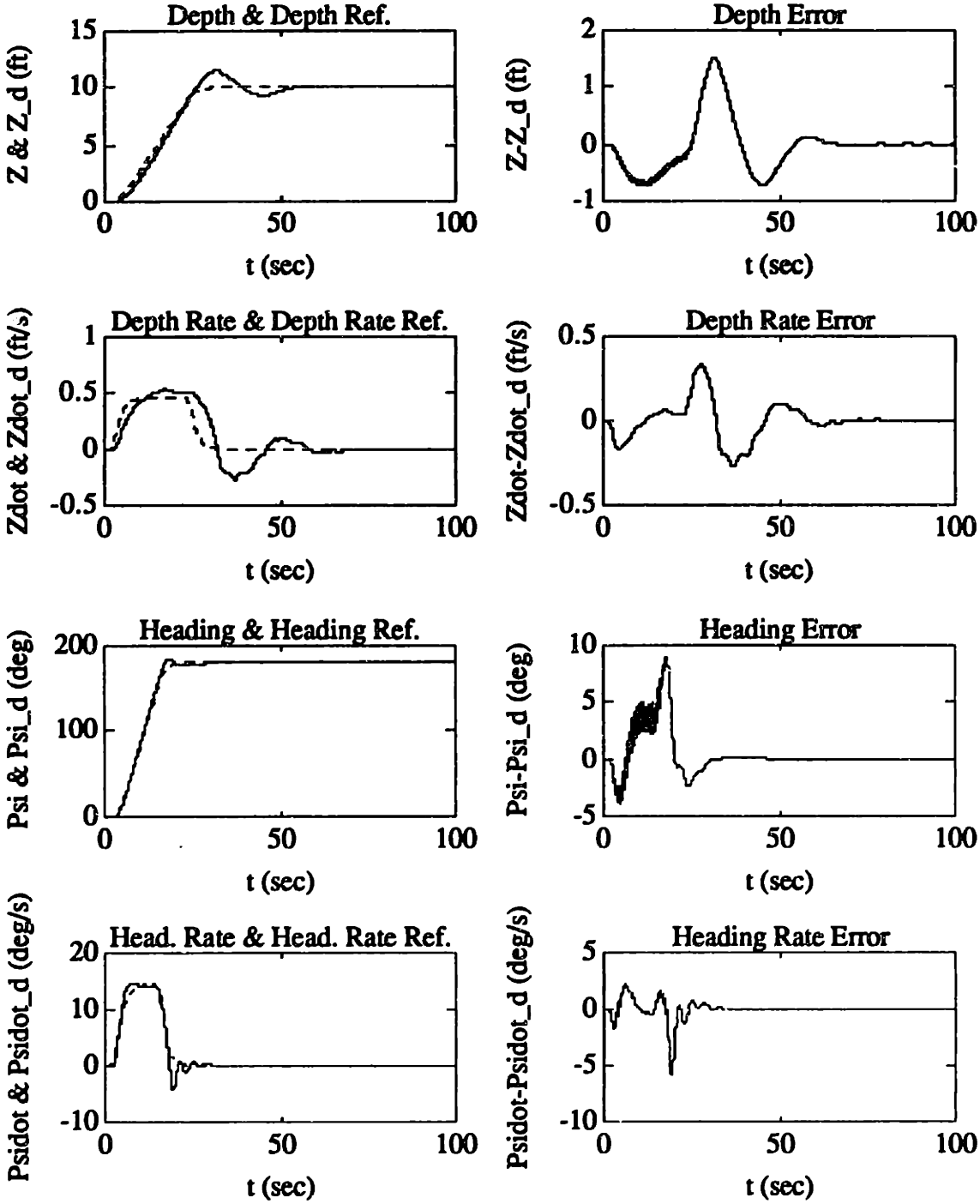

Figure 8.6: "Full-Ahead" Simulation Performance of
Full-Order μ-Synthesis Controller

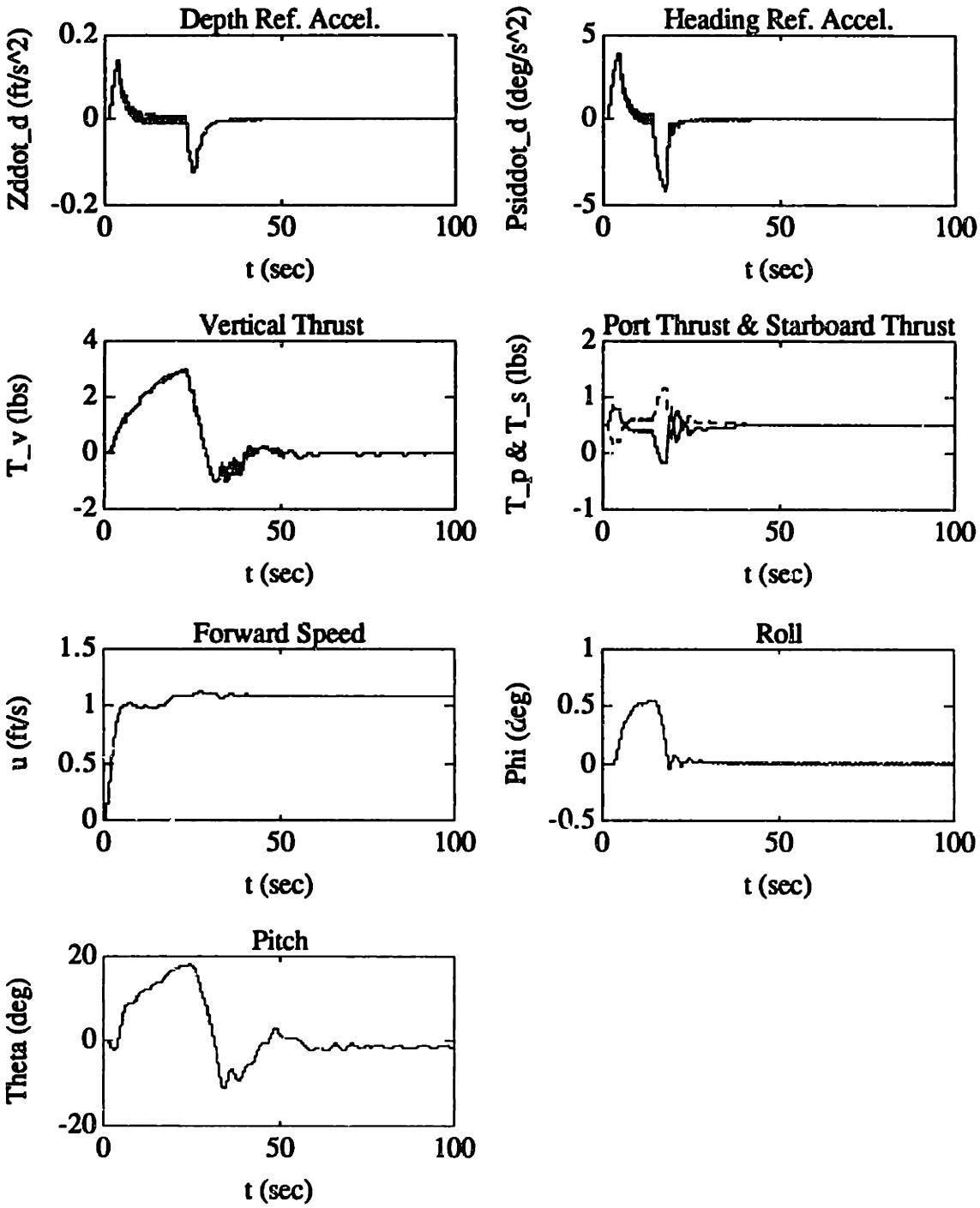

Figure 8.6: "Full-Ahead" Simulation Performance of
Full-Order μ-Synthesis Controller (continued)

From the results of Figure 8.6 and Table 8.4, the "full-ahead" performance of the Full-Order μ-Synthesis controller was similar to the performance of the robust H_∞ controller (with the steady-state error performance and the heading overshoot meeting the nonlinear performance goals of Chapter 6 and 7). The heading response time was slightly slower than the heading response time for the H_∞ controller, but still acceptable. In contrast, the depth response time was improved so as to meet the design specification (but just barely).

"Hovering" Simulation Performance

The second simulated test of the full-order μ-synthesis controller was also done with nominal model parameters and zero sensor noise, but with a commanded total forward thrust of 0.0 lb. As with the robust H_∞ controller, this was done in order to test the robustness of the μ-synthesis controller to low off-nominal axial velocities. The commanded trajectories were identical to the first test. The results of this test are shown Figure 8.7 and Table 8.5. For purposes of clarifying the depth steady-state error, the μ-synthesis performance test simulation is shown for an additional 50 seconds (0 to 150 seconds).

Table 8.5: "Hovering" Performance Test of the AUV Full-Order μ-Synthesis Controller (with Performance Specifications from Chapters 6 and 7 in Parentheses)

Steady-State Depth Error	±0.22 feet (±1.0 feet)
Steady-State Heading Error	0.0 degrees (±5.0 degrees)
Depth Overshoot	0.45 feet (1.0 feet)
Heading Overshoot	3.07 degrees (10.0 degrees)
Depth Response	2.72 seconds (10.0 seconds)
Heading Response	0.4 seconds (5.0 seconds)

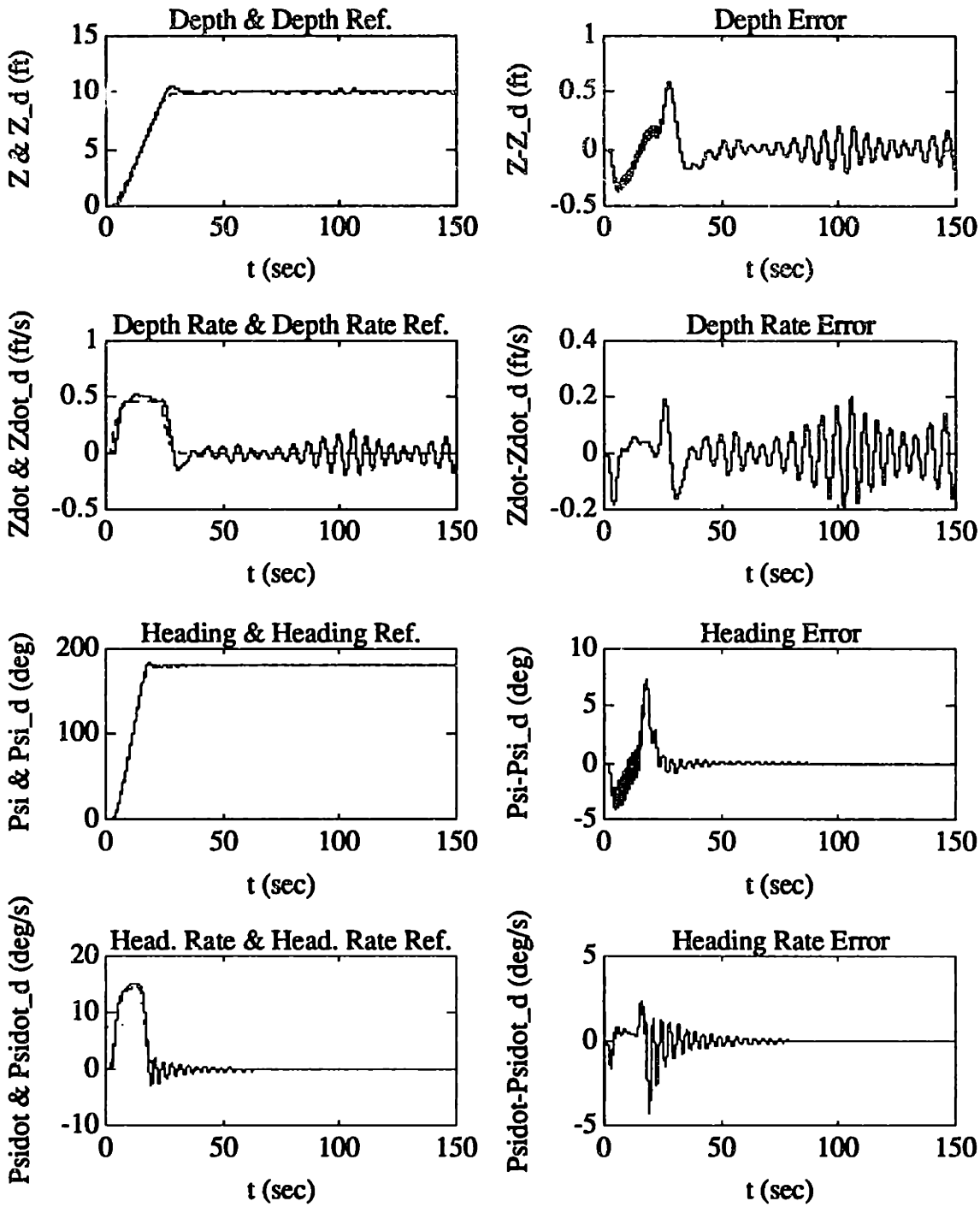

Figure 8.7: "Hovering" Simulation Performance of
Full-Order μ-Synthesis Controller

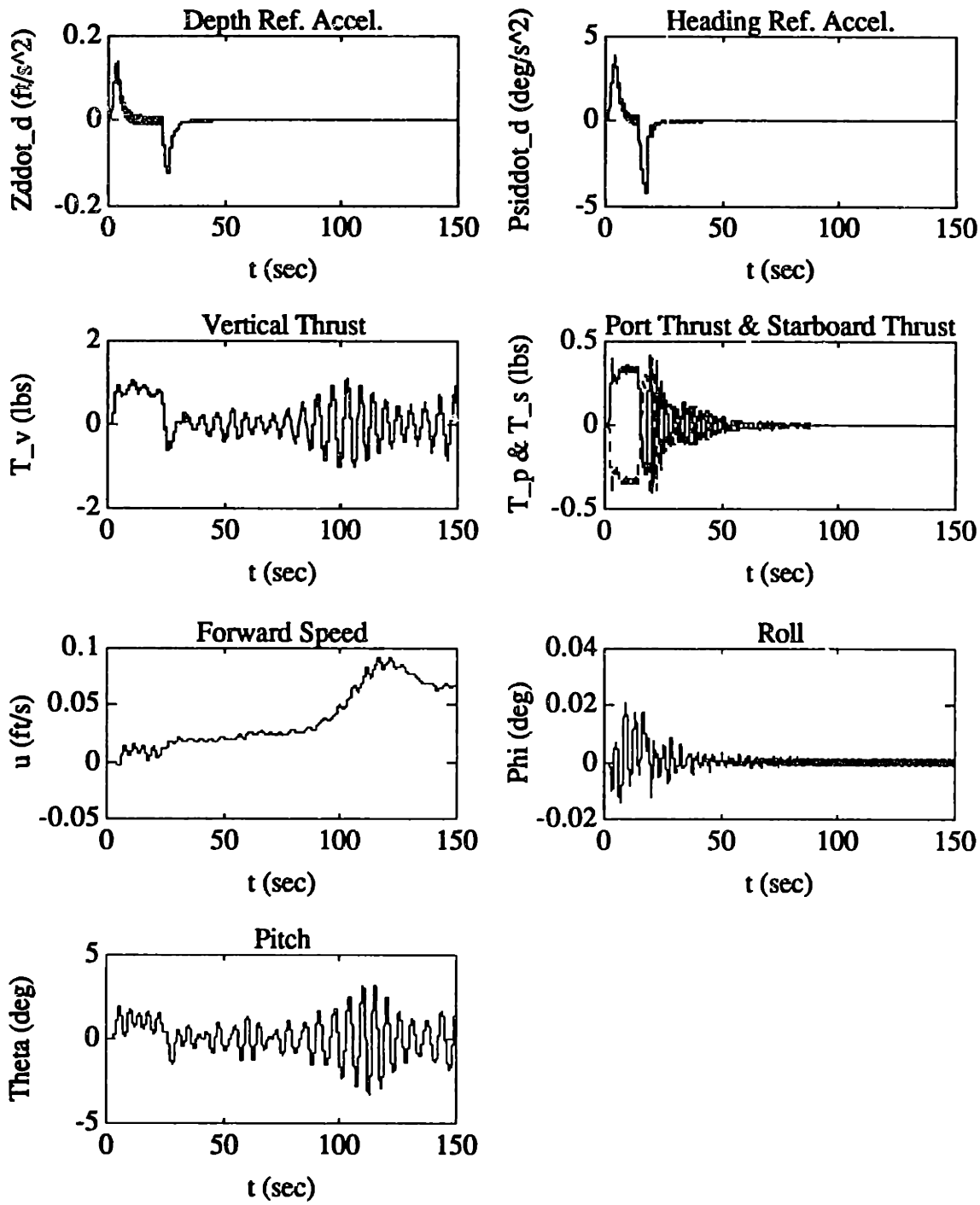

Figure 8.7: "Hovering" Simulation Performance of
Full-Order μ-Synthesis Controller (continued)

From the results of Figure 8.7 and Table 8.5, the "hovering" performance of the full-order μ-synthesis controller essentially met all of the nonlinear performance goals of Chapter 6 and 7, including the depth overshoot. However, note the appearance of an undesirable steady-state oscillation in the depth response (even though the maximum amplitude of this oscillation still falls well within the steady-state depth-error performance goal). From the linear time-domain analysis of Section 5.4.2, this oscillation is caused by the higher gain of the "depth control" portion of the μ-synthesis controller, as compared to the "depth control" portion of the H_∞ controller. The commanded thrust input signals to the AUV vertical thruster are also significantly more oscillatory for this case (with a maximum steady-state magnitude of approximately 1.1 lb.). For the actual *Sea Squirt* vehicle, this could cause an unwanted drain by the vertical thruster motor on the AUV's power source, even though the depth performance would still be good enough for the AUV to complete a "typical" mission.

"Full-Reverse" Simulation Performance

The next simulated test of the AUV full-order μ-synthesis controller was done with nominal model parameters and zero sensor noise, but with a commanded total forward thrust of -1.0 lb. This was done in order to test the robustness of this controller to negative off-nominal axial velocities. The commanded trajectories were identical to the first test. The results of this test are shown Figure 8.8 and Table 8.6.

Table 8.6: "Full-Reverse" Performance Test of the AUV Full-Order μ-Synthesis Controller (with Performance Specifications from Chapters 6 and 7 in Parentheses)

Steady-State Depth Error	$\pm$0.02 feet ($\pm$1.0 feet)
Steady-State Heading Error	0.0 degrees ($\pm$5.0 degrees)
Depth Overshoot	0.95 feet (1.0 feet)
Heading Overshoot	3.43 degrees (10.0 degrees)
Depth Response	6.64 seconds (10.0 seconds)
Heading Response	6.52 seconds (5.0 seconds)

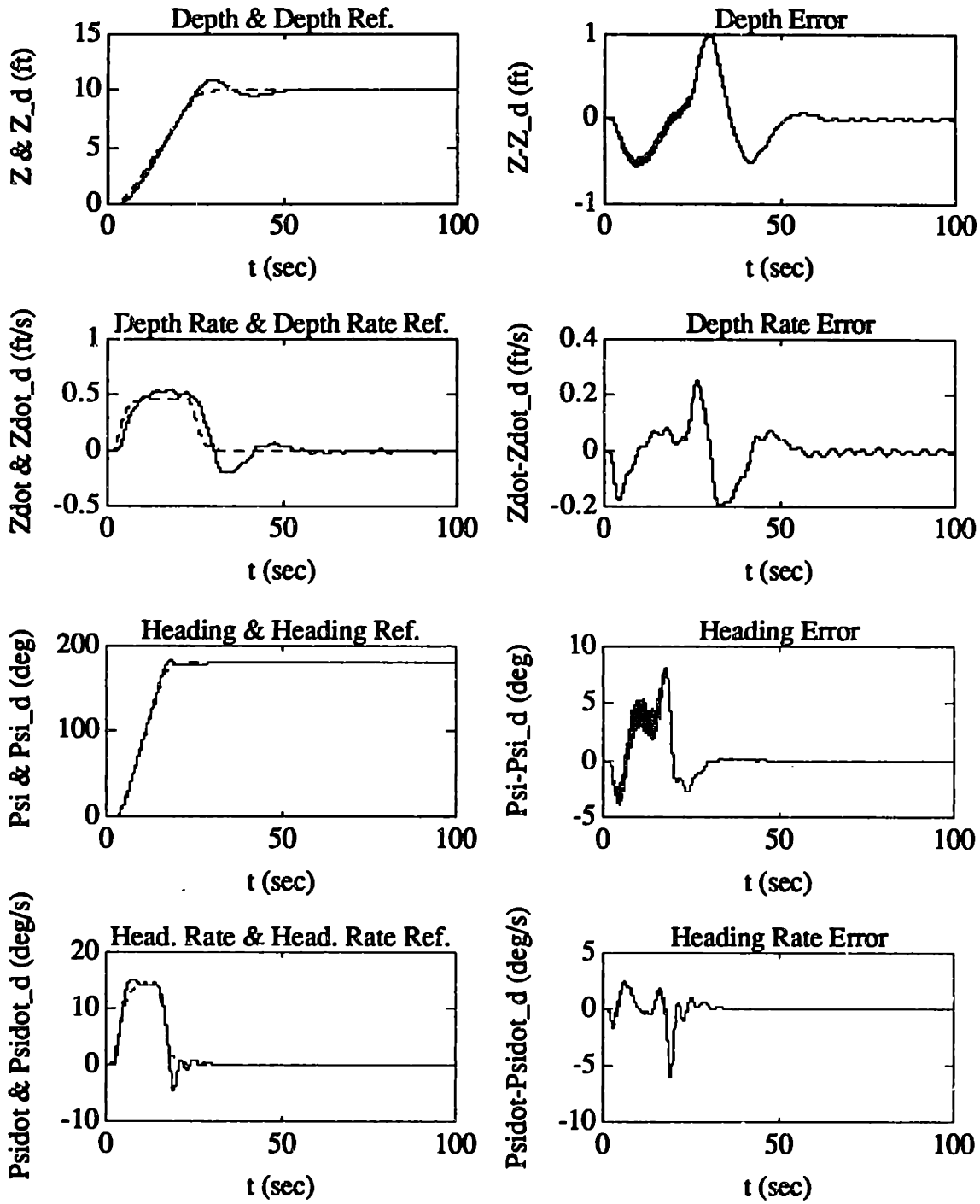

Figure 8.8: "Full-Reverse" Simulation Performance of
Full-Order μ-Synthesis Controller

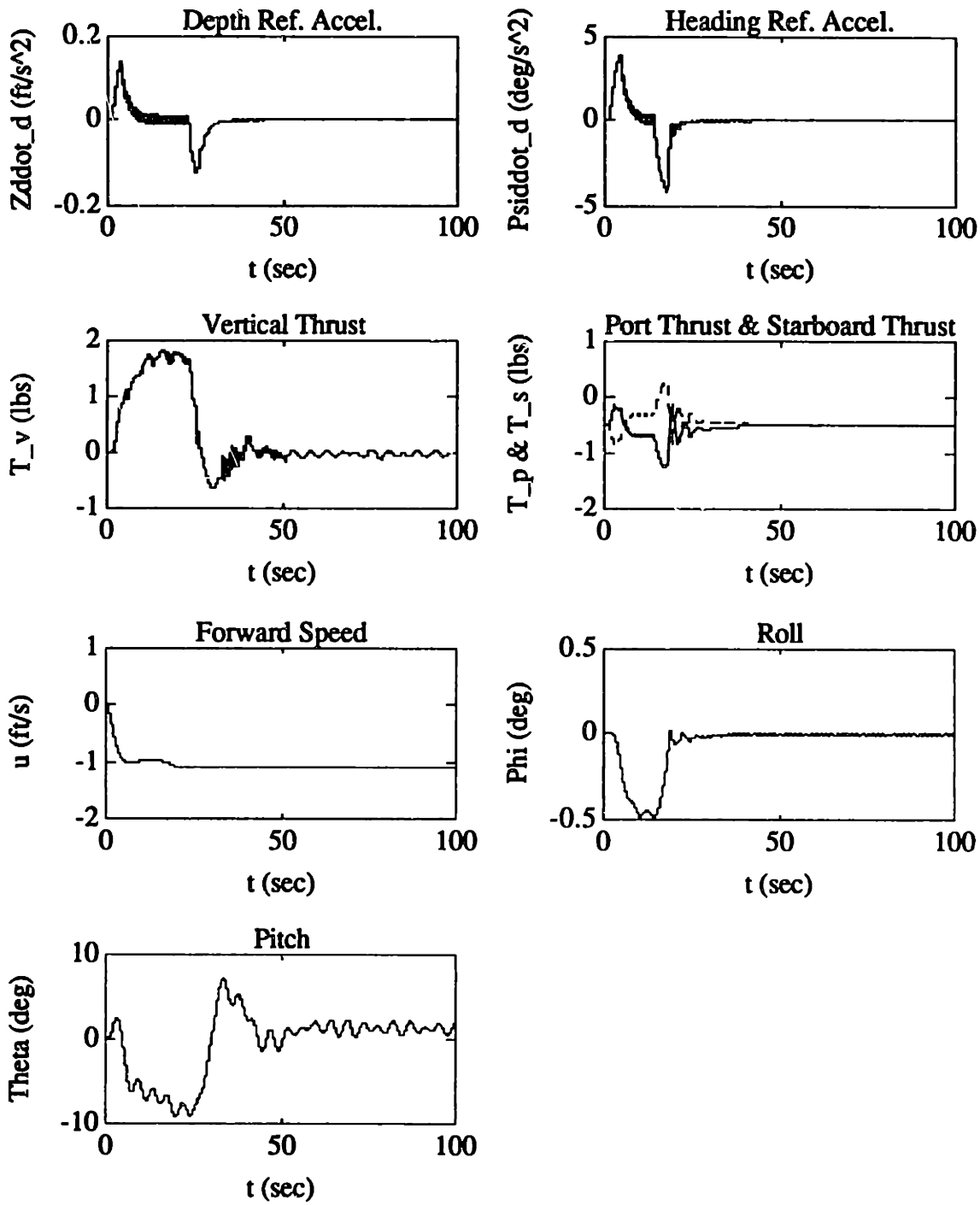

Figure 8.8: "Full-Reverse" Simulation Performance of Full-Order μ-Synthesis Controller (continued)

From the results of Figure 8.8 and Table 8.6, the "full-reverse" steady-state error performance of the Full-Order μ-Synthesis controller met the nonlinear performance goals of Chapter 6 and 7, as well as both the heading overshoot and the depth response time. The heading response time was slightly slower than for the H_∞ controller, but was still acceptable. In contrast, the depth overshoot performance was improved to the point of meeting the nonlinear performance goal, as compared to the H_∞ controller.

"Noisy Full-Ahead" Simulation Performance

The next simulated test was done using nominal model parameters, at the "nominal" commanded forward thrust of 1.0 lb. However, the Gaussian sensor noise inputs were set to the values found Section 4.6 (in order to test the noise performance of the μ-synthesis controller). The commanded heading trajectory was again from 0.0 to 180.0 degrees, and the commanded depth trajectory was from 0.0 to 10.0 ft. The results of this test are shown in Figure 8.9

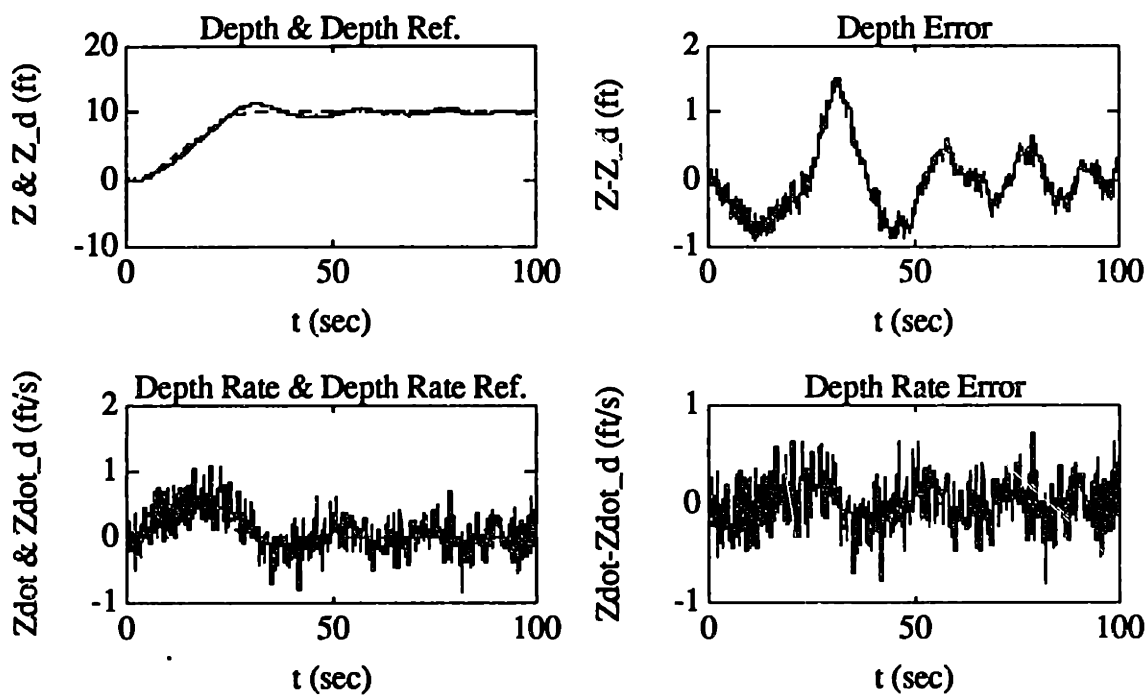

Figure 8.9: "Noisy Full-Ahead" Simulation Performance of Full-Order μ-Synthesis Controller

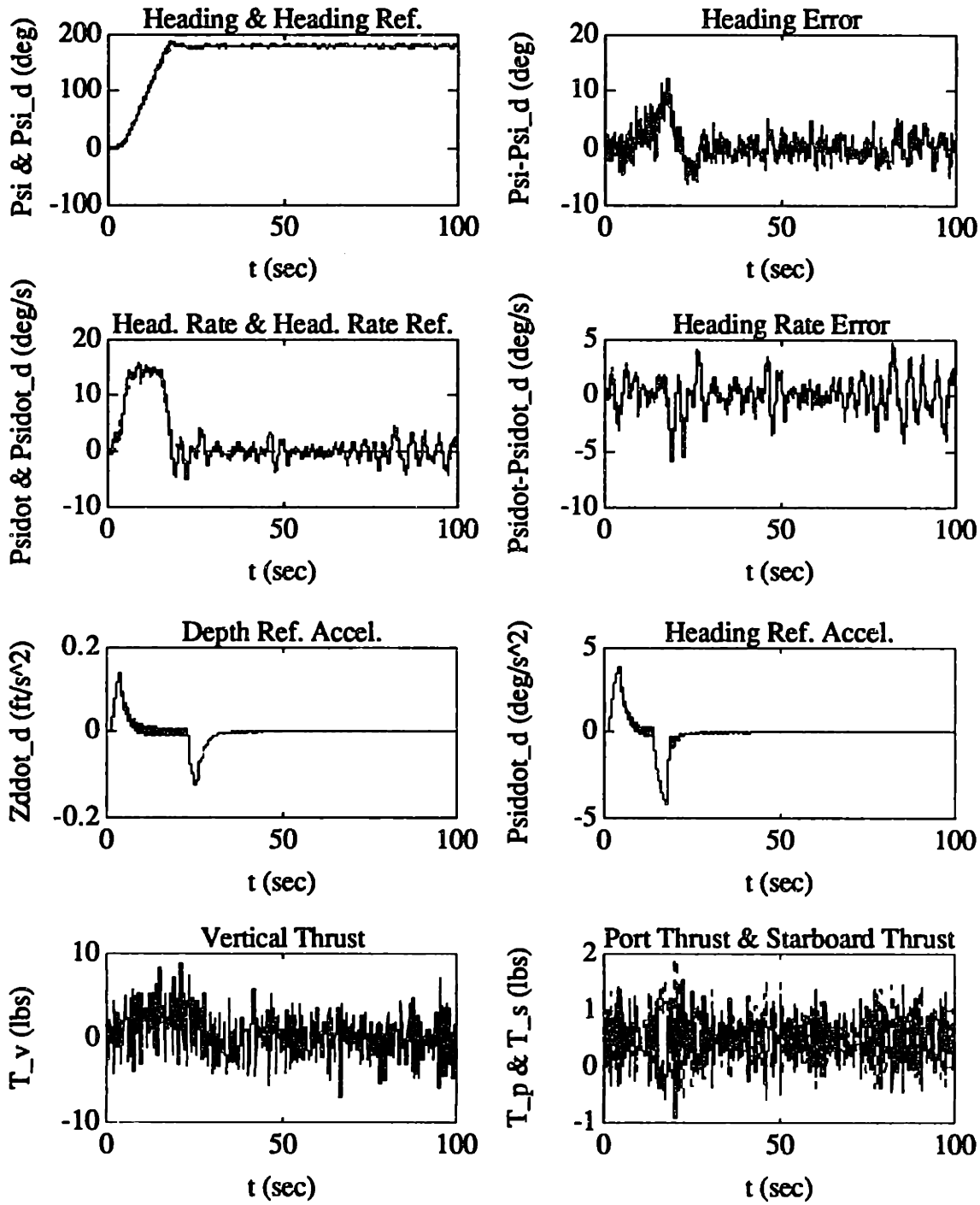

Figure 8.9: "Noisy Full-Ahead" Simulation Performance of Full-Order μ-Synthesis Controller (continued)

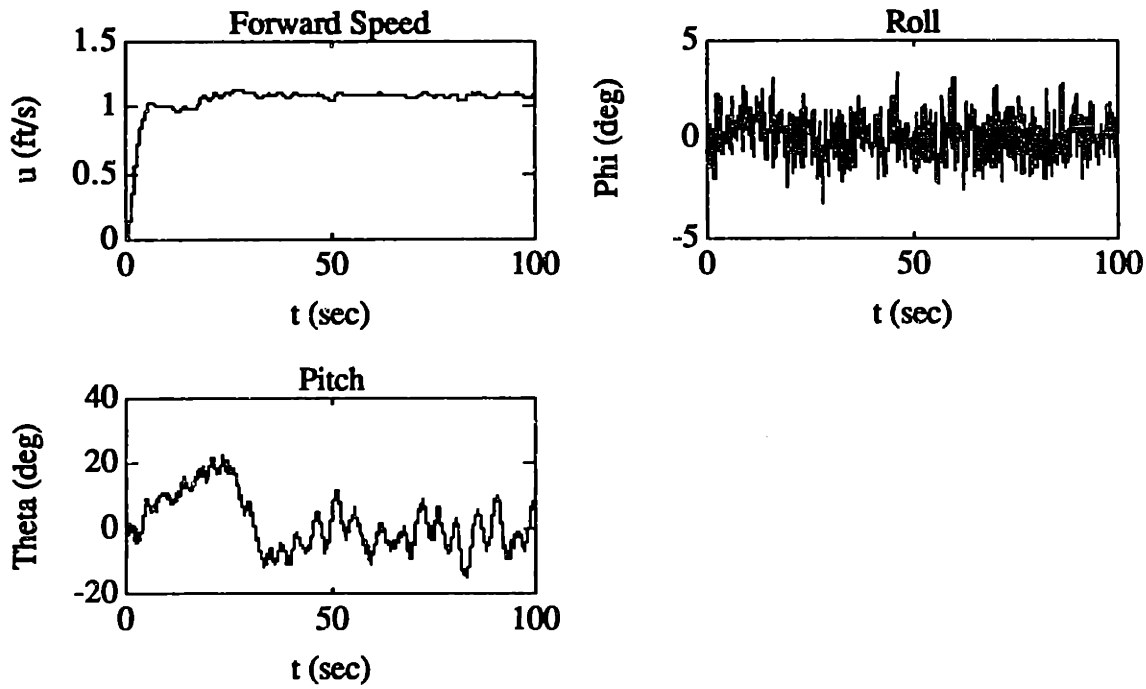

Figure 8.9: "Noisy Full-Ahead" Simulation Performance of Full-Order μ-Synthesis Controller (continued)

From the results of Figure 8.9, it appears that the full-order μ-synthesis controller is reasonably robust to the additive sensor noise (at least for the "full-ahead case"). Similarly to the H_∞ controller, the overshoot and response time characteristics of this control design are essentially unchanged from the noise-free case (with the exception of a slightly larger depth overshoot). The steady-state errors in both the depth and the heading are somewhat larger and more oscillatory than for the noise-free case, but they still meet the design specifications of ±1.0 feet and ±5.0 degrees for depth and heading, respectively. The commanded thrust input signals to the AUV thrusters are also significantly more oscillatory for this case.

8.3 SLIDING-MODE CONTROLLER PERFORMANCE

8.3.1 Initial Sliding-Mode Controller Performance

"Hovering" Simulation Performance

The first simulated test was done with a commanded forward thrust of 0.0 lb., nominal model parameters, and zero sensor noise in order to test (as close as possible) the nominal performance of the initial Sliding-Mode control design of Chapter 6. The commanded heading trajectory was from 0.0 to 180.0 degrees, and the commanded depth trajectory was from 0.0 to 10.0 ft. The results of this test are shown in Figure 8.10 and Table 8.7. As with the H_∞/μ-Synthesis numerical performance results of the previous section, the response time is defined as the time period from where the reference trajectory reaches its final value (within 0.1 feet for depth and within 0.5 degrees for heading) to the where the vehicle first attains this value (within 0.1 feet for depth and within 0.5 degrees for heading). The maximum overshoot is defined as the difference between the maximum value reached by the vehicle and the maximum value reached by the reference trajectory. The numerical results of Table 8.7 are shown together with the (nonlinear) performance specifications from Chapter 6 and Chapter 7.

Table 8.7: "Hovering" Performance Test of the Initial AUV Sliding-Mode Controller (with Performance Specifications from Chapters 6 and 7 in Parentheses)

Steady-State Depth Error	0.0 feet ($\pm$1.0 feet)
Steady-State Heading Error	0.0 degrees ($\pm$5.0 degrees)
Depth Overshoot	0.49 feet (1.0 feet)
Heading Overshoot	12.36 degrees (10.0 degrees)
Depth Response	13.21 seconds (10.0 seconds)
Heading Response	31.33 seconds (5.0 seconds)

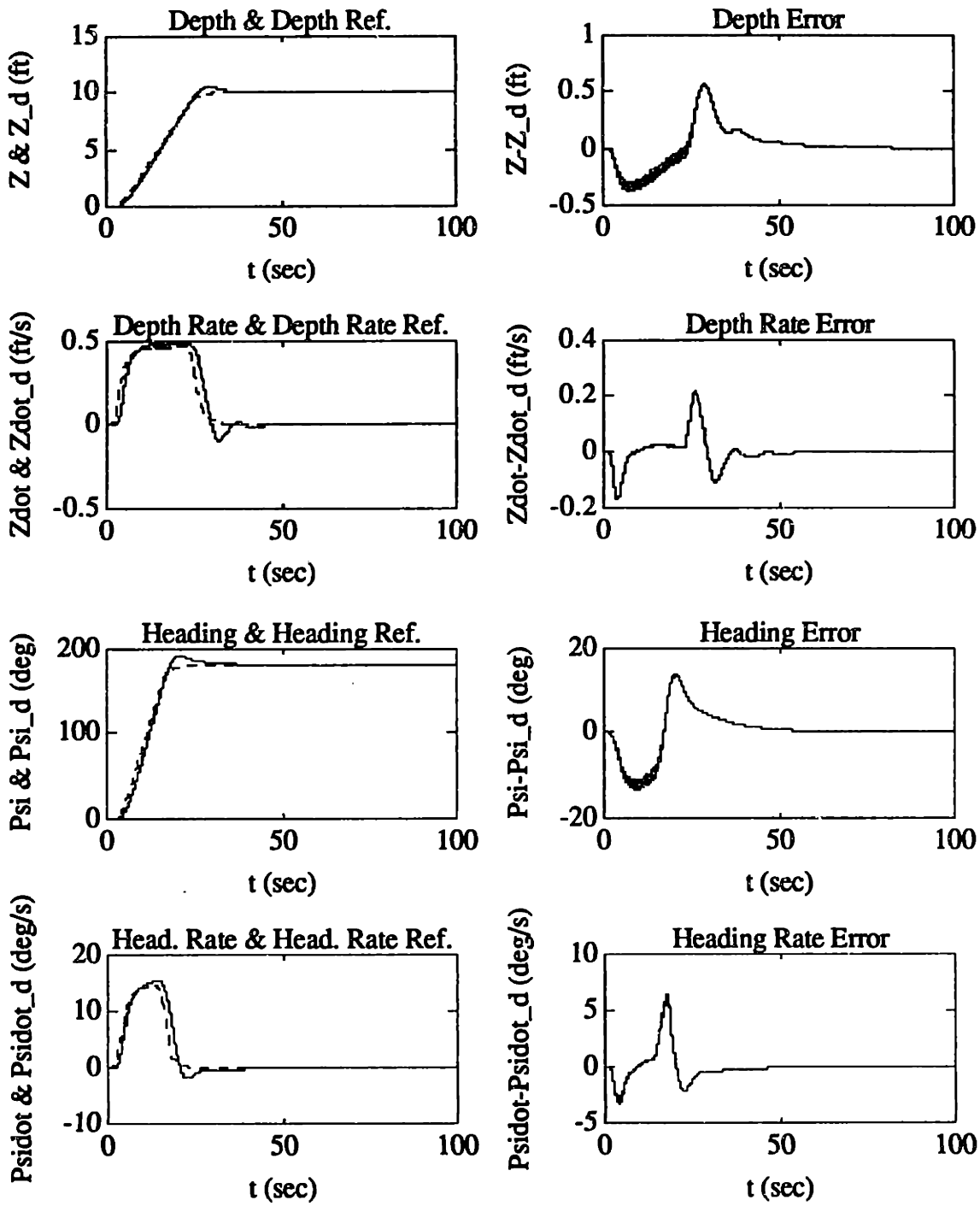

Figure 8.10: "Hovering" Simulation Performance of the Initial Sliding-Mode Controller

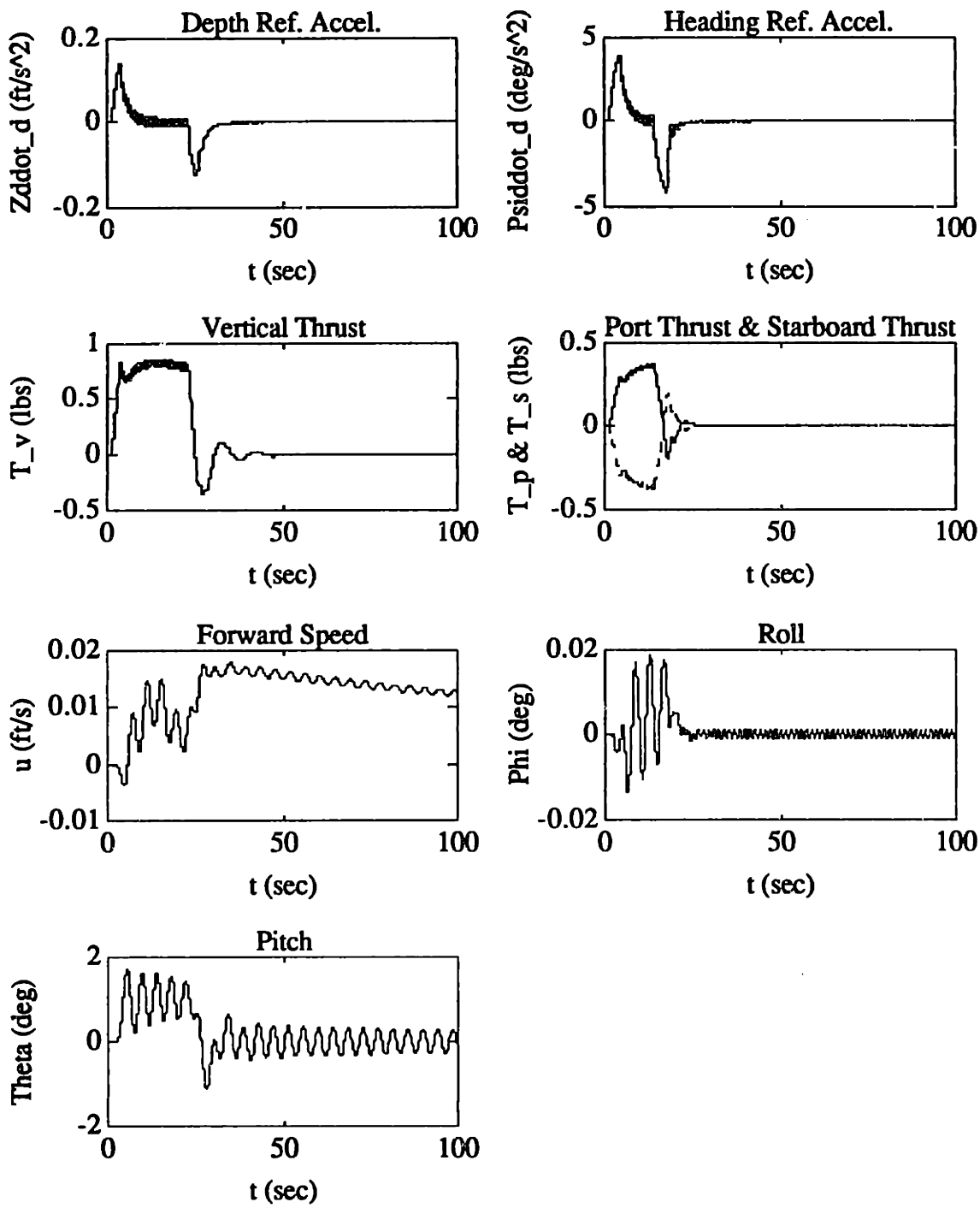

Figure 8.10: "Hovering" Simulation Performance of the Initial Sliding-Mode Controller (continued)

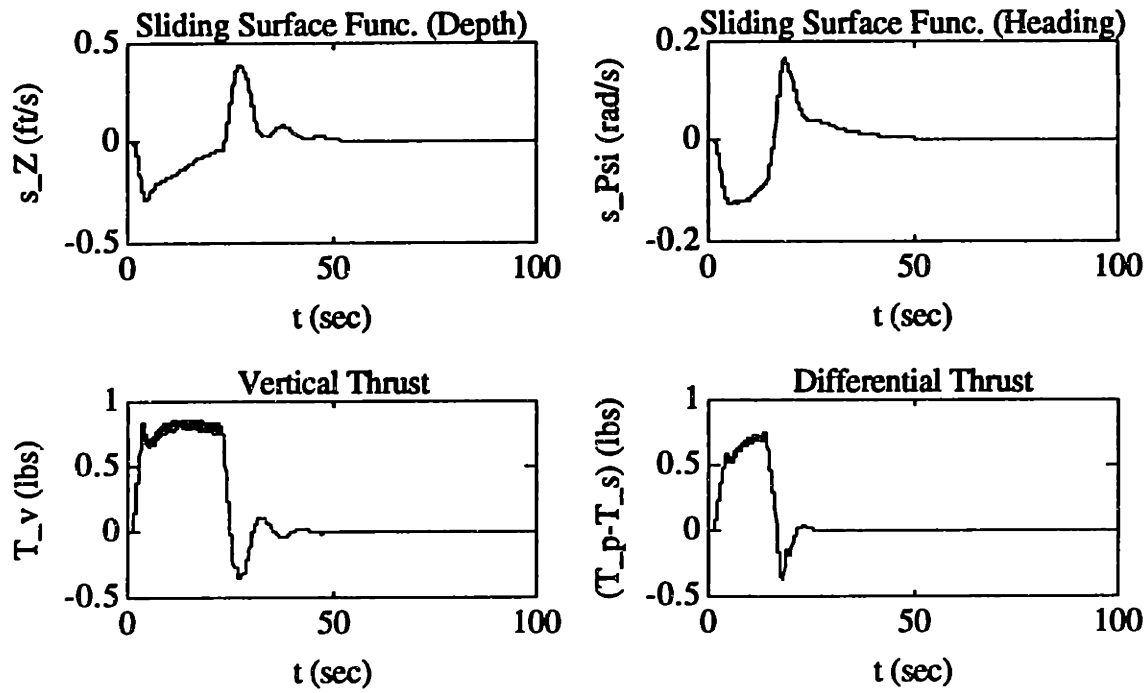

Figure 8.10: "Hovering" Simulation Performance of the
Initial Sliding-Mode Controller (continued)

From the results of Figure 8.10 and Table 8.7, the "hovering" performance of the initial Sliding-Mode controller was virtually identical to its nominal design-model performance (presented in Section 6.3). This indicates that the reduced-order nonlinear model provides a relatively accurate representation of the dynamic behavior of the full-order AUV model at low axial velocities.

The nominal steady-state error performance of the Sliding-Mode controller met the nonlinear performance goals, as well as did the depth overshoot. The heading overshoot was slightly more than specified, but still acceptable. The depth response-time and the heading response-time were slower than specified, but were judged to be acceptable. Roll and pitch were stabilized by this controller, even though their responses were somewhat oscillatory. Note that there is no oscillation in depth due to the oscillatory pitch response, as compared to the H_∞/μ-Synthesis controllers. From the plots of the sliding-surface functions for both depth and heading, the controller remains well within the respective boundary layers.

Full-Ahead" Simulation Performance

The next simulated test of the initial AUV Sliding-Mode controller was done with a commanded forward thrust of 1.0 lb., nominal model parameters, and zero sensor noise in order to test the robustness to significant forward axial speeds. As with the "hovering" case, the commanded heading trajectory was from 0.0 to 180.0 degrees, and the commanded depth trajectory was from 0.0 to 10.0 ft. The results of this test are shown in Figure 8.ii and Table 8.8.

Table 8.8: "Full-Ahead" Performance Test of the Initial AUV Sliding-Mode Controller (with Performance Specifications from Chapters 6 and 7 in Parentheses)

Steady-State Depth Error	0.04 feet ($\pm$1.0 feet)
Steady-State Heading Error	140.22 degrees ($\pm$5.0 degrees)
Depth Overshoot	Over-damped response (1.0 feet)
Heading Overshoot	169.53 degrees (10.0 degrees)
Depth Response	35.41 seconds (10.0 seconds)
Heading Response	13.59 seconds (5.0 seconds)

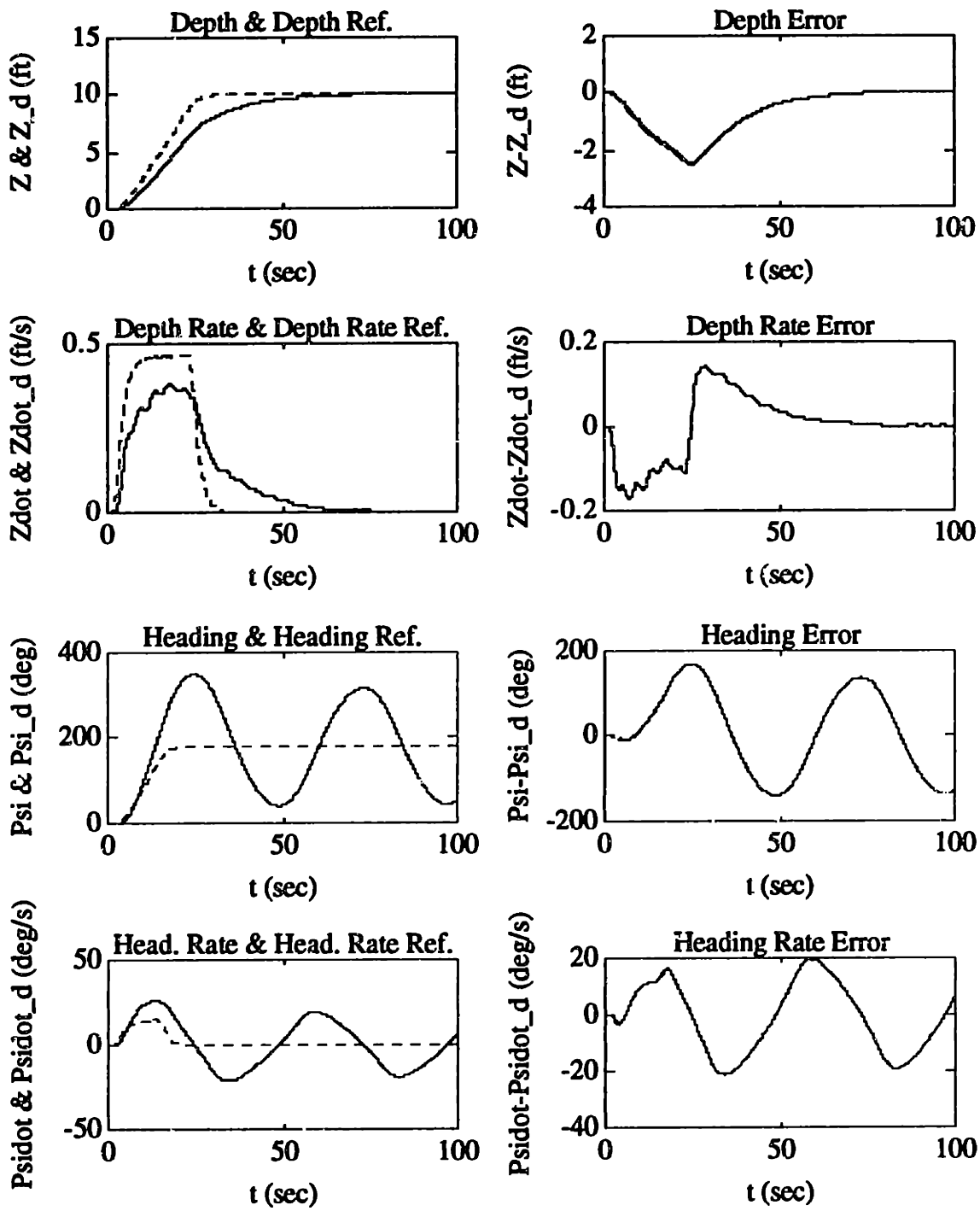

Figure 8.11: "Full-Ahead" Simulation Performance of the Initial Sliding-Mode Controller

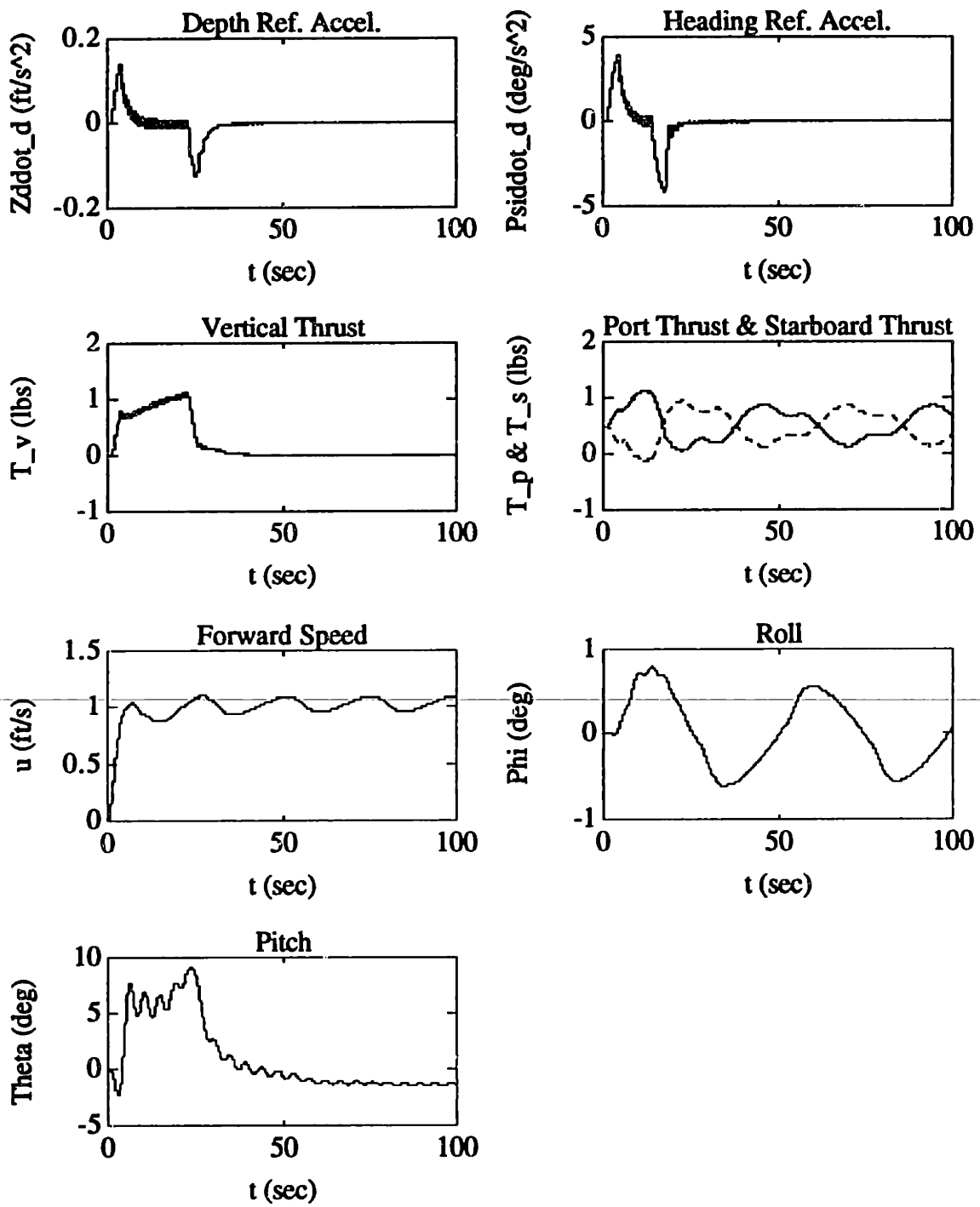

Figure 8.11: "Full-Ahead" Simulation Performance of the Initial Sliding-Mode Controller (continued)

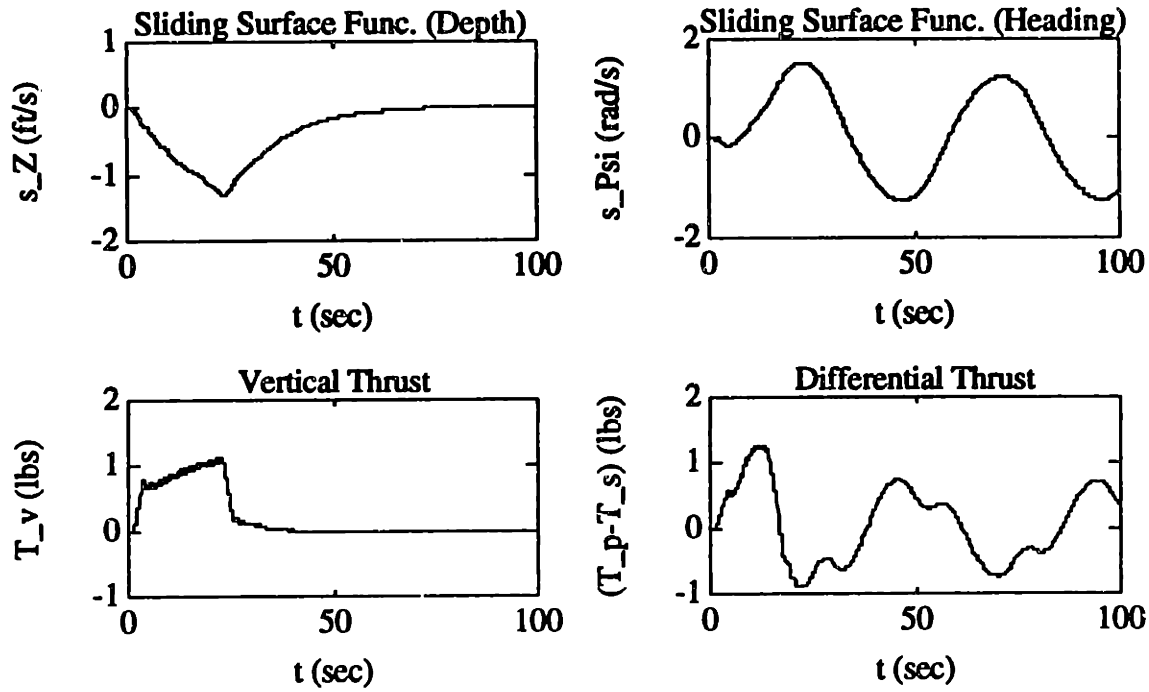

Figure 8.11: "Full-Ahead" Simulation Performance of the Initial Sliding-Mode Controller (continued)

From the results of Figure 8.11 and Table 8.9, the performance of the initial Sliding-Mode controller has degraded significantly to an unacceptable level. For the "full-ahead" case, the heading performance had an overshoot and a steady-state oscillation an order of magnitude higher than the nonlinear performance specifications. The most obvious cause of this undesirable heading performance is the destabilizing Munk moment alluded to earlier in Chapter 4. One implication of the heading oscillation (and the relatively low values for the differential thrust) is that the Sliding-Mode controller does not have enough control authority to counteract this moment.

The depth performance for this case is significantly more sluggish than for the "hovering" case, with an almost 170% increase in the response time. Interestingly, the depth response is now overdamped (i.e., zero overshoot) for this case, as compared to the H∞/μ-Synthesis controllers (which had a *larger* overshoot for the "full-ahead" case than for the "hovering" case). One possible implication of this over-damped response (and the

relatively "fast thrust response) is that the Sliding-Mode controller has a higher tolerance of the effects of the nonlinear hydrodynamic drag.

In spite of its poor performance, the initial Sliding-Mode controller still remains inside the Sliding-surface boundary layers. This implies that one possible solution for improving the overall performance of the Sliding-Mode controller would be to decrease the width of these boundary-layers (so long as they are wide enough not to excite other unmodeled dynamics of the AUV).

8.3.2 Second Sliding-Mode Controller Performance

From the discussion of Section 6.2.4, the following value was calculated for the Sliding-Surface "boundary-layer" matrix, Φ, of the initial Sliding-Mode control design.

$$\Phi = \begin{bmatrix} 11.2 & 0 \\ 0 & 11.1 \end{bmatrix} \tag{8.9}$$

However, recall from the previous section that this initial design exhibited unacceptably poor performance for the "full-ahead" case, even though it stayed well within the boundary-layers given by (8.9). Therefore, an attempt was made to improve the Sliding-Mode performance by decreasing the width of the boundary layers (until oscillations due to other unmodeled AUV dynamics occurred). From this procedure, the following value was selected for the "boundary-layer" matrix of the second Sliding-Mode design.

$$\Phi = \begin{bmatrix} 4.48 & 0 \\ 0 & 1.48 \end{bmatrix} \tag{8.10}$$

From Chapter 6, the guaranteed output tracking precision is then given by

$$\left|\tilde{x}\right| = \left|x - \hat{x}_d\right| \leq \begin{bmatrix} 8.96 \\ 2.96 \end{bmatrix} \tag{8.11}$$

provided that the modeling-error and disturbance bounds are not exceeded. As with the initial Sliding-Mode design, this bound is so conservative as to be essentially useless (with a depth tracking-error bound of *8.96 feet* and a heading tracking-error bound of *2.96 radians* (approximately *169.6 degrees*)). However, this bound is still less conservative than the corresponding bound given in Section 6.2.4. for the initial Sliding-Mode controller.

"Hovering" Simulation Performance

The first simulated test of the second Sliding-Mode controller was done with a commanded forward thrust of 0.0 lb., nominal model parameters, and zero sensor noise in order to test its approximate nominal performance. The commanded heading trajectory was from 0.0 to 180.0 degrees, and the commanded depth trajectory was from 0.0 to 10.0 ft. The results of this test are shown in Figure 8.12 and Table 8.9.

Table 8.9: "Hovering" Performance Test of the Second AUV Sliding-Mode Controller (with Performance Specifications from Chapters 6 and 7 in Parentheses)

Steady-State Depth Error	0.01 feet ($\pm$1.0 feet)
Steady-State Heading Error	$\pm$0.23 degrees ($\pm$5.0 degrees)
Depth Overshoot	0.34 feet (1.0 feet)
Heading Overshoot	7.42 degrees (10.0 degrees)
Depth Response	1.88 seconds (10.0 seconds)
Heading Response	0.64 seconds (5.0 seconds)

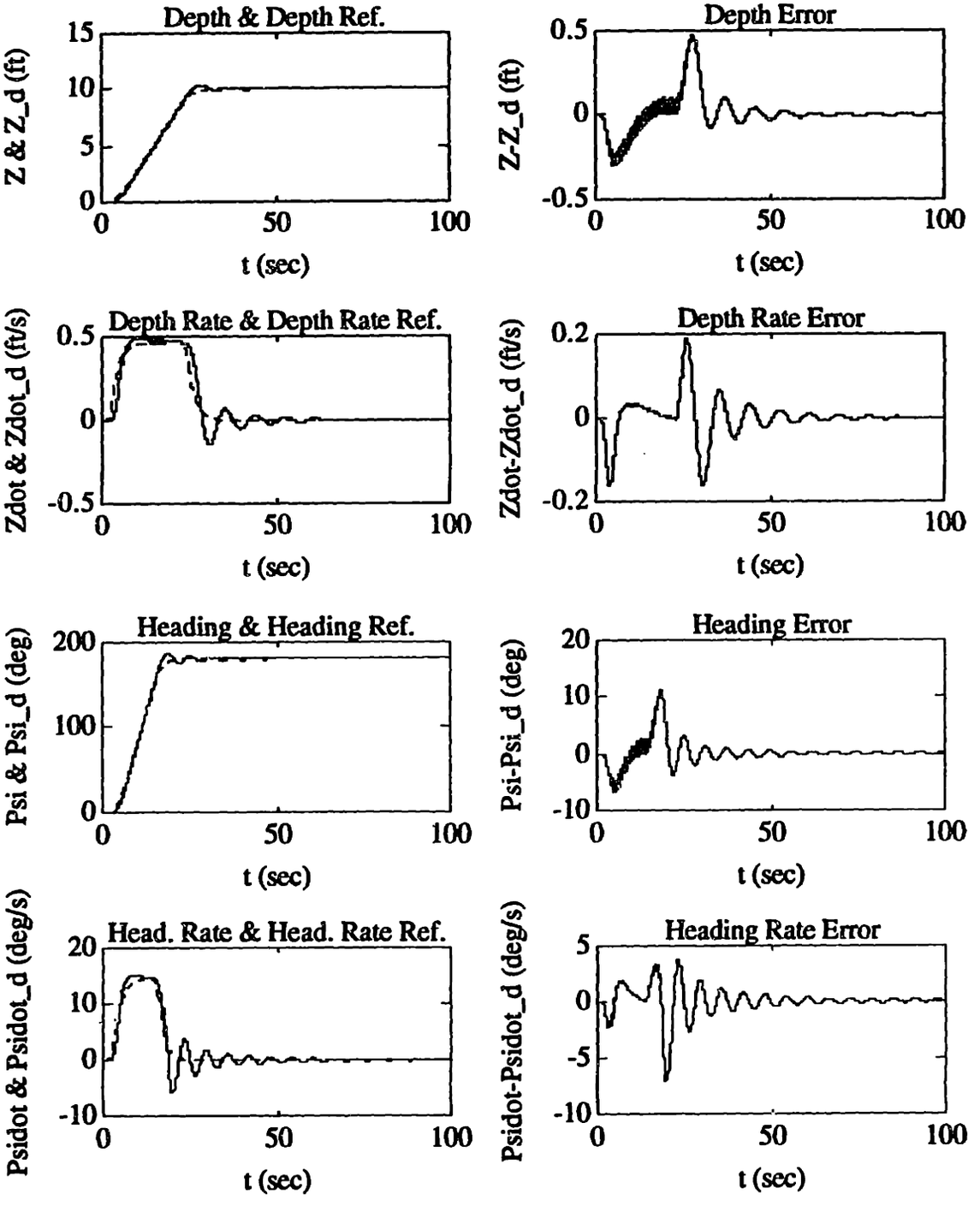

Figure 8.12: "Hovering" Simulation Performance of the Second Sliding-Mode Controller

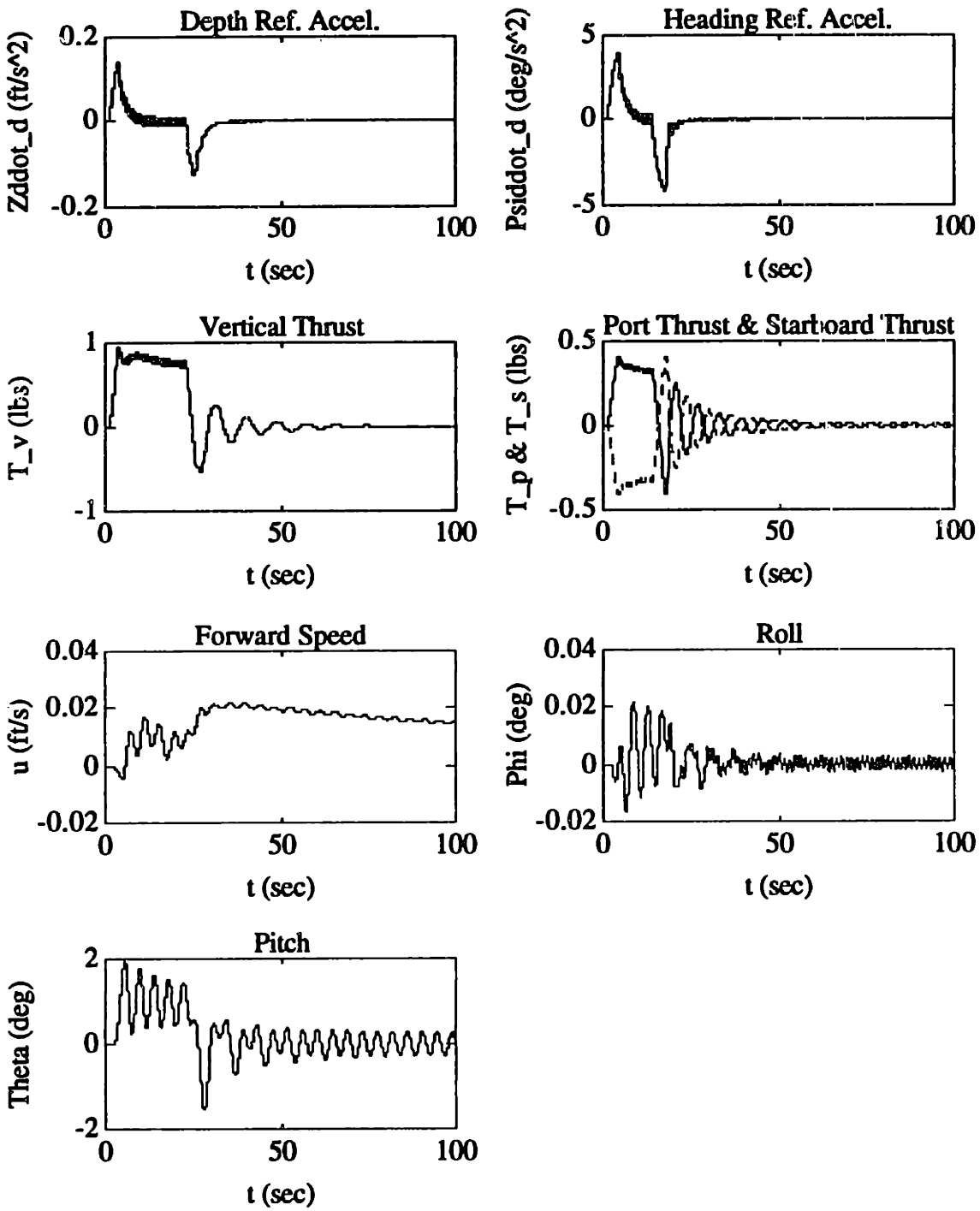

Figure 8.12: "Hovering" Simulation Performance of the Second Sliding-Mode Controller (continued)

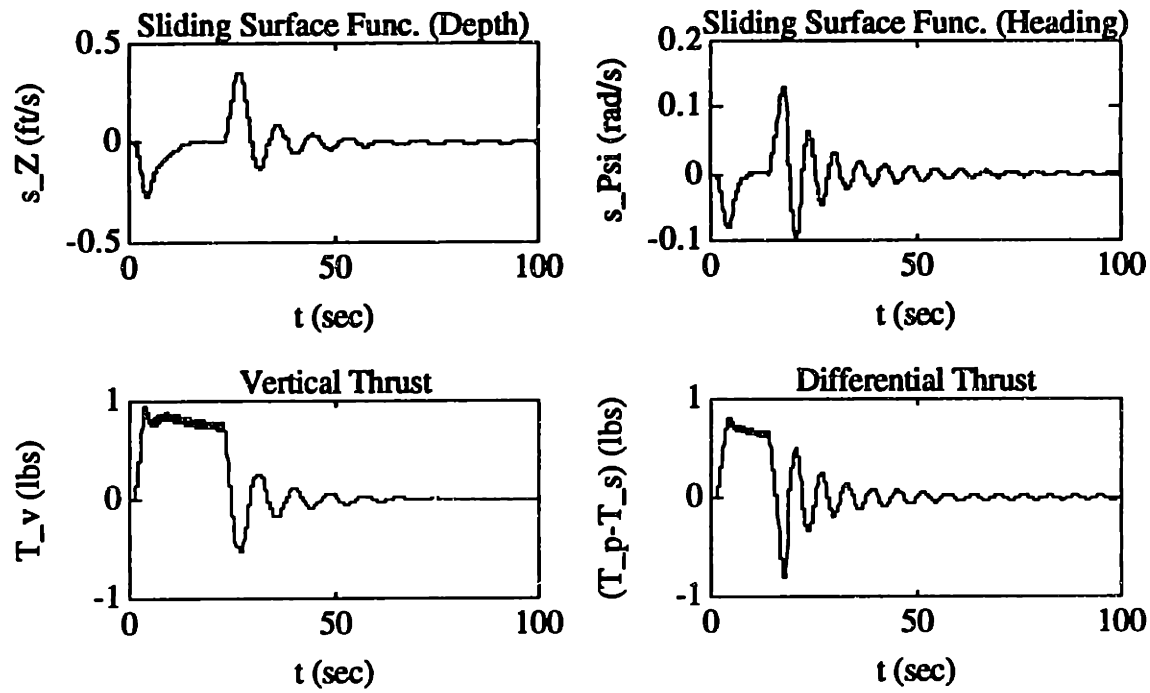

Figure 8.12: "Hovering" Simulation Performance of the Second Sliding-Mode Controller (continued)

The approximately nominal "hovering" performance of the Sliding-Mode controller appears to have been significantly improved by the decrease in boundary-layer width. The heading overshoot was improved to the point of meeting the nonlinear design specification. Similarly, the depth and heading response times were also improved to the point of meeting their respective specifications. The oscillatory roll and pitch responses were nearly unchanged from the initial design case. Note that there appears to be a slight steady-state oscillation in both depth and heading, as compared to the initial Sliding-Mode controller. This implies that any further decrease in the boundary-layer width could raise these steady-state oscillations to unacceptably high levels. From the plots of the sliding-surface functions for both depth and heading, the controller still remains well within the respective boundary layers.

"Full-Ahead" Simulation Performance

The next simulated test of the second AUV Sliding-Mode controller was done with a commanded forward thrust of 1.0 lb., nominal model parameters, and zero sensor noise. As with the initial Sliding-Mode design, this was done in order to test the performance-robustness to significant forward axial speeds. The commanded heading trajectory was from 0.0 to 180.0 degrees, and the commanded depth trajectory was from 0.0 to 10.0 ft. The results of this test are shown in Figure 8.13 and Table 8.10.

Table 8.10: "Full-Ahead" Performance Test of the Second AUV Sliding-Mode Controller (with Performance Specifications from Chapters 6 and 7 in Parentheses)

Steady-State Depth Error	0.03 feet ($\pm$1.0 feet)
Steady-State Heading Error	$\pm$0.22 degrees ($\pm$5.0 degrees)
Depth Overshoot	Over-damped response (1.0 feet)
Heading Overshoot	31.29 degrees (10.0 degrees)
Depth Response	13.59 seconds (10.0 seconds)
Heading Response	10.12 seconds (5.0 seconds)

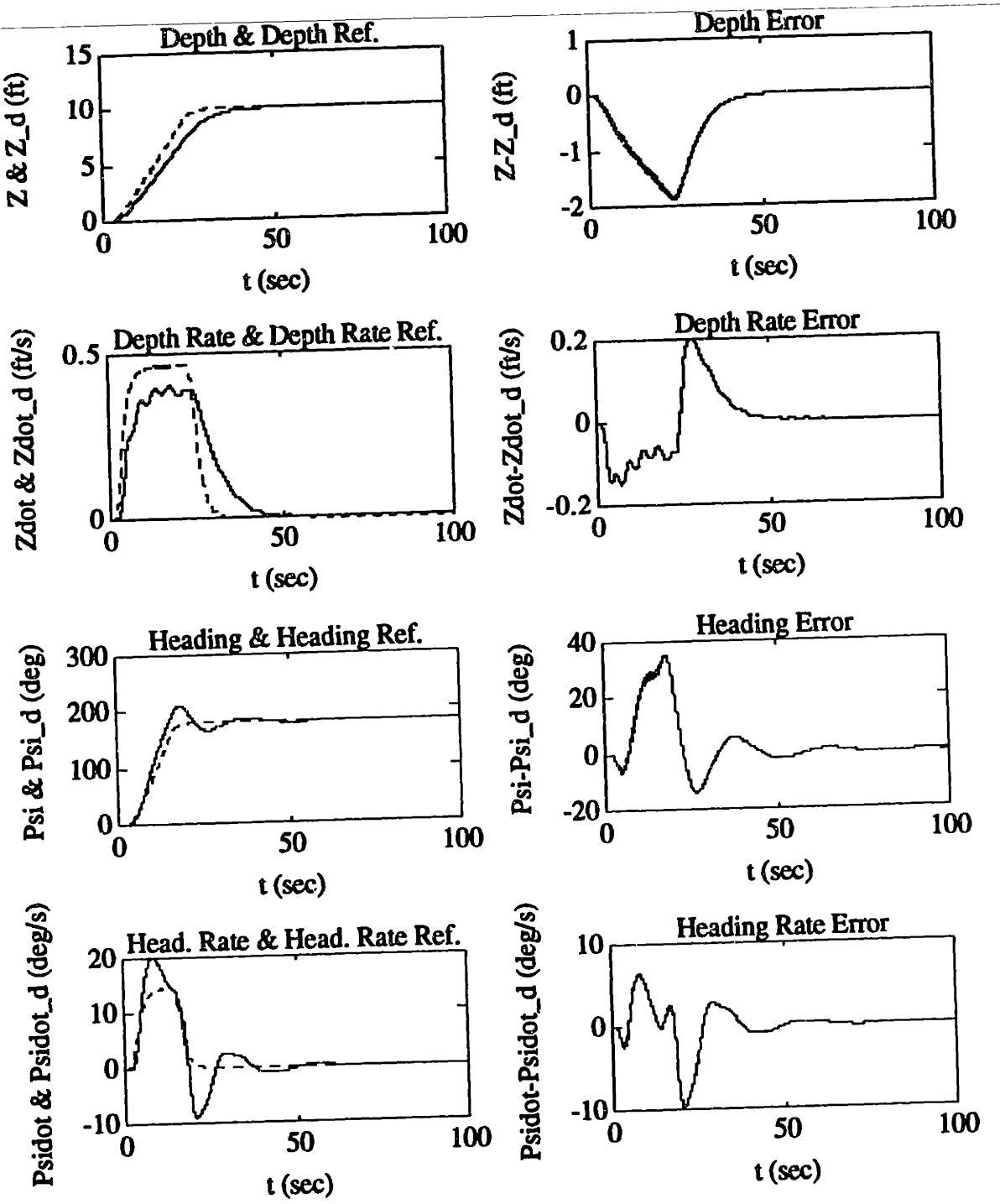

Figure 8.13: "Full-Ahead" Simulation Performance of the Second Sliding-Mode Controller

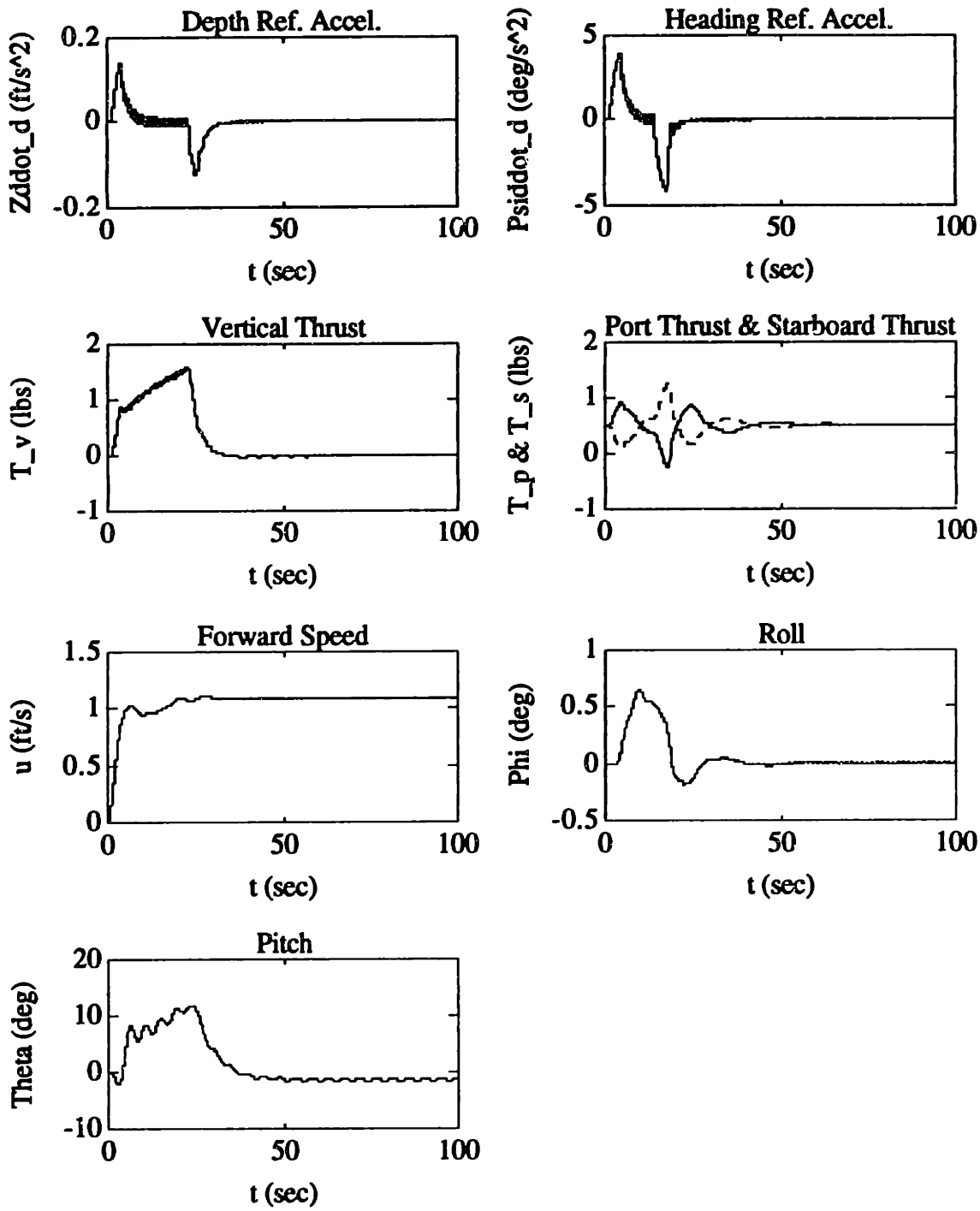

Figure 8.13: "Full-Ahead" Simulation Performance of the Second Sliding-Mode Controller (continued)

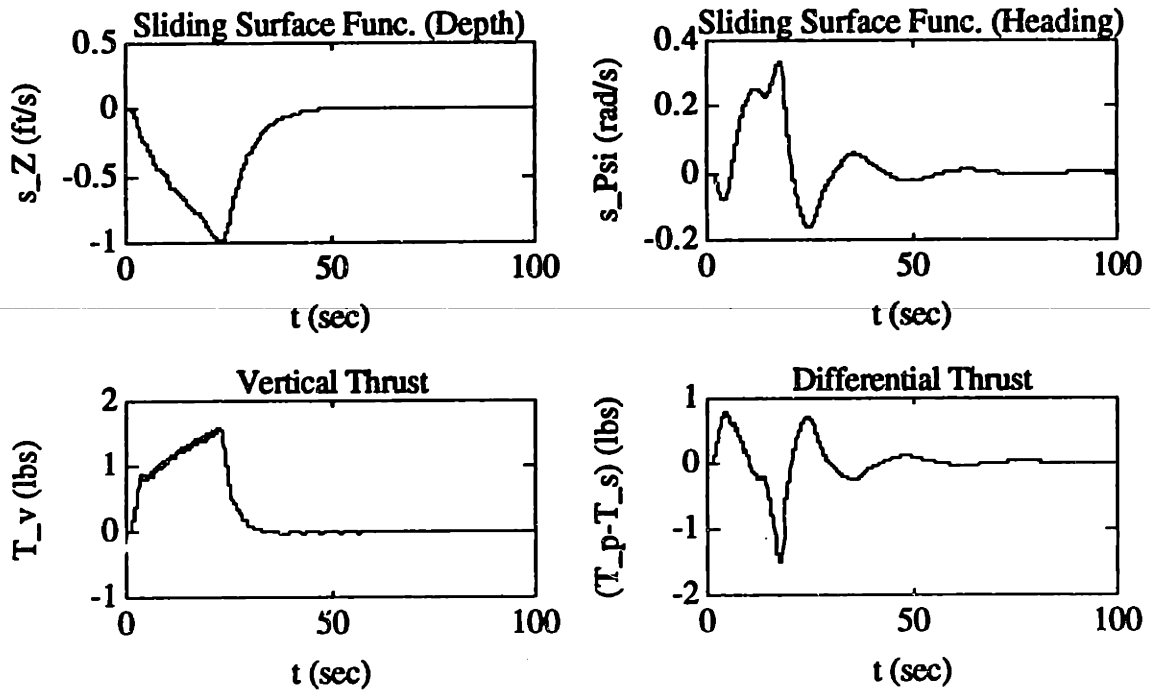

Figure 8.13: "Full-Ahead" Simulation Performance of the Second Sliding-Mode Controller (continued)

The "full-ahead" performance of the Sliding-Mode controller appears to have been significantly improved as well by the decrease in boundary-layer width. The heading performance, especially, appears to have been radically improved. The heading overshoot was greater than the nonlinear design specification, but still acceptable (since any attempt to improve this overshoot would probably increase the steady-state heading oscillation for the "hovering" case). Similarly, the depth response-time and the heading response time were also improved to acceptable levels. From the plots of the sliding-surface functions for both depth and heading, the controller remains well within the respective boundary layers.

"Full-Reverse" Simulation Performance

The next simulated test of the second AUV Sliding-Mode controller was done with a commanded forward thrust of -1.0 lb., nominal model parameters, and zero sensor noise. This was done in order to test the performance-robustness to significant negative axial speeds. The commanded heading trajectory was from 0.0 to 180.0 degrees, and the commanded depth trajectory was from 0.0 to 10.0 ft. The results of this test are shown in Figure 8.14 and Table 8.11.

Table 8.11: "Full-Reverse" Performance Test of the Second AUV Sliding-Mode Controller (with Performance Specifications from Chapters 6 and 7 in Parentheses)

Steady-State Depth Error	0.02 feet ($\pm$1.0 feet)
Steady-State Heading Error	$\pm$0.76 degrees ($\pm$5.0 degrees)
Depth Overshoot	Over-damped response (1.0 feet)
Heading Overshoot	35.85 degrees (10.0 degrees)
Depth Response	10.18 seconds (10.0 seconds)
Heading Response	9.01 seconds (5.0 seconds)

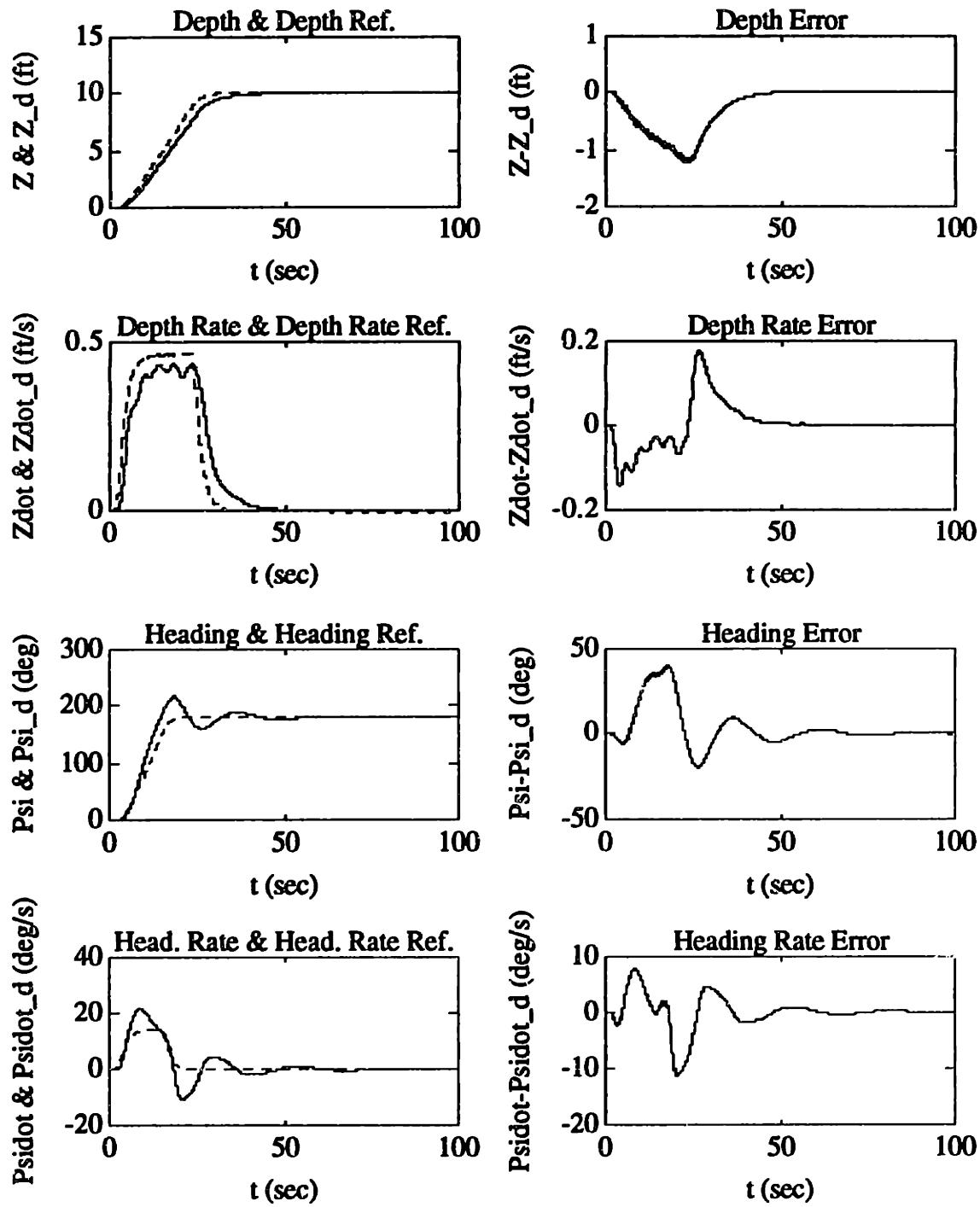

Figure 8.14: "Full-Reverse" Simulation Performance of the Second Sliding-Mode Controller

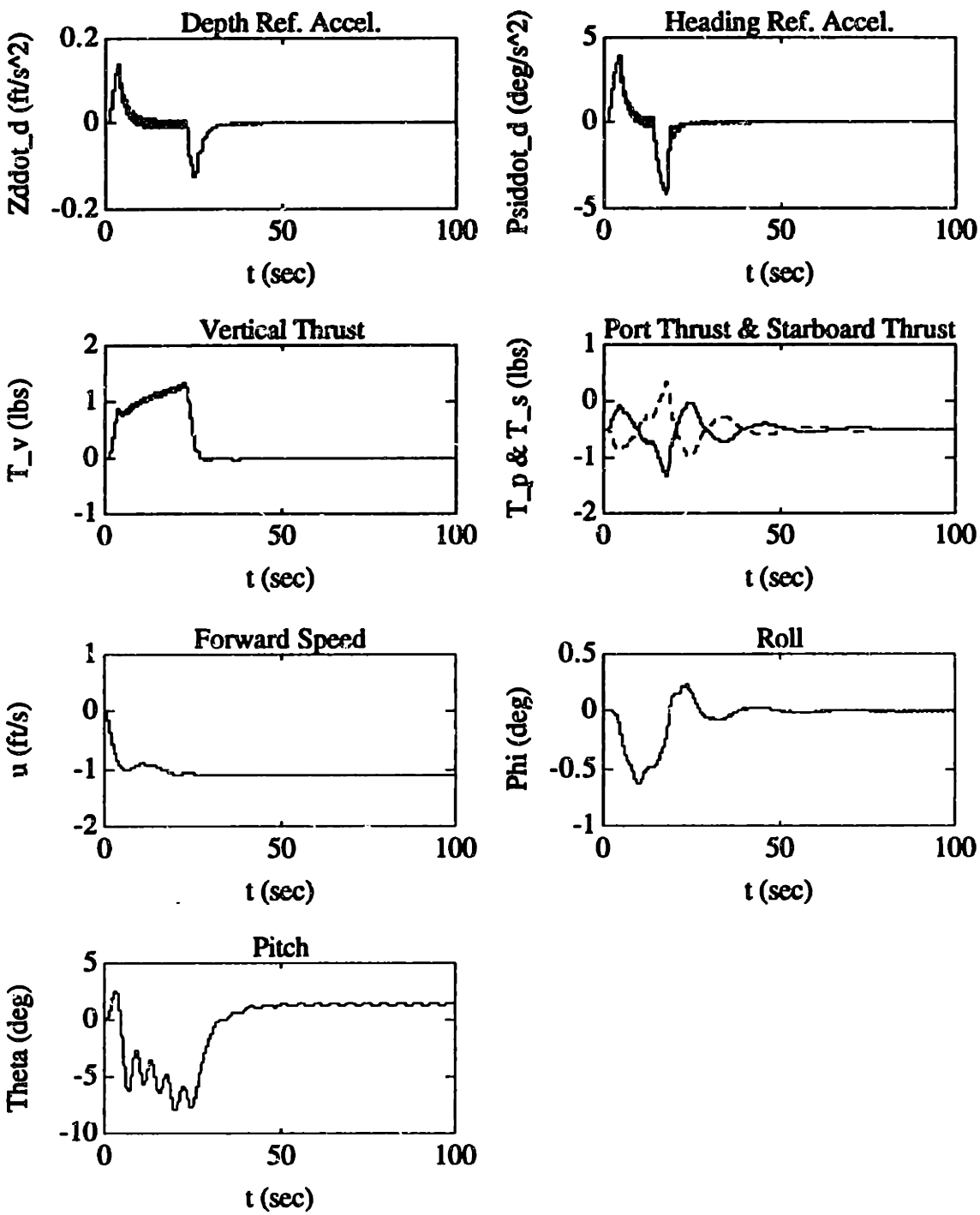

Figure 8.14: "Full-Reverse" Simulation Performance of the Second Sliding-Mode Controller (continued)

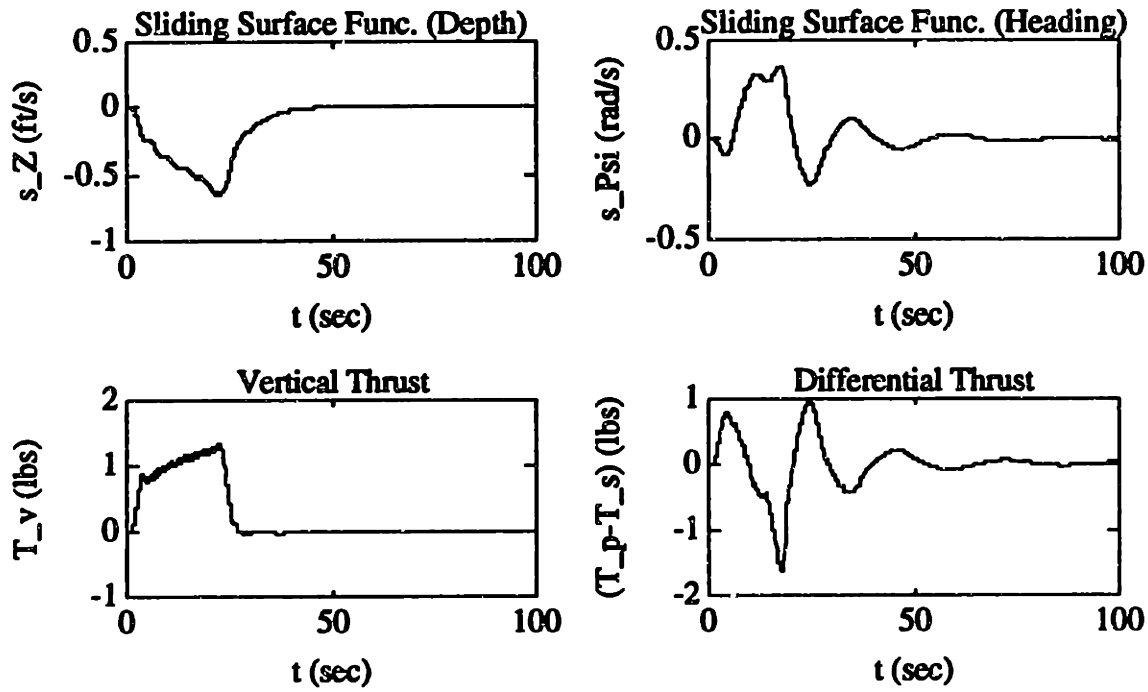

Figure 8.14: "Full-Reverse" Simulation Performance of the Second Sliding-Mode Controller (continued)

The "full-reverse" performance of the second Sliding-Mode controller is very similar to its performance for the "full-ahead" case. The heading overshoot, the depth response time, and the heading response time were greater than the nonlinear design specification, but still acceptable. Again, from the plots of the sliding-surface functions for both depth and heading, the controller remains well within the respective boundary layers.

Compared to the H_∞/μ-Synthesis controllers, the second Sliding-Mode controller appears to have better overall noise-free depth-performance characteristics, possibly since it can accommodate for the effects of the nonlinear hydrodynamic drag forces. However, this controller has worse heading performance, especially at significant axial speeds, since it cannot directly accommodate for the effects of the destabilizing Munk moment uncertainty.

"Noisy Hovering" Simulation Performance

The next simulated test of the second Sliding-Mode controller was done using nominal model parameters, at the "nominal" zero commanded forward thrust. The Gaussian sensor noise inputs were set to the values found Section 4.6 (in order to test the noise performance of this controller). The commanded heading trajectory was again from 0.0 to 180.0 degrees, and the commanded depth trajectory was from 0.0 to 10.0 ft. The results of this test are shown in Figure 8.15.

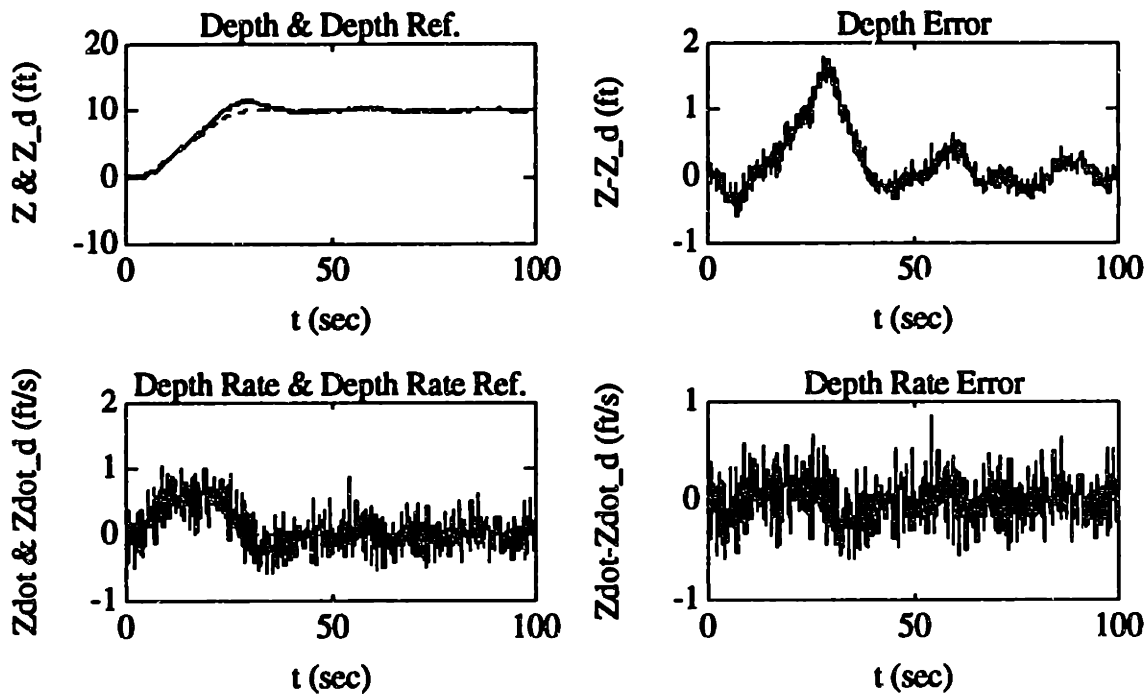

Figure 8.15: "Noisy Hovering" Simulation Performance of the Second Sliding-Mode Controller

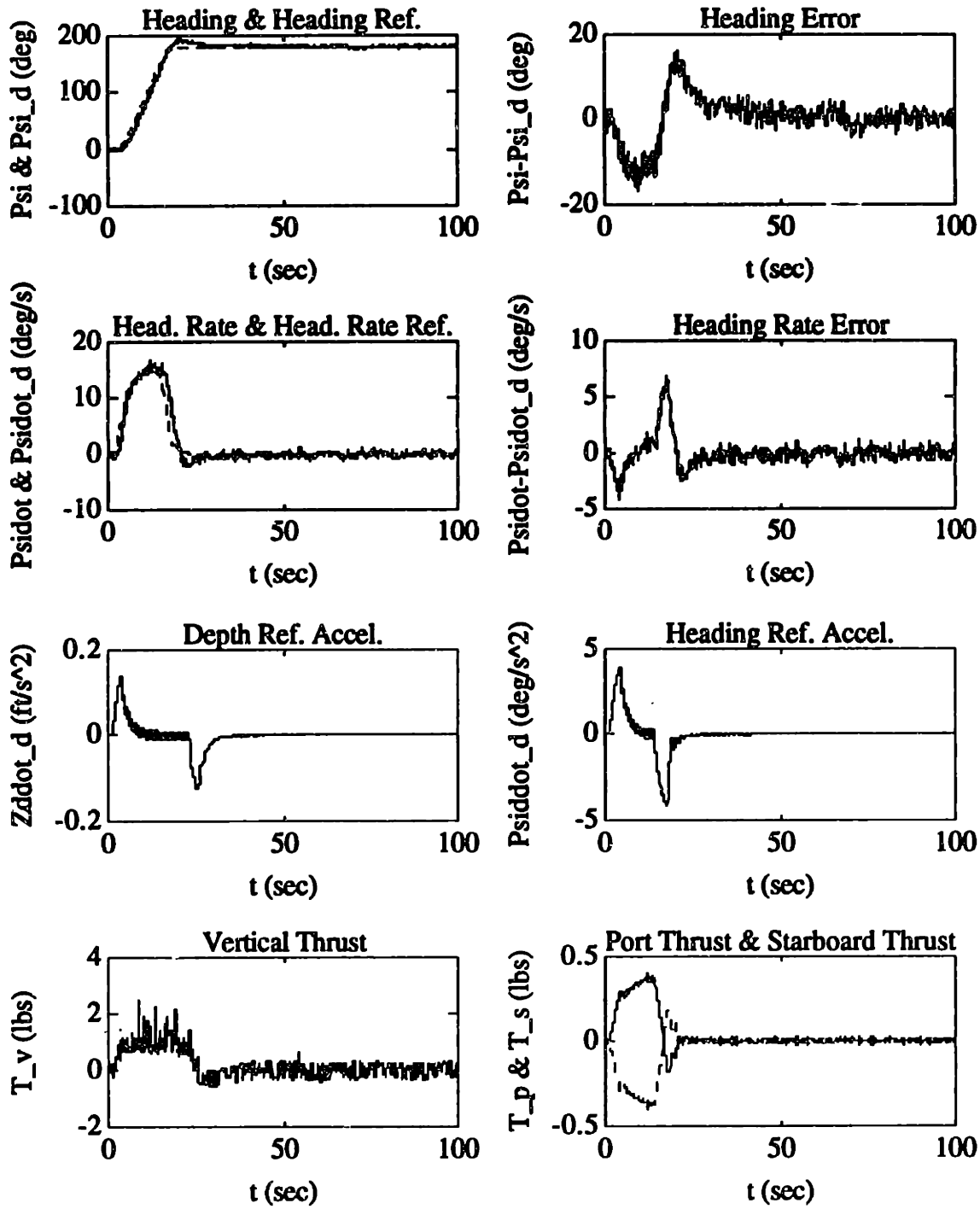

Figure 8.15: "Noisy Hovering" Simulation Performance of the Second Sliding-Mode Controller (continued)

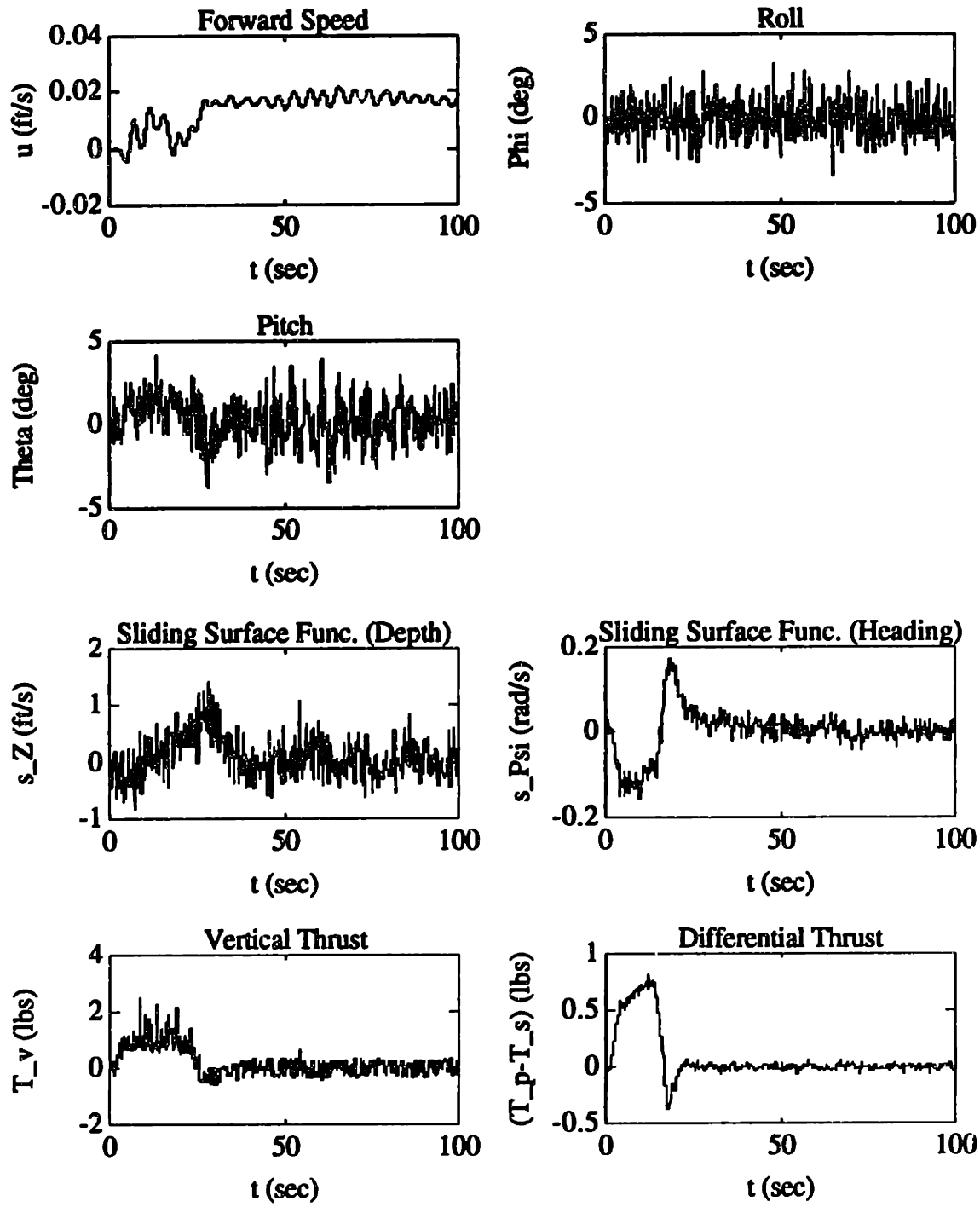

Figure 8.15: "Noisy Hovering" Simulation Performance of the Second Sliding-Mode Controller (continued)

From the results of Figure 8.15, it appears that the second Sliding-Mode controller is reasonably robust to the additive sensor noise (at least for the "hovering" case). The performance characteristics of this control design are essentially unchanged from the noise-free case (with the exception of a larger depth overshoot). The steady-state errors in both the depth and the heading are somewhat larger and more oscillatory, but still meets the design specifications of ±1.0 feet and ±5.0 degrees for depth and heading, respectively. The commanded thrust input signals to the AUV thrusters are also significantly more oscillatory for this case. Compared to the H_∞/μ-Synthesis controllers, however, the thrust commands are somewhat less oscillatory (due to the Sliding-Mode controller having lower gain characteristics). For the actual vehicle, this implies that the slightly better noise characteristics of the Sliding-Mode would probably cause less average power drain on the AUV thruster power supply.

8.3 SLIDING-MODE AUGMENTED CONTROLLER PERFORMANCE

"Hovering" Simulation Performance

The first simulated test of the Sliding-Mode Augmented controller was done with a commanded forward thrust of 0.0 lb., nominal model parameters, and zero sensor noise in order to test (as close as possible) the nominal performance of this controller. The commanded heading trajectory was from 0.0 to 180.0 degrees, and the commanded depth trajectory was from 0.0 to 10.0 ft. The results of this test are shown in Figure 8.16 and Table 8.12. As with the H_∞/μ-Synthesis and Sliding-Mode performance results of the previous sections, the response time is defined as the time period from where the reference trajectory reaches its final value (within 0.1 feet for depth and within 0.5 degrees for heading) to the where the vehicle first attains this value (within 0.1 feet for depth and within 0.5 degrees for heading). The maximum overshoot is defined as the difference between the maximum value reached by the vehicle and the maximum value reached by the reference trajectory. The results of Table 8.12 are shown together with the (nonlinear) performance specifications from Chapter 6 and Chapter 7.

Table 8.12: "Hovering" Performance Test of the
AUV Sliding-Mode Augmented Controller
(with Performance Specifications from Chapters 6 and 7 in Parentheses)

Steady-State Depth Error	0.01 feet (±1.0 feet)
Steady-State Heading Error	0.0 degrees (±5.0 degrees)
Depth Overshoot	0.08 feet (1.0 feet)
Heading Overshoot	1.25 degrees (10.0 degrees)
Depth Response	0.64 seconds (10.0 seconds)
Heading Response	2.0 seconds (5.0 seconds)

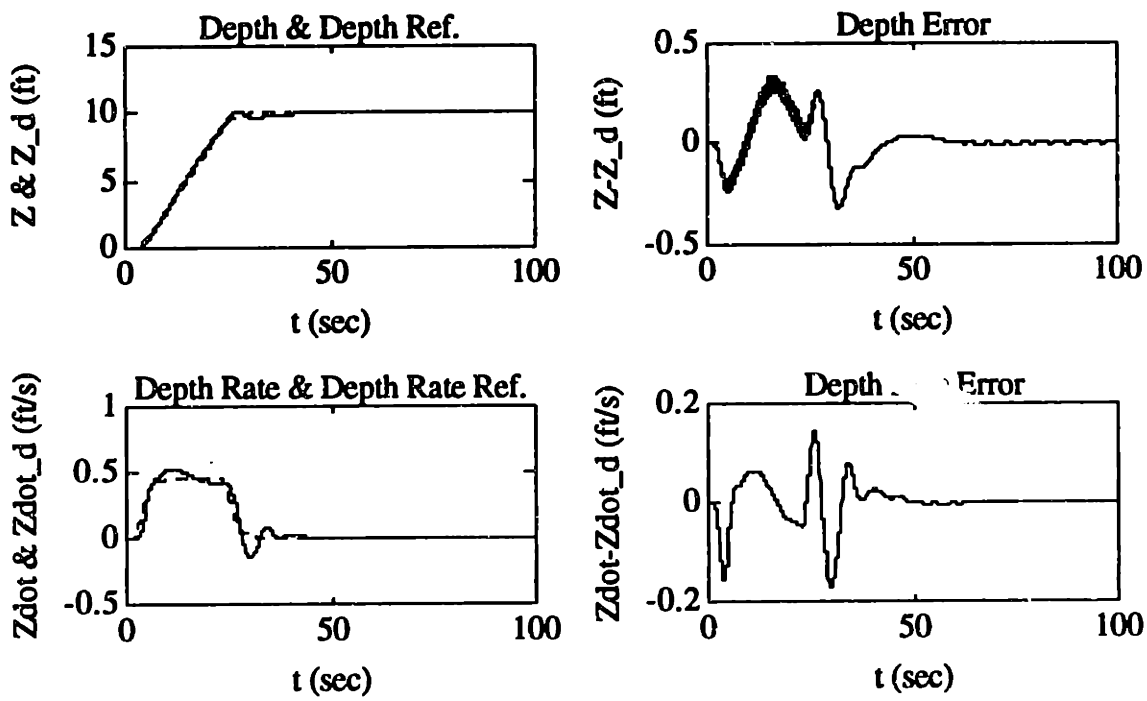

Figure 8.16: "Hovering" Simulation Performance of the
Sliding-Mode Augmented Controller

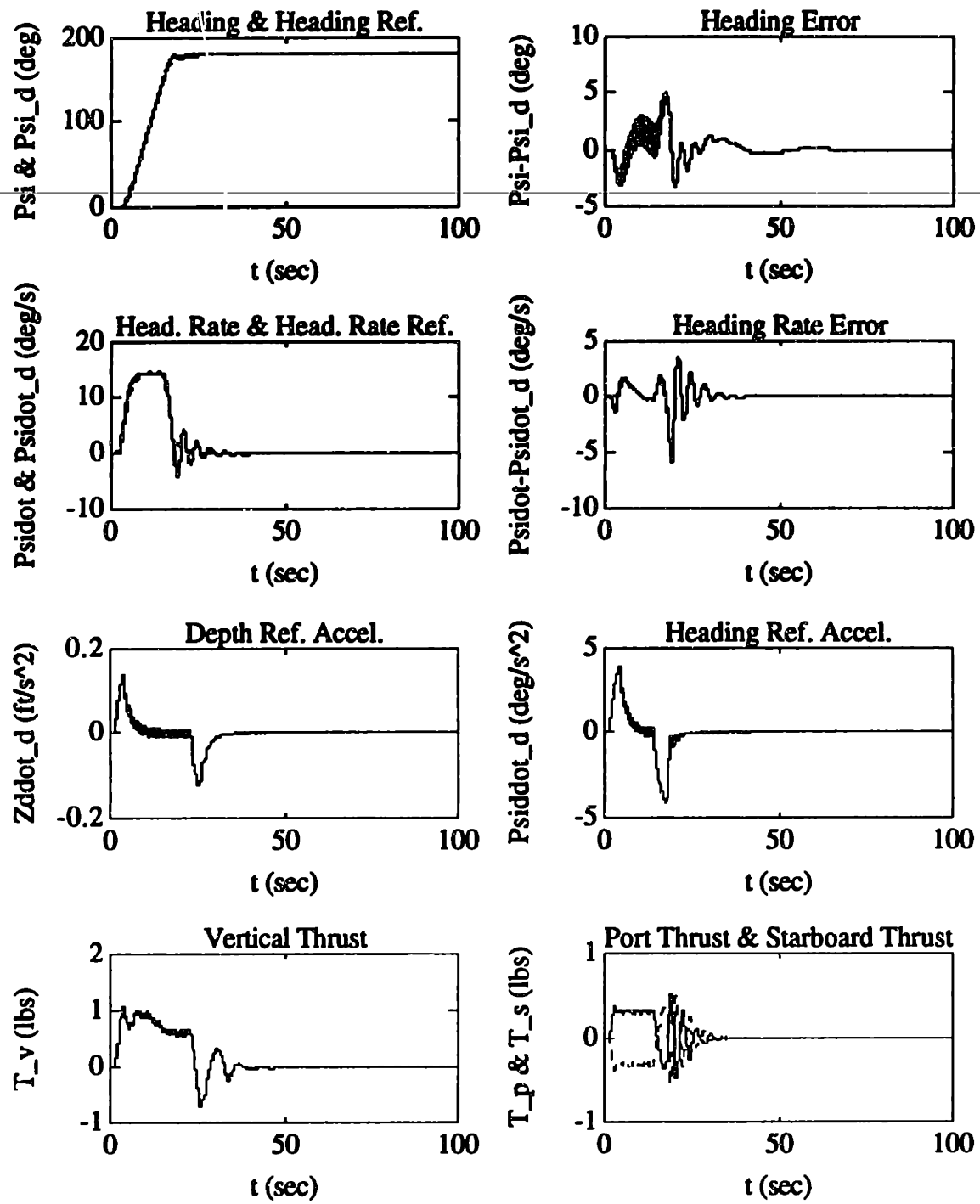

Figure 8.16: "Hovering" Simulation Performance of the Sliding-Mode Augmented Controller (continued)

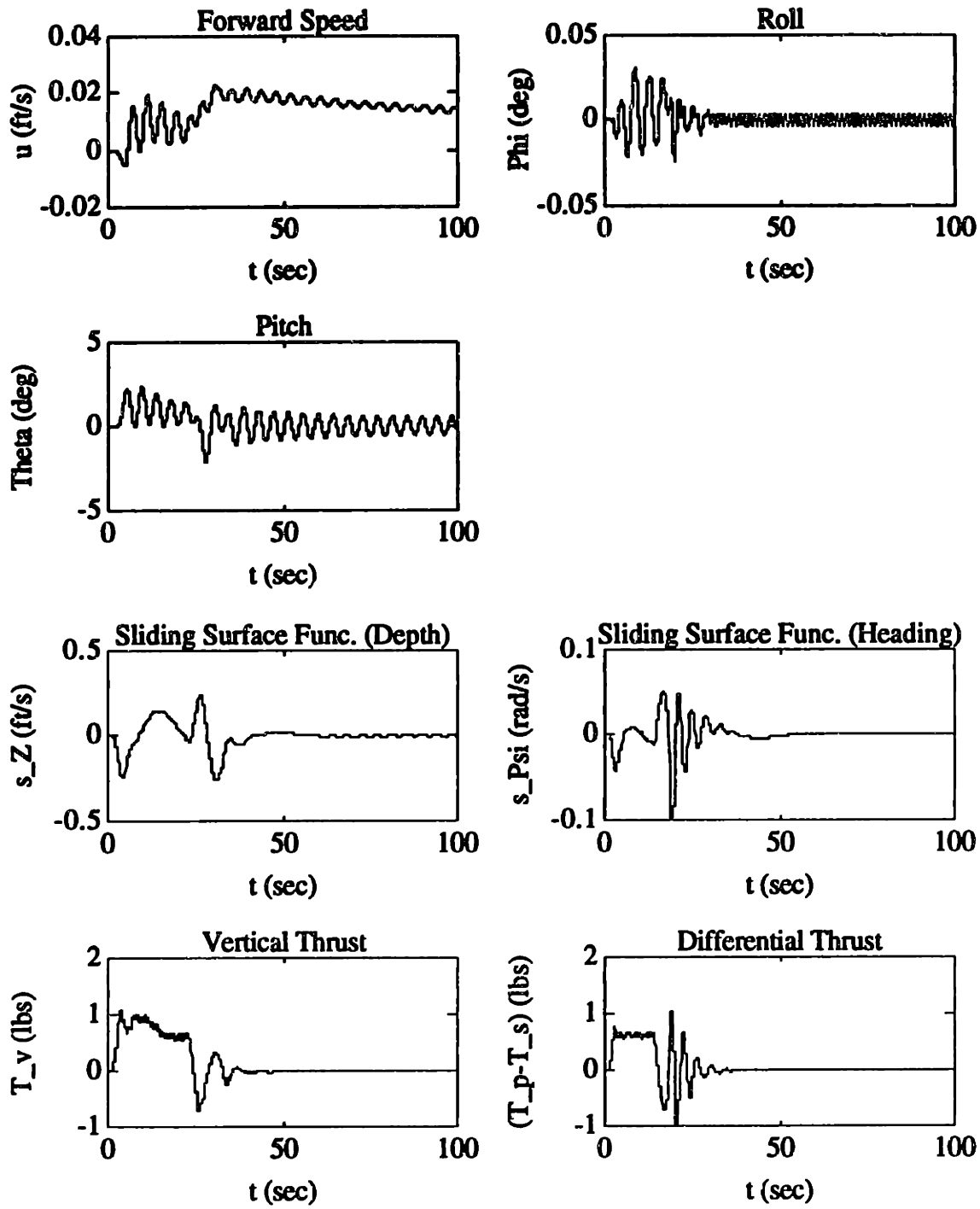

Figure 8.16: "Hovering" Simulation Performance of the Sliding-Mode Augmented Controller (continued)

From the results of Figure 8.16 and Table 8.12, The "hovering" performance of the Sliding-Mode controller met all of the nonlinear performance goals (as compared the H∞/μ-Synthesis controllers and the second Sliding-Mode controller). Roll and pitch were stabilized by this controller, even though their responses were somewhat oscillatory. Note that there is less oscillation in depth due to the oscillatory pitch response, as compared to the H_∞/μ-Synthesis controllers. From the plots of the sliding-surface functions for both depth and heading, the controller remains well within the outer boundary layer. The steady-state values of the sliding-surface functions of the Sliding-Mode Augmented controller remain inside the inner boundary-layer as well (implying a complete reliance in steady-state upon the reduced-order H_∞ controller).

"Full-Ahead" Simulation Performance

The next simulated test of the AUV Sliding-Mode Augmented controller was done with a commanded forward thrust of 1.0 lb., nominal model parameters, and zero sensor noise. As with the previous AUV control designs, this was done in order to test the performance-robustness to significant forward axial speeds. The commanded heading trajectory was from 0.0 to 180.0 degrees, and the commanded depth trajectory was from 0.0 to 10.0 ft. The results of this test are shown in Figure 8.17 and Table 8.13.

Table 8.13: "Full-Ahead" Performance Test of the
AUV Sliding-Mode Augmented Controller
(with Performance Specifications from Chapters 6 and 7 in Parentheses)

Steady-State Depth Error	0.02 feet ($\pm$1.0 feet)
Steady-State Heading Error	0.1 degrees ($\pm$5.0 degrees)
Depth Overshoot	1.03 feet (1.0 feet)
Heading Overshoot	2.53 degrees (10.0 degrees)
Depth Response	15.13 seconds (10.0 seconds)
Heading Response	4.80 seconds (5.0 seconds)

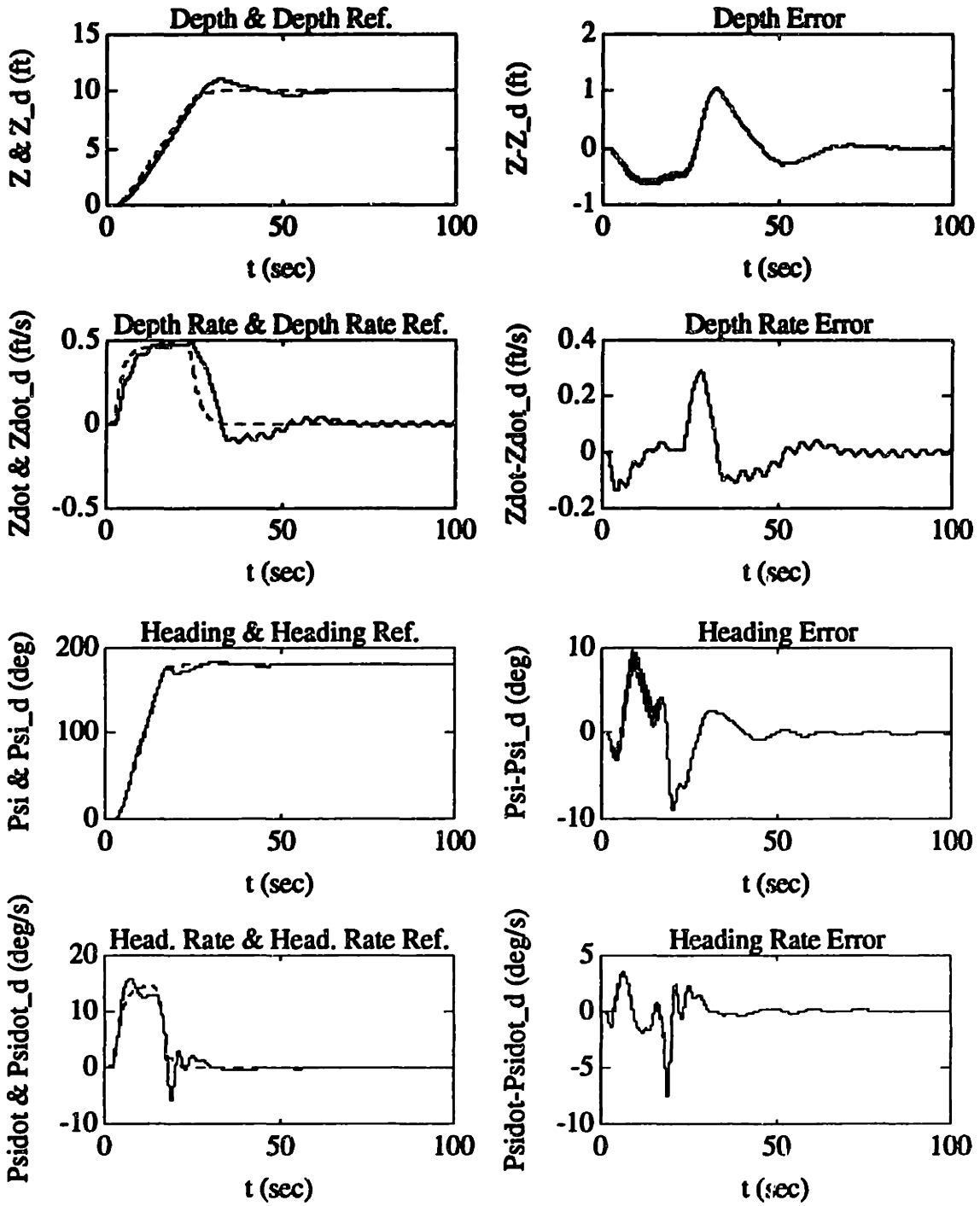

Figure 8.17: "Full-Ahead" Simulation Performance of the Sliding-Mode Augmented Controller

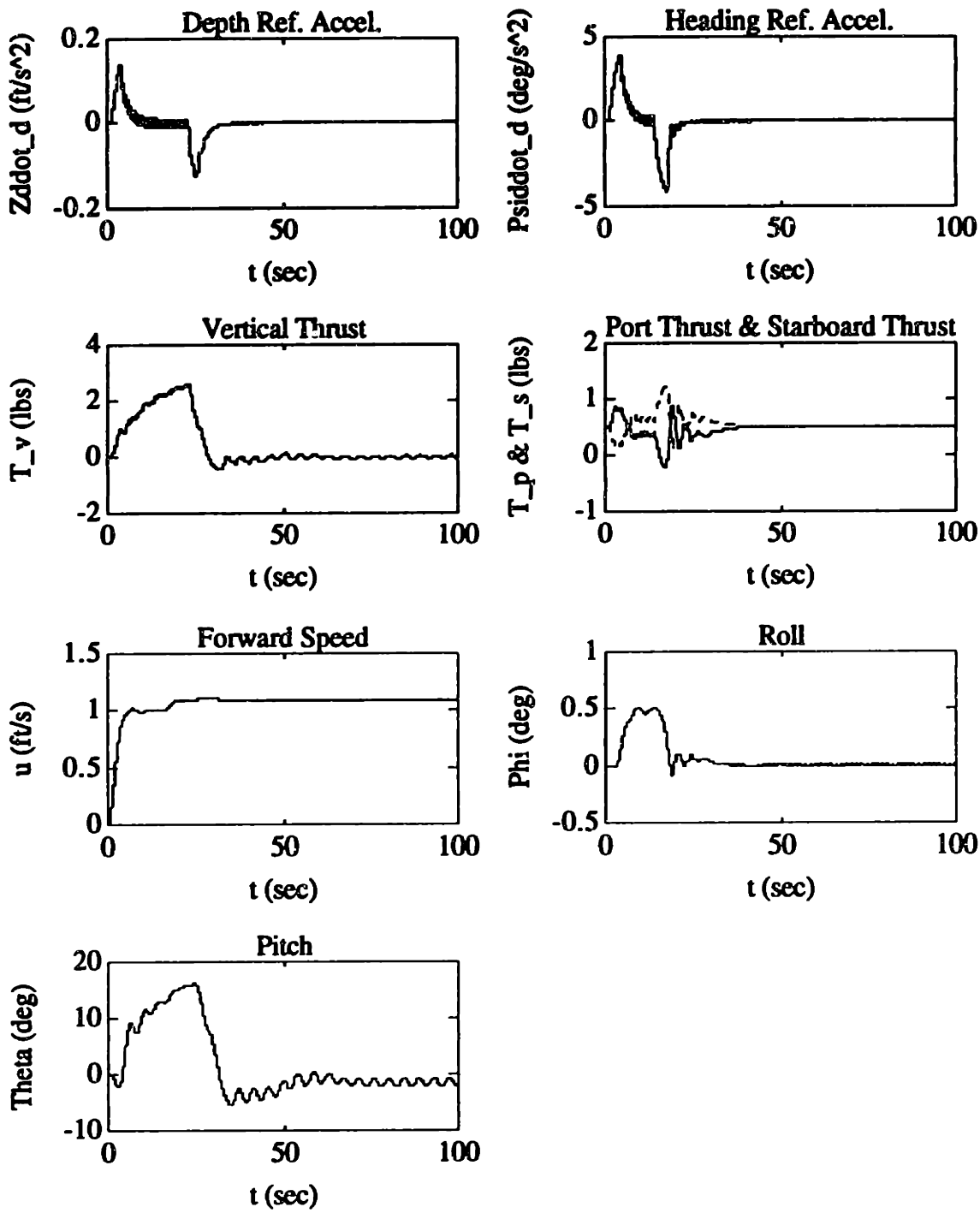

Figure 8.17: "Full-Ahead" Simulation Performance of the Sliding-Mode Augmented Controller (continued)

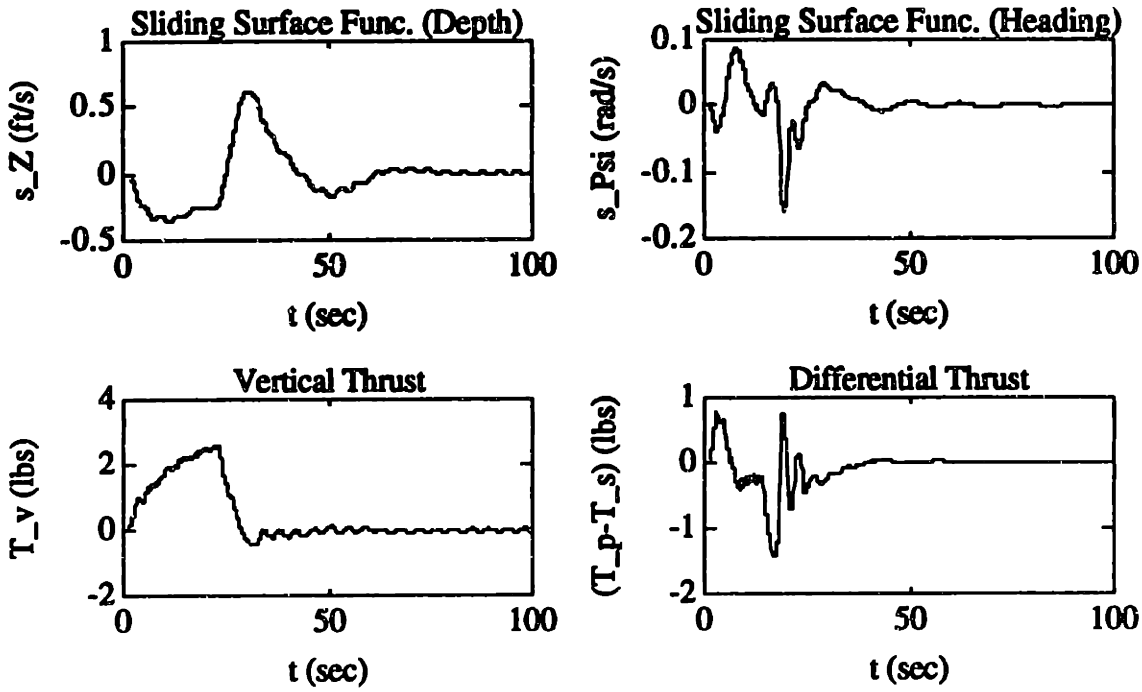

Figure 8.17: "Full-Ahead" Simulation Performance of the Sliding-Mode Augmented Controller (continued)

From the results of Figure 8.17 and Table 8.13, the Sliding-Mode Augmented "full-ahead" heading performance meet the desired design goals of Chapter 7. The heading overshoot was less than either the Sliding-Mode controller or the H_∞/μ-synthesis controllers, possibly since the LTI portion of the Augmented controller compensates for the Munk moment (like the H_∞/μ-controllers), and the Sliding-Mode portion compensates for the nonlinear yawing hydrodynamic "drag". The depth overshoot was slightly larger than the specification, but still acceptable (and smaller than the depth overshoot for the H_∞/μ-Synthesis controllers). The depth response time was slower than the specification, but was still acceptable.

"Full-Reverse" Simulation Performance

The next simulated test of the second AUV Sliding-Mode Augmented controller was done with a commanded forward thrust of -1.0 lb., nominal model parameters, and zero sensor noise. This was done in order to test the performance-robustness to significant negative axial speeds. The commanded heading trajectory was from 0.0 to 180.0 degrees, and the commanded depth trajectory was from 0.0 to 10.0 ft. The results of this test are shown in Figure 8.18 and Table 8.14. For purposes of clarifying the depth steady-state error-performance, the Sliding-Mode Augmented test simulation is shown for an additional 50 seconds (0 to 150 seconds).

Table 8.14: "Full-Reverse" Performance Test of the
AUV Sliding-Mode Augmented Controller
(with Performance Specifications from Chapters 6 and 7 in Parentheses)

Steady-State Depth Error	0.03 feet ($\pm$1.0 feet)
Steady-State Heading Error	0.13 degrees ($\pm$5.0 degrees)
Depth Overshoot	0.57 feet (1.0 feet)
Heading Overshoot	3.03 degrees (10.0 degrees)
Depth Response	11.40 seconds (10.0 seconds)
Heading Response	4.91 seconds (5.0 seconds)

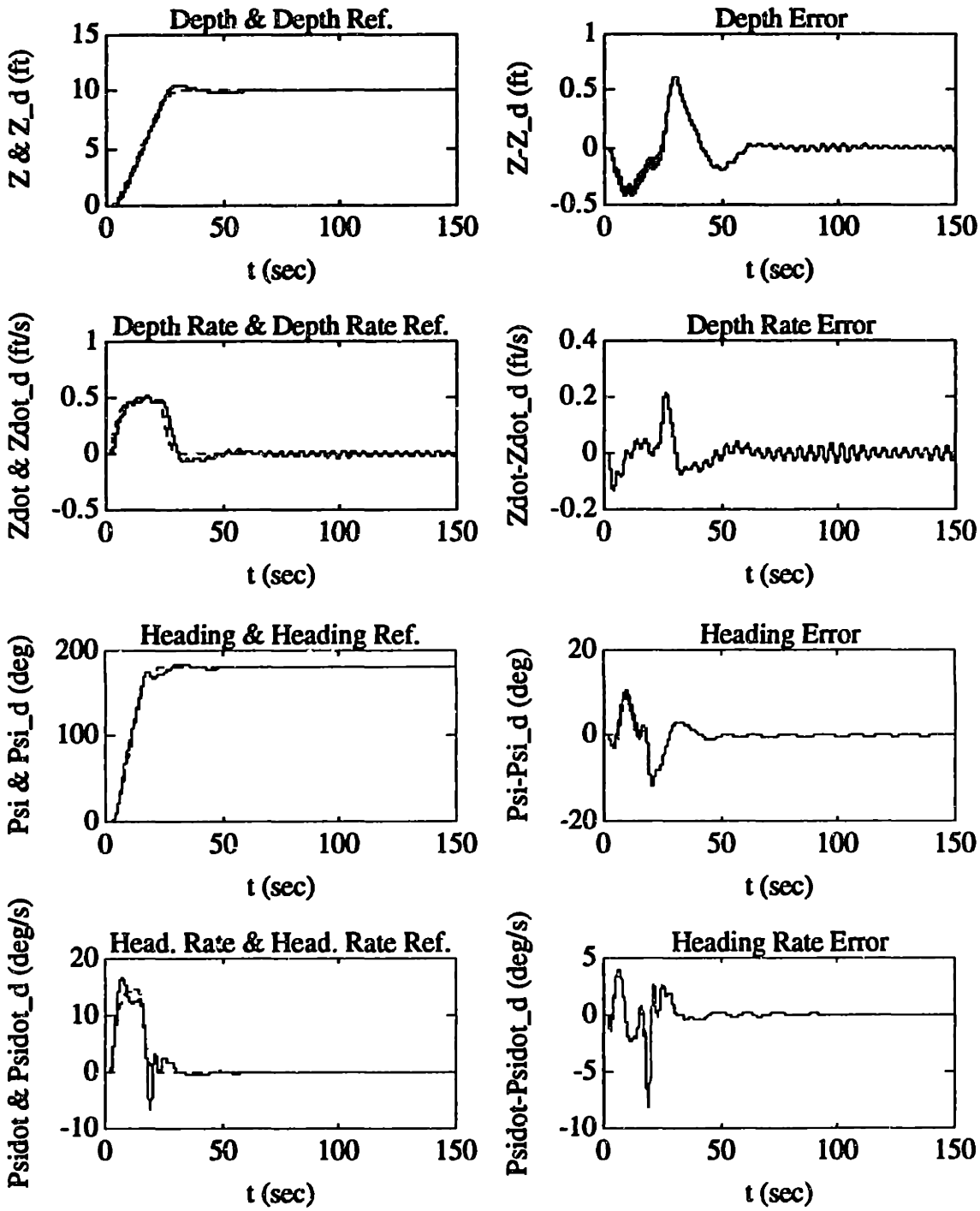

Figure 8.18: "Full-Reverse" Simulation Performance of the Sliding-Mode Augmented Controller

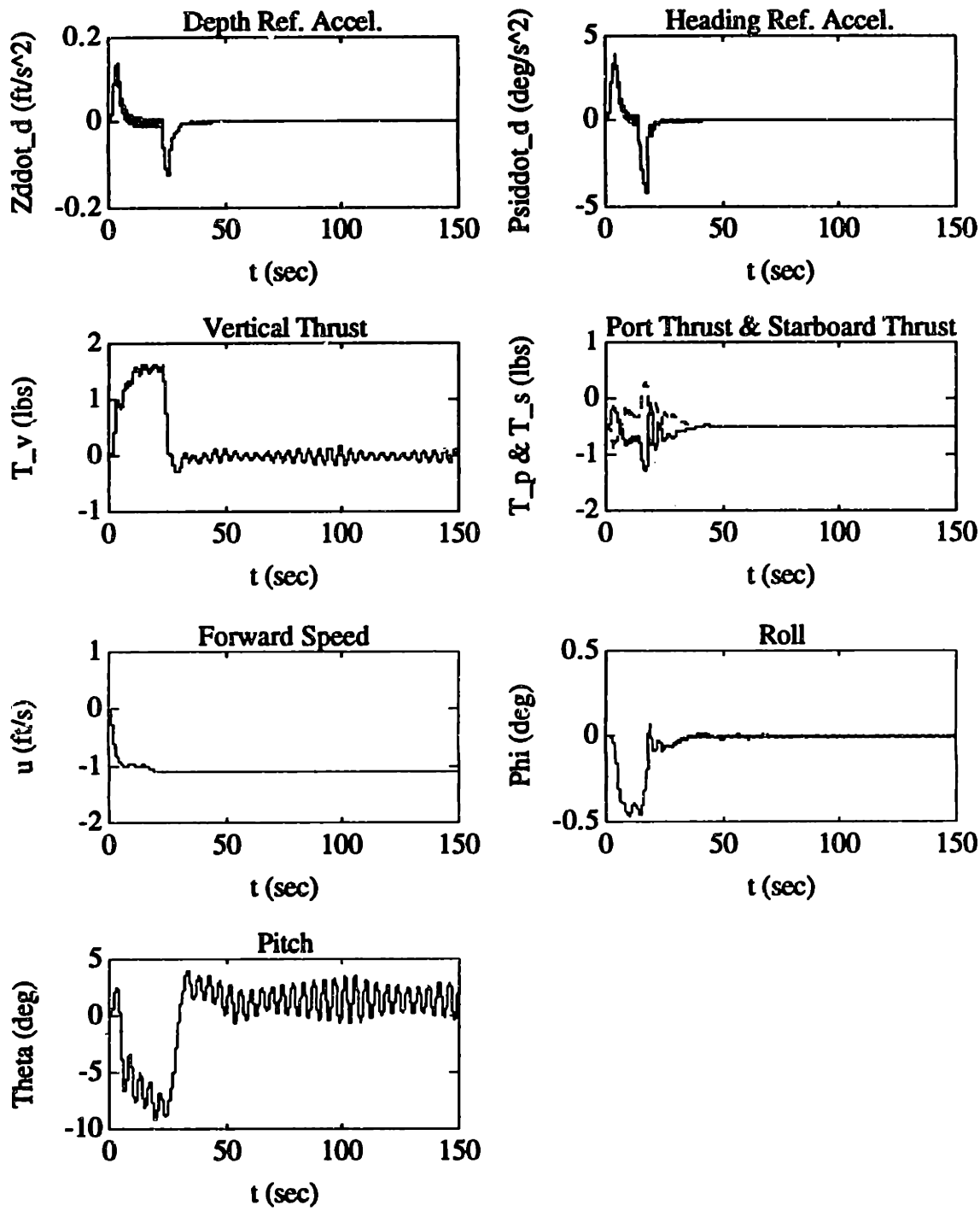

Figure 8.18: "Full-Reverse" Simulation Performance of the Sliding-Mode Augmented Controller (continued)

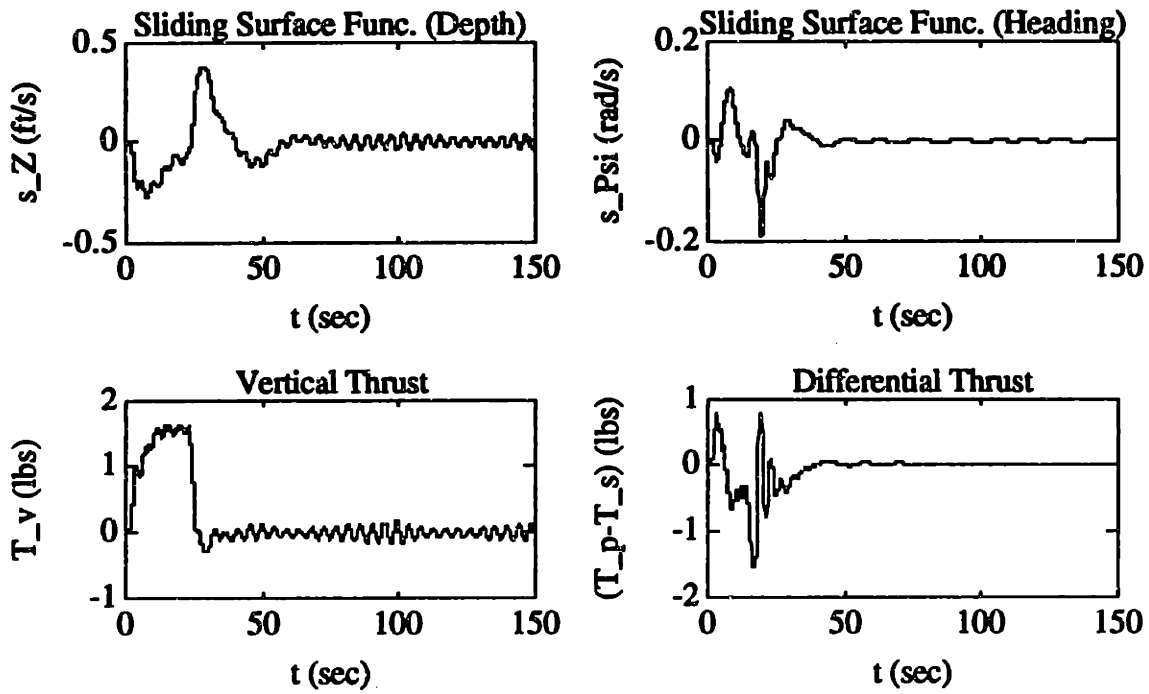

Figure 8.18: "Full-Reverse" Simulation Performance of the Sliding-Mode Augmented Controller (continued)

From the results of Figure 8.18 and Table 8.14, the Sliding-Mode Augmented heading-performance met the desired design goals of Chapter 7 for the "full-reverse" case. Similarly to the "full-ahead" case, the heading overshoot was less than either the Sliding-Mode controller or the H_∞/μ-synthesis controllers, since the LTI portion of the Augmented controller compensates for the Munk moment (like the H_∞/μ-controllers), and the Sliding-Mode portion compensates for the (nonlinear) yawing hydrodynamic "drag". The depth overshoot also met the specification for this case. The depth response time was slower than the specification, but was still acceptable. However, the vertical thrust signal exhibited an undesirable steady-state oscillation with a magnitude of approximately 0.16 lb., due to the apparent excitation of the pitching dynamics. On the actual Sea Squirt vehicle, this could cause an unwanted power drain by the vertical thruster upon the AUV's power source, even though the depth steady-state error-performance would be well within the specifications required for a "typical" mission.

"Noisy Hovering" Simulation Performance

The next simulated test of the Sliding-Mode Augmented controller was done using nominal model parameters, at the "nominal" zero commanded forward thrust. The Gaussian sensor noise inputs were set to the values found Section 4.6 (in order to test the noise performance of this controller). The commanded heading trajectory was again from 0.0 to 180.0 degrees, and the commanded depth trajectory was from 0.0 to 10.0 ft. The results of this test are shown in Figure 8.19.

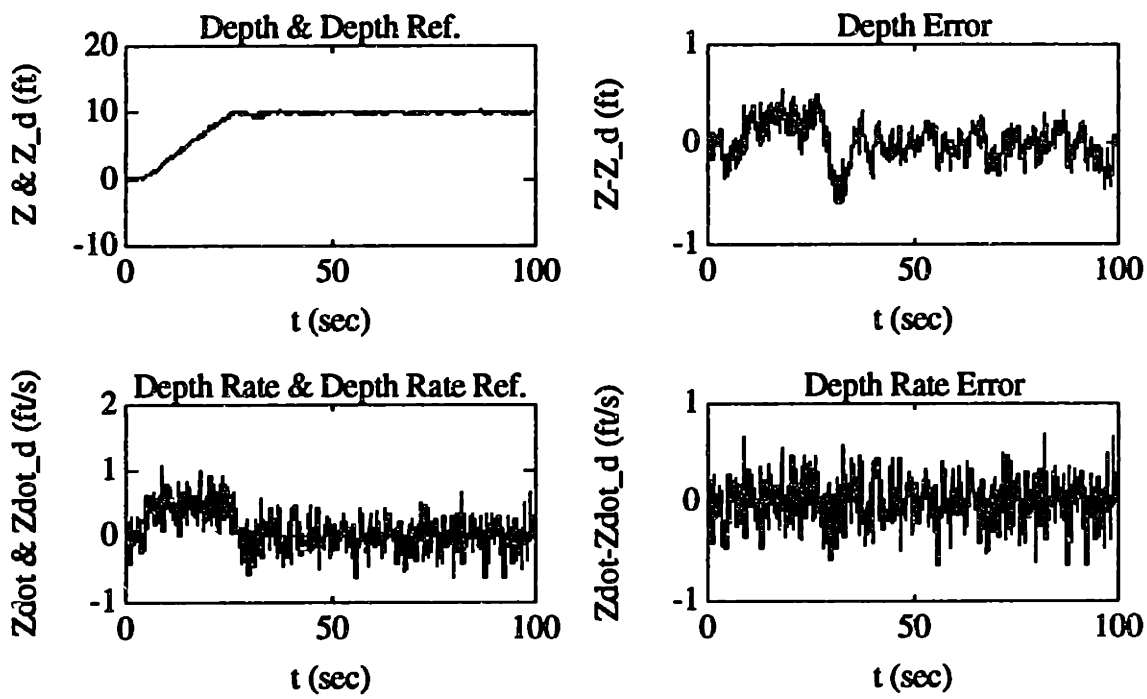

Figure 8.19: "Noisy Hovering" Simulation Performance of the Sliding-Mode Augmented Controller

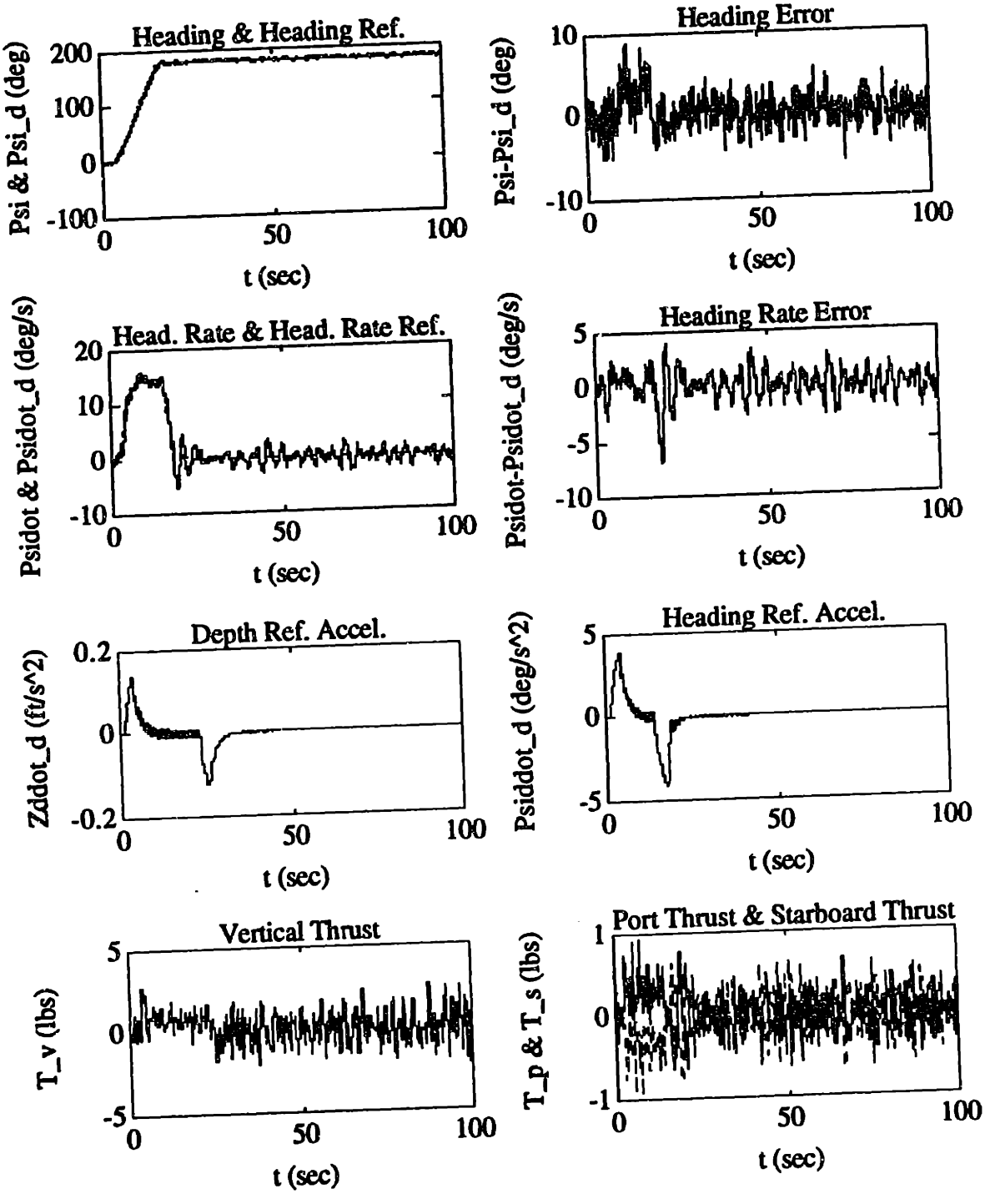

Figure 8.19: "Noisy Hovering" Simulation Performance of the Sliding-Mode Augmented Controller (continued)

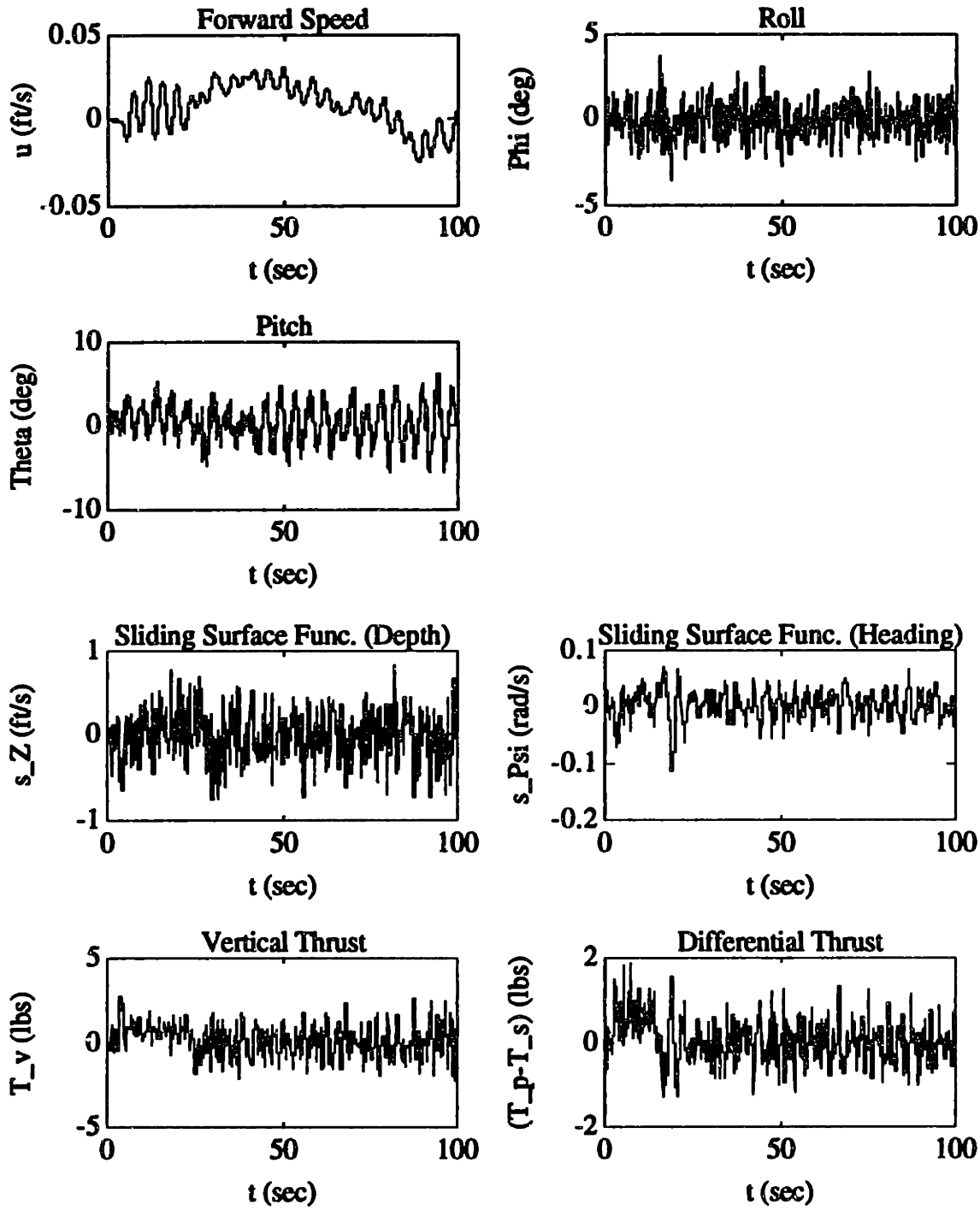

Figure 8.19: "Noisy Hovering" Simulation Performance of the Sliding-Mode Augmented Controller (continued)

From the results of Figure 8.19, it appears that the Sliding-Mode Augmented controller is reasonably robust to the additive sensor noise (at least for the "hovering" case). The overshoot characteristics of this control design somewhat larger than for the noise-free case, but still meets the specifications. The steady-state errors in both the depth and the heading are somewhat larger and more oscillatory than for the noise-free case, but they still meet the design specifications of ±1.0 feet and ±5.0 degrees for depth and heading, respectively. The commanded thrust input signals to the AUV thrusters are also significantly more oscillatory for this case (especially as compared to the lower gain Sliding-Mode controller). Not e that the noise inputs are causing excitation of the pitching dynamics.

Chapter 9

Summary and Conclusions

This thesis presents a comparison between the H_∞/μ-Synthesis and Sliding-Mode robust control-system design methodologies, as applied to the design, implementation, and performance of heading and depth controllers for the *Sea Squirt* AUV. This thesis also presents the theoretical development of the Sliding-Mode Augmented design technique (where a linear time-invariant (LTI) controller is augmented by a Sliding-Mode based controller). The motivation behind the development of this technique was to find a way of incorporating the advantages of both the H_∞/μ-Synthesis methodology and the Sliding-Mode methodology into the AUV control-design process. A comparison is made between an AUV controller designed with this augmented technique and AUV controllers designed with the H_∞/μ-Synthesis methodology and the Sliding-Mode methodology.

Even though the control designs were done specifically for the *Sea Squirt*, the desired goal of this thesis is that the conclusions reached from the results of the comparisons can be applied to controller design for other types of systems as well.

9.1 SUMMARY

The results presented in this thesis are for a full-order, six degree-of-freedom, nonlinear model of the dynamics of the Sea Squirt AUV. However, the full-order nonlinear model, together with its representation for uncertainty, could not be used directly in the design process by either the H_∞/μ-Synthesis methodology or the Sliding-Mode methodology. Therefore, approximations were made of both the nonlinear model and its uncertainty representation.

The H_∞/μ-Synthesis approach required the use of a full-order linear-time invariant (LTI) Taylor-series approximation to the full-order nonlinear model. Revelant parametric uncertainties and known nonlinearities were approximated as LTI perturbations (with bounds found by a numerical comparison between the "nominal" LTI model and several "perturbed" LTI models). This uncertain LTI model was converted into a suitable H_∞/μ-Synthesis design model by the addition of a set of frequency-domain "loopshaping" weighting functions as design parameters. From an analysis of the full-order nonlinear model, the AUV's depth and heading dynamics were found to be approximately decoupled This approximate decoupling allowed a similar decoupling of the respective weighting functions for depth control and heading control, thus allowing for separate (but concurrent) control designs. An H_∞ controller was synthesized using this weighted model together with an H_∞ gamma-iteration algorithm. Synthesis of a feasible design required the scaling of both the nominal (unweighted) full-order LTI model and the LTI perturbation structure. A μ-Synthesis controller was synthesized by applying a μ-based robust design algorithm to the H_∞ design model. Model reduction-and-balancing algorithms were employed at several stages of the H_∞/μ-Synthesis design process in order to minimize the state-order of these controllers. A preliminary analysis of the performance robustness of these control designs to the LTI uncertainties was done by comparing the nominal closed-loop, time-domain, step-response to the time-domain step responses for full-order LTI models with either off-nominal axial velocities or with selected perturbations in the "added mass" hydrodynamic coefficients.

The Sliding-Mode approach required the use of a reduced-order nonlinear approximation to the full-order nonlinear AUV model, together with a reduced-order approximate parametric-uncertainty representation. The approximate decoupling of the AUV's depth and heading dynamics allowed for the decoupling of the respective Sliding-Mode design parameters (thus allowing for decoupled depth and heading control designs). The parameter selection process was based on several design "rule-of-thumb" guidelines from the literature.

The Sliding-Mode Augmented approach required the use of a reduced-order LTI approximation to the full-order AUV model, together with the nonlinear approximation used in the Sliding-Mode methodology. The LTI controller was designed for this reduced-

order model using the H_∞ design technique, in a similar fashion to the design procedure used for the full-order H_∞ design. Similarly, the design of The Sliding-Mode portion of the Sliding-Mode Augmented controller was based on design of the "regular" AUV Sliding-Mode controller.

The H_∞/μ-Synthesis-based controllers, the Sliding-Mode based controller, and the Sliding-Mode Augmented controller, were implemented and tested by using a simulation of the full-order nonlinear model. Both the thruster and sensor dynamics were included in this simulation. All of the control algorithms were implemented in discrete-time, using the sampling time (0.2 seconds) of the actual AUV digital control system. The performance of the controllers was analyzed over the approximate range of "typical" axial velocities commanded by the AUV (i.e., the "full-ahead" case of approximately 1.0 ft/s, the "hovering" case of approximately 0.0 ft/s, and the "full-reverse" case of approximately -1.0 ft/s). The performance of the controllers in the face of additive sensor noise was also analyzed.

As a benchmark, the performance of all of the control designs of this thesis was compared to the Sliding-Mode nonlinear performance goals presented in Chapter 6. With the exception of a slightly slower heading response time, the heading performance of both the H_∞ controller and the μ-Synthesis controller met these specifications over the entire range of axial velocities. The depth performance of both these controllers met these specifications (with the exception of a large axial-velocity dependent depth overshoot). For the "hovering" case, the μ-synthesis controller exhibited a significant steady-state oscillation in the vertical thrust control signal.

For the Sliding-Mode controller with the initial selection of parameters aided by the design guidelines in the literature, the performance for the "hovering" case was nearly identical to the performance for the nominal reduced-order nonlinear design model, meeting the specifications with the exception of a larger heading overshoot, and slower heading and depth response times. For the "full-ahead" case, the performance of the initial Sliding-Mode controller degraded to unacceptable levels (e.g., a heading overshoot and a steady-state heading-error oscillation of approximately an order of magnitude greater than the specification). To improve the performance of the Sliding-Mode controller, the widths of

the sliding-surface "boundary-layer" parameters for both depth and heading control were decreased below the "rule-off-thumb" design guidelines. The "hovering" performance of this second Sliding-Mode controller met all of the nonlinear design specifications. For both "full-ahead" case and the "full-reverse" cases, the performance of the second Sliding-Mode controller met most of the performance goals. The heading response for these two cases exhibited an overshoot that was larger than the specification. However, it was approximately 20% of the "full-ahead" overshoot of the initial Sliding-Mode design. On the other hand, the heading overshoot of the second Sliding-Mode design was about 3 times greater than the corresponding heading overshoot for the H_∞/μ-Synthesis designs. The steady-state heading oscillation of the second Sliding-Mode design was reduced in magnitude for both the "full-ahead" case and the "full-reverse" case, to a level meeting the steady-state heading-error design goal.

For the Sliding-Mode Augmented controller, the heading performance met all of the design specifications over the entire range of axial velocities. The overall depth performance of this controller met these specifications, with the exception of a larger depth overshoot for the "full-ahead" case and a slower depth response time for both the "full-ahead" case and the "full-reverse case". For the "full-reverse" case, the Sliding-Mode Augmented controller exhibited a significant steady-state oscillation in the vertical thrust control signal.

9.2 CONCLUSIONS

Several conclusions can be deduced from the results of the *Sea Squirt* AUV control design efforts presented in this thesis. The first conclusion that can be deduced from the actual control design procedures presented in Chapter 5 and Chapter 6, for the *Sea Squirt* AUV design example (a system with a reasonably high state-order of 10 states, significant nonlinear dynamic effects, unmodeled dynamics, and significant parameter uncertainty), is that *there is no concrete global performance-robustness guarantee to be had from either the H_∞/μ-Synthesis methodology or the Sliding-Mode methodology.* Direct application of the performance-robustness theorems presented by either methodology for the design of the *Sea Squirt* control system would yield either designs or guarantees that are so conservative

as to be essentially useless (or unachievable). The usefulness (and similarity) of these robust approaches, as applied to the *Sea Squirt* control design effort, is that *they provide the control designer with a framework for incorporating knowledge about the uncertainty in the AUV design model directly into the parameters of the design process.* By a careful selection of these design parameters, a tradeoff can be made between the nominal performance of the control designs and the robust-performance. However, a comparison of these design efforts revealed some significant issues, which can be used to draw other design conclusions.

The strength of the LTI H_∞/μ-Synthesis approach, as applied to the *Sea Squirt* AUV control design, is that it provided a consistent framework for dealing with "approximately linear" unmodeled dynamics (e.g., destabilizing Munk moment uncertainty, thruster dynamics, and sensor dynamics). In particular, the H_∞/μ-Synthesis based controllers exhibited consistently better heading performance over the Sliding-Mode based controllers, due to incorporating the effects of the approximately linear Munk-moment uncertainty into the design. Models for the thruster dynamics were also allowed to be directly incorporated in the H_∞/μ-Synthesis design process.

However, the H_∞/μ-synthesis methodology was weak in dealing with the effects of state-dependent nonlinearities (e.g., hydrodynamic drag) on the *Sea Squirt* design. For the designs presented in this thesis, a somewhat *ad hoc* non-rigorous, numerical perturbation scheme (where the state-dependent nonlinearities were approximated by a set of LTI parametric state-space perturbations) was used as an attempt for dealing with this issue. This procedure appeared to reduced the sensitivity of the design to these nonlinearities somewhat, but it was not always obvious how to scale the resulting parametric perturbations.

The strength of the Sliding-Mode design approach was providing a framework for accommodating these (known) state-dependent nonlinearities, as applied to the Sea Squirt AUV design. In particular, the Sliding-Mode based controllers exhibited consistently better depth performance over the H_∞/μ-synthesis based controllers, due to incorporating the effects of the state-dependent nonlinear hydrodynamic "drag" forces into the design process.

In contrast, the Sliding-Mode approach was weak in dealing with the effects of lower frequency unmodeled dynamics on the AUV control design. Higher frequency unmodeled dynamics, such as the sensor and thruster dynamics, were dealt with indirectly by limiting the desired closed-loop bandwidth. However, this approach does not work for the example of the lower frequency unmodeled Munk moment dynamics. For the results presented in this thesis, it was possible to get acceptable performance by decreasing the width of the Sliding-Surface "boundary layer" from the values selected using the "rule-of-thumb" design guidelines. However, it was not obvious by what amount should this boundary layer be decreased. In addition, the heading performance was still not as good as the heading performance of the H_∞/μ-Synthesis controllers (which incorporated the effects of the lower frequency Munk moment dynamics directly into the design).

The Sliding-Mode Augmented approach provided a framework for incorporating the advantages of both H_∞/μ-synthesis and Sliding-Mode into the Sea Squirt design example (where the LTI controller was designed to accommodate for "approximately linear" unmodeled dynamics by using the H_∞ technique, while the Sliding-mode portion was designed to accommodate for known nonlinearities). The benefits of the Sliding-Mode Augmented approach were validated from both the heading and the depth performance results. In particular, the overall heading performance of the Sliding-Mode Augmented controller was superior to either the H_∞/μ-Synthesis controllers or the Sliding-Mode controller (since the LTI portion of this controller was designed to compensate for the Munk-moment uncertainty, while the Sliding-Mode portion was designed to compensate for the nonlinear hydrodynamic "drag" moment about the vehicle's yawing axis). The depth overshoot performance of the Sliding-Mode Augmented controller was better overall than the depth overshoot of the H_∞/μ-Synthesis controllers (since the Sliding-Mode portion of this controller was designed to compensate for the hydrodynamic drag force along the vehicle's vertical axis). However, the steady-state performance of the Augmented Sliding-Mode controller was less robust at negative axial velocities (since the augmented LTI controller was designed using the reduced-order AUV LTI model, which is only valid at low axial velocities).

In terms of the required design effort for the *Sea Squirt* AUV depth and heading controllers, the design process for the H_∞/μ-synthesis controllers was much more

involved. Even though the decoupled nature of the *Sea Squirt* problem allowed for significant simplifications in the design model, it was not obvious how to choose the frequency-domain weighting functions in order to get a reasonable level of performance for the full-order nonlinear model (or even for the full-order "perturbed" LTI models). For the decoupled *Sea Squirt* design problem, the selection process for the Sliding-Mode controller parameters was considerably simpler. However, since the Sliding-Mode methodology presented in this thesis was limited to systems with full-state feedback, more effort was required in deriving the open-loop design model from the full-order nonlinear model.

For the *Sea Squirt* controller, the more difficult part of the Sliding-Mode Augmented design effort was the design of the LTI controller, using the H_∞ design methodology. As with the full-order H_∞ design, it was not obvious how to choose the frequency-domain weighting functions in order to get a reasonable level of performance for the full-order nonlinear model. Similar to Sliding-Mode, the Sliding-Model Augmented technique, in the form presented in this thesis, is limited to systems with full-state feedback. Therefore, it would be useful to derive a form for the Sliding-Mode Augmented control law that does not have this limitation.

Appendix A

Descriptor-System/Two-Riccati H_∞ Optimization Algorithm

In order to use the Descriptor-System/Two-Riccati H_∞ optimization algorithm [10], the design plant must first be converted to the Standard Form (SF) Model, shown in Figure A.1. P(s) is the open-loop SF system, K(s) is a linear controller, and $\Delta(s)$ is a stable norm-bounded block-diagonal perturbation matrix.

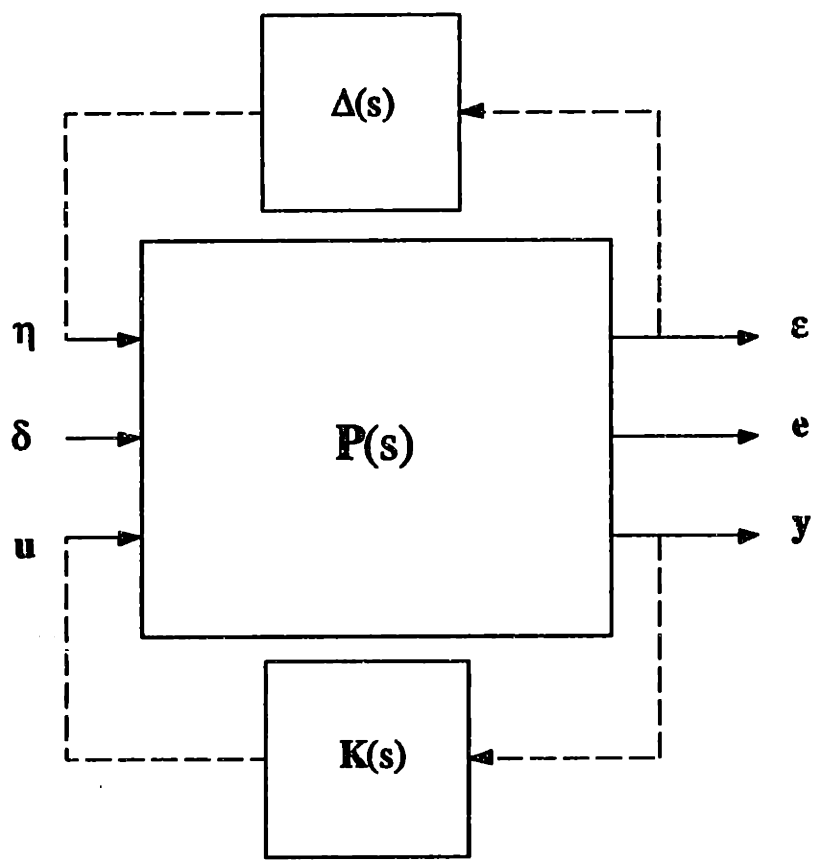

Figure A.1: Standard Form Model

The nine-block transfer-function of the open-loop system, P(s), is given by

$$\begin{bmatrix} \varepsilon \\ e \\ y \end{bmatrix} = \begin{bmatrix} P_{11}(s) & P_{12}(s) & P_{13}(s) \\ P_{21}(s) & P_{22}(s) & P_{23}(s) \\ P_{31}(s) & P_{32}(s) & P_{33}(s) \end{bmatrix} \begin{bmatrix} \eta \\ \delta \\ u \end{bmatrix} \tag{A.1}$$

and the four-block transfer-function of the closed-loop system, G(S), is given by

$$\begin{bmatrix} \varepsilon \\ e \end{bmatrix} = \begin{bmatrix} G_{11}(s) & G_{12}(s) \\ G_{21}(s) & G_{22}(s) \end{bmatrix} \begin{bmatrix} \eta \\ \delta \end{bmatrix} \tag{A.2}$$

Given a scalar, γ, the descriptor-system two-Riccati algorithm attempts to find the family of stabilizing linear controllers, K(s), such that, for the closed-loop system, G(s),

$$\|G(s)\|_\infty = \left\| \begin{bmatrix} G_{11}(s) & G_{12}(s) \\ G_{21}(s) & G_{22}(s) \end{bmatrix} \right\|_\infty < \gamma \tag{A.3}$$

To do this, the nine-block SF system, P(s), is first converted into the four-block open-loop SF system, T(s), given by

$$T(s) = \begin{bmatrix} T_{11}(s) & T_{12}(s) \\ T_{21}(s) & T_{22}(s) \end{bmatrix}$$

$$= \begin{bmatrix} \begin{bmatrix} P_{11}(s) & P_{12}(s) \\ P_{21}(s) & P_{22}(s) \end{bmatrix} & \begin{bmatrix} P_{13}(s) \\ P_{23}(s) \end{bmatrix} \\ \begin{bmatrix} P_{31}(s) & P_{32}(s) \end{bmatrix} & [P_{33}(s)] \end{bmatrix} \tag{A.4}$$

with the transfer-function matrices, T_{11}, T_{12}, T_{21}, and T_{22} having dimensions, $p_1 \times m_1$, $p_1 \times m_2$, $p_2 \times m_1$, and $p_2 \times m_2$, respectively. This implies that the input vectors η and δ are lumped together to form a new input vector given by

$$w = \begin{bmatrix} \eta \\ \delta \end{bmatrix} \tag{A.5}$$

and it implies that the output vectors ε and e are lumped together to form a new output vector given by

$$z = \begin{bmatrix} \varepsilon \\ e \end{bmatrix} \tag{A.6}$$

$T(s)$ is scaled by γ to form $T_\gamma(s)$, which is given by

$$T_\gamma(s) = \begin{bmatrix} \frac{1}{\sqrt{\gamma}}[T_{11}(s)]\frac{1}{\sqrt{\gamma}} & \frac{1}{\sqrt{\gamma}}[T_{12}(s)] \\ [T_{21}(s)]\frac{1}{\sqrt{\gamma}} & T_{22}(s) \end{bmatrix} \tag{A.7}$$

with the state-space representation denoted by

$$T_\gamma(s) \stackrel{s}{=} \left[\begin{array}{c|cc} A & B_1 & B_2 \\ \hline C_1 & D_{11} & D_{12} \\ C_2 & D_{21} & D_{22} \end{array}\right] \tag{A.8}$$

Note that this notation for the state-space representation implies

$$T_\gamma(s) = \begin{bmatrix} C_1 \\ C_2 \end{bmatrix}[sI - A]^{-1}[\, B_1 \quad B_2 \,] + \begin{bmatrix} D_{11} & D_{12} \\ D_{21} & D_{22} \end{bmatrix} \tag{A.9}$$

In order for the H_∞ optimization problem to be well-posed, $(\mathbf{A}, \mathbf{B}_2, \mathbf{C}_2)$ must be stabilizable and detectable; $\mathbf{D}_{12}$ must have full column rank; and $\mathbf{D}_{21}$ must have full row rank. In addition, the following conditions must hold for all real ω

$$\text{rank}\begin{bmatrix} \mathbf{A} - j\omega\mathbf{I} & \mathbf{B}_2 \\ \mathbf{C}_1 & \mathbf{D}_{12} \end{bmatrix} = n + m_2 \tag{A.10}$$

and

$$\text{rank}\begin{bmatrix} \mathbf{A} - j\omega\mathbf{I} & \mathbf{B}_1 \\ \mathbf{C}_2 & \mathbf{D}_{21} \end{bmatrix} = n + p_2 \tag{A.11}$$

where the dimension of $\mathbf{A}$ is $n \times n$.

The next step in the descriptor-system two-Riccati algorithm is to "zero" out $\mathbf{D}_{22}$ (i.e. assume that it is equal to zero for now) which then gives

$$T_{2\gamma}(s) \overset{s}{=} \left[\begin{array}{c|cc} \mathbf{A} & \mathbf{B}_1 & \mathbf{B}_2 \\ \hline \mathbf{C}_1 & \mathbf{D}_{11} & \mathbf{D}_{12} \\ \mathbf{C}_2 & \mathbf{D}_{21} & 0^{p_2 \times m_2} \end{array}\right] \tag{A.12}$$

The following vector transformations are performed

$$\tilde{\mathbf{u}} = \mathbf{S}_u\mathbf{u} \tag{A.13}$$

$$\tilde{\mathbf{y}} = \mathbf{S}_y\mathbf{y} \tag{A.14}$$

$$\tilde{\mathbf{w}} = \mathbf{S}_w\mathbf{w} \tag{A.15}$$

$$\tilde{\mathbf{z}} = \mathbf{S}_z\mathbf{z} \tag{A.16}$$

where the matrices S_u and S_y are nonsingular and the matrices S_w and S_z are unitary. From this, the state-space representation for $T_{2\gamma}(s)$ can be written as

$$T_{2\gamma}(s) \overset{s}{=} \left[\begin{array}{c|cc} A & B_1 S_w^H & B_2 S_u^{-1} \\ \hline S_z C_1 & S_z D_{11} S_w^H & S_z D_{12} S_u^{-1} \\ S_y C_2 & S_y D_{21} S_w^H & 0^{p_2 \times m_2} \end{array}\right]$$

$$= \left[\begin{array}{c|cc} A & \hat{B}_1 & \hat{B}_2 \\ \hline \hat{C}_1 & \hat{D}_{11} & \hat{D}_{12} \\ \hat{C}_2 & \hat{D}_{21} & 0^{p_2 \times m_2} \end{array}\right] \qquad \text{(A.17)}$$

Since the matrices, S_z and S_w, are unitary, the closed-loop H_∞ norm of $T_{2\gamma}(s)$ is unaffected by these transformations.

The goal of performing these transformations is that the scaling matrices, S_u, S_y, S_z, and S_w, can be chosen such that

$$\hat{D}_{12} = S_z D_{12} S_u^{-1} = \begin{bmatrix} 0 \\ I \end{bmatrix} \qquad \text{(A.18)}$$

and

$$\hat{D}_{21} = S_y D_{21} S_w^H = [\, 0 \;\; I \,] \qquad \text{(A.19)}$$

with the previous assumptions that the matrix D_{12} has full column rank and the matrix D_{21} has full row rank. One means of finding the desired scaling matrices is by using the singular-value decompositions of D_{12} and D_{21}.

Next, $\hat{D}_{11}$ is partitioned into submatrices as

$$\hat{D}_{11} = \begin{bmatrix} \hat{D}_{1111} & \hat{D}_{1112} \\ \hat{D}_{1121} & \hat{D}_{1122} \end{bmatrix} \tag{A.20}$$

where $\hat{D}_{1122}$ has m_2 rows and p_2 columns. These submatrices are used to calculate the "all-pass embedding" matrix, F_{opt}, given by

$$F_{opt} = -\left[\hat{D}_{1122} + \hat{D}_{1121}\left(I - \hat{D}_{1111}^T\hat{D}_{1111}\right)^{-1}\hat{D}_{1111}^T\hat{D}_{1112}\right] \tag{A.20}$$

For the cases where either $m_1 = p_2$ or $m_2 = p_1$ (which implies $\hat{D}_{1111}$ is not defined), F_{opt} is simply given by

$$F_{opt} = -\hat{D}_{1122} \tag{A.21}$$

F_{opt} is used to "loop-shift" $T_{2\gamma}$. This produces the following matrices

$$\hat{A} = A + \hat{B}_2 F_{opt} \hat{C}_2 \tag{A.22}$$

$$\tilde{B}_1 = \hat{B}_1 + \hat{B}_2 F_{opt} \hat{D}_{21} \tag{A.23}$$

$$\tilde{C}_1 = \hat{C}_1 + \hat{D}_{12} F_{opt} \hat{C}_2 \tag{A.24}$$

$$\tilde{D}_{11} = \hat{D}_{11} + \hat{D}_{12} F_{opt} \hat{D}_{21} \tag{A.25}$$

Next, the orthogonal complements, $\hat{\mathbf{D}}_{12p}$ and $\hat{\mathbf{D}}_{21p}$, are computed for $\hat{\mathbf{D}}_{12}$ and $\hat{\mathbf{D}}_{21}$, where

$$\begin{bmatrix} \hat{\mathbf{D}}_{12}^T \\ \hat{\mathbf{D}}_{12p}^T \end{bmatrix} \begin{bmatrix} \hat{\mathbf{D}}_{12} & \hat{\mathbf{D}}_{12p} \end{bmatrix} = \begin{bmatrix} \mathbf{I} & 0 \\ 0 & \mathbf{I} \end{bmatrix} \tag{A.26}$$

and

$$\begin{bmatrix} \hat{\mathbf{D}}_{21} \\ \hat{\mathbf{D}}_{21p} \end{bmatrix} \begin{bmatrix} \hat{\mathbf{D}}_{21}^T & \hat{\mathbf{D}}_{21p}^T \end{bmatrix} = \begin{bmatrix} \mathbf{I} & 0 \\ 0 & \mathbf{I} \end{bmatrix} \tag{A.27}$$

Then *stabilizing* symmetric solutions, $\hat{\mathbf{P}}$ and $\hat{\mathbf{S}}$, are found for the following pair of normalized matrix Riccati equations (hence the name "two-Riccati")

$$\mathbf{A}_{r1}^T\hat{\mathbf{P}} + \hat{\mathbf{P}}\mathbf{A}_{r1} - \hat{\mathbf{P}}\mathbf{R}_{r1}\hat{\mathbf{P}} + \mathbf{Q}_{r1} = 0 \tag{A.28}$$

$$\mathbf{A}_{r2}\hat{\mathbf{S}} + \hat{\mathbf{S}}\mathbf{A}_{r2}^T - \hat{\mathbf{S}}\mathbf{R}_{r2}\hat{\mathbf{S}} + \mathbf{Q}_{r2} = 0 \tag{A.29}$$

where

$$\begin{aligned} \mathbf{A}_{r1} &= \hat{\mathbf{A}} \\ &+ \left(\tilde{\mathbf{B}}_1\tilde{\mathbf{D}}_{11}^T\hat{\mathbf{D}}_{12p}\hat{\mathbf{D}}_{12p}^T - \hat{\mathbf{B}}_2\hat{\mathbf{D}}_{12}\right)\left(\mathbf{I} - \tilde{\mathbf{D}}_{11}\tilde{\mathbf{D}}_{11}^T\hat{\mathbf{D}}_{12p}\hat{\mathbf{D}}_{12p}^T\right)^{-1}\tilde{\mathbf{C}}_1 \end{aligned} \tag{A.30}$$

$$\begin{aligned} \mathbf{R}_{r1} &= \hat{\mathbf{B}}_2\hat{\mathbf{B}}_2^T \\ &- \left(\tilde{\mathbf{B}}_1 - \hat{\mathbf{B}}_2\hat{\mathbf{D}}_{12}^T\tilde{\mathbf{D}}_{11}\right)\left(\mathbf{I} - \tilde{\mathbf{D}}_{11}^T\hat{\mathbf{D}}_{12p}\hat{\mathbf{D}}_{12p}^T\tilde{\mathbf{D}}_{11}\right)^{-1}\left(\tilde{\mathbf{B}}_1^T - \tilde{\mathbf{D}}_{11}^T\hat{\mathbf{D}}_{12}\hat{\mathbf{B}}_2^T\right) \end{aligned} \tag{A.31}$$

$$\mathbf{Q}_{r1} = \tilde{\mathbf{C}}_1^T\hat{\mathbf{D}}_{12p}\left(\mathbf{I} - \hat{\mathbf{D}}_{12p}^T\tilde{\mathbf{D}}_{11}\tilde{\mathbf{D}}_{11}^T\hat{\mathbf{D}}_{12p}\right)^{-1}\hat{\mathbf{D}}_{12p}^T\tilde{\mathbf{C}}_1 \tag{A.32}$$

$$A_{r2} = \hat{A} + \tilde{B}_1 \left(I - \hat{D}_{21p}^T \hat{D}_{21p} \tilde{D}_{11}^T \tilde{D}_{11}\right)^{-1} \left(\hat{D}_{21p}^T \hat{D}_{21p} \tilde{D}_{11}^T \tilde{C}_1 - \hat{D}_{21}^T \hat{C}_2\right) \quad \text{(A.33)}$$

$$R_{r2} = \hat{C}_2^T \hat{C}_2 - \left(\tilde{C}_1^T - \hat{C}_2^T \hat{D}_{21} \tilde{D}_{11}^T\right)\left(I - \tilde{D}_{11} \hat{D}_{21p}^T \hat{D}_{21p} \tilde{D}_{11}^T\right)^{-1} \left(\tilde{C}_1 - \tilde{D}_{11} \hat{D}_{21}^T \hat{C}_2\right) \quad \text{(A.34)}$$

$$Q_{r2} = \tilde{B}_1 \hat{D}_{21p}^T \left(I - \hat{D}_{21p} \tilde{D}_{11}^T \tilde{D}_{11} \hat{D}_{21p}^T\right)^{-1} \hat{D}_{21p} \tilde{B}_1 \quad \text{(A.35)}$$

Now, if both the matrices, $\hat{P}$ and $\hat{S}$, are symmetric, and

$$\text{re}\left[\lambda_i\left(\hat{P}\right)\right] > 0 \quad \text{for all } i \quad \text{(A.36)}$$

$$\text{re}\left[\lambda_i\left(\hat{S}\right)\right] > 0 \quad \text{for all } i \quad \text{(A.37)}$$

$$\rho\left(\hat{P}\hat{S}\right) = \max_i \left[\lambda_i\left(\hat{P}\hat{S}\right)\right] < 1 \quad \text{(A.38)}$$

and

$$\bar{\sigma}\left(\begin{bmatrix} \hat{D}_{1111} & \hat{D}_{1112} \end{bmatrix}\right) < 1 \quad \text{(A.39)}$$

$$\bar{\sigma}\left(\begin{bmatrix} \hat{D}_{1111}^T & \hat{D}_{1121}^T \end{bmatrix}\right) < 1 \quad \text{(A.40)}$$

then a stabilizing linear controller exists such that

$$\|G(s)\|_\infty = \left\| \begin{bmatrix} G_{11}(s) & G_{12}(s) \\ G_{21}(s) & G_{22}(s) \end{bmatrix} \right\|_\infty < \gamma \quad \text{(A.41)}$$

If the existence conditions are satisfied, the descriptor-system/two-Riccati algorithm computes the state-space parameterization of all rational stabilizing linear controllers that satisfy (A.41). The first step in calculating this parameterization is to compute $\mathbf{E}_k$, given by

$$\mathbf{E}_k = \mathbf{I} - \hat{\mathbf{S}}\hat{\mathbf{P}} \tag{A.42}$$

Next, the matrices $\tilde{\mathbf{A}}_{k1}$, $\tilde{\mathbf{A}}_{k2}$, and $\tilde{\mathbf{A}}_{k3}$ are computed, where

$$\tilde{\mathbf{A}}_{k1} = -\left[\left(\hat{\mathbf{S}}\tilde{\mathbf{C}}_1^T\tilde{\mathbf{D}}_{11} + \tilde{\mathbf{B}}_1\right)\left(\mathbf{I} - \hat{\mathbf{D}}_{21p}^T\hat{\mathbf{D}}_{21p}\tilde{\mathbf{D}}_{11}^T\tilde{\mathbf{D}}_{11}\right)^{-1} \hat{\mathbf{D}}_{21}^T\hat{\mathbf{D}}_{21}\left(\mathbf{I} - \tilde{\mathbf{D}}_{11}^T\hat{\mathbf{D}}_{12p}\hat{\mathbf{D}}_{12p}^T\tilde{\mathbf{D}}_{11}\right)^{-1}\right] \tag{A.43}$$

$$\tilde{\mathbf{A}}_{k2} = -\left[\hat{\mathbf{S}}\hat{\mathbf{C}}_2^T\hat{\mathbf{D}}_{21}\left(\mathbf{I} - \tilde{\mathbf{D}}_{11}^T\tilde{\mathbf{D}}_{11}\hat{\mathbf{D}}_{21p}^T\hat{\mathbf{D}}_{21p}\right)^{-1} \left(\mathbf{I} - \tilde{\mathbf{D}}_{11}^T\tilde{\mathbf{D}}_{11}\right)\left(\mathbf{I} - \tilde{\mathbf{D}}_{11}^T\hat{\mathbf{D}}_{12p}\hat{\mathbf{D}}_{12p}^T\tilde{\mathbf{D}}_{11}\right)^{-1}\right] \tag{A.44}$$

$$\tilde{\mathbf{A}}_{k3} = \tilde{\mathbf{D}}_{11}^T\hat{\mathbf{D}}_{12p}\hat{\mathbf{D}}_{12p}^T\tilde{\mathbf{C}}_1 + \tilde{\mathbf{B}}_1^T\hat{\mathbf{P}} - \tilde{\mathbf{D}}_{11}^T\hat{\mathbf{D}}_{12}\hat{\mathbf{B}}_2\hat{\mathbf{P}} + \left(\mathbf{I} - \tilde{\mathbf{D}}_{11}^T\hat{\mathbf{D}}_{12p}\hat{\mathbf{D}}_{12p}^T\tilde{\mathbf{D}}_{11}\right)\hat{\mathbf{D}}_{21}^T\hat{\mathbf{C}}_2 \tag{A.45}$$

These matrices are used to calculate the matrix $\tilde{\mathbf{A}}_k$, given by

$$\tilde{\mathbf{A}}_k = \left(\tilde{\mathbf{A}}_{k1} + \tilde{\mathbf{A}}_{k2}\right)\tilde{\mathbf{A}}_{k3} + \mathbf{E}_k\left[\hat{\mathbf{A}} + \left(\tilde{\mathbf{B}}_1\tilde{\mathbf{D}}_{11}^T\hat{\mathbf{D}}_{12p}\hat{\mathbf{D}}_{12p}^T - \hat{\mathbf{B}}_2\hat{\mathbf{D}}_{12}^T\right)\left(\mathbf{I} - \tilde{\mathbf{D}}_{11}\tilde{\mathbf{D}}_{11}^T\hat{\mathbf{D}}_{12p}\hat{\mathbf{D}}_{12p}^T\right)^{-1}\tilde{\mathbf{C}}_1 - \left[\hat{\mathbf{B}}_2\hat{\mathbf{B}}_2^T - \left(\tilde{\mathbf{B}}_1 - \hat{\mathbf{B}}_2\hat{\mathbf{D}}_{12}^T\tilde{\mathbf{D}}_{11}\right)\left(\mathbf{I} - \tilde{\mathbf{D}}_{11}^T\hat{\mathbf{D}}_{12p}\hat{\mathbf{D}}_{12p}^T\tilde{\mathbf{D}}_{11}\right)^{-1}\left(\tilde{\mathbf{B}}_1^T - \tilde{\mathbf{D}}_{11}^T\hat{\mathbf{D}}_{12}\hat{\mathbf{B}}_2\right)\right]\hat{\mathbf{P}}\right] \tag{A.46}$$

The next step is to compute $\tilde{B}_{k1}$ and $\tilde{C}_{k1}$, given by

$$\tilde{B}_{k1} = \left[\left[\tilde{B}_1 + \hat{S}\tilde{C}_1^T\tilde{D}_{11} - \hat{S}\hat{C}_2^T\hat{D}_{21}\left(\tilde{D}_{11}^T\tilde{D}_{11} - I\right)\right]\left(I - \hat{D}_{21p}^T\hat{D}_{21p}\tilde{D}_{11}^T\tilde{D}_{11}\right)\hat{D}_{21}^T\right] \tag{A.47}$$

$$\tilde{C}_{k1} = -\left[\hat{D}_{12}^T\left(I - \tilde{D}_{11}\tilde{D}_{11}^T\hat{D}_{12p}\hat{D}_{12p}^T\right)^{-1}\left[\tilde{C}_1 + \tilde{D}_{11}\tilde{B}_1^T\hat{P} - \left(\tilde{D}_{11}\tilde{D}_{11}^T - I\right)\right]\hat{D}_{12}\hat{B}_2\hat{P}\right] \tag{A.48}$$

Then, $\tilde{R}_{bk2}$ and $\tilde{R}_{ck2}$ are computed by the following Cholesky factorizations

$$\tilde{R}_{bk2}^T\tilde{R}_{bk2} = \hat{D}_{12}^T\left(I - \tilde{D}_{11}\tilde{D}_{11}^T\right)\left(I - \hat{D}_{12p}\hat{D}_{12p}^T\tilde{D}_{11}\tilde{D}_{11}^T\right)^{-1}\hat{D}_{12} \tag{A.49}$$

$$\tilde{R}_{ck2}^T\tilde{R}_{ck2} = \hat{D}_{21}\left(I - \tilde{D}_{11}^T\tilde{D}_{11}\hat{D}_{21p}^T\hat{D}_{21p}\right)^{-1}\left(I - \tilde{D}_{11}^T\tilde{D}_{11}\right)\hat{D}_{21}^T \tag{A.50}$$

$\tilde{R}_{bk2}$ and $\tilde{R}_{ck2}$ are used to compute the following

$$\tilde{B}_{k2} = \left[\hat{B}_2 + \left(\hat{S}\tilde{C}_1^T - \tilde{B}_1\hat{D}_{21p}^T\hat{D}_{21p}\tilde{D}_{11}^T - \hat{S}\hat{C}_2^T\hat{D}_{21}\tilde{D}_{11}\right)\left(I - \tilde{D}_{11}\hat{D}_{21p}^T\hat{D}_{21p}\tilde{D}_{11}^T\right)^{-1}\hat{D}_{12}\right]\tilde{R}_{bk2}^T \tag{A.51}$$

$$\tilde{C}_{k2} = \tilde{R}_{ck2}\left[-\hat{C}_2 - \hat{D}_{21}\left(I - \tilde{D}_{11}^T\hat{D}_{12p}\hat{D}_{12p}^T\tilde{D}_{11}\right)^{-1}\left(\tilde{D}_{11}^T\hat{D}_{12p}\hat{D}_{12p}^T\tilde{C}_1 - \tilde{D}_{11}^T\hat{D}_{12}\hat{B}_2^T\hat{P} + \tilde{B}_1\hat{P}\right)\right] \tag{A.52}$$

$$\tilde{D}_{k12} = \tilde{R}_{bk2}^T \tag{A.53}$$

$$\tilde{D}_{k21} = \tilde{R}_{ck2} \tag{A.54}$$

$$\tilde{D}_{k22} = \left(\tilde{R}_{ck2}^T\right)^{-1} \hat{D}_{21}\tilde{D}_{11}^T \left(I - \tilde{D}_{11}\hat{D}_{21p}^T\hat{D}_{21p}\tilde{D}_{11}^T\right)^{-1} \hat{D}_{12}\tilde{R}_{bk2}^T \tag{A.55}$$

Next, $\tilde{D}_{k11}$ is computed. This matrix is simply given by

$$\tilde{D}_{k11} = F_{opt} \tag{A.56}$$

where F_{opt} is the "all-pass imbedding" matrix defined by (A.20)-(A.21).

The next step in computing the controller parameterization is to reverse the transformation scalings of (A.17), which leads to

$$\hat{B}_{k1} = \tilde{B}_{k1}S_y^{-1} \tag{A.57}$$

$$\hat{C}_{k1} = S_u\tilde{C}_{k1} \tag{A.58}$$

$$\hat{D}_{k11} = S_u\tilde{D}_{k11}S_y^{-1} \tag{A.59}$$

$$\hat{D}_{k12} = S_u\tilde{D}_{k12} \tag{A.60}$$

$$\hat{D}_{k21} = \tilde{D}_{k21}S_y^{-1} \tag{A.61}$$

The final step is to "shift" the original D_{22} matrix back into the system (Recall that this matrix was "zeroed out" for the previous calculations). If both $(I - D_{22}\hat{D}_{k11})$ and $(I + \hat{D}_{k11}D_{22})$ are nonsingular, this "shifting" operation leads to

$$A_k = \tilde{A}_k - \hat{B}_{k1}D_{22}\left(I + \hat{D}_{k11}D_{22}\right)^{-1} \hat{C}_{k1} \tag{A.62}$$

$$B_{k1} = \hat{B}_{k1}\left(I - D_{22}\hat{D}_{k11}\right) \tag{A.63}$$

$$B_{k2} = \tilde{B}_{k2} - \hat{B}_{k1}D_{22}\left(I + \hat{D}_{k11}D_{22}\right)^{-1}\hat{D}_{k12} \tag{A.64}$$

$$C_{k1} = \left(I + \hat{D}_{k11}D_{22}\right)^{-1}\hat{C}_{k1} \tag{A.65}$$

$$C_{k2} = \tilde{C}_{k2} - \hat{D}_{k21}D_{22}\left(I + \hat{D}_{k11}D_{22}\right)^{-1}\hat{C}_{k1} \tag{A.66}$$

$$D_{k11} = \left(I + \hat{D}_{k11}D_{22}\right)^{-1}\hat{D}_{k11} \tag{A.67}$$

$$D_{k12} = \left(I + \hat{D}_{k11}D_{22}\right)^{-1}\hat{D}_{k12} \tag{A.68}$$

$$D_{k21} = \hat{D}_{k21}\left(I - D_{22}\hat{D}_{k11}\right) \tag{A.69}$$

$$D_{k22} = \tilde{D}_{k22} - \hat{D}_{k21}D_{22}\left(I + \hat{D}_{k11}D_{22}\right)^{-1}\hat{D}_{k12} \tag{A.70}$$

These matrices, together with the matrix E_k, represent the descriptor-system form of the state-space parameterization of **K**, given by

$$E_k\dot{x}_k = A_kx_k + B_{k1}y + B_{k2}y_\Phi \tag{A.71}$$

$$u = C_{k1}x_k + D_{k11}y + D_{k12}y_\Phi \tag{A.72}$$

$$u_\Phi = C_{k2}x_k + D_{k21}y + D_{k22}y_\Phi \tag{A.73}$$

with

$$y_\Phi = \Phi(s)u_\Phi \tag{A.74}$$

For this controller parameterization, $\Phi(s)$ can be *any* stable, rational, linear transfer-function, so long as its H_∞ norm is less than unity. A diagram of the Standard Form model, together with this particular controller parameterization, is shown in Figure A.2

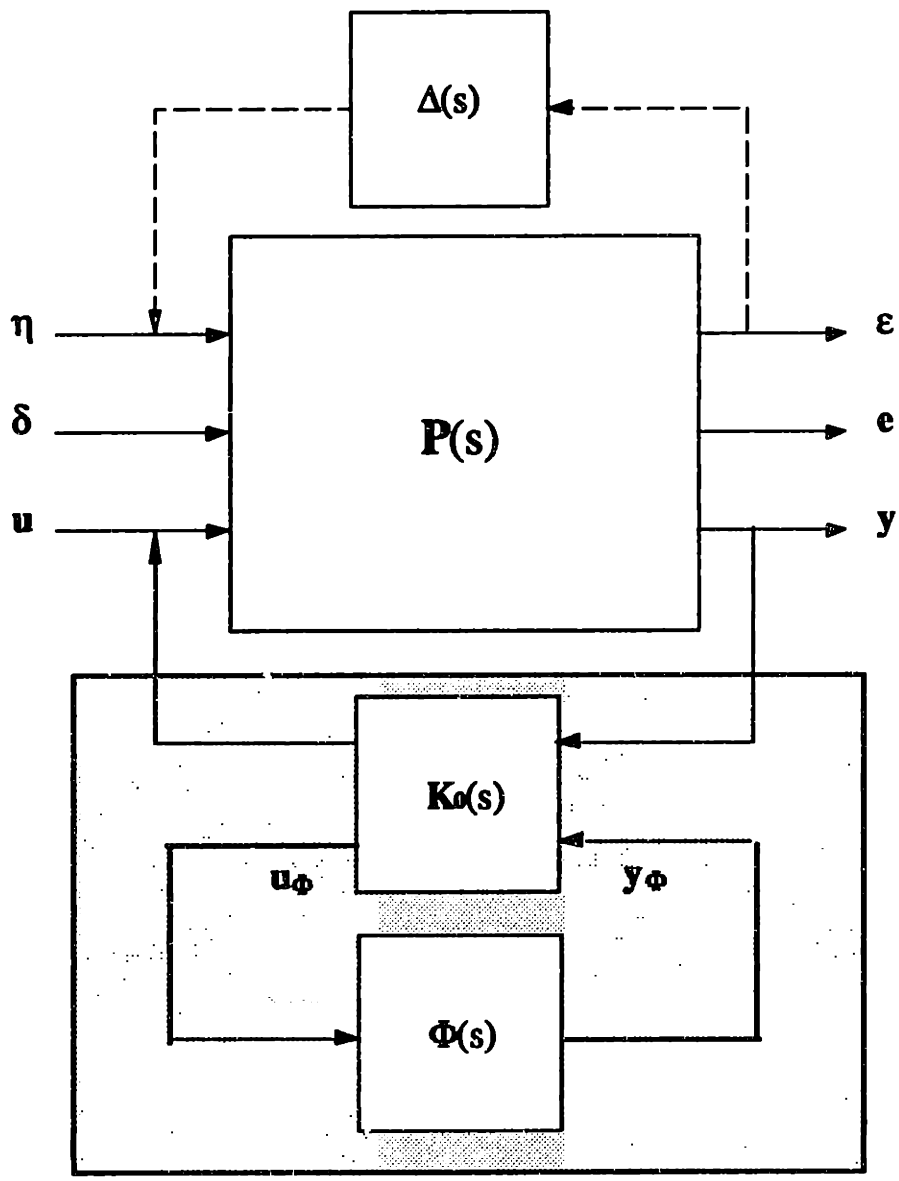

Figure A.2: Standard Form Model with Parameterization for K

For the case where $\Phi(s)$ is exactly equal to zero, this state-space parameterization reduces to $K_{11}(s)$, given by

$$E_k\dot{x}_k = A_k x_k + B_{k1} y \tag{A.75}$$

$$u = C_{k1} x_k + D_{k11} y \tag{A.76}$$

This particular controller is known as the *central* or *maximum-entropy* controller. Note that the central controller also happens to have the same state dimension as the original open-loop Standard-Form model, $P(s)$.

Appendix B

Sliding-Surfaces in State-Space

Suppose the state-space of a dynamic system is described by $R^{(n)\times k}$ (i.e., real-valued, n differentiable, k degrees-of-freedom). This implies that the system state vector, x, can defined by

$$\mathbf{x} = \begin{bmatrix} \hat{\mathbf{x}} \\ \vdots \\ \hat{\mathbf{x}}^{(n-1)} \end{bmatrix} \tag{B.1}$$

where

$$\hat{\mathbf{x}} = \begin{bmatrix} \hat{x}_1 \\ \vdots \\ \hat{x}_k \end{bmatrix} \tag{B.2}$$

From this state description, the following linear hyperplane surface can be defined in the state-space

$$s(\mathbf{x}) = \sum_{p=0}^{n-1} \binom{n-1}{p} \Lambda^p \, \hat{\mathbf{x}}^{(n-1-p)} \tag{B.3}$$

where

$$\binom{n-1}{p} = \frac{(n-1)!}{p!\,((n-1)-p)!} \tag{B.4}$$

If the system states are constrained to the surface $s(x) = 0$, the system dynamics are described by the following linear matrix differential equation

$$\left(\frac{d}{dt} + \Lambda\right)^{n-1} \hat{x} = 0 \qquad \textbf{(B.5)}$$

If Λ is chosen such that the matrix $-\Lambda$ is Hurwitz (i.e. all the eigenvalues of $-\Lambda$ are in the left half-plane), (B.5) describes a stable differential equation, which implies that the state vector solution, $\hat{x}$, (and consequently x) will decay to zero.

Suppose x is initially off the sliding surface (i.e. $s(x)$ is nonzero). One measure of the "distance" from x to the sliding surface is given by the following Lyapunov "virtual energy" function

$$V(x) = s^T(x)s(x) \qquad \textbf{(B.6)}$$

Note that $V(x)$ is greater than zero for all x not on the sliding surface. For x to be "attracted" to the sliding surface implies that this distance, given by $V(x)$, must be constantly decreasing (until it reaches zero). In other words, the time-derivative of $V(x)$ must be less than zero for all states not on the sliding surface.

One way for the dynamic system to satisfy this constantly-decreasing distance condition is for the time-derivative of $V(x)$ to satisfy the following relation for all states not on the sliding-surface

$$\frac{1}{2}\frac{d}{dt}V(x) \leq -\eta\left(V(x)\right)^{1/2} \quad \text{for } x \in \left(R^{(n)\times k} - S(t)\right) \qquad \textbf{(B.7)}$$

where η is a positive constant and $S(t)$ is defined to be the sliding surface, $s(x) = 0$. Substituting (B.6) into (B.5) gives

$$\frac{1}{2}\frac{d}{dt}s^T(x)s(x) \leq -\eta\left(s^T(x)s(x)\right)^{1/2} \quad \text{for } x \in \left(R^{(n)\times k} - S(t)\right) \qquad \textbf{(B.8)}$$

This relation can be simplified further by recognizing the fact that the magnitude of the vector s(x) is always less than or equal to the sum of the magnitudes of its individual elements, i.e.

$$|s(x)| = \left(s^T(x)s(x)\right)^{1/2} \leq \sum_{i=1}^{k} |s_i(x)| = s^T(x)\mathrm{sgn}(s(x)) \tag{B.9}$$

which gives

$$\frac{1}{2}\frac{d}{dt}s^T(x)s(x) \leq -\eta s^T(x)\mathrm{sgn}(s(x)) \quad \text{for } x \in \left(R^{(n)\times k} - S(t)\right) \tag{B.10}$$

where sgn(s(x)) is defined as the vector of the signs of the elements of s(x)

$$\mathrm{sgn}(s(x)) = \begin{bmatrix} \mathrm{sgn}(s_1(x)) \\ \vdots \\ \mathrm{sgn}(s_k(x)) \end{bmatrix} \tag{B.11}$$

If (B.10), also known as the *sliding condition*, is satisfied for all "off" states, it can be shown that the system reaches the sliding surface in a *finite* time, and remains there, as shown in Figure B.1.

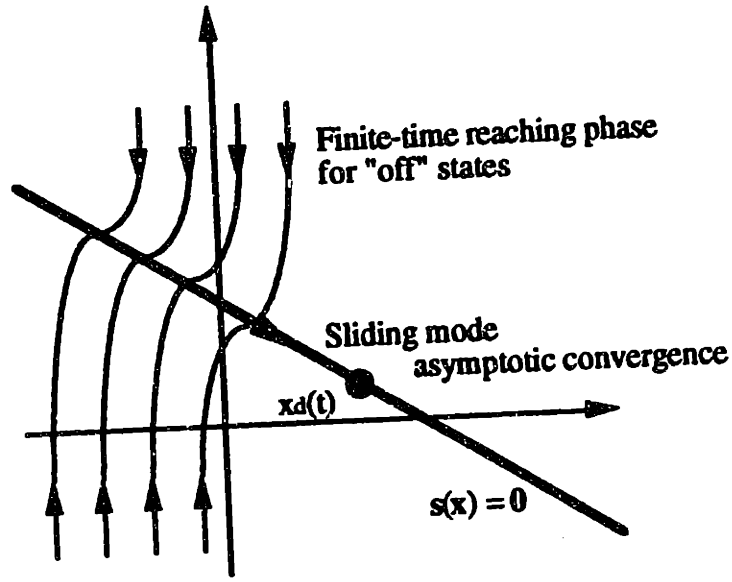

Figure B.1: Graphical Interpretation of the Sliding Condition

Appendix C

AUV Equations of Motion

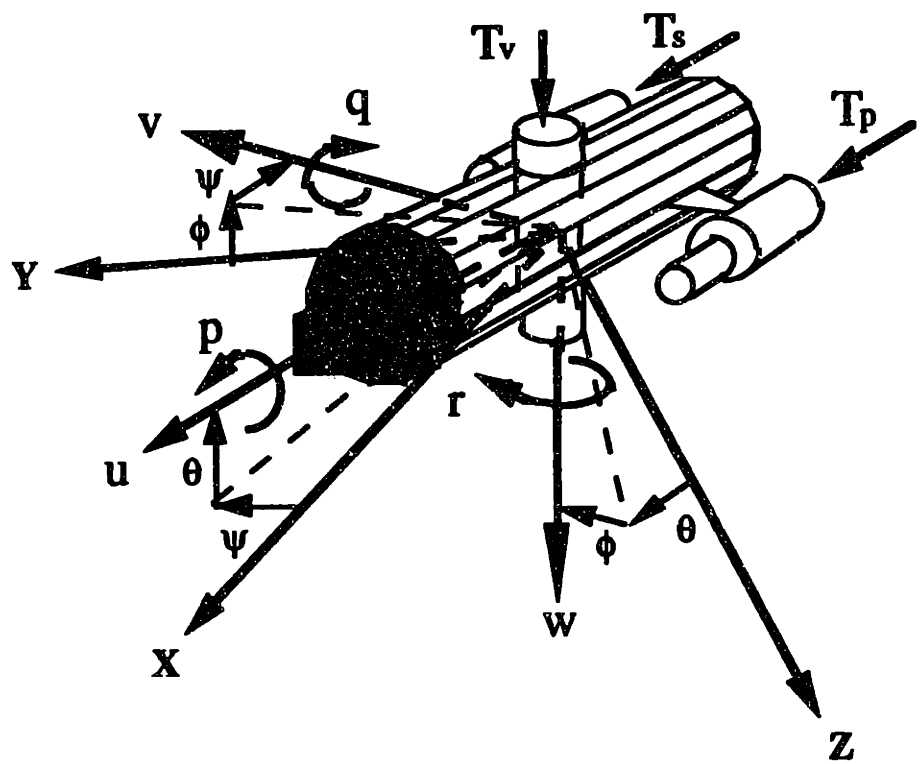

Figure C.1: Definition of AUV EOM Variables

Table C.1: State Variables

Vehicle relative	Fixed-frame relative
u = forward velocity (ft/s)	X = X position (ft)
v = lateral velocity (ft/s)	Y = Y position (ft)
w = vertical velocity (ft/s)	Z = Z position (ft)
p = roll rate (rad/s)	ϕ = roll angle (rad)
q = pitch rate (rad/s)	θ = pitch angle (rad)
r = yaw rate (rad/s)	ψ = yaw angle (rad)

Table C.2: Input Variables

T_V = vertical thrust (lb)
T_P = port thrust (lb)
T_S = starboard thrust (lb)

Axial Force

$$m[\dot{u} - vr + wq - X_g(q^2 + r^2) + Y_g(pq - \dot{r}) + Z_g(pr + \dot{q})] = X_{\dot{u}}\dot{u} + X_{u|u|}u|u| + (W - B)\sin\theta + T_p + T_s + D_u \quad \text{(C.1)}$$

Lateral Force

$$m[\dot{v} - wp + ur - Y_g(r^2 + p^2) + Z_g(qr - \dot{p}) + X_g(qp + \dot{r})] = Y_{\dot{v}}\dot{v} + Y_{\dot{p}}\dot{p} + Y_{\dot{r}}\dot{r} + Y_{v|v|}v|v| + Y_{ur}ur + Y_{uv}|u|v + (W - B)\cos\theta\sin\phi + D_v \quad \text{(C.2)}$$

Vertical Force

$$m[\dot{w} - uq + vp - Z_g(p^2 + q^2) + X_g(rp - \dot{q}) + Y_g(rq + \dot{p})] = Z_{\dot{w}}\dot{w} + Z_{\dot{q}}\dot{q} + Z_{w|w|}w|w| + Z_{uw}|u|w + Z_{uq}uq + (W - B)\cos\theta\cos\phi + T_v + D_w \quad \text{(C.3)}$$

Rolling Moment

$$\begin{aligned} &I_{xx}\dot{p} + (I_{zz} - I_{yy})qr - (\dot{r} + pq)I_{zx} + (r^2 - q^2)I_{yz} \\ &+ (pr - \dot{q})I_{xy} + m[Y_g(\dot{w} - uq + vp) - Z_g(\dot{v} - wp + ur)] \\ &= K_{\dot{p}}\dot{p} + K_{\dot{v}}\dot{v} + K_{p|p|}p|p| + (Y_gW - Y_bB)\cos\theta\cos\phi \\ &- (Z_gW - Z_bB)\cos\theta\sin\phi + T_vY_g + D_p \end{aligned} \qquad \text{(C.4)}$$

Pitching Moment

$$\begin{aligned} &I_{yy}\dot{q} + (I_{xx} - I_{zz})rp - (\dot{p} + qr)I_{xy} + (p^2 - r^2)I_{yz} \\ &+ (qp - \dot{r})I_{yz} + m[Z_g(\dot{u} - vr + wq) - X_g(\dot{w} - uq + vp)] \\ &= M_{\dot{q}}\dot{q} + M_{\dot{w}}\dot{w} + M_{qq|q|}q|q| + M_{uw}uw + M_{uq}uq \\ &- (X_gW - X_bB)\cos\theta\cos\phi \\ &- (Z_gW - Z_bB)\sin\theta - (T_p + T_s)Z_g + T_vX_g + D_q \end{aligned} \qquad \text{(C.5)}$$

Yawing Moment

$$\begin{aligned} &I_{zz}\dot{r} + (I_{yy} - I_{xx})pq - (\dot{q} + rp)I_{yz} + (q^2 - p^2)I_{xy} \\ &+ (rq - \dot{p})I_{zx} + m[X_g(\dot{v} - wp + ur) - Y_g(\dot{u} - vr + wq)] \\ &= N_{\dot{r}}\dot{r} + N_{\dot{v}}\dot{v} + N_{r|r|}r|r| + N_{ur}ur + N_{uv}uv \\ &+ (X_gW - X_bB)\cos\theta\sin\phi \\ &+ (Y_gW - Y_bB)\sin\theta + Y_T(T_p - T_s) + D_r \end{aligned} \qquad \text{(C.6)}$$

In the equations described here, u, v, and w are the linear velocities defined in the vehicle-relative coordinate frame, and p, q, and r are the angular velocities in the vehicle-relative coordinate frame. The positive directions of these velocities are defined according to the right-hand rule as shown in Figure C.1. The vehicle's earth-frame relative angular positions (roll, pitch, and heading) are represented by the Euler angles, ϕ, θ, and ψ, which are defined in the manner also shown in Figure C.1. T_S, T_P, and T_V represent the propulsion forces produced by the starboard, port, and vertical thrusters. D_u, D_v, D_w, D_p, D_q, and D_r represent the disturbance forces and torques with positive directions defined in the vehicle-relative coordinate frame exactly like u, v, w, p, q, and r. Derivatives with respect to time are represented by the dotted terms. The mass of the vehicle is given by m, while the mass moments of inertia are given by I_{xx}, I_{yy}, and I_{zz}. B and W are the AUV's buoyancy and weight, respectively. The locations of the vehicle's center-of-gravity (cg) and center-of-buoyancy (cb) are defined in the vehicle-relative

coordinate frame by (X_g,Y_g,Z_g) and (X_b,Y_b,Z_b). The remaining terms in the EOM are the various hydrodynamic coefficients of the AUV (i.e., $Y_{|v|v}$, N_{ur}, etc.). These terms are used to describe effects such as drag forces, lift forces, and "added mass" forces which act on the AUV.

The kinematic relationships between the vehicle-relative velocities and the Earth-relative positions and Euler angles can be defined by the following equations.

$$\dot{X} = u \cos\theta \cos\psi + v(\sin\phi \sin\theta \cos\psi - \cos\phi \sin\psi) + w(\sin\phi \sin\psi + \cos\phi \sin\theta \cos\psi) \quad \text{(C.7)}$$

$$\dot{Y} = u \cos\theta \sin\psi + v(\cos\theta \cos\psi + \cos\phi \sin\vartheta \sin\psi) + w(\cos\phi \sin\theta \cos\psi - \sin\phi \cos\psi) \quad \text{(C.8)}$$

$$\dot{Z} = - u \sin\theta + v \cos\theta \sin\phi + w \cos\theta \cos\phi \quad \text{(C.9)}$$

$$\dot{\phi} = p + \left[\frac{r \cos\phi + q \sin\phi}{\cos\theta}\right] \sin\theta \quad \text{(C.10)}$$

$$\dot{\theta} = q \cos\phi + r \sin\phi \quad \text{(C.11)}$$

$$\dot{\psi} = \frac{r \cos\phi + q \sin\phi}{\cos\theta} \quad \text{(C.12)}$$

Appendix D

Vehicle Parameters

B	63.32
I_{xx}	.3
I_{yy}	2.3
I_{zz}	2.3
$K_{p\|p\|}$	-.8
$K_{p'}$	-.025
$K_{v'}$	.0079
mass	1.97
$M_{q\|q\|}$	6.5
$M_{q'}$	-.41
M_{uq}	-.32
M_{uw}	1.57
$M_{w\|w\|}$	0.0
$M_{w'}$	-.02
$N_{r\|r\|}$	-5.6
$N_{r'}$	-.38
N_{ur}	-.32
N_{uv}	-1.57
$N_{v'}$	0.0
W	63.32

Xb	.12
X_g	.12
$X_{u\|u\|}$	-.84
$X_{u'}$	-.35
Y_b	0.0
Y_g	0.0
$Y_{p'}$	.0079
$Y_{r'}$	0.0
Y_T	.56
Y_{ur}	.042
Y_{uv}	-.3
$Y_{v\|v\|}$	-3.00
$Y_{v'}$	-1.48
Z_b	0.0
Z_g	.091
$Z_{q'}$	-.02
Z_{uq}	-.042
Z_{uw}	-.28
$Z_{w\|w\|}$	-3.49
$Z_{w'}$	-1.32

Appendix E

Model Reduction

Consider the standard LTI state-space model given by

$$\dot{\mathbf{x}} = \mathbf{A}\mathbf{x} + \mathbf{B}\mathbf{u}$$
$$\mathbf{y} = \mathbf{C}\mathbf{x} + \mathbf{D}\mathbf{u} \qquad \text{(E.1)}$$

The transfer-function matrix of this system is given by

$$\mathbf{G}(s) = \mathbf{D} + \mathbf{C}(s\mathbf{I} - \mathbf{A})^{-1}\mathbf{B} \qquad \text{(E.2)}$$

It can be shown [5] that if the system given by (E.1) is stable, then the controllability and observability gramians, given respectively by

$$\mathbf{P} = \int_0^\infty e^{\mathbf{A}t}\,\mathbf{B}\mathbf{B}^T e^{\mathbf{A}^T t}\,dt \qquad \text{(E.3)}$$

$$\mathbf{Q} = \int_0^\infty e^{\mathbf{A}^T t}\,\mathbf{C}^T\mathbf{C}\,e^{\mathbf{A}t}\,dt \qquad \text{(E.4)}$$

are both (symmetric) positive semi-definite. These gramians can be found by solving the following pair of Lyapunov equations.

$$\mathbf{A}\mathbf{P} + \mathbf{P}\mathbf{A}^T + \mathbf{B}\mathbf{B}^T = 0 \qquad \text{(E.5)}$$

$$\mathbf{A}^T\mathbf{Q} + \mathbf{Q}\mathbf{A} + \mathbf{C}^T\mathbf{C} = 0 \qquad \text{(E.6)}$$

Since these gramians are positive semi-definite, the following real factorizations can be defined

$$\mathbf{P} = \mathbf{R}\mathbf{R}^T \tag{E.7}$$

$$\mathbf{Q} = \mathbf{S}\mathbf{S}^T \tag{E.8}$$

Let the singular value decomposition (SVD) of the matrix, $\mathbf{S}^T\mathbf{R}$, be given by

$$\mathbf{S}^T\mathbf{R} = \mathbf{U}_H\Sigma_H\mathbf{V}_H^T \tag{E.9}$$

Then the SVD of the matrix, $\mathbf{H} = \mathbf{R}^T\mathbf{Q}\mathbf{R}$, is given by

$$\mathbf{H} = \mathbf{V}_H\Sigma_H^2\mathbf{V}_H^T \tag{E.10}$$

The elements of the diagonal matrix, Σ_H, are known as the Hankel Singular Values (HSV). The "relative" controllability and observability of the states of the LTI system given by (E.1) are directly directly dependent on the magnitude of these HSV's [22], which implies that the number of non-minimal (uncontrollable or unobservable) states is exactly equal to the number of zero HSV's.

Let the matrix, Σ_H, be factored as

$$\Sigma_H = \begin{bmatrix} \Sigma_{11} & 0 \\ 0 & \Sigma_{22} \end{bmatrix} \tag{E.11}$$

Now define the following transformation matrices

$$\mathbf{S}_L = \mathbf{S}\mathbf{U}_H\Sigma_{11}^{-1/2} \tag{E.12}$$

$$S_R = R V_H \Sigma_{11}^{-1/2} \qquad \text{(E.13)}$$

Then the "balanced" reduced-order approximation [22], $G_r(s)$, of (E.1) is given by

$$\dot{x}_r = S_L^T A S_R x_r + S_L^T B u$$
$$y = C S_R x_r + D u \qquad \text{(E.14)}$$

where the state-order of this approximation is exactly equal to the number of diagonal elements of Σ_{11}. The H_∞ bound on the additive approximation error is given by

$$\| G(s) - G_r(s) \|_\infty \leq 2 \, \text{trace}[\Sigma_{22}] \qquad \text{(E.15)}$$

Note that both the controllability gramian and observability gramian for the reduced-order model are given by Σ_{11} [22]

The fractional-balanced reduction approach [23] utilizes stable coprime factorizations of the model given by (E.1) and (E.2) to generalize the "balanced" model-reduction to unstable plants. However, the plant is still required to be stabilizable and detectable.

The normalized right coprime factorization (NRCF) of the LTI model, (E.1) and (E.2), is given by

$$G(s) = N(s) D^{-1}(s) + D \qquad \text{(E.16)}$$

where the (stable) transfer-function matrices, N(s) and D(s), are given by

$$N(s) = 0 + C(sI - (A + BK))^{-1} B \qquad \text{(E.17)}$$

$$D(s) = I + K(sI - (A + BK))^{-1} B \qquad \text{(E.18)}$$

The "stabilizing feedback gain" matrix, K, is given by

$$\mathbf{K} = -\mathbf{B}^T\mathbf{Q} \tag{E.19}$$

where **Q** is the solution of the matrix Riccatti equation

$$\mathbf{QA} + \mathbf{A}^T\mathbf{Q} - \mathbf{QBB}^T\mathbf{Q} + \mathbf{C}^T\mathbf{C} = 0 \tag{E.20}$$

The matrix, **Q**, is also the observability gramian of the "fictitious" stable plant given by

$$\begin{bmatrix} \mathbf{D}(s) \\ \mathbf{N}(s) \end{bmatrix} = \begin{bmatrix} \mathbf{I} \\ 0 \end{bmatrix} + \begin{bmatrix} \mathbf{K} \\ \mathbf{C} \end{bmatrix} (s\mathbf{I} - (\mathbf{A} + \mathbf{BK}))^{-1}\mathbf{B} \tag{E.21}$$

The corresponding controllability gramian, **P**, of this fictitious system is given by the solution of the following Lyapunov equation

$$(\mathbf{A} + \mathbf{BK})\mathbf{P} + \mathbf{P}(\mathbf{A} + \mathbf{BK})^T + \mathbf{BB}^T = 0$$

By applying equations similar to (E.7) through (E.15) [23] (and "undoing" the stabilizing feedback from the NRCF), a reduced-order model of the original, possibly unstable plant model can be derived (with a corresponding bound on the modeling approximation error). Extensions of the fractional-balanced approach can also be made to systems with uncontrollable or unobservable unstable modes [22].

References

[1] Athans, M., "6.233J-6.234J Class Notes", MIT, Cambridge, MA., Fall 1989-Spring 1990.

[2] Appleby, B. D., Robust Estimator Design Using the H∞ Norm and μ-Synthesis. Ph.D. Thesis, MIT, Cambridge, MA, February 1990.

[3] Doyle, J. C., "Analysis of Feedback Systems with Structured Uncertainties", IEEE Proceedings, vol. 129, pp. 242-250, 1982.

[4] Doyle, J. C., "Structured Uncertainty in Control System Design", Proceeding of 24th IEEE Conference on Decision and Control, Fort Lauderdale, FL. Dec. 1985 pp. 260-265.

[5] Francis, Bruce A., A Course in H_∞ Control Theory , Lecture Notes in Control and Information Sciences, Vol. 88. Berlin: Springer-Verlang, 1987.

[6] Maciejowski, J. M., Multivariable Feedback Design, Addison Wesley , Reading, MA., 1989.

[7] Youla, D. C., Jabr, H. A., and Bongiorno, J. J., "Modern Wiener-Hopf Design of Optimal Controllers: Part II", IEEE Transactions on Automatic Control, vol. AC-21, pp. 319-338, 1976.

[8] Glover, K., "All Optimal Hankel-Norm Approximations of Linear Multivariable Systems and Their L_∞-Error Bounds", International Journal of Control, vol. 39, no. 6, pp. 1115-1193, 1984.

[9] Doyle, J. C., Glover, K., Khargonekar, P., and Francis, B., "State-Space Solutions to Standard H_2 and H_∞ Control Problems", IEEE Transactions on Automatic Control, vol. AC-34, no. 8, pp. 831-847, 1989.

[10] Limebeer, D. N. J., Kasenally, E. M., and Safonov, M. G., "A Characterization of All Solutions to the Four-Block General Distance Problem", submitted April 1988 to SIAM Journal of Control.

[11] Chiang, R. Y., and Safonov, M. G., Robust Control Toolbox for use with MATLAB™, The Mathworks, 1988.

[12] Safonov, M. G., Chiang, R. Y., and Limebeer, D. N. J.,"Hankel-Model Reduction without Balancing - A Descriptor Approach", Proceeding of IEEE Conference on Decision and Control, Los Angeles, CA., Dec. 9-11, 1987.

[13] Filippov, A. F., "Differential Equations with Discontinuous Right Hand Side", American Mathematical Society Translations, vol. 62, pp. 199-231, 1960

[14] Utkin, V. I., Sliding Mode and its Applications to Variable Structure Systems, Mir., Moscow, 1978

[15] Slotine, J.-J.E., Tracking Control of Nonlinear Systems Using Sliding Surfaces, Ph.D. Thesis, MIT, Cambridge, MA, 1983.

[16] Slotine, J.-J.E. and Li, Weiping, Applied Nonlinear Control, Prentice Hall,Inc., Englewood Cliffs, N. J., 1991.

[17] Bedrossian, N. S., Nonlinear Control Using Linearizing Transformations., Ph.D. Thesis, MIT, Cambridge, MA, September 1991.

[18] Wallar, Eric, Design and Full-Scale Testing of a Sliding Mode Controller for a Small Underwater Vehicle. S.M. Thesis, MIT, Cambridge, MA, July 1989.

[19] Feldman, J., "DTNSRDC Revised Standard Submarine Equations of Motion", DTNSRDC/SPD-0303-09, U.S. Navy, June 1979.

[20] Yoerger, Dana R., "The Influence of Thruster Dynamics on Underwater Vehicle Behavior and Their Incorporation Into Control System Design,"IEEE Oceanic Engineering, vol. 15, pp. 167-78, 1990.

[21] Ogata, K., Discrete-Time Control Systems Prentice Hall,Inc., Englewood Cliffs, N. J., 1987.

[22] Dowdle, John R., "Design Issues for Large-Scale Uncertain Systems", The Charles Stark Draper Laboratory, Inc., Report CSDL R-2174, September 1989

[23] Meyer, D., "A Fractional Approach to Model Reduction", Proceedings 1988 American Control Conference, pp. 1041-1047, 1988